Case No. 84739

IN THE SUPREME COURT OF THE STATE OF NEVADA

ADAM SULLIVAN, P.E., NEVADA STATE ENGINEER, et al.

Appellants,

vs.

LINCOLN COUNTY WATER DISTRICT, et al.

JOINT APPENDIX

VOLUME 9 OF 49

USGS
science for a changing world

Advanced Methods for Modeling Water-Levels and Estimating Drawdowns with SeriesSEE, an Excel Add-In

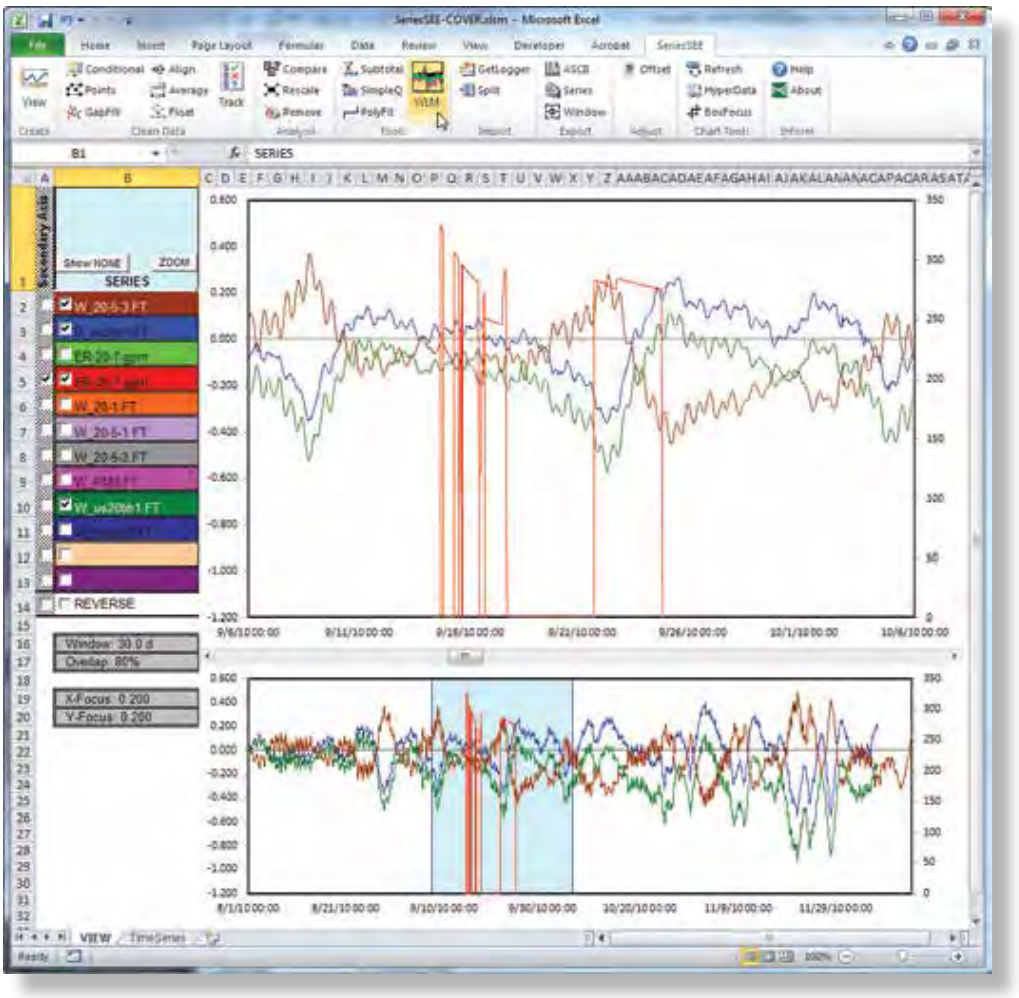

Techniques and Methods 4–F4

U.S. Department of the Interior
U.S. Geological Survey

SE ROA 11371
JA_4133

Cover art: Screen showing SeriesSEE toolbar and example workbook that was created with SeriesSEE

Advanced Methods for Modeling Water-Levels and Estimating Drawdowns with SeriesSEE, an Excel Add-In

By Keith Halford, C. Amanda Garcia, Joe Fenelon, and Benjamin Mirus

U. S. Department of Energy, National Nuclear Security Administration,
Environmental Restoration Program, Underground Test Area Project

Techniques and Methods 4–F4

U.S. Department of the Interior
U.S. Geological Survey

U.S. Department of the Interior
KEN SALAZAR, Secretary

U.S. Geological Survey
Marcia K. McNutt, Director

U.S. Geological Survey, Reston, Virginia: 2012

Suggested citation:
Halford, K., Garcia, C.A., Fenelon, J., and Mirus, B., 2012, Advanced methods for modeling water-levels and estimating drawdowns with SeriesSEE, an Excel add-In, U.S. Geological Survey Techniques and Methods 4–F4, 28 p.

Preface

This report documents a spreadsheet add-in for viewing time series and modeling water levels that was developed in Microsoft® Excel 2010. Use of trade names does not constitute endorsement by the U.S. Geological Survey (USGS). The spreadsheet add-in has been tested for accuracy by using multiple datasets. If users find or suspect errors, please contact the USGS.

Every effort has been made by the USGS or the United States Government to ensure the spreadsheet add-in is error free. Even so, errors possibly exist in the spreadsheet add-in. The distribution of the spreadsheet add-in does not constitute any warranty by the USGS, and no responsibility is assumed by the USGS in connection therewith.

Acknowledgments

The report was prepared in cooperation with the U.S. Department of Energy, National Nuclear Security Administration, Nevada Site Office, Office of Environmental Management under Interagency Agreement DE-AI52-12NA30865.

The tide-challenged authors are indebted to Devin Galloway for clarifying the ebb and flow of tides.

Contents

Figures

Tables

Conversion Factors and Datums

Multiply	By	To obtain
	Length	
foot (ft)	0.3048	meter (m)
mile (mi)	1.609	kilometer (km)
	Volume	
gallon (gal)	3.785	liter (L)
	Flow rate	
gallon per minute (gal/min)	0.06309	liter per second (L/s)
	Transmissivity*	
foot squared per day (ft^2/d)	0.09290	meter squared per day (m^2/d)

Vertical coordinate information is referenced to the North American Vertical Datum of 1988 (NAVD 88).

Horizontal coordinate information is referenced to the North American Datum of 1983 (NAD 83).

Altitude, as used in this report, refers to distance above the vertical datum.

*Transmissivity: The standard unit for transmissivity is cubic foot per day per square foot times foot of aquifer thickness [(ft^3/d)/ft^2]ft. In this report, the mathematically reduced form, foot squared per day (ft^2/d), is used for convenience.

Advanced Methods for Modeling Water-Levels and Estimating Drawdowns with SeriesSEE, an Excel Add-In

By Keith Halford, C. Amanda Garcia, Joe Fenelon, and Benjamin Mirus

Abstract

Water-level modeling is used for multiple-well aquifer tests to reliably differentiate pumping responses from natural water-level changes in wells, or "environmental fluctuations." Synthetic water levels are created during water-level modeling and represent the summation of multiple component fluctuations, including those caused by environmental forcing and pumping. Pumping signals are modeled by transforming step-wise pumping records into water-level changes by using superimposed Theis functions. Water-levels can be modeled robustly with this Theis-transform approach because environmental fluctuations and pumping signals are simulated simultaneously. Water-level modeling with Theis transforms has been implemented in the program SeriesSEE, which is a Microsoft® Excel add-in. Moving average, Theis, pneumatic-lag, and gamma functions transform time series of measured values into water-level model components in SeriesSEE. Earth tides and step transforms are additional computed water-level model components. Water-level models are calibrated by minimizing a sum-of-squares objective function where singular value decomposition and Tikhonov regularization stabilize results. Drawdown estimates from a water-level model are the summation of all Theis transforms minus residual differences between synthetic and measured water levels. The accuracy of drawdown estimates is limited primarily by noise in the data sets, not the Theis-transform approach. Drawdowns much smaller than environmental fluctuations have been detected across major fault structures, at distances of more than 1 mile from the pumping well, and with limited pre-pumping and recovery data at sites across the United States. In addition to water-level modeling, utilities exist in SeriesSEE for viewing, cleaning, manipulating, and analyzing time-series data.

Introduction

Multiple-well, aquifer testing provides the most direct, integrated assessment of bulk hydraulic properties within complex geologic systems (Bohling and others, 2003; Sepúlveda, 2006; Yeh and Lee, 2007; Walton, 2008). The aquifer volume investigated with multi-well aquifer tests increases with increasing distance at which drawdown, or the pumping signal, can be detected (Risser and Bird, 2003; Halford and Yobbi, 2006). Drawdown analyses at distances of more than 1 mile (mi) often fail because environmental water-level fluctuations typically overwhelm the pumping signal. Barometric change, tidal forces, surface-water stage changes, or other external stresses induce these natural water-level changes in wells, which collectively are referred to here as "environmental fluctuations."

Barometric change and tidal forces can induce water-level fluctuations in a well greater than 1 foot (ft) during periods of less than a few days (Fenelon, 2000). Daily barometric changes alone typically exceed 0.3 ft where aquifers are confined or the unsaturated zone is thicker than 500 ft (Weeks, 1979; Merritt, 2004). Episodic recharge events can cause water-level rises that exceed 1 ft (O'Reilly, 1998). Climatic variations in recharge can induce long-term rising trends of more than 3 feet per year that affect detection of small pumping signals (Elliott and Fenelon, 2010; Fenelon, 2000). Drawdowns can be a fraction of the environmental fluctuations in distant observation wells that are more than a mile from a pumping well.

Environmental fluctuations have been modeled previously to differentiate natural water-level changes from pumping responses. Barometric and tidal effects typically are modeled independently and removed from water-level records (Erskine, 1991; Rasmussen and Crawford, 1997; Toll and Rasmussen, 2007). These approaches do not remove regional trends, such as long-term recharge, and are difficult to automate because all significant stresses that affect water levels other than pumping are not simulated simultaneously.

Water levels from background wells can be used to explicitly model water-level changes from recharge responses, surface-water stage changes, or any other external stress (Halford, 2006; Criss and Criss, 2011). A background well monitors water levels that are affected by tidal potential-rock interaction, imperfect barometric coupling, and all other stresses, excluding analyzed pumping, that affect water levels in observation wells. The need for antecedent data and background water levels has long been recognized (Stallman, 1971), but these trends and corrections typically have been estimated qualitatively.

Environmental fluctuations can be simulated as synthetic water levels, which represent the summation of multiple time series of barometric-pressure change, tidal potential, and background water levels, if available (Halford, 2006). Synthetic water levels are fitted to measured water levels for a period just prior to pumping, which should be more than three times greater than the period affected by pumping (Halford, 2006). Amplitude and phase of each time series are adjusted to minimize differences between synthetic and measured water levels. These synthetic water levels are projected into the pumping period, and drawdown is the difference between synthetic and measured water levels. This approach is referred to here as the "projection approach" to water-level modeling. The projection approach becomes unreliable where most of the analyzed period is affected by pumping.

Simultaneous modeling of environmental fluctuations and pumping signals overcomes the limitations of long-term extrapolation by using the projection approach. Environmental fluctuations can be defined during the entire period of record, which includes pumping and prolonged recovery periods. Variable pumping rates, as defined by a schedule of step changes, can be transformed to pumping signals by superimposing multiple Theis functions (Theis, 1935). Simultaneous simulation of all significant stresses affecting water-level changes is discussed as the "Theis-transform approach" to water-level modeling.

These water-level modeling approaches have been implemented in the program SeriesSEE, which is a Microsoft® Excel add-in. Water levels to be modeled, component fluctuations, and period of analysis are defined interactively and viewed in workbooks that are created by SeriesSEE. Water levels are modeled with a FORTRAN program that is called from Excel. Differences between synthetic and measured water levels are minimized with *PEST* (Doherty, 2010a and 2010b). Water-level models are calibrated rapidly because PEST files are created and executed seamlessly.

Water-level modeling with SeriesSEE differs from existing applications that filter environmental fluctuations or simulate pumping (Toll and Rasmussen, 2007; Harp and Vesselinov, 2011). This is because models of environmental fluctuations, Theis transforms, and parameter estimation are integrated in SeriesSEE. BETCO (barometric and earth tide correction) and similar programs simulate barometric and tidal water-level fluctuations but not regional trends and pumping effects (Toll and Rasmussen, 2007). Theis transforms have been applied previously in other water-level models, but environmental fluctuations were simulated with linear trends (Harp and Vesselinov, 2011).

Purpose and Scope

The purpose of this report is to document the approach used in SeriesSEE. This is the supporting software for modeling water levels that respond to environmental fluctuations and pumping. Water levels are modeled so pumping signals can be differentiated from environmental fluctuations. A method for fitting these water-level models to measured series by adjusting the selected parameters of each component is reported. The spreadsheet add-in is compatible with Microsoft® Excel 2010 (version 14.0) or higher. Use of the spreadsheet add-in requires basic knowledge of Excel. Use and applicability of this software is documented in this report. The hydrologic concepts and methods used in the data processing also are described briefly.

Environmental Fluctuations

Environmental fluctuations in measured water levels, or natural water-level changes, can be modeled by using pertinent time series, such as barometric pressure, tidal potential, background water levels, and stream stage. These time series represent potential components used to create synthetic water levels in a water-level model. Relevant components can be selected where a relation is expected with the water-level record. For example, water-level fluctuations in well b4mwh appear to be related to earth tide, barometric pressure fluctuations, recharge, and pumping (fig. 1). Simulating these environmental fluctuations in well b4mwh requires that earth tide, barometric pressure, and background water level (wells rw204 and sct4) components are included so that synthetic water levels can replicate measured water levels.

Barometric Effects

Barometric pressure induced water-level fluctuations are greatest in deep, confined aquifers where the rock matrix absorbs most of the atmospheric load (Merritt, 2004). Fluctuations increase because pressure instantly affects water levels in wells, whereas a stiff rock matrix transfers little of the increased atmospheric load to the confined water column. Atmospherically induced water-level fluctuations typically are less than 0.2 ft during a day. Large barometric-pressure changes from regional storms can cause water-level fluctuations of more than 1 ft during a week.

Barometric changes also measurably affect water levels in unconfined aquifers (Weeks, 1979). Pressure changes do not propagate instantaneously through the unsaturated zone because air is highly compressible. The relatively low pneumatic diffusivity of the unsaturated zone creates substantial phase lags between atmospheric and water-level changes. Unconfined water-level fluctuations can approach the magnitude of confined water-level fluctuations where the depth to water exceeds 500 ft. This is because atmospheric loading through the wellbore is not balanced by diffusion through the unsaturated zone.

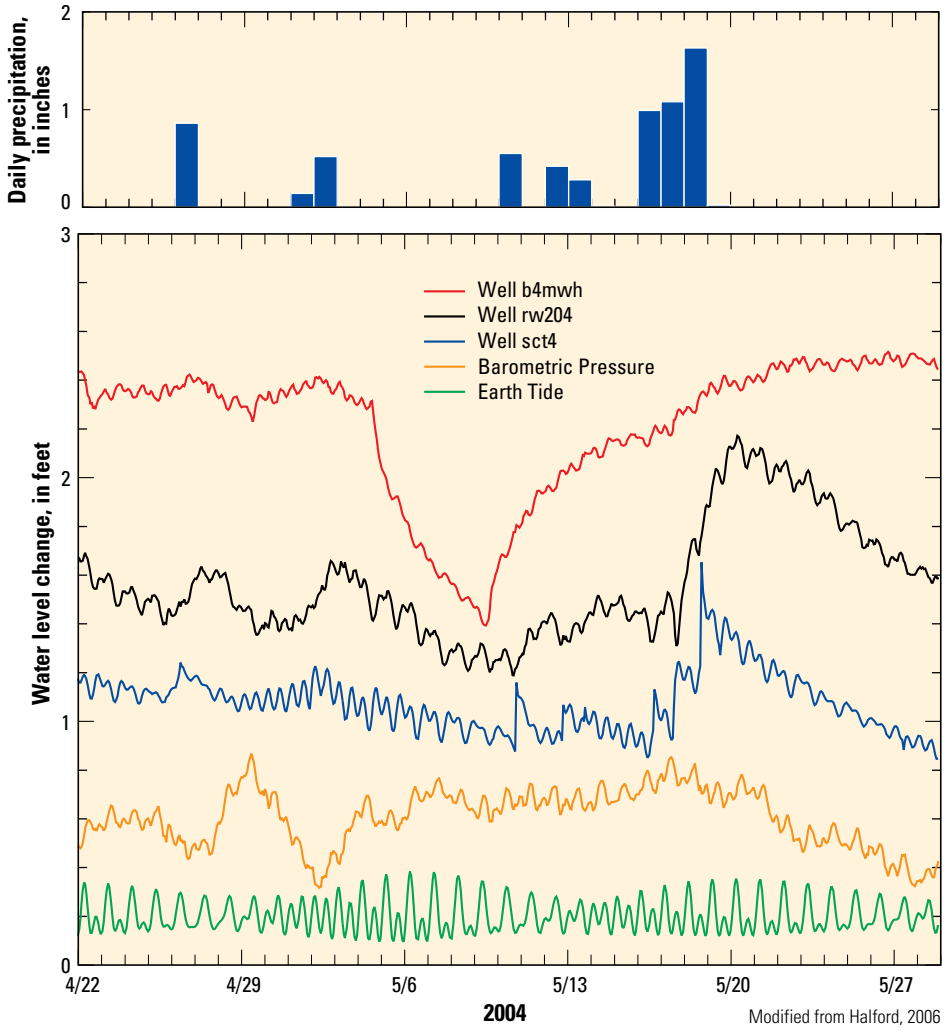

Figure 1. Daily precipitation, groundwater levels, barometric change, and earth tide at Air Force Plant 6, Marietta, Georgia, April 22 to May 28, 2004.

Tidal Effects

Tidal forces distort the crust of the earth, which creates water-level fluctuations in mid-continent wells (Bredehoeft, 1967; Marine, 1975; Hanson and Owen, 1982; Narasimhan and others, 1984). Earth tides periodically deform (dilate and compress) the skeleton of the aquifer system, changing the porosity and causing measurable water-level fluctuations of as much as 0.1 ft or more in wells penetrating aquifers with small storage coefficients (fig. 1). Coupling between the mechanical deformation and the fluid filling the secondary porosity amplifies water-level response in wells hydraulically connected to the secondary-porosity features, such as fractures or faults. The presence of secondary porosity typically renders the formation more compliant to imposed stresses, depending on orientation of the fractures or faults with respect to the principal component directions of the imposed stress. The theoretical crustal strain tensors that result from the two principal lunar daily and semidiurnal tides are largely horizontal and orthogonal to one another. Subvertical fractures with azimuths oriented perpendicular to the strain tensor for a particular tide tend to amplify the strain and, thereby, the water-level response (Bower, 1983).

The diurnal rise and fall of ocean levels are the most common manifestation of varying gravitational forces and are referred to as ocean tides. Ocean tides affect coastal groundwater levels through direct head changes in an aquifer or as loads applied through a confining unit (Merritt, 2004). Ocean-tide effects are better approximated with a nearby tidal gage than calculated tides because wind and coastal geometry also affect ocean tides in addition to direct gravitational forcing.

Background Water Levels

Recharge events, regional pumping, and change in surface-water stage are identifiable stresses that typically affect large areas but are not predicted easily with independent time series such as barometric change and tidal potential. Recharge events and regional pumping stresses can create similar water-level

changes in multiple wells over areas of many square miles. Change in surface-water stages locally affects groundwater levels and can be measured directly. Water levels in wells sufficiently removed from an aquifer test can simulate these regional stresses, local changes in surface-water stages, and any other unidentified pervasive stresses. Water levels in these remote wells are referred to as background water levels (Halford, 2006).

Background water levels can be more effective correctors than independent barometric and tidal time series even where only barometric and tidal stresses are significant (Halford, 2006). Barometric forcing through the unsaturated zone lags behind water-level changes because of the small permeability of unsaturated rock relative to an open well (Weeks, 1979). The complex relation between barometric pressure and water level in a well is explained poorly with barometric efficiency where the unsaturated zone is thick. Background water levels from another well of similar construction better approximate this relation. Likewise, rock properties and fracture orientation in an aquifer control tidal water-level fluctuations as much as tidal forcing. Water levels from background wells can better approximate the rock-tide interaction than theoretical tidal components alone. Independent barometric and tidal time series frequently remain necessary because of differences in rock properties, fracture orientation, and well completions around measured and background wells.

Water-Level Modeling

Water-level modeling assumes that measured water-level fluctuations can be approximated by summing multiple-component fluctuations (Halford, 2006). Input series of barometric pressure, input series of background water levels, and computed earth tides explain most environmental fluctuations (fig. 2). Pumping signals are simulated with multiple Theis solutions that transform pumping schedules to water-level fluctuations.

Water-level model components are summed to create a synthetic water level. A synthetic water level at time, t, is determined:

$$SWL(t) = C_0 + \sum_{i=1}^{n} WLMC_i \qquad (1)$$

where

C_0 is an offset (L) that allows mean values of synthetic water levels to match mean values of measured water levels,

n is the number of water-level model (WLM) components, and

$WLMC_i$ is the i^{th} WLM component in units of the modeled water level.

Water-level model results are denoted with the word synthetic rather than simulated to differentiate between water-level and groundwater-flow model results.

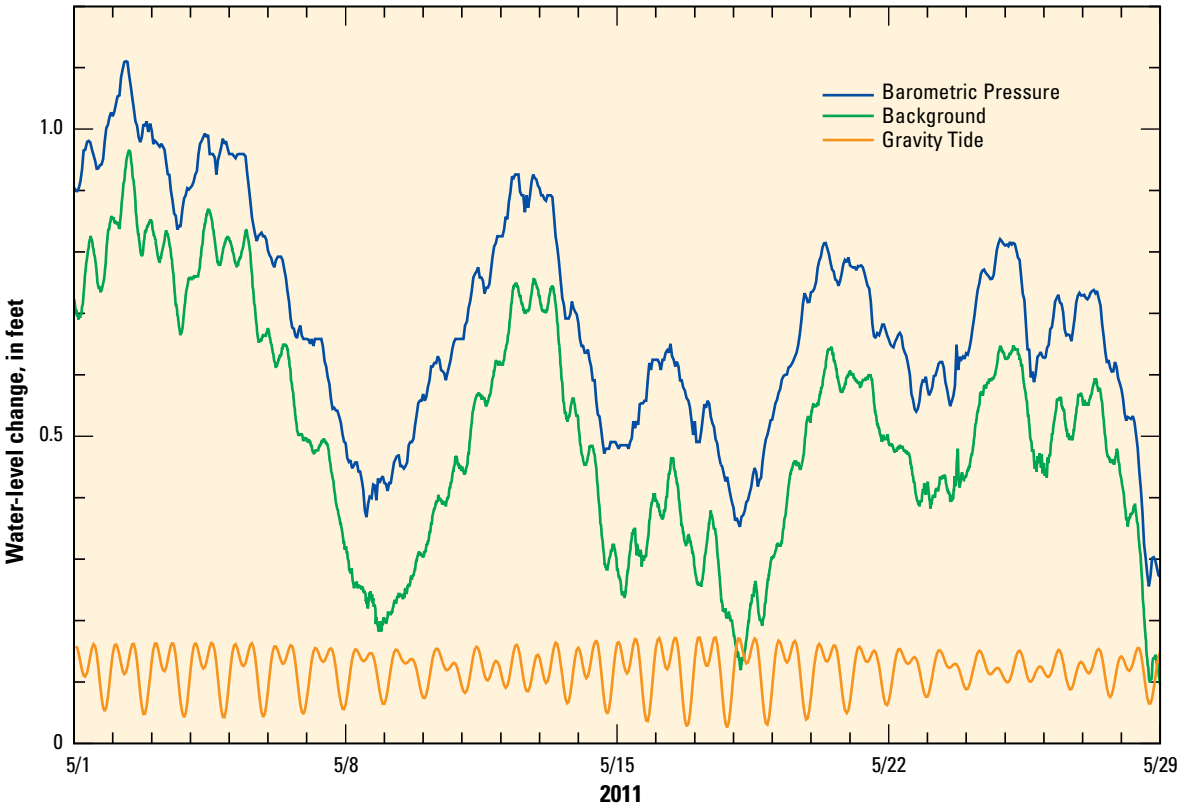

Figure 2. Input series of barometric pressure, input series of background water level, and computed gravity tide.

SE ROA 11384

JA_4146

Water-Level Model Components

Input series are measured water levels, barometric pressures, or pumping schedules that are transformed to represent water-level change. All input series are assumed to be continuous between each discrete measurement where continuity can be piecewise linear or stepwise. Water levels and barometric pressures typically are used as piecewise linear functions. Pumping schedules typically are used as stepwise functions. All input series are transformed into WLM components that are smooth, differentiable functions.

WLM components are created from input series with one of six transforms. The parameters that define each transform generically are referred to as coefficients because characteristics and terminology are not consistent among transforms (table 1). Moving averages are most frequently used to transform interpolated time series of barometric pressure and background water levels into WLM components. Pumping schedules are transformed into water-level fluctuations with Theis transforms. Earth tides are computed for a given observation well location (Harrison, 1971). Transducer displacement, as a result of resetting a transducer in a well, is simulated with the step transform following a user-specified time. Lag and attenuation of barometric-pressure changes between land surface and water table are simulated with the pneumatic-lag transform. Water-level rises from infiltration events are simulated with the gamma transform.

WLM components are smooth functions because values are interpolated linearly between consecutive data pairs or transformed from stepwise data to a smooth function. Interpolation or transformation allows data to be collected at variable intervals within a time series. Collection frequencies can differ among time series and do not need to be synchronized because interpolation or transformation synchronizes comparisons (fig. 3).

Moving Average

Fluctuations of different frequencies exist in input series such as barometric changes and background water levels. Barometric changes exhibit diurnal, weekly, and seasonal fluctuations that differ in amplitude and frequency. Frequency-dependent differences in water-level fluctuations also exist between wells because of differences in well construction and aquifer properties. Diurnal water-level fluctuations will be less where communication between well and aquifer is impeded and wellbore storage is increased. Poorly developed wells with large casing diameters and short screens damp high-frequency water-level fluctuations. Aquifers with large storage coefficients and small transmissivity values also will damp water-level fluctuations.

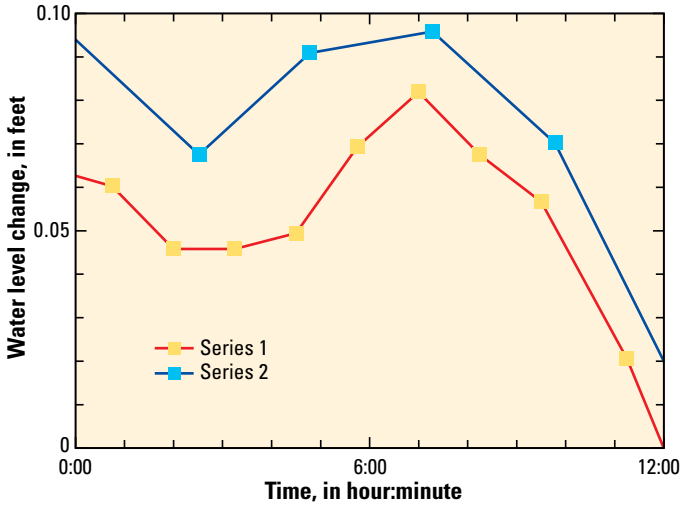

Figure 3. Two time series with different collection frequencies and sampling times.

Table 1. Water-level model (WLM) components.

[— is not applicable]

WLM component	Time series	Coefficient				
		1	2	3	4	5
Moving average	Any series	Multiplier	Phase	Averaging period	—	—
Theis transform	Pumping schedule	Transmissivity	Storage coefficient	Radial distance	Flow-rate conversion	—
Tide	Computed	Multiplier	Phase	Latitude	Longitude	Altitude
Step	—	Time	Offset	—	—	—
Pneumatic lag [a]	Barometric pressure	K_{AIR}	S_{AIR}	Thickness of unsaturated zone	—	—
Gamma[1]	Infiltration	Multiplier	k	n	Time conversion	Multiplication series

[a] Hydraulic properties of the Pneumatic-lag transform, K_{AIR} & S_{AIR}, are with respect to air. K_{AIR} is hydraulic conductivity of air and is about 60 times greater than K_{WATER}.S_{AIR} is average air-filled porosity divided by mean air pressure.

[1] The k and n terms represent scale and shape parameters, respectively in the Gamma Probability Distribution Function.

Input series frequently are composed of multiple signals of different frequencies. These different frequencies can be separated into multiple WLM components with multiple moving averages of the input series (fig. 4). Water levels can be averaged over periods of hours to days where duration of averaging periods and the number of WLM components are arbitrary quantities. More than a half dozen WLM components frequently are created from a single input series because a broad range of averaging periods are more likely to simulate the environmental fluctuations. An excess of WLM components generally does not degrade results. High-frequency signals are approximated indirectly by summing multiple WLM components with ranges of averaging periods. The original input series and WLM component are one and the same where an averaging period of 0 is specified (table 1).

The moving-average transform is applied to ith WLM component at time, *t*:

$$WLMC_i = a_i V_i(t + \phi_i) \quad (2)$$

where

a_i is the amplitude multiplier of the ith component in units of the modeled water level divided by units of the ith component,

Φ_i is the phase-shift of the ith component (t), and

$V_i(t+\Phi_i)$ is the value of the moving average of ith input series at time $t+\Phi_i$ in units of ith component.

Amplitude (a) and phase (Φ) are estimated in equation 2 to minimize differences between synthetic and measured water-levels.

Moving averages are centered about the evaluation time, t, where averaging periods are defined by time, not the number of measurements. For example, a 12-hr, moving average at the time when sampling increased from hourly to 15-minute measurements would average 31 values. Six values were measured prior to the evaluation time, another value was measured at the evaluation time, and 24 values were measured after the evaluation time.

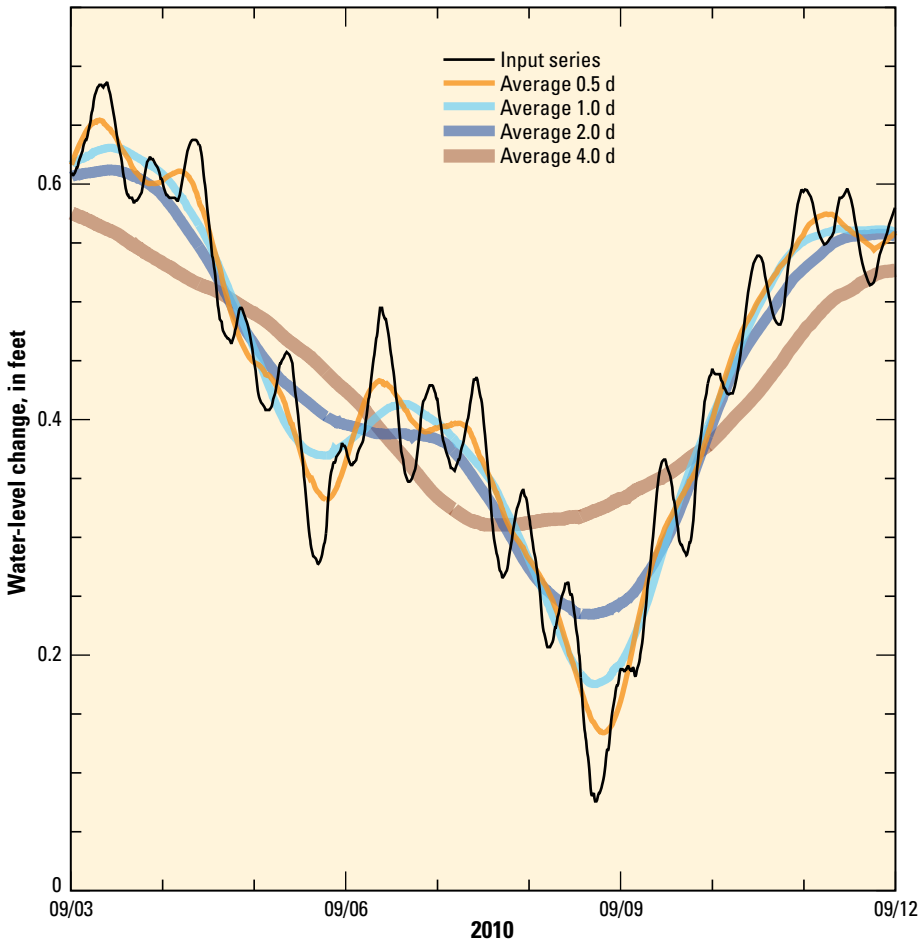

Figure 4. Input series and four additional water-level model components that were created by averaging in periods of 0.5, 1, 2, and 4 days (d).

Theis Transform

Pumping schedules are converted into water-level responses with a simple model: the Theis (1935) solution. Water-level changes or drawdown, *s*, from pumping-rate changes are simulated:

$$WLMC_i = s = \frac{Q}{4\pi T} W(u) = \frac{Q}{4\pi T} W\left(\frac{r^2 S}{4T\Delta t}\right) \quad (3)$$

where

Q is the flow rate (L^3/t),
T is the transmissivity (L^2/t),
$W(u)$ is the exponential integral solution,
u is dimensionless time,
r is the radius (L),
S is the storage coefficient (dimensionless), and
Δt is the elapsed time since the flow rate changed (t).

Multiple Theis solutions are superimposed in time to simulate water-level responses to variable pumping schedules (fig. 5). The effects of multiple pumping wells also can be simulated by superposition in space (Harp and Vesselinov, 2011). Each pumping well with its unique pumping schedule and radial distance is simulated with a WLM component in SeriesSEE. Pumping signals are discussed here as drawdowns, regardless of pumping rate, because discrete drawdown and recovery periods do not exist when variable pumping schedules are simulated.

Superimposed Theis solutions serve as transform functions, where step-wise pumping records are translated into approximate water-level responses at observation wells. Log-transforms of transmissivity (T) and storage coefficient (S) are estimated in equation 3 to minimize differences between synthetic and measured water-levels. Estimates of T and S can characterize correctly the hydraulic properties of an aquifer if assumptions of the Theis solution are honored. These same

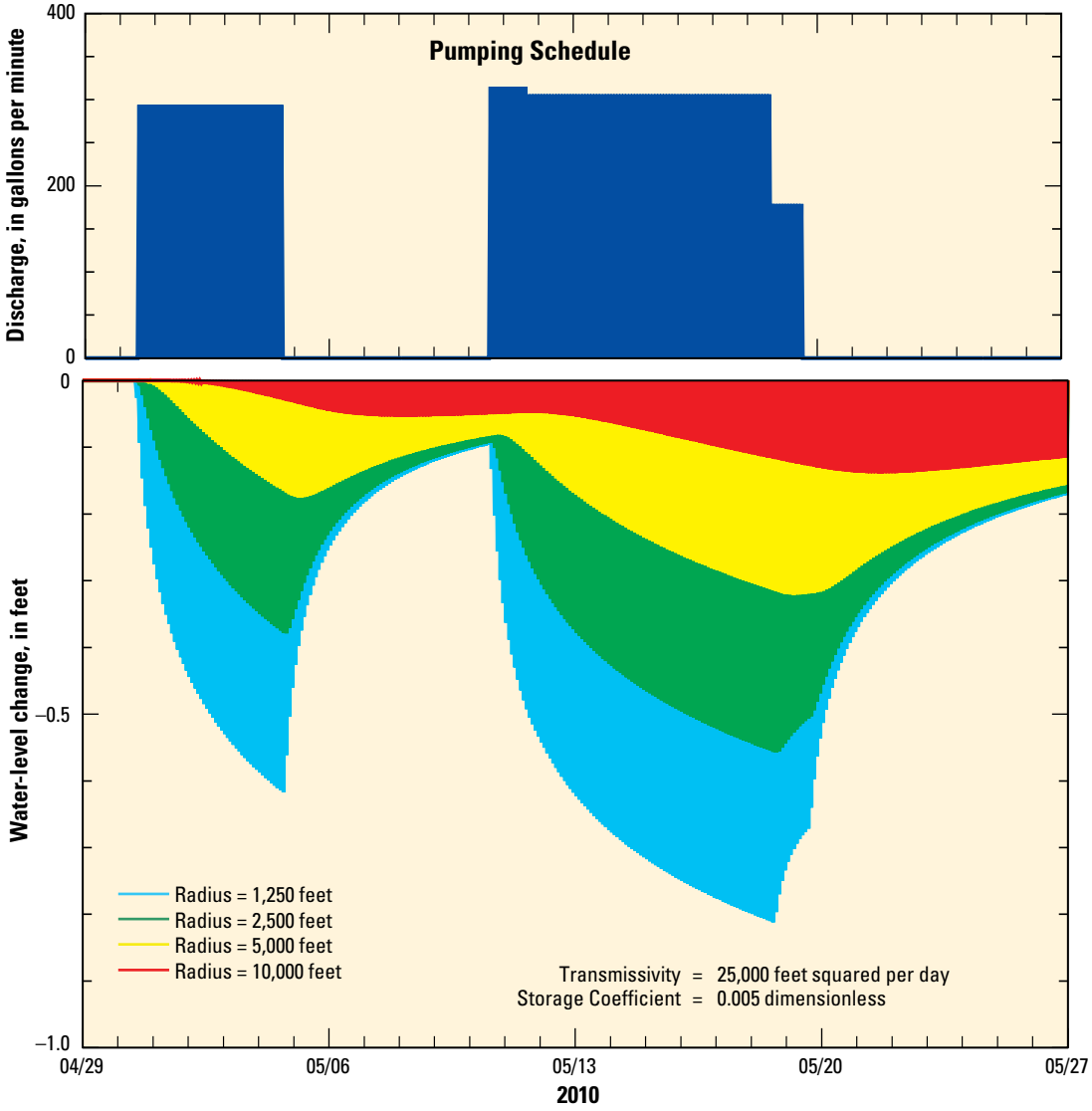

Figure 5. Theis transform of a pumping schedule to water-level changes at radial distances between 1,250 and 10,000 feet from a pumping well for a fixed transmissivity and storage coefficient.

parameters primarily are fitting terms with little physical significance in hydrogeologically complex aquifer systems because assumptions of the Theis solution are violated. This component of the water-level model is referred to as a "Theis transform," here, and applies to the pumping schedule of a single well.

Hydrogeologic complexity and uncertainty are addressed by applying multiple Theis transforms to a single pumping schedule. Relatively fast and slow elements of pumping signals propagate through complex aquifer systems. These fast and slow elements are approximated by Theis transforms with relatively high and low hydraulic diffusivities, respectively.

Computed Tides

The tides are displacements of the particles in a celestial body caused by the forces of attraction in a neighboring body. The terrestrial tides on Earth consist of the atmospheric tides, the earth tides, and the ocean tides and are related to the lunar and solar cycles (Defant, 1958). Simulated tidal forcing and body tides of a solid Earth (oceanless) produced by the moon and sun are computed from gravitational and astronomical theory for a specified point on the Earth for a specified time by using the Harrison (1971) model. Changes in the solid Earth caused by the ocean tides are not considered here. Many of the model parameters, and thus the computed tidal components, are functions of time based on the ephemerides, which are computed in the model but are not included here explicitly.

The earth tides result as the crust undergoes volumetric strains, ε_V, due to variations in tide-generating forces:

$$\varepsilon_V = \frac{1}{3}\left(\varepsilon_{\theta\theta} + \varepsilon_{\lambda\lambda} + \varepsilon_{rr}\right) \tag{4}$$

where, $\varepsilon_{\Theta\Theta}$, $\varepsilon_{\lambda\lambda}$, and ε_{rr} (positive downwards) represent the principal components of the strain-tide tensor with respect to polar north, east, and radial, respectively. Most of the stress close to the Earth's surface is plane stress, and the resultant strain tide is predominately an areal strain, ε_A (Melchior, 1966:

$$\varepsilon_A = \frac{1}{2}\left(\varepsilon_{\theta\theta} + \varepsilon_{\lambda\lambda}\right) \tag{5}$$

The areal strain produced by earth tides is computed from theoretical considerations (Harrison, 1971, 1985; Beaumont and Berger, 1975; Berger and Beaumont, 1976) by using the tidal potential, V (L^2/t^2), as formulated by Bartels (1957, 1985) and computed by Harrison (1971):

$$V = \frac{GMr^2}{R_s^3}\left\{\frac{3\cos^2 z_m - 1}{2} + \frac{r}{R_m}\frac{5\cos^2 z_m - 3\cos^2 z_m}{2}\right\} + \frac{GSr^2}{R_s^3}\left\{\frac{3\cos^2 z_s - 1}{2}\right\} \tag{6}$$

where

G is the Newtonian constant of gravitation ($L^3 / M^1\text{-}t^2$),
M and S are the masses of the moon and sun, respectively (M),
r is the distance between the center of the Earth and the observation point on the Earth's surface (L),
R_m and R_s are the distances of the moon and sun, respectively, from the Earth's center (L), and
z_m and z_s are the zenith angles of the moon and sun, respectively (radians).

The areal strain tide component is formulated as a scaled function of the tidal potential (Munk and McDonald, 1960; Melchior, 1966, Bredehoeft, 1967):

$$\varepsilon_A = \left(2\bar{h} - 6\bar{l}\right)\frac{V}{rg} \tag{7}$$

where

$\bar{h}$ and $\bar{T}$ are Love numbers at the Earth's surface, and
g is the gravitational acceleration (L/t^2).

Areal strain tide is computed by using $\bar{h} = 0.638$ and $\bar{T} = 0.088$ and is expressed in parts per billion strain (dimensionless). The resulting areal 'dry' (in the absence of saturating fluid) tidal dilatation at the Earth's surface, Δ_t can be expressed (Bredehoeft, 1967):

$$\Delta_t = \left[\frac{1-2v}{1-v}\right]\varepsilon_A \tag{8}$$

where v is Poisson's ratio.

The gravity tide oriented downwards normal to the Earth's ellipsoid, g_N, is computed (Harrison, 1971):

$$g_N = \frac{\partial V}{\partial r} - \delta\frac{\partial V}{r\partial\theta} \tag{9}$$

where

Θ is the geocentric polar angle of the observation point (radians), and
δ is the difference between the geodetic and geocentric latitudes.

For example, δ attains a value of about 3.37×10^{-3} radians at 45° latitude. Gravity tide is expressed in terms of microgals (L/t^2).

The tilt tide in a plane tangent to the Earth's ellipsoid along a specified azimuth oriented with respect to 0° N, γ_T is computed (Harrison, 1971):

$$\gamma_T = \frac{1}{g}\left[\left(\frac{\partial V}{r\partial\theta} + \delta\frac{\partial V}{\partial r}\right)\cos\alpha + \frac{1}{r\sin\theta}\frac{\partial V}{\partial\lambda}\sin\alpha\right] \tag{10}$$

where

λ is the terrestrial east longitude of the observation point (radians) and
α is the specified azimuth of tilt (radians).

Tilt tide is expressed in nanoradians.

Dry, gravity, and tilt tides (Table 2) result from changes in gravitational forces as the relative positions of the sun, moon, and earth change (Harrison, 1971). These theoretical earth tides are computed functions that only require the location of an observation well.

Adjustable WLM components are created by multiplying computed dry, gravity, or tilt tide (table 2) by an amplitude. Zenith angles primarily are specified by longitude and time as referenced to Greenwich Mean Time. A phase shift can be applied to the zenith angles through the specified time. Amplitude (a) and phase (Φ) are estimated to minimize differences between synthetic and measured water-levels.

Step Change

Step changes in water-level records are introduced when a transducer is disturbed or replaced. Transducer submergence can change if the hanger position is moved. Replacing a transducer is likely to change submergence because the devices can differ and cable stretch can occur. A step-change WLM component is necessary because shifts of less than 0.03 ft are detectable in WLM results.

A step change in the water-level measurement is simulated as follows:

$$WLMC_i = \Delta h_i \quad \text{for } t \geq t_{STEP}$$
$$WLMC_i = 0 \quad \text{for } t < t_{STEP} \qquad (11)$$

where

Δh_i is the step change of the ith component and t is the time. The step change is estimated in equation 11 to minimize differences between synthetic and measured water-levels.

Pneumatic Lag

The pneumatic lag between barometric-pressure changes at land surface and the water table can be simulated with a one-dimensional diffusion equation instead of being approximated with multiple moving averages. This alternative approach is advantageous for estimating the hydraulic properties of the unsaturated zone and precludes using multiple moving averages of barometric pressure. The propagation of barometric changes through the unsaturated zone is solved analytically by using equivalent solutions for surface-water/groundwater interaction (Rorabaugh, 1964; Barlow and Moench, 1998).

Stage changes of a fully penetrating river that perturb groundwater levels behave similarly to barometric pressure changes that perturb air pressures in the unsaturated zone (fig. 6). This assumes that pressure changes are small relative to the mean air-pressure so air density and specific storage are affected minimally. Barometric changes typically are less than 2 ft while mean air-pressure ranges between 26 and 34 ft (Merritt, 2004; Fenelon, 2005). Boundary conditions for a one-dimensional, confined aquifer are equivalent to boundary conditions of an areally extensive, thick unsaturated zone. The water table is an impermeable boundary because air-filled pores cease to exist.

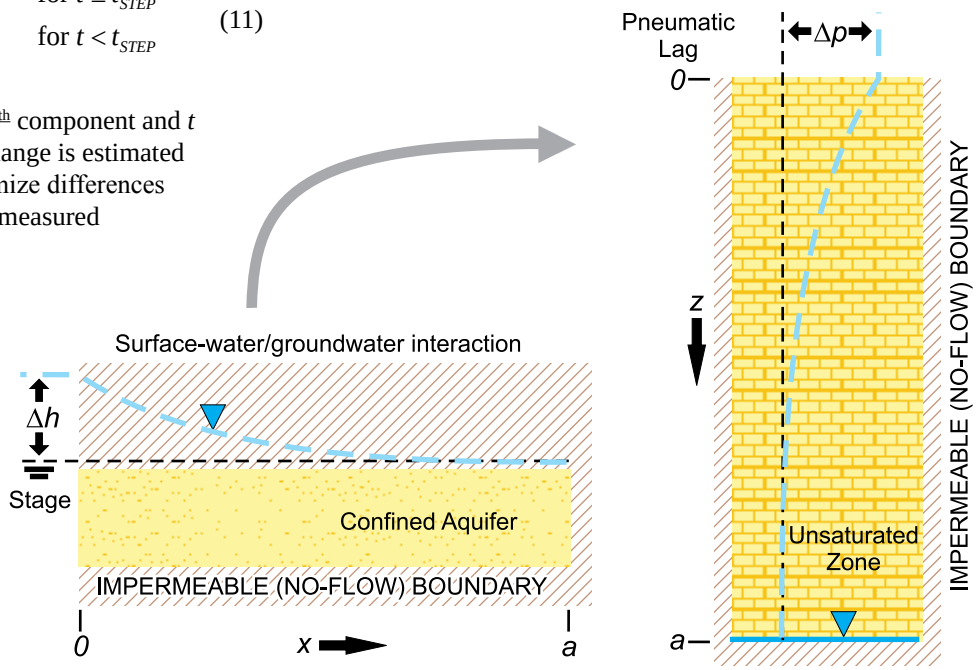

Figure 6. Schematics of one-dimensional, confined aquifer and an areally extensive, thick unsaturated zone that experience similar step-changes to a time-varying specified-head boundary such as a river or barometric-pressure difference.

Table 2. Abbreviations and descriptions of tides that are computed in SeriesSEE.

Tide	DESCRIPTION	Units	Equation
DRY	Areal strain tide	parts per billion	8
GRAVITY	Normal to the Earth ellipsoid	microgals	9
TILT	Plane tangent to the Earth ellipsoid	nanoradians	10

Equivalent hydraulic conductivity and specific storage of the unsaturated zone differ from the confined aquifer solution because the pores are filled with air rather than water. Equivalent hydraulic conductivity is air permeability divided by the viscosity of air and is about 60 times greater than saturated hydraulic conductivity because the ratio of water-to-air viscosity ranges from 70 to 40 for temperatures between 10 and 30°C. Air permeability is affected negligibly by changes in barometric pressure (Baehr and Hult, 1991). Specific storage of the unsaturated zone is the air-filled porosity divided by the mean air pressure.

Pressure change at a given depth in the unsaturated zone from a step-change in pressure at land surface is simulated as follows:

$$WLMC_i = \Delta p - 2\sum_{m=1}^{\infty} \frac{-1^{m+1}}{\left(\pi m - \frac{1}{2}\right)} e^{-\pi^2\left(m-\frac{1}{2}\right)^2 \frac{\Delta t K_{AIR}}{S_{AIR} a^2}} \cos\left(\pi\left(m-\frac{1}{2}\right)\left(1-\frac{z}{a}\right)\right) \qquad (12)$$

where

Δp is the step change in air pressure at land surface (L),
m is an index,
Δt is elapsed time since the step change (t),
K_{AIR} is the air permeability divided by viscosity of air (L/t),
S_{AIR} is air-filled porosity divided by the mean air-pressure (1/L), and
a is the thickness of the unsaturated zone (L).

Multiple step changes are superimposed in time to simulate air-pressure changes at the water table by using barometric-pressure changes at land surface (fig. 7).

Water-table changes are assumed equal and opposite of air-pressure changes at the water table. Log-transforms of K_{AIR} and S_{AIR} are estimated in equation 12 to minimize differences between synthetic and measured water-levels. If the objective of a water-level model is to estimate hydraulic properties of the unsaturated zone by using equation 11, then multiple moving averages of barometric pressure cannot be used as WLM components.

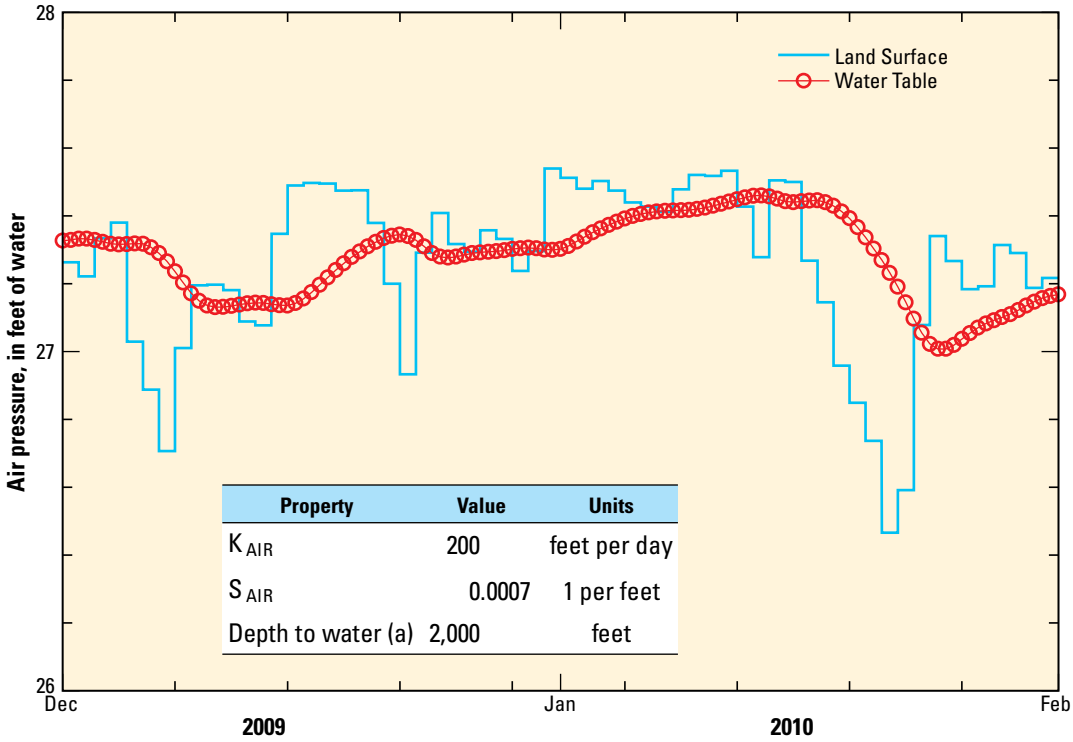

Figure 7. Average daily barometric pressure and simulated air pressure at the water table.

Gamma Transform

The gamma transform was adapted from a Water-Balance/Transfer Function (WBTF) model that simulates recharge to the water table from precipitation (O'Reilly, 2004). The gamma transform retains the transfer function from the WBTF model that translates a discrete pulse of infiltration below the root zone to recharge at the water table. The delay between infiltration and recharge at the water table increases as unsaturated-zone thickness increases. Recharge pulses also are attenuated and prolonged as unsaturated-zone thickness increases. The WBTF model was selected because the transfer function simulates these characteristics (O'Reilly, 2004).

Water-level rise, rather than recharge, is simulated with the gamma transform. Water-level rise equals recharge divided by specific yield, where the aquifer is unconfined, and consequently has a greater magnitude than recharge (fig. 8).

Water-table rise from each infiltration event is simulated as follows:

$$WLMC_i = a_i I \frac{e^{-\frac{\Delta t}{k}}}{k\Gamma(n)}\left(\frac{\Delta t}{k}\right)^{n-1} \quad (13)$$

where

a_i is the amplitude multiplier of the ith component,
I is amount of infiltration during an event (L),
Δt is elapsed time since the infiltration event(t),
k is a scale parameter (t),
n is a shape parameter (dimensionless) , and
$\Gamma(n)$ is the gamma function, (dimensionless), which is equivalent to (n – 1) for integer values of n (Potter and Goldberg, 1987, p. 111).

Multiple step changes are superimposed in time to simulate water-table fluctuations from infiltration events below land surface (O'Reilly, 2004).

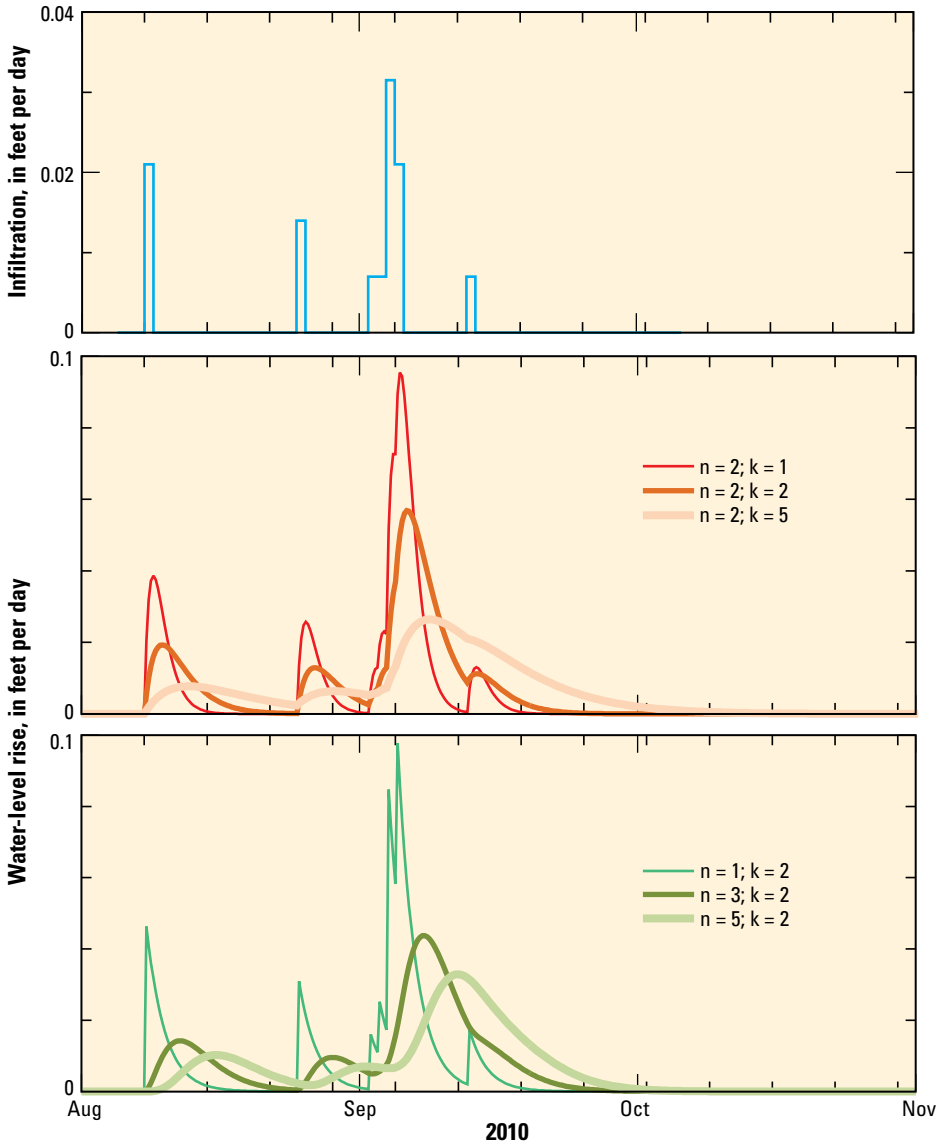

Figure 8. An infiltration schedule and water-level rises simulated with gamma transforms that were defined by six pairs of shape (n) and scale (k) parameters.

Physical significances have been attributed to the fitting parameters a_i, k, and n (O'Reilly, 2004). The amplitude multiplier (a_i) converts recharge to water-level rise and should be proportional to the inverse of the storage coefficient. The scale parameter (k) controls the average delay time imposed by the unsaturated zone (Dooge, 1959). The shape parameter (n) has been characterized as "the number of linear reservoirs necessary to represent the unsaturated zone" by O'Reilly (2004). These explanations are interesting, but estimated values of a_i, k, and n should be interpreted with great skepticism, if at all.

Superimposed gamma transforms translate step-wise precipitation or infiltration records into approximate water-level responses at observation wells. Amplitude (a) and the log-transform of the scale parameter (k) are estimated in equation 13 to minimize differences between synthetic and measured water-levels. The shape parameter (n) is assigned and is not estimated. Multiple gamma transforms should be used with different values of n if the effect of n is investigated.

Calibration

Water-level models must be calibrated to reliably differentiate small pumping responses from environmental fluctuations. Efficient and effective calibration requires a quantitative measure of model misfit so model parameters can be estimated automatically as is done with the parameter estimation software PEST (Doherty, 2010a, 2010b). Differences between synthetic and measured water levels, or residuals, define the goodness-of-fit and are summed in the measurement objective function:

$$\Phi(x)_{MEAS} = \sum_{j=1}^{nobs} \left(SWL(x)_j - MWL_j \right)^2 \qquad (14)$$

where

x	is the vector of parameters being estimated,
nobs	is the number of observations compared,
$SWL(x)_j$	is the j^{th} synthetic water level, and
MWL_j	is the j^{th} measured water level.

Although the sum-of-squares error serves as the measurement objective function, root-mean-square (RMS) error,

$$RMS = \sqrt{\frac{\Phi(x)_{MEAS}}{nobs}} \qquad (15)$$

is reported because RMS is easily compared to measurements.

Residuals are not weighted in the measurement objective function because suspect measured water levels should be discarded rather than assigned a low weight. Each measured water level is assumed equally important so all water levels are weighted equally. Uniform weighting causes differences between synthetic and measured water levels to equally affect the measurement objective function (eq. 14).

Stable parameter-estimation results are ensured with selective parameter transformation and regularization. Log-transforms of hydraulic properties are estimated in the Theis, pneumatic lag, and gamma transforms to scale parameters and precluded negative hydraulic properties (table 3). Regularization avoids estimating insensitive parameters and guides estimates toward preferred values. Parameter estimates have little to no significance because the parameter values generally are not interpreted. Drawdown estimates are interpreted and are the ultimate water-level model result.

Parameter estimation for water-level modeling is unconditionally stable because singular-value decomposition (SVD) regularization is used (Doherty and Hunt, 2010). Insensitive or highly correlated parameters are not estimated and remain at their assigned values if eliminated by SVD regularization.

Tikhonov regularization guides estimates to preferred conditions (Doherty, 2010a, 2010b). Regularization observations are added to define preferred relations between parameters (Doherty and Johnston, 2003). Homogeneity within each of the three parameter groups of amplitude, phase, and hydraulic property was the preferred relation that was enforced with Tikhonov regularization (table 3).

The balance between fitting measurement and regularization observations is controlled by the sum-of-squares measurement error, PHIMLIM, in PEST (Doherty, 2010a, 2010b). An expected RMS error defines PHIMLIM, which equals the square of the expected RMS error times the number of measured water levels (*nobs)*. The expected RMS error defaults to 0.003 (L) in SeriesSEE, but can be changed by the user.

Table 3. Summary of estimable parameters and parameter groups for water-level modeling (WLM) components.

[— is not applicable]

WLM component	Coefficient 1	Parameter group	Coefficient 2	Parameter group
Moving Average	a	Amplitude	ϕ	Phase
Theis Transform	T	Hydraulic Property	S	Hydraulic Property
Tide	a	Amplitude	ϕ	Phase
Step	—	—	a	Amplitude
Pneumatic Lag	K_{AIR}	Hydraulic Property	S_{AIR}	Hydraulic Property
Gamma	a	Amplitude	*k*	Hydraulic Property

Drawdown Estimation

Drawdown estimates from a water-level model are the difference between measured water levels and synthetic water levels without the Theis transforms. Alternatively, drawdowns can be computed directly by summing all Theis transforms and subtracting residuals (fig. 9). The summation of all Theis transforms is the direct estimate of the pumping signal. Residuals represent all unexplained water-level fluctuations. These fluctuations should be random residuals during non-pumping periods, but can contain unexplained components of the pumping signal during pumping and recovery periods. This method of estimating drawdowns is called the Theis-transform approach.

A limited, application of water-level modeling, the projection approach, was developed prior to the Theis-transform approach (Halford, 2006). Synthetic water levels were developed and calibrated during a period prior to pumping with the projection approach. Calibrated, synthetic water levels were then projected forward during pumping and recovery. Drawdown was the difference between projected synthetic values and measured values. This approach ensures that environmental fluctuations and the pumping signal are uncorrelated because pumping is not simulated during model calibration to antecedent water levels.

The projection approach is limited primarily because regional water-level trends are simulated poorly. Excluding pumping and recovery periods from WLM calibration eliminated much of the regional trends from the calibration period. This drawback weakened the projection approach and limited the usefulness of background well information, particularly where pumping and recovery periods were greater than the antecedent data period.

The Theis-transform approach is a more robust application of water-level modeling because environmental fluctuations and pumping signal are simulated during pumping and recovery in addition to antecedent water levels. This allows for calibration of synthetic water-levels to all measured data. The effects of pumping on measured water levels are approximated by using a simple approach, Theis transforms, so that simulations are quick. Efficiency and speed are mandatory because water levels are modeled independently in every observation well. These requirements preclude numerical groundwater-flow models or any other laborious approach for translating pumping schedules to water-level responses.

Drawdown detection with the Theis-transform approach becomes ambiguous when the signal-to-noise ratio is low or where environmental fluctuations and pumping signals can be correlated. Signal and noise are defined herein as the maximum drawdown in a well during an aquifer test and the RMS

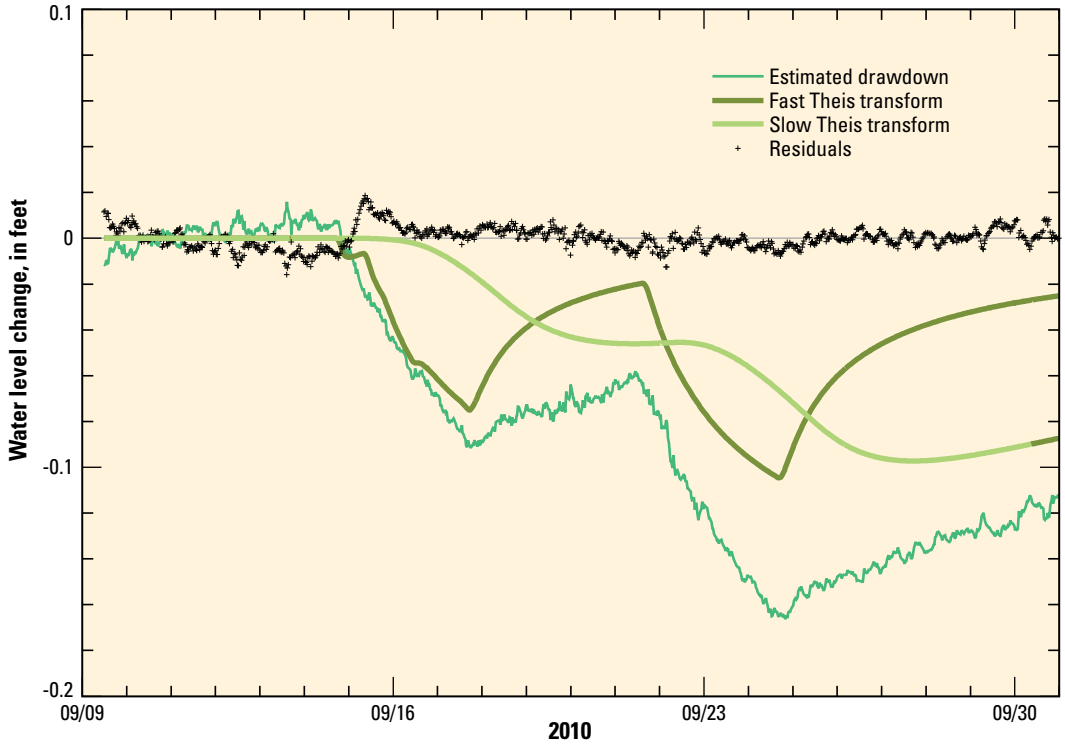

Figure 9. Estimated drawdown from summing Theis transforms and subtracting residuals. Fast and slow Theis transforms represent the relatively fast and slow elements of pumping signals that propagate through a complex aquifer system.

error, respectively. Drawdown has been detected definitively where the signal-to-noise ratio was greater than 10 and correlation was unlikely. Correlation is unlikely where sharply defined pumping signals (saw-tooth shape) exist or considerable recovery has been observed (fig. 10, ER-EC-6 deep, r = 6,800 ft). Correlation between environmental fluctuations and the pumping signal is possible where observed drawdown can be approximated by a linear trend during all or part of the period of analysis (fig. 10, ER-EC-12 shallow, r = 8,900 ft). The potential for correlation increases as hydraulic diffusivity decreases, distance between observation and pumping well increases, or recovery diminishes.

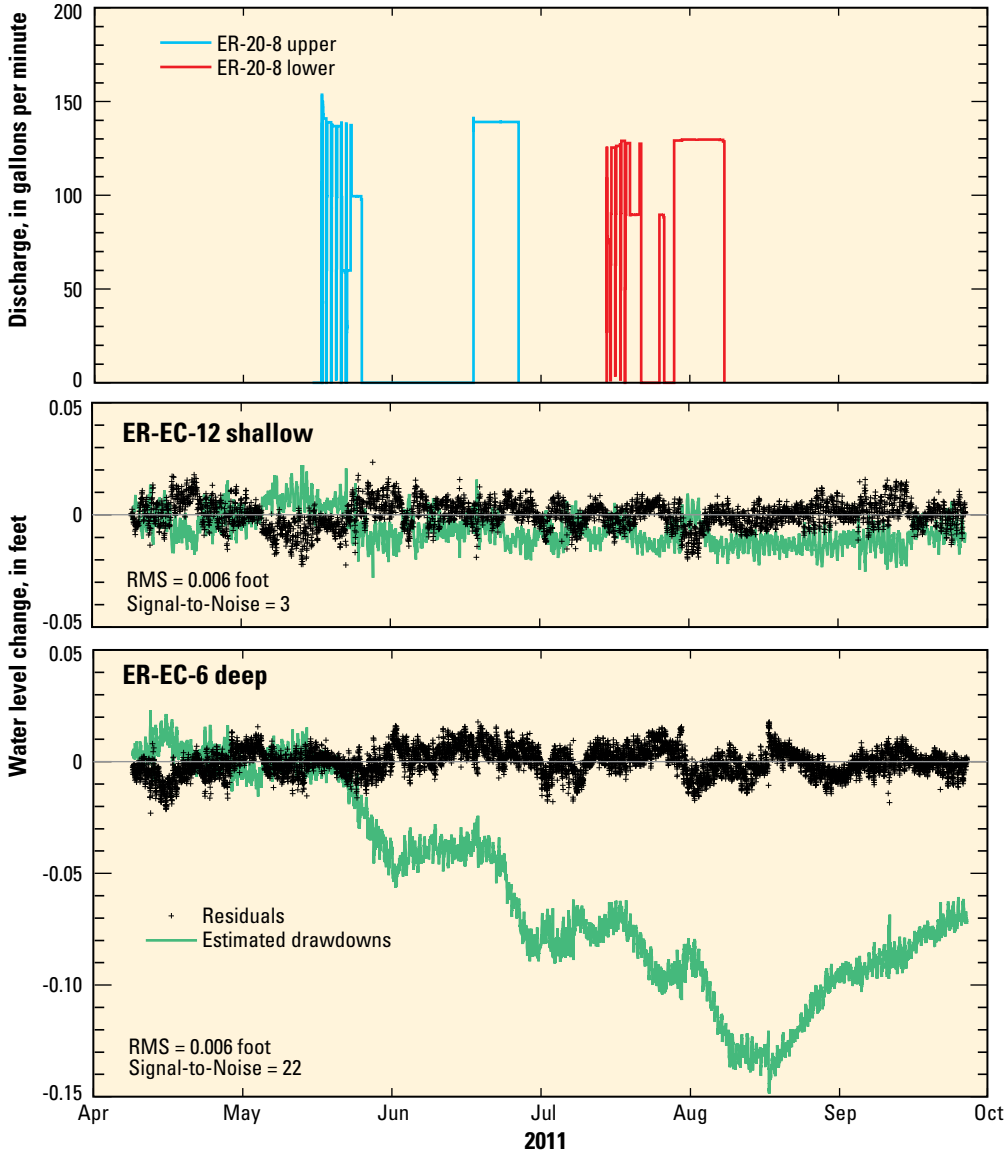

Figure 10. Discharge from pumping wells ER-20-8 upper and ER-20-8 lower, estimated drawdowns, residuals, RMS errors, and signal-to-noise ratios in observation wells ER-EC-12 shallow and ER-EC-6 deep.

SeriesSEE

SeriesSEE is a Microsoft® Excel add-in for viewing, cleaning, manipulating, and analyzing time-series data where water-level modeling is a primary analysis tool. SeriesSEE creates a viewer file from a data workbook that can contain more than 16,000 series. The maximum number of series that can be viewed simultaneously is limited to twelve. Time series are displayed on two charts where all data are shown in one chart, and a magnified subset is shown in the other chart (fig. 11). Borehole geophysical logs also can be viewed, cleaned, manipulated, and analyzed with SeriesSEE, where the two charts are displayed top-to-bottom, rather than left-to-right. SeriesSEE software, installation instructions, and help for all tools can be downloaded in the zipped file, which is described in appendix A.

All source code that was developed for SeriesSEE can be downloaded freely (appendix B). All utilities, except WLM, are processed exclusively with VBA code in the SeriesSEE add-in or supporting add-in files named ***SSmodule_*.SerSee***. Source codes for these files are in the VBA folder of appendix B and are named ***SSmodule_*.xlsm***. Water levels to be modeled, input series, and period of analysis are defined with VBA routines. WLM components are transformed (table 1) and water levels are simulated with the FORTRAN program ***WLmodel,*** which reads ASCII files written by VBA programs. Differences between synthetic and measured water levels are minimized with *PEST* (Doherty, 2010a, 2010b). A copy of

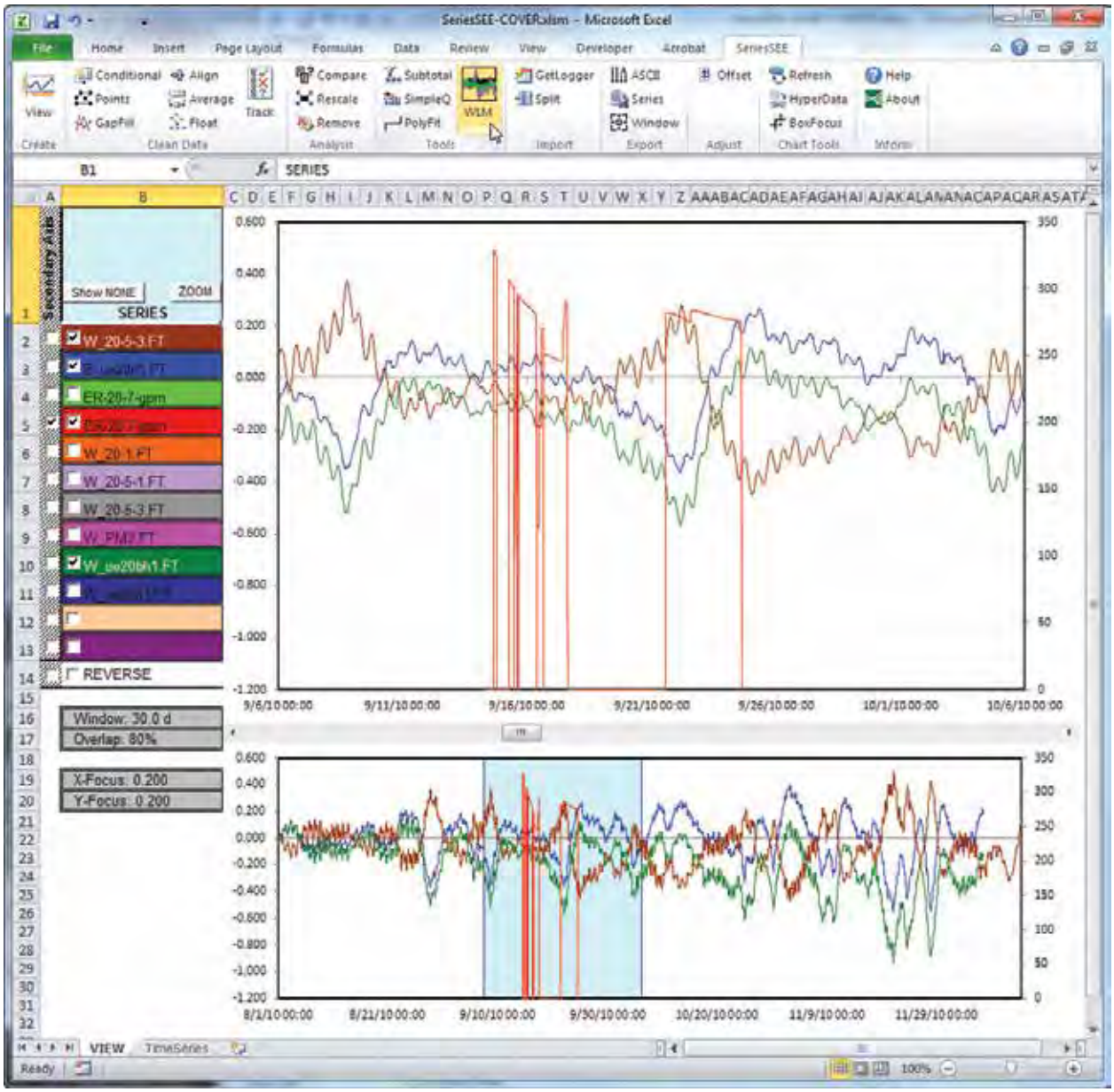

Figure 11. SeriesSEE toolbar and example workbook that was created with SeriesSEE.

PEST exists in the SeriesSEE installation files, but also can be downloaded independently from *http://www.pesthomepage.org/*. The VBA utility WLM writes the PEST control file, ****.pst***, as multiple, commented input files, which are concatenated and stripped of comments with the FORTRAN program ***NoComment***. Source codes and documentation of ***WLmodel*** and ***NoComment*** are in the FORTRAN folder of appendix B.

Data Requirements

Data must be arranged as a continuous series of headers and values where all headers are in a single row (fig. 12). Multiple time columns can be specified, which allows for specification of series with different or irregular sampling intervals. All series are independent, so time columns need not be synchronous. Multiple data series can share a common time column (fig. 12, See columns C, D, and E), but the shared time column must be the first time column to the left of the data series.

A Viewer file is created by selecting a cell in the block of data to be analyzed and pressing the View button (fig. 11). The entire data block is copied from the user's original file into the viewer file by default. All equations within the block of data are converted to values in the viewer file, which breaks all linkages to the user's original workbook. Original data and formulas are not altered in the user's original file because all SeriesSEE operations act on a copy of the data in the viewer file.

Supporting Utilities

SeriesSEE features more than 20 supporting utilities in addition to the viewer creation and water-level modeling utilities already discussed (table 4). Many utilities exist to provide data-handling capabilities that can be used prior to water-level modeling. Related utilities are grouped and labeled as Clean Data, Analysis, Tools, Import, Export, Adjust, and Chart Tools (table 4).

Time-series data generally must be cleaned before analyzing. Cleaning removes erroneous measurements, converts units, reconciles continuous and periodic measurements, and removes step changes from transducer disturbances. All changes between the original and cleaned series can be recorded with explanations for each data change if the track utility is active. Changes and explanations are recorded to an auxiliary workbook that also contains the original and revised series. Utilities in the clean data and analysis groups perform these tasks (table 4).

Simple analysis and inspection of series are supported by utilities in the analysis group (table 4). New series can be created by adding, subtracting, multiplying, or dividing one series by another with the Compare utility. Measurement frequencies of the two series can differ because of interpolation. Smoother series can be created from noisy series with moving averages or LOWESS (LOcally Weighted Scatterplot Smoothing), which is a nonparametric method of fitting a curved line to data (Helsel and Hirsch, 1992, p. 288–291). Potential correlations among multiple series of disparate scales can be inspected by normalizing these series to a common scale with the Rescale utility.

Water-level modeling and other analyses can be expedited and improved by data reduction where there has been oversampling. Data can be reduced by averaging within periods such that 1-minute data are reduced to 1-hour averages with the Subtotal utility. Continuous records of flow rates with many thousands of measurements can be reduced accurately to a few dozen step changes with the SimpleQ utility. Simplified pumping schedules increase the efficiency and speed at which drawdowns can be simulated in WLMs. Geophysical logs are approximated with a simple polyline using the PolyFit utility, PolyFit , which can eliminate extraneous fluctuations and constrain the polyline to monotonic increases. Utilities in the tools group perform these tasks (table 4).

Time series can be imported from ASCII files and database tables to a SeriesSEE data table with utilities in the import group (table 4). Multiple data-logger files are read interactively with the GetLogger utility to create a single SeriesSEE data table. Database tables with site identifiers, times, and water levels grouped into three columns can be reformatted to a SeriesSEE data table with the Split utility.

	A	B	C	D	E	F	G	H	I
1	DATE-TIME	W_20-1.FT	DATE-TIME	B_ue20n1.FT	W_ue20n1.FT	DATE-TIME	W_20-5-1.FT	DATE-TIME	W_20-5-3.FT
2	08/01/2010 00:00:06	0.000	08/01/201		0.000	08/01/2010 00:00:07	0.000	08/01/2010 00:00:06	0.000
3	08/01/2010 00:30:06	-0.002	08/01/201		-0.002	08/01/2010 00:10:07	0.002	08/01/2010 00:10:06	-0.005
4	08/01/2010 01:10:06	0.002	08/01/201		-0.002	08/01/2010 00:20:07	-0.002	08/01/2010 00:20:06	-0.007
5	08/01/2010 01:20:06	0.007	08/01/201		-0.005	08/01/2010 00:30:07	0.000	08/01/2010 00:30:06	-0.009
6	08/01/2010 02:00:06	0.012	08/01/201		-0.007	08/01/2010 01:10:07	0.000	08/01/2010 00:40:06	-0.012
7	08/01/2010 02:30:06	0.016	08/01/201		-0.005	08/01/2010 01:20:07	0.005	08/01/2010 00:50:06	-0.014
8	08/01/2010 03:00:06	0.014	08/01/201		-0.007	08/01/2010 01:30:07	0.002	08/01/2010 01:00:06	-0.016
9	08/01/2010 03:30:06	0.012	08/01/201		-0.005	08/01/2010 01:40:07	0.005	08/01/2010 01:10:06	-0.018
10	08/01/2010 04:10:06	0.009	08/01/2010 03:15:00	-0.004	-0.002	08/01/2010 01:50:07	0.002	08/01/2010 01:30:06	-0.021
11	08/01/2010 04:40:06	0.007	08/01/2010 03:45:00	-0.003	-0.002	08/01/2010 02:00:07	0.005	08/01/2010 01:50:06	-0.023
12	08/01/2010 05:00:06	0.000	08/01/2010 04:00:00	0.001	0.000	08/01/2010 02:10:07	0.007	08/01/2010 02:00:06	-0.025
13	08/01/2010 05:40:06	0.000	08/01/2010 04:30:00	0.001	-0.002	08/01/2010 02:30:07	0.009	08/01/2010 02:40:06	-0.025
14	08/01/2010 06:10:06	-0.002	08/01/2010 04:45:00	0.004	0.000	08/01/2010 03:00:07	0.007	08/01/2010 02:50:06	-0.028

HEADINGS
Date and time entries should be captioned "DATE-TIME". Date series headings should start with text. Short descriptors of series will be comprehensible if the first 2 characters are unique.

Figure 12. Format of headers and values for creating a viewer file with SeriesSEE.

Table 4. Summary of available tools in SeriesSEE.

Group	Utility	Description	Name
Create	View	Create Viewer file by selecting a cell in a block of data in an original source file, which is copied to the viewer file. All equations are converted to values in the Viewer file.	View
Clean Data	Conditional	Bad data conditionally can be commented and/or eliminated.	Conditional
	Points	Bad data in a single series can be commented and/or eliminated graphically.	Points
	GapFill	Data gaps from the cleaning process can be filled by linear interpolation, loaded with a dummy value, eliminated altogether, or gaps can be created for alignment.	GapFill
	Align	Shift data segments. Estimate shift with simple water-level models that use a few guide series. Alternatively, shifts can be assigned from other estimates.	Align
	Average	Data reduction by averaging where oversampled.	Average
	Float	Float series to tape downs without changing slope of transducer data.	Float
	Track	Force an explanation to be appended to each data change in an auxillary workbook that also contains the original and revised series.	Track
Analysis	Compare	Create new series by addition, subtraction, multiplication, and division of existing series. Second series interpolated to times in the first series. Series can also be smoothed with a moving average or LOWESS curve.	Compare
	Rescale	Series can be normalized to common scales.	Rescale
	Remove	Removes derived series that are created by Compare or Rescale.	Remove
Tools	Subtotal	Data reduction tool where selected series are binned by time periods or depth intervals to compute statistics.	Subtotal
	SimpleQ	Reduces pumping rates to a simple schedule.	SimpleQ
	PolyFit	Geophysical logs are approximated with a simple polyline.	PolyFit
	WLM	Model water levels interactively in a new workbook, where water levels are simulated with a FORTRAN program and differences are minimized with PEST.	WLM
Import	GetLogger	Series from data-logger files are read interactively and concatenated in a SeriesSEE format.	GetLogger
	Split	Split 3 columns of site identifiers, time, and water levels into SeriesSEE input where a new series is identified at each change in site identifier.	Split
Export	ASCII	Output from tracking workbooks to selected ASCII formats.	ASCII
	Series	Export individual series with options to create drawdown observations. Drawdown observations require shifting, binning, and truncating to a time window.	Series
	Window	Data are copied to a new workbook and reduced to a user-specified period.	Window
Adjust	Offset	Individual, selected, or all series can be shifted such that the average, minimum, maximum, or first value will equal zero.	Offset
Chart Tools	Refresh	Refresh the list of available series after manually adding or deleting series on the data page.	Refresh
	HyperData	Create temporary hyperlinks between visible series and charted data in the Viewer file.	HyperData
	BoxFocus	Magnify subareas of plot. First click adds a rectangle. Second click re-scales both axes to rectangle area. Third click restores plot.	BoxFocus
Inform	Help	Controls and usage of SeriesSEE are explained.	Help
	About	Display ad copy about SeriesSEE.	About

Series can be viewed and inspected at scales as fine as discrete measurements with utilities in the "adjust" and "chart tools" groups (table 4). Series can be shifted so that all measurements fluctuate about a common reference with the Offset utility, which eases comparisons among series (fig. 13). Subareas of charts in SeriesSEE viewer and auxiliary files can be magnified interactively with the BoxFocus utility. Discrete measurements can be selected graphically and connected to the cell with the numerical value in the Viewer file with the HyperData utility, which creates temporary hyperlinks between charted points and the cell with the plotted value.

Each SeriesSEE utility is fully documented in the help system, which can be called with the Help utility or from context sensitive help calls in each utility (appendix A). Each group, utility, form, and auxiliary workbook is explained briefly, and step-by-step instructions (fig. 14). Complex utilities such as water-level modeling are documented with multiple pages that explain each form and action.

Water-Level Modeling

Water levels are modeled interactively with the WLM utility in SeriesSEE. Water levels to be modeled, input series, period of analysis, and WLM components are defined through the use of data-entry forms. A new workbook for modeling water levels is created with user-specified information from these forms. Fitting periods and WLM components can be modified in the WLM workbook.

Analytical models that transform WLM components in the FORTRAN program ***WLmodel*** have been verified (table 5). The analytical models for moving average and step transforms were verified against intrinsic functions in Excel. The analytical models for Theis, tide, pneumatic lag, and gamma transforms were verified against solutions that were computed with published programs. Source problems, programs, and comparisons between ***WLmodel*** output and published programs are documented fully in appendix C.

Differences between synthetic and measured water levels are minimized with PEST. Parameter estimates, transformed WLM components, synthetic water levels, and differences are imported automatically into the WLM workbook after PEST finishes. Model fit is defined by RMS error and evaluated graphically. Parameters are estimated and WLM results are evaluated iteratively until the user deems the fit to be adequate.

Table 5. Summary of verification tests for analytical models in the FORTRAN program WLmodel.

WLM Component	SeriesSEE Label	Verification Source
Moving Average	SERIES	Excel function
Theis Transform	THEIS	Barlow and Moench, 1999
Tide	TIDE	Harrison, 1971
Step	STEP	Excel function
Pneumatic Lag	AIR-LAG	Barlow and Moench, 1998
Gamma	GAMMA	O'Reilly, 2004

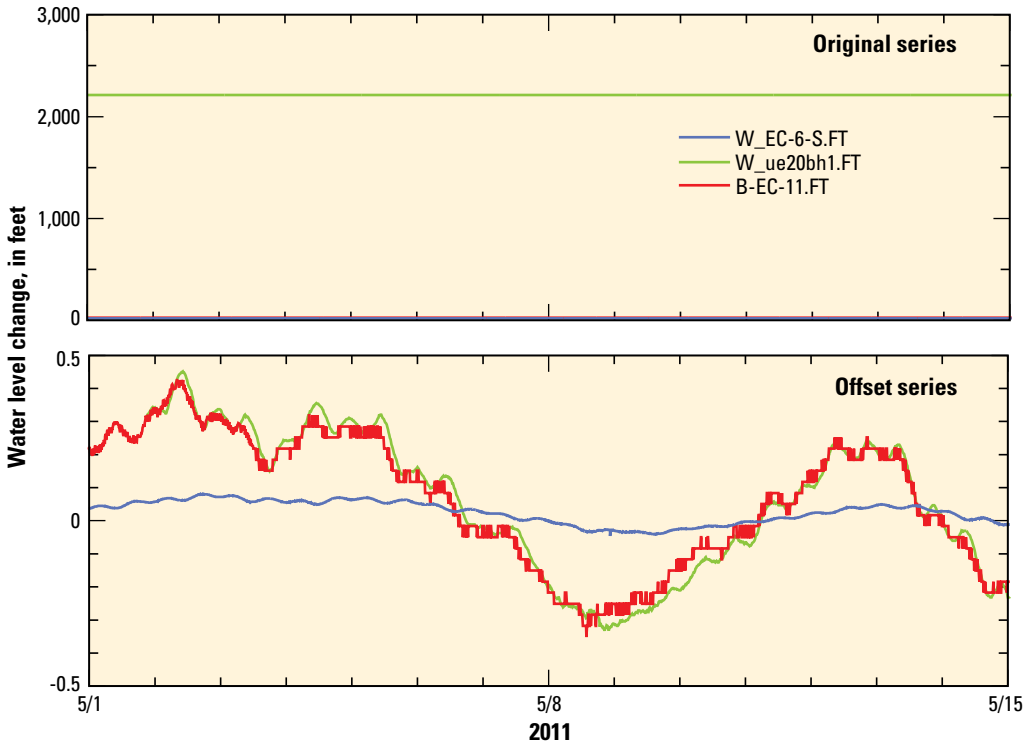

Figure 13. Shifting series to a common reference with the offset utility.

SE ROA 11398

JA_4160

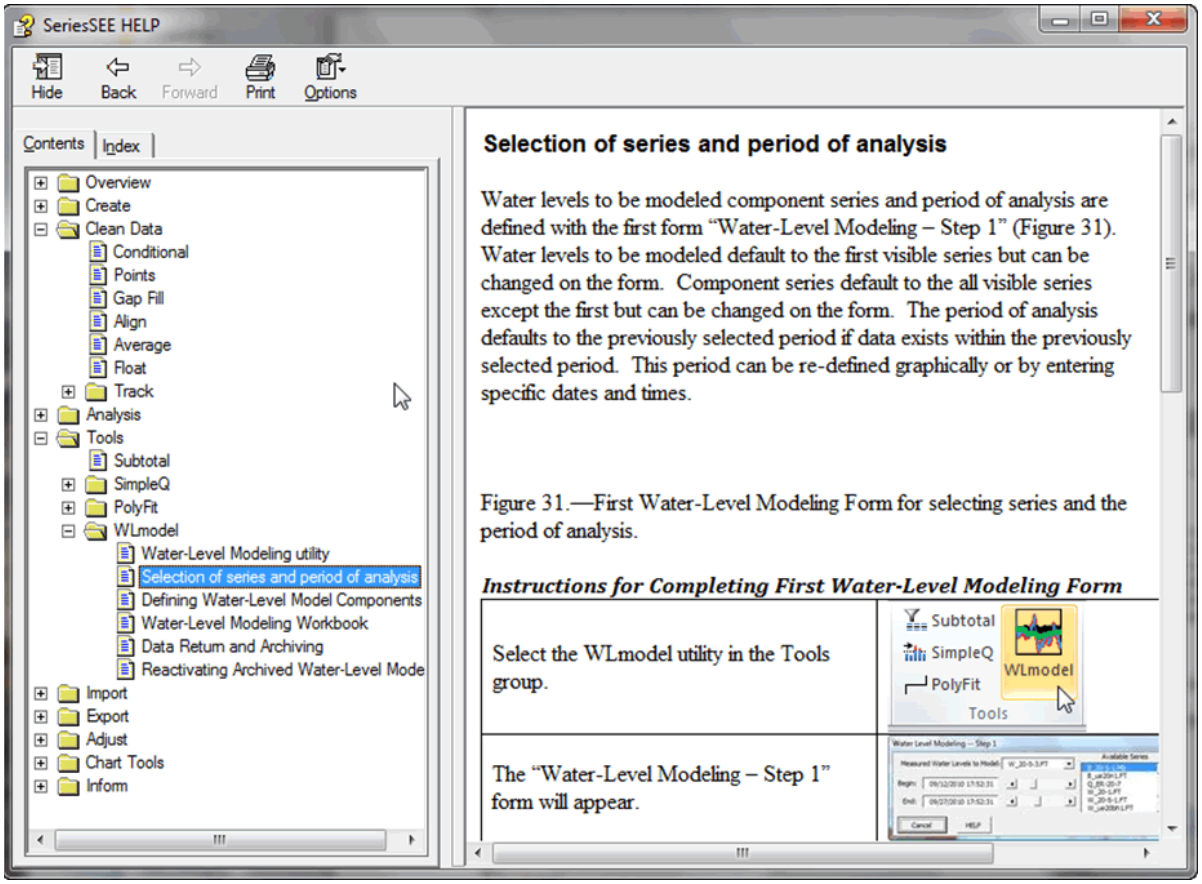

Figure 14. Table of contents and an explanation page in the help system for SeriesSEE.

Drawdowns and transformed WLM components are returned to the SeriesSEE viewer once the user accepts a WLM, where drawdowns are the sum of all Theis transforms minus differences between synthetic and measured water levels. Drawdowns and transformed WLM components are selected individually, so the number of returned series can range from 0 to all WLM components. The WLM workbook can be archived as a macro-free workbook with re-activation capabilities.

Applications of Water-Level Modeling

Water-level modeling applications of SeriesSEE are demonstrated with a hypothetical example and a field investigation at Pahute Mesa, Nevada National Security Site (NNSS). The hypothetical example emulated the complex hydrogeology beneath Pahute Mesa so that known drawdowns could be simulated in a complex aquifer system. Limitations of the Theis-transform approach were investigated with these known drawdowns. Environmental noise, which was the record of water levels in background well ER EC-6 shallow (table 6), was added to known drawdowns. The field investigation demonstrated that drawdowns much smaller than environmental fluctuations can be detected across a major fault structure more than 1 mile from the pumping well. Explanations, data sets, and ancillary software for the hypothetical example and field investigation are in appendixes D and E, respectively.

Water-level modeling was developed and tested with data from Pahute Mesa, NNSS, (fig. 15) because detection of distant drawdowns is imperative and complicated by more than 2,000 ft of unsaturated zone. Migration of radionuclides from underground testing of nuclear devices drives the need to quantify groundwater flow and transport beneath Pahute Mesa (Laczniak and others, 1996). The great depth to water and accessibility limit the number of wells, which typically penetrate a mile of volcanic rock and are more than 1-mi apart (Fenelon and others, 2010). Environmental water-level fluctuations are substantial beneath Pahute Mesa because of the thick unsaturated zone and high hydraulic diffusivity of the volcanic rocks.

The aquifer system beneath Pahute Mesa comprises layered sequences of volcanic rocks that have been faulted into distinct structural blocks (Warren and others, 2000). Rhyolitic lavas or welded ash-flow tuffs such as in the Benham and Topopah Springs aquifers, respectively, comprise aquifers. Bedded and non-welded, zeolitized tuffs typically comprise confining units (Blankennagel and Weir, 1973; Prothro and Drellack, 1997; Bechtel Nevada, 2002). More than a half

Table 6. Site information and completion depths for wells at Pahute Mesa, Nevada National Security Site that were used in hypothetical example and field investigation.

Well name: Names are listed in alphabetical order. Bold part of name is well site as shown on Figure 15.
U.S. Geological Survey site identification number: Unique 15-digit number identifying well.
Latitude/Longitude: Latitude and longitude coordinates, referenced to North American Datum of 1927.
Land-surface altitude: Altitude, referenced to National Geodetic Vertical Datum of 1929.
Open intervals: Depth, in feet below land surface, of the top and bottom of open annulus.

Well Name	U.S. Geological Survey site identification number	Latitude (degrees, minutes, seconds)	Longitude (degrees, minutes, seconds)	Land-surface altitude (feet)	Open intervals
ER-20-5 #1	371312116283801	37°13'12.2"	116°28'37.8"	6,242	2,249–2,655
ER-20-6 #3	371533116251801	37°15'33.1"	116°25'17.5"	6,466	2,436–2,807
ER-EC-6 shallow	371120116294805	37°11'19.6"	116°29'48.1"	5,604	1,606–1,948
ER-EC-11 main	371151116294102	37°11'51.2"	116°29'41.1"	5,656	3,196–3,385 3,590–4,148
PM-3-1	371421116333703	37°14'20.7"	116°33'36.6"	5,823	1,872–2,192
UE-20n 1	371425116251902	37°14'25.1"	116°25'19.0"	6,461	2,308–2,834
ER-20-7	371247116284502	37°12'47.0"	116°28'44.8"	6,209	2,292–2,924
ER-20-8 main	371135116282601	37°11'35.1"	116°28'26.3"	5,848	2,440–2,940 3,070–3,442

dozen faults with offsets in excess of 500 ft have been mapped previously in Pahute Mesa (McKee and others, 2001), and additional faults are mapped with each new well (for example, National Security Technologies, LLC, 2010).

Hypothetical Example

The reliability of differentiating environmental fluctuations and pumping responses with water-level models was tested with a hypothetical aquifer system. Drawdown from a hypothetical aquifer test was simulated where the hydrogeologic complexity and distribution of hydraulic properties were assigned. The hypothetical aquifer system is comprised of ash-fall tuff, bedded tuff, welded tuff, and lava units that are flat-lying, laterally isotropic, and homogeneous (fig. 16). A fault 1,500 ft east of the pumping well, P1, bisects the aquifer system, vertically displaces hydrogeologic units 1,000 ft, and alters hydraulic properties around the structure.

The hypothetical aquifer system was simulated with a three-dimensional MODFLOW model (Harbaugh, 2005). The model domain was discretized laterally into 135 columns of 135 rows with a variably spaced grid (fig. 16). Cell sizes ranged in width from 10 ft by the pumping well to 40,000 ft at the model edges. Model edges were about 200,000 ft away from the pumping well, P1, and were simulated as no-flow boundaries. The model grid extended vertically from an impervious base at sea level to the water table at 4,200 ft above sea level. Vertical discretization was uniform, with 200-ft thick layers except for a 1-ft thick layer at the water table. The thickness differed so that the storage coefficient and specific storage were equivalent, and it allowed specific yield to be assigned directly in a layer. Changes in saturated thickness of the aquifer were not simulated because maximum drawdown at the water table was small relative to the total thickness.

Hydraulic properties typical of volcanic units were assigned to the hypothetical aquifer system. Ash-fall tuff, bedded tuff, welded tuff, and lava were assigned hydraulic conductivities of 0.001, 0.1, 3, and 50 ft/d, respectively. Horizontal-to-vertical anisotropy of one was assigned to all units. A uniform value of 0.02 was assigned for specific yield. The specific storage of all hydrogeologic units was 2×10^{-6} 1/ft.

Hypothetical aquifer-test results were simulated and analyzed during a 3-month period that was divided into five stress periods. The antecedent, pumping, recovery, pumping, and recovery periods were 21, 10, 10, 10, and 40 days, respectively. Pumping rates were 500 gpm during the second and fourth stress periods. Flow and drawdown in pumping and observation wells were simulated and sampled with the Multi-Node Well (MNW) package (Harbaugh, 2005). Flow to the pumping well was distributed proportionally to cell transmissivities by the MNW package.

Water levels with a "known" pumping signal and environmental fluctuations (noise) shown in figure 17 for well O3 were created by adding simulated drawdowns from MODFLOW to measured water levels in well EREC-6 shallow (fig. 17). Simulated drawdowns from MODFLOW in well O3, which is 7,800 ft from well P1, were interpolated in time to match measured water levels in well EREC-6 shallow. Simulated drawdowns from MODFLOW and simulated drawdowns with environmental noise added are in appendix D in the file .\WLMs\00_Hypo+Meas2SeriesSEE.xlsx.

Drawdowns were estimated by modeling "measured" water levels in well O3. Environmental fluctuations were simulated with computed tides, barometric pressure and background water levels in wells PM-3 and UE-20n 1 (fig. 17). Pumping effects were simulated with a Theis transform of the hypothetical pumping schedule. The water-level model was calibrated during the period from November 18, 2010, to March 6, 2011.

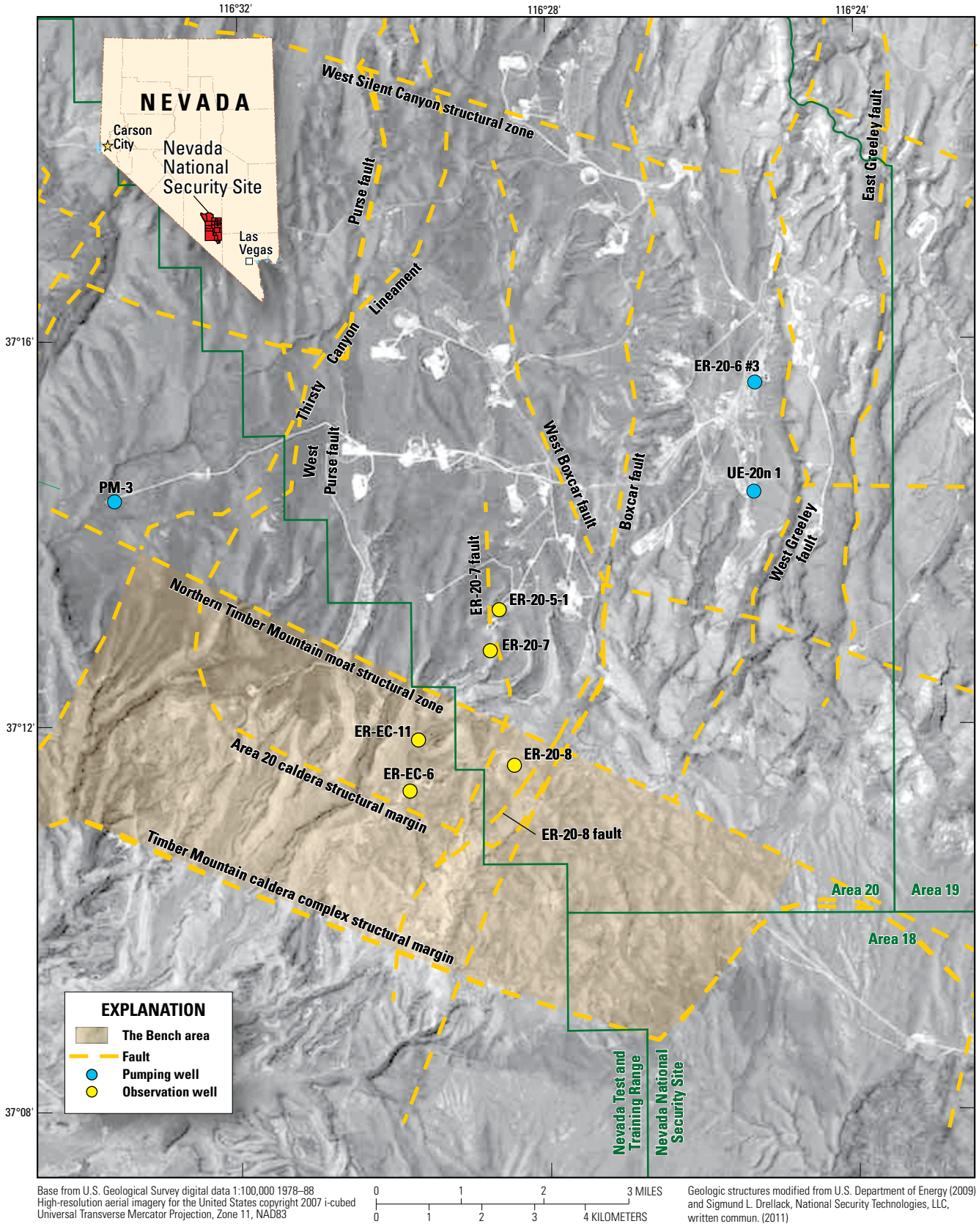

Figure 15. Background wells, observation wells, pumping well, and selected fault structures at Pahute Mesa Nevada National Security Site.

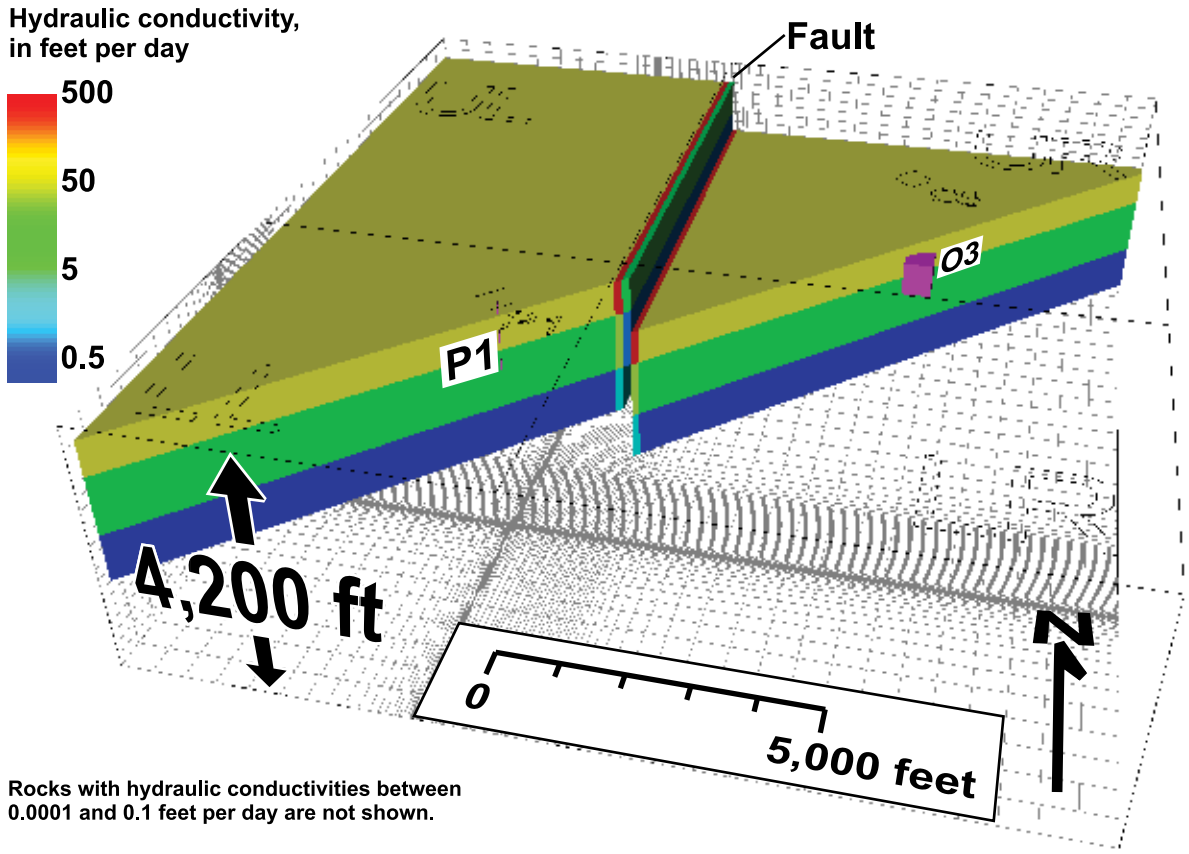

Figure 16. Hydraulic conductivity distribution of a subset of a hypothetical aquifer system that has been bisected by a fault, showing well locations and labeled quadrants (upper left, UL; upper right, UR; lower right, LR; lower left, LL).

Drawdowns that were estimated from "measured" water levels in well O3 agreed with known drawdowns within the noise of the data set (fig. 18). A maximum drawdown of 0.18 ft was estimated which was identical to the known maximum. The RMS error of differences between synthetic and measured water levels was 0.013 ft. The RMS error of differences between synthetic and known drawdowns was 0.015 ft.

Drawdowns alternatively were estimated in well O3 by modeling the original MODFLOW results with Theis transforms. No other WLM components were considered because environmental fluctuations did not exist in the original MODFLOW results. This alternative water-level model also was calibrated during the period from November 18, 2010, to March 6, 2011.

Drawdowns that were estimated directly from MODFLOW results could be replicated almost perfectly with Theis transforms. Differences between MODFLOW results and a single Theis transform could be reduced to a RMS error of less than 0.006 ft. RMS error declined to less than 0.0006 ft with the addition of a second Theis transform (fig. 18). Deviations of less than 0.001 ft approach the accuracy of the numerical solution of the hypothetical aquifer test.

The simplicity of Theis transforms did not introduce error because MODFLOW results could be replicated near perfectly with Theis transforms. Differences between known drawdowns and drawdowns that were estimated from "measured" water levels differed because of noise in the measured input series.

The hypothetical model and SeriesSEE input were created with **HypoFrame**, which is a workbook for simulating hypothetical aquifer tests and creating water levels with known pumping signals and environmental noise. Hypothetical aquifer systems must have flat-lying geologic units of uniform thickness and laterally isotropic, homogeneous hydraulic conductivity. A hypothetical aquifer system can be subdivided into four quadrants by two intersecting faults. Rock sequences in each quadrant can be displaced vertically within each quadrant. The **HypoFrame** workbook and documentation are in appendix D.

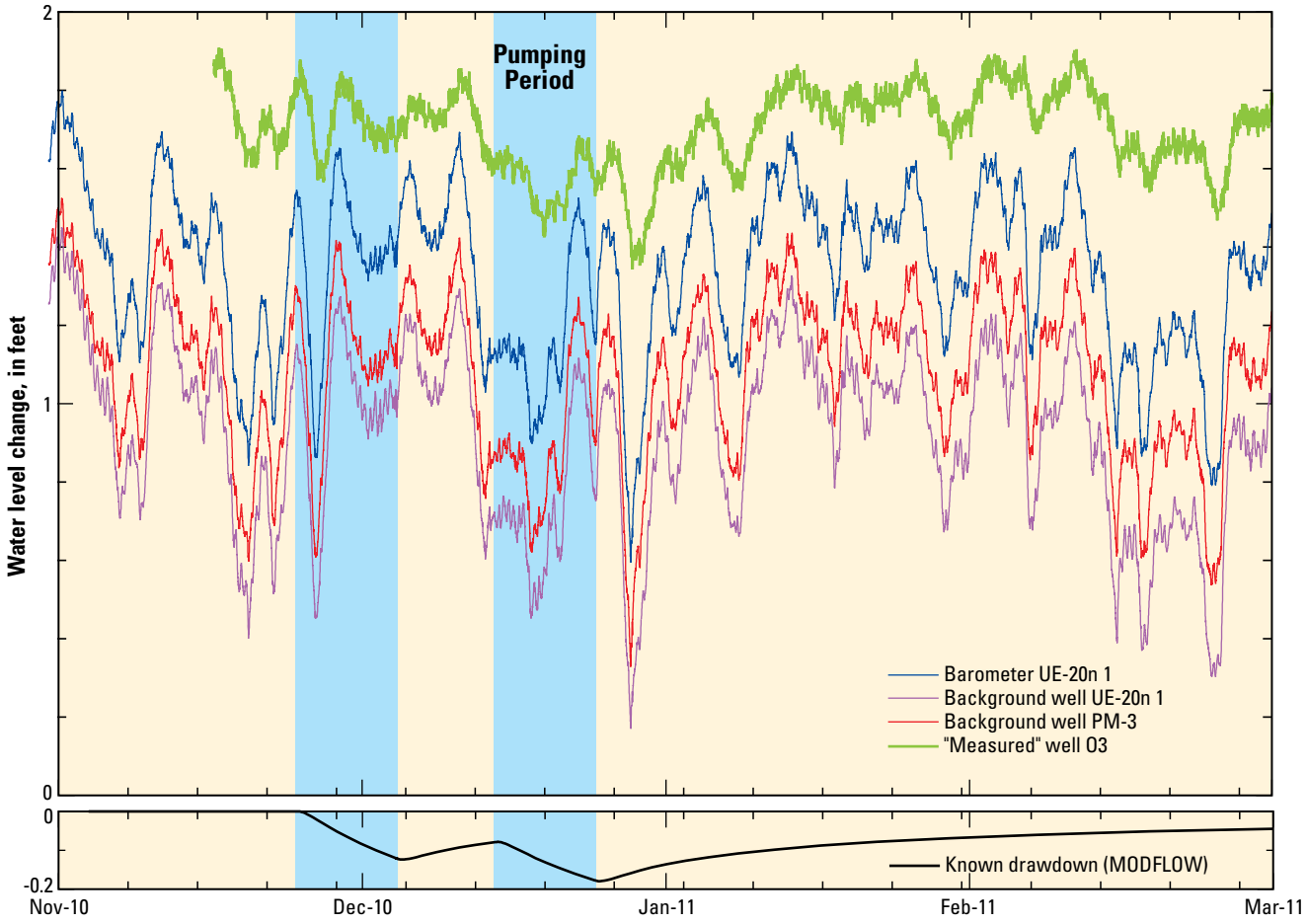

Figure 17. Barometric pressure, background water levels, and water levels with known drawdowns in hypothetical well 03.

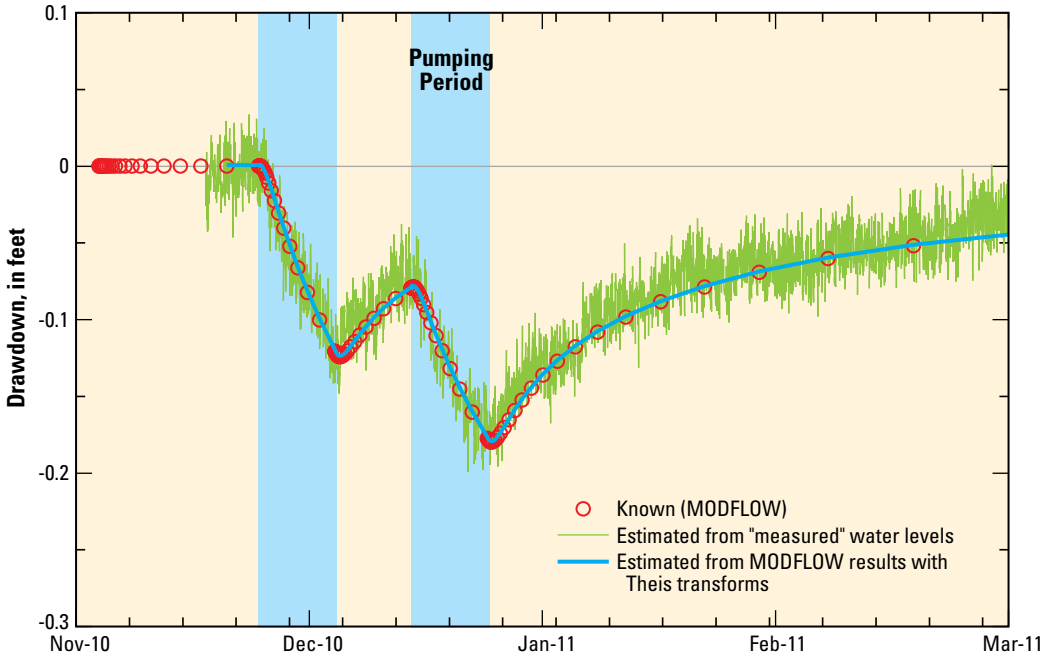

Figure 18. Known drawdowns (MODFLOW), drawdowns estimated from "measured" water levels, and drawdowns estimated directly from MODFLOW results in well 03.

Pahute Mesa Example

Water-level modeling was tested in a complex hydrogeologic system by estimating drawdown from two aquifer tests beneath Pahute Mesa (Halford and others, 2011). The upper and lower zones of well ER-20-8 main produced water from the Tiva Canyon and Topopah Spring aquifers sequentially between June 16, 2011, and August 8, 2011. Each well was pumped a total of 20 d, where pumping periods were evenly divided between well development and a constant-rate test (fig. 19).Drawdown from pumping both zones was estimated in observation well ER-20-7, which is screened in the Topopah Spring aquifer. Pumping and observation wells are 1.4 mi apart and penetrate different structural blocks (fig. 15).

Drawdown in well ER-20-7 was estimated with multiple Theis transforms in the water-level model. Environmental fluctuations were simulated with computed tides, barometric pressure, and background water levels from well UE-20bh-1 (fig. 15). Pumping effects were simulated with two Theis transforms for each of the two pumping schedules (fig. 19). The fitting period was from April 20, 2011, to November 11, 2011. Synthetic water levels matched measured water levels with a RMS error of 0.004 ft.

Drawdown in well ER-20-7 also was estimated with an identical water-level model, except that WLM components with background water levels were negated. Synthetic water levels matched measured water levels with a RMS error of 0.027 ft during the same fitting period from April 20, 2011, to November 11, 2011 (fig. 19). Each drawdown estimate was the difference between a synthetic water level without Theis transforms and a measured water level.

Poor drawdown estimates from the water-level model without background water levels demonstrates the need to simulate as much of the environmental fluctuations as possible. Antecedent conditions were simulated poorly where estimated drawdowns should be zero. Estimated drawdowns unambiguously were wrong during October and November when net water-level rises from pumping were estimated (fig. 19).

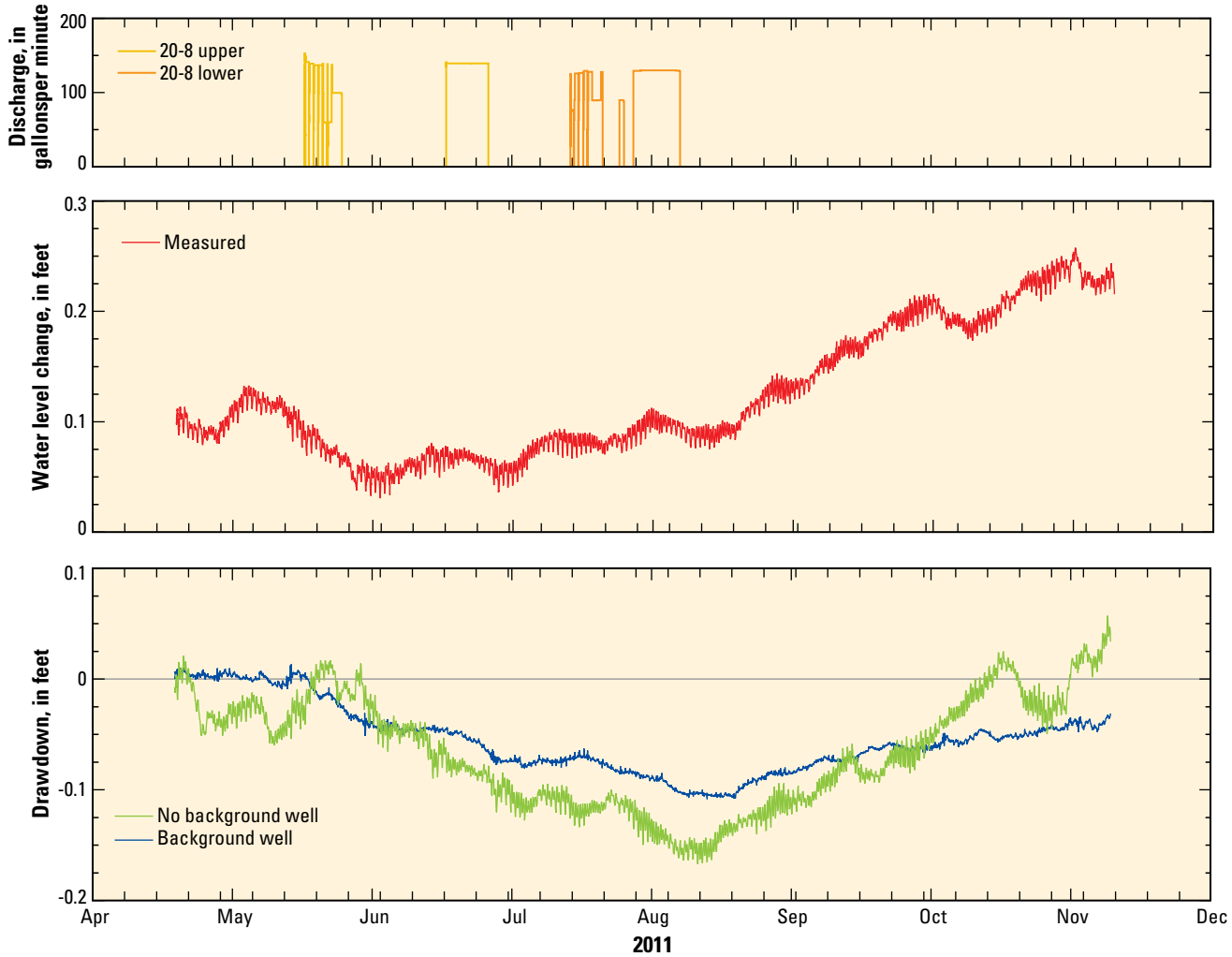

Figure 19. Measured water levels, synthetic water levels, Theis transforms, and estimated drawdowns in well ER-20-7 from pumping ER-20-8 main upper and lower zones, Pahute Mesa, Nevada National Security Site.

Water-Level Modeling Strategies

Estimating drawdowns that have been obscured by environmental fluctuations is the primary goal of the water-level modeling approach. This approach is most effective and efficient where many WLM components are specified and fitting periods are great. This approach has been summarized, sometimes derisively, as the flak-gun, fishing-with-dynamite, and kitchen-sink approaches. All phrases accurately depict testing many WLM components simultaneously. Unique contributions from each WLM component remain unknown, but pumping signals are not correlated with environmental fluctuations. The flak-gun approach was adopted here.

The flak-gun approach uses WLM components that could have been excluded. This is not a problem because mechanisms exist to negate WLM components. Amplitudes tending to zero will negate a WLM component. Multiple WLM components also can negate one another by summing to zero. Likewise, Theis transforms also are negated by a large transmissivity or storage coefficient value where pumping signals are below detection or absent. Negated WLM components aesthetically are lacking, but do not affect results. Systematic investigation of WLM components is possible with SeriesSEE, but has not been automated.

The flak-gun approach has many advantages, especially when estimating drawdowns in dozens of wells. Reporting is easier because the same input series and WLM components were used in all of the water-level models. Water-level models calibrate quickly after analyzing the first or second well because WLM components are defined with fair initial estimates of amplitude and phase. The flak-gun approach can fail when the fitting period decreases and correlation becomes possible between pumping signals and environmental fluctuations.

Correlation between weak pumping signals and environmental fluctuations is possible and requires further investigation. Nebulous drawdown estimates can be investigated with multiple water-level models where water levels initially are simulated without Theis transforms. An alternative water-level model is created by adding a Theis transform to the initial water-level model. The initial transmissivity and storage coefficient should create a small but measureable maximum deflection in the added Theis transform. Drawdowns likely were not detected if the RMS error cannot be reduced by more than 30 percent.

Input series of greater duration potentially can degrade with time as pressure transducers fail. For example, multiple input series could be good for the first four months, while one input series degrades during the last two months. Degradation likely will be apparent in the WLM residuals as scatter increases. Identifying the onset of failure in a specific input series requires modeling water levels during subsets of the fitting period. Degrading input series can be investigated manually with SeriesSEE, but an automated tool would be a better approach.

Summary and Conclusions

Pumping responses can be differentiated reliably from environmental fluctuations with water-level modeling. Water-level modeling approximates measured water-level fluctuations by summing multiple component fluctuations. Environmental fluctuations primarily are composed of barometric and background water-level input series and computed tide components. Pumping signals are modeled by superimposing multiple Theis transforms, where step-wise pumping records of flow are transformed into water-level changes. The summation of all component fluctuations is a synthetic water-level series.

Water-levels can be modeled robustly with the Theis-transform approach because environmental fluctuations and pumping signals are simulated simultaneously. Long-term trends are well simulated because environmental fluctuations are defined with entire periods of record. Fitting periods are extended greatly where pumping and recovery affect a majority of the record. Multiple Theis responses with different hydraulic diffusivities are summed to approximate lithologic variability.

Water-level modeling with Theis transforms has been implemented in the program SeriesSEE, which is a Microsoft® Excel add-in. Water levels to be modeled, input series, period of analysis, and water-level model components are defined interactively and viewed in workbooks that are created by SeriesSEE. Water levels are modeled with a FORTRAN program that is called from Excel. Differences between synthetic and measured water levels are minimized with PEST.

Water-level model components are transformations of input series. Moving average, Theis, pneumatic-lag, and gamma transforms are available transforms in SeriesSEE. Moving averages most frequently transform input series of barometric pressure and background water levels. Pumping schedules are transformed into water-level fluctuations with Theis transforms. Pneumatic-lag transforms barometric pressure changes at land surface to lagged and attenuated responses at the water table. Water-level rises from infiltration events are simulated with the gamma transform. Earth tides and step transforms are purely computed quantities that do not require input series.

Many utilities exist in SeriesSEE for viewing, cleaning, manipulating, and analyzing time-series data in addition to water-level modeling. Supporting utilities exist because data handling frequently consumes more time and effort than water-level modeling. Each SeriesSEE utility is documented with a brief explanation and step-by-step instructions that are accessed through context sensitive help.

Water-level models must be calibrated to reliably differentiate small pumping responses from environmental fluctuations. Differences between synthetic and measured water levels define goodness-of-fit. Sum-of squares of differences are minimized by PEST where singular value decomposition and Tikhonov regularization are used to assure stable results, not to inform estimated parameter values. Preferred homogeneity within amplitude, phase, and hydraulic property parameters is enforced with Tikhonov regularization.

Drawdown estimates from a water-level model are the summation of all Theis transforms minus residuals. The summation of all Theis transforms is the direct estimate of the pumping signal. Residuals represent all unexplained water-level fluctuations. These fluctuations should be random residuals during non-pumping periods, but can contain unexplained components of the pumping signal during pumping and recovery periods.

The simplicity of Theis transforms did not introduce error because results from a hydrogeologically complex MODFLOW model could be replicated near perfectly with Theis transforms. Differences between known drawdowns and drawdowns that were estimated from "measured" water levels differed because of noise in the measured input series. Estimated drawdowns are affected minimally by the Theis-transform approach relative to the inaccuracies that result from noise in the data sets.

Drawdowns much smaller than environmental fluctuations have been detected across a major fault structure more than 1 mile from the pumping well beneath Pahute Mesa, Nevada National Security Site. A maximum drawdown of 0.1 ft was estimated in well ER-20-7 during an 8-month period of analysis. Drawdown estimates in well ER-20-7 were consistent with a plausible pattern of drawdowns at all observation wells. Drawdowns could not have been detected without water-level modeling as implemented in SeriesSEE.

References

Baehr, A.L., and Hult, M.F., 1991, Evaluation of unsaturated zone air permeability through pneumatic tests: Water Resources Research, v. 27, no. 10, p. 2605–2617.

Barlow, P.M., and Moench, A.F., 1998, Analytical Solutions and Computer Programs for Hydraulic Interaction of Stream-Aquifer Systems: United States Geological Survey, Open-File Report 98-415A, 85 p.

Barlow, P.M., and Moench, A.F., 1999, WTAQ—A computer program for calculating drawdowns and estimating hydraulic properties for confined and water-table aquifers: U.S. Geological Survey Water-Resources Investigations Report 99-4225, 84 p.

Bartels, J., 1957, Gezeitenkrafte: Encyclopedia of Physics, vol. 48, 734: Berlin, Springer.

Bartels, J., 1985, Tidal forces (English translation), in Harrison J.C. (ed.) Earth Tides: New York, Van Nostrand Reinhold, p. 25–63.

Beaumont, C., and Berger, J., 1975, An analysis of tidal strain observations from the United States of America: I. The laterally homogeneous tide: Bulletin of the Seismological Society of America, v. 65, no. 6, p. 1613–1629.

Berger, J., and Beaumont, C., 1976, An analysis of tidal strain observations from the United States of America II. The inhomogeneous tide: Bulletin of the Seismological Society of America, v. 66, no. 6, p. 1821–1846.

Bechtel Nevada, 2002, A hydrostratigraphic model and alternatives for the groundwater flow and contaminant transport model of Corrective Action Units 101 and 102—Central and western Pahute Mesa, Nye County, Nevada: U.S. Department of Energy Report DOE/NV/11718–706.

Blankennagel, R.K., and Weir, J.E., Jr., 1973, Geohydrology of the eastern part of Pahute Mesa, Nevada Test Site, Nye County, NV: U.S. Geological Survey Professional Paper 712-B (Also available at *http://pubs.usgs.gov/pp/0712b/report.pdf*.)

Bower, D.R., 1983, Bedrock fracture parameters from the interpretation of well tides: Journal of Geophysical Research, v. 88, no. B6, p. 5025–5035.

Bohling, G.C., Zhan, X., Knoll, M.D., and Butler J.J., 2003, Hydraulic tomography and the impact of a priori information: An alluvial aquifer example. Kansas State Geological Survey Open-File Report 2003-71. Lawrence, Kansas: Kansas State Geological Survey.

Bredehoeft, J.D., 1967, Response of well-aquifer systems to earth tides: Journal of Geophysical Research, v. 72, no. 12, p. 3075–3087.

Criss, R. E. and Criss, E.M., 2011. Prediction of well wevels in the alluvial aquifer along the Lower Missouri River: Ground Water. doi: 10.1111/j.1745-6584.2011.00877.x

Defant, A., 1958, Ebb and Flow: Ann Arbor, University of Michigan Press.

Doherty, J., 2010b, Addendum to the PEST manual: Brisbane, Australia, Watermark Numerical Computing.

Doherty, J., 2010a, PEST, Model-independent parameter estimation—User manual (5th ed., with slight additions): Brisbane, Australia, Watermark Numerical Computing.

Doherty, J.E., and Hunt, R.J., 2010, Approaches to highly parameterized inversion—A guide to using PEST for groundwater-model calibration: U.S. Geological Survey Scientific Investigations Report 2010–5169, 59 p.

Doherty, J. and Johnston, J.M., 2003, Methodologies for calibration and predictive analysis of a watershed model: Journal of the American Water Resources Association, v. 39, no. 2, p. 251–265.

Dooge, J.C.I., 1959, A general theory of the unit hydrograph: Journal of Geophysical Research, v. 64, no. 2, p. 241–256.

Elliot, P.E., and Fenelon, J.M., 2010, Database of groundwater levels and hydrograph descriptions for the Nevada Test Site area, Nye County, Nevada, 1941–2010: U.S. Geological Survey Data Series 533. (Also available at *http://pubs.usgs.gov/ds/533/*.)

Erskine, A. D., 1991, The effect of tidal fluctuation on a coastal aquifer in the UK: Ground Water, v. 29, p. 556–562. doi: 10.1111/j.1745-6584.1991.tb00547.x

Fenelon, J.M., 2000, Quality assurance and analysis of water levels in wells on Pahute Mesa and vicinity, Nevada Test Site, Nye County, Nevada: U.S. Geological Survey Water-Resources Investigations Report 00-4014. (Also available at *http://pubs.usgs.gov/wri/WRIR00-4014/*.)

Fenelon, J.M., 2005, Analysis of ground-water levels and associated trends in Yucca Flat, Nevada Test Site, Nye County, Nevada, 1951–2003: U.S. Geological Survey Scientific Investigations Report 2005-5175, 87 p., at URL: *http://pubs.water.usgs.gov/sir2005-5175*.

Fenelon, J.M., Sweetkind, D.S., and Laczniak, R.J., 2010, Groundwater flow systems at the Nevada Test Site, Nevada: A synthesis of potentiometric contours, hydrostratigraphy, and geologic structures: U.S. Geological Survey Professional Paper 1771.

Halford, K.J., 2006, Documentation of a spreadsheet for time-series analysis and drawdown estimation: U.S. Geological Survey Scientific Investigations Report 2006-5024. (Also available at http://pubs.usgs.gov/sir/2006/5024/PDF/SIR2006-5024.pdf.)

Halford, K.J., Fenelon, J.M., and Reiner, S.R., 2010, Aquifer-test package—Analysis of ER-20-8 #2 and ER-EC-11 multi-well aquifer tests, Pahute Mesa, Nevada National Security Site: unpublished U.S. Geological Survey aquifer-test package, accessed August 30, 2011, at URL: *http://nevada.usgs.gov/water/AquiferTests/er_wells.cfm?studyname=er_wells*.

Halford, K.J., and Yobbi, D.K., 2006, Estimating hydraulic properties using a moving-model approach and multiple aquifer tests: Ground Water, v. 44, no. 2, p. 284–291.

Hanson, J.M., and Owen, L.B., 1982, Fracture orientation analysis by the solid earth tidal strain method: Presented at the 57th Annual Fall Technical Conference and Exhibition of the Society of Petroleum Engineers of AIME, American Institute of Mechanical Engineers, New Orleans, Louisiana, September 26–29, 1982.

Harbaugh, A.W., 2005, MODFLOW-2005, the U.S. Geological Survey modular ground-water model -- the ground-water flow process: U.S. Geological Survey Techniques and Methods 6-A16.

Harp, D. R., and Vesselinov, V.V., 2011, Identification of pumping influences in long-term water level fluctuations: Ground Water, v. 49, p. 403–414. doi: 10.1111/j.1745-6584.2010.00725.x

Harrison, J.C., 1971, New computer programs for the calculation of earth tides: Cooperative Institute for Research in Environmental Sciences, National Oceanic and Atmospheric Administration/University of Colorado.

Harrison, J.C., 1985, Earth Tides: New York, Van Nostrand Reinhold.

Helsel, D.R., and Hirsch, R.M., 1992, Statistical methods in water resources: New York, Elsevier Science Publishing, 522 p.

Laczniak, R.J., Cole, J.C., Sawyer, D.A., and Trudeau, D.A., 1996, Summary of hydrogeologic controls on ground-water flow at the Nevada Test Site: U.S. Geological Survey Water-Resources Investigations Report 96-4109. (Also available at http://pubs.usgs.gov/wri/wri964109/.)

Marine, I.W., 1975, Water level fluctuations due to earth tides in a well pumping from slightly fractured rock: Water Resources Research, v. 11, no. 1, p. 165–173.

McKee, E.H., Phelps, G.A., and Mankinen, E.A., 2001, The Silent Canyon Caldera—A three-dimensional model as part of a Pahute Mesa—Oasis Valley, Nevada, hydrogeologic model: U.S. Geological Survey Open-File Report 01-297.

Melchior, P., 1966, The Earth Tides: London, Pergamon Press.

Merritt, M.L., 2004, Estimating Hydraulic Properties of the Floridan Aquifer System by Analysis of Earth-Tide, Ocean-Tide, and Barometric Effects, Collier and Hendry Counties, Florida: U.S. Geological Survey Water-Resources Investigations Report 03-4267.

Munk, W.H., and MacDonald, G.J.F., 1960, The Rotation of the Earth: A Geophysical Discussion: London, Cambridge University Press.

Narasimhan, T.N., Kanehiro, B.Y., and Witherspoon, P.A., 1984, Interpretation of earth tide responses of three deep, confined aquifers: Journal of Geophysical Research, v. 89, no. B3, p. 1913–1924.

National Security Technologies, LLC, 2010, Completion report for the well ER-20-7, Correction Action Units 101 and 102--central and western Pahute Mesa: U.S. Department of Energy Report DOE/NV—1386.

O'Reilly, A.M., 1998, Hydrogeology and simulation of the effects of reclaimed-water application in west Orange and southeast Lake Counties, Florida: U.S. Geological Survey Water-Resources Investigations Report 97-4199.

O'Reilly, A.M., 2004, A Method for Simulating Transient Ground-Water Recharge in Deep Water-Table Settings in Central Florida by Using a Simple Water-Balance/Transfer-Function Model: U.S. Geological Survey Scientific Investigations Report 2004-5195, 49 p.

Potter, M.C., and Goldberg, Jack, 1987, Mathematical methods (2d ed.): Englewood Cliffs, N.J., Prentice-Hall, 639 p.

Prothro, L.B., and Drellack, S.L., Jr., 1997, Nature and extent of lava-flow aquifers beneath Pahute Mesa, Nevada Test Site: Bechtel Nevada, Technical Report DOE/NV-11718-156.

Rasmussen, T.C., and Crawford, L.A., 1997, Identifying and removing barometric pressure effects in confined and unconfined aquifers: Ground Water, v. 35, no. 3, p. 502–511.

Risser, D.W. and Bird, P.H., 2003, Aquifer tests and simulation of ground-water flow in Triassic sedimentary rocks near Colmar, Bucks and Montgomery Counties, Pennsylvania: U.S. Geological Survey Water-Resources Investigations Report 2003-4159.

Rorabaugh, M.I., 1964, Estimating changes in bank storage and ground-water contribution to streamflow: International Association of Scientific Hydrology, Publication 63, p. 432–441.

Sepúlveda, N., 2006, Ground-water flow model calibration program MODOPTIM and its application to a well field in Duval County, Florida: USGS Scientific Investigations Report 2005-5233. Reston, Virginia: USGS.

Stallman, R.W., 1971, Aquifer-Test Design, Observation, and Data Analysis: USGS Techniques of Water-Resources Investigations, Book 3, Chapter B1.

Theis, C.V., 1935, The relation between the lowering of the piezometric surface and the rate and duration of discharge of a well using groundwater storage: American Geophysical Union Transactions, v. 16, p. 519–524.

Toll, N.J., and Rasmussen, T.C., 2007, Removal of barometric pressure effects and earth tides from observed water levels: Ground Water, v. 45, no. 1, p. 101–105.

Walton, W. C., 2008, Upgrading aquifer test analysis: Ground Water, v. 46, p. 660–662. doi: 10.1111/j.1745-6584.2008.00442.x

Warren, R.G., Cole, G.L., and Walther, D., 2000, A structural block model for the three-dimensional geology of the Southwestern Nevada Volcanic Field: Los Alamos National Laboratory Report LA-UR-00-5866.

Weeks, E.P., 1979, Barometric fluctuations in wells tapping deep unconfined aquifers: Water Resources Research, v. 15, no. 5, p. 1167–1176.

Yeh, T.C., and Lee, C.H., 2007, Time to change the way we collect and analyze data for aquifer characterization. Technical commentary: Ground Water, v. 45, no. 2, p. 116–118.

Appendix A. SeriesSEE add-in

The SeriesSEE add-in, example data sets, and installation instructions in the zipped file, AppendixA_SeriesSEE.v.1.00.zip, can be accessed and downloaded at *http://pubs.usgs.gov/tm/tm4-F4/*. The SeriesSEE add-in, supporting modules, templates, and compiled FORTRAN codes are in the subfolder AddIN. Examples of geophysical log, data logger input, other time series, and water-level modeling data sets are in the subfolders Example_BOREHOLE, Example_LOGGER, Example_TIME, and Example_WLM, respectively. An Adobe PDF version of the help files, SeriesSEE.V1.00_Explain.pdf, is in the root directory because compressed help files that are on servers can be disabled, *http://support.microsoft.com/kb/896358.* Contents of all subdirectories are reported in README file in the root directory of the unzipped AppendixA_SeriesSEE.v.1.00.zip file.

Appendix B. Source Codes for SeriesSEE

Source code for SeriesSEE exists as FORTRAN, XML, and VBA codes in the zipped file, AppendixB_Codes-SeriesSEE.v1.00.zip, which can be accessed and downloaded at *http://pubs.usgs.gov/tm/tm4-F4/*. The FORTRAN codes NoComment and WLmodel support PEST and solve water-level models, respectively, and are in the FORTRAN subfolder. All VBA code are in the SeriesSee.V*.xlsm and SSmodule_*.xlsm files in the VBA subfolder. The XML that defines SeriesSEE commands and buttons in the Excel ribbon are in the XML subfolder. Contents of all subdirectories are reported in a README file in the root directory of the unzipped AppendixB_Codes-SeriesSEE.v1.00.zip file.

Appendix C. Verification of Analytical Solutions

Analytical solutions that were computed with the FORTRAN program WLmodel and published results of the same solutions in the zipped file, AppendixC_Verification.zip, can be accessed and downloaded at *http://pubs.usgs.gov/tm/tm4-F4/*. The analytical models for pneumatic lag, gamma, moving average, step, Theis, and tide are verified against known solutions in the subfolders AirLAG, Gamma, MovingAverage, Step, Theis, and Tide, respectively. Contents of all subdirectories are reported in a README file in the root directory of the unzipped AppendixC_Verification.zip file.

Appendix D. Hypothetical Test of Theis Transforms

The Excel program, HypoFrame, measured water levels, measured barometric changes, and reported water-level models in the zipped file, AppendixD_HypotheticalAquifer.zip, can be accessed and downloaded at *http://pubs.usgs.gov/tm/tm4-F4/*. HypoFrame is a workbook for simulating hypothetical aquifer tests and creating water levels with known pumping signals and environmental fluctuations. The premise and usage of HypoFrame are documented in the compressed help file 00_HypoFrame-HELP.chm. Measured water levels and barometric changes that serve as environmental fluctuation sources and background water levels are in the file 00_Meas+Back-for-Analysis.xlsx. Reported water-level models and tools for viewing parameter correlation are in the subfolder WLMs.

Appendix E. Pahute Mesa Example

Measured water levels, measured barometric changes, pumping signals, and reported water-level models in the zipped file, AppendixE_PahuteMesaExample.zip, can be downloaded at *http://pubs.usgs.gov/tm/tm4-F4/*. The zip file contains the pumping response in well ER-20-7 from the ER-20-8 main upper and lower aquifer tests.

SE ROA 11410

SE ROA 11411

OPEN ACCESS Freely available online

PLOS ONE

An Ecohydraulic Model to Identify and Monitor Moapa Dace Habitat

James R. Hatten[1]*, Thomas R. Batt[1], Gary G. Scoppettone[2], Christopher J. Dixon[1]

1 U.S. Geological Survey, Western Fisheries Research Center, Columbia River Research Laboratory, Cook, Washington, United States of America, **2** U.S. Geological Survey, Western Fisheries Research Center, Reno Field Station, Reno, Nevada, United States of America

Abstract

Moapa dace (*Moapa coriacea*) is a critically endangered thermophilic minnow native to the Muddy River ecosystem in southeastern Nevada, USA. Restricted to temperatures between 26.0 and 32.0°C, these fish are constrained to the upper two km of the Muddy River and several small tributaries fed by warm springs. Habitat alterations, nonnative species invasion, and water withdrawals during the 20th century resulted in a drastic decline in the dace population and in 1979 the Moapa Valley National Wildlife Refuge (Refuge) was created to protect them. The goal of our study was to determine the potential effects of reduced surface flows that might result from groundwater pumping or water diversions on Moapa dace habitat inside the Refuge. We accomplished our goal in several steps. First, we conducted snorkel surveys to determine the locations of Moapa dace on three warm-spring tributaries of the Muddy River. Second, we conducted hydraulic simulations over a range of flows with a two-dimensional hydrodynamic model. Third, we developed a set of Moapa dace habitat models with logistic regression and a geographic information system. Fourth, we estimated Moapa dace habitat over a range of flows (plus or minus 30% of base flow). Our spatially explicit habitat models achieved classification accuracies between 85% and 91%, depending on the snorkel survey and creek. Water depth was the most significant covariate in our models, followed by substrate, Froude number, velocity, and water temperature. Hydraulic simulations showed 2–11% gains in dace habitat when flows were increased by 30%, and 8–32% losses when flows were reduced by 30%. To ensure the health and survival of Moapa dace and the Muddy River ecosystem, groundwater and surface-water withdrawals and diversions need to be carefully monitored, while fully implementing a proactive conservation strategy.

Citation: Hatten JR, Batt TR, Scoppettone GG, Dixon CJ (2013) An Ecohydraulic Model to Identify and Monitor Moapa Dace Habitat. PLoS ONE 8(2): e55551. doi:10.1371/journal.pone.0055551

Editor: Z. Daniel Deng, Pacific Northwest National Laboratory, United States of America

Received August 13, 2012; **Accepted** December 24, 2012; **Published** February 7, 2013

Funding: Funding was provided by U.S. Fish and Wildlife Service (Nevada Fish and Wildlife Office) Interagency agreements 85320-7-H437 and F11RG00507; the Conservation Initiatives portion of the Southern Nevada Public Lands Management Act; and the Southern Nevada Water Authority. The funders had no role in study design, data collection and analysis, decision to publish, or preparation of the manuscript.

Competing Interests: The authors have the following interest. This study was partly funded by the Southern Nevada Water Authority. There are no patents, products in development or marketed products to declare. This does not alter the authors' adherence to all the PLOS ONE policies on sharing data and materials, as detailed online in the guide for authors.

* E-mail: jhatten@usgs.gov

Introduction

Anthropogenic factors negatively affect aquatic communities in the southwestern U.S. Specifically, in the Southern Xeric Basin and Range ecoregion [1], 82% of sampled stream reaches have disturbed riparian zones, 73% contain non-native vertebrates, 53% have serious streambed stability issues, 42% have mercury in fish, and 33% have reduced habitat complexity [2]. Aggravating this situation is the higher than average human growth rate in the arid southwest, contributing to the 15–60 m declines in groundwater levels region-wide, depending on location [3]. Thus it is no surprise that the desert southwest has an inordinate number of federally listed fishes, including Moapa dace *Moapa coriacea* [4]. Further complicating this picture is the looming threat of climate change, which will likely result in warmer air and water temperatures, reduced winter snowpack, and lower summer streamflows [5,6]. Collectively, these conditions make it imperative that wise water management practices are implemented to conserve the native aquatic biota in the arid southwest.

The Moapa dace is a thermophilic minnow endemic to the Muddy River, Clark County, Nevada [7]. Inhabiting water temperatures between 26.0 and 32.0°C, Moapa dace is restricted to the upper reaches of the Muddy River ecosystem where the river originates from thermal springs emanating from a deep carbonaceous aquifer [8,9]. The Moapa dace occurs only in the upper reaches of the Muddy River ecosystem (a.k.a. Warm Springs Area) because its water cools in a downstream direction [10]. In addition, seven other aquatic species of special concern inhabit the Muddy River ecosystem (three fish, two snails, and two insects), with each species having a unique life history and habitat preferences [11]. The Moapa White River springfish *Crenichthys baileyi moapae* is a cohabitating endemic thermophile that occurs in similar locations as Moapa dace. Virgin River chub *Gila seminuda* were known to occur throughout the main stem Muddy River, while speckled dace *Rhinichthys osculus moapae* inhabited the river downstream of the Warm Springs Area.

Moapa dace habitat was altered with the development of spring discharge in the Warm Springs Area for agricultural and recreational use [11,12]. The introduction of western mosquitofish *Gambusia affinis* by the 1930s and shortfin molly *Poecilia mexicana* in the 1960s also contributed to Moapa dace decline [13,14]. To insure persistence of Moapa dace and the Moapa White River springfish, the Moapa Valley National Wildlife Refuge (hereafter

"Refuge") was established in 1979 and subsequently expanded [11]. The Refuge is now comprised of three spring provinces (i.e., groups of springs) representing less than 10% of the two endemic's historic habitat. Still, the Refuge has been important to native fish persistence, especially Moapa dace and White River springfish. Moapa dace reproduce in the spring-fed tributaries to the Muddy River in water temperatures between 30 and 32°C [12].

The Refuge was instrumental in averting the extinction of Moapa dace after the 1995 invasion of blue tilapia *Oreochromis aureus* into the Warm Springs Area. Following the invasion, the two thermal endemic species were extirpated from about 90% of their former range [15,16], including critical adult foraging habitat in the mainstem Muddy River. While tilapias were prevented from accessing the Refuge by installation of temporary barriers, they have nonetheless temporarily severed the connectivity between springbrook and mainstem habitats. Readers may view a video of Moapa dace and Moapa White River springfish foraging and feeding in the Refuge (see Video S1).

Repatriation of Moapa dace to its historic range (i.e., Muddy River) is important because fragmented populations have a much greater chance of extinction [17,18]. The largest, oldest, and most fecund Moapa dace occurred in the larger water volume of the main stem Muddy River [12] - life history traits which enhance the species' probability of persistence [19]. In 2005 the primary water purveyor for Clark County, Southern Nevada Water Authority [20], purchased the Warm Springs Area for the protection of the area's biota, which provided the opportunity for tilapia extirpation from the Warm Springs Area.

With the establishment of Refuge and the Warm Springs Natural Area (WSNA), a substantial portion of the Moapa dace historic habitat is now under protection. However, in recent years there has been concern as to the sustainability of springs feeding the Muddy River [21]. Specifically, there has been pumping from the Muddy River's ground-water source, which may increase further, translating into decreased spring discharge [21]. To manage Moapa dace populations on the Refuge and WSNA, while sustaining the seven other sensitive aquatic species, managers need to understand the effect reduced streamflow has on the dace population and the larger Muddy River ecosystem.

In this paper we examine the potential effects of surface-water reductions on the availability of Moapa dace habitat by simulating an increase or decrease in the three primary Refuge springbrooks by 30% relative to baseflow. While Moapa dace are more sensitive to flow reduction than some species (e.g., Moapa White River springfish) [14], our results have implications for all aquatic species in the Warm Springs and Muddy River ecosystem. By providing a methodology that couples fine-grain hydrodynamic data, GIS, and habitat use observations, our approach can be applied to any aquatic ecosystem, large or small, provided the necessary physical and biological data are available.

Materials and Methods

Study Site

The Moapa Valley National Wildlife Refuge is situated near the southern edge of the Warm Springs Area (Fig. 1). Approximately 47 hectares, the Refuge contains three spring provinces - each of which feed a springbrook - referred to herein as the Plummer, Pedersen, and Apcar springbrooks. The three springbrooks eventually converge to form the Refuge Springbrook, a tributary to the Muddy River. Just prior to their acquisition, the Plummer and Pedersen properties were public resorts with their springbrooks feeding large and small swimming pools. In contrast, Apcar Springbrook had been altered to provide water for local municipal and irrigation purposes. At the time of each acquisition, no Moapa dace and few to no Moapa White River springfish occurred on each of the three properties. Following acquisition by the U.S. Fish and Wildlife Service, substantial habitat rehabilitation was undertaken at each of the three spring provinces aimed at creating suitable native fish habitat. Major rehabilitation modifications included channel realignment, removal of hundreds of nonnative fan palms *Wahingtonia filifera*, and channel excavation. Other rehabilitation actions included riparian vegetation planting, in-stream log placement, and cattail *Tyha* sp. removal [20].

The Pedersen Springbrook system was the first U.S. Fish and Wildlife Service acquisition (1979 and 1984), and habitat modification on that system began in the mid-1980s. This springbrook is fed by the highest springs within the Warm Springs Area and they are suspected to be the most sensitive to ground-water pumping [21]. Of the seven springs feeding the Pedersen Springbrook, two of the highest are equipped with flow gages, as is the Pedersen Springbrook where it leaves the Refuge 200 m downstream from the convergences of the spring tributaries (Fig. 1). The Pedersen Springbrook is also distinguished by the absence of western mosquitofish and shortfin molly; a small barrier prevents nonnative fishes access to the Refuge reach of the springbrook.

Purchased in 2001, hundreds of fan palms were removed from the Apcar system in 2007 and the springbrook rerouted to what was judged to be its historic course in 2009. Moapa dace began colonizing the newly excavated 163-m-long springbrook within months after its construction, but density was low at the time of our study and probably below carrying capacity. Streamflow in the Apcar Springbrook had the greatest potential for fluctuation in discharge due to water diversion for municipal use.

The Plummer Springbrook was used in the development and testing of our habitat models because it harbored the greatest density of Moapa dace during our five years of study (unpublished survey data, U.S. Fish and Wildlife Service, Las Vegas Field Office). The Plummer Springbrook has three tributaries converging 45 m upstream from where the springbrook leaves the Refuge at Warm Springs Road. With the assistance of The Nature Conservancy this property and spring province was acquired by the U.S. Fish and Wildlife Service in the late 1990s and a major rehabilitation of the spring province and springbrook occurred in 2006 and 2007. The rehabilitated springbrook is composed of small pools, riffles, glides, and small falls; it also has a public viewing chamber and is the focus of the Refuge's visitor center.

Hydrodynamic Modeling

We simulated the hydraulic conditions in the three Refuge springbrooks with River2D [22], a two-dimensional (2D), depth-averaged model [23]. Developed for streams and rivers, River2D has been extensively verified [24–26]. One of River2D's strengths is its variable-size mesh that can be optimized to obtain fine-scale details in areas of interest. Given the small size of the Refuge springbrooks, we constructed a mesh with 8–12 cm resolution to accurately discern hydraulic features associated with Moapa dace. We avoided one- and three-dimensional models because they produce data too coarse- (1-D) or fine-scale (3-D) to efficiently model Moapa dace foraging habitat (i.e., <1 m^2), while providing the flexibility to map and compare habitat across the entire Refuge [27]. Three products output by River2D are depth-averaged velocity, water depth, and Froude number, calculated at each intersection (node) of a triangulated irregular mesh, for a given flow. The Froude number is a dimensionless hydraulic variable that can objectively identify pool, riffle, and glide features [28,29].

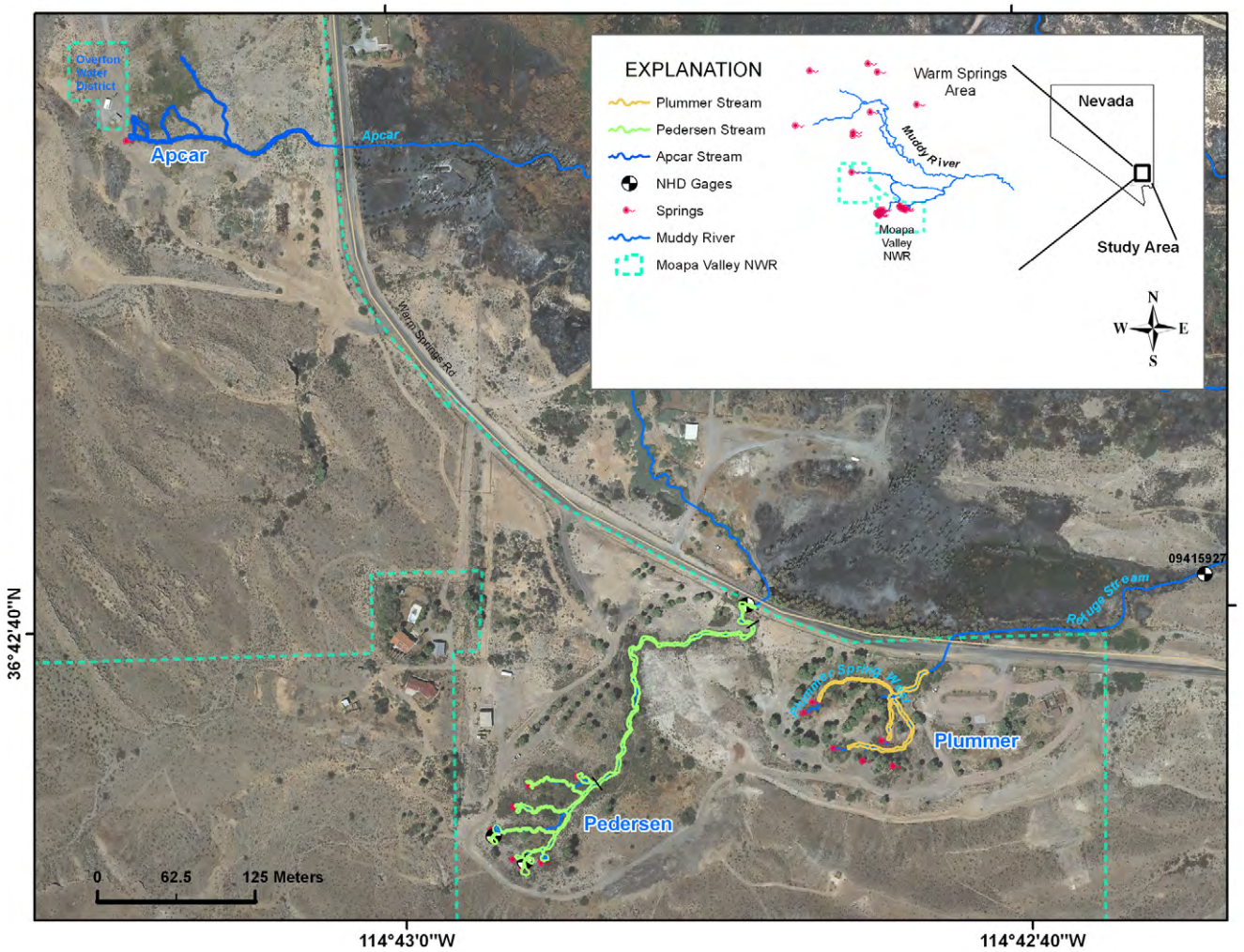

Figure 1. A map of the project area with the three spring-fed creeks displayed inside the Refuge boundary. Culverts route the springbrooks under the road located on the Refuge boundary.
doi:10.1371/journal.pone.0055551.g001

To insure confidence in the predictability of our 2-D-hydrodynamic model, we followed the methodology and steps in the on-line manual http://www.river2d.ualberta.ca and real-life applications [30,31]. Refer to File S1 for details related to bathymetry, substrate, or water temperature; File S2 for hydrodynamic boundary conditions; and File S3 for a calibration chart of Plummer Creek (0.071 cms). We could not verify simulations that were higher or lower than the baseflows for each springbrook since their flows were unwavering during and proceeding the study period. Nor could we manually change the inflows at each springhead for verification purposes due to the endangered status of Moapa dace. Thus, we relied exclusively on the calibration of the baseflow simulations and the depth-averaged St.Venant equations [22] to reach equilibrium (inflow equals outflow) for each flow simulation (see Hydrodynamic and Habitat Modeling Accuracies section in Discussion for details as to how this may affect our simulations).

Snorkel Surveys

Three snorkel surveys were conducted during the spring of 2009 on Plummer Springbrook between April 20 and May 28. Spaced approximately two weeks apart, snorkel surveys covered the entire Plummer Springbrook from the spring head to the culvert, located at the Refuge boundary (Fig. 1). Snorkel surveys began at the downstream of the springbrook as it left the Refuge and the snorkeler crawled upstream until a subject Moapa dace was sighted. After it was judged the fish was unaffected by the snorkeler's presence, its location was marked on a map as accurately as possible. Fish habitat use is influenced by size and life stage [32] and for our model we used dace ranging from about 40 to 85 mm fork length (FL), the largest observed on the Plummer Springbrook. Fish 40 mm FL were in the late juvenile stage [12], but used the same habitat as adults. For model construction, we drew polygons around dace locations to create occupied patch boundaries, with larger dace clusters producing the biggest patch boundaries. All locations outside of occupied patch boundaries were considered empty since no dace were observed in the snorkel surveys. A map of Moapa dace habitat was completed by joining the presence-absence polygons into one continuous surface representing Plummer Springbrook from the spring head to the Refuge boundary, with no areas unsurveyed.

Three follow-up snorkel surveys were conducted in the next 18 months: January 30, 2010; August 10, 2010; and January 30, 2011. The last survey date was unique because all three Refuge springbrooks were surveyed, while only Plummer Springbrook was surveyed on the other two dates. Thus, the first two snorkel surveys

were used to calibrate and verify the habitat model in Plummer Springbrook, while the third survey was used to verify the model on Pedersen and Apcar springbrooks following extrapolation of the model. This approach allowed us to perform an independent verification of the habitat model over both space and time.

Environmental Database

We constructed an environmental database for habitat modeling by georeferencing all data to a common coordinate system (UTM, Zone 11, NAD83), with each variable rendered as a grid with 12X12-cm (0.014 m^2) resolution (Table 1). Five predictor variables were created from River2D and field surveys for each springbrook; the principal variables were water depth (DEP), velocity (VEL), Froude number (FRD), substrate (SUB3), and water temperature (TMP). Additional variables were created for modeling purposes through the aggregation of substrate and Froude values into different size classes. Specifically, Froude number was reclassified into pool, riffle, and glide classes with FRD thresholds (pool: Fr <0.18; riffle >0.41; with glide intermediate) [29], while six substrate classes (fines, small gravel, medium gravel, large gravel, cobble, boulder) were aggregated into three classes (fines, gravels, cobble/boulder). Lastly, higher-order terms (e.g., quadratic, cubed) were created for each continuous variable for curvilinear model testing.

Habitat Modeling

We used cell-based (raster) modeling [33] and logistic regression [34] to build and test numerous Moapa dace habitat models for Plummer Springbrook. We employed logistic regression because it is well suited for the examination of the relationship between a binary response (i.e., presence or absence) and various explanatory variables [34,35]. We constructed a set of candidate habitat models for comparison and hypothesis testing with presence/absence snorkel data (spring 2009), physical variables (2D hydrodynamic data and substrate maps), logistic regression, and cell-based modeling. We used ArcGIS (version 9x; Redlands, CA) for database construction, SPSS (Chicago, Ill) for logistic regression, and ARC/INFO GRID (ESRI, 1992) for cell-based modeling.

A couple of challenges we faced when developing a model were spatial errors in the observations ($\sim$ 0.5–1 m) and an uneven distribution of dace, reflecting habitat preferences at certain locations. We dealt with spatial errors by randomly generating locations inside of occupied patch boundaries, reasoning that the fish were moving and feeding at the time of observation. We preserved the unequal distribution of dace by generating the same number of random points in each patch as the mean number observed in the snorkel surveys. Lastly, we characterized the larger, unused (background) portion of Plummer Springbrook by generating more absences than presences [36,37], with a minimum spacing of 12 cm (309 absences versus 141 presences; Fig. 2). Our approach reduced spatial autocorrelation by ensuring that no cell was sampled twice and that its neighboring cells were empty, while capturing habitat preferences through the unequal allocation of random points that were informed by snorkel abundance data. Following the compilation of random points, we attributed each location with its respective environmental features (e.g., velocity, depth) with a GIS.

We evaluated the predictive capability of combinations of covariates on dace occurrence with multivariate logistic regression. Given the field work that had been conducted to date on the Refuge, we held an a priori assumption that a combination of geomorphic features and hydraulic conditions was important for Moapa dace (Table 1). We used backward elimination and the likelihood-ratio test to identify significant covariates, starting with a full model and then progressively removing one or more variables and examining the change in Akaike's information criterion (AIC) [38]. We checked for nonlinearity between the logit and a continuous variable with quadratic, cubic, and log terms [39]. We evaluated 11 candidate models, comparing their performance with AIC model weights [38], Nagelkerke's pseudo-R^2 [40], Hosmer–Lemeshow goodness-of-fit statistic $\hat{C}$ [34], a binary classification table [41], and a Receiver Operating Characteristic (ROC) area-under-the-curve (AUC) [42].

Model Application and Verification

We generated spatially explicit maps of predicted Moapa dace habitat in Plummer Springbrook with cell-based modeling techniques [33], populating each model with its respective predictor variables (grids). We examined model accuracy with snorkel data described previously. We focused only on presence locations for verification purposes since the differences in Moapa dace numbers ($\sim$4X, this paper) on the three Refuge springbrooks were large, reflecting the recent history of habitat modifications and enhancement on each stream, versus the quality of habitat, making a comparison of model commission meaningless among streams.

We constructed a binary habitat map for each model by applying a probability cutpoint (threshold) of 0.3, which we obtained through trial and error during the model development and testing phase on Plummer Springbrook, balancing omission and commission errors [37]. Specifically, grid cells with a probability >0.3 were assigned a value of 1 (habitat), while cells with probabilities ≤ 0.3 were converted to zero (non-habitat). We used a GIS to overlay dace locations and habitat maps, calculating accuracy as the percentage of dace locations that fell within predicted suitable areas. Since there was some error in assigning locations of dace observed in the field to a map, we considered any

Table 1. Predictor variables used for Moapa dace habitat modeling.

Variable	Type	Description
VEL	Continuous	Depth-averaged velocity (m/s) obtained from 2D hydrodynamic model
DEP	Continuous	Water depth (m) obtained from 2D boundary conditions
FRD	Continuous	Froude values greater than 1 are super-critical flow; values <1 are sub-critical flow
SUB3	Categorical	Three substrate classes: 1 = fines, 2 = gravels, 3 = cobbles/boulders
SUB7	Categorical	Seven substrate classes: the three groups (SUB3) are further subdivided by size
TMP	Continuous	Temperature °C

doi:10.1371/journal.pone.0055551.t001

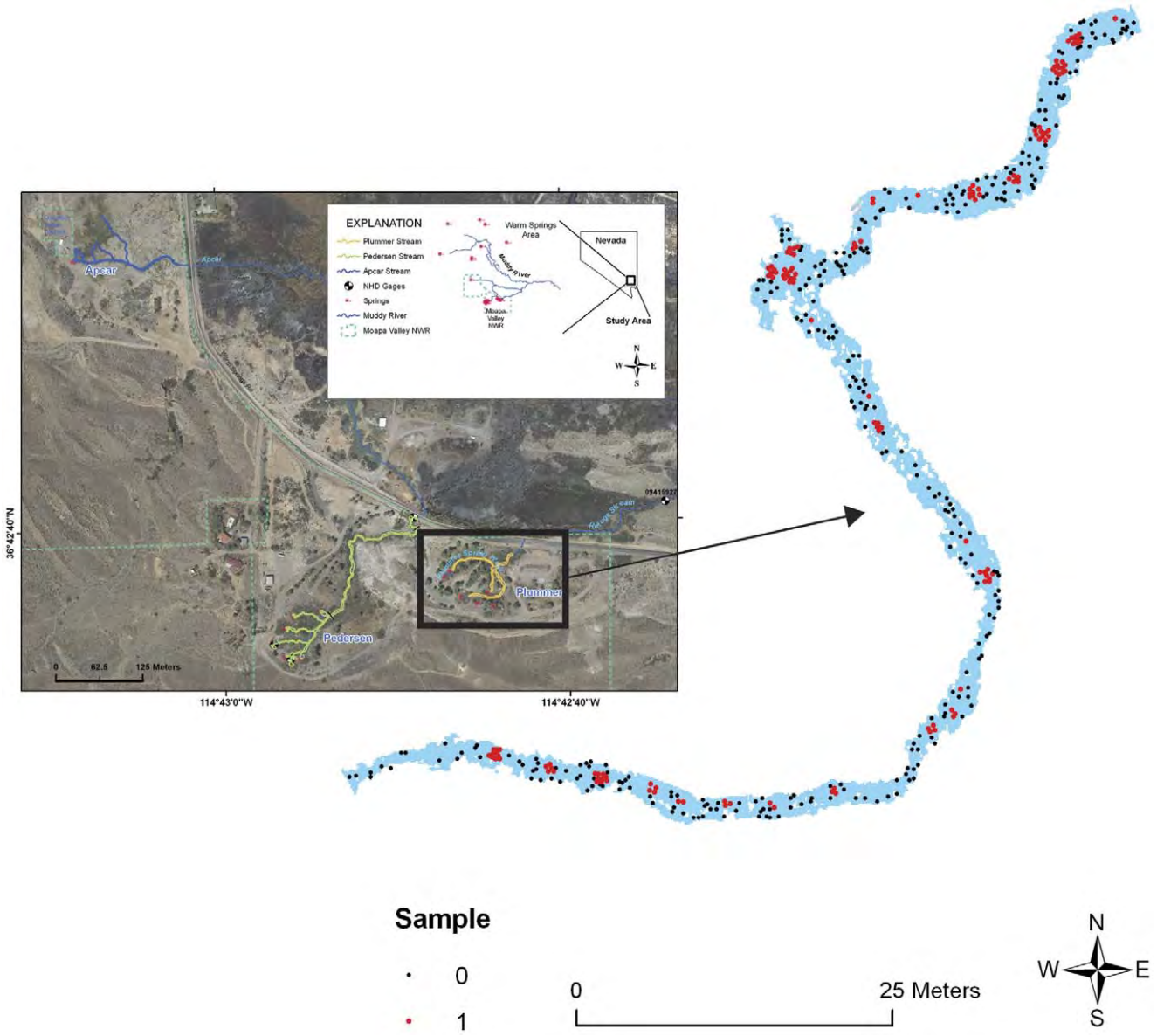

Figure 2. Random sample locations used for model development inside and outside of occupied dace patches in Plummer Springbrook. Snorkel surveys in the spring of 2009 were conducted to determine the locations of Moapa dace (shown in red), while absence locations were generated randomly outside of known dace sites with a GIS (309 absences and 141 presences).
doi:10.1371/journal.pone.0055551.g002

dace that fell within two cells (~24 cm) of an occupied patch to be a correct classification.

We assessed model fit by examining the density of presence locations found within discrete probability classes [31,37]. Specifically, we created 20% interval classes from the continuous probabilities output from the habitat model, overlaid dace locations, and calculated the density of dace within each probability class (number of dace/cell/probability class). A good fit to the model should be demonstrated by an increasing number of dace locations inside of higher probability classes.

Extrapolating the models to Apcar and Pedersen springbrooks required that we not change the model coefficients or probability threshold that were obtained on Plummer Springbrook, only the predictor grids (substrate, velocity, depth, Froude number). Applying the Plummer Springbrook habitat model to Plummer, Apcar, and Pedersen springbrooks ensured a true test of our habitat model in a spatial and temporal perspective.

Hydraulic Habitat Simulations

We conducted habitat simulations over a range of flows by ramping up or drawing down the flow in each Refuge springbrook by 30% relative to its baseflow, in 10% increments, calculating the amount of habitat at each flow with the habitat model. We tabulated the amount of predicted dace habitat for each flow simulation and displayed the results in bar graphs. Due to different reach lengths and base flows of the three springbrooks, we standardized our results for comparison purposes in two ways. First, we divided the amount of predicted habitat for each habitat-flow simulation by the length of springbrook, resulting in the amount of predicted habitat per-linear-meter of channel. Second, we divided the difference between each habitat-flow simulation

from its base-flow habitat estimate, producing the magnitude of change relative to its baseflow.

Results

Hydrodynamic Modeling

Two-dimensional hydraulic simulations for Plummer, Pedersen, and Apcar springbrooks achieved velocity and depth accuracies from 74%–91% (RMSE) and 84%–92%, respectively (see File S3). Each 2D springbrook simulation produced distinct patterns in depths and velocities, with pools and riffles easily discerned by their shapes and profiles (see File S4). Applying Froude thresholds to velocity and depth data revealed that Plummer Springbrook was comprised of 70% pools, 18% glides, and 12% riffles (baseflow = 0.071 cms). In contrast, Pedersen Springbrook was comprised of 50% pools, 33% glides, and 17% riffles (baseflow = 0.108 cms). Lastly, Apcar was comprised of 67% pools, 15% glides, and 18% riffles (baseflow = 0.066 cms).

Snorkel Surveys

Snorkel surveys in Plummer Springbrook (20 April through 28 May, 2009) revealed that dace were located at similar locations in different surveys, but moved significantly between sites (CV ~ 60%). However, overall abundance changed little between surveys (<5%), with an average of 141 dace, or 1.1 fish per-linear-meter of stream channel inside the Refuge. The two follow-up snorkel surveys in Plummer Springbrook detected 127 dace on 30 Jan 2010 (0.96 fish/m) and 161 dace on 30 Jan 2011 (1.2 fish/m). In contrast, only 62 dace were detected on Pedersen Springbrook on 30 Jan 2011 (0.26 fish/m) and 34 dace on Apcar Springbrook (0.21 fish/m). Thus, Plummer Springbrook had ~4 times the number of dace per-linear-meter of springbrook than the other two refuge streams.

Habitat Modeling

We saw distinct differences in velocity and depth conditions selected by Moapa dace, as compared to random background locations, in Plummer Springbrook at a baseflow of 0.071 cms (Fig. 3A), and a small difference in temperature (Fig. 3B). The further apart each group's medians, the stronger the evidence for habitat selectivity, while the closer the quartiles are within a group (i.e., 0 or 1), the smaller (more specific) the niche. The largest differences in median values between each sample group, listed in descending order of importance, were water depth, Froude number, stream temperature, and velocity. For the categorical variable substrate (Fig. 3C), the largest number of absence locations occurred inside cobble/boulder areas, while the largest number of presence locations occurred inside gravel areas.

Univariate logistic regression revealed that water depth had the closest association with dace locations during the spring of 2009 (Table 2; baseflow = 0.071 cms), followed in descending order of importance by substrate (3 classes), Froude number (continuous), velocity, and water temperature. Water depth obtained a good fit across 10 probability deciles ($\hat{C} = 0.5$), explained 37% of the variability, achieved 75.1% overall classification accuracy (binary; probability threshold = 0.3), and achieved an AUC of 0.82. The next closest univariate was substrate, with an AUC of 0.71. Of the univariables, only temperature had a non-significant AUC.

Of the 13 models we tested (Table 2) the top performer (according to AIC) contained a depth and substrate variable, plus a Froude variable (Model 1). Model 2 was also strongly supported by AIC (ΔAIC = 1.78), but contained a velocity variable in place of the Froude variable. We could not pair velocity into most models that contained Froude due to high colinearity, but we could pair

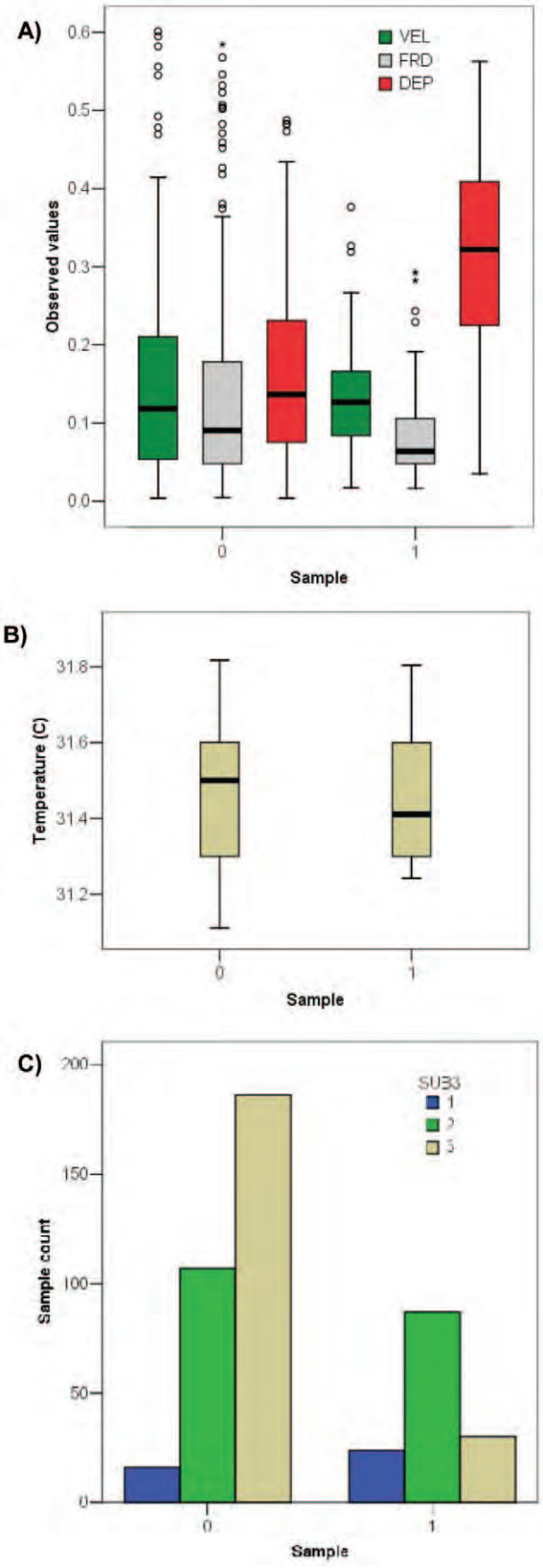

Figure 3. Box-and-whisker plots and bar graphs display the range of environmental values found at 450 sample locations in Plummer Springbrook (see Fig. 2). Panel A displays the distribution of velocity (m/sec), depth (m), and Froude values; panel B shows temperature values; panel C portrays the number of presence or absence sample locations found within three substrate classes (1 = fines, 2 = gravels, 3 = cobble/boulder).
doi:10.1371/journal.pone.0055551.g003

depth with Froude - even though Froude incorporates depth into its computation. There was moderate support for Models 3–7 (ΔAIC between 3 and 6), with no support for the remaining six models (ΔAIC >79). The critical variable that resulted in the large gap in AIC scores between Models 1 thru 7 and Models 8 thru 13 was depth. Whenever depth was in a model, it was either strongly (Models 1,2) or moderately (Models 3–7) supported. No other covariate influenced the multivariate models to the magnitude of depth, with substrate a distant second, followed by Froude number, velocity, and temperature. Depth was also the best univariate model (Model 6), achieving equal model-fit statistics as the top five models, with the exception of its AIC score (ΔAIC = 4.455). The two temperature models (5 and 7) were only moderately supported by AIC, but Model 5 achieved the best overall model fit ($\hat{C} = 0.821$) and tied model 1 for best R^2 (0.403) and AUC (0.838), while Model 7 obtained the best overall classification accuracy (76.6%), indicating temperature played a small role in dace habitat selection in Plummer Springbrook.

We selected Model 2 for model extrapolation into Apcar and Pedersen springbrooks, and for hydraulic-habitat simulations (i.e., ramping up and drawing down flows), because it was strongly supported by AIC, achieved a reasonably good model fit ($\hat{C} = 0.608$), and velocity is easier to interpret than the Froude number. We also found little difference in performance between these two models from an accuracy or spatially explicit perspective (model parameters for Models 1 and 2 are listed in Table 3). We retained covariates in Models 1 or 2 if they improved the overall fit

Table 3. Model parameters and coefficients for Model 1 (top) and Model 2 (bottom): outputs were obtained from multiple logistic regression on Plummer Creek, with samples collected in the spring of 2009 ($n = 450$; 309 absences and 141 presences).

Model 1					
Variable	***B***	**S.E.**	**Wald**	**df**	**Sig.**
DEP	12.745	4.402	8.383	1	0.004
DEP_2	−8.956	7.822	1.311	1	0.252
FRD	4.778	6.065	0.621	1	0.431
FRD_2	−22.941	20.594	1.241	1	0.265
SUB3 (reference)			10.44	2	0.005
SUB3 (class 1)	1.134	0.442	6.595	1	0.01
SUB3 (class 2)	0.8	0.282	8.031	1	0.005
Constant	−3.838	0.626	37.634	1	0
Model 2					
DEP	13.935	4.426	9.913	1	0.002
DEP_2	−10.923	7.746	1.989	1	0.158
SUB3 (reference)			10.272	2	0.006
SUB (class 1)	1.126	0.447	6.345	1	0.012
SUB (class 2)	0.796	0.282	7.979	1	0.005
vel252b	4.238	5.135	0.681	1	0.409
vel252b_2	−15.174	14.272	1.13	1	0.288
Constant	−4.047	0.604	44.914	1	0

See Table 1 for variable definitions; variables with an underscore (e.g., Dep_2) are squared terms.
doi:10.1371/journal.pone.0055551.t003

Table 2. Model results for univariate and multivariate logistic regression, listed from best to worst according to AIC score ($n = 450$; 309 absences and 141 presences).

Model	LL	NPar	AIC	ΔAIC	w	$\hat{C}$	R^2	OA	AUC	Variables
1	407.461	8	423.461	0.000	0.484	0.685	0.403	76.20	0.838	*DEP, FRD, SUB3
2	409.241	8	425.241	1.780	0.199	0.608	0.399	76.20	0.835	*DEP, VEL, SUB3
3	421.035	3	427.035	3.574	0.081	0.499	0.372	75.70	0.826	*DEP, FRD
4	419.037	4	427.037	3.576	0.081	0.797	0.377	75.05	0.826	*DEP, VEL, FRD
5	407.284	10	427.284	3.828	0.072	0.821	0.403	76.30	0.838	*DEP,FRD,TMP,SUB3
6	421.916	3	427.916	4.455	0.052	0.499	0.370	75.10	0.823	DEP
7	408.963	10	428.963	5.502	0.031	0.488	0.400	76.55	0.835	*DEP,VEL,TMP,SUB3
8	494.787	4	502.787	79.326	0.000	NA	0.188	69.45	0.708	SUB3
9	491.44	8	507.440	83.979	0.000	NA	0.197	68.65	0.724	SUB7
10	519.993	2	523.993	100.532	0.000	0.040	0.118	59.50	0.664	FRD
11	522.173	3	528.173	104.712	0.000	0.247	0.112	61.65	0.670	VEL
12	527.814	4	535.814	112.353	0.000	NA	0.096	59.60	0.598	FRD3
13	559.568	1	561.568	138.107	0.000	0.000	0.000	54.90	0.500	TMP

Statistics presented are twice the negative log-likelihood value (−2L), the number of parameters (NPar), change in AIC score when compared to the best model (ΔAIC), AIC model weight (w), Hosmer-Lemeshow goodness-of-fit statistic ($\hat{C}$), Nagelkerke pseudo R-squared (R^2), overall classification accuracy (OA), ROC area-under-the-curve (AUC), and the principal variables in each model (higher-order terms not shown. For variable descriptions, see Table 1; * denotes the variable that had the greatest influence on the model's log likelihood. Quadratic terms are not shown in the Variables field.
doi:10.1371/journal.pone.0055551.t002

of the model ($\hat{C}$), regardless of statistical significance (Table 3). While quadratic terms improved the fit of both models, indicating non-linear relationships, logarithmic and cubic functions failed to improve model fit.

Interpretation of the odds ratios (exp β) and model coefficients for Models 1 or 2 provided information about the habitat preferences of dace. Specifically, dace were approximately three times as likely to occur on sandy substrates as a cobble-boulder substrate, and approximately two times as likely on a gravel surface. Interpretation of the squared terms revealed that in small springbrooks dace about 40 to 85 mm FL preferred water depths between 0.64 and 0.71 m, a Froude value of 0.1 (non-stagnant pool), and a velocity of 0.14 m/s. These values changed slightly when other models were examined, but they were not as well supported by AIC as Models 1 or 2.

Model Application and Verification

Model 2 produced a mean probability for dace habitat in Plummer Springbrook of 0.21 (baseflow 0.071 cms), with a maximum of 0.83 and a minimum of 0. Applying a habitat probability threshold of 0.3, 26.8% (0.007 ha) of Plummer Springbrook was predicted to be dace habitat at a baseflow of 0.069 cms (see File S4). Model 2 achieved 88% accuracy in August 2010 when challenged with independent snorkel data (22 out of 25 sites correct), 90.5% accuracy in January 2010 (19 of 21), and 91.1% in January 2011 (41 out of 45).

Model 2 obtained a good fit when we examined dace density per probability class in Plummer Springbrook, using snorkel data in the spring of 2009 (Fig. 4). For this analysis we merged probability classes 4 and 5 since the model's probabilities topped out at 84%, producing too few cells or fish observations in class 5 to stand alone. Thus, we calculated dace densities inside four probability classes: 0–20%, 20.1–40%, 40.1–60%, and >60%. The following equation describes the relationship between dace density and the four probability classes in Plummer Springbrook.

$$D = 0.009X - 0.0077.$$

where D is the density of dace per cell (0.0144 m^2) for a given probability class. Our density estimate for Plummer Springbrook appeared to represent future dace conditions too since the numbers of dace in the two future snorkel surveys bracketed the numbers observed in the spring of 2009, with the locations approximately the same.

The mean probability of dace occurrence in Pedersen Springbrook, using Model 2, was 22.2% (baseflow 0.108 cms), with a maximum probability of 85.3%, and a minimum of 0%. Applying a 30% probability threshold resulted in 29.3% (0.013 ha) of the springbrook predicted to be dace habitat (see File S4). When we challenged the habitat model to independent snorkel data collected in January 2011, the model achieved 84.6% accuracy (22 of 26 sites correctly classified). The mean model probability for Apcar Springbrook, using Model 2, was 30.8% (baseflow 0.066 cms), with a maximum probability of 86% and a minimum of 0%. Applying a 30% probability threshold resulted in 42.7% (0.013 ha) of Apcar Springbrook predicted to be dace habitat (see File S4). When we challenged the habitat model to independent snorkel data collected in January 2011, the model achieved 90% accuracy (18 of 20 sites).

Hydraulic Habitat Simulations

When we supplied the habitat model with seven flows, starting at a 30% increase over baseflow and then descending in 10% increments - until a 30% reduction was achieved - habitat (per-linear-meter of stream channel) appeared to decrease steadily in Plummer and Apcar springbrooks (Fig. 5A). This pattern was not the same for Pedersen Springbrook, where the maximum habitat was obtained at a 10% increase over baseflow, before leveling out. The amount of predicted habitat per-linear-meter of springbrook revealed that Apcar Springbrook is expected to produce the most dace habitat over the range of flows. The slope of the increase for Plummer Springbrook appeared similar to Apcar, but the amount of predicted habitat per-linear-meter of channel was approximately 30% less. In contrast, Plummer and Pedersen springbrooks had different slopes (reactions), but the amount of predicted habitat per-linear-meter of springbrook was similar at the top and bottom of the flow simulations. However, Pedersen Springbrook appeared more responsive to flows between minus 20% and plus 20% compared with Plummer Springbrook. When we simulated how dace habitat in each springbrook would change in relation to its baseflow prediction (Fig. 5B), Plummer Springbrook appeared the most sensitive, with potential losses of approximately 30% and increases of 10%. Pedersen Springbrook appeared to be the second most sensitive to flow modifications, with potential habitat losses of 15% and gains of 2%. In contrast, Apcar Springbrook gained or lost approximately 5% of its predicted dace habitat in relation to its baseflow, indicating it was least sensitive to flow alteration.

Discussion

Hydrodynamic and Habitat Modeling Accuracies

The accuracy rate of our 2D hydrodynamic flow simulations ranged from 73–91%, under baseflow conditions, which is consistent with other 2D studies on large and small streams [26,30,43]. We were unable to calibrate or validate non-baseflow simulations given the unvarying springheads over the study period. Calibration typically involves changing mesh configuration or roughness values to achieve closer agreement between simulated and measured water surface elevations and velocities [23,30]. Thus, our flow simulations may have bias that could affect habitat classification, but the baseflow had good verification results and it was the midrange of our flow simulations. To our knowledge these are some of the smallest streams where 2D fish-habitat modeling has been conducted and we are satisfied given the 85–91% accuracies Model 2 achieved with temporally and spatially independent snorkel-survey data. Furthermore, the excellent linear fit between the model's probability classes and dace densities demonstrated that the model provided useful information about the quality of dace habitat (i.e., higher dace numbers informed the model of preferred hydrogeomorphic conditions).

Habitat-flow Simulations

Plummer and Apcar springbrooks produced proportionately more habitat as flows increased, while Pedersen springbrook reached a plateau after a 10% increase, suggesting a geomorphic constraint. In contrast, Plummer and Apcar springbrooks appeared relatively unconstrained by geomorphology and thus dace might benefit from increased flows. Conversely, habitat simulations consistently showed in each springbrook that reduced flows produce less Moapa dace habitat. A reduction in habitat is typically followed by a reduction in population number, thus the information in this study is important when considering population dynamics in relation to streamflow [44].

Because Refuge springbrooks are close to spring heads, Refuge habitat experienced a very narrow temperature range and our analysis garnered only moderate support for the two temperature

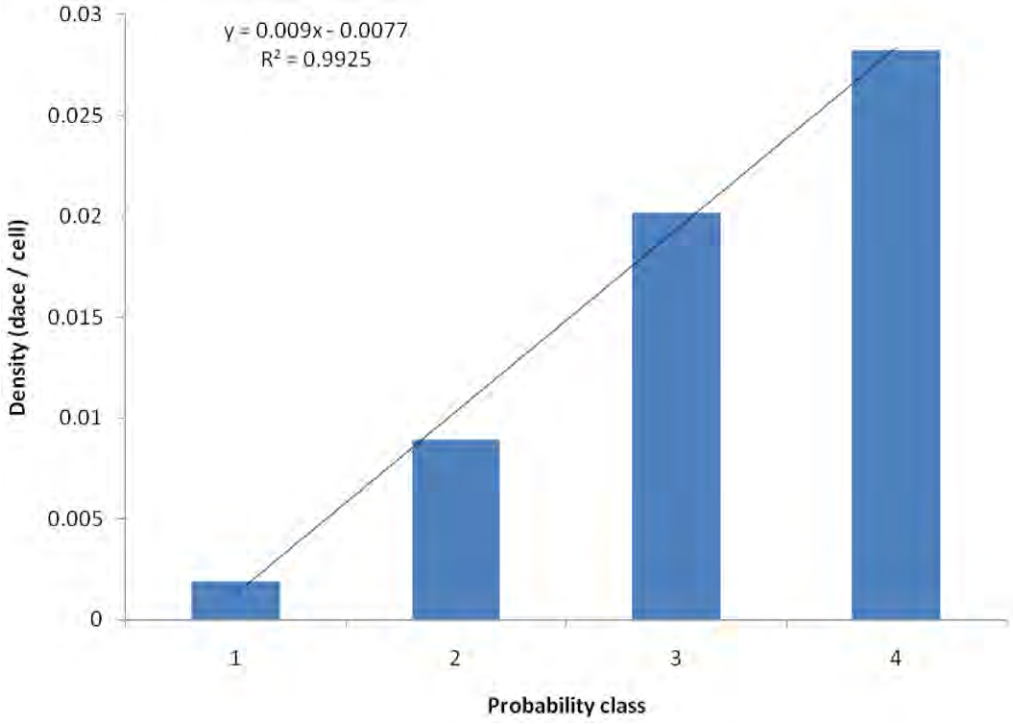

Figure 4. The relationship between Moapa dace density and four probability classes in Plummer Creek, as output by Model 2. Probability classes are 1 (0–20%), 2 (20.1–40%, 3 (40.1–60%), and 4 (>60%). Dace densities were obtained by averaging three back-to-back snorkel surveys (spring of 2009), counting the number of dace within each probability class, and dividing by the number of cells (0.0144 m^2) found within each probability class.
doi:10.1371/journal.pone.0055551.g004

models (Table 2, Models 5,7). Had we had the opportunity to study Moapa dace in its historic range in the Muddy River, where waters are cooler, the influence of temperature in our models would likely be greater because larger, older fishes frequently inhabit cooler water [45,46]; a phenomena previously observed in Moapa dace [12]. A reduction in springflows on the Refuge or Muddy River could result in stream cooling [47], which may reduce the area currently suitable for rearing, foraging, and spawning (26°−32°C).

Detection

Moapa dace have patchy distribution and congregate in predictable hydraulic conditions, as defined by our model. Foraging primarily upon drift [12], Moapa dace presumably select hydraulic conditions that promote optimal foraging [48], hence their patchy distribution. They are also quite transient, frequently moving among patches [14], with an average movement of 68 m between bi-monthly sampling events, and ~30% leaving the refuge entirely (Mark Hereford, USGS Biologist, personal communication). As more information is gathered through tagging and genetic analysis, we will gain a better understanding of dace migration rates on and off the refuge, particularly at finer temporal and spatial scales. Until this occurs, we chose not to incorporate detection probabilities into our modeling approach [49].

Habitat selection can be density dependent with only higher quality habitat used when population numbers are low [50,51]. The Plummer Springbrook was inhabited by well over 50% of the Moapa dace population during the period of our study and presumably virtually all available habitats were occupied during our snorkel surveys. We are confident based upon our extrapolation tests (temporally and spatially) that the habitat model we developed for Plummer Springbrook, and extrapolated to Pedersen and Apcar springbrooks, captured the essential features that comprise dace habitat. Namely, water depth, substrate composition, Froude number, and velocity, with temperature a distant last.

Habitat Restoration-Rehabilitation

Habitat rehabilitation in the three Refuge springbrooks was crudely modeled on sites observed to support congregations of foraging Moapa dace before they became restricted to the Refuge (Unpublished report: G. Gary Scoppettone). Most sites were in the upper Muddy River where the catchment basin intermittently floods, producing flows well beyond the historic 1.1 m^3/s attributed solely to thermal springs [9]. The cut and fill alluviation produced by intermittent flooding most likely built and destroyed Moapa dace habitat in the main-stem Muddy River in a dynamic process that has occurred for thousands of years. These dynamic flooding-erosion processes generally decrease in an upstream direction [52], thus catchments with smaller or reduced drainage areas are not as dynamic. The Refuge springbrooks have all been cut off from their respective sub- catchment basins and thus the quality of Moapa dace habitat will likely degrade in time due to emergent and submergent vegetation. Without intermittent flooding to maintain or generate new dace habitat, the Refuge springbrooks will need to be continually monitored for habitat quality, with habitat restoration conducted on an as-needed basis.

Our habitat models provide targets and thresholds for managers in the development, evaluation, and monitoring of dace habitat. For example, the amount of predicted habitat from our models can be used as an indicator of the effectiveness of a restoration or

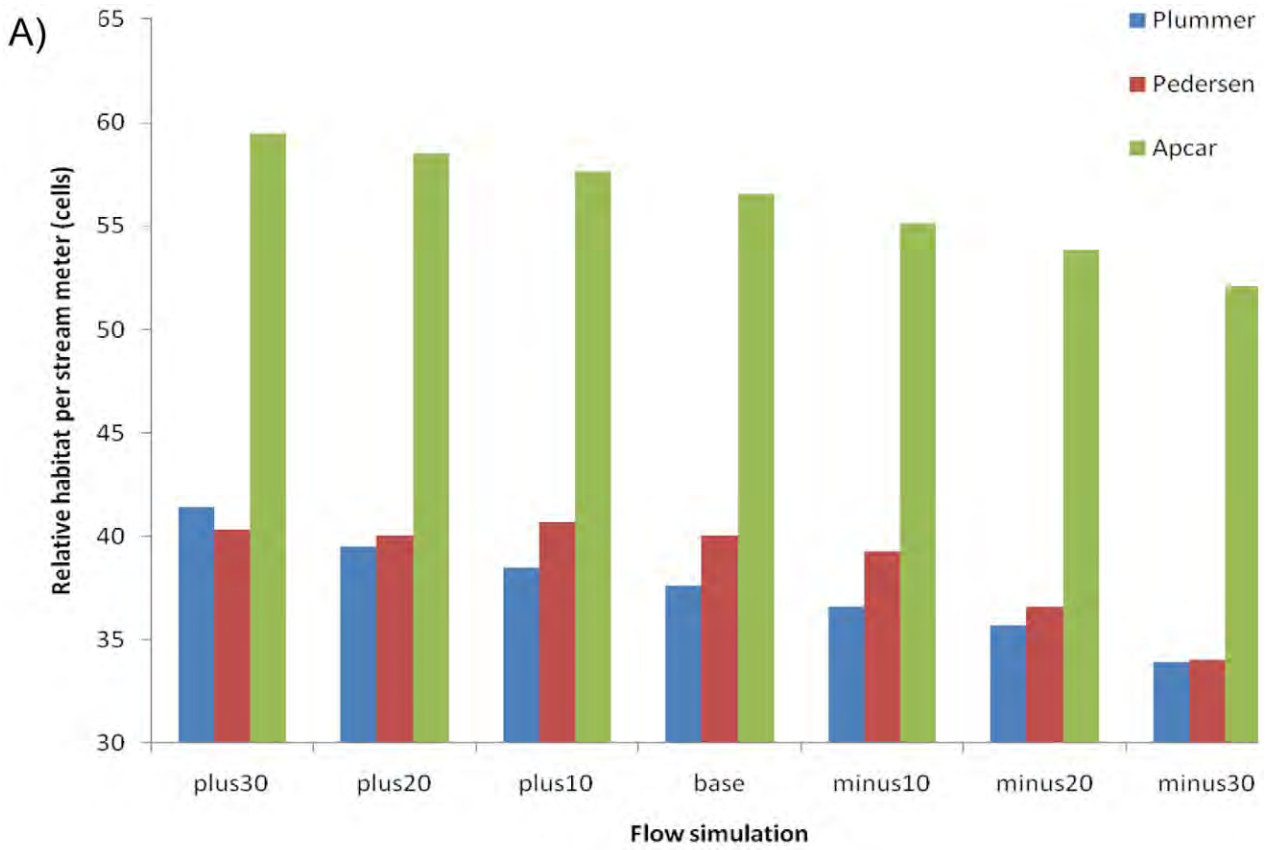

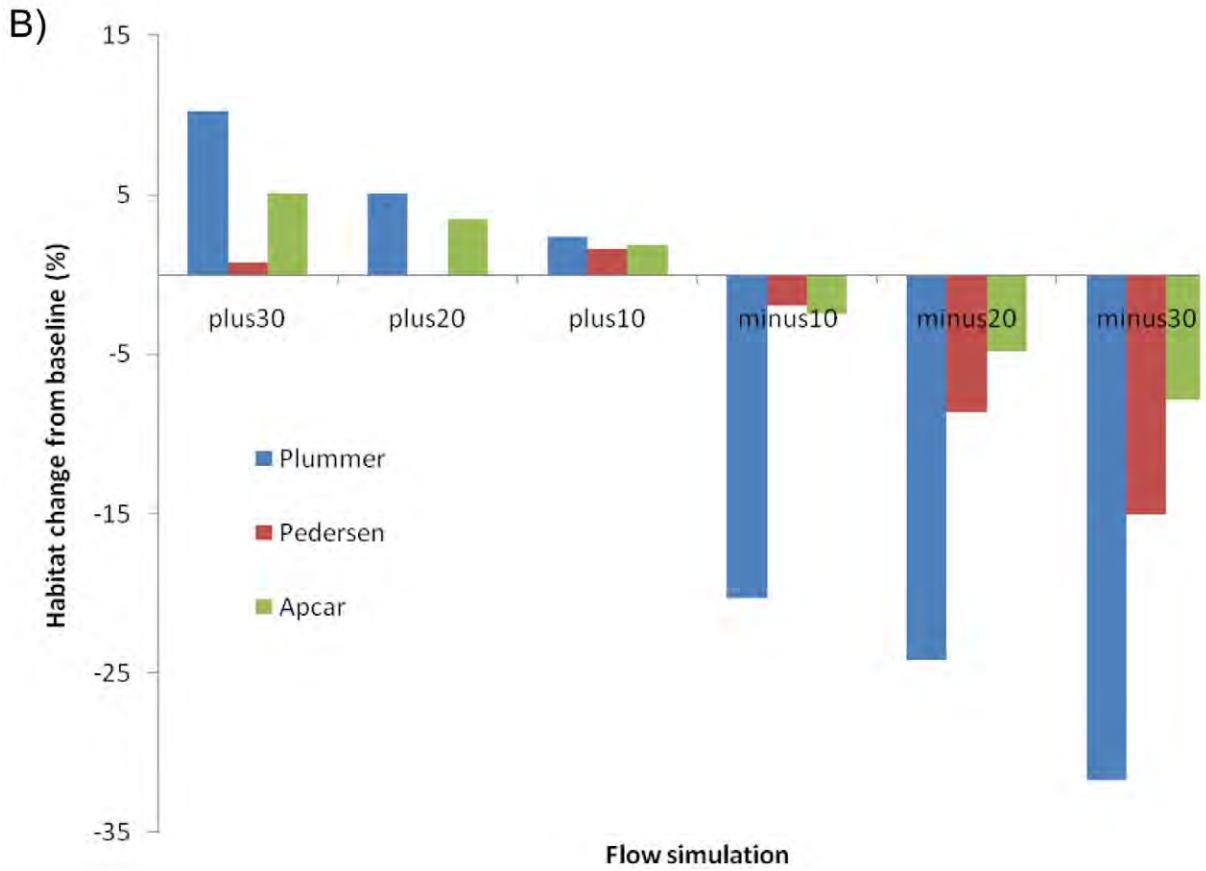

Figure 5. Habitat-discharge relations among Plummer, Pedersen, and Apcar creeks, in 10% flow increments. In panel A, the amount of predicted habitat by flow is presented after standardizing the data by stream length. In panel B, the relative change in habitat in relation to baseflow was calculated in 10% flow increments.
doi:10.1371/journal.pone.0055551.g005

enhancement activity. In addition, changes in habitat quantity or quality could be assessed by calculating habitat prior to and after a restoration or enhancement activity, calculating the mean probability for a given reach, or habitat quantity through application of a probability threshold (30% for our models). It is also possible to use the habitat models to simulate the benefits of a given restoration or enhancement activity before committing the funds for on-the-ground efforts to implement the proposal. Simulating an enhancement activity would involve modifying the bathymetry, rerunning the 2D hydraulic model, and recomputing habitat. One could compare multiple scenarios when determining the most optimum use of resources for the restoration or enhancement of dace habitat. The final evaluation criterion for any project should be the number of dace observed prior to and following a restoration or enhancement activity, with the models providing guidance on the achievement and monitoring of dace habitat over space and time.

Conclusion

This study indicates that a reduction in spring discharge within Moapa Valley National Wildlife Refuge will cause a reduction in important refugial habitat for Moapa dace, and may exacerbate native-nonnative interactions [53,54]. The Muddy River's carbonate aquifer is being closely monitored to prevent breaching its sustainability (personal communication, Lee Simons, U.S. Fish and Wildlife Service, Las Vegas, Nevada). However, there are concerns that pumping from the aquifer may cause an unintended overdraft and a reduction in spring discharge [21]. Another looming threat to sustaining the Muddy River's carbonate aquifer is global climate change. The southwest is expected to get warmer and drier in the next century, with spring and summer streamflows predicted to be significantly reduced [5,6]. While it is unknown how climate change will affect the groundwater in the vicinity of the Refuge, it will probably decrease as the climate warms and dries. Our model provides important information to managers charged with protecting and recovery of Moapa dace in an era of potential reduction in thermal spring discharge feeding the Muddy River.

The focus of this study was Moapa dace, but our results have implications for seven other aquatic species listed as sensitive in the Muddy River ecosystem [11]. Each species has its own specific habitat requirements, by life stage, but they all share the Muddy River ecosystem and a threat to one species is a concern for all. We have shown that reduced flows on the Refuge will threaten Moapa dace habitat, while increased flows would provide benefits. Until we know more about the habitat preferences of all aquatic species in the Muddy River ecosystem, a water conservation strategy that minimizes any net loss in habitat is desirable.

Supporting Information

File S1 Background information on substrate and bathymetric surveys.
(DOC)

File S2 Detailed boundary conditions for River2D hydraulic simulations.
(DOC)

File S3 2D hydrodynamic model calibration and verification charts for each springbrook.
(DOC)

File S4 2D hydrodynamic model output and habitat maps for each springbrook.
(DOC)

Video S1 A typical sandy-bottom plunge-pool habitat selected by Moapa dace. Identified by their fusiform body and deeply forked tail with black spot at its base, Moapa dace are actively working the water column for drift items. Also in the video are Moapa White River springfish identified by their square tail. Both species are thermal endemic, typically occurring in water temperatures from 26 to 32°C and are restricted to the headwaters of the Muddy River, Clark County, Nevada where the river originates from a series of thermal springs. Video provided by Pete Rissler (U.S. Geological Survey).
(MP4)

Acknowledgments

We thank staff from the U.S. Geological Survey Columbia River Research Laboratory (Adam St Saviour, Anita Lahey) and Reno Field Station (Antonio Salgado, Peter Rissler, Danielle Johnson, and Mark Hereford) for providing assistance in the collection of field data in the Moapa Valley National Wildlife Refuge; Amy LaVoie, Lee Simons, Allison Manwaring, Cynthia Martinez, Janet Bair, and Amy Sprunger, U.S. Fish and Wildlife Service, for scientific, administrative, and moral support; Robert Johnson, David Syzdek, and Cailin Doyle, Southern Nevada Water Authority (provided field assistance, LiDAR and photography). We also thank three anonymous reviewers, and Alec Maule (USGS), for providing useful comments that greatly improved this paper. Any use of trade, firm, or product names is for descriptive purposes only and does not imply endorsement of the U.S. Government.

Author Contributions

Performed snorkel and habitat surveys: GGS CJD. Conceived and designed the experiments: JRH. Performed the experiments: JRH TRB. Analyzed the data: JRH TRB GGS CJD. Wrote the paper: JRH GGS TRB.

References

1. Omernik JM (1987) Ecoregions of the conterminous United States. Annals of the Association of American Geographers 77, 118–125.
2. Stoddard JL, Peck DV, Paulsen SG, Van Sickle J, Hawkins CP, et al. (2005) An Ecological Assessment of Western Streams and Rivers. EPA 620/R-05/005, U.S. Environmental Protection Agency, Washington, DC. Available: http://www.epa.gov/emap/west/html/docs/wstriv.html. Accessed 2012 Nov 24.
3. Stonestrom DA, Harrill JR (2007) Ground-water recharge in the arid and semiarid southwestern United States-climatic and geologic framework. U.S. Geological Survey Professional Paper 1703-A, 27 p. Available: http://pubs.usgs.gov/pp/pp1703/a/pp1703a.pdf. Accessed 2012 Nov 24.
4. Minckley WL, Deacon JE (1991) Battle against extinction: native fish management in the American West. Tucson: University of Arizona Press. 517 p.
5. Seager R, Ting MF, Held I, Kushnir Y, Lu J, et al. (2007) Model projections of an imminent transition to a more arid climate in southwestern North America. Science 316: 1181–1184.
6. Subhrendu G, Pruitt T (2011) West-Wide Climate Risk Assessments: Bias-Corrected and Spatially Downscaled Surface Water Projections. Technical Memorandum No. 86-68210-2011-01. U.S. Department of the Interior, Bureau of Reclamation, Technical Service Center, Denver, Colorado. Available: http://www.usbr.gov/WaterSMART/docs/west-wide-climate-risk-assessments.pdf. Accessed 2012 Jul 6.

7. U.S. Department of the Interior (1973) Threatened wildlife of the United States. U.S. Bureau of Sport Fisheries and Wildlife Resources Publication 114.
8. Hubbs CL, Miller RR (1948) Two new relict genera of cyprinid fishes from Nevada. Occas pap Mus Zool. Univ. Mich 507: 1–30.
9. Eakin TE (1966) A regional interbasin groundwater system in the White River Area, southeastern Nevada. Water Resour Res 2: 251–271.
10. Garside LJ, Schilling JH (1979) Thermal waters of Nevada. Nevada Bureau of Mines and Geology. Bulletin 91. Reno: Mackay School of Mines and Geology, University of Nevada. 163 p.
11. U.S. Fish and Wildlife Service (1995) Recovery plan for the rare aquatic species of the Muddy River ecosystem. Portland, Oregon. 60 pp. Available: http://water.nv.gov/hearings/past/dry/browseable/exhibits%5CUSFWS/Exhibit%20601%20recovery%20plan%20for%20aquatic%20spp%20MRS.pdf. Accessed 2012 Jul 6.
12. Scoppettone GG, Burge HL, Tuttle PL (1992) Life history, abundance, and distribution of Moapa dace (*Moapa coriacea*). Great Basin Nat 52: 216–225.
13. Deacon JE, Bradley WG (1972) Ecological distribution of fishes of Moapa (Muddy) River in Clark County, Nevada. Trans Am Fish Soc 101: 408–419.
14. Scoppettone GG (1993) Interactions between native and nonnative fishes of the upper Muddy River, Nevada. Trans Am Fish Soc 122: 599–608.
15. Scoppettone GG, Rissler PH, Nielsen MB, Harvey JE (1998) The status of *Moapa coriacea* and *Gila seminude* and status information on other fishes of the Muddy River, Clark County, Nevada. Southwest Nat 43: 115–122.
16. Scoppettone GG, Salgado JA, Nielsen MB (2005) Blue tilapia (*Oreochromis aureus*) predation on fishes in the Muddy River system, Clark County, Nevada. West N Am Nat 65: 410–414.
17. Groom MJ, Meffe GK, Carroll CR (2006) Principles of Conservation Biology, 3rd Edition. Sunderland: Sinauer Associates 793 p.
18. Fahrig L (2002) Effect of habitat fragmentation on the extinction threshold: a synthesis. Ecol Appl 12: 346–353.
19. Stearns SC (1992) The evolution of life histories. New York: Oxford University Press. 249 p.
20. Galati L (2011) Warm Springs Natural Area Stewardship Plan. Southern Nevada Water Authority, Las Vegas, NV. Available: http://www.snwa.com/env/wsna_stewardship.html. Accessed 2012 Jul 2.
21. Mayer TD, Congdon RD (2008) Evaluating climate variability and pumping effects in statistical analyses. Ground Water 46: 212–227.
22. Ghanem AH, Steffler PM, Hicks FE, Katopodis C (1996) Two dimensional finite element flow modeling of physical fish habitat. Regul River 12: 185–200.
23. Steffler P, Blackburn J (2002) River2D. Two-Dimensional Depth Averaged Model of River Hydrodynamics and Fish Habitat. Introduction to Depth Averaged Modeling and User's Manual. University of Alberta. September, 2002. 119 pp. Available: http://www.river2d.ualberta.ca/Downloads/documentation/River2D.pdf. Accessed 2012 Jul 6.
24. Ghanem AH, Steffler PM, Hicks FE, Katopodis C (1995) Dry area treatment for two dimensional finite element shallow flow modeling. Proceedings of the 12th Canadian Hydrotechnical Conference, Ottawa, Ontario.
25. Waddle T, Steffler PM, Ghanem A, Katopodis C, Locke A (1996) Comparison of one and two dimensional hydrodynamic models for a small habitat stream. Ecohydraulics 2000 Conference, Quebec City, June. 10 p.
26. Hatten JR, Batt TR (2010) Hydraulic alterations resulting from hydropower development in the Bonneville Reach of the Columbia River. Northwest Sci 84: 207–222.
27. Lane SN, Mould DC, Carbonneau PE, Hardy RJ, Bergeron NE (2006) Fuzzy modelling of habitat suitability using 2D and 3D hydrodynamic models : biological challenges., in River Flow 2006 : International Conference on Fluvial Hydraulics, Lisbon, Portugal, 6–8 September 2006; proceedings. London: Taylor & Francis, 2043–2054.
28. Jowett IG, Richardson J, Biggs BJF, Hickey CW, Quinn JM (1991) Microhabitat preferences of benthic invertebrates and the development of generalized *Deleatidium* spp. habitat suitability curves, applied to four New Zealand rivers. New Zeal J Mar Fresh 25: 187–199.
29. Jowett IG (1993) A method for objectively identifying pool, run, and riffle habitats from physical measurements. New Zeal J Mar Fresh 27: 241–248.
30. Tiffan KF, Garland RD, Rondorf DW (2002) Quantifying flow-dependent changes in subyearling fall chinook salmon rearing habitat using two-dimensional spatially explicit modeling. N Am J Fish Manage 22: 713–726.
31. Hatten JR, Tiffan KF, Anglin DR, Haeseker SL, Skalicky JJ, et al. (2009) A spatial model to assess the effects of hydropower operations on Columbia River fall Chinook salmon spawning habitat. N Am J Fish Manage 29: 1379–1405.
32. Lobb MD III, Orth DJ (1991) Habitat use by an assemblage of fish in a warmwater stream. Trans. Am. Fish. Soc. 120: 65–78.
33. Environmental Systems Research Institute (ESRI) (1992) Cell-based Modeling with GRID, 2nd ed. Redlands: ESRI. 267 p.
34. Hosmer DW, Lemeshow S (2000) Applied logistic regression. New York: John Wiley & Sons. 373 p.
35. Keating KA, Cherry S (2004) Use and interpretation of logistic regression in habitat selection studies. J Wildl. Manage 68: 774–789.
36. Kvamme L (1985) Determining empirical relationships between the natural environment and prehistoric site locations: a hunter-gatherer example. Pages 208–238 *in* C. Carr, editor. For concordance in archaeological analysis. Westport Publishers, Kansas City, Kansas, USA.
37. Hatten JR, Paradzick CE (2003) A multiscaled model of Southwestern Willow Flycatcher breeding habitat. J. Wildl. Manage. 67: 774–788.
38. Burnham KP, Anderson DR (2002) Model selection and multimodel inference: a practical information theoretic approach, 2nd edition. New York: Springer. 488 p.
39. Box GEP, Tidwell PW (1962) Transformation of the independent variables. Technometrics 4: 531–550.
40. Nagelkerke NJD (1991) A note on general definition of the coefficient of determination. Biometrika 78: 691–692.
41. Story M, Congalton RG (1986) Accuracy assessment: a user's perspective. Photogramm Eng Remote Sens. 52: 397–399.
42. Egan JP (1975) Signal detection theory and ROC analysis. New York: Academic Press. 277 p.
43. Waddle T (2010) Field evaluation of a two-dimensional hydrodynamic model near boulders for habitat calculation. River Res Appl 26: 730–741.
44. Williams BK, Nichols JD, Conroy MJ (2002) Analysis and management of animal populations. San Diego: Academic Press. 817p.
45. Ricker WE (1979) Growth rates and models. Pages 677–743 *in* W.S. Hoar, D. J. Randall, and J.R. Brett, editors. Fish Physiology; Bioenergetics and Growth. VIII. Academic Press, New York, San Francisco, London.
46. Glencross BD, Felsing M (2006) Influence of fish size and water temperature on the metabolic demand by barranmundi, *Lates calcarifer* (Bloch), in freshwater. Aquac Res 37: 1055–1062.
47. Hauer FR, Hill WR (2006) Temperature, light and oxygen. Pages 103–119 in Hauer FR and Lamberti GA, editors, Methods in stream ecology. Amsterdam, Boston, Heidelberg, London: Academic Press. 877 p.
48. Grossman G D, Rincon PA, Farr MD, Ratazcjczak RE (2002) A new optimal foraging model predicts habit use by drift-feeding stream minnows. Ecol Freshw Fish 11: 2–10.
49. MacKenzie DI, Nichols JD, Royle JA, Pollock KH, Bailey LL, et al. (2006) Occupancy estimation and modeling: Inferring patterns and dynamics of species occurrence. San Diego: Academic Press. 344 p.
50. Guthric CG, Moorhead DL (2002) Density-dependent habitat selection: evaluating isoleg theory with a Lotka-Volterra model. Oikos 97: 184–194.
51. Lindberg WJ, Frazer TK, Portier KM, Vose F, Loftin J, et al. (2006) Density-dependent habitat selection and performance by a large mobile reef fish. Ecol Appl 16: 731–746.
52. Hauer FR, Lamberti GA (2006) Methods in stream ecology. Amsterdam, Boston, Heidelberg, London: Academic Press. 877 p.
53. Scoppettone GG, Rissler PH, Gourley C, Martinez C (2005) Habitat restoration as a means of controlling non-native fish in a Mojave Desert Oasis. Restor Ecol 13: 247–256.
54. Lamouroux N, Cattaneo F (2006) Fish assemblages and stream hydraulics: consistent relations across spatial scales and regions. River Res Appl 22: 727–737.

Hilderbrand, R. H., A. C. Watts, and A. M. Randle 2005. The myths of restoration ecology. *Ecology and Society* **10**(1): 19. [online] URL: http://www.ecologyandsociety.org/vol10/iss1/art19/

Perspective

The Myths of Restoration Ecology

Robert H. Hilderbrand[1], *Adam C. Watts*[2], *and April M. Randle*[3]

Key Words: *carbon copy; command and control; cookbook; ecological restoration; fast forward; field of dreams; myths; resilience; restoration ecology; Sisyphus complex*

INTRODUCTION

Humanity's ever-increasing ability to effect environmental change on a number of spatial and temporal scales requires tough decisions about how we view, value, and manage ecosystems. For example, advances in agriculture that support vastly more people per unit area than hunting and gathering are clearly a positive outcome for society. However, many beneficial land-use practices, including agriculture, may ultimately degrade ecosystems. To function as a society, some amount of ecosystem alteration must occur to support the human population, but we are ultimately dependent on ecosystem services. Our actions both intentionally and unwittingly alter the goods and services of many ecosystems on which we rely, and by entering into this relationship of altering ecosystems, we incur responsibility to our neighbors and to future generations. However, the difficult decisions have largely been avoided by the expectations and confidence in conservation and, in particular, ecological restoration.

Given the widespread alteration of natural systems, it is clear that conservation measures alone will not suffice to protect ecosystem functions, services, and habitat for a large number of species in the future. Conservation has traditionally been a rearguard measure to prevent further degradation rather than a means for increasing resources or natural capital. As such, simple maintenance as opposed to enhancement of ecosystems may often leave ecosystems and species vulnerable. Despite conservation policies such as roadless areas and the "No Net Loss" concept for U.S. wetlands, losses continue to exceed gains (Dahl and Allord 1996), and gains are often not functionally equivalent to losses (Zedler 2000a, National Research Council 2001). Increasing human population growth and resource consumption continue to place additional stresses on systems and demands *more* capacity and services, rather than simple maintenance of current services. Thus, we must either alter consumption or rely on our ability to create, restore, and enhance ecosystems and their services.

Despite our dependence on healthy ecosystems, society has made the decision to continue life as usual until a loss of valued goods and services is realized; then, society will expect and rely on science to clean up the mess *and* make it look natural. Many government policies concerning development and extractive resource use already assume the ability to mitigate ecosystem damage through the restoration of degraded land or creation of new habitats. However, many restorations are not successful either in structure (Lockwood and Pimm 1999) or function (Kentula 1996, Zedler and Callaway 1999) when compared with reference ecosystems. Such results underscore the need to evaluate our underlying beliefs and expectations in restoration.

The incredible complexity of nature forces us to simplify the systems we study in order to develop theory and generalities by reducing them to understandable subsets. Although we cannot function without theory and conceptual models, their creation often ignores the variability that is so important to accurately describe, predict, and re-create current and future system attributes. In essence, restoration ecology strives to (re-)create complex systems from simplified guiding principles

[1]University of Maryland Center for Environmental Science Appalachian Laboratory, [2]University of Florida, [3]University of Pittsburgh

or myths. Failure to recognize the limitations and tacit assumptions can lead to failures because of the over-application of over-simplified concepts to complex systems (Holling 1995, Holling and Meffe 1996). We believe the same is true in ecological restoration.

We believe that many unsatisfactory restorations result from a failure to recognize and address uncertainty, and from a focus on inappropriate time scales. Ecological restoration is trying to do in a matter of years what takes decades or centuries under natural conditions. Expecting complete restoration on human time scales is unreasonable, even where full recovery may eventually occur. Nonetheless, many of our underlying beliefs tacitly assume that systems will return to a "natural" state in fairly short order if they are just nudged in the right direction through adjustments to physical attributes or by regulating species composition. Additional problems arise in defining what is "natural" and in our inability to accept that systems are dynamic and may have multiple trajectories leading to numerous possible outcomes. Finally, because we are extrapolating from oversimplified concepts, ignoring uncertainty may result in surprise and failure because we have not created a system capable of adapting or responding to future drivers or events. Therefore, restorations should not be one-time events, but are likely to require periodic attention and adaptive management to increase the chances of responsive, adaptive, and successful projects.

Based on our experiences as researchers and practitioners in conservation and restoration ecology, we propose five central myths (Table 1) under which many ecological restoration and management projects seem to be conceived and implemented. Myths have value because they help us to organize and understand complex systems and phenomena. Identifying myths can help make the tacit explicit by revealing assumptions that are otherwise hidden (Holling 1982). However, they remain simplified and potentially misguided models for understanding and application (Holling 1982, Timmerman 1986). The first Myth, the Carbon Copy, addresses the goal-setting process, and as such, it forms the basis of how restorations are evaluated. The Carbon Copy is closely tied to the remaining four myths, which involve the process of restoration and management: the Field of Dreams; Fast Forwarding; the Cookbook; and Command and Control: the Sisyphus Complex. We believe that describing these myths will be useful in understanding how some management or restoration strategies are conceived, designed, and implemented. For example, adherence to different myths may direct actions in divergent directions, as could be the case when choosing between a focus on ecosystem structure (Carbon Copy) or on key processes (Field of Dreams). Examining these myths may also help us better understand why some restoration projects do not meet our expectations. In the pages below, we briefly describe each myth and its assumptions, and give examples where the myth exists.

Our objective is not to abandon what we propose to be prevalent myths in ecological restoration—there are elements of truth in each—but to recognize that there are tacit assumptions associated with each myth. Failure to recognize these assumptions can lead to conflict and disappointing results despite large expenditures of time and effort. Our challenge is to recognize the limitations and not accept sometimes dogmatic beliefs without critical examination. We do not claim that every project is rooted in myth, but suggest that many perceived failures may be traced to over-reliance on one or more of the myths. We do not condemn restoration ecology, but rather provide a means of self-examination so readers can identify from their own experiences what worked and possible reasons for perceived failures.

THE MYTH OF THE CARBON COPY

The myth of the Carbon Copy relates to the selection of restoration goals and end points, and maintains that we can restore or create an ecosystem that is a copy of a previous or ideal state. The myth is rooted in the Clementsian (1936) idea that ecosystems develop in a predictable fashion toward a specified, static, end point or climax. Accordingly, any disturbance or degrading activity will reset the system, resulting in a phase of rebuilding and a return to the previous trajectory of ecosystem development. However, restoration sites are different from those where secondary succession occurs after disturbance (Zedler 2000*b*), and restoring or creating an ecosystem of specific composition becomes quite difficult. Most successes appear to be only transitory (Lockwood and Pimm 1999). Despite the shortcomings, the myth of a carbon copy persists in ecological

Table 1. The myths of restoration and their core issues

Restoration Myth	Core Issues
Carbon Copy	Community assembly predictable; a single endpoint exists
Field of Dreams	Sole focus on physico-chemical conditions; systems self-organize
Fast Forward	Succession and ecosystem development can be accelerated
Cookbook	Methodology overused and not sufficiently validated
Command and Control: Sisyphus Complex	Nature is controllable; Treating symptoms will fix the problem

restoration. The main reason is that the underpinnings of restoration ecology involve ecological succession and assembly rules (Young 2000), which tend to reinforce subconsciously the concept of a static, climax end point. Indeed, van der Valk (1998) described restoration as accelerated succession. Ecology is rich with examples of succession (Glenn-Lewin et al. 1992), and there is little doubt of its importance in community and ecosystem development (Odum 1969), or potential in restoration (e.g., van der Valk 1998). The main issue is the extent to which succession is equilibrial and can be predicted or controlled to arrive at a predefined state under human time scales. Most landscapes are a mosaic of different vegetation types that shift through both space and time (Bormann and Likens 1979, Pickett and White 1985), and identifying a single state as the only end point is not realistic for most systems.

The myth of the Carbon Copy has influenced resource agencies, such as the U.S. National Park Service, that have mandates to restore and manage some systems to pre-settlement conditions. At its extreme, the Carbon Copy emphasizes a natural or primeval state that existed before European settlement, and becomes the restoration or management objective. As the natural state existed before corruption by modern influences or before a need for restoration, its return is the objective. Although the purpose of restoration and management outside of legislative mandates should guide the goals and end points, a de facto end point is all too often what the system was like in an undisturbed state.

Restoration to a pre-disturbance state may be desirable when concerns are for the "naturalness" of the system, but many difficulties exist during implementation. Few would debate that a pre-disturbance state is, in most cases, preferable to a degraded one, but the ability to (re-)create a system resembling pre-disturbance may be difficult, if not impossible. Given the sheer number of non-native species that have invaded and been integrated into virtually every ecosystem, it is arguably impossible to achieve a pre-settlement target condition. Even if such a goal could be achieved, selection of the appropriate target remains in question—do we restore for the ecosystem of 1500 AD, 500 AD, or 1000 BC? Another difficulty arises when the underlying parameters and drivers have changed (e. g., Ehrenfeld 2000) or the system is too degraded to achieve pre-disturbance conditions (Hobbs and Norton 1996). Changes such as a rise in sea level, atmospheric acid deposition, and altered hydrology because of urbanization, dams, and water withdrawals may all substantially alter both structure and function as a result of changes in salinity, soil and water chemistry, and hydrography and geomorphology, respectively. Thus, we may aim at a target that is not only moving, but also at a target that is no longer attainable at a specific locale.

Tension and conflict arise when the Carbon Copy is an unrealistic or inappropriate goal. Pre-disturbance or "pristine" conditions are often in conflict with stakeholder wishes, particularly in more urbanized situations (Shore 1997). Even setting goals that recognize multiple end points can be politically and socially problematic when various stakeholders each desire a different and conflicting

result. In these cases, a pre-disturbance condition may not represent the best solution, when the objective is to maximize an ecosystem service, function, or aesthetic. Rather than focus on restoring to some primeval state, a more profitable approach would be to accept that ecosystems are dynamic and focus on repairing damaged systems to the extent possible (Hobbs and Harris 2001).

The Carbon Copy myth prevails in extractive resource industries, such as forestry and mining, and its foundations are used as arguments to justify access to resources in undisturbed environments—the belief being that these systems will return to their previous state after disturbance. Although few ecologists pretend that the more destructive forms of mining can be fully restored, the belief in this ability is promoted by those backing the extraction industries. Despite limited success, the Carbon Copy myth has resurged in the USA in the form of the "No Net Loss" paradigm of wetland protection policy and mitigation (Zedler 1996), which assumes that created or restored wetlands provide equivalent ecological services, function, and value as those destroyed. Although success stories exist, many now consider the assumptions invalid because few created or restored wetlands have achieved structure or function equivalent to existing wetlands (Zedler and Callaway 1999, National Research Council 2001, Seabloom and van der Valk 2003), and natural wetlands continue to disappear without equivalent replacement (Whigham 1999).

An alternative to creating a carbon copy of species complement is to create a system equivalent in function to the pre-disturbance state. Restored systems can be functionally superior to pre-disturbance systems, as in the case of wetlands engineered for nutrient removal (e.g., Peterson 1998). The growing field of ecological engineering is rich with examples of such enhanced systems (Ansola et al. 1995, Kadlec and Knight 1996, Knowlton et al. 2002, Kangas 2003), and will become ever more important to society as we continue to degrade natural systems. Functional replacement could be more easily accomplished than replacement of taxonomic composition because of the shared ecological function of many species (Stanturf et al. 2001). The danger in this approach is that some functions may be enhanced yet more subtle functions (e.g., species' habitats) or indirect interactions (e.g., heightened predation due to habitat differences) may suffer. Questions that remain include the resilience of functional replacements to disturbances and their acceptability to society. The heightened public awareness of invasive species modifying ecosystems and the potentially foreign look of a functional replacement may be socially unpalatable.

THE MYTH OF THE FIELD OF DREAMS

The Field of Dreams stems from the notion that all one needs is the physical structure for a particular ecosystem, and biotic composition and function will self-assemble—if you build it, they will come. Similarly, restoration of a process, such as fire or hydrologic regime, is expected to re-create pre-disturbance structure. Although re-creating the physical template and drivers are a necessary first step, it is rarely a final step and sometimes a misstep (e.g., Smith 1997). A fundamental assumption of this myth is that the community and ecosystem assembly process follow a repeatable trajectory, and uncertainty is implicitly ignored. Although there are some encouraging generalizations emerging about community assembly (Christensen and Peet 1984, Drake 1990, Keddy 1999), community assembly is in many ways reminiscent of Rudyard Kipling's (1902) *Just So Stories*: communities are historically contingent products (Parker 1997), and much uncertainty still exists given the influences of initial conditions (Grace 1987) and stochastic or neutral assembly (Hubbell 2001). Failure to accept uncertainty and the dynamic nature of community assembly can lead to the traps of the Carbon Copy myth.

The Field of Dreams approach is common in both wetland and stream restoration, where emphasis is often on re-creating physical attributes with little attention paid to biotic responses. For example, the Rosgen approach (Rosgen 1994, 1998) is probably the most widely used stream restoration method in North America, but it deals almost exclusively with geomorphic attributes of stream channels. Restoration goals in systems such as urban watersheds often involve preventing streambed erosion and destruction of buried utilities, such as sewer and water lines. Although stabilization of the stream channel is quite important, stopping at a geomorphic end point is similar to ensuring that mining excavations in terrestrial landscapes are filled after a job is completed, and then not proceeding with revegetation. Similar examples exist for wetland restorations (van der Valk 1998), where the concept of self-design (Mitsch and

Wilson 1996, Mitsch et al. 1998) is embraced after the hydrologic conditions are restored. Restoration sites do become revegetated, but may be of different species composition and degree of cover (Seabloom and van der Valk 2003), owing to dispersal limitations of many wetland species (Galatowitsch and van der Valk 1996). Thus, the effectiveness of self-design depends on the restoration goals, but adopting a concept of self-design does implicitly recognize and embrace the existence of multiple end points.

An effective restoration of the physical variables will create the template for biotic recovery, but physical structure does not always beget biotic structure, and biotic structure does not necessarily result in similar ecosystem functions across sites. The concept of self-organization, or self-design, is an intuitively appealing approach and is very attractive to resource managers who have limited time and budgets. A self-assembling ecosystem would substantially cut down on the amount of effort required to restore ecosystems, and we feel this is why the Field of Dreams is commonly employed. However, its effectiveness in restoring structure and function is still debatable (Simenstad and Thom 1996, Zedler and Callaway 1999, National Research Council 2001), and restored areas may be quite different from undisturbed sites (Seabloom and van der Valk 2003). In defense of self-assembly, composition of restored sites is expected to approach reference sites given sufficient time (Mitsch 1997). Effective restoration using this approach must overcome issues of recolonization and dispersal, stochasticity in community assembly, and assembly of energy transfer pathways. One commonly used strategy to circumvent these limitations is to jumpstart the process by adding organisms, but our understanding of accelerating ecosystem development is incomplete and may lead to the myth of Fast-Forwarding.

THE MYTH OF FAST-FORWARDING

The myth of Fast-Forwarding is based on the idea that one can accelerate ecosystem development by controlling pathways, such as dispersal, colonization, and community assembly, to reduce the time required to create a functional or desired ecosystem. This idea stems from the initial floristics model of succession (Egler 1954) in which the process of ecosystem development is accelerated by controlling initial species composition and succession to achieve the desired end point (van der Valk 1998). The major assumption is that we can reliably recreate key processes and links between the biota and physical environment. A driving force behind this approach is the need to demonstrate rapid recovery of disturbed lands in order, for example, to have insurance or mitigation performance bonds returned quickly.

Many types of restoration projects justifiably use a fast-forwarding approach to jumpstart the recovery process by using species desired in the ecosystem. As most restorations include plantings to get the ball rolling and stabilize the terrain, it is logical to try to advance the successional process, and this is why the practice is so common. However, relying on the premise that fast-forwarding will produce the desired ecosystem trajectory and speed the recovery process may result in disappointment. Little evidence exists for achieving desired trajectories or functions within the shortened time spans promised by fast-forwarding (Simenstad and Thom 1996, Zedler and Callaway 1999, Campbell et al. 2002, Wilkins et al. 2003). As with other myths, there is some element of truth, and successes using fast-forwarding have occurred (e.g., Clewell 1999). Successful projects typically require multiple plantings and a considerable amount of attention to ensure survival of plantings in systems that may be "premature" for the species' arrival. Even when successful, certain ecological processes, such as the development of tree hollows for cavity-nesting animals, soil development, mycorrhyzal associations, and hydrologic regimes, present more difficult challenges and may take years or decades. Mitsch and Wilson (1996), for example, point out that the 5-year span in which "'quick-fix' wetlands" are expected to become sufficient replacements for lost or damaged areas is improbably short, and that 15–20 years is a much more realistic expectation. Long-term monitoring (5–15 years) of restoration projects is indicating that a more likely time horizon is several decades for a restoration to resemble a pre-disturbance target (Zedler and Callaway 1999, Wilkins et al. 2003). Many ecological restoration projects—even ecological restoration itself—aim for rapid progress from a damaged state toward some more-or-less specific target. There is nothing inherently wrong with such a goal, however, we should not be so intent on attaining a specific point that the system's potential future state (i.e., after restoration efforts cease and natural processes take over) is ignored.

THE MYTH OF THE COOKBOOK

When a particular restoration experience is successful in one area or ecosystem, we naturally want to apply the same techniques in other restoration efforts; after all, science has little relevance if the results are not repeatable. We refer to the over-use or continued use of a locally unsuccessful restoration prescription because it worked somewhere else, or is in the published literature, as the myth of the Cookbook. Perpetrators of this myth assume that similar physical and ecological systems respond identically and predictably to restoration techniques. Although a reasonable starting point, systems that appear very similar may exhibit considerable differences in variables that regulate slow processes (e.g., carbon storage), and the same management prescription applied to two such systems may have vastly different results. The difficulty arises when approaches are adopted that ignore uncertainty. A non-adaptive technique forces us down a path with few alternatives to a changing world.

The myth of the cookbook arises often in stream restoration, and possibly wetland restoration and creation, where recipes for restoration exist (Rosgen 1998). Cookbook approaches seem to be most often present in engineering approaches to restorations. We are not denouncing the goal of standard methods, but we believe that there is still too much uncertainty to commit totally to one technique in a given situation. Even in chemistry, where well developed standard methods exist, a good yield from a single reaction may be 90% and a complex set of reactions may yield less than 50%, meaning that half the reactions did not go as they should. Given the complexity of many restorations, the practice is fairly successful relative to the chemistry analogy. However, incomplete chemical reactions can be precipitated, discarded, or otherwise dealt with quickly and inexpensively, but we do not have the luxury to treat degraded systems similarly, nor can we accept such a failure rate given the high financial cost. The positive side is that systems are rarely in worse condition after a restoration even if the project did not meet the stated goals.

To resource professionals plagued by a lack of information, time, and budget, cookbook approaches may be the only realistic approach. The opportunity to use a successful restoration effort as a template for a similar system is a start, and may be preferable to inaction. It may also be advisable to replicate certain elements of proven restoration techniques, because some valid generalities may be made concerning the responses of a wide range of ecosystems to the same actions (Zedler 2000*a*). However, idiosyncrasies of each system (unique ecological histories, differing assembly rules, or even differing functional roles of components of two similar ecosystems) may result in elements of surprise and crisis when a uniform, cookbook approach is used without detailed knowledge of the ecological characteristics of the ecosystem to be restored. As the community or ecosystem to be restored becomes less and less similar to the system in which a given restoration approach was successful, the potential for unforeseen responses and failure increases dramatically.

By defining the myth of the Cookbook, we do not advocate reinventing the wheel with every new project. One of the major goals of restoration ecology is to develop a suite of methods that can be used in a given situation to best effect. We believe this desire or belief in repeatable methods is why the cookbook remains. Problems arise when a method is over used or used in the wrong situation just because the method exists and is understood. A number of approaches (e.g., Kershner 1997, Clewell et al. 2000, Richter et al. 2003) provide general guidance, but allow for site-specific adjustments to deal with uncertainty. A more cautious approach, acknowledging our inability to predict the exact response of an ecosystem to manipulation, would be the application of a varied management or restoration regime across a landscape. Techniques aimed at discovering and mimicking the character of natural systems would be more likely to find successful solutions (Mitsch and Wilson 1996), while likely contributing to the resilience of the system (Holling et al. 2002).

THE MYTH OF COMMAND AND CONTROL AND THE SISYPHUS COMPLEX

The myth of Command and Control (Holling and Meffe 1996) describes the “pathology of natural resources management” where goals are achieved by active intervention and unending control, or manipulation of physical and biological components of the ecosystem. This myth, articulated by Holling and Meffe (1996), assumes we have the knowledge, abilities, and foresight to actively control ecosystem structure and function to manage for a particular ecosystem state indefinitely into the future. Exerting

command and control invariably decreases system resilience by reducing the range of natural variation and adaptive capacity for the system to respond to disturbances (Gunderson 2000). As resilience decreases, the likelihood of a disturbance shifting the system into an undesired or degraded state increases, and control is wrested from the manager.

Practice of Command and Control recalls the story of Sisyphus, one of the most unenviable characters in Greek mythology because he is compelled by the Gods to forever push a heavy boulder uphill. Just as he nears the top, Sisyphus becomes exhausted, and the boulder rolls back down to the plain below, where Sisyphus must begin again. Like Sisyphus, we can become trapped in an endless cycle of effort to compel ecosystems to remain in single, transient, or unstable states, resulting in repeated episodes of surprise and crisis that can mimic the ball-in-cup analogy of system dynamics (Lewontin 1969, Holling 1973, Beisner et al. 2003), with the ball rolling around the cup and away from the manager's desired state. The Sisyphus Complex emerges when we act through Command and Control to hold a dynamic system static or force a system to exist in a transient state. In any restoration, some amount of Command and Control is required to perform the restoration. Additional nudges to physical or biological components will likely occur in the years after the restoration as well. There is nothing wrong with some tinkering—we cannot exist without having some effect on our surroundings. Actions to be avoided are those that are long term in nature or will decrease the natural range of variability in key processes, such as fire regime or hydrology.

The Sisyphus Complex often occurs when the dominant, large-scale drivers of the system have changed and are either not noticed or conveniently ignored. When we fall into the Sisyphus Complex, we become fixated on treating symptoms rather than the root of the problem and so become susceptible to failure. Urban stream restorations often occur in response to severely eroded stream channels, and a more flashy hydrograph that results from increases in impervious surface area higher in the watershed. Many such restorations fail (sometimes multiple times) despite tremendous expense and effort, because the altered driver (the hydrograph) and the root cause (impervious surfaces) were not addressed. Other general examples include coastal beach restoration in the face of ongoing, natural erosion; rare species stocking/reintroduction programs that ignore the root causes of rarity; and attempting to direct succession to end points incompatible with environmental conditions. Sometimes the Sisyphus Complex results from social or political mandates to do something despite credible science to the contrary. In these situations, we must make every effort for science to influence decision making so that the inevitable repeated failures are not perceived as employment justification or incompetence on the part of science.

MOVING BEYOND THE MYTHS

Myths have value because they help us to organize and understand complex systems and phenomena, and provide a starting point toward the restoration and management of degraded ecosystems. We feel this is why the myths of restoration exist and persist. We hope that proposing these myths (whether the reader agrees with them or not) will begin a dialog leading to a deeper thinking about and greater understanding of natural systems and advancing the science of restoration ecology and management.

Identifying myths has several implications for restoration design. A common theme in the myths is a failure to recognize and address uncertainty. Ignoring uncertainty often results in surprise and failure, because we have not created a system capable of adapting or responding to future drivers or chance events, and we are unable to exert ultimate control over the system. An alternative approach would be designing for resilience by planning for surprise. Although we cannot anticipate all future events, we can manage and restore in ways that allow for uncertainty. Planning for resilience should allow systems a greater ability to deal with and recover from surprise and future change by focusing on a diversity of approaches, functions, and taxa.

When viewed in the context of designing for resilience, restorations become experiments in adaptive management or adaptive restoration (Zedler 2000b). Restoration projects with decision points along the way allow for critical assessment and possible intervention with contingency plans if things are not proceeding appropriately. Rapid learning can also be achieved by using a diversity of restoration techniques and approaches likely to be successful within the larger restoration. Assessing the performance of multiple approaches may increase cost, but it allows for testing multiple hypotheses and adaptive learning, and may cost less in the long run. If more than one approach is

successful, the restoration toolbox quickly expands, and much about the system is learned. If, however, no approach works, we will have quickly learned the inability of several techniques compared with the time it would take to gain the same results one restoration at a time. The challenge is to implement and design multiple approaches so that each can be assessed independently of others, as well as independently of adaptive responses that may occur along decision points after periodic evaluations. Multiple approaches within a larger restoration will also likely increase system resilience because the system created by each approach may have differential response to and recovery from disturbances. Maximizing species diversity in restorations is likely to increase response diversity (Elmqvist et al. 2003) and may increase the likelihood of a restoration containing species resistant or resilient to future conditions and disturbances. Although the concept that diversity begets ecosystem stability may itself be an emerging myth, it seems worth pursuing for other reasons as well.

Recognizing mythologies may also aid the goal-setting process. The forest primeval no longer exists and may not be attainable—exotic species, historic disturbance regimes, and changes in climatic and landscape drivers all serve to ensure that there never was, and probably never will be a single, repeatable end point. More realistically, goals should include multiple scientifically defensible end points of functional or structural equivalence. Although maintaining biotic or ecological integrity is a noble goal, invasive species are too entrenched in many systems to consider their presence a restoration failure, particularly when some may have similar roles as native species. Providing for alternative solutions to future conditions by setting multiple end points implicitly increases resilience by increasing the adaptive capacity and response diversity of the system. In addition to being more realistic and attainable, having several possible end points may also reduce tension within and among practitioners and stakeholders.

Restoration projects should expand goals and expectations beyond quantitative targets or ranges for ecological attributes, such as vegetation density, biogeochemical processes, and hydroperiods. Approaches that consider ecological capital, connectivity, and variability are likely to improve the ecological resilience of restored systems, and therefore, their ability to absorb disturbances or insults without resulting in a permanent change in fundamental system attributes. One size does not fit all, even when situations may appear very similar. Any ecological restoration or management effort involves both explicit and implicit attempts to prescribe and predict the ecological future of a site. These efforts require extrapolating far beyond our predictive abilities, and we must be aware of our limitations as scientists, as well as our tendency as humans to rely on partial truths and assumptions when implementing ecological restoration and management projects.

We conclude by suggesting a final myth of restoration ecology, but one held by society—the Bionic World. The myth of the Bionic World is a belief that science and technology will solve the pressing issues of human population growth, finite resources, and altered ecosystems. In the Bionic World, degraded landscapes will be fixed or reconstructed with the precision and surety of the "Bionic Woman" and the "Six Million Dollar Man" in the U.S. television shows of the 1970s. If we follow this logic, we have no tough choices to make about how we view and treat our surroundings, and decisions can be put off until the economic markets demand or justify a solution. Let's hope they're right, but until supporting evidence emerges, we must maintain what we have.

Responses to this article can be read online at:
http://www.ecologyandsociety.org/vol10/iss1/art19/responses/

Acknowledgments:

This work was conducted as part of the Theories for Sustainable Futures Working Group supported by the National Center for Ecological Analysis and Synthesis, a Center funded by the National Science Foundation (Grant #DEB-94-21535), the University of California at Santa Barbara, and the State of California. The authors thank Guy Barnett, Katia Engelhardt, Lance Gunderson, Buzz Holling, and two anonymous referees for helpful comments throughout manuscript preparation. R. H. was partially supported by a D. H. Smith Conservation Research Fellowship from The Nature Conservancy. This is publication DHS 2004-07 of the David H. Smith Research Fellowship Program, University of Maryland Center for Environmental Science Appalachian Laboratory scientific contribution

number 3813.

LITERATURE CITED

Ansola, G., C. Fernandez, and E. de Luis. 1995. Removal of organic matter and nutrients from urban wastewater by using an experimental emergent aquatic macrophyte system. *Ecological Engineering* **5**:13-19.

Beisner, B. E., D. T. Haydon, and K. Cuddington. 2003. Alternative stable states in ecology. *Frontiers in Ecology and the Environment* **1**:376–382.

Bormann, F. H., and G. E. Likens. 1979. *Pattern and process in a forested ecosystem*. Springer–Verlag, New York, New York, USA.

Campbell, D. A., C. A. Cole, and R. P. Brooks. 2002. A comparison of created and natural wetlands in Pennsylvania, USA. *Wetlands Ecology and Management* **10**:41–49.

Christensen, N. L., and R. K. Peet. 1984. Convergence during secondary forest succession. *Journal of Ecology* **72**:25–36.

Clements, F. E. 1936. Nature and structure of the climax. *Journal of Ecology* **24**:252–284.

Clewell, A. F. 1999. Restoration of riverine forest at Hall Branch on phosphate-mined land, Florida. *Restoration Ecology* **7**:1–14.

Clewell, A., J. Rieger, and J. Munro. 2000. *Guidelines for developing and managing ecological restoration projects*. Society for Ecological Restoration, Tucson, Arizona, USA.

Dahl, T. E., and G. J. Allord. 1996. History of wetlands in the conterminous United States. Pages 19–26 *in* J. D. Fretwell, J. S. Williams, and P. J. Redman, editors. *National water summary on wetland resources*. United States Geological Survey. Water Supply Paper **2425**. Reston, Virginia, USA.

Drake, J. A. 1990. Communities as assembled structures: do rules govern pattern? *Trends in Ecology and Evolution* **5**:159–164.

Egler, F. E. 1954. Vegetation science concepts. I. initial floristic composition—a factor in old-field vegetation development. *Vegetatio* **4**:412–417.

Ehrenfeld, J. G. 2000. Evaluating wetlands within an urban context. *Ecological Engineering* **15**:253–265.

Elmqvist, T., C. Folke, M. Nystrom, G. Peterson, J. Bengtsson, B. Walker, and J. Norberg. 2003. Response diversity, ecosystem change, and resilience. *Frontiers in Ecology and the Environment* **1**:488–494.

Galatowitsch, S., and A. van der Valk. 1996. The vegetation of restored and natural prairie wetlands. *Ecological Applications* **6**:102–112.

Glenn-Lewin, D. C., R. K. Peet, and T. T. Veblen. 1992. *Plant succession: theory and prediction*. Chapman and Hall, London, UK.

Grace, J. B. 1987. The impact of preemption on the zonation of two *Typha* species along lakeshores. *Ecological Monographs* **57**:283–303.

Gunderson, L. H. 2000. Resilience in theory and practice. *Annual Review of Ecology and Systematics* **31**:425–439.

Hobbs, R. J., and J. A. Harris. 2001. Restoration ecology: repairing the Earth's ecosystems in the new millennium. *Restoration Ecology* **9**:239–246.

Hobbs, R. J., and D. A. Norton. 1996. Towards a conceptual framework for restoration ecology. *Restoration Ecology* **4**:93–110.

Holling, C. S. 1973. Resilience and stability of ecological systems. *Annual Review of Ecology and Systematics* **4**:1–23.

Holling, C. S. 1982. Myths of ecology and energy. Pages 8–16 *in* L. C. Ruedisili and M. W. Firebaugh, editors. *Perspectives on energy: issues, ideas, and environmental dilemmas.* Oxford University Press, New York, New York, USA.

Holling, C. S. 1995. What barriers? What bridges? Pages 3–34 *in* L. H. Gunderson, C. S. Holling, and S. S. Light, editors. *Barriers and bridges to the renewal of ecosystems and institutions*. Columbia University Press, New York, New York, USA.

Holling C. S., S. R. Carpenter, W. A. Brock, and L. H. Gunderson. 2002. Discoveries for sustainable futures. Pages 395–418 *in* L. H. Gunderson, and C. S. Holling, editors. *Panarchy: understanding transformations in human and natural systems*. Island Press, Washington, D.C., USA.

Holling, C. S., and G. K. Meffe. 1996. Command and control and the pathology of natural resource management. *Conservation Biology* **10**:328–337.

Hubbell, S. P. 2001. *The unified neutral theory of biodiversity and biogeography*. Monographs in Population Biology **32.** Princeton University Press. Princeton, New Jersey, USA.

Kadlec, R. H., and R. L. Knight. 1996. *Treatment wetlands.* Lewis Publishers, Boca Raton, Florida, USA.

Kangas, P. C. 2003. *Ecological engineering: principles and practice.* Lewis Publishers, Boca Raton, Florida, USA.

Keddy, P. 1999. Wetland restoration: the potential for assembly rules in the service of conservation. *Wetlands* **19**:716–732.

Kentula, M. E. 1996. Wetland restoration and creation. Pages 87–92 *in* J. D. Fretwell, J. S. Williams, and P. J. Redman, editors. *National water summary on wetland resources. United States Geological Survey.* Water Supply Paper **2425.** Reston, Virginia, USA.

Kershner, J. L. 1997. Setting riparian/aquatic restoration objectives within a watershed context. *Restoration Ecology* **5**:15–24.

Kipling, R. 1902. *Just so stories.* Airmont Publishing Company, New York, New York, USA.

Knowlton, M. F., C. Cuvellier, and J. R. Jones. 2002. Initial performance of a high capacity surface-flow treatment wetland. *Wetlands* **22**:522–527.

Lewontin, R. C. 1969. The meaning of stability. *Brookhaven Symposium in Biology* **22**:13–24.

Lockwood, J. L., and S. L. Pimm. 1999. When does restoration succeed? Pages 363–392 *in* E. Weiher and P. A. Keddy, editors. *Ecological assembly rules: perspectives, advances and retreats.*Cambridge University Press, Cambridge, UK.

Mitsch, W. J. 1997. *Olentangy River Wetland Research Park at the Ohio State University*. Annual Report 1996. School of Natural Resources, Ohio State University, Columbus, Ohio, USA.

Mitsch, W. J., and R. F. Wilson. 1996. Improving the success of wetland creation and restoration with know-how, time, and self-design. *Ecological Applications* **6**:77–83.

Mitsch, W. J., X. Wu, R. W. Nairn, P. E. Weihe, N. Wang, R. Deal, and C. E. Boucher. 1998. Creating and restoring wetlands. *BioScience* **48**:1019–1030.

National Research Council. 2001. *Compensating for wetland losses under the Clean Water Act.* National Academy Press, Washington, D.C., USA.

Odum, E. P. 1969. The strategy of ecosystem development. *Science* **164**:262–270.

Parker, V. T. 1997. The scale of successional models and restoration objectives. *Restoration Ecology* **5**:301–306.

Peterson, H. G. 1998. Use of constructed wetlands to process agricultural wastewater. *Canadian Journal of Plant Science* **78**:199–210.

Pickett, S. T. A., and P. S. White. 1985. *The ecology of natural disturbance and patch dynamics.* Academic Press, New York, New York, USA.

Richter, B. D., R. Matthews, D. L. Harrison, and R. Wigington. 2003. Ecologically sustainable water management: managing river flows for ecological integrity. *Ecological Applications* **13**:206–224.

Rosgen, D. L. 1994. A classification of natural rivers. *Catena* **22**:169–199.

Rosgen, D. L. 1998. *River restoration and natural channel design course handbook.* Wildland Hydrology, Pagosa Springs, Colorado, USA.

Seabloom, E. W., and A. G. van der Valk. 2003. Plant diversity, composition, and invasion of

restored and natural prairie pothole wetlands: implications for restoration. *Wetlands* **23**:1–12.

Shore, D. 1997. The Chicago wilderness and its critics. II. Controversy erupts over restoration in Chicago area. *Restoration and Management Notes* **15**:25–31.

Simenstad, C. A., and R. M. Thom. 1996. Functional equivalency trajectories of the restored Gog-Le-Hi-Te estuarine wetland. *Ecological Applications* **6**:38–56.

Smith, S. 1997. *Changes in the hydraulic and morphological characteristics of a relocated stream channel.* Thesis, University of Maryland, College Park, Maryland, USA.

Stanturf, J. A., S. H. Schoenholtz, C. J. Schweitzer, and J. P. Shepard. 2001. Achieving restoration success: myths in bottomland hardwood forests. *Restoration Ecology* **9**:189–200.

Timmerman, P. 1986. Mythology and surprise in the sustainable development of the biosphere. Pages 436–454 *in* W. C. Clark and R. E. Munn, editors. *Sustainable development of the biosphere.* Cambridge University Press, Cambridge, UK.

van der Valk, A. G. 1998. Succession theory and restoration of wetland vegetation. Pages 657–667 *in* A. J. McComb and J. A. Davis, editors. *Wetlands for the future.* Gleneagles Publishing, Adelaide, Australia.

Whigham, D. F. 1999. Ecological consequences of wetland preservation, restoration, creation and assessment. *Science of the Total Environment* **240**:31–40.

Wilkins, S., D. A. Keith, and P. Adam. 2003. Measuring success: evaluating the restoration of a grassy eucalypt woodland on the Cumberland Plain, Sydney, Australia. *Restoration Ecology* **11**:489–503.

Young, T. P. 2000. Restoration ecology and conservation biology. *Biological Conservation* **92**:73–83.

Zedler, J. B. 1996. Ecological issues in wetland mitigation: an introduction to the forum. *Ecological Applications* **6**:33–37.

Zedler, J. B. 2000a. Progress in wetland restoration ecology. *Trends in Ecology and Evolution* **15**:402–407.

Zedler, J. B. 2000b. *Handbook for restoring tidal wetlands.* CRC Press, Boca Raton, Florida, USA.

Zedler, J. B., and J. C. Callaway. 1999. Tracking wetland restoration: do mitigation sites follow desired trajectories? *Restoration Ecology* **7**:69–73.

Technical Memo

To: Jeff Johnson and Sean Collier, Southern Nevada Water Authority
From: Justin Huntington, Charles Morton, Matt Bromley, Ryan Liebert, Desert Research Institute
Date: June 4, 2013
Re: Analysis of Evapotranspiration for the Muddy River Springs Area

Purpose and Scope

This technical memo provides estimates of evapotranspiration (*ET*) for the Muddy River Springs area from 2001-2012. This work is part of a larger effort toward mapping historical *ET* along the Muddy River and Muddy River Springs (Figure 1) utilizing surface energy balance and vegetation indices from 2001-2012. The Muddy River Springs focused study area (Figure 2) primarily consists of pasture grass, mesquite trees, cotton woods, palm trees, and several species of vines (DeMeo et al., 2008). Previous studies have estimated *ET* in the Muddy River Springs area using a water budget approach (Eakin 1964; 1966), and more recently with *ET* station measurements and remote sensing (DeMeo et al., 2008). This study builds on previous work, and attempts to identify trends in *ET* over the study period of 2001-2012 to identify potential impact on *ET* due to land management and vegetation changes.

Surface Energy Balance and Vegetation Index Approaches

Surface energy balance estimates are made in this study using the Mapping EvapoTranspiration at high Resolution with Internalized Calibration, METRIC, model (Allen et al., 2007). METRIC relies Landsat imagery and locally collected meteorological data to calculate actual *ET*. METRIC recently has been applied by state and federal agencies to estimate ET from rainfed and irrigated vegetation in Nevada, New Mexico, Oregon, Wyoming, Montana, Nebraska, and Colorado (Hendrickx, 2010; Kjaersagaard and Allen, 2010; Sullivan et al., 2011; Snyder et al., 2012). This study also applies a vegetation index reference ET fraction approach to estimate actual *ET* in the Muddy River Springs area similar to Allen et al. (2011), Tasumi and Allen (2007), and Singh and Irmak (2009).

Methods

Estimating actual *ET* required numerous weather data and image processing steps that are briefly described below. Landsat 5 Thematic Mapper (TM) and 7 Enhanced Thematic Mapper Plus (ETM+) images were acquired for the study period of 2001-2012 from the U.S. Geological Survey (USGS) Global Visualization web page (http://glovis.usgs.gov/) totaling 323

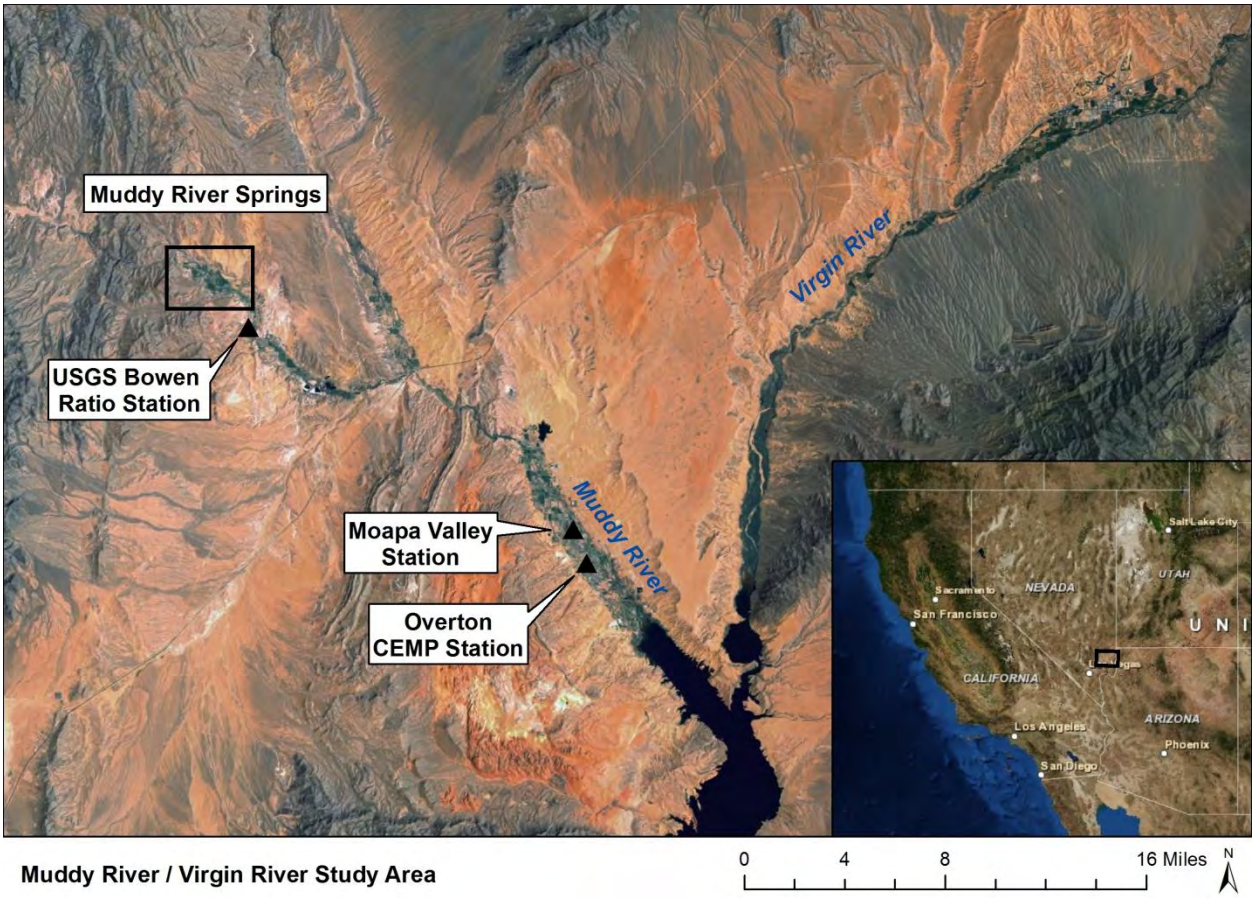

Figure 1. General study area with highlighted Muddy River Springs area.

images (Table A1). Landsat data processing was handled using Python scripts, many of which are described in Morton (2013). General processing steps include performing radiometric and atmospheric corrections using the Landsat Ecosystem Disturbance and Adaptive Processing System (LEDAPS) (Masek et al., 2006) to compute at surface reflectance, with following computations of the Normalized Difference Vegetation Index (NDVI), surface temperature, albedo, and various energy balance components following Allen et al. (2007) and Morton et al. (2013). The land surface energy balance is simulated by METRIC as

$$LE = R_n - H - G$$

where LE is latent heat flux (W/m^2), R_n is net radiation (W/m^2), H is sensible heat flux (W/m^2), and G is ground heat flux in (W/m^2). The reader is referred to Allen et al. (2007) and Morton et al. (2013) for detail on METRIC and how each component of the energy balance is computed from Landsat data. Once LE is computed for each pixel, the equivalent amount of instantaneous ET (mm/hr) is computed by dividing by the latent heat of vaporization (λ). Instantaneous ET at the time of the Landsat image is estimated over the day as

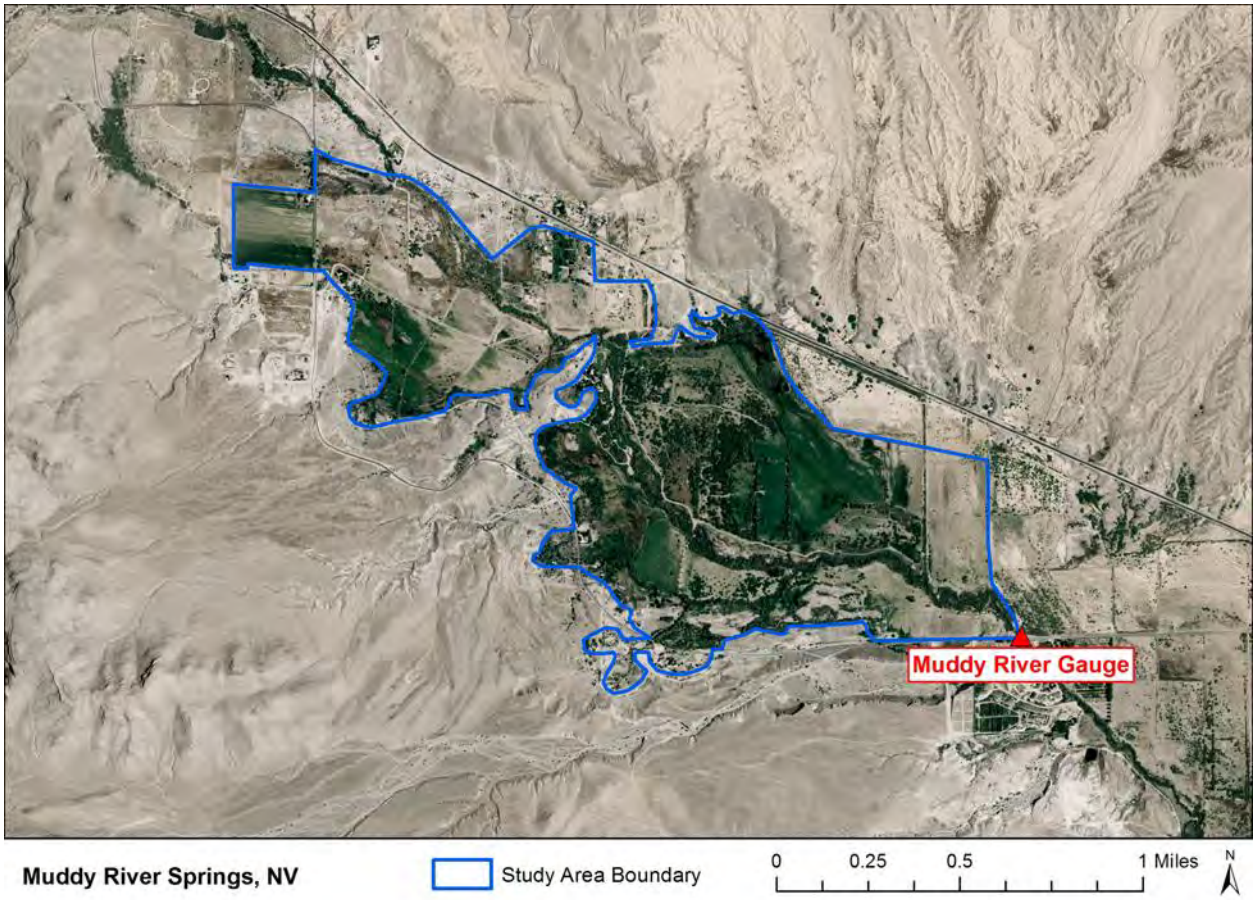

Figure 2. Warm Springs (Muddy River Springs) study area for estimating ET from 2001-2012.

$$ET_{24} = (ET_{inst} / ET_r) * ET_{r24}$$

where the ratio of ET_{inst} (mm/hr) to ET_r (mm/hr) is the reference ET fraction (ET_rF) measured at the satellite overpass time and ET_{r24} is the cumulative ET_r for the day (mm/day). Seasonal total *ET* is estimated by linearly interpolating the daily ET_rF per pixel in between Landsat images, and multiplying daily ET_rF pixel values by the ET_{r24} for respective days. The reference *ET* fraction is commonly referred to as the crop coefficient. In this method, the computation and application of ET_rF simulates vegetation growth stages and phenology changes, roughness of the vegetation surface to account for turbulent effects, and vegetation geometry. Simply put, the effects of weather are incorporated into ET_r, whereas the effects that distinguish vegetated and bare surfaces from the reference surface are integrated into the ET_rF (Allen et al., 1998). There are many physiological and physical variables that determine *ET*, and the ET_r*ET_rF method incorporates the majority of these variables (Bos et al., 2008).

The vegetation index reference *ET* fraction approach is similar to the METRIC surface energy balance approach for estimating *ET* through time, but ET_rF is derived from the NDVI instead of an instantaneous surface energy balance. The reason for applying both approaches is due to the fact that it currently requires a relatively large amount of time and effort to process METRIC for multiple years, whereas it requires significantly less time and effort to compute

NDVI. Heilman et al. (1982) proposed a linear relationship between a vegetation index and fraction of reference ET, and has been supported by various other studies (Choudhury et al., 1994; Tasumi et al., 2005; Tasumi and Allen, 2007; Singh and Irmak, 2009; Calera-Belmonte et al., 2005). If no local calibration data exists, Allen et al. (2011) suggests that ET_rF can be generally estimated as

$$ET_rF = 1.25 * NDVI$$

where ET_rF is the relative fraction of the alfalfa reference ET. NDVI is defined as

$$NDVI = (\rho_{NIR} - \rho_{Red}) / (\rho_{NIR} + \rho_{Red})$$

where ρ is the at-surface reflectance, *NIR* is near infrared waveband from 0.76 to 0.90 µm, *Red* is the visible waveband from 0.63 to 0.69 µm. The relationship suggested by Allen et al. (2011) was modified in this work to more accurately represent the conditions specific to the study area using METRIC derived ET_rF and NDVI for all pixels in the Muddy River Springs study area (Figure 2). Seasonal average slopes between ET_rF and NDVI for 2006-2012 were found to vary between 1.21 and 1.37, with an average of 1.30, and intercepts ranging from 0.02 to 0.1, with an average of 0.06, and R^2 values ranging from 0.66 to 0.80, with an average of 0.74. Figure 3 illustrates an example of the correlation between ET_rF and NDVI for 2006. The fairly large scatter exists due to the fact that NDVI is not capable of detecting evaporation from wet soil due to irrigation, where METRIC is able to detect soil evaporation using the Landsat derived surface temperature, which results in high ET_rF and low NDVI. Additionally, NDVI is not able to detect acute vegetation stress due to water limitations, whereas the use of surface temperature in METRIC detects this acute water stress, which results in relatively high NDVI and low ET_rF due to low predicted evaporation by METRIC. While the use of NDVI does have limitations, for the sake of simplicity and providing the ability to estimate changes in *ET* for years before 2006 over the Muddy River Springs area, the equation

$$ET_rF = 1.30 * NDVI + 0.06$$

was applied in this work over the Muddy River Springs area to all cloud free Landsat 5 TM and 7 ETM+ images from 2001-2012 period (Table A1). A typical annual time series of spatially averaged NDVI from 2006 is illustrated for the Muddy River Springs study area in Figure 4, where greenup and senescence periods are clearly evident. Once NDVI is transformed into ET_rF at each pixel, ET_rF is linearly interpolated per pixel in between Landsat image dates, and then multiplied by the ET_r, ET_rF, to estimate *ET*.

Reference ET (ET_r) Estimates

Hourly weather data of solar radiation, air temperature, dewpoint temperature, and windspeed collected at SNWA's Moapa agricultural weather station and DRI's Overton Community Environmental Monitoring Program (CEMP) weather station (Figure 1) were downloaded and quality assured and controlled (QAQCed) according to Allen et al. (1996).

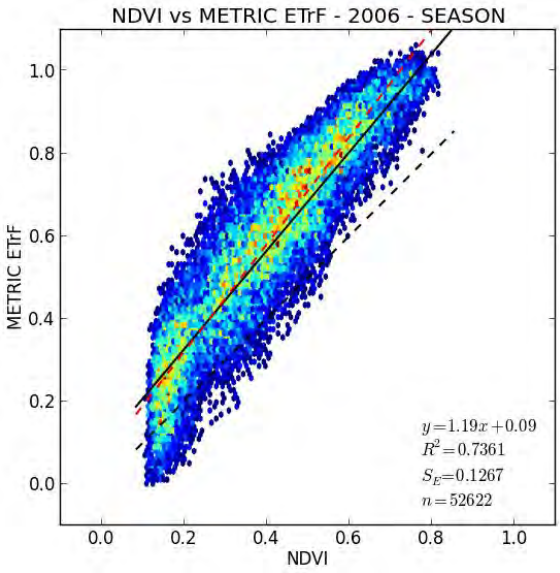

Figure 3. Scatter plot of ET_rF and NDVI for the 2006 growing season (February-November). Colors of the scatter plot represent point density where red is high density, and blue is low density. The red hatched line is the average regression line used to compute ET_rF from NDVI in this study, and the black hatched line is the 1:1 line.

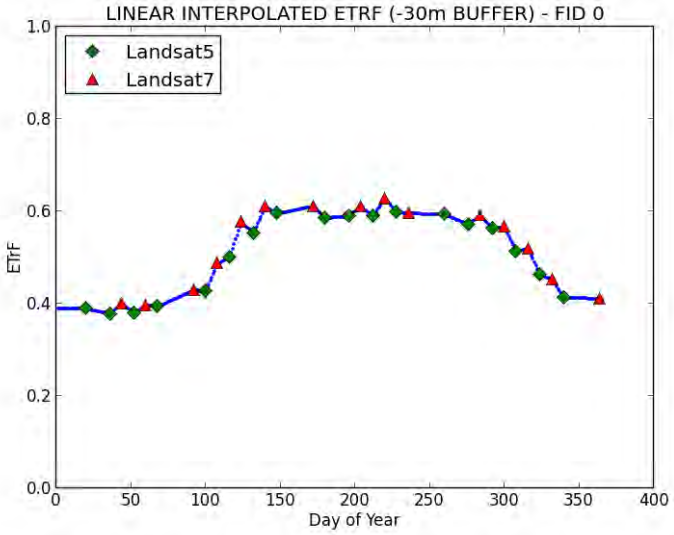

Figure 4. Time series of NDVI derived ET_rF for 2006 spatially averaged over the Muddy River Springs area shown in Figure 2. Interpolation of ET_rF in between Landsat image dates occurs on a pixel by pixel basis; however, this figure shows interpolation ET_rF averaged over the study area simply for illustrative purposes.

Overton CEMP weather data was analyzed from 2001-2012, and SNWA Moapa weather data was analyzed from 2010-2012, the available period of record for Moapa. Following adjustment procedures outlined in Allen et al. (1998) and Allen et al. (2011a), reported windspeed measured at respective measurement heights were logarithmically transformed to 2m height equivalent windspeed estimates, as required for input into the ASCE standardized reference ET equation. Windspeed measurement heights are 2.3m and 6m (7.5ft and 20ft) at the Moapa and Overton stations, respectively. Many years of solar radiation (R_s) measurements required some level of correction to better match clear sky solar radiation curves (R_{so}). Such needed corrections are common due to pyronometer sensor calibration drift (Allen, 1996). Figure 5 illustrates raw and corrected R_s from the Overton CEMP station. In this case it is evident that sensor calibration is in error due to the fact that measured R_s over a day never reaches the theoretical R_s that would occur for a clear sky day (R_{so}). Overton CEMP hourly solar radiation data was found to be corrupt from 2011 and 2012 and the data were not salvageable. Therefore, Moapa QAQCed hourly R_s was used to fill Overton CEMP hourly R_s for years 2011 and 2012. After QAQC was completed, ET_r was computed for both stations utilizing the standardized reference ET equation (ASCE-EWRI, 2005) for an alfalfa reference surface using the Ref-ET program (Allen, 2011).

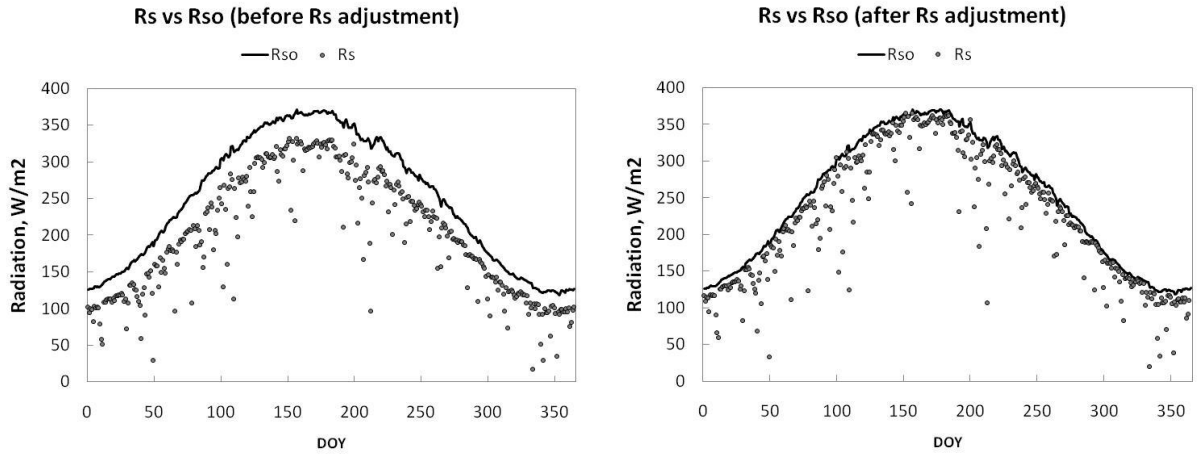

Figure 5. Overton CEMP 2007 measured solar radiation (R_s) (left), and corrected solar radiation to the theoretical clear sky solar radiation (R_{so}) (right) following recommendations of Allen (1996). Solar radiation corrections are typically needed due to pyronometer calibration drift, as is evident in this figure.

Because the desired study period was from 2001-2012 and Moapa weather data was only available from 2010-2012, a comparative analysis between Overton and Moapa computed ET_r was completed to potentially develop ET_r adjustment factors for Overton computed ET_r to simulate Moapa ET_r from 2001-2010. Figures 6 and 7 illustrate monthly ET_r computed from Overton and Moapa weather data for 2010-2012. It is evident that ET_r is nearly the same for most months, even though the Overton CEMP station is not located in an optimal reference environment that reflects the climate of agricultural and active *ET* conditions. As previously discussed, 2011 and 2012 Moapa R_s was substituted for Overton R_s, however, from inspection

of Figure 6 it is evident that 2011 Moapa ET_r is lower than Overton ET_r during mid-summer months. After investigating the potential cause of this difference, it was found that, raw, pre-QAQCed hourly windspeed for the Moapa station was often zero at night and during some hours of the day. In comparing windspeed between Moapa and Overton for 2010 and 2012, it was found that Overton 2m equivalent windspeed was typically lower than Moapa, except for this mid-summer period of 2011, where Moapa was lower than Overton. Due to the consistency of Overton having lower 2m equivalent windspeed in all months except for these three mid-summer months, and the fact that there were many reported zero values, it was assumed that the Moapa measured windspeed was in error for this period.

Due to the nearly identical computed ET_r between Overton and Moapa, Overton computed ET_r was utilized in this work to estimate *ET* using METRIC and NDVI-ET_rF approaches from 2001-2009, and 2011, while Moapa computed ET_r was used to estimate *ET* for 2010 and 2012. Growing season (February-November) and annual ET_r from 2001-2012 is illustrated in Figure 8 where it is evident that ET_r has generally decreased from 2001. This is significant, because any decreasing trends in ET_r will cause decreasing trends in *ET*. This result was cause for concern due to possible sensor drift and or data quality, therefore, an analysis was conducted to investigate if any trends were present in driving ET_r weather variables of solar radiation, temperature, dewpoint, and windspeed. While the analysis showed slight decreasing trends in annual averages, a more focused analysis was conducted for warm season months of May-September, since most of the annual *ET* occurs during these months. Results of the warm season trend analysis indicate that warm season average daily maximum and minimum temperatures, windspeed, and solar radiation all have decreasing trends from 2001-2012, while warm season average daily minimum temperature minus dewpoint temperature (i.e. dewpoint depression) is rising during this same period, indicating drying conditions (Appendix Figures A1-A5).

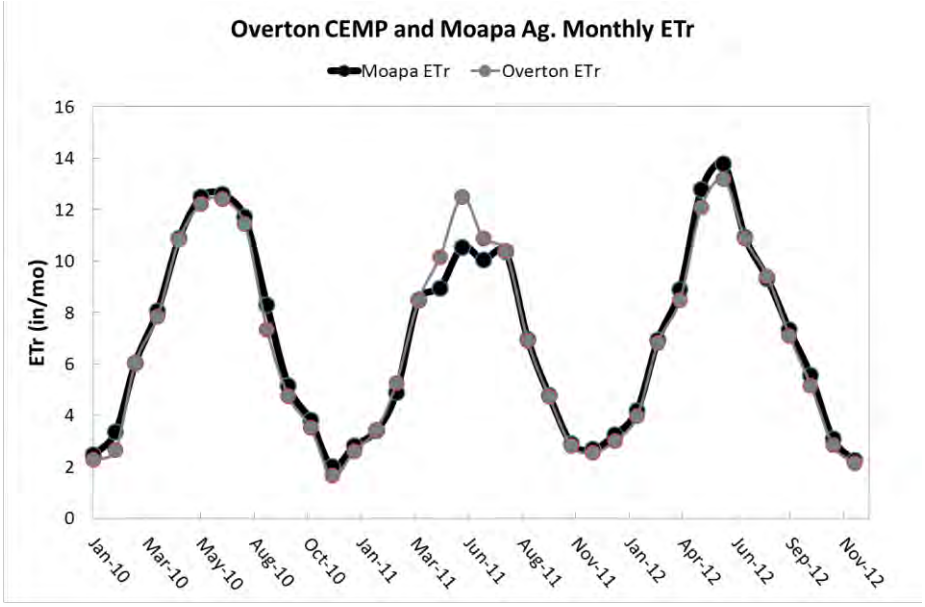

Figure 6. Monthly time series comparison of ET_r from Overton CEMP and Moapa agricultural weather stations

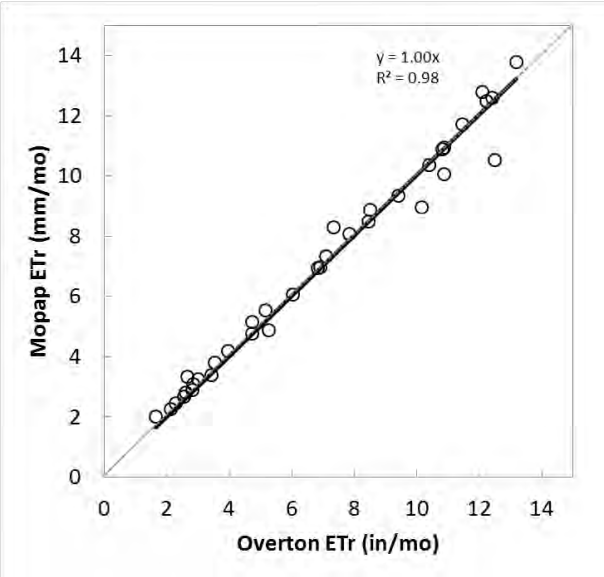

Figure 7. Scatter plot comparison of monthly ET_r from Overton CEMP and Moapa agricultural weather stations.

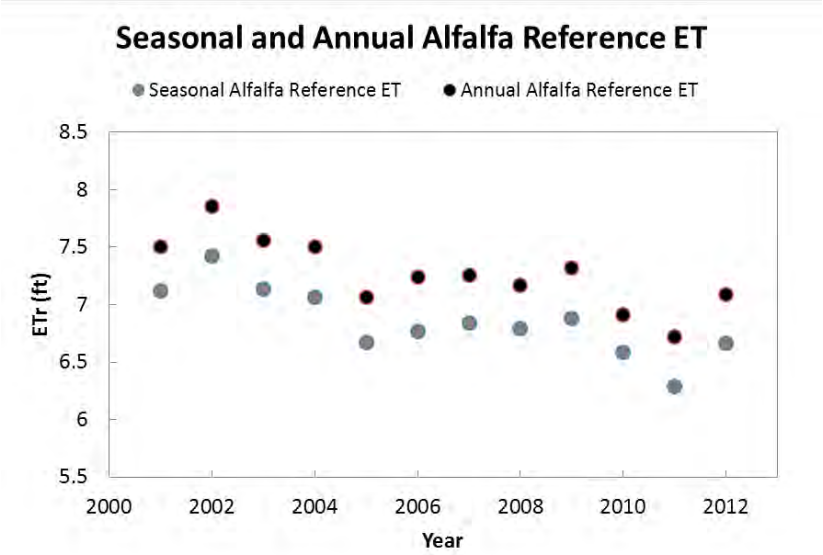

Figure 8. Seasonal (February – November) and annual ET_r from 2001-2012. As illustrated, ET_r has generally decreased over the study period of 2001-2012.

To confirm that these trends are real and not an artifact of possible weather station sensor drift, weather data from the closest weather station measuring temperature and windspeed was acquired and analyzed over the same period for warm season months of May-September. Results indicate very similar trends, where warm season average daily maximum and minimum temperatures and windspeed exhibit decreasing trends from 2001-2012, and warm season average daily minimum temperature minus dewpoint temperature is rising during the same period (Appendix Figures A6-A9). The comparative weather variable trend analysis between Overton and Nellis weather stations suggests that the trend in Overton computed ET_r from 2001-2012 is likely real and not artificial, and thus thought to be valid.

Evapotranspiration Estimates

Annual and seasonal *ET* from the Muddy River Springs study area was estimated using METRIC and the NDVI approaches, as previously described, by utilizing all available and cloud free images during each year from 2001-2012 (listed in Table A1). Mechanically, for both approaches, ET_rF is estimated for each image date and linearly interpolated, per pixel, in between image dates, and then multiplied by the respective daily reference *ET* (ET_r), to estimate the daily *ET*. Graphically, Figure 4 illustrates interpolation of ET_rF in between image dates for the Muddy River Springs area. Figure 9 illustrates respective ET_r, and the product of Figure 4 and Figure 9 for respective days results in estimated daily *ET* for 2006, shown in Figure 9. The use of ET_r to estimate *ET* in between image dates is critical for properly accounting for daily variations in atmospheric water demand (i.e., solar radiation, windspeed, temperature, humidity), and resulting impacts on *ET*. The translation of the daily variability in ET_r to *ET* can be seen in Figure 9, a process that would be missing, and in error, if *ET* were to be simply interpolated in between image dates (shown as green triangles on right panel of Figure 9).

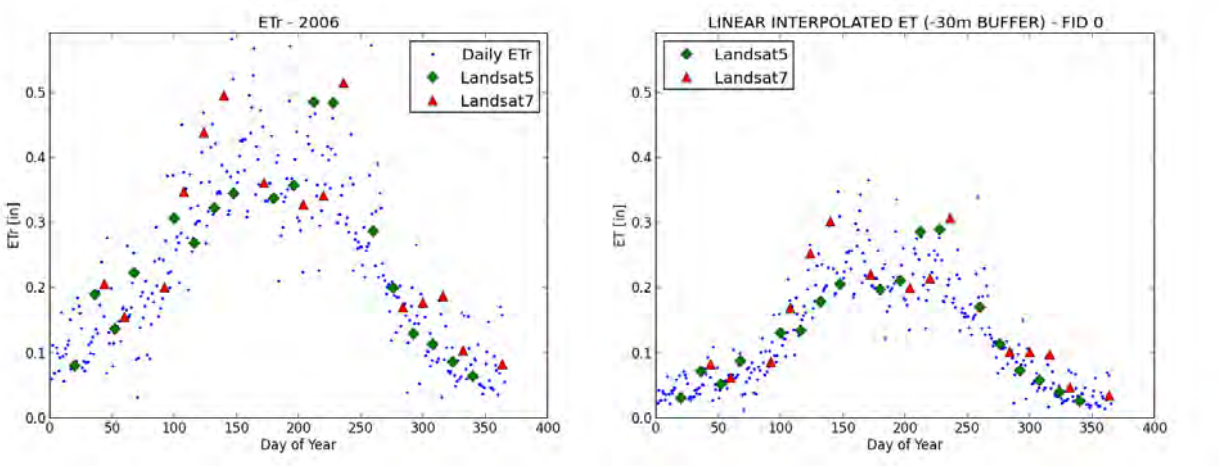

Figure 9. Daily reference *ET*, ET_r, (left) is multiplied by daily interpolated ET_rF (shown in Figure 4) to estimate daily *ET* for 2006 (right).

Seasonal (February-November) and annual *ET* totals were estimated utilizing METRIC from 2006-2012 and NDVI from 2001-2012, and results are shown in Figure 10 and Figure 11. A slight decrease in METRIC estimated *ET* is noticeable, however, this is largely due to the decrease in ET_r over this period, as the ratio of METRIC *ET* to ET_r (ET_rF) is fairly stable, as shown in Figure 12. The trend in NDVI estimated *ET* from 2001-2012 is more pronounced. The ratio of NDVI estimated *ET* to ET_r (ET_rF) is also fairly stable for 2006-2012, but decreases over the entire study period of 2001-2012 (Figure 13). Because *ET* is a function of precipitation (*PPT*), and *PPT* is highly variable from year to year, normalizing *ET* by removing the influence of *PPT* is needed for trend analysis. To accomplish this, annual *PPT* was subtracted from seasonal and annual METRIC and NDVI estimated *ET*. Monthly and annual *PPT* totals for the Muddy River Springs area were estimated from 2001-2011 using 800m spatial resolution PRISM data (Daly et al., 1994) for a single pixel within the study area to remove potential elevation biases from spatial averaging multiple pixels that fell outside the study area. A comparison between measured *PPT* at the Overton COOP station and estimated PRISM *PPT* for a single pixel at the Overton COOP station location is shown in Figure 14, where the correspondence between COOP measured and PRISM estimated *PPT* is good, although this was expected since the PRISM process uses the COOP station as a control point. Missing *PPT* in the Overton COOP precipitation record was filled with *PPT* from the Overton CEMP station, which totaled 424 days from 2001-2007. A comparison was also made between the Overton COOP *PPT* and Muddy River Springs area PRISM 800m *PPT* (Figure 15). Because 800m PRISM *PPT* was not available for 2012, and effectively no bias exists between Overton COOP *PPT* and 800m PRISM *PPT* for the Muddy River Springs area, Overton COOP monthly *PPT* was used for the Muddy River Springs area for 2012.

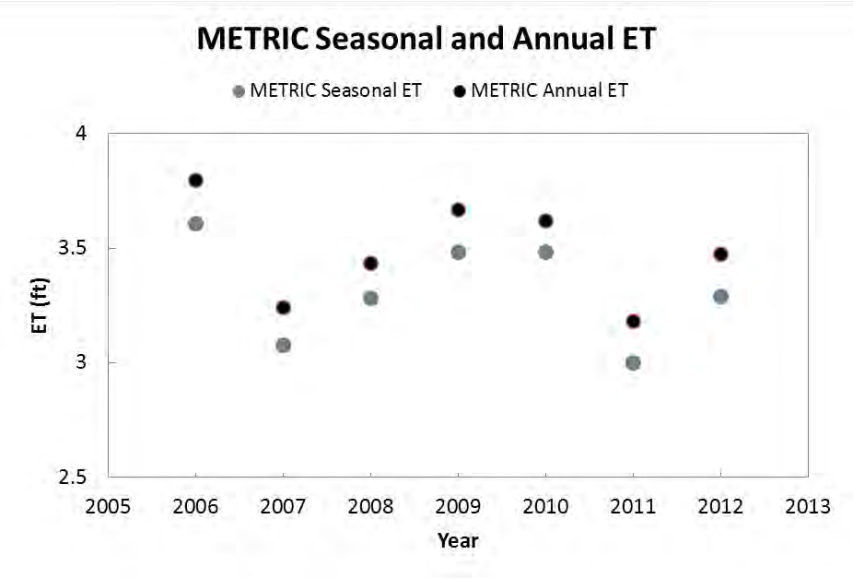

Figure 10. Seasonal and annual METRIC derived *ET* from 2006-2012. Seasonal totals are for the growing season, estimated to be February-November.

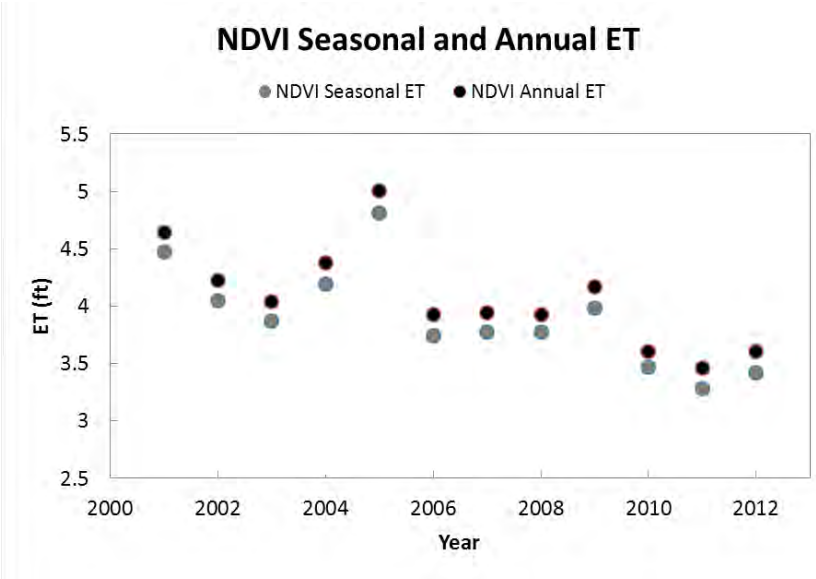

Figure 11. Seasonal and annual NDVI derived *ET* from 2001-2012. Seasonal totals are for the growing season, estimated to be February-November.

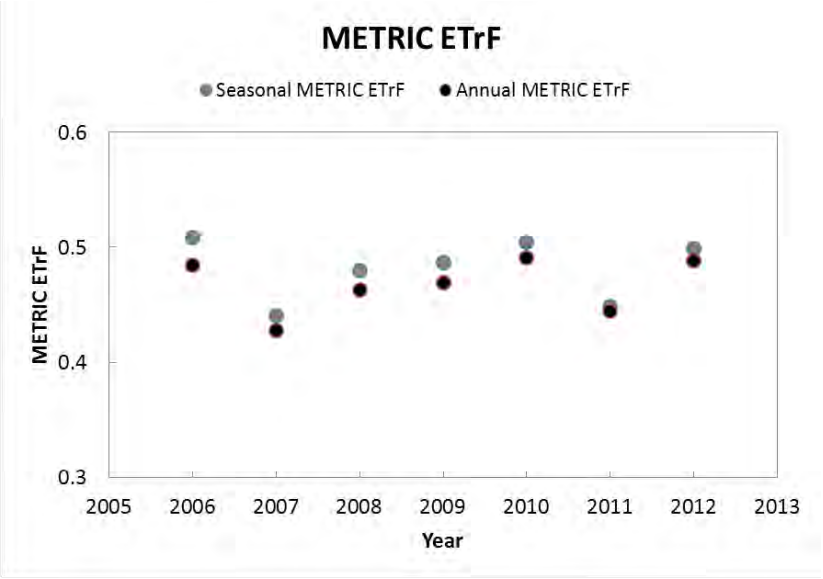

Figure 12. Seasonal and annual METRIC derived ET_rF from 2006-2012.

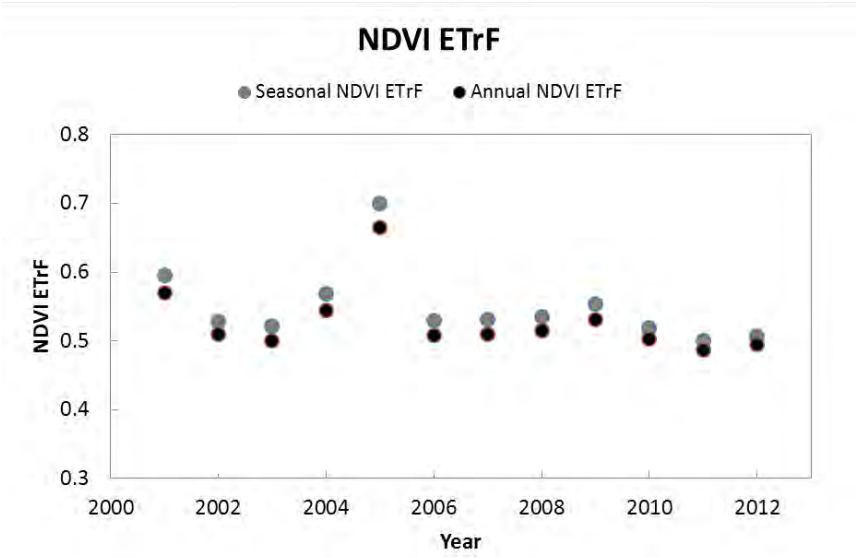

Figure 13. Seasonal and annual NDVI derived ET_rF from 2001-2012.

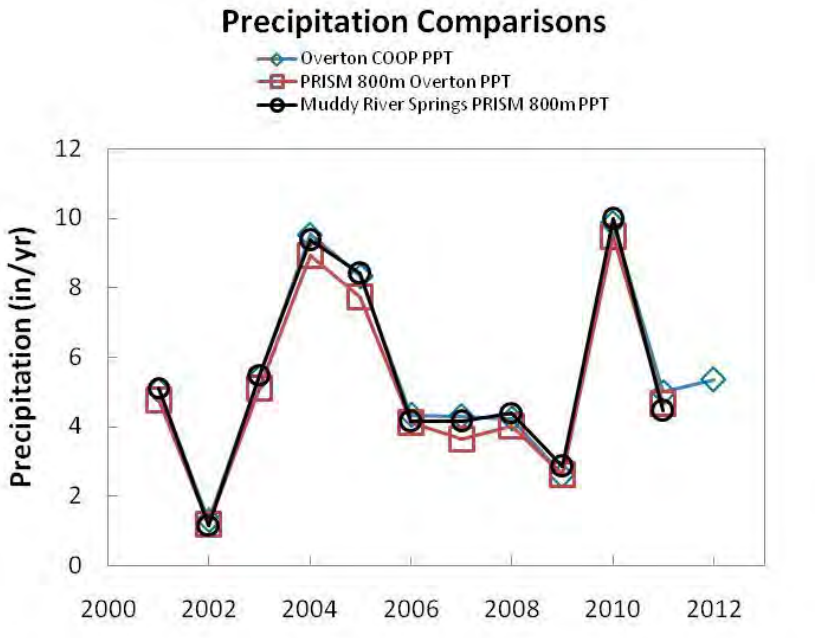

Figure 14. Comparison of Overton COOP *PPT*, 800m PRISM *PPT* for the Overton COOP location, and 800m PRISM *PPT* for the Muddy River Springs area. PRISM *PPT* at the 800m spatial resolution was not available for 2012, therefore, Overton COOP data was used due to the low bias between Overton COOP and Muddy River Springs PRISM *PPT* (Figure 15, right).

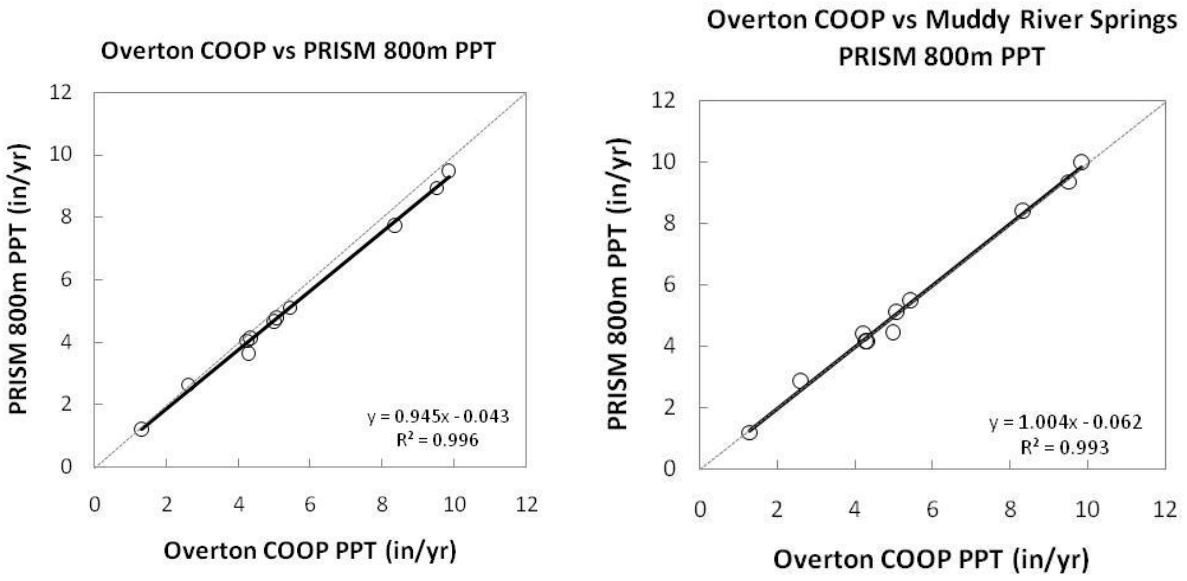

Figure 15. Overton COOP *PPT* vs. 800m PRISM *PPT* for the Overton COOP location (left), and Overton COOP *PPT* vs. 800m PRISM *PPT* for the Muddy River Springs area (right). PRISM *PPT* at the 800m spatial resolution was not available for 2012, therefore, Overton COOP data was used due to the low bias between Overton COOP and Muddy River Springs PRISM PPT.

Utilizing PRISM and COOP *PPT* estimates, seasonal and annual METRIC and NDVI estimated *ET-PPT* was computed (Figures 16 and 17). As previously mentioned, reduced *ET* over the study period is largely due to the decline in ET_r from 2001-2012, and this impact is also evident in the estimated *ET-PPT*. Both METRIC and NDVI estimated ET_rF of *ET-PPT* slightly decline over the 2006-2012 and 2001-2012 periods by 0.07 and 0.10, respectively, indicating that *ET* has declined independent of ET_r and *PPT* due to changes in vegetation and or water management in the study area (Tables A7 and A10). METRIC and NDVI annual estimated ET and ET_rF for 2006-2012 are illustrated in Figures 18 and 19, where it is evident that NDVI estimated *ET* is slightly higher than METRIC estimated *ET* (Figures 20-22). This is due to the fact that bare soil evaporation, potential vegetation stress, and changing surface conditions causes the relationship between NDVI and ET_rF for the Muddy River Springs area to be different from year to year, therefore no average regression will perform well over all years. Average annual METRIC estimated *ET* and *ET-PPT* for 2006-2012 is 3.5 ft/yr and 3.1 ft/yr, respectively. Average annual NDVI estimated *ET* and *ET-PPT* for 2006-2012 is 3.8 ft/yr and 3.4 ft/yr, respectively. For the period of 2006-2012, annual bias between NDVI and METRIC estimated *ET* and ET_rF ranges from 0 to 0.7 ft/yr, and 0.01 to 0.08, respectively, and the average annual bias is 0.32 ft/yr and 0.04, respectively (Figure 23).

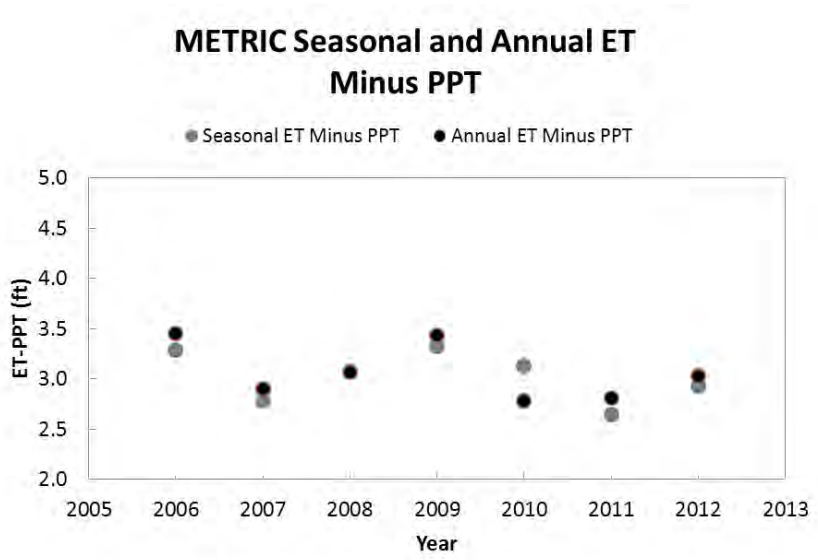

Figure 16. Seasonal and annual METRIC derived *ET-PPT* from 2006-2012.

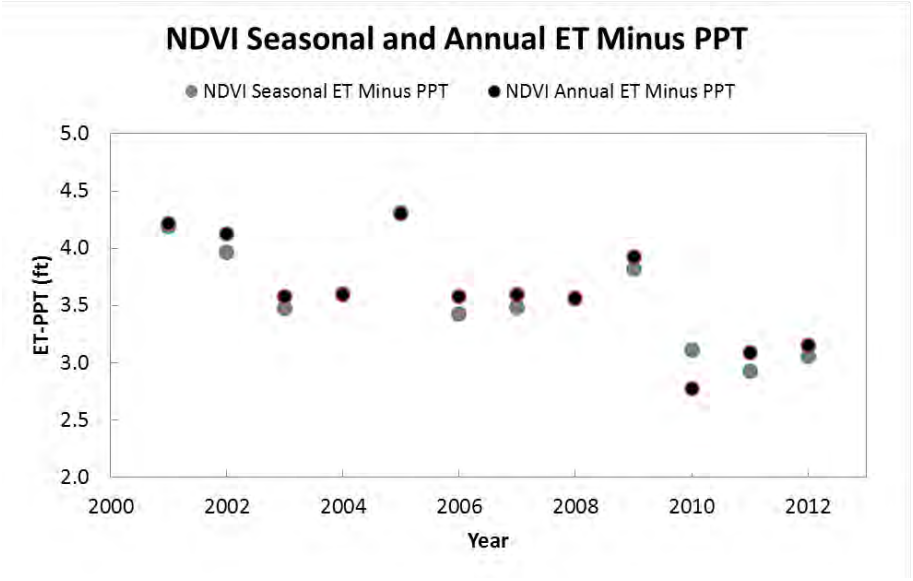

Figure 17. Seasonal and annual NDVI derived *ET-PPT* from 2001-2012.

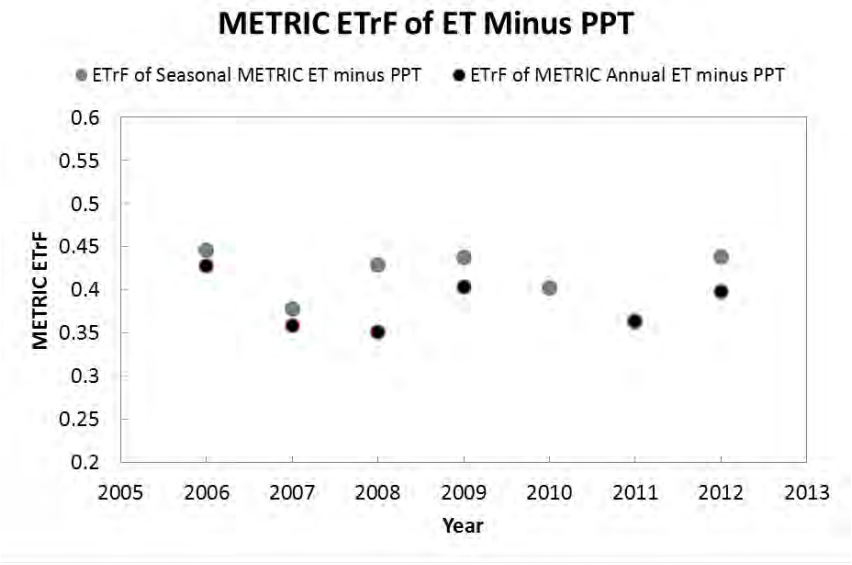

Figure 18. Seasonal and annual METRIC derived ET_rF from 2006-2012.

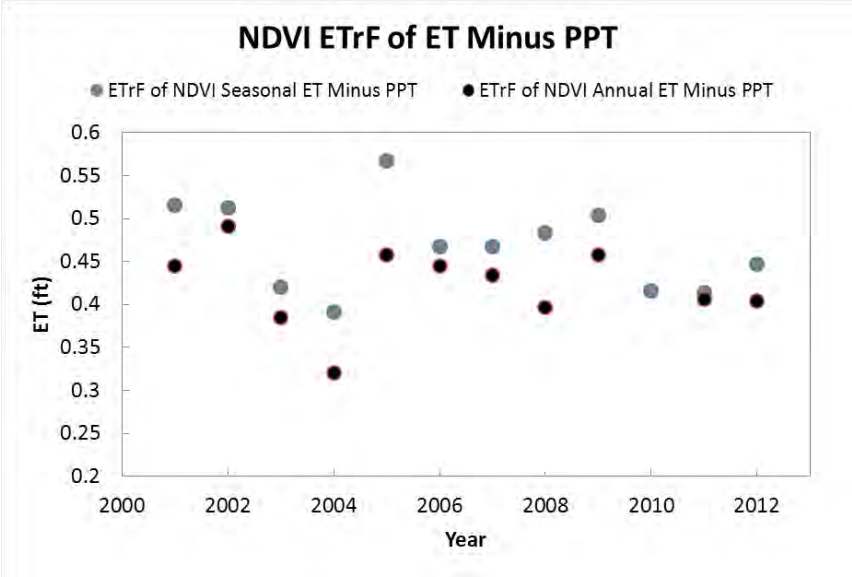

Figure 19. Seasonal and annual NDVI derived ET_rF from 2001-2012.

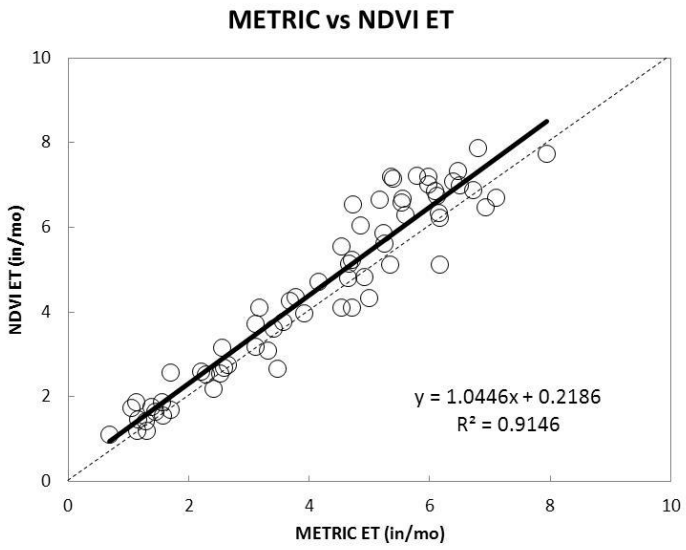

Figure 20. METRIC and NDVI estimated monthly *ET* from 2006-2012.

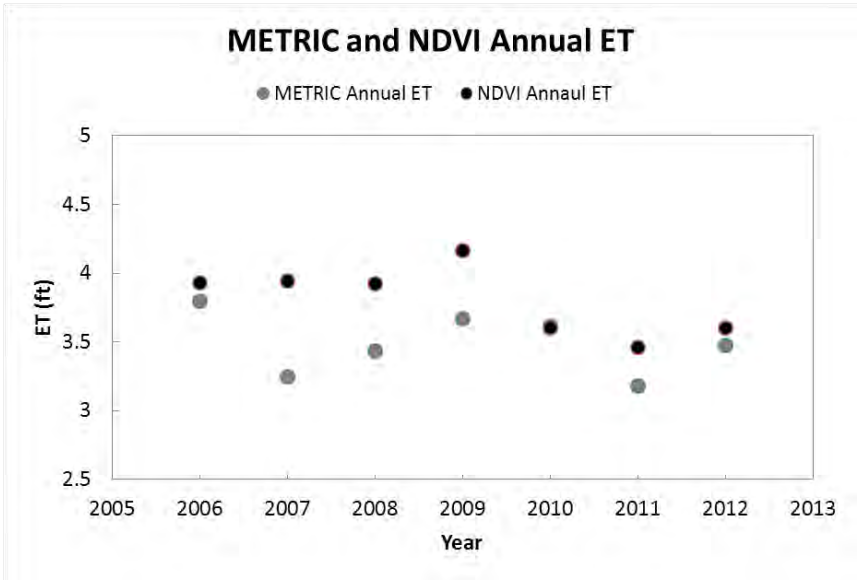

Figure 21. METRIC and NDVI estimated annual *ET* from 2006-2012.

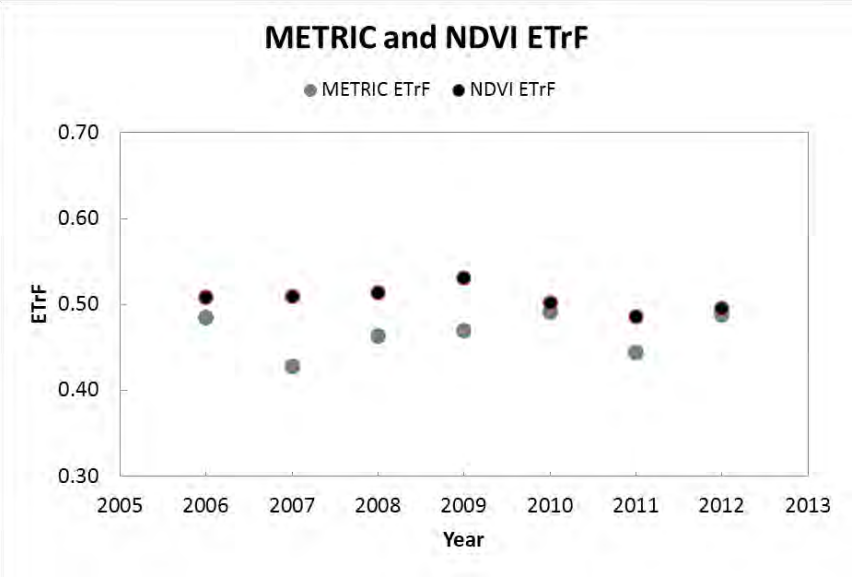

Figure 22. METRIC and NDVI estimated annual *ETrF* from 2006-2012.

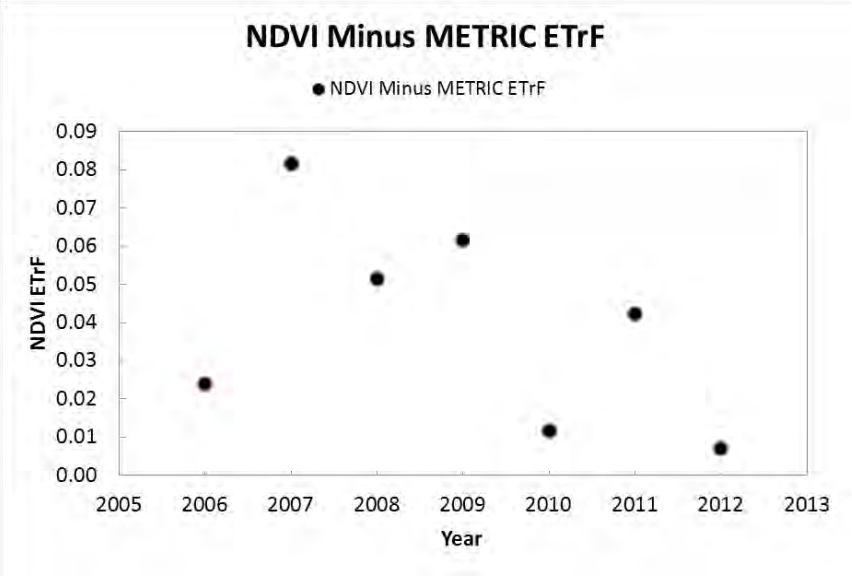

Figure 23. NDVI minus METRIC estimated annual *ETrF* from 2006-2012.

Considering that METRIC estimated *ET* relies on a surface energy balance based on surface temperature, and NDVI strictly relies on optical reflectance and a simple linear index, and the fact that the average annual bias between NDVI and METRIC ET_rF is only 0.04, the comparison between NDVI and METRIC estimated *ET* is thought to be fairly good. As previously mentioned, the use of NDVI does have weaknesses, especially in detecting bare soil evaporation, however, due to the fact that bare soil evaporation is thought to be a fairly small component of *ET* in the Muddy River Springs area due to irrigation practices and moderate vegetation cover. For this reason, the use of NDVI for estimating *ET* is considered to be fairly robust in this work.

Evapotranspiration Reductions

Average METRIC and NDVI estimated annual *ET-PPT* reductions for the Muddy River Springs area for the period of 2006-2012 range from -0.062 ft/yr to -0.11 ft/yr, respectively, with total reductions of METRIC and NDVI annual *ET-PPT* over the 2006-2012 period being -0.43ft and -0.77ft, respectively. Average NDVI estimated annual *ET-PPT* decline for the Muddy River Springs area over the period of 2001-2012 is estimated to be -0.095 ft/yr, with a total reduction in annual *ET-PPT* of -1.14 ft (Tables A6 and A9). For the period 2006-2012, METRIC and NDVI estimated annual *ET-PPT* volume reductions over the 797 acre Muddy River Springs study area are estimated to be -344 ac-ft and -613 ac-ft, respectively. For the period 2001-2012, the NDVI estimated annual *ET-PPT* volume reduction over the 797 acre study area is estimated to be -910 ac-ft. These results along with monthly, seasonal, and annual results of METRIC *ET*, ET_r, PRISM *PPT*, NDVI *ET*, METRIC *ET-PPT*, NDVI *ET-PPT*, METRIC ET_rF, and NDVI ET_rF are listed in Appendix Tables A2-A10. Differences in reductions between METRIC and NDVI from 2006-2012 are due to differences in the computed slopes in ET-PPT during this period. METRIC estimates of *ET* and *ET-PPT* are noticeably lower than NDVI estimates of *ET* and *ET-PPT* for 2007-2009, a period of relatively low precipitation, potentially causing water limited stress conditions that NDVI is not sensitive to. To support this argument METRIC seems to compare well with NDVI estimated *ET* and *ET-PPT* during years of relatively higher precipitation. Also, calibration of METRIC during 2007-2009 could possibly be abnormally low, however, it is thought that calibration during these years are relatively robust and consistent.

Comparison to Previous ET Work

For comparison purposes, METRIC and NDVI derived *ET* was compared to a recent study by DeMeo et al. (2008), who estimated *ET* in the Muddy River Springs area using the Bowen Ratio Energy Balance (BREB) approach from July 2003-October 2006. The Bowen ratio station location is shown in Figure 24, and is surrounded by a dense grove of 10 to 15 ft tall mesquite trees (DeMeo et al., 2008) (Figure 25). DeMeo et al. (2008) reports the average annual *ET* to be 3.6 ft/yr from summing 2003-2006 daily average *ET* estimates from the Muddy River Bowen station. No monthly totals were reported. To compare METRIC *ET* and NDVI *ET* to the Muddy River station estimated *ET* for respective years, 20 minute *ET* data was acquired from the USGS and summed into daily and monthly totals. METRIC and NDVI *ET* estimates were extracted from a 75m buffer around the USGS Muddy River station (Figure 24). Previous work has shown that roughly 80% of the turbulent fluxes measured at many Nevada ET stations with surrounding riparian and shrubland vegetation originates within a 30 to 100m radius of the *ET* station, with the lower range being associated with taller riparian vegetation (Moreo et al., 2007; Allander et al., 2009).

Monthly METRIC and NDVI *ET* estimates were compared to Bowen ratio station *ET* estimates from 2003-2006 (Figures 25 and 26). Results suggest that METRIC and NDVI over predict *ET* at the low *ET* range, but is fairly accurate at the moderate to high *ET* range. The comparisons are considered favorable given that a large part of the annual *ET* in the study area is derived from high *ET* months.

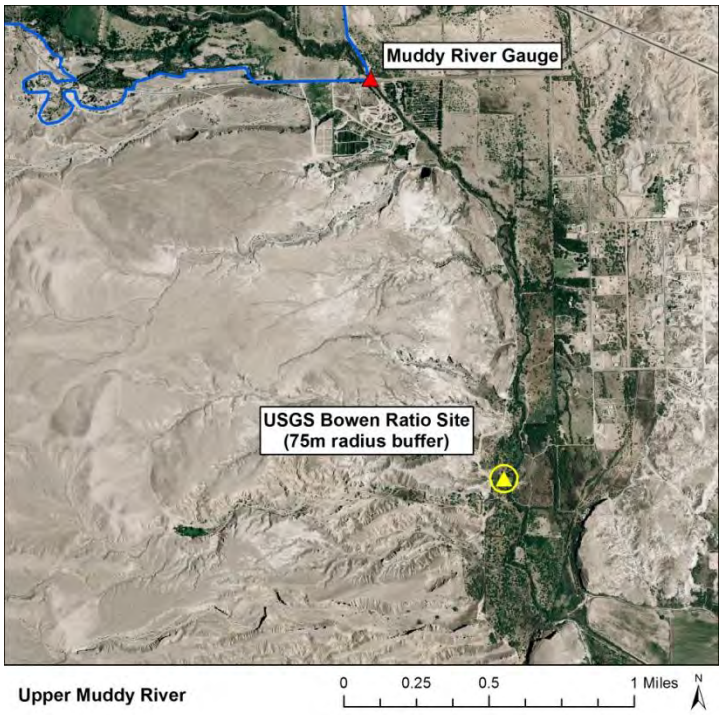

Figure 24. USGS Bowen Ratio Energy Balance station to compare METRIC and NDVI ET estimates to for 2003-2006.

Figure 25. USGS Bowen Ratio Energy Balance station located in the Muddy River area. Modified figure from DeMeo et al. (2008).

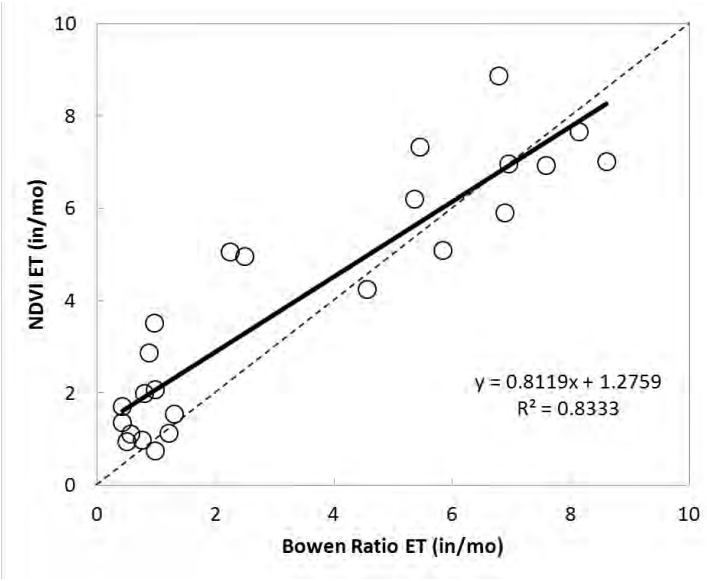

Figure 25. Bowen Ratio Energy Balance estimated monthly ET and NDVI estimated monthly ET from 2003-2006 (with several months of missing data).

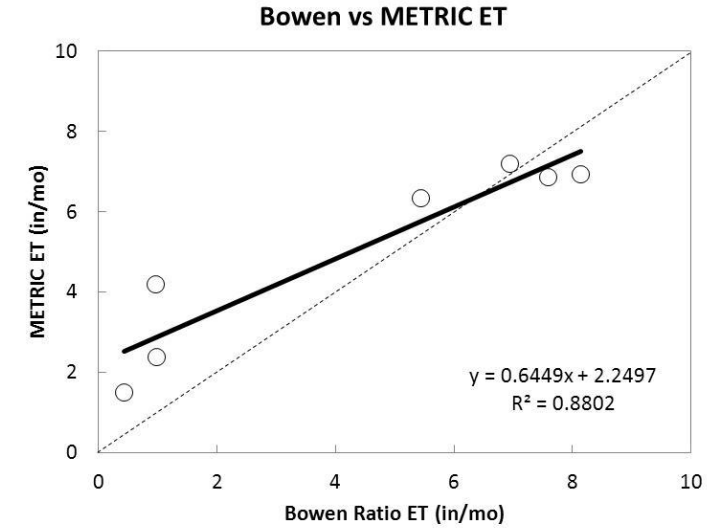

Figure 26. Bowen Ratio Energy Balance estimated monthly ET and METRIC estimated monthly ET from February-August of 2006 (only data available for METRIC comparison).

While the DeMeo et al. (2008) study from 2003-2006 estimated the average *ET* to be 3.6 ft/yr, there were over 271 missing days, many of which were in the spring and summer of 2004 and 2005. As previously indicated, annual *ET* totals reported by DeMeo et al. (2008) were computed by summing period of record daily average *ET* rates (i.e., 365 daily average values). Using daily averages from multiple years is a general approach for gap filling daily *ET* data, and in this case for computing an average annual *ET* rate, however, such averaging and filling approaches do not consider *ET* variability caused by precipitation. For example, a large portion of summer 2005, which was exceptionally wet in the preceding months, was filled with daily average summer values from 2004 and 2006, which were preceded by relatively wet and dry periods, respectively (Figure 14, Table A5). The impact of this type of summation is likely causing a biased low average annual *ET* estimate in this case. As a result of missing data, an accurate comparison of METRIC and NDVI estimated annual *ET* is not possible. For reporting purposes, Bowen station NDVI estimated *ET* ranged from 5.6 ft/yr to 3.9 ft/yr for 2005 and 2006, respectively, with an average annual estimate of 4.3 ft/yr from 2003 -2006. For purposes of making a more respective cumulative *ET* comparison, a comparison was made between the Bowen station, METRIC, and NDVI *ET* over the longest continuous record at the Bowen *ET* station from February-August 2006. Results indicate that Bowen station, METRIC, and NDVI estimated *ET* over this period is 30.5 in, 35.4 in, and 36.2 in, respectively (Figure 27).

Comparing to previous work of DeMeo et al. (2008) revealed that METRIC and NDVI estimated *ET* is likely biased high during low *ET* periods. This bias could be due to inaccuracies of METRIC during the cool season caused by small differences in METRIC surface temperatures at extreme ET conditions (i.e., hot and cold pixel temperature values at dry and well irrigated conditions are nearly the same). Additionally, NDVI bias during the cool period likely exists due to the presence of background NDVI from bare soil and vegetation during fall and winter senescence and dormancy periods, along with inaccuracies in the statistical model between NDVI and ET_rF. In general, the comparison between Bowen station *ET* and METRIC and NDVI estimated *ET* is considered fairly robust given that *ET* estimates generally fall within the uncertainty of Bowen station *ET* estimates, which is likely around 10-15% (Allander et al., 2009). It is difficult to judge the quality of these Bowen ratio *ET* data given that there is extremely limited description on Bowen ratio station instrumentation, and station setup and deployment, such as reporting the make and model of net radiometer and ground heat flux plates, number of soil heat flux plates used, discussion on methods for computing soil heat storage and soil heat flux, filtering of erroneous Bowen ratio values, QAQC of net radiation and ground heat flux, soil moisture measurements, etc., all of which are critical aspects for *ET* measurement reporting (Allen et al., 2011b).

Summary

This study evaluated over 300 Landsat TM and ETM+ images to assess potential changes in *ET* over the Muddy River Springs area from 2001-2012. Results suggest that *ET* has declined from 2001-2012 independent of *PPT* changes. Changes in *ET* are primarily due to to changes in ET_r, and to a lesser extent, due to changes in ET_rF. Reduction of annual *ET-PPT* ranges between -600 to -900 ac-ft. The -600 ac-ft rounded value is derived from the METRIC estimated *ET-PPT* rate of change of -0.062 ft/yr over the period of 2006-2012, and applied to the 12 year period

of 2001-2012 (Table A6). The -900 ac-ft rounded value is derived from the NDVI estimated *ET-PPT* rate of change of -0.095 ft/yr over the period of 2001-2012, and is applied to the 12 year period of 2001-2012 (Table A9). Comparisons between METRIC and NDVI, and Bowen ratio station estimated *ET* in the Muddy River Springs area from 2003-2006 are favorable and are generally within the uncertainty of Bowen station *ET* estimates.

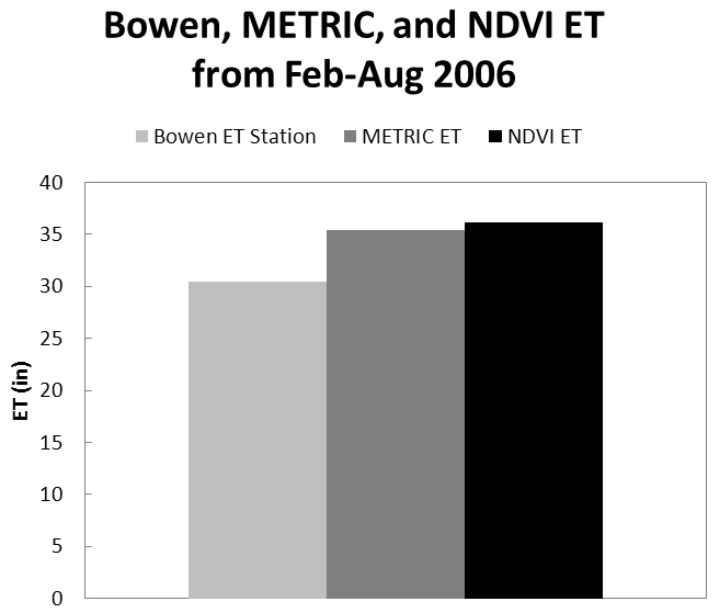

Figure 27. Comparison of total estimated ET from Feb-Aug. 2006 between the Bowen station METRIC, and NDVI. The Feb-Aug. 2006 period was the longest continuous data record for the Bowen station.

References

Allander, K. K., J. L. Smith, and M. J. Johnson (2009). Evapotranspiration from the lower Walker River basin, west-central Nevada, water years 2005–07, U.S. Geol. Sur. Sci. Invest. Rep. 2009-5079, 62 pp.

Allen, R.G. (1996). Assessing Integrity of Weather Data for use in Reference Evapotranspiration estimation. Journal of Irrigation and Drainage Engineering, ASCE. 122(2), 97-106 pp.

Allen, R.G., Pereira, L.S., Raes, D. and Smith, M. (1998). Crop Evapotranspiration: Guidelines for Computing Crop Water Requirements. Irrigation and Drainage Paper 56, Food and Agriculture Organization of the United Nations, Rome, 300 p.

Allen, R. G. (2011). *REF-ET: Version - Windows 3.1.10*. University of Idaho.

Allen, R.G., Pereira, L., Howell, T., and M. E. Jensen (2011a). Evapotranspiration information reporting: I. Factors governing measurement accuracy. *Agricultural Water Management*, 98, 899-920.

Allen, R.G., Pereira, L., Howell, T., and M. E. Jensen (2011b). Evapotranspiration information reporting: II. Recommended documentation. *Agricultural Water Management*, 98, 921-929.

ASCI-EWRI (2005). The ASCE Standardized Reference Evapotranspiration Equation. Report 0-7844-0805-X, ASCE Task Committee on Standardization of Reference Evapotranspiration. Reston, VA., American Society of Civil Engineers.

Bos, M., Kselik, R., Allen, R., & Molden, D. (2008). *Water Requirements for Irrigation and the Environment.* Springer.

Calera-Belmonte, A., Jochum, A.M., Cuesta-Garcia, A., Montoro-Rodriguez, A., Lopez- Fuster, P. (2005). Irrigation management from space: towards user-friendly products. *Irrigation Drainage Systems* 19, 337–353.

Choudhury, B.J., Ahmed, N.U., Idaho, S.B., Reginato, R.J., Daughtry, C.S.T. (1994). Relations between evaporation coefficients and vegetation indices: studies by model simulation. *Remote Sensing Environment* 50, 1–17.

Daly, C., R. P. Neilson, and D. L. Phillips (1994). A statistical-topographic model for mapping climatological precipitation over mountainous terrain. *Journal of Applied Meteorology* 33, 140-158.

DeMeo, G.A., Smith, J.L., Damar, N.A., and Darnell, Jon (2008). Quantifying ground-water and surface-water discharge from evapotranspiration processes in 12 hydrographic areas of the Colorado Regional Ground-Water Flow System, Nevada, Utah, and Arizona: U.S. Geological Survey Scientific Investigations Report 2008-5116, 22 p.

Eakin, T.E. (1964). Ground-water appraisal of Coyote Spring and Kane Spring Valleys and Muddy River Springs area, Lincoln and Clark Counties, Nevada: Nevada Department of Conservation and Natural Resources, Ground-Water Resources Reconnaissance Series, Report 25, 40 p.

Eakin, T. E. (1966). A Regional Interbasin Groundwater System in the White River Area, Southeastern Nevada. *Water Resources Research* 2, 251-271.

Heilman, J. L., Heilman, W. E., and Moore, D. G. (1982). Evaluating the Crop Coefficient Using Spectral Radiance. *Agronomy Journal 74*, 967-971.

Hendrickx, J.M.H. (2010). ET Mapping in the Green River Basin - Second Stage, Growing Season (2009). Final Report to the University of Wyoming. Soil Hydrology Associates, LLC, Los Lunas, NM.

Groeneveld, D.P., W.M. Baugh, J.S. Sanderson, and D.J. Cooper (2007). Annual Groundwater Evapotranspiration Mapped from Single Satellite Scenes. *Journal of Hydrology* 344:146-156. DOI:10.1016/j.jhydrol.2007.07.002.

Kjaersagaard, J. and R.G. Allen (2010). Remote Sensing Technology to Produce Consumptive Water Use Maps for the Nebraska Panhandle. Final completion report submitted to the University of Nebraska. 60 p.

Masek, J. G., E. F. Vermote, N. Saleous, R. Wolfe, F. G. Hall, F. Huemmrich, F. Gao, J. Kutler, and T. K. Lim (2006). A Landsat surface reflectance data set for North America, 1990–2000, *Geoscience Remote Sensing Letters* 3, 68–72.

Moreo, M.T., R.J. Laczniak, and D.I. Stannard (2007). Evapotranspiration Rate Measurements of Vegetation Typical of Groundwater Discharge Areas in the Basin and Range Carbonate-Rock Aquifer System, White Pine County, Nevada, and Adjacent Areas in Nevada and Utah, September 2005-August 2006. U.S. Geological Survey Scientific Investigations Report 2007-5078, 36 pp. http://pubs.usgs.gov/sir/2007/5078.

Morton, C., Huntington, J.L., Pohll, G., Allen, R., McGwire, K., Bassett, S. (2013). Assessing Calibration Uncertainty and Automation for Estimating Evapotranspiration from Agricultural Areas Using METRIC. *Journal of the American Water Resources Association.* In Press.

Nagler, P.L., R.L. Scott, C. Westenburg, J.R. Cleverly, E.P. Glenn, and A.H. Huete (2005). Evapotranspiration on Western U.S. Rivers Estimated Using the Enhanced Vegetation Index from MODIS and Data from Eddy Covariance and Bowen Ratio Flux Towers. *Remote Sensing of Environment* 97(3):337-351. DOI:10.1016/j.rse.2005.05.011

Schuepp, P.H., LeClerc, M.Y., Macpherson, J.I., and Desjardins, R.L. (1990). Footprint prediction of scalar fluxes from analytical solutions of the diffusion equation: Boundary-Layer Meteorology, v. 50, p. 355-373.

Singh, R. and Irmak, A. (2009). Estimation of crop coefficients using satellite remote sensing. *Journal of Irrigation Drainage Engineering, ASCE* 135 (5), 597–608.

Smith, J.L., R.J. Laczniak, M.T. Moreo, and T.L. Welborn (2007). Mapping Evapotranspiration units in the Basin and Range Carbonate-Rock Aquifer System, White Pine County, Nevada, and Adjacent Areas in Nevada and Utah. U.S. Geological Survey Scientific Investigations Report 2007–5087, 31 p. http://pubs.usgs.gov/sir/2007/5087/

Snyder, D.T., Risley, J.C., and Haynes, J.V. (2012). Hydrological information products for the Off-Project Water Program of the Klamath Basin Restoration Agreement: U.S. Geological Survey Open-File Report 2012–1199, 20 p., http://pubs.usgs.gov/of/2012/1199

Sullivan, A., Huntington, J., and Morton, C. (2011). Remote Sensing of Consumptive Use in the Walker River Basin, Nevada. American Water Resource Association Annual Conference, Albuquerque, NM, 2011. http://www.awra.org/meetings/ABQ2011/doc/abs/Sess%2029%20abs.pdf, http://awra.org/annual2011/doc/pres/S29-Sullivan.pdf

Tasumi, M., Allen, R.G. (2007). Satellite-based ET mapping to assess variation in ET with timing of crop development. *Agriculture Water Management* 88 (1–3), 54–62.

Tasumi, M., Allen, R.G., Trezza, R., and Wright, J.L. (2005). Satellite-based energy balance to assess within-population variance of crop coefficient curves. *Journal Irrigation Drainage Engineering* 131 (1), 94–109.

Appendix

Table A1. Listing of Landsat scenes and ET and precipitation results using METIC, NDVI, and EVI methods. Landsat 5 (TM), Landsat ETM, and Landsat ETM SLC off were all used for NDVI and METRIC ET estimates. Landsat ETM SLC off did not impact the quality of ET estimates in the Muddy River Springs area, as SLC gaps were not present in the study area due to the Muddy River Springs area being located in the center of Landsat ETM scenes.

Count	SCENE_ID	DATE	YEAR	DOY	SENSOR	NDVI ET	METRIC ET
1	LT50390352001006XXX02	1/6/2001	2001	6	LANDSAT_TM	x	
2	LE70390352001014EDC00	1/14/2001	2001	14	LANDSAT_ETM	x	
3	LE70390352001030EDC00	1/30/2001	2001	30	LANDSAT_ETM	x	
4	LE70390352001046EDC00	2/15/2001	2001	46	LANDSAT_ETM	x	
5	LT50390352001054XXX02	2/23/2001	2001	54	LANDSAT_TM	x	
6	LE70390352001062EDC01	3/3/2001	2001	62	LANDSAT_ETM	x	
7	LE70390352001078EDC00	3/19/2001	2001	78	LANDSAT_ETM	x	
8	LT50390352001102XXX02	4/12/2001	2001	102	LANDSAT_TM	x	
9	LT50390352001118XXX02	4/28/2001	2001	118	LANDSAT_TM	x	
10	LE70390352001126EDC00	5/6/2001	2001	126	LANDSAT_ETM	x	
11	LT50390352001134AAA02	5/14/2001	2001	134	LANDSAT_TM	x	
12	LE70390352001142EDC00	5/22/2001	2001	142	LANDSAT_ETM	x	
13	LT50390352001150AAA02	5/30/2001	2001	150	LANDSAT_TM	x	
14	LE70390352001158EDC00	6/7/2001	2001	158	LANDSAT_ETM	x	
15	LT50390352001166XXX02	6/15/2001	2001	166	LANDSAT_TM	x	
16	LE70390352001174EDC00	6/23/2001	2001	174	LANDSAT_ETM	x	
17	LT50390352001182LGS03	7/1/2001	2001	182	LANDSAT_TM	x	
18	LE70390352001190EDC00	7/9/2001	2001	190	LANDSAT_ETM	x	
19	LT50390352001214LGS01	8/2/2001	2001	214	LANDSAT_TM	x	
20	LE70390352001222EDC00	8/10/2001	2001	222	LANDSAT_ETM	x	
21	LT50390352001230LGS01	8/18/2001	2001	230	LANDSAT_TM	x	
22	LE70390352001238EDC00	8/26/2001	2001	238	LANDSAT_ETM	x	
23	LT50390352001246LGS01	9/3/2001	2001	246	LANDSAT_TM	x	
24	LT50390352001262LGS01	9/19/2001	2001	262	LANDSAT_TM	x	
25	LE70390352001270EDC00	9/27/2001	2001	270	LANDSAT_ETM	x	
26	LE70390352001286EDC00	10/13/2001	2001	286	LANDSAT_ETM	x	
27	LT50390352001310LGS01	11/6/2001	2001	310	LANDSAT_TM	x	
28	LE70390352001318EDC00	11/14/2001	2001	318	LANDSAT_ETM	x	
29	LT50390352001342LGS01	12/8/2001	2001	342	LANDSAT_TM	x	
30	LE70390352001350EDC00	12/16/2001	2001	350	LANDSAT_ETM	x	
31	LT50390352001358LGS01	12/24/2001	2001	358	LANDSAT_TM	x	

32	LE70390352002017EDC00	1/17/2002	2002	17	LANDSAT_ETM	x	
33	LE70390352002033EDC00	2/2/2002	2002	33	LANDSAT_ETM	x	
34	LT50390352002041EDC01	2/10/2002	2002	41	LANDSAT_TM	x	
35	LT50390352002057LGS01	2/26/2002	2002	57	LANDSAT_TM	x	
36	LE70390352002081EDC00	3/22/2002	2002	81	LANDSAT_ETM	x	
37	LT50390352002089LGS01	3/30/2002	2002	89	LANDSAT_TM	x	
38	LE70390352002097EDC00	4/7/2002	2002	97	LANDSAT_ETM	x	
39	LT50390352002105LGS01	4/15/2002	2002	105	LANDSAT_TM	x	
40	LT50390352002121LGS03	5/1/2002	2002	121	LANDSAT_TM	x	
41	LE70390352002129EDC00	5/9/2002	2002	129	LANDSAT_ETM	x	
42	LT50390352002137LGS01	5/17/2002	2002	137	LANDSAT_TM	x	
43	LE70390352002145EDC01	5/25/2002	2002	145	LANDSAT_ETM	x	
44	LE70390352002161EDC00	6/10/2002	2002	161	LANDSAT_ETM	x	
45	LT50390352002169LGS03	6/18/2002	2002	169	LANDSAT_TM	x	
46	LE70390352002177EDC00	6/26/2002	2002	177	LANDSAT_ETM	x	
47	LT50390352002185EDC02	7/4/2002	2002	185	LANDSAT_TM	x	
48	LE70390352002193EDC00	7/12/2002	2002	193	LANDSAT_ETM	x	
49	LT50390352002201LGS01	7/20/2002	2002	201	LANDSAT_TM	x	
50	LE70390352002209EDC00	7/28/2002	2002	209	LANDSAT_ETM	x	
51	LE70390352002225EDC00	8/13/2002	2002	225	LANDSAT_ETM	x	
52	LT50390352002233LGS01	8/21/2002	2002	233	LANDSAT_TM	x	
53	LE70390352002241EDC00	8/29/2002	2002	241	LANDSAT_ETM	x	
54	LE70390352002257EDC00	9/14/2002	2002	257	LANDSAT_ETM	x	
55	LT50390352002265LGS01	9/22/2002	2002	265	LANDSAT_TM	x	
56	LE70390352002273EDC00	9/30/2002	2002	273	LANDSAT_ETM	x	
57	LT50390352002281LGS01	10/8/2002	2002	281	LANDSAT_TM	x	
58	LE70390352002289EDC00	10/16/2002	2002	289	LANDSAT_ETM	x	
59	LT50390352002297LGS01	10/24/2002	2002	297	LANDSAT_TM	x	
60	LE70390352002305EDC00	11/1/2002	2002	305	LANDSAT_ETM	x	
61	LE70390352002337EDC00	12/3/2002	2002	337	LANDSAT_ETM	x	
62	LE70390352002353EDC00	12/19/2002	2002	353	LANDSAT_ETM	x	
63	LT50390352002361LGS01	12/27/2002	2002	361	LANDSAT_TM	x	
64	LE70390352003020EDC00	1/20/2003	2003	20	LANDSAT_ETM	x	
65	LT50390352003028LGS01	1/28/2003	2003	28	LANDSAT_TM	x	
66	LE70390352003052EDC01	2/21/2003	2003	52	LANDSAT_ETM	x	
67	LE70390352003068EDC00	3/9/2003	2003	68	LANDSAT_ETM	x	
68	LT50390352003092LGS01	4/2/2003	2003	92	LANDSAT_TM	x	
69	LE70390352003100EDC00	4/10/2003	2003	100	LANDSAT_ETM	x	
70	LE70390352003116EDC00	4/26/2003	2003	116	LANDSAT_ETM	x	
71	LT50390352003124LGS01	5/4/2003	2003	124	LANDSAT_TM	x	
72	LT50390352003140LGS01	5/20/2003	2003	140	LANDSAT_TM	x	

73	LE70390352003148EDC00	5/28/2003	2003	148	LANDSAT_ETM	x	
74	LT50390352003156LGS01	6/5/2003	2003	156	LANDSAT_TM	x	
75	LT50390352003172EDC03	6/21/2003	2003	172	LANDSAT_TM	x	
76	LT50390352003188PAC02	7/7/2003	2003	188	LANDSAT_TM	x	
77	LE70390352003212EDC02	7/31/2003	2003	212	LANDSAT_ETM_SLC_OFF	x	
78	LT50390352003220PAC04	8/8/2003	2003	220	LANDSAT_TM	x	
79	LE70390352003244EDC01	9/1/2003	2003	244	LANDSAT_ETM_SLC_OFF	x	
80	LT50390352003252PAC02	9/9/2003	2003	252	LANDSAT_TM	x	
81	LE70390352003260EDC02	9/17/2003	2003	260	LANDSAT_ETM_SLC_OFF	x	
82	LE70390352003276EDC02	10/3/2003	2003	276	LANDSAT_ETM_SLC_OFF	x	
83	LT50390352003284LGS01	10/11/2003	2003	284	LANDSAT_TM	x	
84	LE70390352003308EDC01	11/4/2003	2003	308	LANDSAT_ETM_SLC_OFF	x	
85	LT50390352003348PAC02	12/14/2003	2003	348	LANDSAT_TM	x	
86	LE70390352003356EDC01	12/22/2003	2003	356	LANDSAT_ETM_SLC_OFF	x	
87	LT50390352004015PAC02	1/15/2004	2004	15	LANDSAT_TM	x	
88	LE70390352004023EDC01	1/23/2004	2004	23	LANDSAT_ETM_SLC_OFF	x	
89	LE70390352004039EDC01	2/8/2004	2004	39	LANDSAT_ETM_SLC_OFF	x	
90	LT50390352004063PAC02	3/3/2004	2004	63	LANDSAT_TM	x	
91	LE70390352004071EDC02	3/11/2004	2004	71	LANDSAT_ETM_SLC_OFF	x	
92	LT50390352004079PAC02	3/19/2004	2004	79	LANDSAT_TM	x	
93	LE70390352004087EDC02	3/27/2004	2004	87	LANDSAT_ETM_SLC_OFF	x	
94	LE70390352004103EDC02	4/12/2004	2004	103	LANDSAT_ETM_SLC_OFF	x	
95	LE70390352004119EDC03	4/28/2004	2004	119	LANDSAT_ETM_SLC_OFF	x	
96	LE70390352004135EDC01	5/14/2004	2004	135	LANDSAT_ETM_SLC_OFF	x	
97	LT50390352004143PAC02	5/22/2004	2004	143	LANDSAT_TM	x	
98	LE70390352004151EDC01	5/30/2004	2004	151	LANDSAT_ETM_SLC_OFF	x	
99	LT50390352004159PAC02	6/7/2004	2004	159	LANDSAT_TM	x	
100	LE70390352004167EDC01	6/15/2004	2004	167	LANDSAT_ETM_SLC_OFF	x	
101	LT50390352004175PAC02	6/23/2004	2004	175	LANDSAT_TM	x	
102	LT50390352004191PAC01	7/9/2004	2004	191	LANDSAT_TM	x	
103	LT50390352004207PAC02	7/25/2004	2004	207	LANDSAT_TM	x	
104	LT50390352004223PAC01	8/10/2004	2004	223	LANDSAT_TM	x	
105	LT50390352004239PAC01	8/26/2004	2004	239	LANDSAT_TM	x	
106	LE70390352004247EDC02	9/3/2004	2004	247	LANDSAT_ETM_SLC_OFF	x	
107	LE70390352004263EDC02	9/19/2004	2004	263	LANDSAT_ETM_SLC_OFF	x	
108	LT50390352004271EDC00	9/27/2004	2004	271	LANDSAT_TM	x	
109	LT50390352004287PAC01	10/13/2004	2004	287	LANDSAT_TM	x	
110	LT50390352004303PAC01	10/29/2004	2004	303	LANDSAT_TM	x	
111	LT50390352004319PAC01	11/14/2004	2004	319	LANDSAT_TM	x	
112	LT50390352004351PAC01	12/16/2004	2004	351	LANDSAT_TM	x	
113	LE70390352004359EDC00	12/24/2004	2004	359	LANDSAT_ETM_SLC_OFF	x	

114	LT50390352005017PAC01	1/17/2005	2005	17	LANDSAT_TM	x	
115	LT50390352005033PAC01	2/2/2005	2005	33	LANDSAT_TM	x	
116	LT50390352005065PAC01	3/6/2005	2005	65	LANDSAT_TM	x	
117	LE70390352005089EDC00	3/30/2005	2005	89	LANDSAT_ETM_SLC_OFF	x	
118	LE70390352005105EDC00	4/15/2005	2005	105	LANDSAT_ETM_SLC_OFF	x	
119	LT50390352005129PAC01	5/9/2005	2005	129	LANDSAT_TM	x	
120	LE70390352005137EDC00	5/17/2005	2005	137	LANDSAT_ETM_SLC_OFF	x	
121	LT50390352005145EDC00	5/25/2005	2005	145	LANDSAT_TM	x	
122	LE70390352005153EDC00	6/2/2005	2005	153	LANDSAT_ETM_SLC_OFF	x	
123	LT50390352005161PAC01	6/10/2005	2005	161	LANDSAT_TM	x	
124	LE70390352005169EDC00	6/18/2005	2005	169	LANDSAT_ETM_SLC_OFF	x	
125	LT50390352005177PAC01	6/26/2005	2005	177	LANDSAT_TM	x	
126	LT50390352005193PAC01	7/12/2005	2005	193	LANDSAT_TM	x	
127	LT50390352005209PAC01	7/28/2005	2005	209	LANDSAT_TM	x	
128	LT50390352005225PAC01	8/13/2005	2005	225	LANDSAT_TM	x	
129	LE70390352005233EDC00	8/21/2005	2005	233	LANDSAT_ETM_SLC_OFF	x	
130	LT50390352005241PAC01	8/29/2005	2005	241	LANDSAT_TM	x	
131	LE70390352005249EDC00	9/6/2005	2005	249	LANDSAT_ETM_SLC_OFF	x	
132	LT50390352005257PAC01	9/14/2005	2005	257	LANDSAT_TM	x	
133	LE70390352005265EDC00	9/22/2005	2005	265	LANDSAT_ETM_SLC_OFF	x	
134	LT50390352005273PAC01	9/30/2005	2005	273	LANDSAT_TM	x	
135	LT50390352005289PAC01	10/16/2005	2005	289	LANDSAT_TM	x	
136	LE70390352005297EDC00	10/24/2005	2005	297	LANDSAT_ETM_SLC_OFF	x	
137	LT50390352005321PAC01	11/17/2005	2005	321	LANDSAT_TM	x	
138	LE70390352005345EDC00	12/11/2005	2005	345	LANDSAT_ETM_SLC_OFF	x	
139	LT50390352006020EDC00	1/20/2006	2006	20	LANDSAT_TM	x	
140	LT50390352006036PAC01	2/5/2006	2006	36	LANDSAT_TM	x	x
141	LE70390352006044EDC00	2/13/2006	2006	44	LANDSAT_ETM_SLC_OFF	x	
142	LT50390352006052PAC01	2/21/2006	2006	52	LANDSAT_TM	x	
143	LE70390352006060EDC00	3/1/2006	2006	60	LANDSAT_ETM_SLC_OFF	x	
144	LT50390352006068PAC01	3/9/2006	2006	68	LANDSAT_TM	x	x
145	LE70390352006092EDC00	4/2/2006	2006	92	LANDSAT_ETM_SLC_OFF	x	
146	LT50390352006100PAC01	4/10/2006	2006	100	LANDSAT_TM	x	x
147	LT50390352006116PAC01	4/26/2006	2006	116	LANDSAT_TM	x	x
148	LE70390352006124EDC00	5/4/2006	2006	124	LANDSAT_ETM_SLC_OFF	x	
149	LT50390352006132PAC01	5/12/2006	2006	132	LANDSAT_TM	x	x
150	LE70390352006140EDC00	5/20/2006	2006	140	LANDSAT_ETM_SLC_OFF	x	
151	LT50390352006148PAC01	5/28/2006	2006	148	LANDSAT_TM	x	x
152	LE70390352006156EDC00	6/5/2006	2006	156	LANDSAT_ETM_SLC_OFF	x	
153	LE70390352006172EDC00	6/21/2006	2006	172	LANDSAT_ETM_SLC_OFF	x	
154	LT50390352006180PAC01	6/29/2006	2006	180	LANDSAT_TM	x	x

155	LT50390352006196PAC01	7/15/2006	2006	196	LANDSAT_TM	x	x
156	LE70390352006204EDC00	7/23/2006	2006	204	LANDSAT_ETM_SLC_OFF	x	
157	LT50390352006212PAC02	7/31/2006	2006	212	LANDSAT_TM	x	x
158	LE70390352006220EDC00	8/8/2006	2006	220	LANDSAT_ETM_SLC_OFF	x	
159	LT50390352006228PAC01	8/16/2006	2006	228	LANDSAT_TM	x	x
160	LE70390352006236EDC00	8/24/2006	2006	236	LANDSAT_ETM_SLC_OFF	x	
161	LT50390352006260PAC01	9/17/2006	2006	260	LANDSAT_TM	x	x
162	LT50390352006276PAC01	10/3/2006	2006	276	LANDSAT_TM	x	x
163	LE70390352006284EDC00	10/11/2006	2006	284	LANDSAT_ETM_SLC_OFF	x	
164	LT50390352006292PAC01	10/19/2006	2006	292	LANDSAT_TM	x	x
165	LE70390352006300EDC00	10/27/2006	2006	300	LANDSAT_ETM_SLC_OFF	x	
166	LT50390352006308PAC01	11/4/2006	2006	308	LANDSAT_TM	x	x
167	LE70390352006316EDC00	11/12/2006	2006	316	LANDSAT_ETM_SLC_OFF	x	
168	LT50390352006324PAC01	11/20/2006	2006	324	LANDSAT_TM	x	x
169	LE70390352006332EDC00	11/28/2006	2006	332	LANDSAT_ETM_SLC_OFF	x	
170	LT50390352006340PAC01	12/6/2006	2006	340	LANDSAT_TM	x	x
171	LE70390352006364EDC00	12/30/2006	2006	364	LANDSAT_ETM_SLC_OFF	x	
172	LT50390352007007PAC01	1/7/2007	2007	7	LANDSAT_TM	x	
173	LE70390352007015EDC00	1/15/2007	2007	15	LANDSAT_ETM_SLC_OFF	x	
174	LT50390352007023PAC01	1/23/2007	2007	23	LANDSAT_TM	x	
175	LE70390352007047EDC00	2/16/2007	2007	47	LANDSAT_ETM_SLC_OFF	x	x
176	LT50390352007055PAC01	2/24/2007	2007	55	LANDSAT_TM	x	x
177	LE70390352007063EDC00	3/4/2007	2007	63	LANDSAT_ETM_SLC_OFF	x	
178	LT50390352007071PAC01	3/12/2007	2007	71	LANDSAT_TM	x	
179	LT50390352007103PAC01	4/13/2007	2007	103	LANDSAT_TM	x	
180	LE70390352007111EDC00	4/21/2007	2007	111	LANDSAT_ETM_SLC_OFF	x	
181	LT50390352007119PAC01	4/29/2007	2007	119	LANDSAT_TM	x	x
182	LE70390352007127EDC00	5/7/2007	2007	127	LANDSAT_ETM_SLC_OFF	x	x
183	LT50390352007135PAC01	5/15/2007	2007	135	LANDSAT_TM	x	x
184	LE70390352007143EDC00	5/23/2007	2007	143	LANDSAT_ETM_SLC_OFF	x	x
185	LT50390352007151PAC01	5/31/2007	2007	151	LANDSAT_TM	x	x
186	LE70390352007159EDC00	6/8/2007	2007	159	LANDSAT_ETM_SLC_OFF	x	x
187	LT50390352007167PAC01	6/16/2007	2007	167	LANDSAT_TM	x	x
188	LE70390352007175EDC00	6/24/2007	2007	175	LANDSAT_ETM_SLC_OFF	x	x
189	LT50390352007183PAC01	7/2/2007	2007	183	LANDSAT_TM	x	x
190	LE70390352007191EDC00	7/10/2007	2007	191	LANDSAT_ETM_SLC_OFF	x	
191	LT50390352007199PAC01	7/18/2007	2007	199	LANDSAT_TM	x	x
192	LT50390352007215PAC01	8/3/2007	2007	215	LANDSAT_TM	x	x
193	LE70390352007223EDC00	8/11/2007	2007	223	LANDSAT_ETM_SLC_OFF	x	x
194	LT50390352007247PAC01	9/4/2007	2007	247	LANDSAT_TM	x	x
195	LE70390352007255EDC00	9/12/2007	2007	255	LANDSAT_ETM_SLC_OFF	x	x

196	LE70390352007287EDC00	10/14/2007	2007	287	LANDSAT_ETM_SLC_OFF	x	x
197	LE70390352007303EDC00	10/30/2007	2007	303	LANDSAT_ETM_SLC_OFF	x	x
198	LE70390352007319EDC00	11/15/2007	2007	319	LANDSAT_ETM_SLC_OFF	x	x
199	LE70390352007351EDC00	12/17/2007	2007	351	LANDSAT_ETM_SLC_OFF	x	
200	LE70390352008018EDC00	1/18/2008	2008	18	LANDSAT_ETM_SLC_OFF	x	
201	LT50390352008026EDC00	1/26/2008	2008	26	LANDSAT_TM	x	
202	LT50390352008042EDC00	2/11/2008	2008	42	LANDSAT_TM	x	
203	LT50390352008058PAC01	2/27/2008	2008	58	LANDSAT_TM	x	
204	LE70390352008066EDC00	3/6/2008	2008	66	LANDSAT_ETM_SLC_OFF	x	x
205	LT50390352008074PAC01	3/14/2008	2008	74	LANDSAT_TM	x	
206	LE70390352008082EDC00	3/22/2008	2008	82	LANDSAT_ETM_SLC_OFF	x	x
207	LE70390352008098EDC00	4/7/2008	2008	98	LANDSAT_ETM_SLC_OFF	x	x
208	LT50390352008106PAC01	4/15/2008	2008	106	LANDSAT_TM	x	
209	LE70390352008114EDC00	4/23/2008	2008	114	LANDSAT_ETM_SLC_OFF	x	x
210	LT50390352008122PAC01	5/1/2008	2008	122	LANDSAT_TM	x	x
211	LE70390352008130EDC00	5/9/2008	2008	130	LANDSAT_ETM_SLC_OFF	x	x
212	LT50390352008138PAC01	5/17/2008	2008	138	LANDSAT_TM	x	x
213	LT50390352008154PAC01	6/2/2008	2008	154	LANDSAT_TM	x	x
214	LE70390352008162EDC00	6/10/2008	2008	162	LANDSAT_ETM_SLC_OFF	x	
215	LT50390352008170PAC01	6/18/2008	2008	170	LANDSAT_TM	x	x
216	LE70390352008178EDC00	6/26/2008	2008	178	LANDSAT_ETM_SLC_OFF	x	x
217	LT50390352008234PAC01	8/21/2008	2008	234	LANDSAT_TM	x	x
218	LE70390352008242EDC00	8/29/2008	2008	242	LANDSAT_ETM_SLC_OFF	x	x
219	LT50390352008250PAC01	9/6/2008	2008	250	LANDSAT_TM	x	x
220	LE70390352008258EDC00	9/14/2008	2008	258	LANDSAT_ETM_SLC_OFF	x	x
221	LT50390352008266PAC01	9/22/2008	2008	266	LANDSAT_TM	x	x
222	LE70390352008274EDC00	9/30/2008	2008	274	LANDSAT_ETM_SLC_OFF	x	x
223	LT50390352008282PAC01	10/8/2008	2008	282	LANDSAT_TM	x	x
224	LE70390352008290EDC00	10/16/2008	2008	290	LANDSAT_ETM_SLC_OFF	x	x
225	LT50390352008298PAC01	10/24/2008	2008	298	LANDSAT_TM	x	x
226	LE70390352008322EDC00	11/17/2008	2008	322	LANDSAT_ETM_SLC_OFF	x	x
227	LE70390352008338EDC00	12/3/2008	2008	338	LANDSAT_ETM_SLC_OFF	x	
228	LE70390352009004EDC00	1/4/2009	2009	4	LANDSAT_ETM_SLC_OFF	x	
229	LT50390352009012PAC01	1/12/2009	2009	12	LANDSAT_TM	x	
230	LE70390352009020EDC00	1/20/2009	2009	20	LANDSAT_ETM_SLC_OFF	x	
231	LT50390352009092PAC01	4/2/2009	2009	92	LANDSAT_TM	x	x
232	LT50390352009108PAC01	4/18/2009	2009	108	LANDSAT_TM	x	x
233	LE70390352009116EDC00	4/26/2009	2009	116	LANDSAT_ETM_SLC_OFF	x	x
234	LE70390352009132EDC02	5/12/2009	2009	132	LANDSAT_ETM_SLC_OFF	x	x
235	LT50390352009140PAC01	5/20/2009	2009	140	LANDSAT_TM	x	x
236	LE70390352009148EDC00	5/28/2009	2009	148	LANDSAT_ETM_SLC_OFF	x	x

237	LT50390352009172PAC01	6/21/2009	2009	172	LANDSAT_TM	x	x
238	LE70390352009180EDC00	6/29/2009	2009	180	LANDSAT_ETM_SLC_OFF	x	x
239	LT50390352009188PAC01	7/7/2009	2009	188	LANDSAT_TM	x	x
240	LE70390352009196EDC00	7/15/2009	2009	196	LANDSAT_ETM_SLC_OFF	x	x
241	LE70390352009212EDC00	7/31/2009	2009	212	LANDSAT_ETM_SLC_OFF	x	x
242	LT50390352009220PAC01	8/8/2009	2009	220	LANDSAT_TM	x	x
243	LE70390352009228EDC00	8/16/2009	2009	228	LANDSAT_ETM_SLC_OFF	x	x
244	LT50390352009236PAC01	8/24/2009	2009	236	LANDSAT_TM	x	x
245	LT50390352009252PAC01	9/9/2009	2009	252	LANDSAT_TM	x	x
246	LE70390352009260EDC00	9/17/2009	2009	260	LANDSAT_ETM_SLC_OFF	x	x
247	LT50390352009268PAC01	9/25/2009	2009	268	LANDSAT_TM	x	x
248	LT50390352009284PAC01	10/11/2009	2009	284	LANDSAT_TM	x	x
249	LE70390352009292EDC00	10/19/2009	2009	292	LANDSAT_ETM_SLC_OFF	x	x
250	LE70390352009308EDC00	11/4/2009	2009	308	LANDSAT_ETM_SLC_OFF	x	x
251	LE70390352009324EDC00	11/20/2009	2009	324	LANDSAT_ETM_SLC_OFF	x	x
252	LT50390352009332PAC01	11/28/2009	2009	332	LANDSAT_TM	x	x
253	LE70390352009340EDC00	12/6/2009	2009	340	LANDSAT_ETM_SLC_OFF	x	
254	LT50390352009348PAC01	12/14/2009	2009	348	LANDSAT_TM	x	
255	LT50390352010015PAC01	1/15/2010	2010	15	LANDSAT_TM	x	
256	LT50390352010031PAC01	1/31/2010	2010	31	LANDSAT_TM	x	
257	LT50390352010047PAC01	2/16/2010	2010	47	LANDSAT_TM	x	x
258	LE70390352010071EDC00	3/12/2010	2010	71	LANDSAT_ETM_SLC_OFF	x	
259	LT50390352010079PAC01	3/20/2010	2010	79	LANDSAT_TM	x	
260	LE70390352010087EDC00	3/28/2010	2010	87	LANDSAT_ETM_SLC_OFF	x	x
261	LE70390352010103EDC00	4/13/2010	2010	103	LANDSAT_ETM_SLC_OFF	x	x
262	LT50390352010111PAC01	4/21/2010	2010	111	LANDSAT_TM	x	
263	LT50390352010127PAC01	5/7/2010	2010	127	LANDSAT_TM	x	x
264	LE70390352010135EDC00	5/15/2010	2010	135	LANDSAT_ETM_SLC_OFF	x	x
265	LT50390352010143PAC01	5/23/2010	2010	143	LANDSAT_TM	x	x
266	LE70390352010151EDC00	5/31/2010	2010	151	LANDSAT_ETM_SLC_OFF	x	x
267	LE70390352010167EDC00	6/16/2010	2010	167	LANDSAT_ETM_SLC_OFF	x	x
268	LT50390352010175EDC00	6/24/2010	2010	175	LANDSAT_TM	x	x
269	LE70390352010183EDC00	7/2/2010	2010	183	LANDSAT_ETM_SLC_OFF	x	
270	LE70390352010199EDC00	7/18/2010	2010	199	LANDSAT_ETM_SLC_OFF	x	x
271	LE70390352010215EDC00	8/3/2010	2010	215	LANDSAT_ETM_SLC_OFF	x	x
272	LT50390352010223EDC00	8/11/2010	2010	223	LANDSAT_TM	x	x
273	LE70390352010231EDC00	8/19/2010	2010	231	LANDSAT_ETM_SLC_OFF	x	x
274	LT50390352010239EDC00	8/27/2010	2010	239	LANDSAT_TM	x	x
275	LE70390352010247EDC00	9/4/2010	2010	247	LANDSAT_ETM_SLC_OFF	x	x
276	LE70390352010263EDC00	9/20/2010	2010	263	LANDSAT_ETM_SLC_OFF	x	x
277	LT50390352010271EDC00	9/28/2010	2010	271	LANDSAT_TM	x	x

278	LE70390352010279EDC00	10/6/2010	2010	279	LANDSAT_ETM_SLC_OFF	x	
279	LT50390352010287EDC00	10/14/2010	2010	287	LANDSAT_TM	x	x
280	LE70390352010311EDC00	11/7/2010	2010	311	LANDSAT_ETM_SLC_OFF	x	x
281	LT50390352010319PAC01	11/15/2010	2010	319	LANDSAT_TM	x	x
282	LE70390352010327EDC00	11/23/2010	2010	327	LANDSAT_ETM_SLC_OFF	x	
283	LT50390352010335EDC00	12/1/2010	2010	335	LANDSAT_TM	x	x
284	LE70390352011042EDC00	2/11/2011	2011	42	LANDSAT_ETM_SLC_OFF	x	x
285	LT50390352011082PAC01	3/23/2011	2011	82	LANDSAT_TM	x	x
286	LE70390352011090EDC00	3/31/2011	2011	90	LANDSAT_ETM_SLC_OFF	x	x
287	LE70390352011106EDC00	4/16/2011	2011	106	LANDSAT_ETM_SLC_OFF	x	x
288	LT50390352011114PAC01	4/24/2011	2011	114	LANDSAT_TM	x	x
289	LT50390352011146PAC01	5/26/2011	2011	146	LANDSAT_TM	x	x
290	LE70390352011154EDC00	6/3/2011	2011	154	LANDSAT_ETM_SLC_OFF	x	x
291	LT50390352011162PAC01	6/11/2011	2011	162	LANDSAT_TM	x	x
292	LE70390352011170EDC00	6/19/2011	2011	170	LANDSAT_ETM_SLC_OFF	x	x
293	LT50390352011178PAC01	6/27/2011	2011	178	LANDSAT_TM	x	x
294	LT50390352011194PAC01	7/13/2011	2011	194	LANDSAT_TM	x	x
295	LE70390352011202EDC00	7/21/2011	2011	202	LANDSAT_ETM_SLC_OFF	x	x
296	LT50390352011210PAC01	7/29/2011	2011	210	LANDSAT_TM	x	x
297	LE70390352011218EDC00	8/6/2011	2011	218	LANDSAT_ETM_SLC_OFF	x	x
298	LT50390352011226PAC01	8/14/2011	2011	226	LANDSAT_TM	x	x
299	LE70390352011234EDC00	8/22/2011	2011	234	LANDSAT_ETM_SLC_OFF	x	x
300	LT50390352011242PAC01	8/30/2011	2011	242	LANDSAT_TM	x	x
301	LE70390352011250EDC00	9/7/2011	2011	250	LANDSAT_ETM_SLC_OFF	x	x
302	LT50390352011258PAC01	9/15/2011	2011	258	LANDSAT_TM	x	x
303	LE70390352011266EDC00	9/23/2011	2011	266	LANDSAT_ETM_SLC_OFF	x	x
304	LE70390352011298EDC00	10/25/2011	2011	298	LANDSAT_ETM_SLC_OFF	x	x
305	LT50390352011306PAC01	11/2/2011	2011	306	LANDSAT_TM	x	x
306	LE70390352011330EDC00	11/26/2011	2011	330	LANDSAT_ETM_SLC_OFF	x	x
307	LE70390352012013EDC00	1/13/2012	2012	13	LANDSAT_ETM_SLC_OFF	x	
308	LE70390352012029EDC00	1/29/2012	2012	29	LANDSAT_ETM_SLC_OFF	x	
309	LE70390352012061EDC00	3/1/2012	2012	61	LANDSAT_ETM_SLC_OFF	x	x
310	LE70390352012093EDC00	4/2/2012	2012	93	LANDSAT_ETM_SLC_OFF	x	x
311	LE70390352012109EDC04	4/18/2012	2012	109	LANDSAT_ETM_SLC_OFF	x	x
312	LE70390352012125EDC00	5/4/2012	2012	125	LANDSAT_ETM_SLC_OFF	x	x
313	LE70390352012141EDC00	5/20/2012	2012	141	LANDSAT_ETM_SLC_OFF	x	x
314	LE70390352012157EDC00	6/5/2012	2012	157	LANDSAT_ETM_SLC_OFF	x	x
315	LE70390352012173EDC00	6/21/2012	2012	173	LANDSAT_ETM_SLC_OFF	x	x
316	LE70390352012189EDC01	7/7/2012	2012	189	LANDSAT_ETM_SLC_OFF	x	x
317	LE70390352012205EDC00	7/23/2012	2012	205	LANDSAT_ETM_SLC_OFF	x	
318	LE70390352012221EDC00	8/8/2012	2012	221	LANDSAT_ETM_SLC_OFF	x	x

319	LE70390352012237EDC00	8/24/2012	2012	237	LANDSAT_ETM_SLC_OFF	x	x
320	LE70390352012269EDC00	9/25/2012	2012	269	LANDSAT_ETM_SLC_OFF	x	x
321	LE70390352012301EDC00	10/27/2012	2012	301	LANDSAT_ETM_SLC_OFF	x	x
322	LE70390352012317EDC00	11/12/2012	2012	317	LANDSAT_ETM_SLC_OFF	x	x
323	LE70390352012333EDC00	11/28/2012	2012	333	LANDSAT_ETM_SLC_OFF	x	x

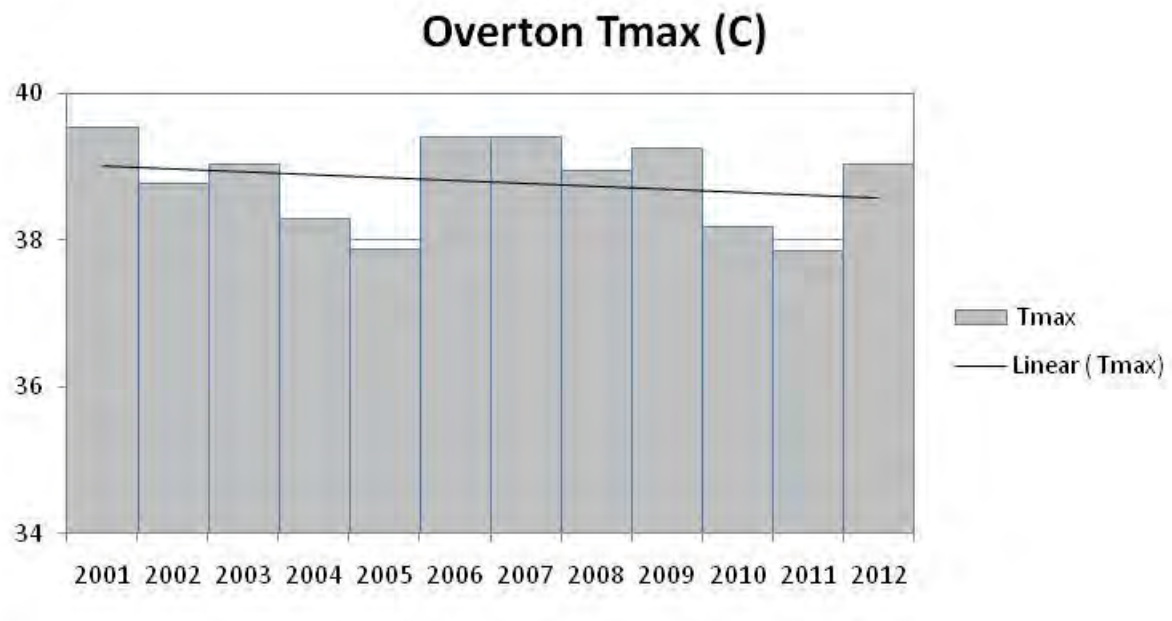

Figure A1. Overton CEMP warm season (May-September) average daily maximum temperature (Tmax).

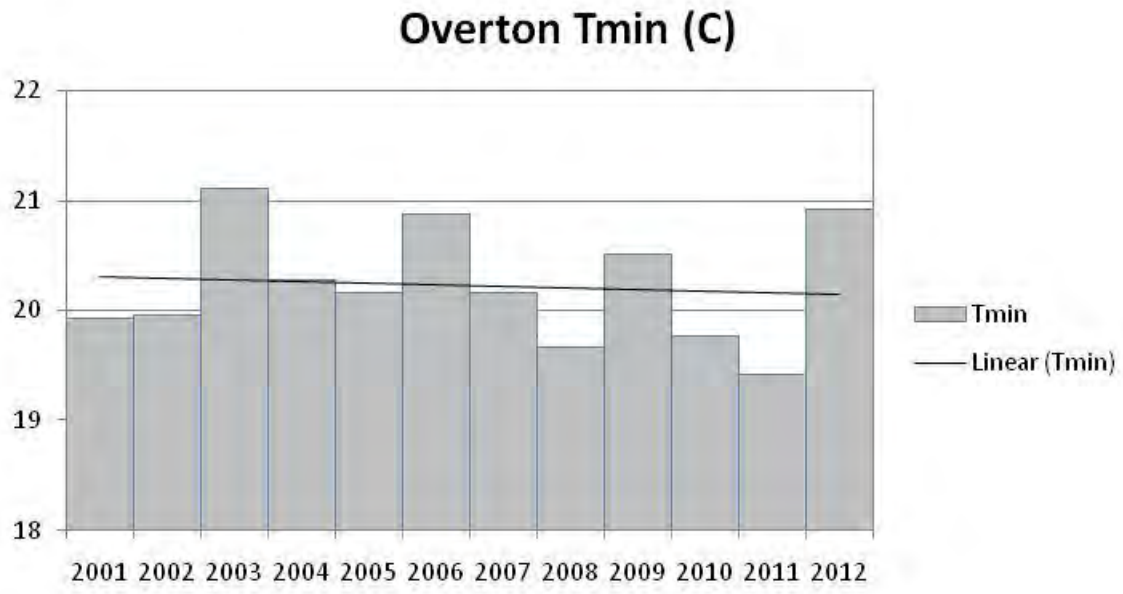

Figure A2. Overton CEMP warm season (May-September) average daily minimum temperature (Tmin).

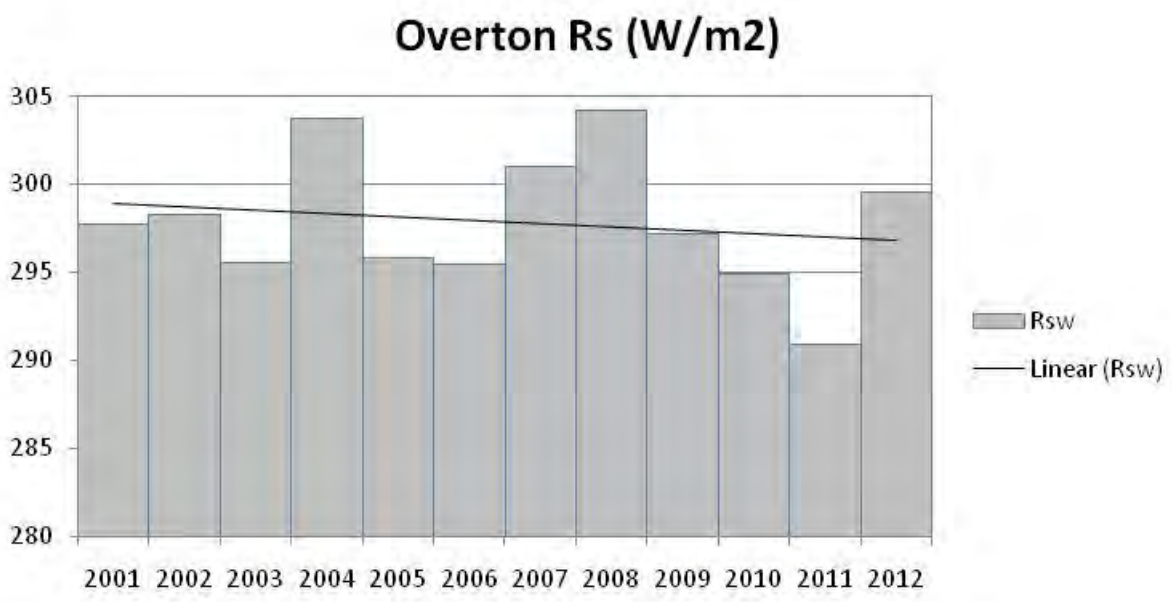

Figure A3. Overton CEMP warm season (May-September) average daily solar radiation (Rs).

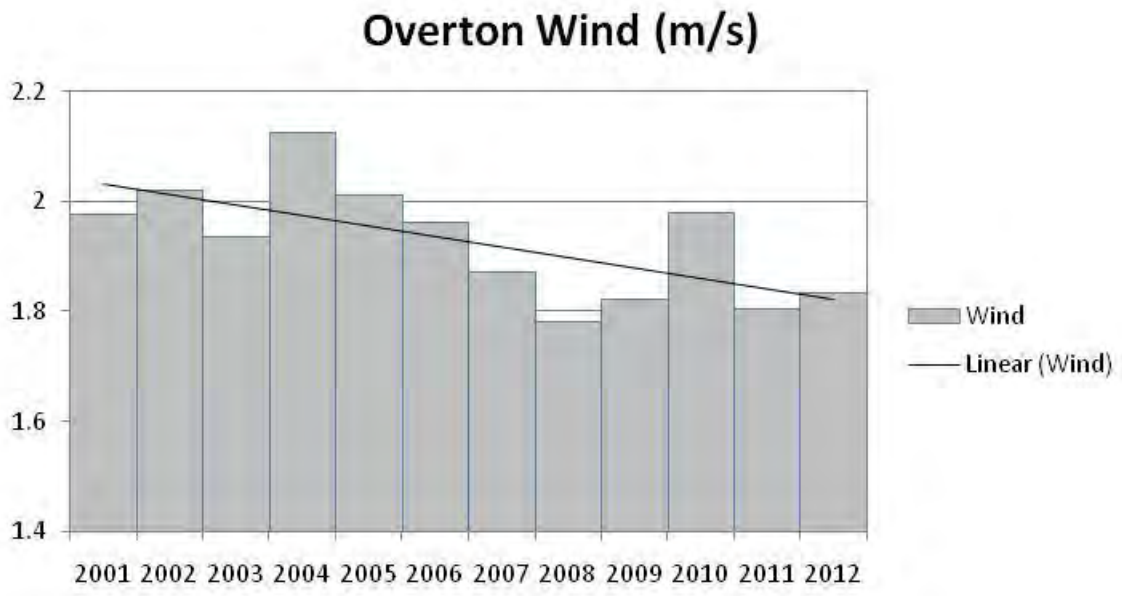

Figure A4. Overton CEMP warm season (May-September) average daily 6m height windspeed.

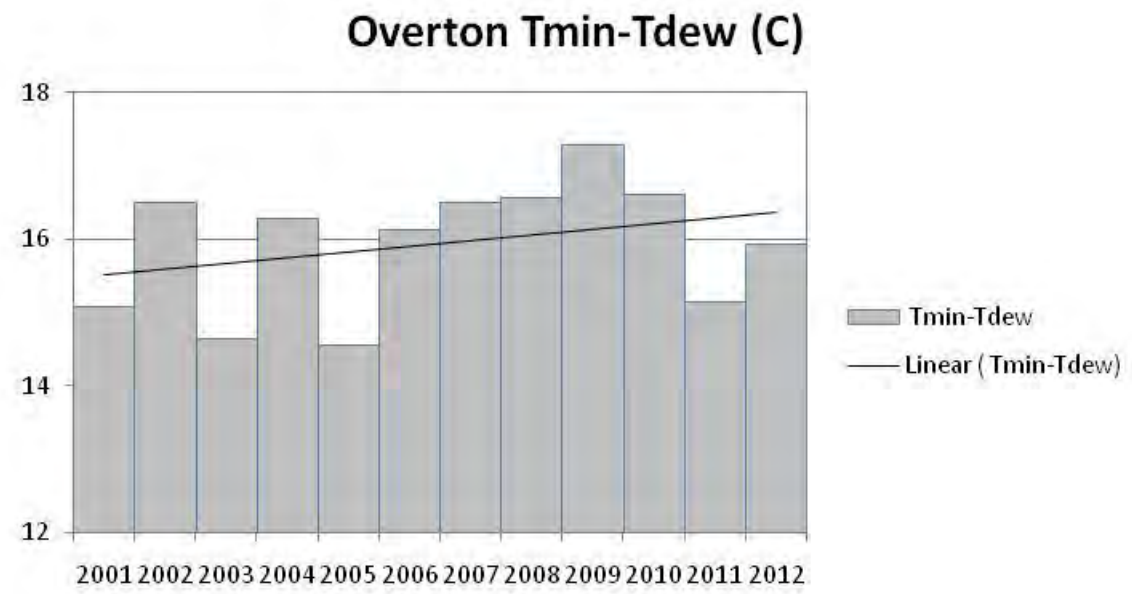

Figure A5. Overton CEMP warm season (May-September) average daily minimum temperature minus dewpoint temperature (i.e. dewpoint depression).

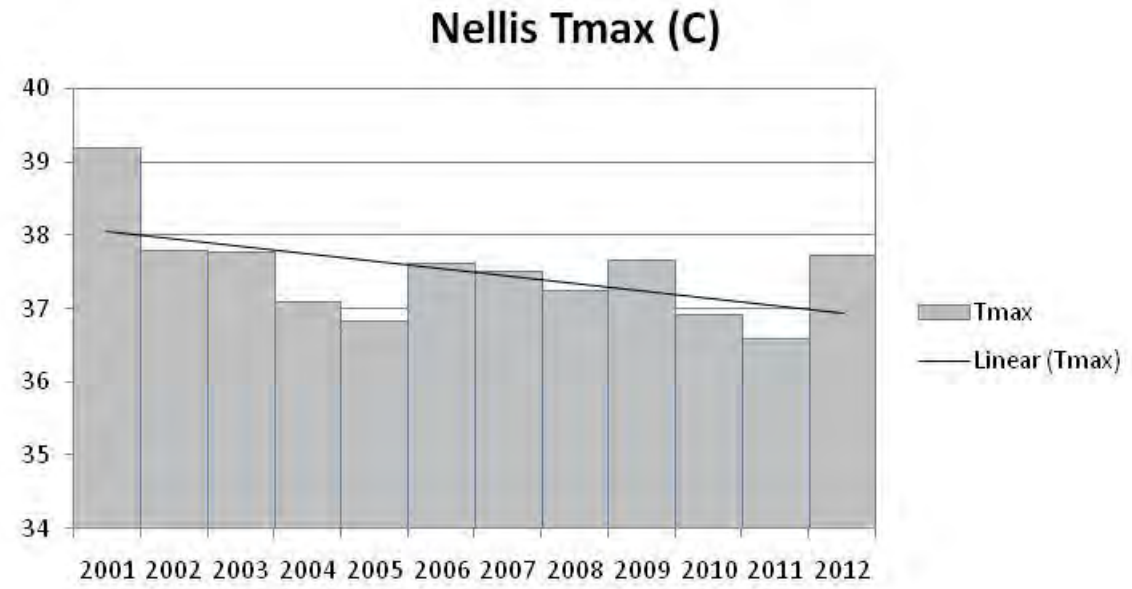

Figure A6. Nellis AFB warm season (May-September) average daily maximum temperature (Tmax).

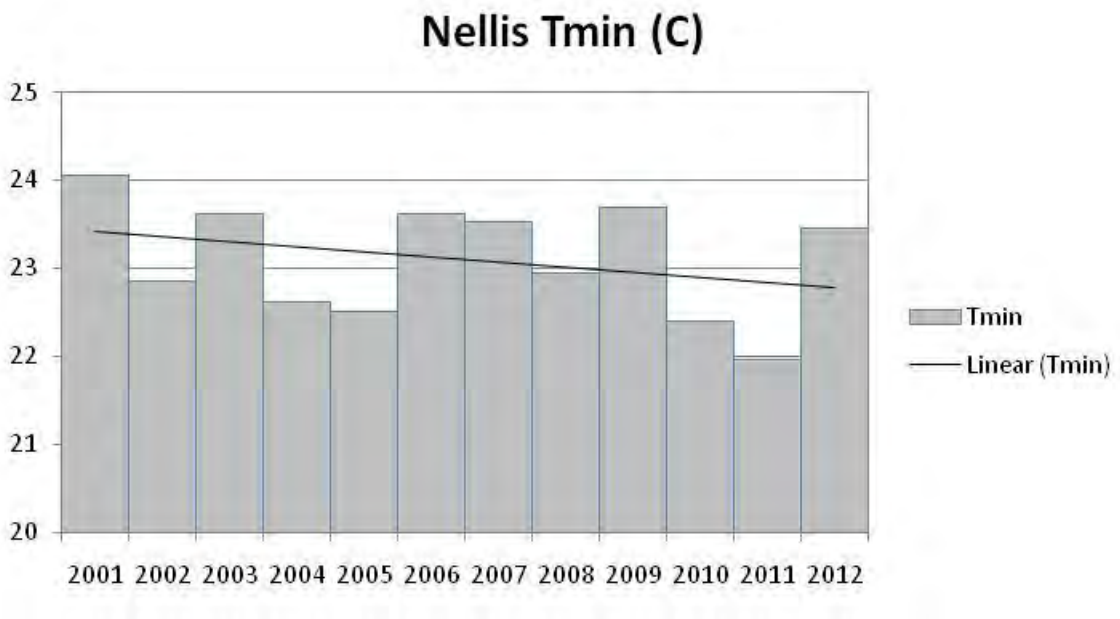

Figure A7. Nellis AFB warm season (May-September) average daily minimum temperature (Tmin).

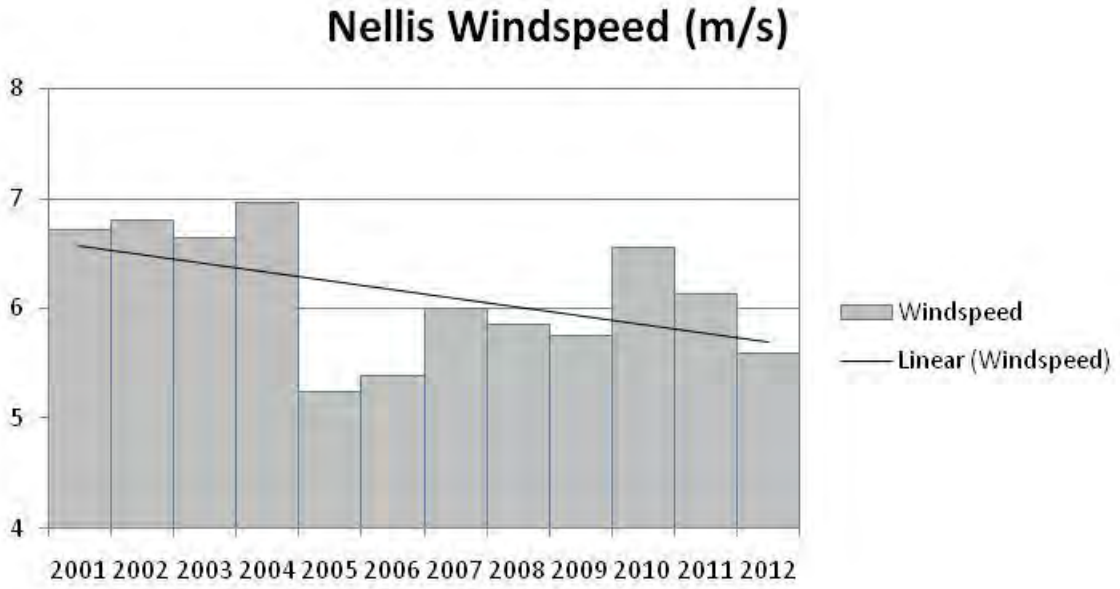

Figure A8. Nellis AFB warm season (May-September) average daily 10m height windspeed.

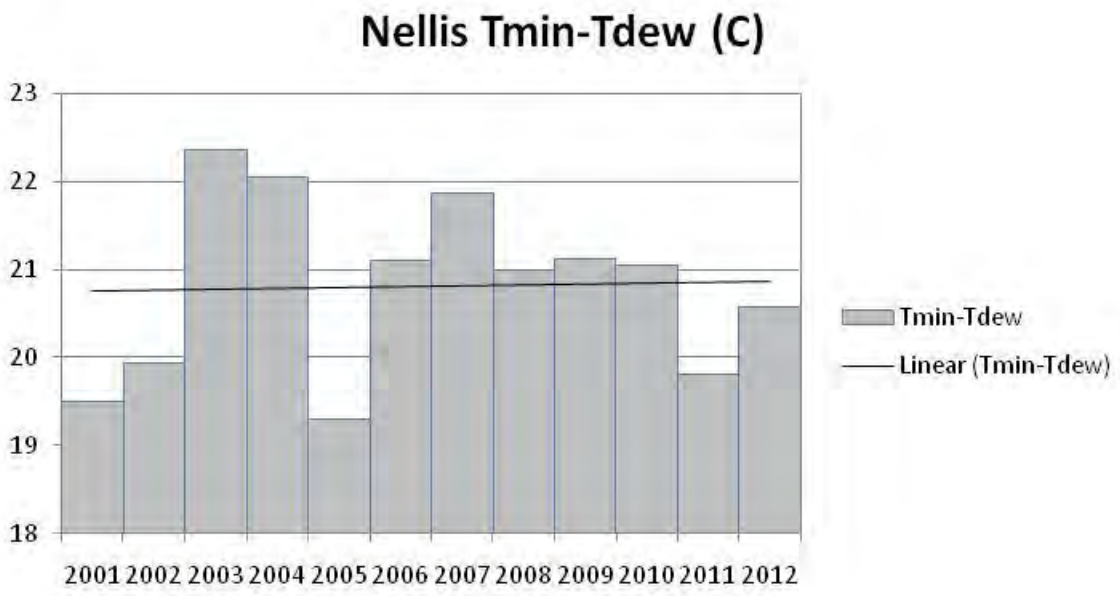

Figure A9. Nellis AFB warm season (May-September) average daily minimum temperature minus dewpoint temperature (i.e. dewpoint depression).

Table A2. Muddy River Springs METRIC *ET* from 2006-2012.

Warm Springs Area METRIC ET (ft)

Month	2006	2007	2008	2009	2010	2011	2012
1	0.11	0.09	0.09	0.10	0.08	0.08	0.11
2	0.12	0.10	0.10	0.10	0.11	0.06	0.13
3	0.20	0.21	0.19	0.23	0.29	0.09	0.18
4	0.38	0.31	0.35	0.26	0.42	0.28	0.30
5	0.54	0.39	0.40	0.46	0.58	0.39	0.47
6	0.54	0.45	0.45	0.48	0.66	0.50	0.53
7	0.59	0.46	0.50	0.57	0.51	0.51	0.44
8	0.51	0.43	0.51	0.56	0.38	0.51	0.44
9	0.41	0.39	0.39	0.44	0.31	0.33	0.39
10	0.22	0.21	0.26	0.26	0.14	0.22	0.28
11	0.10	0.12	0.14	0.13	0.09	0.11	0.13
12	0.09	0.08	0.07	0.09	0.06	0.10	0.08
Seasonal (ft)	3.61	3.08	3.28	3.48	3.48	3.00	3.29
Annual (ft)	3.80	3.24	3.44	3.67	3.62	3.18	3.48

Mean Seasonal (ft)	3.32
Mean Annual (ft)	3.49
Seasonal Slope (ft/yr)	-0.03
Annual Slope (ft/yr)	-0.03
Warm Springs Area (acres)	797
2006-2012 Seasonal Change (ft)	-0.23
2006-2012 Seasonal Change (ac-ft)	-181
2006-2012 Annual Change (ft)	-0.23
2006-2012 Annual Change (ac-ft)	-181

Table A3. Overton CEMP alfalfa reference *ET* (ET_r) for estimating of METRIC *ET* and NDVI *ET*.

Alfalfa Reference ET (ft)

Month	2001	2002	2003	2004	2005	2006	2007	2008	2009	2010	2011	2012
1	0.21	0.25	0.25	0.24	0.17	0.27	0.25	0.23	0.25	0.19	0.22	0.25
2	0.27	0.38	0.29	0.26	0.26	0.35	0.29	0.30	0.25	0.22	0.29	0.33
3	0.39	0.52	0.49	0.62	0.52	0.45	0.53	0.55	0.56	0.50	0.44	0.57
4	0.73	0.76	0.78	0.71	0.65	0.73	0.70	0.82	0.72	0.65	0.70	0.71
5	1.04	1.00	0.93	1.00	0.90	1.00	0.96	0.91	0.93	0.90	0.85	1.01
6	1.14	1.13	1.14	1.04	1.05	1.02	1.02	1.01	0.94	1.02	1.04	1.10
7	1.14	1.08	1.05	1.04	0.97	0.94	0.99	0.98	1.00	1.03	0.91	0.91
8	0.92	1.05	0.86	0.94	0.80	0.95	0.90	0.88	0.90	0.95	0.87	0.78
9	0.73	0.71	0.77	0.76	0.75	0.68	0.71	0.63	0.75	0.61	0.57	0.59
10	0.48	0.46	0.58	0.46	0.50	0.40	0.46	0.45	0.54	0.40	0.39	0.43
11	0.29	0.35	0.23	0.24	0.27	0.25	0.28	0.26	0.29	0.29	0.23	0.24
12	0.17	0.17	0.18	0.20	0.22	0.21	0.17	0.15	0.19	0.14	0.21	0.18
Seasonal (ft)	7.12	7.43	7.13	7.06	6.67	6.76	6.84	6.79	6.88	6.59	6.29	6.66
Annual (ft)	7.51	7.85	7.56	7.51	7.06	7.24	7.26	7.17	7.32	6.92	6.72	7.09

2001-2012 Mean Seasonal (ft)	6.85
2001-2012 Mean Annual (ft)	7.27
2006-2012 Mean Seasonal (ft)	6.69
2006-2012 Mean Annual (ft)	7.10
2001-2012 Seasonal Slope (ft/yr)	-0.068
2001-2012 Annual Slope (ft/yr)	-0.069
2006-2012 Seasonal Slope (ft/yr)	-0.057
2006-2012 Annual Slope (ft/yr)	-0.064
2001-2012 Seasonal Change (ft)	-0.82
2006-2012 Seasonal Change (ft)	-0.40
2001-2012 Annual Change (ft)	-0.83
2006-2012 Annual Change (ft)	-0.45

Table A4. Muddy River Springs METRIC fraction of alfalfa reference ET (ET_rF) from 2006-2012. Values with * indicate that NDVI was used to estimate ET_rF using function described in text.

METRIC ETrF

Month	2006	2007	2008	2009	2010	2011	2012
1	0.39*	0.36*	0.37*	0.38*	0.40*	0.39*	0.42*
2	0.34	0.33	0.33*	0.39*	0.49	0.20	0.38*
3	0.45	0.40	0.35	0.41*	0.57	0.22	0.32
4	0.52	0.45	0.42	0.37	0.64	0.40	0.42
5	0.54	0.41	0.45	0.50	0.64	0.46	0.46
6	0.53	0.44	0.44	0.51	0.65	0.48	0.48
7	0.63	0.47	0.51	0.56	0.50	0.57	0.48
8	0.53	0.48	0.58	0.62	0.40	0.59	0.57
9	0.60	0.55	0.61	0.59	0.50	0.57	0.66
10	0.55	0.47	0.58	0.48	0.36	0.55	0.64
11	0.39	0.41	0.54	0.44	0.30	0.45	0.56
12	0.34*	0.38*	0.38*	0.38*	0.45*	0.45*	0.45*
Seasonal	0.51	0.44	0.48	0.49	0.50	0.45	0.50
Annual	0.48	0.43	0.46	0.47	0.49	0.44	0.49

Mean Seasonal	0.48
Mean Annual	0.47
Seasonal Slope	0.0005
Annual Slope	0.0026
Seasonal Change	0.003
Annual Change	0.018

Table A5. Muddy River Springs PRISM Precipitation from 2001-2012.

Warm Springs Area PRISM Precipitation (ft)

Month	2001	2002	2003	2004	2005	2006	2007	2008	2009	2010	2011	2012
1	0.123	0.001	0.004	0.010	0.192	0.016	0.013	0.069	0.025	0.187	0.002	0.003
2	0.122	0.000	0.154	0.156	0.215	0.001	0.025	0.050	0.107	0.115	0.073	0.018
3	0.073	0.006	0.072	0.016	0.046	0.092	0.004	0.006	0.000	0.053	0.026	0.023
4	0.016	0.000	0.041	0.083	0.044	0.007	0.010	0.000	0.014	0.009	0.010	0.037
5	0.001	0.000	0.002	0.001	0.004	0.001	0.000	0.017	0.001	0.002	0.021	0.000
6	0.000	0.000	0.000	0.002	0.009	0.010	0.000	0.000	0.002	0.000	0.000	0.000
7	0.013	0.014	0.012	0.009	0.033	0.069	0.052	0.034	0.021	0.003	0.043	0.007
8	0.033	0.000	0.056	0.027	0.039	0.000	0.039	0.021	0.002	0.047	0.004	0.142
9	0.000	0.019	0.009	0.009	0.004	0.015	0.075	0.005	0.005	0.002	0.048	0.068
10	0.000	0.029	0.001	0.119	0.104	0.121	0.000	0.020	0.002	0.108	0.095	0.063
11	0.023	0.015	0.044	0.171	0.007	0.000	0.090	0.055	0.004	0.014	0.030	0.000
12	0.022	0.013	0.065	0.176	0.005	0.016	0.039	0.089	0.054	0.292	0.018	0.085
Seasonal (ft)	0.281	0.084	0.389	0.593	0.505	0.315	0.294	0.208	0.158	0.353	0.351	0.358
Annual (ft)	0.426	0.097	0.458	0.779	0.701	0.346	0.346	0.366	0.238	0.832	0.371	0.446

2001-2012 Mean Seasonal (ft)	0.32
2001-2012 Mean Annual (ft)	0.45
2006-2012 Mean Seasonal (ft)	0.29
2006-2012 Mean Annual (ft)	0.42
2001-2012 Seasonal Slope (ft/yr)	0.000
2001-2012 Annual Slope (ft/yr)	0.006
2006-2012 Seasonal Slope (ft/yr)	0.014
2006-2012 Annual Slope (ft/yr)	0.029
Warm Springs Area (acres)	797
2001-2012 Seasonal Change (ft)	0.00
2001-2012 Seasonal Change (ac-ft)	-3
2006-2012 Seasonal Change (ft)	0.10

2006-2012 Seasonal Change (ac-ft)	78
2001-2012 Annual Change (ft)	0.07
2001-2012 Annual Change (ac-ft)	53
2006-2012 Annual Change (ft)	0.20
2006-2012 Annual Change (ac-ft)	162

Table A6. Muddy River Springs METRIC ET minus PRISM precipitation from 2006-2012.

Warm Springs Area METRIC ET minus PRISM Precipitation (ft)

Month	2006	2007	2008	2009	2010	2011	2012
1	0.09	0.07	0.02	0.07	-0.11	0.08	0.10
2	0.12	0.07	0.05	-0.01	-0.01	-0.02	0.11
3	0.11	0.21	0.18	0.22	0.24	0.07	0.16
4	0.37	0.31	0.35	0.25	0.41	0.28	0.26
5	0.54	0.39	0.39	0.46	0.57	0.37	0.47
6	0.53	0.45	0.45	0.48	0.66	0.50	0.53
7	0.52	0.41	0.46	0.55	0.51	0.47	0.43
8	0.51	0.39	0.49	0.56	0.33	0.51	0.30
9	0.40	0.32	0.38	0.43	0.30	0.28	0.33
10	0.10	0.21	0.24	0.26	0.03	0.12	0.21
11	0.10	0.03	0.09	0.13	0.07	0.08	0.13
12	0.07	0.04	-0.02	0.03	-0.23	0.08	-0.01
Seasonal (ft)	3.29	2.78	3.07	3.33	3.13	2.65	2.93
Annual (ft)	3.45	2.90	3.07	3.43	2.79	2.81	3.03

Mean Seasonal (ft)	3.03
Mean Annual (ft)	3.07
Seasonal Slope (ft/yr)	-0.046
Annual Slope (ft/yr)	-0.062
Warm Springs Area (acres)	797
2006-2012 Seasonal Change (ft)	-0.32
2006-2012 Seasonal Change (ac-ft)	-258
2006-2012 Annual Change (ft)	-0.43
2006-2012 Annual Change (ac-ft)	-344

Table A7. Muddy River Springs ETrF of METRIC ET minus PRISM precipitation (METRIC ET-PPT)/ETr from 2006-2012.

METRIC ETrF of ET minus PRISM Precipitation

Month	2006	2007	2008	2009	2010	2011	2012
1	0.33	0.30	0.07	0.28	-0.59	0.38	0.41
2	0.34	0.24	0.16	-0.03	-0.03	-0.06	0.33
3	0.24	0.39	0.34	0.40	0.47	0.16	0.28
4	0.51	0.43	0.42	0.35	0.62	0.39	0.37
5	0.54	0.41	0.43	0.50	0.64	0.43	0.46
6	0.52	0.44	0.44	0.51	0.65	0.48	0.48
7	0.56	0.41	0.47	0.54	0.49	0.52	0.47
8	0.53	0.43	0.55	0.62	0.35	0.59	0.39
9	0.58	0.45	0.60	0.58	0.50	0.48	0.55
10	0.25	0.47	0.54	0.48	0.09	0.30	0.50
11	0.39	0.09	0.33	0.43	0.25	0.33	0.56
12	0.34	0.23	-0.15	0.18	-1.67	0.36	-0.03
Seasonal	0.45	0.38	0.43	0.44	0.40	0.36	0.44
Annual	0.43	0.36	0.35	0.40	0.15	0.36	0.40

Mean Seasonal	0.41
Mean Annual	0.35
Seasonal Slope	-0.003
Annual Slope	-0.010
Seasonal Change	-0.02
Annual Change	-0.07

Table A8. Muddy River Springs NDVI ET from 2001-2012.

Warm Springs Area NDVI Estimated ET (ft)

Month	2001	2002	2003	2004	2005	2006	2007	2008	2009	2010	2011	2012
1	0.09	0.10	0.09	0.09	0.08	0.11	0.09	0.09	0.10	0.08	0.08	0.11
2	0.10	0.15	0.11	0.09	0.14	0.14	0.10	0.10	0.10	0.10	0.09	0.13
3	0.19	0.21	0.19	0.26	0.36	0.18	0.21	0.21	0.23	0.22	0.16	0.22
4	0.45	0.37	0.38	0.42	0.48	0.34	0.36	0.39	0.34	0.36	0.30	0.31
5	0.72	0.55	0.54	0.60	0.67	0.58	0.55	0.50	0.55	0.54	0.43	0.52
6	0.77	0.65	0.64	0.66	0.79	0.61	0.60	0.60	0.60	0.64	0.58	0.59
7	0.74	0.63	0.60	0.66	0.68	0.56	0.56	0.60	0.66	0.43	0.53	0.49
8	0.58	0.61	0.51	0.60	0.61	0.57	0.56	0.56	0.57	0.46	0.52	0.43
9	0.46	0.44	0.45	0.49	0.57	0.40	0.44	0.40	0.47	0.35	0.33	0.34
10	0.30	0.27	0.34	0.29	0.34	0.23	0.26	0.27	0.31	0.21	0.22	0.26
11	0.16	0.17	0.12	0.13	0.16	0.12	0.15	0.14	0.16	0.15	0.12	0.13
12	0.08	0.07	0.07	0.10	0.11	0.09	0.08	0.07	0.09	0.06	0.10	0.08
Seasonal (ft)	4.47	4.05	3.87	4.19	4.81	3.74	3.78	3.77	3.98	3.47	3.28	3.42
Annual (ft)	4.64	4.23	4.04	4.38	5.00	3.93	3.94	3.93	4.17	3.60	3.46	3.60

2001-2012 Mean Seasonal (ft)	3.90
2001-2012 Mean Annual (ft)	4.08
2006-2012 Mean Seasonal (ft)	3.63
2006-2012 Mean Annual (ft)	3.80
2001-2012 Seasonal Slope (ft/yr)	-0.089
2001-2012 Annual Slope (ft/yr)	-0.090
2006-2012 Seasonal Slope (ft/yr)	-0.081
2006-2012 Annual Slope (ft/yr)	-0.081
Warm Springs Area (acres)	797
2001-2012 Seasonal Change (ft)	-1.07
2001-2012 Seasonal Change (ac-ft)	-851
2006-2012 Seasonal Change (ft)	-0.56

2006-2012 Seasonal Change (ac-ft)	-450
2001-2012 Annual Change (ft)	-1.07
2001-2012 Annual Change (ac-ft)	-856
2006-2012 Annual Change (ft)	-0.57
2006-2012 Annual Change (ac-ft)	-451

Table A9. Muddy River Springs NDVI ET minus PRISM Precipitation from 2001-2012.

Warm Springs Area NDVI Estimated ET minus PRISM Precipitation (ft)

Month	2001	2002	2003	2004	2005	2006	2007	2008	2009	2010	2011	2012
1	-0.04	0.10	0.09	0.08	-0.11	0.09	0.07	0.02	0.07	-0.11	0.08	0.10
2	-0.02	0.15	-0.05	-0.06	-0.07	0.14	0.07	0.05	-0.01	-0.02	0.02	0.11
3	0.12	0.20	0.12	0.25	0.31	0.09	0.21	0.20	0.22	0.17	0.13	0.19
4	0.43	0.37	0.34	0.34	0.43	0.34	0.35	0.39	0.33	0.35	0.29	0.28
5	0.72	0.55	0.53	0.60	0.67	0.58	0.55	0.49	0.55	0.54	0.41	0.52
6	0.77	0.65	0.64	0.66	0.78	0.60	0.60	0.60	0.60	0.64	0.58	0.59
7	0.73	0.62	0.59	0.65	0.65	0.49	0.51	0.57	0.64	0.42	0.48	0.48
8	0.55	0.61	0.45	0.57	0.57	0.57	0.52	0.54	0.57	0.41	0.51	0.28
9	0.45	0.42	0.44	0.48	0.57	0.39	0.36	0.39	0.46	0.35	0.28	0.28
10	0.30	0.24	0.33	0.17	0.24	0.11	0.26	0.25	0.31	0.11	0.13	0.19
11	0.14	0.16	0.08	-0.04	0.16	0.12	0.06	0.09	0.15	0.13	0.09	0.13
12	0.06	0.06	0.01	-0.08	0.10	0.07	0.04	-0.02	0.03	-0.23	0.08	-0.01
Seasonal (ft)	4.19	3.97	3.48	3.60	4.31	3.42	3.48	3.57	3.82	3.11	2.93	3.06
Annual (ft)	4.21	4.13	3.58	3.60	4.30	3.58	3.59	3.56	3.93	2.77	3.09	3.16

2001-2012 Mean Seasonal (ft)	3.58
2001-2012 Mean Annual (ft)	3.63
2006-2012 Mean Seasonal (ft)	3.34
2006-2012 Mean Annual (ft)	3.38
2001-2012 Seasonal Slope (ft/yr)	-0.089
2001-2012 Annual Slope (ft/yr)	-0.095
2006-2012 Seasonal Slope (ft/yr)	-0.095
2006-2012 Annual Slope (ft/yr)	-0.110
Warm Springs Area (acres)	797
2001-2012 Seasonal Change (ft)	-1.06
2001-2012 Seasonal Change (ac-ft)	-849
2006-2012 Seasonal Change (ft)	-0.66

2006-2012 Seasonal Change (ac-ft)	-528
2001-2012 Annual Change (ft)	-1.14
2001-2012 Annual Change (ac-ft)	-910
2006-2012 Annual Change (ft)	-0.77
2006-2012 Annual Change (ac-ft)	-613

Table A10. Muddy River Springs ETrF of NDVI ET minus PRISM precipitation (NDVI ET-PPT)/ETr) from 2001-2012.

NDVI ETrF of ET minus PRISM Precipitation

Month	2001	2002	2003	2004	2005	2006	2007	2008	2009	2010	2011	2012
1	-0.17	0.42	0.36	0.32	-0.66	0.33	0.30	0.07	0.28	-0.59	0.38	0.41
2	-0.07	0.39	-0.17	-0.24	-0.27	0.39	0.26	0.16	-0.03	-0.07	0.07	0.33
3	0.30	0.40	0.25	0.40	0.60	0.20	0.39	0.38	0.40	0.33	0.29	0.34
4	0.60	0.49	0.44	0.47	0.66	0.46	0.50	0.48	0.46	0.54	0.41	0.39
5	0.69	0.55	0.57	0.60	0.74	0.58	0.57	0.54	0.59	0.60	0.48	0.52
6	0.68	0.57	0.56	0.63	0.74	0.59	0.58	0.59	0.64	0.63	0.56	0.54
7	0.64	0.57	0.56	0.63	0.67	0.52	0.51	0.58	0.63	0.41	0.54	0.53
8	0.59	0.58	0.52	0.61	0.71	0.60	0.57	0.61	0.63	0.43	0.59	0.36
9	0.62	0.59	0.57	0.63	0.76	0.57	0.51	0.62	0.62	0.58	0.49	0.46
10	0.62	0.53	0.57	0.37	0.48	0.27	0.58	0.55	0.57	0.27	0.32	0.45
11	0.48	0.46	0.32	-0.18	0.58	0.49	0.20	0.32	0.52	0.44	0.37	0.54
12	0.36	0.34	0.05	-0.39	0.48	0.34	0.23	-0.15	0.18	-1.67	0.36	-0.03
Seasonal	0.52	0.51	0.42	0.39	0.57	0.47	0.47	0.48	0.50	0.42	0.41	0.45
Annual	0.45	0.49	0.38	0.32	0.46	0.45	0.43	0.40	0.46	0.16	0.41	0.40

Mean Seasonal	0.47
Mean Annual	0.40
Seasonal Slope	-0.005
Annual Slope	-0.008
Seasonal Change	-0.06
Annual Change	-0.10

ground water

The AEM and Regional Carbonate Aquifer Modeling

by Cady Johnson[1] and Martin Mifflin[2]

Abstract

The analytic element method (AEM) has been applied to a 15,000-km^2 area of the Paleozoic carbonate rock terrain of Nevada. The focus is the Muddy River springs area, which receives 1.44 m^3/s (51 ft^3/s) of regionally derived ground water, and forms the Muddy River. The study was undertaken early in 2000 to support the development of a cooling water supply for a gas-fired generation facility 20 km south of the Muddy River springs. The primary objectives of the AEM modeling were to establish a better understanding of regional fluxes and boundary conditions and to provide a framework for examination of more local transient effects using MODFLOW. Geochemical evidence available in 2000 suggested two separate flow fields, one in the north discharging at the springs, and a southern area of small hydraulic gradients. To be conservative, however, hydraulic continuity between the two areas was maintained in the 2000 AEM model. Using new monitoring well data collected in the south, and analyses confirming that seasonal pumping effects in the north are not propagated to the south, a later AEM model that included a barrier calibrated with relative ease. The analytic element model was well suited for simulating an area larger than the immediate area of interest, was easy to modify as more information became available, and facilitated the stepwise development of multiple conceptual models of the site.

Introduction

In 1989, Las Vegas Valley Water District (LVVWD) filed landmark applications for all unappropriated water, ~2.7 $\times$ 10^6 m^3/d (800,000 acre-ft/year) in 26 hydrographic basins of eastern Nevada, later reduced to a maximum of 6.1 $\times$ 10^5 m^3/d (180,800 acre-ft/year) in 17 basins. Alarmed by the potential impacts on springs and associated habitats, the National Park Service (NPS), U.S. Fish and Wildlife Service, Bureau of Land Management, and Bureau of Indian Affairs requested that the USGS quantitatively evaluate the effects of this pumping on regional flow and spring discharge. A highly generalized finite-difference model of the Carbonate Rock Province of the Great Basin was developed, consisting of two layers of 3660 cells, each 8.05 km (5 miles) wide by 12.1 km (7.5 miles) long (Schaefer and Harrill 1995). A flow reduction on the order of 11% was predicted at the Muddy River springs after 100 years of pumping. Conceptually, these results were not unanticipated but offer no guidance as to where the ground water resources might be developed to minimize or prevent impacts.

Beginning in 2000, the analytic element method (AEM) was adopted as a primary modeling strategy in evaluating flow patterns and boundary conditions in a large (15,000 km^2) area of carbonate rock terrain in southeastern Nevada, characterized by interbasin ground water flow and overlapping an area targeted for development by LVVWD. This application of the AEM, using GFLOW 2000 from Haitjema Software, was a departure from traditional methods in the region; previous modeling efforts generally relied on flux estimates based on hydrographic basin water budgets. In the AEM method, fluxes are determined from Darcian and mass conservation principles using aquifer characteristics and water-level data, with measured discharge of the Muddy River springs as a calibration target. The operational challenge of fitting model components to the geologic framework was aided by generally good regional exposures and was anchored by information from four local areas where characteristics of the carbonate aquifer were known from multiwell pumping experiments.

[1]Corresponding author: Mifflin & Associates Inc., HCR 38, Box 126, Las Vegas, NV 89124; ircady@yahoo.com; maihydrogeol@starband.net

[2]Mifflin & Associates Inc., HCR 38, Box 126, Las Vegas, NV 89124

Received June 2003, accepted May 2005.

doi: 10.1111/j.1745-6584.2005.00132.x

The primary objective of the study was to forecast impacts of a 25- to 45-year, 8.6×10^6 m^3/year (7000 acre-ft/year) pumping stress. Calpine Corporation would use the water for power generation at the proposed 750-MW Moapa Paiute Energy Center (MPEC). The MPEC wellfield targeted Paleozoic carbonate rocks that underlie much of the western portion of the Reservation. The first test well, ECP-1, yielded ~6.3×10^{-2} m^3/s (1000 US gallons/min) for a 7-d constant-discharge test. The fundamental question for the Calpine project was the relationship of the carbonate aquifer of the site area to the Muddy River springs, the flows of which support the endemic Moapa dace, an endangered fish that inhabits the spring areas, and to senior water rights on the Muddy River, which originates at the springs and is fully appropriated under Nevada water law. Potential long-term impacts on another major spring complex, Rogers and Blue Point Springs, located ~40 km southeast of the MPEC in the Lake Mead National Recreation Area, were a concern of the NPS.

The area extending some 15 km northwest from the Muddy River springs is a zone of extremely high transmissivities, with small hydraulic gradients indicating flow toward the Muddy River springs (Ertec Western Inc. 1981). In contrast, hydraulic gradients between 2 and 30 km south of the springs were not known at the beginning of this study, nor were the properties of the aquifer, so fluxes within the carbonate rock terrain of the Reservation could not be estimated (Mifflin 1992; Dettinger 1989). Ground water flux in the project area is of great practical interest from the standpoint of tribal water rights as the magnitude and pattern may ultimately determine the allowable level of development based on Nevada water law.

The objective of this paper is to describe the application of the AEM to a poorly understood subregional area with hydrogeology dominated by highly transmissive carbonate rock terrain, and supporting analyses that allowed for refinement of subregional boundary conditions. The paper's scope includes monitoring well databases through the end of the year 2002 and brief observations on data acquired since 2002.

Hydrogeology

In the broadest terms, the hydrogeologic setting of the study area is one of ground water discharge from large springs at the southeastern margin of the Carbonate Rock Province of the eastern Great Basin (Figure 1 inset). Thinning and major facies changes in the carbonate rock section occur as a northeast-trending "hinge line" passing through the study area (Tschanz and Pampeyan 1970, 5); the hinge line represents the approximate boundary between the continental shelf and "miogeosyncline" for much of Paleozoic time. Also, overthrusts of the Sevier orogenic belt (Armstrong 1968) are exposed in a corresponding zone that extends from the Spring Mountains to the southwest to east of upper Moapa Valley (Figure 2). Regional-scale thrust faults, dismembered by Tertiary extension (Axen et al. 1990), ramp to the surface and place carbonate rocks above much less permeable Mesozoic red beds along a northeast trend. The combined effects of stratigraphic thinning and structurally induced damming by Mesozoic and Cenozoic lithologies are thought to induce regional ground water discharge in the study area.

The oasis at the headwaters of the Muddy River, which supplies the entire base flow of this perennial stream, is referred to herein as the Muddy River springs area. The temperature, chemical characteristics, and temporal stability of discharge from these springs clearly indicate the "regional" character of the aquifer system that sustains their flow (Mifflin 1968). Flow in the Muddy River at Warm Springs Road has been monitored intermittently since 1913 by the USGS (site ID 09416000, "Muddy River near Moapa, Nevada") and reported as average daily flow. From the inception of monitoring until the early 1960s, base flow averaged ~1.3 m^3/s (47 ft^3/s).

Figures 1 (inset) and 2 (solid yellow lines) illustrate a series of hydrographic basins in the Carbonate Rock Province (Mifflin 1968, 1988; Dettinger et al. 1995) that were delineated by Eakin (1966) as the combined catchment for the White River flow system (WRFS), with a terminal discharge area at the Muddy River springs (H1 in Figure 1) in upper Moapa Valley (Figures 2 and 3). In Figure 2, Pahranagat Valley (PV) is the location of three large springs classified as "regional" in the Mifflin (1968) study along with the Muddy River springs. The two northernmost basins of the Eakin (1966) WRFS in Figure 2, Long Valley and Jakes Valley, were subsequently noted by Mifflin and Wheat (1979) to display pluvial-climatic-state hydrologic evidence of leaking to the west into Newark Valley (to balance basin surface water catchment areas with pluvial lake areas in these basins). If these two northernmost basins' contributions are removed from Eakin's (1966) classical water balance that was derived for discharge measured at Muddy River springs, a balance is achieved at Pahranagat Valley. Eakin's balance requires the majority of discharge for the Muddy River springs to be derived from flow that passes from Pahranagat Valley south through Coyote Spring Valley and then southeastward to the springs (F3 to K2 to K3 to H1 in Figure 1). Water discharging in Pahranagat Valley is, however, almost devoid of fluoride and isotopically much lighter than Muddy River springs. Muddy River springs' fluoride and stable isotope compositions are more akin to water in upper (northern) Meadow Valley Wash (Figure 2) than to those in Pahranagat Valley (Thomas et al. 1996).

The Muddy River spring area hydrology is locally complex, with an alluvial aquifer comprising coarse gravel lenses inset into the fine-grained Muddy Creek Formation (Schmidt et al. 1996). Between 1987 (Mifflin & Associates Inc. 1987) and 1996 (Mifflin and Adenle 1996), the status of known wells and springs in the upper Moapa Valley was documented on a quarterly basis. The alluvial aquifer is supplied by subsurface inflow from the northwest of roughly 8.3×10^4 m^3/d (34 ft^3/s) from the carbonate rock flow system. An additional 4.1×10^4 m^3/d (17 ft^3/s), or one third of the total ground water discharge (Figure 4), issues from large springs via carbonate-cemented conduits through the alluvial gravels. Roughly 0.1 m^3/s (4 ft^3/s) is lost to evapotranspiration on an annualized basis. A well-developed seasonal cone of depression forms around

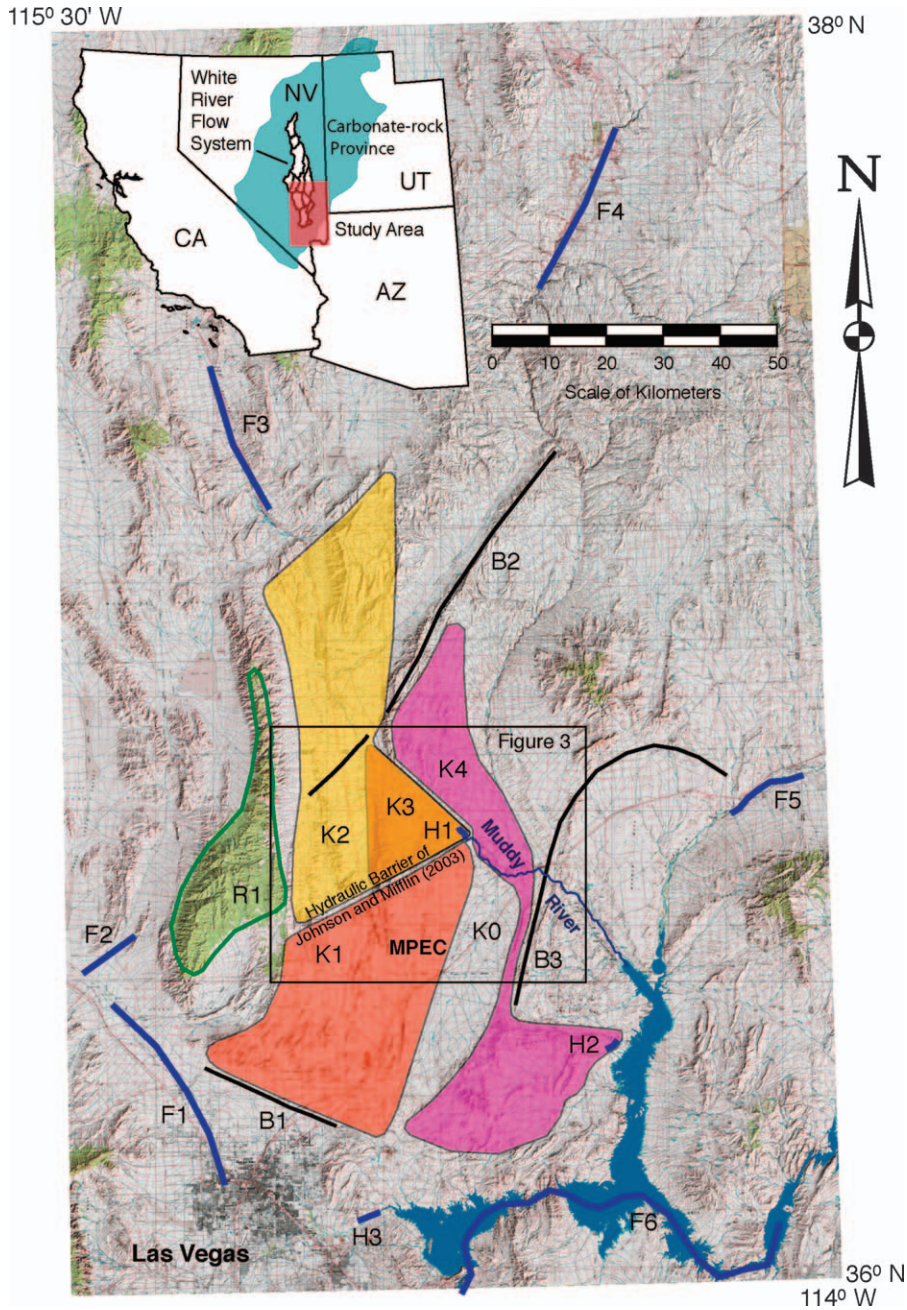

Figure 1. Analytic element representation of the study area, showing hydraulic conductivity domains (K), no-flow barriers (B), far-field features (F), near-field discharge (H), and recharge (R); see reference Table 1 for details.

Nevada Power Company's production wells in the alluvial aquifer and migrates down-valley toward the Muddy River springs during the summer pumping season; there was recovery each winter until 1997. Flow reductions are attributed to effects of the pumping cone on seepage flux from the unconfined alluvial aquifer into the headwaters channels of the Muddy River.

Upstream of the spring area near the Nevada Power Company (NPC) Lewis Well Field (Figure 5), there is local hydraulic continuity between the carbonate aquifer, source for the Arrow Canyon well, and the alluvial aquifer, local source for the Lewis wells. Between this important zone of inflow to the alluvial aquifer and Big Muddy Spring, the alluvial aquifer remains unconfined, but evidence for hydraulic connection with the carbonate aquifer is absent. Near Big Muddy Spring, the alluvial aquifer discharges via seepage into headwaters channels of the Muddy River, and spring outflow channels combine flows to establish the total discharge represented by the Muddy River gauge (Figure 5). Spring conduits (active and relic) are encased by highly cemented zones and, for the most part, hydraulically isolated from the alluvial aquifer. Two wells (LDS East and Central), finished in conduit-cemented gravels (relic conduits), respond instantaneously to pumping stress changes, suggesting a high degree of hydraulic continuity with the carbonate aquifer based on the response characteristics and elevated temperatures. Downstream of the spring area, the alluvial aquifer becomes confined and hydraulically separated from the river channel and remains so southeastward to where monitoring

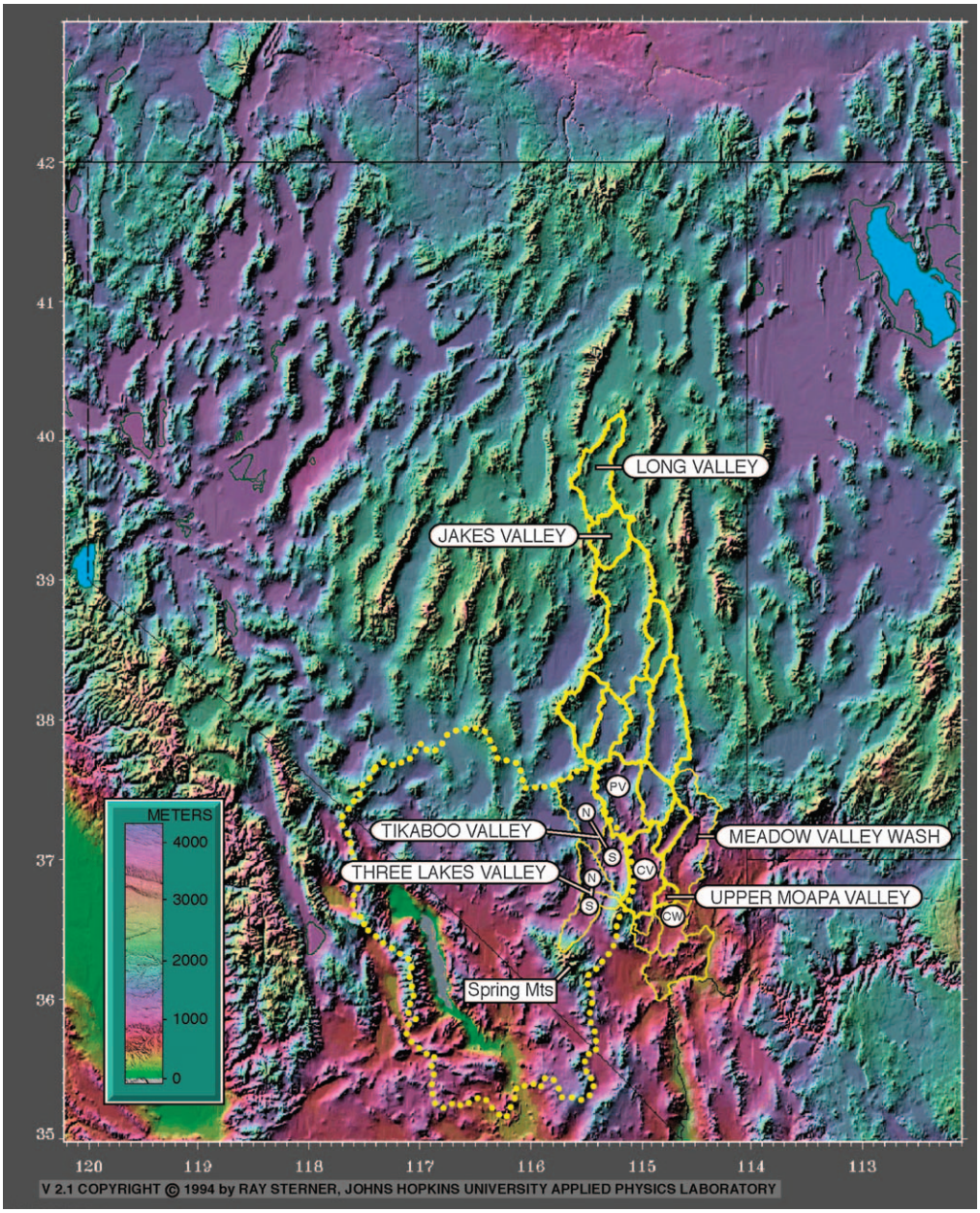

Figure 2. Regional topography showing Eakin's (1966) WRFS delineation (bold outline); flanking southern basins (narrow outline); Death Valley Regional Flow System (dotted) (U.S. Department of Energy 2002); and north (N) and south (S) subdivisions of Tikaboo and Three Lakes Valleys (Southern Nevada Water Authority 2003). PV = Pahranagat Valley; CV = Coyote Spring Valley; CW = California Wash. Base map mosaic copyright 1994 to 2002 by Andrew D. Birrell, used with permission.

well control ends. The Warm Springs Road Muddy River gauging station is located on the reach where there is no hydraulic continuity between the alluvial aquifer and river channel.

In 1985, NPC expanded its monitoring activities to include carbonate aquifer water levels in addition to monthly production totals from each of its wells in the Muddy River springs area. Monitoring records from carbonate rock aquifers became available in 1986, when NPC wells EH-4 and EH-5b were fitted with chart recorders and the USGS began taking monthly water-level measurements in MX-4. Seasonal fluctuations and long-term decline followed by recovery after the drought years of 1987 to 1992 are evident in all the three records. In the California Wash hydrographic basin (Figure 2), a water resources appraisal was conducted for LVVWD in 1990 (Wildermuth et al. 1990), but no potentiometric data were available from carbonate rock aquifers within 18 km of the proposed MPEC facility until 1998 (Terracon; unpublished data). Systematic monitoring in this southern area began late in 2000, and the first full year of record was 2001 (Figure 6).

Basin Water Budgets, Interbasin Flow, and Subregional Fluxes

Hydrographic basin water budgets are the fundamental accounting system used by the Nevada Division of Water Resources to administer the State's limited but uncertain ground water resource. Using the Maxey-Eakin

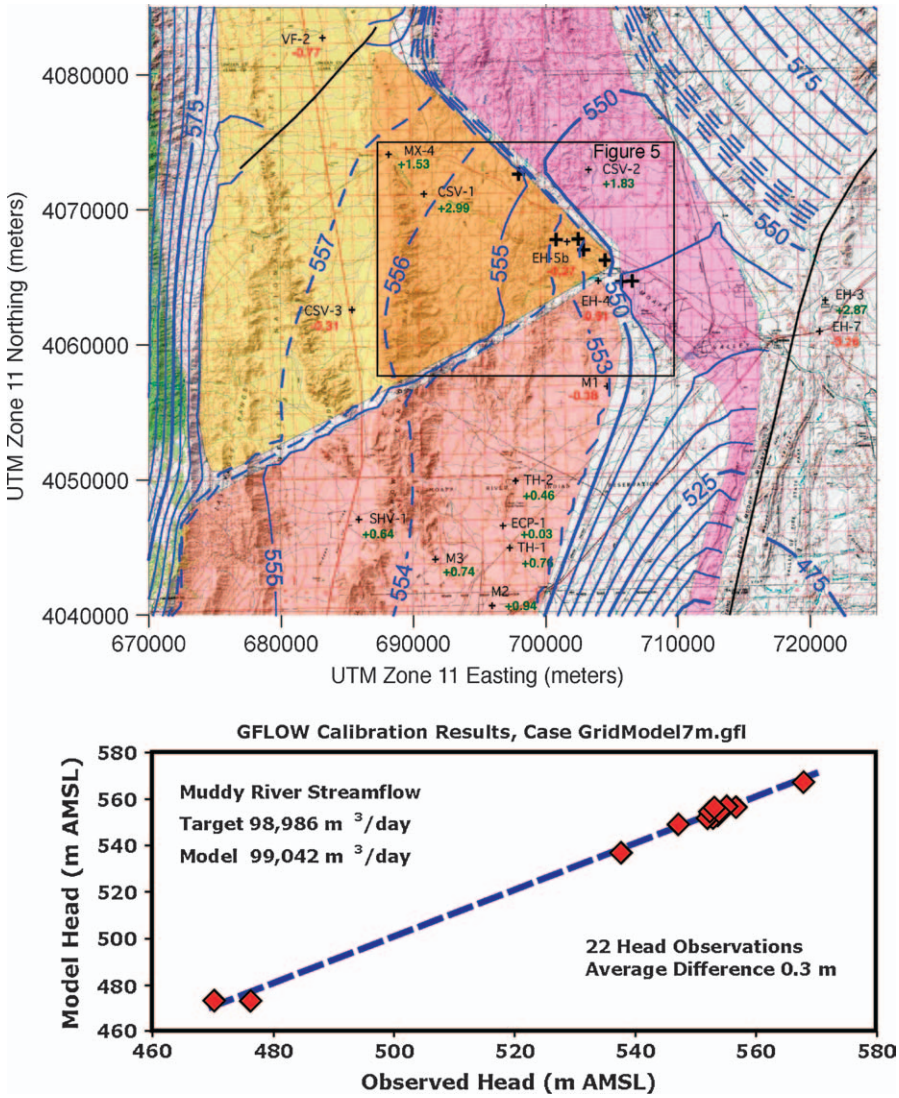

Figure 3. AEM model results for year 2001 conditions with calibration summary, showing head contours (meters above mean sea level) and residuals (meters + or −) at monitoring well locations. Contour interval is 1 m where dashed, 5 m elsewhere. "+" indicates model locations of ground water extraction by Nevada Power Company and Moapa Valley Water District.

method for estimating recharge (Maxey and Eakin 1949), percentages of precipitation falling within elevation zones were designated as recharge, with higher recharge efficiencies associated with the higher elevation (precipitation) zones. The contributions of each elevation zone to recharge were adjusted iteratively so that their sum would balance with discharge estimates in several control basins. Recharge estimates, established in this way as empirical percentages of precipitation assigned to elevation zones in the control basins, were then extrapolated to hydrographic basins throughout the Great Basin. The Maxey-Eakin method relies on two basic assumptions that appear to hold in the control areas:

- The hydrographic basin is also a hydrologically closed basin.
- The efficiency of recharge is uniform regardless of terrain lithology.

However, neither of the above assumptions is necessarily met in the more general case of the Carbonate Rock Province. The carbonate lithologies are likely more efficient in capturing greater percentages of incident precipitation, and hydrologic closure for many hydrographic basins remains uncertain.

The Eakin (1966) water budget approach is based on a "series" configuration of interbasin flow; water is transferred through a series of discrete compartments (basins) down a regional gradient. The method as generally applied does not accommodate "parallel" configurations, proposed by Tóth (1962, 1963) and explored through modeling analyses by Freeze and Witherspoon (1966, 1967, 1968). In suitable hydrogeologic environments, regional interbasin flow may bypass more localized ground water flow systems. The observed geographic distributions of the "regional"-class springs of Mifflin (1968) suggest that the parallel configuration of interbasin flow may be common and frequently unidentified by the basin water budget analytical procedure.

The efficiency of recharge for a given precipitation zone could be significantly greater in carbonate terrain than assigned in the Maxey-Eakin method, but there has been little comprehensive study to determine how much more efficient. The AEM-derived fluxes are independent

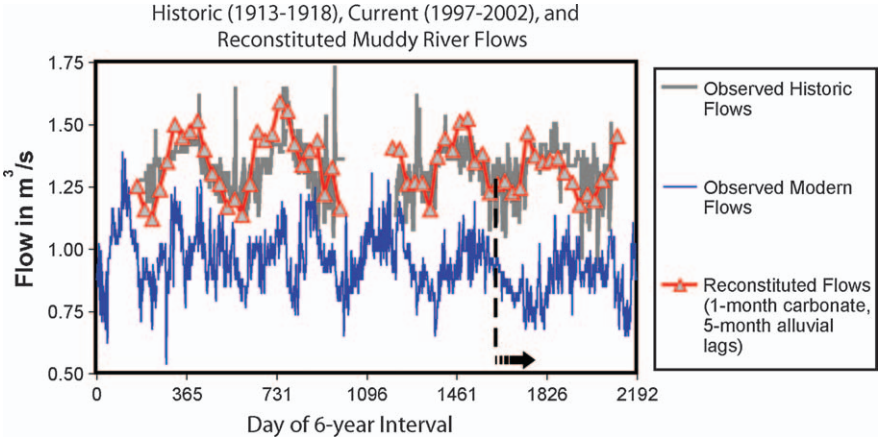

Figure 4. Flow reductions due in part to ground water pumping, accompanied by time lag in occurrence of seasonal discharge pattern of the Muddy River. The Muddy River responds to surface diversions immediately, to pumpage from the carbonate aquifer the following month and does not sense extractions from the alluvial aquifer until 5 months after they occur. Lag relations are attributable to depletion of storage in the alluvial aquifer, observed in monitoring records.

of hydrographic basin water budgets, thereby providing an alternative to Maxey-Eakin–derived flux estimates and their implicitly assumed configurations of interbasin flow. With evidence accumulating that the Muddy River springs are not the terminus of the WRFS (two independent lines of evidence suggest it terminates at Pahranagat Valley and excludes Jakes Valley and Long Valley), the AEM is elevated in importance for evaluating subregional fluxes related to interbasin flows.

The AEM Model and Supporting Analyses

Table 1 summarizes the features and properties of the AEM model as constituted in Figure 1. The AEM was selected to support a fast-track, year-2000 effort to locate a wellfield site, conduct aquifer characterization, establish a monitoring network, and provide an impact assessment for the proposed ground water extraction that would supply MPEC (Johnson et al. 2001). In the subregion of the study area, only four widely spaced areas with aquifer testing in carbonate aquifers were available to suggest material properties for the model (Ertec Western Inc. 1981; Mifflin & Associates Inc. unpublished Bonneville Pacific/Nevada Cogeneration Associates data; Buqo 1994; Johnson et al. 2001). Even less aquifer test data were available from Muddy River alluvium (Mifflin & Associates Inc. 1987) and the Muddy Creek Formation (Johnson et al. 1986). Regional relationships of hydrochemistry and water temperature (Thomas et al. 1996), a few key continuous monitoring well records (USGS, Nevada Power Company, and Mifflin & Associates Inc. unpublished), and distribution of pumping stress (unpublished data in files of Nevada State Engineer) were also available. Major structural features and the resulting distribution of lithologies are complex, but the carefully documented flux of the Muddy River spring area, pumping records, and Muddy River flow records tightly constrain the magnitude of ground water discharge.

In the early efforts toward constructing an AEM representation of the area, reviews of the regionally estimated fluxes, mixing models based on basin water budgets, and isotopic mass balance (Kirk and Campana 1990; Thomas et al. 1996, 2001) were considered in efforts to constrain the more troublesome uncertainties, such as recharge fluxes in adjacent mountainous terrain. The result of these efforts, facilitated by stepwise AEM modeling, was a set of revised conceptual models that addressed uncertainties and inconsistencies in prior analyses, some of which (notably Eakin 1966) have stood unquestioned for decades.

The model has been based on an infinite aquifer, 1524 m (5000 feet) in thickness throughout its stages of development. Two primary observations governed the thickness estimate: measured thicknesses of carbonate rock in the stratigraphic section (Longwell et al. 1965) and ground water temperatures in the 29°C to 35°C range (9°C to 15°C above the mean annual temperature) from Coyote Spring Valley to the Muddy River springs area and south beyond the MPEC site (Johnson et al. 2001). Although this is a remarkable thickness for widespread vertical hydraulic continuity, available evidence supports this order of magnitude thickness of transmissive rock and active ground water circulation in the subregion. The fundamental assumption in application of the AEM is that Dupuit-Forchheimer approximation of the flow field (Freeze and Cherry 1979; Haitjema 1995) is appropriate. In considerations of regional flow, where vertical variations in fluid potential are much less than those that occur over the lateral extent of the model domain, calculations based on Dupuit-Forchheimer flow should compare favorably with more rigorous methods (Haitjema 1995).

Monitoring records were instrumental in driving the evolution of the conceptual model of the area and its AEM representation (Figure 3). In 2000, no monitoring records suggestive of the hydraulic barrier between K1 and K3 existed. A feature limiting or blocking southward ground water flow from the Muddy River springs (H1) area was suspected based on incompatible water chemistries between the spring area discharge water and the southern flow field (K1). Available water-level data suggested that any lateral flow from the K3/H1 spring area southward should result in compatible hydrochemical

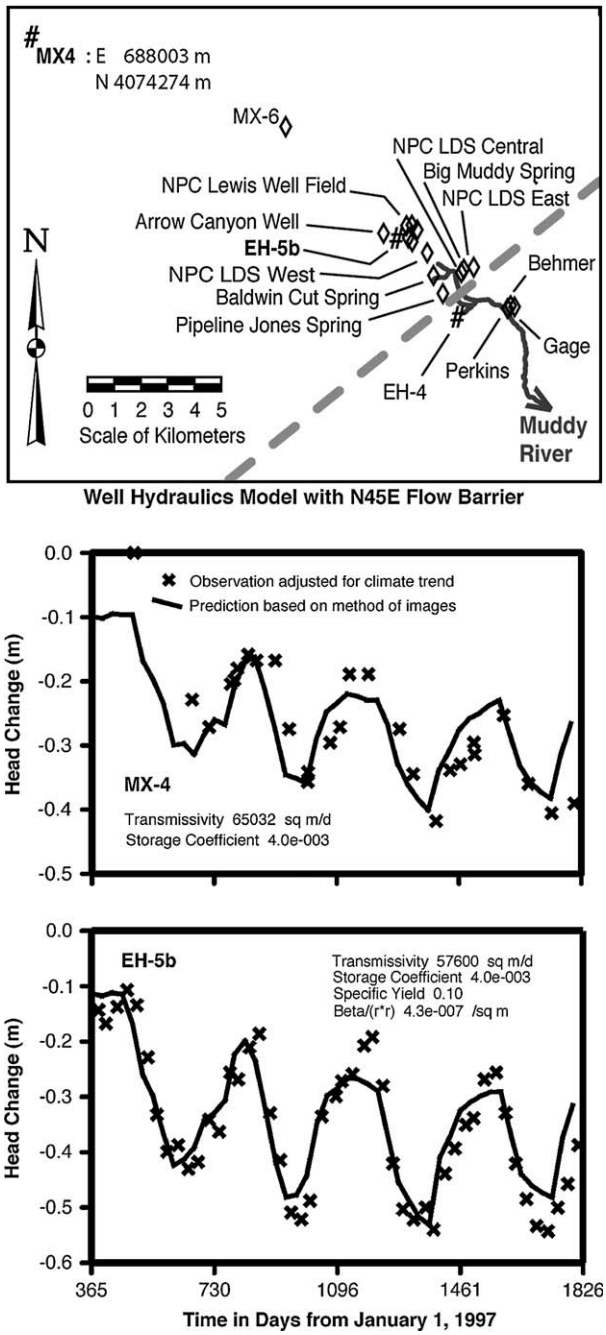

Figure 5. Parameter estimation for Zone K3, based on monthly stress periods, 1997 to 2001, and fitting 1998 to 2001 water levels. Image-well boundary trending N45E through EH-4 location (dashed line) was assumed. Raw measurements by USGS (at MX-4) and NPC (at EH-5b) were detrended to remove -8.32×10^{-2} m/year climate effect, based on southern flow field records (Figure 6).

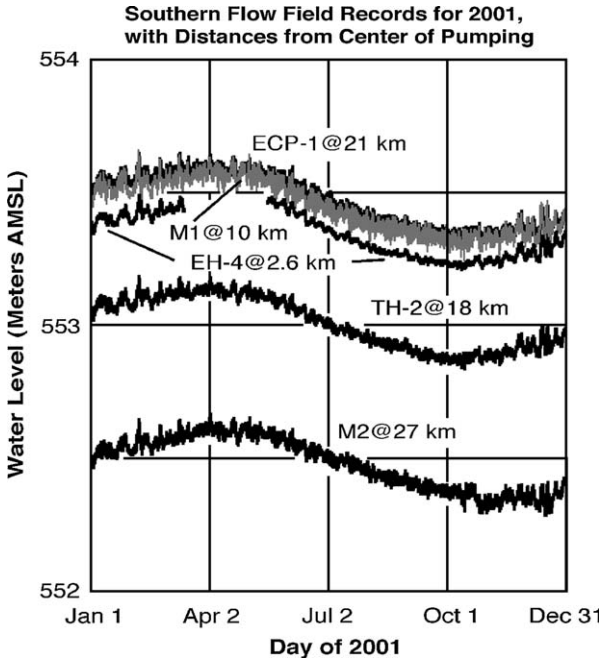

Figure 6. Evidence for hydraulic barrier between southern (Zone K1) and northern flow fields (Zones K2 and K3). Signals are essentially identical from 2.6 to 27 km south of the weighted center of pumping, indicating no distance-drawdown relationship and therefore no pumping effects.

evolution. A decision was made to adopt a conservative modeling approach by allowing hydraulic continuity to carry through from the northern domain to the southern domain in accord with the apparent continuity of carbonate rock (Schmidt et al. 1996), which, in retrospect, made the early AEM calibration difficult. In this manner, conservative analyses of impacts on spring flows were obtained, and the available evidence suggesting a barrier was discussed but not embedded in the AEM or derivative MODFLOW modeling analyses of the transient pumping impacts (Johnson et al. 2001).

As the Reservation area (northern K1) monitoring records accumulated during 2001, the first physical (as contrasted to hydrochemical) evidence for a barrier between the areas was developing. The characteristic pumping-induced asymmetry of the EH-5b and MX-4 monitoring well hydrographs is not present in those from K1; instead, a uniform annual water-level fluctuation cycle and long-term decline are characteristic of the southern records. Two of these wells (EH-4 and M1) are closer to the pumping area than MX-4, and one (TH-2) is about the same distance; yet, no clearly defined asymmetry of the seasonal pulse is evident in the 2001 data. These observations encouraged further analyses in an attempt to better understand the periodicities and regional multiyear water-level declines. It should be noted that the 2002 to 2004 monitoring records indicate the same downward trend and congruent hydrographs in the K1 domain.

Figure 3, a realization from the second-generation AEM model, incorporates a low-permeability "hydraulic barrier" of K0 material between the K1 and K3 domains in Figure 1. In the model, the barrier terminates at its northeast end against the K4 domain, which supplies the flow to Rogers and Blue Point Springs, H2. The area where the barrier approaches K4 presents the greatest uncertainty in the model, which is quite sensitive to the poorly constrained conditions there. Structural elements responsible for the barrier may in fact continue far to the northeast, the area where the Weiser Syncline (B3) terminates in a large drag fold against the Mormon Mountains (Axen et al. 1990), but no monitoring well records are available to support this idea. The southwestern extent of the barrier is suggested by an abrupt transition between upright and overturned beds in the Arrow Canyon Range,

and the northern termination of the Dry Lake Thrust Fault (Page 1992).

The Figure 3 AEM realization, with a "soft" or "leaky" version of the barrier of Johnson and Mifflin (2003), calibrates well with water-level data and observed spring flow. A hydraulic barrier between K1 and K3 was established as a fundamental model component on the basis of (1) the Figure 4 analyses of sources of ground water pumped in the Muddy River springs area (K3); (2) the Figure 5 parameter estimation based on EH-5b and MX-4 monitoring well hydrographs in K3; and (3) the Figure 6 Reservation area (K1) monitoring well records that became available in 2001. These analyses and monitoring well records, when combined with the geochemical differences between the water of the K1 and K3 domains (Johnson et al. 2001), support the inclusion of the low-permeability zone between these areas depicted in Figures 1 and 3. The northeast-southwest trend passing just north of monitoring well EH-4 is constrained to that location and orientation by the affinity of the EH-4

Table 1
Features and Properties of the MPEC Analytic Element Model (from Figure 1)

Far-Field Controls		
F1	Corn Creek to Las Vegas	Specified heads 892 to 652 m
F2	Divide Well to Cow Camp	Specified heads 895 to 867 m
F3	Pahranagat Valley	Specified heads 1100 to 900 m
F4	Upper Meadow Valley Wash	Specified heads 1500 to 1300 m
F5	Virgin River	Specified heads 500 to 450 m
F6	Colorado River	Specified heads 250 to 200 m
Inhomogeneities		
K0	Far-field zone	$K = 0.064$ m/d, obtained by calibration
K1	Southern flow field	$K = 6.1$ m/d from 7-d aquifer test reported by Johnson et al. (2001). Bounded on south and west by Las Vegas Shear Zone and Gass Peak Thrust, respectively (Longwell et al. 1965); on north by subregional hydraulic barrier described by Johnson and Mifflin (2003 and this study), and on east by down-faulted Tertiary (K0) sediments of California Wash (Johnson et al. 1986; Langenheim et al. 2001, 2002)
K2	Northern flow field	$K = 12.2$ m/d, obtained by calibration. Bounded on west by Gass Peak Thrust, on north by Menard Lake Fault, and on east by Delamar Mountains Thrust and fold belt (Tschanz and Pampeyan 1970)
K3	Arrow Canyon zone	$K = 36.6$ m/d from analysis of seasonal pumping response, 1997 to 2001 (Johnson and Mifflin 2003 and this study). Bounded on west by normal fault on west side of Arrow Canyon Range
K4	Glendale cell	$K = 5.5$ m/d, obtained by calibration. Isotopic data reviewed by Pohlmann et al. (1998)
Near-Field Discharge		
H1	Muddy River springs	Specified heads 536 to 530 m, hydraulic resistance 1.35 d
H2	Rogers/Blue Point Springs	Specified heads 488 to 463 m, hydraulic resistance 2.7 d
H3	Southern receptor zone	Specified heads 450 to 396 m at south end along Las Vegas Wash, hydraulic resistance 2 d
No-flow barriers		
B1	Las Vegas Shear Zone	Accounts for large hydraulic gradient between southern flow field (K1) and Las Vegas Valley, and absence of candidate outflow component in Las Vegas Valley ground water (Johnson et al. 2001)
B2	Kane Springs Wash Fault	Diverts flow from north around area of exposed basement rock in Mormon Mountains (Tschanz and Pampeyan 1970); southwestward extension in Coyote Spring Valley required to fit VF-2 and CSV-3 water levels (Figure 3)
B3	Weiser Syncline	Continuous feature per Axen et al. (1990), bent and rotated clockwise at northern end by Moapa Peak Shear Zone; required to match EH-3 and EH-7 water levels (Figure 3)
Recharge		
R1	Sheep Range	0.7 cm/year in forested highlands, by calibration. Recharge area encompasses 420 km^2, total 2.94×10^6 m^3/year (2380 acre-ft/year). Previous estimates include 2000 acre-ft/year (Eakin 1966), 5000 to 6000 acre-ft/year (Kirk and Campana 1990) and 14,000 acre-ft/year (Thomas et al. 1996)

hydrograph with several others to the south (Figure 6), which as a group are distinct from those northwest of the barrier (Figure 5), and by the need for a no-flow boundary in close proximity to the center of pumping for the image-well analysis of Figure 5.

Figure 4 reconstitutes Muddy River flows for the period 1997 to 2002 by adding monthly surface water diversions and ground water pumpage to base flows, with carbonate aquifer pumpage delayed 1 month and alluvial aquifer pumpage delayed 5 months. The exercise is simple addition by spreadsheet, with the lags obtained by trial-and-error comparison of trial results with the 1913 to 1918 record. These lag estimates are compatible with a cone of depression that develops each summer in the alluvial aquifer, migrating down-valley over the pumping season until it intersects the headwaters channels of the Muddy River, then recovering completely by the next pumping season (Mifflin and Adenle 1996). The reconstituted record compares remarkably well with the 1913 to 1918 Muddy River record in both timing and magnitude of seasonal flows. Three key relationships are recognized:

- The flux reaching the spring area has remained constant for almost a century.
- The seasonal variability of flows in the 1913 to 1918 record is likely due to evapotranspiration in the heavily vegetated headwaters area of the Muddy River based on the close correlation of flow differences to seasonal temperatures.
- All ground water diversions of the 1997 to 2002 record are manifested by 1:1 decreases in Muddy River discharge.

The latter point, all water is accounted for in the Muddy River springs system, has bearing on the multiyear downward trend observed in all the monitoring wells in K1, K2, K3, and K4 during the 1997 to 2004 drought. When the analysis of Figure 5 was performed, the data in K3 were detrended according to the rate that is characteristic throughout the K1 domain, where the long-term decline is attributed entirely to drought. The analysis, performed with Aquifer^{win32} from Environmental Simulations Inc. (Reinholds, PA) attempted to replicate the pumping-induced hydrographs of monitoring wells EH-5b and MX-4 of the K3 domain. The forcing function for the well hydraulics analysis was based on monthly production totals from 10 wells that produced at a combined average rate of 2.14×10^4 m^3/d (8.74 ft^3/s) in 2001, a typical year (Table 2) with pumping heavily weighted toward the summer months. To match the hydrographs, a no-flow boundary condition was necessary (from image-well analysis), consistent with the "hydraulic barrier" proposed by Johnson and Mifflin (2003). The derived parameter estimates also proved consistent with the AEM calibration of K3 with Muddy River spring discharge, adding additional confidence in the interpretation of the "barrier" as well as the interpretation of the asymmetrical hydrographs as representing a pumping signal.

Figure 6, the synchronous, but geographically widely distributed 2001 hydrographs of the new monitoring wells in the Reservation area of K1, and EH-4 near the Muddy River spring area, are suggestive of a barrier and encouraged the above analyses. The synchronicity, identical amplitudes both near and far from the pumping center, and absence of a hint of the asymmetry seen in the EH-5b and MX-4 signals (Figure 5) suggest that the periodicity in these wells cannot be a porous-media response to seasonal pumping in K3 to the north. On the other hand, a loading or tidal mechanism for this magnitude of annual aquifer response does not seem reasonable. It is conceivable that a seasonal pumping signal could be propagated southward, with little attenuation along fractures of the Hogan Spring Fault Zone (Schmidt et al. 1996), thus supplying a similar response to the larger K1 area. A 7-d aquifer test (Johnson et al. 2001), however, produced a porous-medium response with no evidence of direct fracture connections between ECP-1, TH-1, and TH-2 (Figure 3). Though the periodicity observed in the K1 domain remains enigmatic, the weight of the evidence indicates that the annual periodicity in the southern flow field is not directly related to seasonal pumping in upper Moapa Valley.

Table 2
Ground Water Diversions, 2001

Well ID	Annualized Q (m^3/d)
Arrow Canyon	8224
MX-6	1046
Lewis 1	369
Lewis 2	64
Lewis 3	1462
Lewis 4	1243
Lewis 5	1351
LDS West	2365
LDS Central	3215
LDS East	2046
Behmer	2761
Perkins	1654

Note: Behmer and Perkins data were used in the regional AEM model but not in the well hydraulics model since they are located southeast of the image-well boundary.

Benefits of the AEM Approach

AEM modeling facilitated a realistic, simple beginning of hydrogeologic assessment but also allowed the easy incorporation of complexity as additional data became available. The ability to simulate a large domain was important for maintaining flexibility in the site area while minimizing boundary artifacts and was easily accommodated by the AEM assumption of an infinite aquifer. A strength of the method lies in the mechanics of its implementation, a logical progression from embedding what is known and easily seen at the land surface to exploring the effects of changes to the underlying conceptual models. The ease of adding and deleting analytic elements helps to determine if a conceptual model with added complexity makes sense or should be discarded. In practice, the AEM approach allows many more realizations within a given time frame (project duration) than alternative methods.

Testing multiple conceptual models is critically important for understanding the effects of adding features that may not exist, or omitting key features that do. The more sparse the constraining databases, the more important this insight—as demonstrated by our initial failure to embed the hydraulic barrier between the northern (K3) and southern (K1) flow fields. Hydrochemical evidence alone, however compelling in terms of indicating a non-Muddy River springs–type water source for southern water, was insufficient to negate the possibility of hydraulic continuity between the northern and southern areas. Moreover, assuming a hydraulic barrier on the basis of hydrochemical evidence alone would likely have been challenged due to its importance for estimating impacts of pumping on the regional spring flows. The quantitative framework provided by the AEM model, and the field data collected after the initial modeling, provided a more encompassing and defensible conceptual model for the site area. While the modeling was a critical part of the investigation, the value and information content of the continuous water-level monitoring cannot be overstated.

Conclusion

The AEM proved to be a powerful approach for conceptualizing ground water flow in a large subregion with poorly understood regional flow in carbonate rock aquifers. During the work, two aspects stood out: (1) its suitability for developing regionally appropriate models while removing the potential for boundary condition artifacts on the local scale of interest, and (2) the ease in which minor or major changes are accommodated and conceptual model hypotheses are "tested." Elements of an existing AEM model were easily modified, removed, or supplemented without starting over. Finally, we believe that the AEM fosters development of a conceptual model that is compact yet complete—a characteristic that is well suited for evaluations of competing models that are often the de facto decision framework for ground water resource management.

Acknowledgments

The authors wish to acknowledge and thank Calpine Corporation, the Moapa Band of Paiute Indians, and Nevada Power Company for support and cooperation during this investigation, and specifically recognize Nevada Power Company for supporting the initial carbonate rock monitoring wells EH-4 and EH-5b, without which these analyses would not have been possible.

References

Armstrong, R.L. 1968. Sevier orogenic belt in Utah. *Geological Society of America Bulletin* 79, no. 4: 429–458.

Axen, G.J., B.P. Wernicke, M.F. Skelly, and W.J. Taylor. 1990. Mesozoic and Cenozoic tectonics of the Sevier thrust belt in the Virgin River Valley area, southern Nevada. *Geological Society of America Memoir* 176, 123–153.

Buqo, T.S. 1994. Results of long-term testing of the Arrow Canyon well. Prepared for Moapa Valley Water District, 22 p. Logandale, Nevada, MVWD (unpublished)

Dettinger, M.D. 1989. Distribution of carbonate-rock aquifers in southern Nevada and the potential for their development—Summary of findings, 1985–1988. Program for the study and testing of carbonate-rock aquifers in eastern and southern Nevada. Summary Report 1.

Dettinger, M.D., J.R. Harrill, D.L. Schmidt, and J.W. Hess. 1995. Distribution of carbonate-rock aquifers and the potential for their development, southern Nevada and adjacent parts of California, Arizona, and Utah. USGS Water-Resources Investigations Report 91-4146.

Eakin, T.E. 1966. A regional interbasin groundwater system in the White River area, southeastern Nevada. *Water Resources Research* 2, no. 2: 251–271.

Ertec Western Inc. 1981. MX siting investigation—Water resources program—Results of regional carbonate aquifer testing—Coyote Spring Valley, Nevada. Unpublished report prepared for U.S. Department of the Air Force, Ballistic Missile Office, Norton Air Force Base, California: 190 p. (unpublished)

Freeze, R.A., and J.A. Cherry. 1979. *Groundwater*. Prentice-Hall, Englewood Cliffs, New Jersey.

Freeze, R.A., and P.A. Witherspoon. 1968. Theoretical analysis of regional groundwater flow: 3. Quantitative interpretations. *Water Resources Research* 4, no. 3: 581–590.

Freeze, R.A., and P.A. Witherspoon. 1967. Theoretical analysis of regional groundwater flow: 2. Effect of water-table configuration and subsurface permeability variation. *Water Resources Research* 3, no. 2: 623–634.

Freeze, R.A., and P.A. Witherspoon. 1966. Theoretical analysis of regional groundwater flow: 1. Analytical and numerical solutions to the mathematical model. *Water Resources Research* 2, no. 4: 641–656.

Haitjema, H.M. 1995. *Analytic Element Modeling of Groundwater Flow*. Academic Press, San Diego, California.

Johnson, C., C. Brick, and S. Tyler. 1986. Construction, development and testing of NPC wells EH-2 and EH-2A. Water Resources Center, Desert Research Institute, University of Nevada system. Reno, Nevada (unpublished)

Johnson, C., and M. Mifflin. 2003. Evidence for a sub-regional hydraulic barrier in southeastern Nevada (abstract). In *Geological Society of America 115th annual meeting*, Seattle, Washington. Geological Society of America, Denver, Colorado.

Johnson, C., M. Mifflin, R.J. Johnson, and H. Haitjema. 2001. Hydrogeologic and groundwater modeling analyses for the Moapa Paiute Energy Center, a Calpine company project in cooperation with the Moapa Band of Paiute Indians, Moapa Indian Reservation, Clark County, Nevada: 218 p. Mifflin and Associates, Inc., Las Vegas, Nevada. (unpublished)

Kirk, S.T., and M.E. Campana. 1990. A deuterium-calibrated groundwater flow model of a regional carbonate-alluvial system. *Journal of Hydrology* 119, no. 4: 357–388.

Langenheim, V.E., J.J. Miller, W.R. Page, and J.A. Grow. 2001. Thickness and geometry of Cenozoic deposits in the California Wash area, Nevada, based on gravity and seismic-reflection data. USGS Open-File Report 01-393.

Langenheim, V.E., W.R. Page, J.J. Miller, and J.A. Grow. 2002. Geophysical and geological constraints on the hydrogeological framework of the California Wash region, southern Nevada (abstract). In *Geological Society of America, Rocky Mountain Section, 54th annual meeting*, May 7–9, 2002. Geological Society of America, Denver, Colorado.

Longwell, C.R., E.H. Pampeyan, B. Bowyer, and R.J. Roberts. 1965. Geology and mineral deposits of Clark County, Nevada. *Nevada Bureau of Mines and Geology Bulletin* 62, 218.

Maxey, G.B., and T.E. Eakin. 1949. Ground water in White River Valley, White Pine, Nye, and Lincoln Counties, Nevada. Nevada State Engineer. *Water Resources Bulletin* 8, 59.

Mifflin & Associates Inc. 1987. Hydrogeologic assessment, upper Muddy River valley, Nevada. Unpublished report prepared

on behalf of Nevada Power Company and California Department of Water Resources: 396 p. (unpublished)

Mifflin, M.D. 1992. The Arrow Canyon Range cell, carbonate aquifer and upper Muddy River valley groundwater monitoring—A summary of local and regional evidence and interpretations. Mifflin & Associates Inc., Las Vegas, Nevada: 18 p. (unpublished)

Mifflin, M.D. 1988. Region 5, Great Basin. In *The Geology of North America: Hydrogeology*, vol. 0–2, ed. W. Back and P.R. Seaber, 69–78. Decade of North American Geology. Geological Society of America, Denver, Colorado.

Mifflin, M.D. 1968. Delineation of groundwater flow systems in Nevada. Water Resources Center, Desert Research Institute, University of Nevada System. Desert Research Institute, Reno, Nevada. Publication no. 42004.

Mifflin, M.D., and O.A. Adenle. 1996. 1995 hydrologic impacts from groundwater withdrawals in the upper Muddy River valley, Nevada. Unpublished report prepared for Nevada Power Company. Mifflin & Associates Inc.:227 p. (unpublished)

Mifflin, M.D., and M.M. Wheat. 1979. Pluvial lakes and estimated pluvial climates of Nevada. *Nevada Bureau of Mines and Geology Bulletin* 94, 57.

Neuman, S.P. 1972. Theory of flow in unconfined aquifers considering delayed response of the water table. *Water Resources Research* 8, no. 4: 1031–1045.

Page, W.R. 1992. Preliminary geologic map of the Paleozoic rocks in the Arrow Canyon Range quadrangle, Clark County, Nevada. USGS Open-File Report 92-681.

Pohlmann, K.F., D.J. Campagna, J.B. Chapman, and S. Earman. 1998. Investigation of the origin of springs in the Lake Mead National Recreation Area. Desert Research Institute, University and Community College System of Nevada, Reno, Nevada. Publication no. 41161.

Schaefer, D.H., and J.R. Harrill. 1995. Simulated effects of proposed groundwater pumping in 17 basins of east-central and southern Nevada. USGS Water-Resources Investigations Report 95-4173.

Schmidt, D.L., W.R. Page, and J.B. Workman. 1996. Preliminary geologic map of the Moapa West quadrangle, Clark County, Nevada. USGS Open-File Report 96-521.

Southern Nevada Water Authority (SNWA). 2003. Hydrology of Tikaboo Valley and Three Lakes Valleys, Clark and Lincoln Counties, Nevada: 70 p. appendix. Las Vegas, Nevada (unpublished)

Thomas, J.M., S.C. Calhoun, and W.B. Apambire. 2001. A deuterium mass-balance interpretation of ground water sources and flows in southeastern Nevada. Division of Hydrologic Sciences, Desert Research Institute, University and Community College System of Nevada, Reno, Nevada. Publication no. 41169.

Thomas, J.M., A.H. Welch, and M.D. Dettinger. 1996. Geochemistry and isotope hydrology of representative aquifers in the Great Basin region of Nevada, Utah, and adjacent states. USGS Professional Paper 1409-C.

Tóth, J. 1963. A theoretical analysis of groundwater flow in small drainage basins. *Journal of Geophysical Research* 68, no. 16: 4795–4812.

Tóth, J. 1962. A theory of groundwater motion in small drainage basins in central Alberta. *Journal of Geophysical Research* 67, no. 11: 4375–4387.

Tschanz, C.M., and E.H. Pampeyan. 1970. Geology and mineral deposits of Lincoln County, Nevada. Nevada Bureau of Mines and Geology Bulletin 73. Reno, Nevada.

U.S. Department of Energy. 2002. Final environmental impact statement for a geologic repository for the disposal of spent nuclear fuel and high-level radioactive waste at Yucca Mountain, Nye County, Nevada. Office of Civilian Radioactive Waste Management. DOE/EIS-0250. Volume I. Impact Analyses.

Wildermuth, M.J., J.H. Hwang, R. Broadbent, and M.C. Inada. 1990. Cooperative water resources development program, final hydrologic report for California Wash, hydrographic basin 218. James M. Montgomery Consulting Engineers, Inc.: 47 p. Las Vegas, Nevada. (unpublished)

ground water

Evaluating Climate Variability and Pumping Effects in Statistical Analyses

by Timothy D. Mayer[1] and Roger D. Congdon[2]

Abstract

As development of ground water resources reaches the limits of sustainability, it is likely that even small changes in inflow, outflow, or storage will have economic or environmental consequences. Anthropogenic impacts of concern may be on the scale of natural variability, making it difficult to distinguish between the two. Under these circumstances, we believe that it is important to account for effects from both ground water development and climate variability. We use several statistical methods, including trend analysis, cluster analysis, and time series analysis with seasonal decomposition, to identify climate and anthropogenic effects in regional ground water levels and spring discharge in southern Nevada. We discuss the parameterization of climate and suggest that the relative importance of various measures of climate provides information about the aquifer system response to climate. In our system, which may be characteristic of much of the arid southwestern United States, ground water levels are much more responsive to wet years than to dry years, based on the importance of selected climate parameters in the regression. Using cluster analysis and time series seasonal decomposition, we relate differences in amplitude and phase in the seasonal signal to two major forcings—climate and pumping—and distinguish between a regional recharge response to an extremely wet year and a seasonal pumping/evapotranspiration response that decays with distance from the pumping center. The observed spring discharge data support our hypothesis that regional spring discharge, particularly at higher elevation springs, is sensitive to relatively small ground water level changes.

Introduction

Ground water sustainability is defined as "development and use of ground water in a manner that can be maintained for an indefinite time without causing unacceptable environmental, economic, or social consequences" (Alley et al. 1999). Increasingly, attention is being placed on how to manage ground water resources in a sustainable manner (Bredehoeft 2002, 1997; Sophocleous 1997; Alley and Leake 2004). Many areas of ground water development in the United States are approaching or exceeding their limits of sustainability. Under these conditions, it is likely that even small changes in inflow, outflow, or storage will affect water supply or biological resources. Anthropogenic impacts of concern may be on the scale of natural variability, a condition that confounds analyses and makes it difficult to distinguish between the two. Moreover, it is often the variability of flows and water level fluctuations that determines the extreme conditions limiting water availability and threatening biological resources.

Ground water systems tend to react more slowly than surface water systems to short-term climate variability. Because of this, many past studies on ground water flow have neglected climate variability and used long-term average climate conditions or recharge, particularly in temporal simulations of ground water flow (Hanson et al. 2004). At short time scales of interest or where there is extensive aquifer development, this approach has provided acceptable simulations and predictions of large-scale changes in ground water storage (Hanson et al. 2004). However, it is becoming apparent that climate variability and change need to be accounted for in the

[1]Corresponding author: U.S. Fish and Wildlife Service, 911 NE 11th Ave., Portland, OR 97232-4181; (503) 231-2395; fax (503) 231-6260; tim_mayer@fws.gov

[2]U.S. Forest Service, 333 Broadway Blvd., Albuquerque, NM 87102; (505) 842-3835; rcongdon@fs.fed.gov

Received March 2007, accepted August 2007.

doi: 10.1111/j.1745-6584.2007.00381.x

management and analyses of ground water resources (Winter et al. 1999; Alley et al. 1999; Gleick and Adams 2000; Hanson et al. 2004; Weber and Stewart 2004; Scanlon et al. 2005). We believe that this is especially true in systems where the effects of ground water development and climate variability are approximately equal in scale and where these effects have economic or environmental consequences.

When considering climate variability explicitly, one of the first and most important questions is how to represent climate. There are a number of measures available to parameterize climate, including raw precipitation data and several precipitation and drought indexes (Hayes 2006). The indexes differ in their statistical distribution and centering and how they measure deviations from historical norms. Our study examines issues regarding climate parameterization while investigating the effects of climate variability and ground water development on the Muddy River Springs area (MRSA), a regional spring system about 100 km north of Las Vegas, Nevada (Figures 1 and 2). We use statistical analyses to examine water levels and spring discharge for a period that includes a significant increase in ground water development and several years of drought and record precipitation. We begin by examining and characterizing temporal and spatial trends in ground water levels in the system. The long-term well records in the area integrate the combined effects of multiple factors such as climate, seismic activity, barometric pressure, earth tides, evapotranspiration (ET), confined or unconfined conditions, and pumping from different aquifers. The effect of each of these factors varies in frequency and magnitude, but our preliminary analyses indicated that the two main factors affecting the system at scales of concern appear to be climate and ground water pumping.

After identifying and evaluating trends in ground water levels, we examine the relationship between ground water levels in the carbonate rock aquifer and regional spring discharge in the MRSA. We show that in this system, spring discharge is affected by rather small changes in ground water levels resulting from climate and pumping effects. We hypothesize that changes in spring discharge will be proportional to those in hydraulic head at each spring. The higher the elevation of the spring, the smaller the initial hydraulic head and the more sensitive the spring is to water level changes. Our examination of changes in spring discharge in relation to spring elevation and ground water level changes validates our hypothesis. The methods and results we present here are useful in quantifying and assessing climate variability and pumping-related impacts to ground water levels and springs in other regional spring systems, especially where those impacts are at similar scales.

Study Site and Setting

Much of the eastern Great Basin is underlain by a thick sequence of limestone and dolomite rocks known as the carbonate rock province (Harrill and Prudic 1998). Beneath southern Nevada, these carbonate rocks are

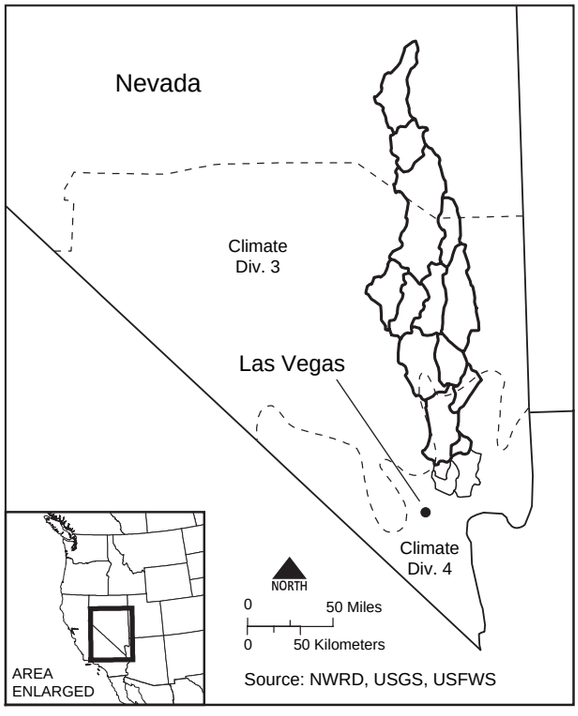

Figure 1. Map of southeastern Nevada showing Eakin's (1966) original White River ground water flow system (bold outline), adjacent southern basins (narrow outline), and the boundaries of Nevada Climate Divisions 3 and 4.

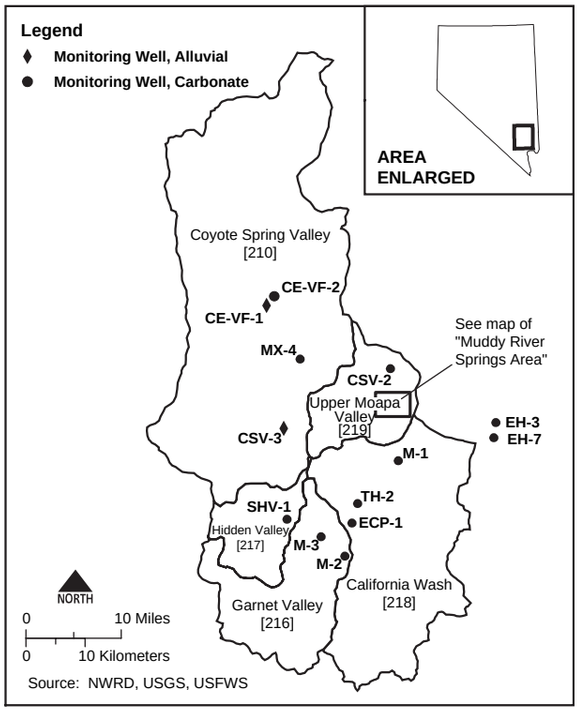

Figure 2. Map of five hydrographic basins within, or adjacent to, the southern portion of the White River ground water flow system, with carbonate and alluvial wells discussed in the text.

widely distributed and permeable enough to facilitate ground water flow at a regional scale. One such regional flow system is the White River ground water flow system, originally defined by Eakin (1966) to encompass 13 topographic basins, extend more than 400 km, and terminate at the MRSA (Figure 1). The flow system consists of numerous local basin fill aquifers underlain by a large regional carbonate rock aquifer that transmits ground water from basin to basin, beneath topographic divides. Much of the flow in the regional carbonate rock aquifer occurs where rocks have been fractured or where openings have been enlarged by dissolution (Prudic et al. 1993; Dettinger et al. 1995). Eakin (1966) identified the regional ground water flow system based on (1) the hydrologic properties of the rocks in the area; (2) the movement of ground water inferred from hydraulic gradients; (3) the relative distribution and quantities of estimated recharge and discharge in the system; (4) the relative uniformity of the discharge of the principal springs; and (5) the chemical composition and warm temperature of the discharge from the principal springs. Additional geologic, isotopic, and numerical studies have confirmed the existence of the regional flow system with minor differences (Harrill et al. 1988; Kirk and Campana 1990; Dettinger et al. 1995; Thomas et al. 1996; GeoTrans Inc. 2001, 2003; Johnson and Mifflin 2006).

Using a water budget approach, Eakin (1966) estimated that 78% of the recharge to the regional flow system occurs as precipitation in the higher elevation mountain ranges of the four northern basins in the flow system and 62% of the discharge from the regional flow system occurs from springs in the Pahranagat and Upper Moapa valleys in the southern part of the flow system. The MRSA in the Upper Moapa Valley (Figure 2) was reported to be the terminal discharge of the regional flow system (Eakin 1966; Harrill et al. 1988; Prudic et al. 1993), although other researchers hypothesize that additional subsurface flow continues beyond the springs to the southeast (Johnson and Mifflin 2006). The springs are located upgradient of a normal fault that juxtaposes low-permeability rock of the Muddy Creek Formation against the carbonate rock aquifer (Dettinger et al. 1995). Eakin (1966) estimated that approximately 1.4 m^3/s of discharge occurs here from about 20 springs. The springs are thermal, discharging at a nearly constant temperature of 32°C (Scoppettone et al. 1992). They occur within a 2-km radius and form the headwaters of the Muddy River. The occurrence of spring discharge at the terminus of regional ground water flow systems is characteristic of the carbonate rock province (Harrill and Prudic 1998).

The MRSA supports eight rare, endemic, aquatic species, including the Moapa dace (*Moapa coriacea*), a federally listed endangered fish since 1967 (U.S. Fish and Wildlife Service, 1996; Scoppettone et al. 1998). The Moapa dace is thermophilic and occurs typically in water temperatures ranging from 26°C to 32°C (Deacon and Bradley 1972). Because the Muddy River cools as it flows downstream, the fish are restricted to the thermal headwater springs (Cross 1976). Like many native fish of the southwestern United States, the Moapa dace have declined due to habitat alteration and introduction of nonnative fish (Deacon and Bradley 1972; Scoppettone et al. 1998). The Moapa Valley National Wildlife Refuge, a 47-ha area of springs and wetlands located in the MRSA, was established in 1979 for the protection of Moapa dace (Figure 3).

The transmissivity of the carbonate rock aquifer in the MRSA and surrounding area is quite variable but can be extremely high. Estimated transmissivities range from 200 m^2/d in several carbonate wells in Coyote Spring Valley to 20,000 m^2/d or higher in wells directly upgradient or adjacent to the springs in the MRSA (Bunch and

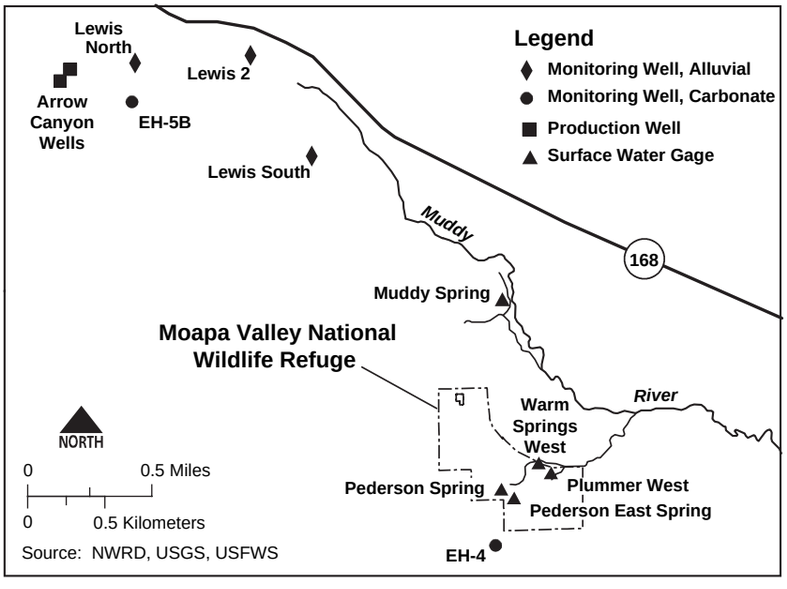

Figure 3. Close-up of MRSA showing Moapa Valley NWR boundaries, Muddy River and tributaries, carbonate production wells, carbonate monitoring wells, alluvial monitoring wells, and spring monitoring sites.

Harrill 1984; Buqo 1994; Dettinger et al. 1995). High-permeability zones such as this are commonly found upgradient of areas of regional spring discharge. Dettinger et al. (1995) analyzed 39 well tests in southern Nevada and found that wells located up to 16 km upgradient of regional springs show transmissivities about 10 to 20 times greater, on average, than those located farther away. The high transmissivity of the carbonate rock aquifer has resulted in a fairly uniform potentiometric surface over an extensive area in and around the MRSA.

There are three primary hydrogeological units in the Upper Moapa Valley: the Quaternary alluvial fill, the Tertiary Muddy Creek Formation, and the Paleozoic carbonate system (Pohlmann 1994). The alluvial fill material provides a shallow, high-yield aquifer that is recharged from the underlying carbonate aquifer. The Muddy Creek Formation underlies the alluvial fill in much of the valley and is considered a semiconfining unit. The Paleozoic carbonates extend below and underlie the other units and are part of the regional carbonate rock aquifer of the White River flow system. Vertical hydraulic gradients in this area are upward from the carbonate rock aquifer to the alluvial fill aquifer.

Like many areas of the southwestern United States, southern Nevada is experiencing tremendous population growth. Municipalities and other water users are turning to the regional carbonate rock aquifer to meet future demand. Ground water in both the shallow alluvial aquifer and the deeper carbonate rock aquifer in the MRSA has been developed. Pumping in the alluvial aquifer for irrigation has been ongoing since World War II, with many of the irrigation water rights being acquired and changed to industrial purposes by power interests since the 1960s. Pumping in the carbonate rock aquifer for municipal supply purposes started in 1986 and increased significantly beginning in 1998. Most of the carbonate pumping now occurs at two adjacent wells: the Arrow Canyon wells 1 and 2, located about 3.5 km northwest of the wildlife refuge (Figure 3).

Theoretical Ground Water Level/Spring Discharge Relationships

Many public agencies and private organizations are concerned that ground water development of the carbonate rock aquifers may negatively impact regional spring systems like the MRSA and the biological resources associated with those systems. It is well established that spring discharge in the MRSA emanates from the regional carbonate aquifer (Eakin 1966; Prudic et al. 1993; Thomas et al. 1996). The potentiometric surface of the carbonate rock aquifer is greater than the land surface elevation of the springs. This hydraulic head differential causes ground water in the carbonate rock aquifer to rise to the land surface, through fissures and fractures, manifesting itself as spring discharge. We are assuming that the flow at a spring is governed by Darcy's law, or some similar proportionality, which states that flow through a porous medium is proportional to the hydraulic head differential or hydraulic gradient (Fetter 1994). The greater the hydraulic head differential between the elevation of the spring orifice and the hydraulic head of the aquifer, the greater the spring discharge, other factors being equal.

All ground water pumping leads to the development of a drawdown cone around the pumping center. As the drawdown cone extends to the springs, the hydraulic head differential at the springs will be reduced. Darcy's law states that a reduction in the hydraulic head differential will result in a proportional decrease in flow. The elevations of spring pool orifices in the MRSA vary by more than 20 m (Southern Nevada Water Authority 2003). The uniform potentiometric surface of the carbonate rock aquifer underlying the MRSA means that the head differential at the various springs decreases with increasing elevation of the spring orifice. We hypothesize that the springs in the system with the smallest head differential, the highest elevation springs, will be proportionately most sensitive to any decline in the potentiometric surface of the carbonate rock aquifer resulting either from ground water pumping or climate effects.

Methods

Climate Data

Each state in the nation has been divided into 1 to 10 climate divisions. These are areas of climate uniformity with water resource data aggregately assessed through principal component analysis, based on information from 10 to 50 individual stations (Guttman and Quayle 1996). Monthly divisional climate data and indexes, including monthly temperature and precipitation, Standard Precipitation Index (SPI), and various Palmer Drought Index (PDI), are compiled back to 1895 for each climate division in the country. We evaluated two climate parameterizations in the study: precipitation and SPI. Monthly precipitation data and SPI were obtained for two of Nevada's four climate divisions: Climate Divisions 3 (South Central) and 4 (Extreme Southern) (Western Regional Climate Center, 2006). Divisions 3 and 4 encompass the north-central and south portions, respectively, of the White River flow system (Figure 1). We calculated moving averages of the monthly precipitation, defined back from points in time, for various time scales for each division.

The SPI is a recently developed normalized index of drought (McKee et al. 1993), designed to explicitly express the fact that it is possible to simultaneously experience wet and dry conditions on multiple time scales. For SPI, historical precipitation data are used to compute the probability distribution of the monthly and seasonal observed precipitation totals (the past 2, 3, 6 months, etc., up to 72 months), and the probabilities are normalized to a cumulative normal distribution. The mean of SPI is then 0 for any particular location and time scale, and the units are normalized variates or standard deviations away from the mean. Positive SPI values indicate greater than average precipitation, while negative values indicate less than average precipitation. Values of 2.0 and -2.0 are defined as extremely wet and extremely dry conditions, respectively. Because SPI is a standardized measure of

precipitation, SPI values from different climate divisions are comparable.

Ground Water and Surface Water Data

Water level data are available for a number of carbonate and alluvial monitoring wells for varying periods (Berger et al. 1988; Southern Nevada Water Authority 2006; USGS 2006). Figures 2 and 3 and Table 1 give the location, aquifer type (carbonate or alluvial), well level elevation, period of record, and frequency of measurements of all monitoring wells investigated in this study. Of particular interest are two carbonate monitoring wells, EH-5B and EH-4, located in the MRSA near the pumping center and the springs (Figure 3). Both wells have monthly measurements dating back to 1987, with continuous measurements beginning in 1997.

Monthly pumping data are available for the alluvial production wells from 1983 through 2005 and for the carbonate production wells from 1992 to 2005 (Las Vegas Valley Water District 2001; Moapa Valley Water District 2005; Nevada Power Co., unpublished data). Annual carbonate pumping from 1987 to 1992 was estimated by Las Vegas Valley Water District (2001). We grouped and averaged annual volumes for both carbonate and alluvial pumping for an 11-year period (1987 to 1997) and a 9-year period (1998 to 2005), based on the availability of pumping and monitoring data and the significant increase in pumping from the carbonate rock aquifer that began in 1998.

Four USGS surface water gauging stations in the MRSA are considered in this study: Pedersen Spring (site no. 09415910), Pedersen East Spring (site no. 09415908), Muddy Springs (site no. 09415900), and Warm Springs West (site no. 09415920) (Table 1; Figure 3). All four sites record spring discharge continuously. The gauges at Pedersen Spring and Pedersen East Spring are V-notch weirs that measure two small springs on the wildlife refuge. These are the highest elevation springs in the area. The weir at the Pedersen Spring gauge developed a leak in 2003, and we use flow data only from 1998 through water year 2002. The gauge at Pedersen East Spring was recently installed, in April 2002.

The gauges at Warm Springs West and Muddy Springs are Parshall flumes that were installed in 1985 and have operated since that year, except for a 21-month gap from October 1994 to June 1996. Warm Springs

Table 1
Monitoring Site Name, Basin, Aquifer, Period of Record, and Frequency of Measurements

Well Name	Hydrographic Basin	Aquifer	Water Level Elevation[1] (m)	Period of Record	Frequency of Measurements
EH-5B	Upper Moapa Valley	Carbonate	553.4	1987–2005	Periodic[2] to 1997, continuous from 1997
EH-4	Upper Moapa Valley	Carbonate	553.4	1987–2005	Periodic to 1997, continuous from 1997
CSV-2	Upper Moapa Valley	Carbonate	547.4	1985–2005	Periodic, continuous from 1991 to 1994 and 1999 to 2005
Lewis North	Upper Moapa Valley	Alluvial	552.3	1987–2005	Periodic
Lewis South	Upper Moapa Valley	Alluvial	546.8	1987–2005	Periodic
Lewis 2	Upper Moapa Valley	Alluvial	547.9	1988–2005	Periodic
EH-3	Lower Moapa Valley	Carbonate	Unknown	1987–2005	Periodic
EH-7	Lower Moapa Valley	Carbonate	Unknown	1987–2005	Periodic
MX-4	Coyote Spring Valley	Carbonate	555.2	1985–2005	Periodic, continuous from 1990 to 1996 and 1999 to 2005
CE-VF-2	Coyote Spring Valley	Carbonate	566.0	1987–2005	Periodic, continuous from 2004
CE-VF-1	Coyote Spring Valley	Alluvial	584.3	1988–2005	Periodic
CSV-3	Coyote Spring Valley	Alluvial	556.0	1987–2005	Periodic
SHV-1	Hidden Valley	Carbonate	554.2	1985–2005	Periodic, continuous from 2001
M-1	California Wash	Carbonate	553.5	2001–2005	Continuous
ECP-1	California Wash	Carbonate	553.5	2001–2005	Continuous
TH-2	California Wash	Carbonate	553.1	2001–2005	Continuous
M-2	Garnet Valley	Carbonate	552.5	2001–2005	Continuous
M-3	Garnet Valley	Carbonate	553.1	2001–2005	Continuous

Spring Name	Hydrographic Basin	Aquifer	Spring Orifice Elevation (m)	Period of Record	Frequency of Measurements
Pedersen Spring	Upper Moapa Valley	Carbonate	552	1998–2002	Continuous
Pedersen East Spring	Upper Moapa Valley	Carbonate	551	2002–2005	Continuous
Warm Springs West	Upper Moapa Valley	Carbonate	548 (average elevation)	1998–2005	Continuous
Muddy Springs	Upper Moapa Valley	Carbonate	535	1998–2005	Continuous
Plummer West	Upper Moapa Valley	Carbonate	536	1998–2004	Periodic

[1]Water level elevation as of January 2001.
[2]Periodic means one or two measurements a month.

West measures the collective discharge from five spring groups upstream on the refuge, including the Pedersen Spring and Pedersen East Spring groups. The Muddy Springs gauge measures the outflow from Muddy Springs, the largest and lowest elevation spring in the area.

Several factors affected the quality of records at these surface water stations prior to 1998, including an unmeasured irrigation diversion above one station, a fire that may have affected another station, a gap in the records because of lack of funding, and some unexplained variability or discontinuities in the flow records. For these reasons, we use data only from 1998 on for these sites. In addition to these four sites, the U.S. Fish and Wildlife Service made monthly measurements of spring discharge at the Plummer West spring (Table 1; Figure 3) from June 1998 to November 2004 using a 45° V-notch weir installed at the outflow of the spring pool. This spring is lower in elevation relative to other springs in the immediate area and does not contribute to the collective flow measured at the Warm Springs West site. A theoretical rating was used to convert stage to discharge at this site. The measurements stopped when the weir was removed because of habitat restoration at the spring.

Elevation Data

The Southern Nevada Water Authority completed a comprehensive elevation survey of numerous wells and stream gauges in the MRSA and surrounding basins, including several of the monitoring sites in this study (Southern Nevada Water Authority 2003, 2005). We referenced elevations from the survey and used a level to determine the elevations of spring monitoring sites not included in the survey (Table 1). The spring elevations were used in combination with the ground water elevations in carbonate monitoring wells to estimate the hydraulic head differential at each spring or spring group.

Statistical Analyses

We used a *t*-test to compare the average pumping volumes for two periods, pre- and post-1998, based on a fourfold increase in pumping from the carbonate rock aquifer that occurred beginning in 1998. Temporal trends in the two carbonate monitoring wells, EH-5B and EH-4, in the MRSA were analyzed pre- and post-1998 periods as well. We evaluated three main stressors: climate, alluvial pumping/ET, and carbonate pumping. We excluded seismic activity, barometric pressure, and earth tides on the grounds that effects from these factors are minor and short term, at least for our scales of interest (Pohlmann 1994; Fenelon and Moreo 2002; Waddell and Roemer 2006).

Explanatory variables for the multiple regressions used in the trend analysis were initially evaluated through automated stepwise procedures (Helsel and Hirsch 1992; Ott 1993) using the statistical software SPSS. We then used regression diagnostics, regression statistics, and residual plots to select variables, to test regression assumptions, and to evaluate multicollinearity among variables, which can cause the values of coefficients to be unstable or their signs to be unreasonable (Helsel and Hirsch 1992). These steps were done iteratively, using the data from the EH-5B and EH-4 carbonate monitoring wells, different explanatory variables, and different periods of record, until we developed a common subset of explanatory variables that applied to both wells. We relied on the variance inflation factor, standardized coefficients, PRESS statistic, and adjusted r^2 to help us evaluate variables and regressions. Candidate explanatory variables for the multiple regressions included a wide range of divisional climate statistics from Divisions 3 and 4, including monthly precipitation, 6- to 36-month moving averages of monthly precipitation, 4- to 72-month SPI, and higher order transforms of all moving averages and SPIs. We address some of the differences and implications of using various climate parameterizations in a later section.

We did not quantitatively model pumping or ET in the statistical analysis. The alluvial pumping/ET signal was assumed to be seasonal and was represented with the periodic functions, sine and cosine, with the time variable used to test the assumption that there were no long-term changes resulting from alluvial pumping/ET. We interpreted coefficients from the sine and cosine terms in the regressions to define the amplitude and phase of the seasonal periodicity (Helsel and Hirsch 1992). These authors suggest always adding both sine and cosine terms, even if one of the pair is not statistically significant, to allow the regression to determine the phase shift from the data rather than arbitrarily.

Carbonate pumping was represented with a binary variable, which was changed from zero to one during periods of increased carbonate pumping. This was done for two reasons. First, we did not have actual monthly pumping data for the entire record; only annual pumping data were available. Second, this approach permitted us to use analysis of covariance to quantify any statistically significant changes that occurred coincident with periods of increased pumping (Helsel and Hirsch 1992; Ott 1993). The key variables in the analysis of covariance approach are the interaction terms or the products of the binary variable with time, sine, and cosine. The regression coefficients and statistics associated with these terms indicate changes in time, amplitude, or phase during periods of increased carbonate pumping. Our approach implicitly assumes that a threshold level of carbonate pumping exists below which there are no measurable effects. Preliminary statistical analysis showed this assumption to be acceptable in our system for the period of interest, but such an approach would not be appropriate in all cases.

For the analysis of spatial trends in carbonate and alluvial monitoring wells throughout the system, we considered the period January 2001 to September 2005, a period encompassing extreme climate variability and increased carbonate pumping. Continuous data, when available, were averaged to monthly values. Several months of data were missing in 2004 for some of the carbonate wells in California Wash. We estimated these missing data based on regressions with TH-2, a carbonate well located in the same basin with a complete record for the period. Spatial trends in all wells in the southern portion of the flow system were compared through hierarchical cluster analysis, using average linkage and correlation

coefficient distance, and through time series seasonal decomposition. We tested for statistically significant seasonality through regression analysis using the sine and cosine of time, as mentioned previously. In those wells with seasonality, we used a seasonal decomposition procedure in the time series analysis in SPSS to compute and compare the amplitude and phase of the seasonality at all wells for four complete years, January 2001 to December 2004. In the seasonal decomposition procedure, the time series is separated into seasonal, trend, and cycle components. The seasonal index is the average deviation of each month's water level from the level that was due to the other components that month, expressed in the original measurement units. The seasonal index provided an objective measure to compare the relative amplitude and phase of the seasonality for all wells. We also examined the recharge response to the extremely wet year in 2005 for all wells.

For the analysis of spring discharge/ground water relationships, we considered the period 1998 to 2005, when spring discharge data are most reliable. For each spring, we normalized flow to the initial flow value in the period of record and then plotted the normalized flow as a function of carbonate water levels at EH-5B. The slopes for linear regressions of normalized flow vs. ground water elevation were computed and compared, based on the elevations of the spring orifices and the assumed hydraulic head differential at each spring.

Results and Discussion

Climate Data

Figure 4a shows total winter precipitation in Climate Divisions 3 and 4 for the period 1985 to 2005. Winter precipitation and late spring snowmelt, rather than summer precipitation, have been shown to be the principal sources of recharge in the fractured carbonate rock of this area (Winnograd et al. 1998). Winter precipitation was quite variable during this period, particularly in Climate Division 4. The winter totals of 2005, 1993, and 1992 were the highest, second highest, and third highest October to March precipitation totals, respectively, in Climate Division 4 since recordkeeping began in 1895. The winter total of 2002 was the second lowest October to March total in Division 4 since 1895.

The 12-, 24-, and 60-month SPI for Nevada Climate Divisions 3 and 4 from 1980 through 2005 are shown in Figure 5. The SPI plots show that both wet and dry conditions have been experienced simultaneously in each division, depending on the time scale of interest. There is less variability in the SPI values at longer time scales.

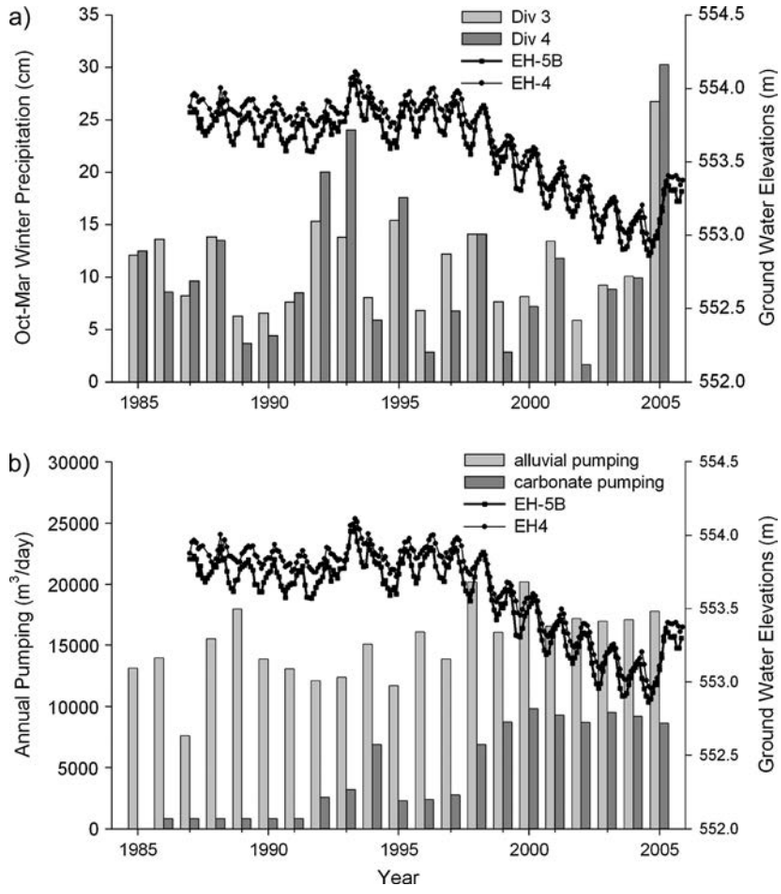

Figure 4. Water levels in carbonate monitoring wells EH-5B and EH-4 for the period 1985 to 2005 with October to March winter precipitation in Nevada Climate Divisions 3 and 4 (a, top plot) and annual alluvial and carbonate pumping (b, bottom plot).

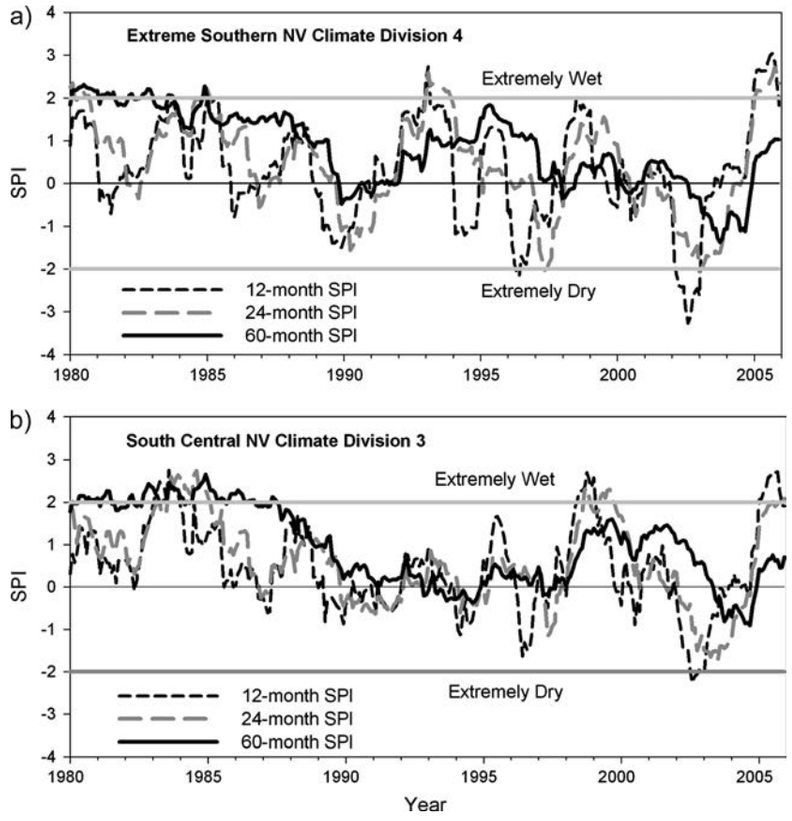

Figure 5. The 12-, 24-, and 60-month SPI for Nevada Climate Divisions 4 (a, top plot) and 3 (b, bottom plot) for 1980 to 2005. The definition of the terms *extremely wet* and *extremely dry* is discussed in the text.

Generally, conditions have been more variable for Division 4 (Extreme Southern Nevada) than Division 3 (South Central Nevada). Considering the 12- and 24-month SPI, Division 4 (Figure 5a) was extremely wet in 1992 and 1993 and extremely dry in 1996 and 1997. In contrast, Division 3 (Figure 5b) was normal or slightly above normal in 1992 and 1993 and not as dry in 1996 and 1997 but was extremely wet in 1998 and 1999. Both climate divisions experienced extremely dry conditions in 2002 and extremely wet conditions in 2005.

One purpose of this study was to discuss the implications of using various climate parameterizations in this type of statistical analysis. Specifically, we explore the difference in using raw precipitation data, in the form of moving average precipitation, vs. a drought index such as the SPI. Generally, the two parameters track similar trends. Moving averages become normally distributed and linearly related to SPI at longer time scales, as a consequence of the larger sample sizes and the Central Limit Theorem (Ott 1993). Guttman (1998) reported that the SPI spectral characteristics conform to what is expected for a moving average process.

A major difference between the two variables is with their units and frequency distributions. The units of SPI are normalized variates, and the frequency distribution is symmetric and centered about a mean of 0. The absolute value of SPI is 0 under average conditions and increases as conditions become either wet or dry. Any regression term containing SPI, or any of its higher order transforms, is the product of the regression coefficient and the value of SPI at that time step. Such a term will have the least amount of influence on the predicted water level under average conditions, when the product is close to zero, and will be larger and more influential, although opposite in sign, as the conditions become wetter or drier. We characterize the regression response to this parameterization as symmetric, in the sense that both wet and dry years will be influential in determining the simulated water level. The PDI (Palmer 1965) and other standardized precipitation or drought indexes centered on zero (see Hayes [2006] for a description of several common indexes) will have similar characteristics.

By contrast, the units of precipitation are nonstandardized values and are always positive, and the frequency distribution of moving average precipitation at shorter time scales is asymmetric and positively skewed (McKee et al. 1993). The square or cubic transform of this variable increases this skewness. Any product in the regression containing precipitation, or any of its higher order transforms, will have the least amount of influence on the predicted water level under dry conditions, or low values of precipitation, and will be more influential as conditions get wetter and precipitation values increase. We characterize the regression response to this parameterization as asymmetric, in the sense that wet years will be more influential in determining the simulated water level than dry years. We propose that the relative importance of these two parameters, moving average precipitation vs.

SPI, in a regression analysis, will have implications about whether the system responds asymmetrically to only wet or dry conditions or symmetrically to both wet and dry conditions.

We excluded two other common climate parameterizations in this study, the PDI and the cumulative rainfall departure from normal, on the basis of critical reviews of these parameterizations. The PDI is a widely used measure of meteorological drought severity (Palmer 1965). Alley (1984) criticized the PDI as being complex to calculate, using somewhat arbitrary rules to designate droughts or wet periods, and being limited in geographical extent. Guttman (1998) compared the PDI and the SPI and reported that the spectral characteristics of the PDI varied geographically, while those of the SPI did not. He concluded that the PDI is a complex structure with a long memory, while the SPI is an easily interpreted, moving average process.

The cumulative rainfall departure from normal measures the accumulated departure of precipitation from a mean defined for some time period. Weber and Stewart (2004) criticized the measure as being problematic for nonnormally distributed precipitation, a common condition in arid environments. Furthermore, they pointed out that the calculated departure is extremely variable depending on the starting and ending points and the length of the period for which the mean is defined.

Pumping and ET

The pumping from the carbonate rock aquifer increased slowly from 1987 to 1997 and then considerably after 1998 (Figure 4b). Carbonate pumping averaged 2200 m^3/d for the period 1987 to 1997 and 8870 m^3/d for the period 1998 to 2005, a statistically significant fourfold increase ($p = 0.000$). The higher values pumped in 1993 and 1994 compared with other years in the earlier period are partly due to a 121-d aquifer test conducted from December 1993 to April 1994 (Buqo 1994).

Annual alluvial pumping increased slightly over the same period from 13,500 m^3/d for the period 1987 to 1997 to 17,750 m^3/d for the period 1998 to 2005 ($p = 0.005$) (Figure 4b). By comparison, we estimated ground water discharge from the alluvial aquifer through phreatophyte ET in the MRSA to be about 5000 m^3/d, based on preliminary information from a USGS study of ET in the area (G.A. DeMeo, written communication, 2006). Based on these estimates, alluvial pumping seems to place a greater demand on the alluvial aquifer than ET. Ground water discharge through ET does not occur in the southern part of the flow system outside the MRSA because of the greater depths to alluvial ground water in other areas. Both alluvial and carbonate pumping are generally greatest during the months of May through September, when demand is highest. Minimum pumping occurs in January in both aquifers.

Temporal Trends in Two Carbonate Monitoring Wells

Ground water elevations in the carbonate rock aquifer in the MRSA, as measured in wells EH-5B and EH-4, show a strong seasonal trend, with minimum annual elevations usually observed in the fall (Figure 4). Two other trends are evident in the ground water level data: annual increases in 1992, 1993, and 2005 and a multiyear decrease beginning in 1998. The increases in 1992, 1993, and 2005 correspond to years of high winter precipitation, especially in Division 4 (Extreme Southern Nevada) (Figure 4a). The decrease beginning in 1998 coincides with the fourfold increase in pumping from the carbonate rock aquifer that occurred at the same time in the MRSA (Figure 4b). The initial water level elevations and the magnitude of increases and declines in both wells are similar, despite the distance separating the two wells and their varying proximities to the pumping center. This is indicative of the uniformity of the potentiometric surface in the carbonate rock aquifer in the MRSA, as a result of the high transmissivities.

We first examined data statistically from EH-5B and EH-4 data for the years 1987 to 1998, a period of minimal carbonate pumping. For both wells, the optimum explanatory variables determined through stepwise multiple regression analysis were sine, cosine, the cube of the Division 4 24-month moving average monthly precipitation, the Division 3 30-month SPI, the Division 4 60-month SPI, time, and carbonate pumping. These seven explanatory variables explained between 65% and 75% of the variance of the data for the period. The most influential terms in the regression, based on the standardized coefficients and the t values, were the sine/cosine, followed by the cubic transform of the Division 4 24-month moving average monthly precipitation. The regression coefficient for time for this period was positive but very small, meaning that there was no long-term decline associated with the alluvial and carbonate pumping that occurred prior to 1998. The effect of the 121-d aquifer test in 1994 in the carbonate rock aquifer, as measured with the carbonate binary pumping variable, was statistically significant but short-lived, appearing to extend about 2 months after the completion of the aquifer test.

The importance of the cubic transform of Division 4 24-month moving average precipitation in the regression is interesting for several reasons. First, the selection of this term, rather than lower order terms of the 24-month moving average, implies that the system is quite responsive to wet years since the cube leads to right skewness in the data and emphasizes wet years. We are using climate division data, which are primarily based on valley floor weather stations, as a surrogate measure of recharge in the system. But the proportion of recharge in mountainous areas during wet years may be much greater than is indicated by the precipitation data from valley floor weather stations. The importance of the cubic transform over lower order terms in the regression may be an indication of the greater proportion of recharge in wetter years.

Second, the fact that a higher order transform of precipitation was selected rather than higher order transforms of SPI means that the system response appears to be asymmetric and more sensitive to wet years than to dry years, as described previously. An example of this asymmetry can be observed in the response of water levels to the extremely wet period in 1992 to 1993 and the lack of a response to the extremely dry period in 1996

to 1997. This sensitivity to wet years, often associated with El Niño events, has been described for other ground water systems in the arid southwestern United States (Hanson et al. 2004; Scanlon et al. 2006).

Finally, the stepwise selection of a precipitation variable from Climate Division 4 ahead of Division 3 states that precipitation in the southern portion of the flow system is quite important. In the original conceptual flow model (Eakin 1966), most of the recharge was believed to occur in the north and recharge in the southern portion was believed to be minor. Our results may contradict this and support greater recharge in the southern portion of the flow system, as suggested by Johnson and Mifflin (2006). Higher precipitation rates, thin soils, and the exposure of high-permeability carbonates at the surface all likely contribute to greater recharge in the high-elevation areas of the southern portion of the flow system.

Next, we extended the regressions for both carbonate monitoring wells to December 2002. This period includes 5 years of increased carbonate pumping, 1998 to 2002, and the extreme drought of 2002. We used the same seven explanatory variables as in the previous regressions, along with three interaction terms of carbonate pumping with time, sine, and cosine. The interaction terms capture any change in the slope with time and the periodicity, corresponding to the period of increased carbonate pumping after 1998. The regressions explained between 95% and 96% of the variance in the two carbonate monitoring wells for the period 1987 to 2002 (Figure 6). The adjusted r^2 values improved considerably from regressions for the previous 1987 to 1998 period, in part because the long-term decline beginning in 1998 dominates the variance and this trend is simulated very well by the regression equations. The regression equations for the 1987 to 2002 period are shown subsequently:

$$\begin{aligned}\text{EH-5B monthly water level (m)} &= 1.78 \times 10^{-5}(t) \\ &+ 0.085\left[\sin(2\pi t)\right] + 0.048\left[\cos(2\pi t)\right] \\ &+ 1.61 \times 10^{-5}(\text{D4 24 m avg})^3 + 0.039(\text{D3 30 m SPI}) \\ &+ 0.023(\text{D4 60 m SPI}) + 6.033(\$\text{bc}\$) \\ &- 1.77 \times 10^{-4}(\$\text{bc}\$ \times t) + 0.013\left[\$\text{bc}\$ \times \sin(2\pi t)\right] \\ &+ 0.027\left[\$\text{bc}\$ \times \cos(2\pi t)\right] + 553.09\end{aligned}$$

$$\begin{aligned}\text{EH-4 monthly water level (m)} &= 8.22\text{E} \times 10^{-6}(t) \\ &+ 0.066\left[\sin(2\pi t)\right] - 0.009\left[\cos(2\pi t)\right] \\ &+ 1.21 \times 10^{-5}(\text{D4 24 m avg})^3 + 0.042(\text{D3 30 m SPI}) \\ &+ 0.012(\text{D4 60 m SPI}) + 6.320(\$\text{bc}\$) \\ &- 1.85 \times 10^{-4}(\$\text{bc}\$ \times t) + 0.026\left[\$\text{bc}\$ \times \sin(2\pi t)\right] \\ &+ 0.033\left[\$\text{bc}\$ \times \cos(2\pi t)\right] + 553.55\end{aligned}$$

where t = time (day of year); sin and cos = the sine and cosine terms for the periodicity; D4 24 m avg = the 24-month moving average precipitation (mm) for Climate Division 4; D3 30 m SPI = the 30-month SPI for Climate

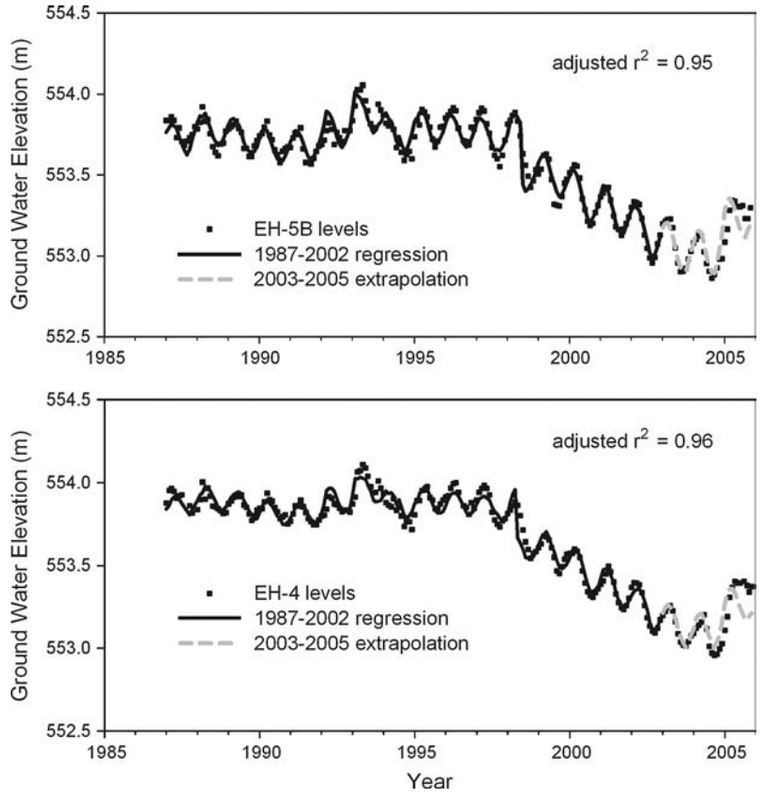

Figure 6. Water levels in carbonate monitoring wells EH-5B and EH-4 for 1987 to 2005 with multiple regressions for 1987 to 2002 and extrapolations of the regression for the period 2003 to 2005.

Division 3; D4 60 m SPI = the 60-month SPI for Climate Division 4; bc = the binary variable for the carbonate pumping; bc $\times$ t = the interaction term of the carbonate binary variable and time; and bc $\times$ $\sin(2\pi t)$ and bc $\times$ $\cos(2\pi t)$ = the interaction terms of the carbonate binary variable and the periodicity.

Coefficients and prediction values from the regressions for each well were basically equal for the two periods, 1987 to 1998 and 1987 to 2002, and the two regressions plot on top of each other during the overlapping years. Only the value of the regression coefficient for the carbonate binary variable changed between the two periods. The coefficient for the interaction term with time was negative and statistically significant, indicating that ground water levels began declining coincident with the increased carbonate pumping in 1998. The interaction terms with sine and cosine indicated that the amplitude of the seasonal pattern increased by 2.7 cm and the phase shifted 2 to 3 weeks earlier in both wells after 1998, although only the phase shift in EH-5B was statistically significant. Extrapolations of the 1987 to 1998 regressions beyond 1998 with climate terms alone were unable to simulate the long-term decline that began in 1998. To simulate this decline, we had to add the binary variable to account for increased carbonate pumping. We infer from these results that the long-term decline in carbonate levels beginning in 1998 is a result of the increased carbonate pumping that began at the same time.

The regressions for the period 1987 to 2002 were extrapolated for 3 years from 2003 to 2005, using the same explanatory variables, in an attempt to validate the statistical model (Figure 6). The regressions appear to simulate the ground water trends in these years for both wells, continuing to decline through 2004 and then increasing in 2005 in response to the extremely wet year. The wet year response in 2005, as predicted by the regressions, is based on the responses observed and fitted statistically in the 1987 to 2002 regressions. While the extremely wet years in 1992, 1993, and 2005 caused large increases in water levels, the extremely dry conditions of 2002 appear to have relatively little effect on water levels. This demonstrates what we interpret to be the sensitivity and asymmetry in the system response to wet years over dry years.

Spatial Trends in Carbonate and Alluvial Monitoring Wells

Most of the carbonate wells examined in this study show similar behavior, with a seasonal pattern imposed over a long-term declining trend from 1998 until 2004 and a large increase in response to the 2005 wet year (Figure 7). We assume that these wells are responding to the same climate and pumping signals as described for EH-5B and EH-4 previously. The multiyear declining trend through 2004 observed in most of the carbonate wells is most likely a result of the increased carbonate pumping in the MRSA. CE-VF-2 and SHV-1, the two more distant carbonate wells, do not appear to start declining until about 2000 rather than 1998.

Figure 8 presents the results from the cluster analysis of all wells examined in this study. Nine of the 11 carbonate wells are very similar to each other, with a similarity level more than 97. However, even within this group, there are subtle but important differences in the amplitude and phase, as indicated by the results from the time series seasonal decomposition (Figure 9). EH-5B has the greatest amplitude and the earliest phase in comparison to the other carbonate wells. It also has more of a characteristic pumping-induced asymmetry, as observed by Johnson and Mifflin (2006), in contrast to the other carbonate wells, which are more symmetric and sinusoidal. The seasonal amplitude, phase, and asymmetry may be related to the proximity of EH-5B to the Arrow Canyon production wells (Figure 3) and other alluvial production wells. MX-4 and M3 have slightly smaller amplitudes and later phases compared with the other carbonate wells. There is a north-south trending thrust fault separating these two wells from the MRSA and California Wash. The stratigraphic position of the carbonate rocks may be shifted across the fault, and this may be part of the reason for the smaller amplitude and later phase in the wells west of the fault. We observed no evidence of pumping-induced asymmetry in the hydrograph for MX-4, in contrast to Johnson and Mifflin (2006). CE-VF-2 and SHV-1, two other carbonate wells farther west of the thrust fault and the MRSA, partitioned quite differently from the main group of carbonate wells because of a lack of seasonality and, in the case of SHV-1, a much smaller decline and recharge response.

In general, carbonate wells located closer to the MRSA tend to have larger amplitudes and earlier phase shifts than those farther away, with the most distant wells in Hidden Valley and Coyote Spring Valley showing no seasonality and a delayed drawdown as well. Such a pattern could be suggestive of a muted or attenuated signal with distance from the source, although this is more clearly evident in the upgradient direction than in California Wash or Garnet Valley. Given the complex geology and the fractured nature of the flow system, responses may not be expected to be isotropic or solely a simple function of linear distance. Johnson and Mifflin (2006) postulated the presence of a hydraulic barrier between California Wash and the MRSA based on their modeling results, but we found no evidence here to support the existence of such a barrier.

The alluvial monitoring wells responded and partitioned quite differently from the carbonate wells and from each other (Figures 7 and 8). The three alluvial wells in the MRSA partitioned into two separate clusters, which are quite unique from the carbonate wells in the same basin. The amplitude is much greater and the phase is earlier than in the adjacent carbonate wells (Figure 9). These differences may be due to the different hydraulic properties of the unconfined alluvial aquifer and the fact that the seasonal signal is partly a result of alluvial pumping in the same aquifer. There is also more of a pumping-induced asymmetry observed in the seasonal pattern, particularly in Lewis North, the closest alluvial well to the Arrow Canyon production wells. Only one of these three wells, Lewis North, shows a long-term decline through 2004 (Figure 7). CSV-3, an alluvial well in Coyote Spring Valley, has poorly defined seasonality, a long-term

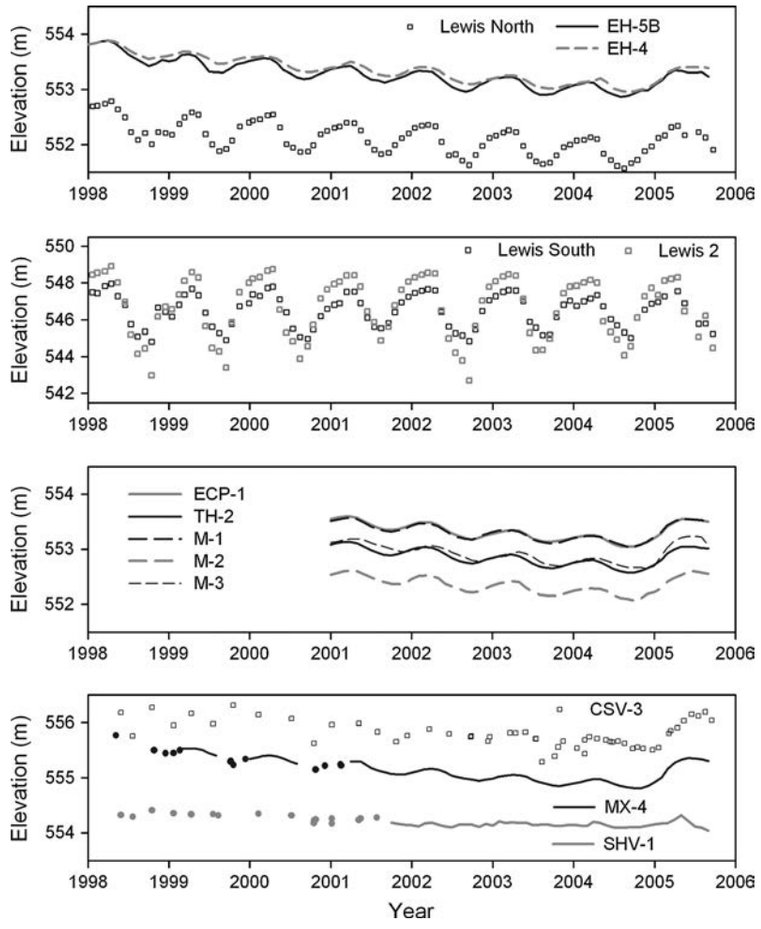

Figure 7. Hydrographs from representative carbonate and alluvial monitoring wells in the MRSA (top two plots), California Wash and Garnet Valley (third plot), and Coyote Spring Valley and Hidden Valley (bottom plot) for the period 1998 to 2005. Lines represent periods of continuous data in the carbonate wells. Symbols represent periodic measurements, open for alluvial wells and closed for carbonate wells. Note the different scales on the vertical axes. Three wells discussed in the text, CSV-2, CE-VF-1, and CE-VF-2, are not plotted.

decline beginning in 2000, and a response to the 2005 wet year. It was partitioned with CE-VF-2, a carbonate well in the same basin with a very similar hydrograph. CE-VF-1, a second alluvial well in northern Coyote Spring Valley, showed no seasonality or long-term decline or recharge response. It partitioned very differently from any of the other wells (Figure 8).

The response to the extremely wet year in 2005 varied by aquifer type. The timing and magnitude of the response are quite uniform in most of the carbonate wells, with the exception of SHV-1 (Figure 7). The 2005 wet year response is more dampened and short-lived in two alluvial wells, Lewis North and CSV-3, and not present at all in the other three alluvial monitoring wells (Figure 7). The widespread and rapid response to the 2005 wet year in the carbonate rock aquifer is surprising. We assumed that climate responses in the regional carbonate aquifer would be attenuated. We believe that the uniform, widespread wet year response, as well as the importance of Division 4 precipitation in the regression analysis, suggests that the carbonate rock aquifer is directly recharged from higher elevation areas in the southern portion of the flow system. The carbonate lithologies are exposed at the surface at higher elevations and are likely quite efficient in capturing recharge, as suggested by others (Winnograd and Thordarson 1975; Winnograd et al. 1998; Johnson and Mifflin 2006). Thomas et al. (1996) postulated that most of the recharge to the Sheep Mountains on the west side of Coyote Spring Valley must flow north and east into the basin and the MRSA because of noncarbonate barriers to westward, southward, and southeastward flow. The results from this study support these conclusions.

The trends described in this study appear to be unique to the southern portion of the White River flow system. They are completely lacking in the records for other wells outside the flow system including EH-7 and EH-3, two carbonate monitoring wells located east of the MRSA (Figure 2), and several other carbonate monitoring wells located to the west of Coyote Spring Valley and the Sheep Mountains. The relevance of these spatial relationships is that they indicate that both climate and pumping impacts are propagated at approximately the same scale throughout much of the southern portion of this system. The area is hydraulically connected through the carbonate rock aquifer. Climate and pumping effects are small but spatially extensive, in part because of the high

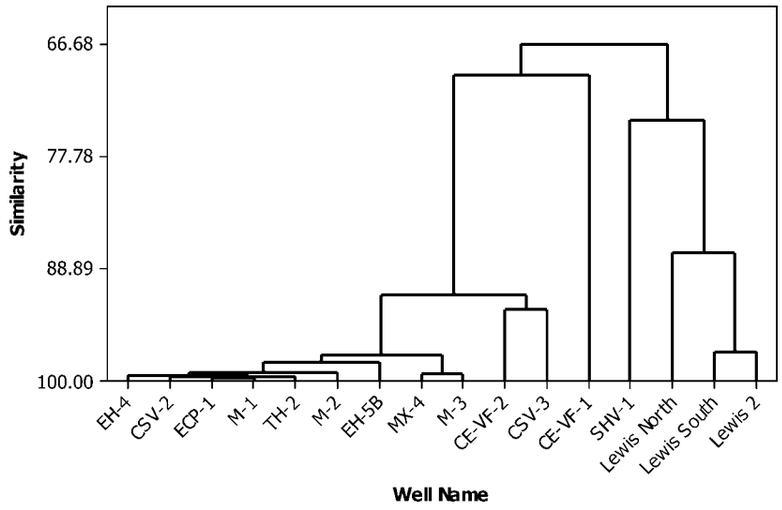

Figure 8. Cluster tree of 11 carbonate and 5 alluvial wells, using average linkage and correlation coefficient distances, with water levels from the period January 2001 to September 2005. The five alluvial wells are Lewis North, Lewis South, and Lewis 2 (all in the MRSA) and CSV-3 and CE-VF-1 (in Coyote Spring Valley).

transmissivity of the carbonate rock aquifer. Next, we examine what these effects mean for regional spring discharge.

Trends in Spring Discharge

Ultimately, much of the interest in ground water level trends relates to effects on spring discharge. Since 1998, we have observed a small but widespread pumping-induced decline in carbonate water levels in the MRSA and adjacent basins, followed by a sharp increase in water levels in response to the record precipitation in 2005. Trends in spring discharge are similar to carbonate water level trends, decreasing through 2004 and increasing after that. The springs essentially behave as artesian flowing wells. However, there are differences in the responses among individual springs, as discussed subsequently.

We hypothesized that because the drawdown is widespread and fairly uniform in the carbonate rock aquifer underlying the MRSA, the sensitivity of any one spring to declines in the water level should be related more to the elevation of the spring orifice and the initial hydraulic head rather than the proximity to pumping. Higher

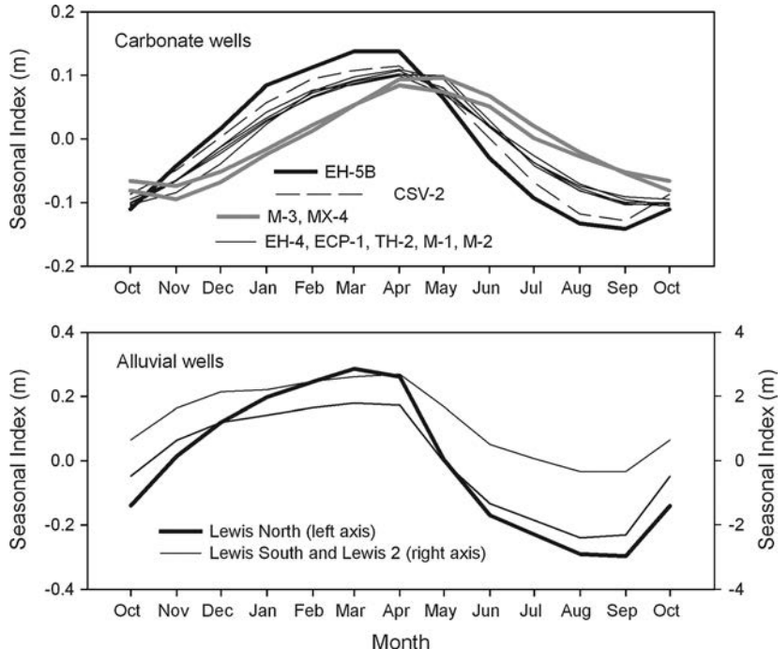

Figure 9. Seasonal indexes for carbonate and alluvial monitoring wells with statistically significant seasonality, based on time series seasonal decomposition of water level data for a 4-year period from January 2001 to December 2004. The seasonal index is the average deviation of each month's water level (in meters), from the level that was due to the other components that month.

elevation springs will be proportionately more sensitive to a uniform decline in ground water levels than lower elevations springs because of their smaller hydraulic head. The elevations of the spring orifices are presented in Table 1. Figure 10 presents normalized spring discharge for several springs of different elevations as a function of ground water elevation at EH-5B. Higher elevation springs have generally steeper regression slopes, meaning that they lose proportionately more flow for a given decline in head than the lower elevation springs. The fairly uniform water level declines or increases observed in the carbonate rock aquifer head result in much greater proportions of head loss or gain at higher elevation springs, with commensurate changes in flow. This indicates that the sensitivity of the various springs to ground water level declines is partly a function of their elevation and initial hydraulic head.

The higher elevation springs may represent some of the most important habitat for thermophilic, aquatic species in the Muddy River Springs ecosystem. Temperatures in the thermal water are warmer at the headwaters of the springs (Cross 1976), and there is generally less habitat disturbance and fewer introduced species in the headwater areas, especially at some of the smaller higher elevation springs. The position of these springs in the landscape means that they are very important in terms of habitat value and more susceptible to pumping-related impacts.

Conclusions

When ground water development approaches the limits of sustainability, even small changes in inflow, outflow, or storage can have economic or environmental consequences. In this study, we explore the premise that under such conditions, anthropogenic impacts of concern may be on the same scale as climate variability and both will need to be accounted for explicitly in any analysis. We use statistical methods to examine the response of water levels and spring discharge in a regional flow system in southern Nevada to climate and pumping. We consider the issue of climate parameterization and evaluate the use of several measures of climate variability, including raw precipitation data and several precipitation and drought indexes. Ultimately, the cubic transform of 24-month moving average precipitation was the most useful measure in our system because it captures the integrated water level response to precipitation over time and the asymmetric response of the system to wet conditions over dry conditions. This sensitivity to wet years, often

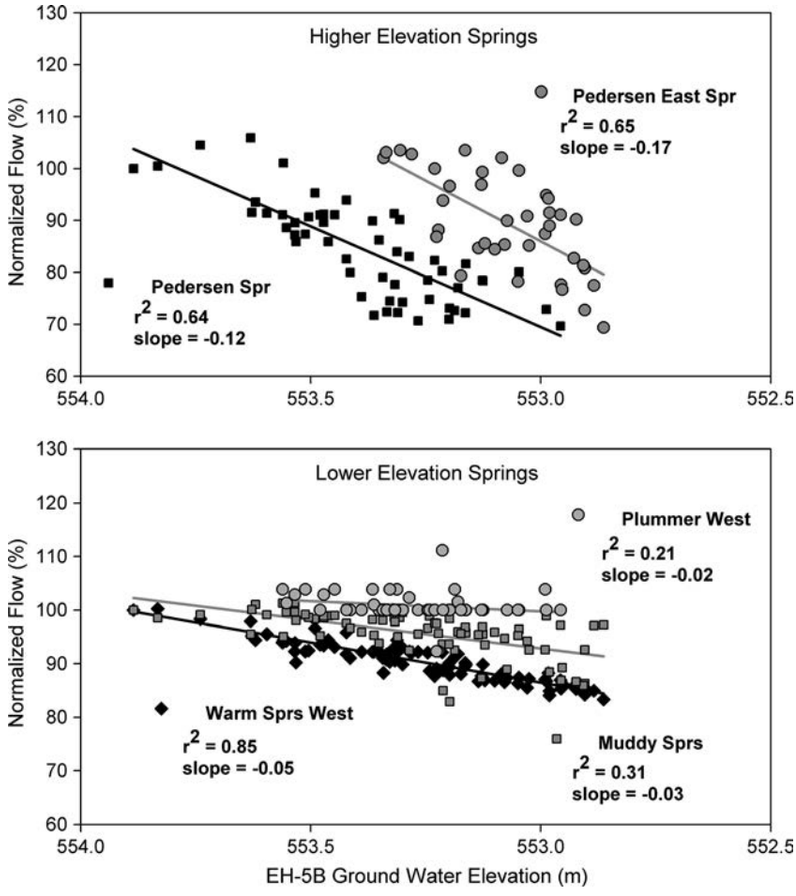

Figure 10. Normalized flow at various springs in the MRSA as a function of EH-5B levels. Values on the *x* axis are from high to low. Periods of record for each spring are given in the text.

associated with El Niño events, has been described for other ground water systems in the arid southwestern United States (Hanson et al. 2006; Scanlon et al. 2006).

Using cluster analysis and time series seasonal decomposition, we show that both climate and pumping impacts are propagated at approximately the same scale throughout much of the flow system. Relatively small changes in carbonate water levels are observed to cause corresponding changes in regional spring discharge. The sensitivity of any one spring to changes in water levels is, in part, related to the elevation and hydraulic head at the spring. The higher the elevation of the spring, the less hydraulic head at the spring initially and the more sensitive the spring is to ground water level changes. This is important since these springs represent some of the most important habitat for aquatic species in the Muddy River Springs ecosystem. Our statistical results give strong inference that the carbonate rock aquifer and the regional springs are well connected and responding to changes in climate and pumping and that the system is reaching the limits of sustainability.

Acknowledgments

We thank Rick Waddell and Bill Van Liew for helping formulate the ideas presented in this article, and Dan Craver for helping prepare figures. We also thank two reviewers, Scott James (associate editor) and Randall Hanson, for their comments and feedback during the review process.

References

Alley, W.M. 1984. The Palmer Drought Severity Index: Limitations and assumptions. *Journal of Climate and Applied Meteorology* 23, no. 7: 1100–1109.

Alley, W.M., and S.A. Leake. 2004. The journey from safe yield to sustainability. *Ground Water* 42, no. 1: 12–16.

Alley, W.M., T.E. Reilly, and O.L. Franke. 1999. Sustainability of ground-water resources. USGS Circular 1186. Reston, Virginia: USGS.

Berger, D.L., K.C. Kilroy, and D.H. Schaefer. 1988. Geophysical logs and hydrologic data for eight wells in the Coyote Spring Valley area, Clark and Lincoln counties, Nevada. USGS Open-File Report 87-679. Reston, Virginia: USGS.

Bredehoeft, J.D. 2002. The water budget myth revisited: Why hydrologists model. *Ground Water* 40, no. 4: 340–345.

Bredehoeft, J.D. 1997. Safe yield and the water budget myth. *Ground Water* 35, no. 6: 929.

Bunch, R.L., and J.R. Harrill. 1984. Compilation of selected hydrologic data from MX missile-siting investigation, east-central Nevada and western Utah. USGS Open-File Report 84-702. Reston, Virginia: USGS.

Buqo, T.S. 1994. Results of long-term testing of the Arrow Canyon Well. Logandale, Nevada: Moapa Valley Water District.

Cross, J.N. 1976. Status of the native fish fauna of the Moapa River (Clark County, Nevada). *Transactions of the American Fisheries Society* 105, no. 4: 503–508.

Deacon, J.E., and W.G. Bradley. 1972. Ecological distribution of the fishes of the Moapa (Muddy) River in Clark County, Nevada. *Transactions of the American Fisheries Society* 101, no. 3: 408–419.

Dettinger, M.D., J.R. Harrill, and D.L. Schmidt. 1995. Distribution of carbonate-rock aquifers and their potential for development, southern Nevada and adjacent parts of California, Arizona, and Utah. USGS Water Resources Investigations Report 91-4146. Reston, Virginia: USGS.

Eakin, T.E. 1966. A regional interbasin groundwater system in the White River Area, southeastern Nevada. *Water Resources Research* 2, no. 2: 251–271.

Fenelon, J.M., and M.T. Moreo. 2002. Trend analysis of groundwater levels and spring discharge in the Yucca Mountain Region, Nevada and California. USGS Water Resources Investigations Report 02-4178. Reston, Virginia: USGS.

Fetter, C.W. 1994. *Applied Hydrogeology*, 3rd ed. Upper Saddle River, New Jersey: Prentice Hall.

GeoTrans Inc. 2003. Addendum to groundwater modeling of the Muddy River Area and surrounding basins with an emphasis on evaluating pending groundwater applications in Coyote Spring Valley. Portland, Oregon: U.S. Fish and Wildlife Service.

GeoTrans Inc. 2001. Groundwater modeling of the Muddy River Area and surrounding basins with an emphasis on evaluating pending groundwater applications in Coyote Spring Valley. Portland, Oregon: U.S. Fish and Wildlife Service.

Gleick, P.H., and D.B. Adams. 2000. Water: The potential consequences of climate variability and change for the water resources of the United States. The report for the Water Sector Team of the National Assessment of the Potential Consequences of Climate Variability and Change for the US Global Research Program. Oakland, California: Pacific Institute for Studies in Development, Environment, and Security.

Guttman, N.B. 1998. Comparing the Palmer Drought Index and the Standardized Precipitation Index. *Journal of the American Water Resources Association* 34, no. 1: 113–121.

Guttman, N.B., and R.G. Quayle. 1996. A historical perspective of U.S. Climate Divisions. *Bulletin of the American Meteorological Society* 77, no. 2: 293–304.

Hanson, R.T., M.W. Newhouse, and M.D. Dettinger. 2004. A methodology to assess relations between climate variability and variations in hydrologic time series in the southwestern United States. *Journal of Hydrology* 287, no. 1–4: 252–269.

Harrill, J.R., and D.E. Prudic. 1998. Aquifer systems in the Great Basin region of Nevada, Utah, and adjacent states—Summary report. USGS Professional Paper 1409-A. Reston, Virginia: USGS.

Harrill, J.R., J.S. Gates, and J.M. Thomas. 1988. Major groundwater flow systems in the Great Basin region of Nevada, Utah, and adjacent states. USGS Hydrologic Investigations Atlas HA-694-C, 2 sheets, scale 1:1,000,000. Reston, Virginia: USGS.

Hayes, M.J. 2006. What is drought? Drought indices. http://www.drought.unl.edu/whatis/indices.htm (accessed May 17, 2006).

Helsel, D.R., and R.M. Hirsch. 1992. *Statistical Methods in Water Resources*. New York: Elsevier Publishing.

Johnson, C., and M. Mifflin. 2006. The AEM and regional carbonate aquifer modeling. *Ground Water* 44, no. 1: 24–34.

Kirk, S.T., and M.E. Campana. 1990. A deuterium-calibrated groundwater flow model of a regional carbonate-alluvial system. *Journal of Hydrology* 119, no. 4: 357–388.

Las Vegas Valley Water District. 2001. Water resources and ground-water modeling in the White River and Meadow Valley flow systems, Clark, Lincoln, Nye, and White Pine counties, Nevada. Las Vegas, Nevada: Las Vegas Valley Water District.

McKee, T.B., N.J. Doeskin, and J. Kliest. 1993. The relationship of drought frequency and duration to time scales. In *Eight Conference on Applied Climatology, American Meteorological Society*; January 17–23, 1993, Anaheim, California, 179–186. Fort Collins: Colorado State University.

Moapa Valley Water District. 2005. Muddy Springs Area monitoring report. Logandale, Nevada: Moapa Valley Water District.

Ott, L.R. 1993. *An Introduction to Statistical Methods and Data Analysis*, 4th ed. Belmont, California: Wadsworth Inc.

Palmer, W.C. 1965. Meteorological drought. U.S. Weather Bureau Research Paper 45. Washington, D.C.: NOAA Library and Information Services.

Pohlmann, K.F. 1994. 1993 ground-water levels in the Upper Muddy River Valley. Prepared for Nevada Power Co. Las Vegas, Nevada: Desert Research Institute, University of Nevada-Reno.

Prudic, D.E., J.R. Harrill, and T.J. Burbey. 1993. Conceptual evaluation of regional ground-water flow in the carbonate-rock province of the Great Basin, Nevada, Utah, and adjacent states. USGS Open-File Report 93-170. Reston, Virginia: USGS.

Scanlon, B.R., K.E. Keese, A.L. Flint, L.E. Flint, C.B. Gaye, W.M. Edmunds, and I. Simmers. 2006. Global synthesis of ground water recharge in semi-arid and arid regions. *Hydrological Processes* 20, no. 15: 3335–3370.

Scanlon, B.R., D.G. Levitt, R.C. Reedy, K.E. Keese, and M.J. Sully. 2005. Ecological controls on water-cycle response to climate variability in deserts. *Proceedings of the National Academy of Sciences* 102, no. 17: 6033–6038.

Scoppettone, G.G., P.H. Rissler, M.B. Nielsen, and J.E. Harvey. 1998. The status of *Moapa coriacea* and *Gila seminude* and status information on other fishes of the Muddy River, Clark County, Nevada. *Southwestern Naturalist* 43, no. 2: 115–122.

Scoppettone, G.G., H.L. Burge, and P.L. Tuttle. 1992. Life history, abundance, and distribution of Moapa dace *(Moapa coriacea). Great Basin Naturalist* 52, no. 3: 216–225.

Sophocleous, M. 1997. Managing water resources systems: Why "safe yield" is not sustainable. *Ground Water* 35, no. 4: 561.

Southern Nevada Water Authority. SNWA portal. 2006. http://www.snwawatershed.org (accessed May 6, 2006).

Southern Nevada Water Authority. 2005. Addendum #1 to survey of wells and stream gages in the Black Mountains area, California Wash Basin, Coyote Spring Valley, Garnet Valley, Hidden Valley, and the Muddy River Springs area, Nevada. Las Vegas, Nevada: Southern Nevada Water Authority.

Southern Nevada Water Authority. 2003. Survey of wells and stream gages in the Black Mountains area, California Wash Basin, Coyote Spring Valley, Garnet Valley, Hidden Valley, and the Muddy River Springs area, Nevada. Las Vegas, Nevada: Southern Nevada Water Authority.

Thomas, J.M., A.H. Welch, and M.D. Dettinger. 1996. Geochemistry and isotope hydrology of representative aquifers in the Great Basin of Nevada, Utah, and adjacent states. USGS Professional Paper 1409-C. Reston, Virginia: USGS.

U.S. Fish and Wildlife Service. 1996. *Recovery plan for rare aquatic species of the Muddy River ecosystem*. Las Vegas, Nevada: Las Vegas Field Office, U.S. Fish and Wildlife Service.

USGS. 2006. Surface-water data for Nevada. http://waterdata.usgs.gov/NV/nwis/ (accessed May 3, 2006).

Waddell, R., and G. Roemer. 2006. Evaluation of effects of barometric pressure changes and earth tides on water levels in the regional carbonate aquifer, California Wash, Nevada. Presented at the Annual Meeting of the Nevada Water Resources Association; February 21–23, 2006, Mesquite, Nevada. Reno: Nevada Water Resources Association.

Weber, K., and M. Stewart. 2004. A critical analysis of the cumulative rainfall departure concept. *Ground Water* 42, no. 6–7: 935–938.

Western Regional Climate Center. 2006. Historical climate information. http://www.wrcc.dri.edu/ (accessed May 13, 2006).

Winnograd, I.J., and W. Thordarson. 1975. Hydrogeologic and hydrochemical framework, south-central Great Basin, Nevada-California, with special reference to the Nevada test site. USGS Professional Paper 712-C. Reston, Virginia: USGS.

Winnograd, I.J., A.C. Riggs, and T.B. Coplen. 1998. The relative contributions of summer and cool-season precipitation to groundwater recharge, Spring Mountains, Nevada, USA. *Hydrogeology Journal* 6, no. 1: 77–93.

Winter, T.C., J.W. Harvey, O.L. Franke, and W.M. Alley. 1999. Ground water and surface water a single resource. USGS Circular 1139. Reston, Virginia: USGS.

VANISHING FISHES OF NORTH AMERICA

Dr. R. Dana Ono
Dr. James D. Williams
Anne Wagner

paintings by Aleta Pahl

Stone Wall Press, Inc.
1241 30th Street NW
Washington, DC 20007

- Th
de
th
- Di
an
th
- Co
Pa
ref
- Ap
or
cer

Bot
water
water
not on
of exti
surviv
teen N
than fi
extinct
Onc
concen
species
100° F.
advanc
in these
could c
ment of
gram. A
smallest
world (
10 feet
water).
This b
gered an
fishes th
concise
color pla

dust jacket designed by Hasten Graphic Design
painting by Aleta Pahl
color photograph by James D. Williams

ISBN 0-913276-43-X

Printed in the United States of America.

Library of Congress Cataloging in Publication Data
Catalog Card No. 82-062896
Ono, R. Dana, James D. Williams, and Anne Wagner
Vanishing Fishes of North America
Washington, D.C.: Stone Wall Press, Inc.

The woundfin was first placed on the Department of Interior's Endangered Species List in 1967. Biologists attempted to transplant the woundfin into four streams in Arizona at the periphery of the woundfin's historic range, but the efforts failed. In 1979, a group of biologists sponsored by the U.S. Fish and Wildlife Service formed the Woundfin Recovery Team and developed a Woundfin Recovery Plan. The goal is to establish self-sustaining populations of the woundfin in the Virgin River and at least two other streams in the woundfin's historic range to secure the woundfin from extinction. The recovery team's success will depend to a large extent on the outcome of the proposed Virgin River energy and water projects. In the final analysis, survival of the woundfin depends on whether the Virgin River habitat is eventually upgraded and stabilized.

The reason for saving the woundfin and preventing the further deterioration of the Virgin River ecosystem is stated in the conclusion of one of the Allen-Warner project technical reports: "Irrigation projects in the southwest are generally shown to be short-lived in a geologic timescale, whereas continued productivity of a natural ecosystem is a long-term phenomenon. Therefore, we are trading a relatively short-term use of a natural resource for economic gain for long-term productivity of a natural ecosystem. Consequently, we are losing the availability of the knowledge contained in the ecosystem, a long-term benefit to man."

Moapa Dace
Moapa coriacea

The Moapa River originates from the warm outflow of more than twenty thermal springs in the northeastern part of Clark County, Nevada, and flows southward for 26 miles into the Overton Arm of Lake Mead. Before Hoover Dam was built and the Colorado River and the lower portion of the Virgin River were impounded, the Moapa River emptied into the Virgin River just above its confluence with the Colorado River. Heading south, the warm crystalline headwaters of the Moapa River cooled a little and picked up sediments, taking on the turbid appearance that earned the river its Paiute Indian name of "moapa" or muddy.

Five native fishes inhabit the Moapa River: the Moapa speckled dace, *Rhinichthys osculus moapae;* the roundtail chub, *Gila robusta;* the Moapa White River springfish, *Crenichthys baileyi moapae;* the desert sucker, *Catostomus clarki;* and the Moapa dace, *Moapa coricea.* A sixth native species, the woundfin, *Plagopterus argentissimus,* has been found in the Moapa River, but is not a permanent resident. As a result of the physical and chemical alterations of the river, the depletion of its headspring waters for commercial and domestic uses, and the introduction of exotic fish species, all of the native fishes in the Moapa River are either endangered or threatened.

The endangered Moapa dace is endemic to the headwaters of the Moapa River where the springs and their outflow maintain the water temperature between 82° and 90°F. Historically this habitat was chemically and physically

very stable compared to downstream areas. The Moapa dace can tolerate the cooler temperatures and increased turbidity of the downstream waters, but is most abundant in the headwaters. In the upstream areas, it appears to prefer crystalline clear pool areas that support an abundant algal growth. The pools are three to fifteen feet wide, six inches to five feet deep, and are partially overgrown by a canopy of streambank vegetation. The gentle currents of the pools and streams flow over a substrate of gravel and pebbles, occasionally interrupted by sandy or muddy areas.

The Moapa dace, the only species of the genus *Moapa,* is among the smallest of the endangered fishes of the Colorado River basin. The Moapa dace reaches sexual maturity when only 1.3 to 3 inches long. Its small scales are deeply embedded in the skin, giving the skin the leathery texture from which the fish's scientific name "*coriacea*," which means leathery, is derived. The Moapa dace is colored deep olive along its back and sides, with greenish brown patches on its upper sides and a wide, black stripe along the middle of its back. Its sides have a shining golden brown band that contrasts sharply with lighter colors of the sides. The Moapa dace is distinguishable from the similar roundtail chub and Moapa speckled dace by its prominent back stripe and by a black spot at the base of its tail. Virtually no detailed information exists on the life history of this tiny fish. The Moapa dace lives in schools and feeds primarily on insects. Like many warm spring desert fishes, they spawn year round, with peak spawning activities in the spring and summer.

Between 1933 and 1950 the Moapa dace was abundant in the Moapa River headwaters, and ichthyologists estimated that the species occupied 25 springs and about 10 miles of spring outflows. By 1964, the Moapa dace was rare in collections from the same area. In 1969, the International Union for Conservation of Nature and Natural Resources (IUCN) Red Data Book on the status of freshwater fishes estimated that the Moapa dace population numbered 500 to 1000 individuals. By 1977, the IUCN estimated that only "a few hundred" Moapa dace remained in the river. Current estimates indicate that the species exists in only three springs and less than two miles of outflow. Reproduction has been documented only in a one hundred yard stretch of outflow from one spring.

The dramatic decline in the Moapa dace population coincided with the introduction and establishment of at least two exotic fishes—the mosquitofish, *Gambusia affinis,* and the shortfin molly, *Poecilia mexicana*—which competed for the limited habitat resources and introduced new parasites. Ichthyologists estimate that a total of nine exotic species have been introduced into the Moapa River, seven of which have become common to abundant since the early 1970s.

The Moapa dace has also suffered from destruction of habitat. Most of the Moapa River headwater springs are on private property and have been lined with gravel or cement and channeled into irrigation canals or water conduits and chlorinated for human consumption. In addition, much of the vegetation that once formed a protective canopy over the springs and pools has been cleared, further altering the environment. The only surviving populations of the Moapa dace are found in springs on agricultural land owned by the Church of the Latter Day Saints and on a section of private land managed by the Moapa Valley Water Users District.

7–6
Thermal headwater springs and pools are prime habitat for the Moapa dace. These springs are located in the headwaters of the Moapa River. Photo by J. D. Williams.

In 1967 the U.S. Fish and Wildlife Service listed the Moapa dace as an endangered species. They later, in 1979, purchased twelve acres of land and the water rights for several headsprings and established the Moapa National Wildlife Refuge. Under the provisions of a Recovery Plan developed in 1982, the Fish and Wildlife Service will delist the Moapa dace after restoring the species to five of approximately twenty of the species' original habitats. To accomplish this goal the U.S. Fish and Wildlife Service plans to reintroduce the Moapa dace into existing spring outflows and newly constructed stream and pool habitats on the Moapa National Wildlife Refuge. The dace also will be introduced into the Upper Plummer Springs, one of the original spring habitats of the Moapa dace that is currently part of the Desert Warm Springs Resort.

LIFE HISTORY, ABUNDANCE, AND DISTRIBUTION OF MOAPA DACE (*MOAPA CORIACEA*)

G. Gary Scoppettone, Howard L. Burge, and Peter L. Tuttle

Reprinted from the
GREAT BASIN NATURALIST
Volume 52, No. 3
September 1992

Great Basin Naturalist 52(3), pp. 216–225

LIFE HISTORY, ABUNDANCE, AND DISTRIBUTION OF MOAPA DACE (*MOAPA CORIACEA*)

G. Gary Scoppettone[1], Howard L. Burge[1, 2], and Peter L. Tuttle[1, 3]

ABSTRACT.—Moapa dace (*Moapa coriacea*) is a federally listed endangered fish endemic to the spring-fed headwaters of the Muddy River, Clark County, Nevada. Species life history, abundance, and distribution were studied from March 1984 to January 1989. Reproduction, which was observed year-round, peaked in spring and was lowest in fall. It occurred in headwater tributaries of the Muddy River, within 150 m of warm water spring discharge in water temperatures ranging from 30 to 32 C. Females matured between 41 and 45 mm in fork length (FL). Egg abundance increased with female size (r^2 = .93); counts ranged from 60 for a 45-mm-FL female to 772 for one 90-mm FL. The oldest of eight fish, aged by the opercle method, was a 90-mm-FL, 4+-year-old female. Adults are omnivorous but tended toward carnivory; 75% of matter by volume consumed was invertebrates and 25% plants and detritus. Fish size was generally commensurate with flow, the largest fish occurring in the greatest flow. Adults were near bottom, in focal velocities ranging from 0 to 55 cm/s. Juveniles occupied a narrower range of depths and velocities than adults, and larvae occupied slack water. From December 1984 to September 1987, the total adult population ranged from 2600 to 2800. Although these numbers are higher than previously believed for Moapa dace, they are still sufficiently low to warrant its endangered status. The dependency of Moapa dace's different life history stages to various areas and habitat types of the Warm Springs area suggests that all remaining habitat is necessary for their survival.

Key words: Moapa coriacea, *Moapa dace, life history, reproduction biology, fecundity, age-growth, food habits, habitat use, body size, Muddy River, Nevada.*

The Moapa dace (*Moapa coriacea*) is a thermophilic minnow endemic to the Muddy River system, Clark County, Nevada. First collected in 1938, it has historically been relegated to the headwater area where the Muddy River originates from a series of warm springs (Hubbs and Miller 1948). La Rivers (1962) called the Moapa dace and its coinhabitant, Moapa White River springfish (*Crenichthys baileyi moapae*), thermal endemics because of their apparent affinity for warm water. Rarely exceeding 12 cm in fork length (FL), Moapa dace have morphological similarities to roundtail chub (*Gila robusta*) and speckled dace (*Rhinichthys osculus*), which also inhabit the Muddy River (Hubbs and Miller 1948). They are more similar, however, to the genus *Agosia*, which occurs in other lower Colorado River drainages; the two genera are speculated to have a common ancestor (Hubbs and Miller 1948). Moapa dace are distinguished by small embedded scales and a bright black spot at the base of the caudal fin.

Little was known of Moapa dace life history prior to this study. La Rivers (1962) identified them as methodical schoolers; a cursory gut examination by him indicated that they foraged primarily on arthropods and some vegetative matter. In a systematic sampling effort, Deacon and Bradley (1972) collected Moapa dace in 28–30 C water; one specimen was collected in 19.5 C water. Within the confines of its limited distribution, Moapa dace have been captured in a variety of habitats, including spring pools and slow- to fast-moving water, and in association with various substrates and submergent vegetation (Hubbs and Miller 1948).

Past ichthyofaunal surveys suggested a declining Moapa dace population (Deacon and Bradley 1972, Cross 1976). These surveys were qualitative and produced neither an estimate of the number of dace remaining nor the relative population decrease between surveys. Ono et al. (1984) thought that only several hundred Moapa dace persisted and that their distribution had been further restricted within the already limited historic habitat, confining them to the

[1]U.S. Fish and Wildlife Service, National Fisheries Research Center, Reno Substation, Reno, Nevada, USA 89502.
[2]Present address: U.S. Fish and Wildlife Service, Dworshak Fisheries Assistance Office, Ahsahka, Idaho, USA 83520.
[3]Present address: U.S. Fish and Wildlife Service, Great Basin Complex, Reno, Nevada, USA 89502.

main stem of the upper Muddy River and a semi-isolated headwater spring system about 130 m long. The purpose of this study is to expand information on Moapa dace life history, abundance, and distribution. Life history information includes reproductive biology, habitat use, food habits, and age and growth.

Study Area

The Muddy River is at the northern edge of the Mohave Desert, where average annual precipitation is 15 cm usually in the form of rain. Carpenter (1915) described historic terrestrial vegetation which included greasewood (*Sarcobatus vermiculatus*), shadscale (*Atriplex confertifolia*), creosote bush (*Larrea tridentata*), and mesquite (*Prosopis* sp.). Stream banks were lined with willows (*Salix* sp.), screw-bean (*Prosopis pubescens*), cottonwood (*Populus* sp.), and mesquite (Carpenter 1915, Harrington 1930). Prior to the completion of Hoover Dam (aka Boulder Dam) in 1935, the Muddy (aka Moapa) River was about 48 km long and discharged into the Virgin River, which joined the Colorado River (Hubbs and Miller 1948). Today, it is about 40 km long and discharges into the Overton arm of Lake Mead (Fig. 1). Source springs of the Muddy River probably originate from Paleozoic carbonate rocks (Garside and Schilling 1979) and occur within a 2-km radius. As is typical of warm springs, the water is relatively rich in minerals. Garside and Schilling (1979) list sodium and calcium as predominant cations, and carbonate and sulfate as predominant anions; total dissolved solids were 854 ppm and pH was 7.7. Water emerges at 32 C and cools and increases in turbidity downstream (Cross 1976). Although spring discharge is relatively constant at about 1.1 m^3/s, the Muddy River flow fluctuates because of rain, agricultural diversions, evaporation, and transpiration (Eakin 1964). The headwater region, the historic range of the Moapa dace, is known as the Warm Springs area (Fig. 1). During our study the area was used primarily for agriculture, and up to 0.25 m^3/s of river discharge was being diverted to irrigate alfalfa, barley, and pasture. Spring outflows had been channelized, and several were converted into irrigation ditches, some lined with concrete. Earthen tributary channels had scant to thick riparian corridors of fan palm (*Washingtonia filifera*), tamarisk (*Tamarix* sp.), arrow weed (*Pluchea sericea*). Two nonnative fishes successfully established in the Warm Springs area: mosquitofish (*Gambusia affinis*), present when Moapa dace were discovered in 1938 (Hubbs and Miller 1948), and shortfin molly (*Poecilia mexicana*), introduced in the early 1960s (Hubbs and Deacon 1964). Besides Moapa dace and springfish, roundtail chub and speckled dace are the only native fishes occurring within the Warm Springs area, but they are rare and in greater abundance downstream (Cross 1976, Deacon and Bradley 1972).

In 1979 the Moapa National Wildlife Refuge (NWR) was established in historic habitat at the southern edge of the Warm Springs area for the preservation and perpetuation of the Moapa dace (Fig. 1). The refuge stream originates from five small springs occurring in a radius of 70 m and having a cumulative discharge of abut 0.09 m^3/s (Fig. 2). Fan palms are the predominant riparian vegetation. In 1984 Moapa dace larvae and adults were reintroduced into the upper Refuge Stream, and by January 1986 there was a stable reproductive population of 120 adults (authors, unpublished data). They were isolated by a 75-cm-high waterfall. Springfish were the only other fish present, and they were abundant.

Materials and Methods

Reproductive biology.—Among our objectives was to quantify duration of the reproductive period and the season of peak larvae recruitment. To this end, a segment of the upper Refuge Steam system was snorkeled at 30- to 90-day intervals from February 1986 to January 1989 and larvae were enumerated (Fig. 2). This is the area in which virtually all reproduction on the Moapa NWR occurred. Dace 7–15 mm TL were considered larvae. This range approximates the proto- to metalarvae stages of the similar-sized speckled dace (Snyder 1981). Snorkeling enabled us to locate reproduction sites in the headwater Muddy River system and to determine the abundance and distribution of adult Moapa dace as well as to quantify habitat use for all life stages. Areas with larvae close to swim-up size (about 7 mm TL) were considered reproduction sites. Fish used for food habit analysis and aging were also used to determine fecundity.

Habitat use.—We defined habitat use in terms of stream depth and velocity at foraging sites and at suspected spawning areas. Depth measurements included focal and total, while

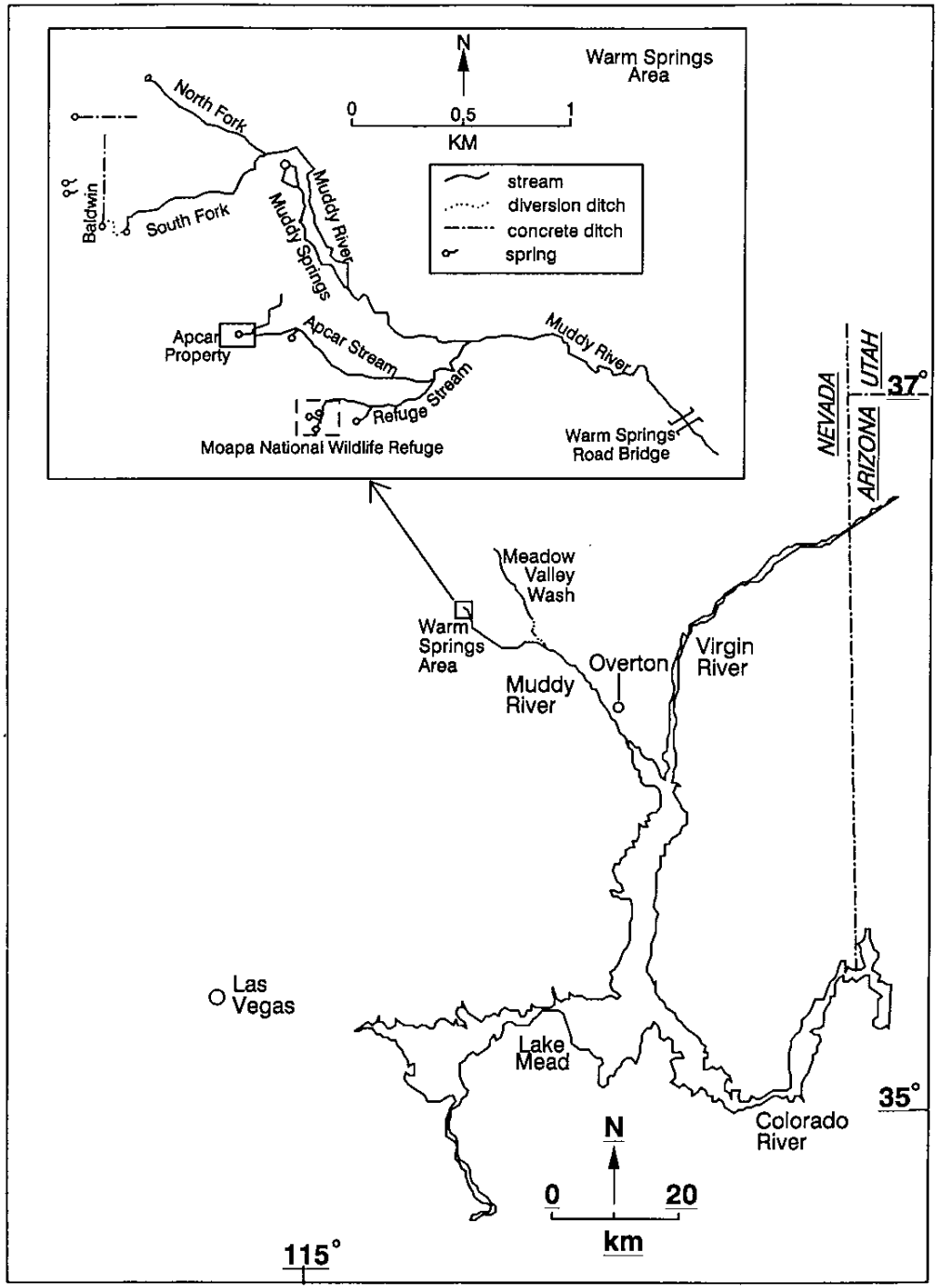

Fig. 1. Map showing relationship of the Muddy to the Virgin River and Lake Mead, Nevada, and relationship of the Warm Springs area to the Muddy River (below). Warm Springs area or headwaters of the Muddy River showing tributary streams to the upper Muddy River and relationship of the Moapa National Wildlife Refuge (above).

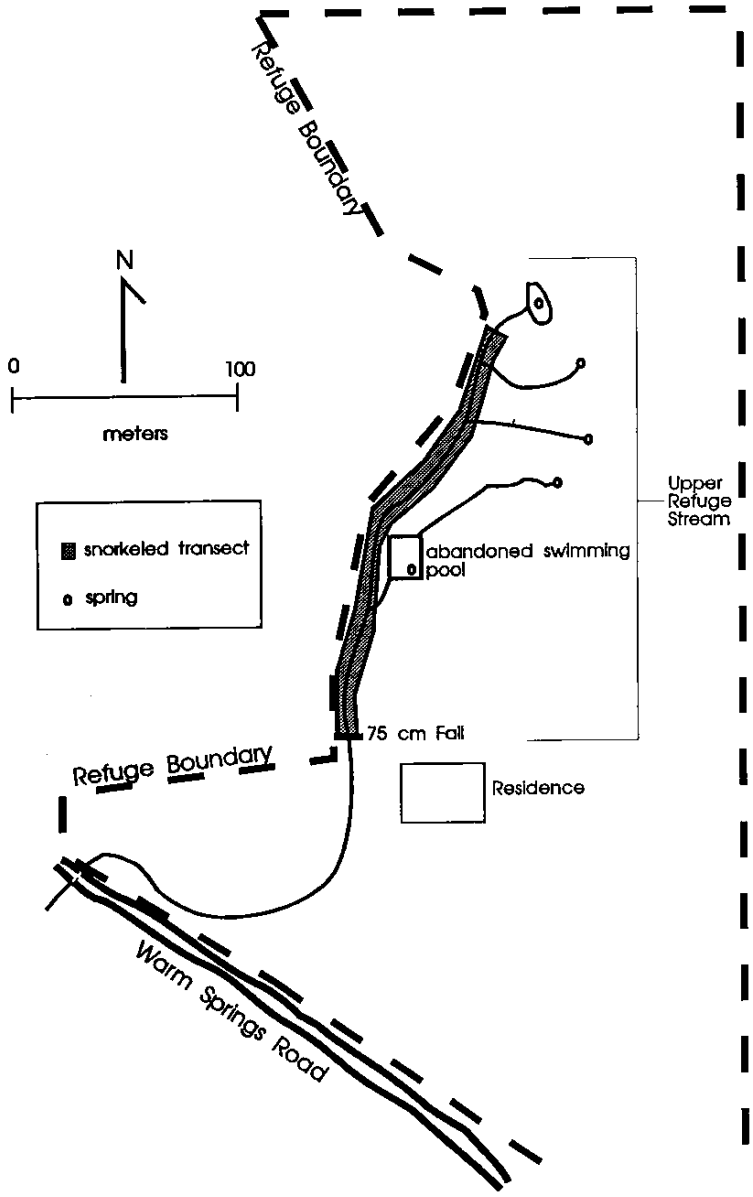

Fig. 2. Map of Moapa National Wildlife Refuge; shaded site indicates the reach of the upper Refuge Stream where larvae snorkel counts were made from February 1986 to January 1989.

velocity measurements included focal and mean water column, as prescribed by Bovee (1986). Dissolved oxygen and temperature were also measured. Fish were located using mask and snorkel. A Marsh and McBirney model 201D digital flow meter mounted on a calibrated rod

Yellow Springs Instrument model 57 dissolved oxygen meter for temperature and dissolved oxygen. Sampling occurred from 1984 to 1986. Adult habitat was also defined by contrasting body size with quantity of stream flow; it was our subjective evaluation that larger fish were

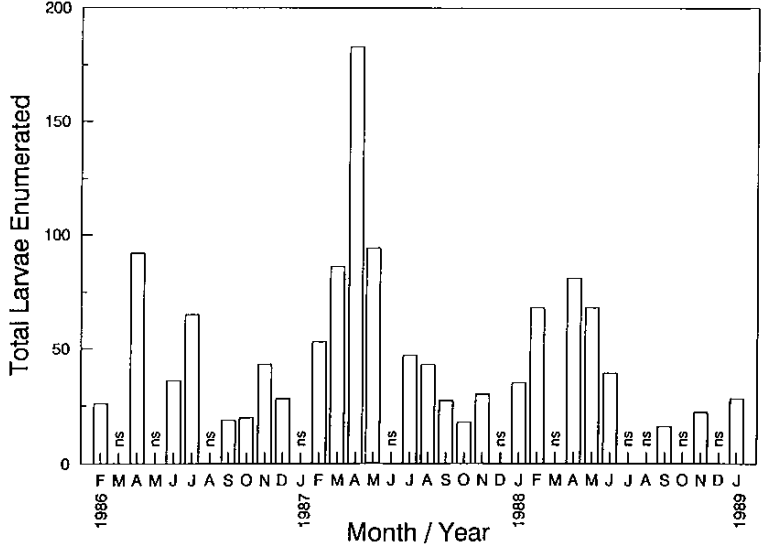

Fig. 3. Abundance of Moapa dace larvae from February 1986 to January 1989 in the Muddy River system on the Moapa National Wildlife Refuge, Nevada. Bars represent a single day's count for the month. NS indicates not sampled.

hypothesis in the summer of 1986 when samples of adults were minnow-trapped from the Muddy River, Muddy Spring Stream, Refuge Stream, and Apcar Stream and their length frequencies compared. Discharge for each stream was measured using standard U.S. Geological Survey methods (Rantz et al. 1982) near each fish sample. A one-way factorial ANOVA was used to test whether there was a significant difference between length frequency among fishes and different water volumes.

AGE AND GROWTH.—The opercle bone was used for estimating age as described by Casselman (1974). Eight specimens, collected in summer 1985 and 1986, were aged. Flesh was scraped with a scalpel and the bone allowed to dry. Glycerin was used to highlight the more transparent region of the bone, which was assumed to have the greatest calcium concentration and to have been formed in the winter when food is scarce. The more opaque region signifies greater concentration of protein associated with growth (Casselman 1974).

FOOD HABIT.—Food habit analyses were made from 10 Moapa dace taken 9–11 November 1984 from each of three upper Muddy River tributaries (Apcar, South Fork, and Muddy Spring). They were captured by seining and with unbaited minnow traps fished no longer than 10 minutes. Ranging from 42 to 71 mm FL, they were preserved in 10% formalin solution. Contents in the anterior third of the gut were examined using a dissecting microscope and quantified by frequency of occurrence (Windell 1971) and by percent composition (Hynes 1950).

ABUNDANCE AND DISTRIBUTION.—The abundance and distribution of adult Moapa dace (>40 mm FL) were determined by snorkeling the upper Muddy River system beginning from 200 m downstream of Warm Springs Road bridge (Fig. 1). Except for 1984, the surveys included 5.3 km of the upper Muddy River and 7.5 km of its spring-fed tributaries (Refuge Stream system, Apcar Stream, Muddy Spring, South Fork, and North Fork). In 1984 the survey area was the same except that only the upper 130 m of the Apcar Stream was snorkeled rather than its entire stream length. Snorkeling was conducted over periods of four to six days when turbidity was low (between 1.4 and 5.0 NTU) because no agricultural return flows were entering the stream. Counts were made 6–10 December 1984, 6–10 June 1986, and 16–22 September 1987. Each observer enumerated Moapa dace twice at three areas of relatively high concentrations (30–60 fish), and the range of results was then calculated. These sites were chosen because the greatest variation among observers was expected among them. For the three sites, variation was less than 15% in counts

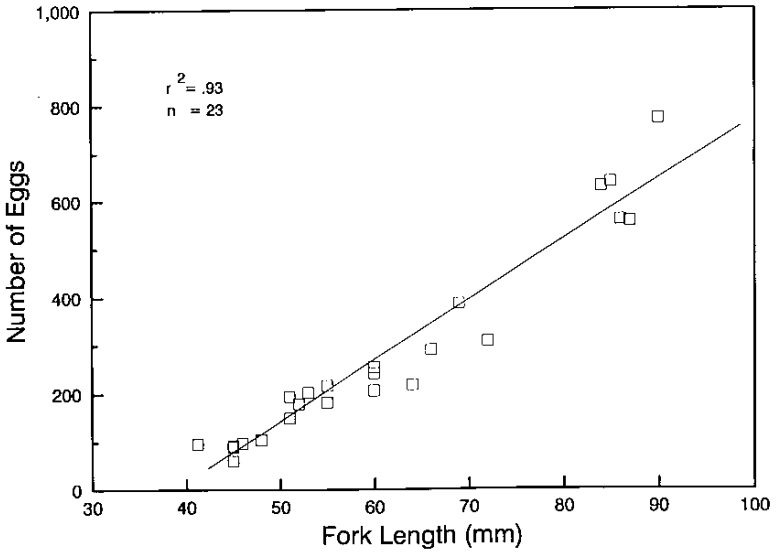

Fig. 4. Moapa dace fecundity as a function of fork length.

between individuals; thus, we conservatively estimated a 15% variation in our population counts.

Results and Discussion

Reproductive Biology

Moapa dace larvae were found year-round, indicating year-round reproduction. On the Moapa NWR peak larval recruitment was in spring, the low in autumn (Fig. 3). Fish at other reproductive sites in the Warm Springs area exhibited this same general trend. Seasonal fluctuation in larval recruitment was probably linked to availability of food. In the upper Muddy River system the abundance of benthic and drifting invertebrates is much lower in winter than in spring (Scoppettone, unpublished data). Naiman (1976) documented substantial seasonal fluctuation in primary productivity in another southwestern warm springs where production is lowest in winter; presumably most invertebrate population fluctuates with primary production.

Recently emerged larvae were found within 150 m of spring discharge over sandy silt bottoms in temperatures of 30–32 C and dissolved oxygen of 3.8–7.3 mg/L. Whether spawning occurs only at these headwater sites or is successful only at these sites is unknown. Visual cues such as sexual dichromatism, pronounced

females were not readily apparent, and spawning was not observed during our study. However, we indirectly identified and quantified spawning habitat. The presence of hundreds of protolarvae in a concrete irrigation channel immediately downstream of the Baldwin springhead (Fig. 1) indicated that reproduction had taken place. Progenitors apparently came from the South Fork, entering Baldwin Spring outflow through a diversion channel (Fig. 1). The concrete irrigation channel had homogeneous water depth and velocity, and substrate was sandy silt. Several depressions in the sand were similar to "redds" described for longfin dace (*Agosia chrysogaster;* Minckley and Willard 1971). Depth and velocity at the suspected redds were representative of the outflow channel and similar to other suspected spawning areas in the Warm Springs area. Depth ranged from 15.0 to 19.0 cm, near-bed velocities from 3.7 to 7.6 cm/sec, and mean water column velocity from 15.2 to 18.3 cm/sec.

Similar to the longfin dace, which reproduces during much of the year (Kepner 1982), eggs in the skein of Moapa dace were in different stages of development. All visible eggs were counted, but because they are intermittently deposited and develop throughout a given year, our counts do not represent absolute annual fecundity. However, egg production increased

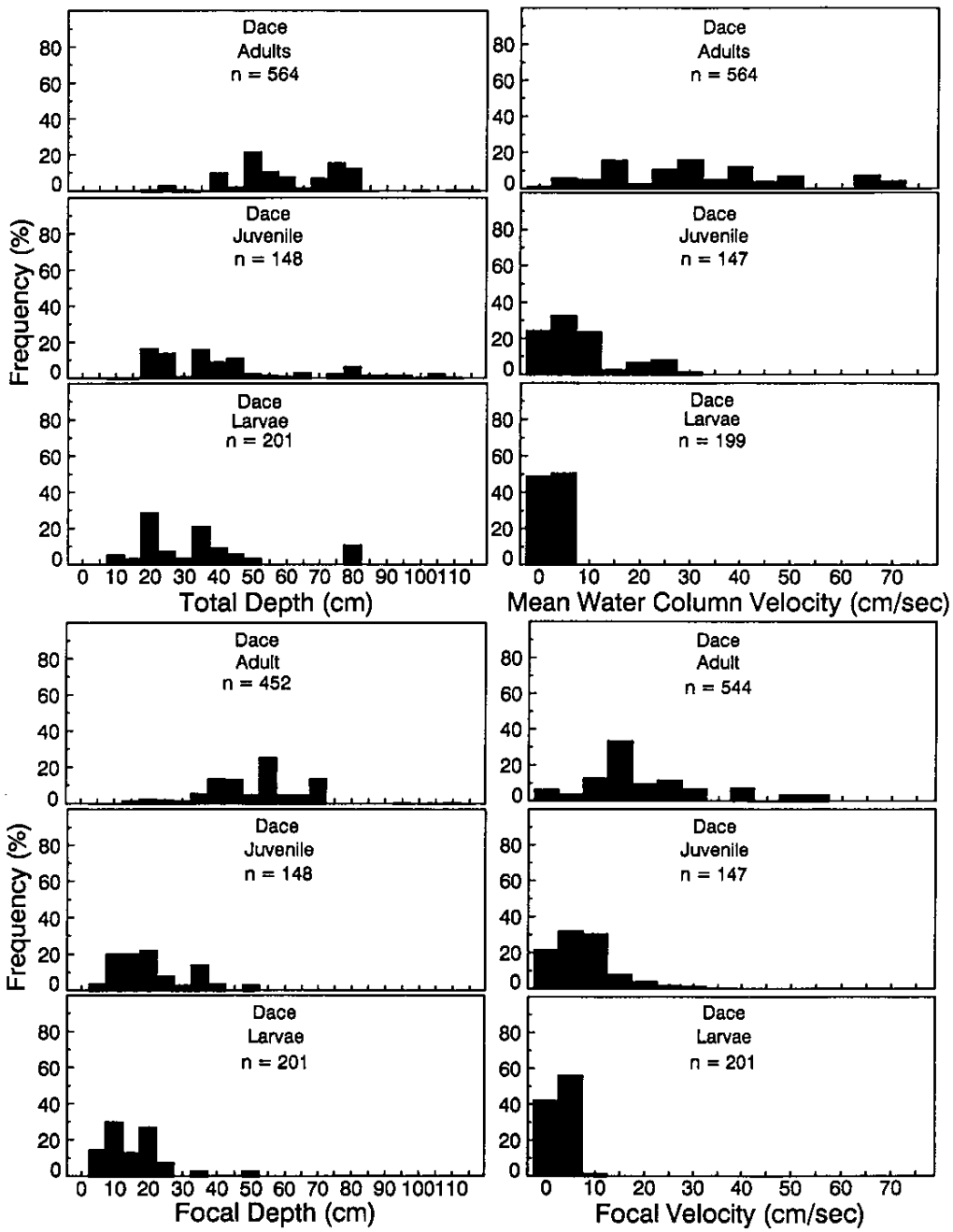

Fig. 5. Mean water column and focal point velocities, total depth, and focal point depth used by Moapa dace adults, juveniles, and larvae in the upper Muddy River system (Warm Springs area), Nevada, 1984 through 1986.

TABLE 1. Fork length, sex, and estimated age of eight Moapa dace collected from the upper Muddy River system, Nevada, in 1985 and 1986. Age was determined by the opercle method.

FL (mm)	Sex	Collection date	Age
45	Unknown	4/86	0+
55	Unknown	7/86	1+
61	Unknown	7/86	1+
67	Female	4/86	2+
69	Female	04/22/86	2+
77	Unknown	10/09/85	3+
80	Unknown	10/11/85	3+
90	Female	10/08/85	4+

ranged from 60 in a 45-mm-FL individual to 772 in a 90-mm-FL dace. Eggs were just developing in a 41-mm-FL female and were mature in a 45-mm-FL fish, suggesting that females mature at lengths in this range.

Habitat Use

Again, Moapa dace larvae were found exclusively in the upper reaches of spring-fed tributaries, while juveniles occurred primarily in tributaries but were more far-ranging. Adults were present in tributaries and in the main river, with larger fish generally found in the larger water volumes. There were significant differences in length frequencies among adults from different water volumes ($p \leq .006$). In the Muddy River, in a flow of about 0.50 m^3/s, mean FL was 73 mm (n = 78, SD = 16 mm); Muddy Spring had a flow of 0.20 m^3/s, and the mean FL was 64 mm (n = 72, SD = 14 mm); the Refuge Stream flowed at 0.17 m^3/s, and mean FL was 56 mm (n = 64, SD = 8 mm); the Apcar Stream flowed at 0.06 m^3/s, and mean FL was 51 mm (n = 89, SD = 5 mm).

Larvae occurred and fed in the mid- to upper region of the column. They were found most frequently in zero water velocity (Fig. 5). As size increased, individuals tended to occupy faster water and occur lower in the water column. Juvenile Moapa dace occupied focal and mean water column velocities ranging from 0 to 46 cm/s. Adults were found in a wide range of water depths and velocities, but they tended to orient at the bottom in low to moderate current. Water column depth ranged from 15 to 113 cm and focal point depth from 9 to 107 cm. Mean water column velocity ranged from 2 to 77 cm/s and focal point velocity from 0 to 55 cm/s. Water

TABLE 2. Food items ingested by 21 Moapa dace by percent composition (Hynes 1950) and percent frequency of occurrence (Windell 1971). Nine other guts examined were empty.

Food items	% composition	% of occurrence
GASTROPODA		
Tyronia clathrata	1.1	4.8
OLIGOCHAETE	27.0	23.8
AMPHIPODA		
Hyallela azteca	1.7	9.5
HEMIPTERA		
Pelocoris shoshone	4.5	4.8
HOMOPTERA		
Aphiidae	9.0	4.8
TRICHOPTERA		
Dolophilodes	5.1	9.5
Nectopsyche	4.5	9.5
LEPIDOPTERA		
Paragyractis	4.5	9.5
COLEOPTERA		
Stenelmis calida	1.1	4.8
Dytiscidae (larvae)	9.0	4.8
DIPTERA		
Chironomidae	4.5	4.8
Unidentified insect parts	3.3	9.5
Filamentous algae	18.5	42.3
Vascular plants	3.4	9.5
Detritus	2.8	14.3

27 to 32 C and dissolved oxygen from 3.5 to 8.4 mg/L.

Age Growth

Annulus formation is typically associated with an annual period of slower growth caused by seasonal changes in environmental conditions such as temperature or food resources (Tesch 1971). Although seasonal water temperatures do not change substantially in the Warm Springs area, there is an apparent reduction of potential food during the winter (Scoppettone, unpublished data). We were unsuccessful in aging Moapa dace by the scale method because scales were small, embedded, and extremely difficult to remove from live specimens. Also, environmental conditions in waters of the Warm Springs area were sufficiently constant that annuli were not readily apparent. Assumed annuli on opercular bones were presumed to be associated with slower growth during the winter. Ages of the eight fish examined ranged from 0+ for a 43-mm-FL individual to 4+ for a 90-mm-FL female (Table 1).

Food Habit

Nine of 30 guts examined were empty and

TABLE 3. Estimated number of Moapa dace adults in six tributary streams in the Warm Springs area, Muddy River system, Nevada, 6–14 December 1984, 13–18 June 1986, and 16–22 September 1987.

Stream name	December 1984	Variation in count	June 1986	Variation in count	September 1987	Variation in count
Muddy River	475	±71	1230	±185	1165	±175
Refuge System	370	±56	406	±61	806	±121
Apcar	200	±30	565	±85	475	±72
South Fork	300	±45	185	±28	100	±15
North Fork	15	±2	30	±5	60	±9
Muddy Spring	1450	±218	160	±24	200	±30
Total	2810	±422	2581	±387	2806	±421

*Only the upper 130 m of stream was sampled in 1984.

but what had been consumed indicated Moapa dace to be omnivorous tending toward carnivory; 75% by composition was invertebrates while 25% was plant material and detritus (Table 2). Among 21 dace guts, oligochaetes represented the largest volume (27.0%) of foodstuffs consumed, followed by filamentous algae (18.5%). In terms of frequency of occurrence filamentous algae occurred in 42.3% of the guts while oligochaetes were in 23.8%. The structure of the pharyngeal teeth also suggests an omnivorous diet; they are strongly hooked but have a well-developed grinding surface (La Rivers 1962). The presence of detritus and gastropods indicates at least some foraging from the benthos, and we observed fish in the field occasionally pecking at substrate. However, the greatest time in foraging is expended on drift feeding (authors, unpublished data), although our data set does not strongly support this observation.

Abundance and Distribution

Moapa dace were more widespread and numerous than had been previously reported (Ono et al. 1984); they were in five headwater tributaries and the upper Muddy River to about 100 m downstream from the Warm Springs Road bridge (Fig. 2). Numbers ranged from about 2600 in 1986 to 2800 in 1984 and 1987. The numerical distribution for the three years suggests movement by the adult population (Table 3). In 1984 the Muddy Spring stream supported about 50% of the population (1450 adults), with only 16% (450 adults) found in the river. In June 1986 we could account for only 7% of the population in the Muddy Spring stream, while almost 50% of the total was in the river. In 1987 the mainstream river again supported most adult Moapa dace (1200). The distribution of adult Moapa dace was patchy and clumped. [illegible] summer 1986, 79% of the observed dace in the main stem Muddy River were in groups of 10 or more, and 37% were in groups of 30 or more. In tributaries, groups were generally smaller, with 52% of the adults in groups of 10 or more and only 13% in groups of 30 or more.

CONCLUSION

Moapa dace are dependent upon the link between the upper river and its tributaries. The main stem river typically harbors the largest, and presumably the longest-lived, and most fecund fish; yet tributaries are important for reproduction and as larvae and juvenile nursery habitat. Age and growth information suggests that three years is the mean age of fish in the river and that adults in smaller tributaries are one to two years old.

Although the Moapa dace population is more widespread and abundant than previously believed, its existence remains in jeopardy. Widespread movement and obligatory spawning near warm water spring discharge suggest that species survival depends on access to the entire headwater Muddy River system (Warm Springs area), river and tributaries alike. Every effort should be made to preserve all of its remaining habitat.

ACKNOWLEDGMENTS

William Burger and Dana Winkleman assisted in snorkel surveys, and Michael Parker and Nadine Kanim assisted in estimating fish populations. Peter Rissler helped to determine habitat use. Michael Parker conducted gut analysis. Glen Clemmer, Randy McNatt, and Tom

helped with editing and Stephanie Byers with graphics.

LITERATURE CITED

BOVEE, K. D. 1986. Development and evaluation of habitat suitability criteria for use in the instream flow incremental methodology. Instream Flow Information Paper 21. U.S. Fish and Wildlife Service Biological Report 86(7). 235 pp.

CARPENTER, E. 1915. Ground water in southern Nevada. U.S. Geological Survey Water-Supply Paper 365: 1–86.

CASSELMAN, J. M. 1974. Analysis of hard tissue of pike *Esox lucius* L. with special reference to age and growth. Pages 13–27 *in* T. B. Bagenal, ed., Proceedings of an international symposium on the ageing of fish. European Inland Fisheries Commission of FAO, The Fisheries Society of the British Isles and The Fish Biological Association. Unwin Brothers.

CROSS, J. N. 1976. Status of the native fauna of the Moapa River (Clark County, Nevada). Transactions of the American Fisheries Society 105: 503–508.

DEACON, J. E., and W. G. BRADLEY. 1972. Ecological distribution of the fishes of the Moapa (Muddy) River in Clark County, Nevada. Transactions of the American Fisheries Society 101: 408–419.

EAKIN, T. E. 1964. Ground-water appraisal of Coyote Springs and Kane Spring valleys and Muddy River Springs Area, Lincoln and Clark counties, Nevada. Nevada Department of Conservation and Natural Resources, Ground-Water Resources—Reconnaissance Series. Report 25.

GARSIDE, L. J., and J. H. SCHILLING. 1979. Thermal waters of Nevada. Nevada Bureau of Mines and Geology, Bulletin 91. Mackay School of Mines, University of Nevada, Reno. 163 pp.

HARRINGTON, M. R. 1930. Archaeological exploration in southern Nevada. Southwest Museum Papers No. 4. Reprinted in 1970. 126 pp.

HUBBS, C., and J. E. DEACON. 1964. Additional introductions of tropical fishes into southern Nevada. Southwestern Naturalist 9: 249–251.

HUBBS, C. L., and R. R. MILLER. 1948. Two new relict genera of cyprinid fishes from Nevada. University of Michigan Museum of Zoology Occasional Papers 507: 1–30.

HYNES, H. B. N. 1950. The food of freshwater sticklebacks (*Gasterosteus aculeatus* and *Pygosteus pungitius*) with a review of methods used in studies of the food of fishes. Journal of Animal Ecology 19: 35–58.

KEPNER, W. G. 1982. Reproductive biology of longfin dace (*Agosia chrysogaster*) in a Sonoran Desert stream, Arizona. Unpublished master's thesis, Arizona State University, Tucson.

LA RIVERS, I. 1962. Fishes and fisheries of Nevada. Nevada Fish and Game Commission, Reno. 782 pp.

MINCKLEY, W. L., and W. E. WILLARD. 1971. Some aspects of biology of the longfin dace, a cyprinid fish characteristic of streams in the Sonoran Desert. Southwestern Naturalist 15: 459–464.

NAIMAN, R. J. 1976. Primary production, standing stock, and export of organic matter in a Mohave Desert thermal stream. Limnology and Oceanography 21: 60–73.

ONO, R. D., J. D. WILLIAMS, and A. WAGNER. 1984. Vanishing fishes of North America. Stone Wall Press, Inc.

RANTZ, S. E. and OTHERS. 1982. Measurement and computation of streamflow: volume 1. Measurement of stage and discharge. Geological Survey Water-Supply Paper 2175.

SNYDER, D. E. 1981. Contributions to a guide to the cypriniform fish larvae of the Upper Colorado River System in Colorado. U.S. Bureau of Land Management, Denver. Colorado Contract YA-5612-CT8-129. 81 pp.

TESCH, F. W. 1971. Age and growth. *In:* W. E. Ricker, ed., Methods for assessment of production in fresh waters. IBP Handbook No. 3. Blackwell Scientific Publication, Oxford and Edinburgh.

WINDELL, J. T. 1971. Food analysis and rate of digestion. *In:* W. E. Ricker, ed., Methods for assessment of production in fresh waters. IBP Handbook No. 3. Blackwell Scientific Publication, Oxford and Edinburgh.

Received 1 August 1991
Accepted 15 September 1992

Doc No. HAM-ED-0001

Southern Nevada Water Authority

Geology of White Pine and Lincoln Counties and Adjacent Areas, Nevada and Utah: The Geologic Framework of Regional Groundwater Flow Systems

November 2007

SOUTHERN NEVADA
WATER AUTHORITY

Geology of White Pine Counties and Adjacent Areas, Nevada and Utah: The Geologic Framework of Regional Groundwater Flow Systems

By: Gary L. Dixon,[1] Peter D. Rowley,[2] Andrew G. Burns, James M. Watrus, David J. Donovan,[3] and E. Bartlett Ekren[4]

November 2007

1. Southwest Geology, Inc., Blackfoot, ID
2. Geologic Mapping, Inc., New Harmony, UT
3. Southern Nevada Water Authority, Las Vegas, NV
4. Geology Unlimited, White Sulphur Springs, MT

SOUTHERN NEVADA WATER AUTHORITY
Groundwater Resources Department
Water Resources Division
snwa.com

CONTENTS

CONTENTS (CONTINUED)

CONTENTS (CONTINUED)

THIS PAGE INTENTIONALLY LEFT BLANK

FIGURES

FIGURES (CONTINUED)

PLATES

This Page Intentionally Left Blank

TABLES

THIS PAGE INTENTIONALLY LEFT BLANK

ACKNOWLEDGEMENTS

We are deeply grateful to Yvonne Honore for doing much of the preparation, word processing, and formatting of the manuscript and its many rewrites. We also acknowledge with sincere gratitude Judy Brandt for her preparation and digitization of the plates and their many revisions. Geophysics by Ed Mankinen, Darcy McPhee, Daniel Scheirer, and their colleagues of the U.S. Geological Survey (USGS) helped significantly in the interpretation of the structural geology of the area. Ken Albright provided leadership and guidance at all steps along the way. We thank M.A. Kuntz of the USGS for a detailed technical review of the manuscript. For the later EIS stage, Lisa Luptowitz helped us wend our way through the labyrinth. Helpful EIS review comments from members of cooperating agencies included those of Dan Netcher, Heidi Hadley, and Robert Boyd of BLM; Patrick Plumley of Plumley & Associates for ENSR; Lari Knochenmus and Donald Sweetkind of the USGS; and one or more anonymous reviewers from the Reno office of U.S. Fish & Wildlife Service. We thank Casey Collins and Derek Sloop for making many of the changes to the text, plates, and figures following EIS reviews. Paul Sholar did a nontechnical review of the report.

THIS PAGE INTENTIONALLY LEFT BLANK

ACRONYMS

AMT	audiomagnetotelluric
BLM	U.S. Bureau of Land Management
DVFS	Death Valley Flow System
GSLDFS	Great Salt Lake Desert Flow System
GVFS	Goshute Valley Flow System
HGU	hydrogeologic unit
MVFS	Meadow Valley Flow System
SNWA	Southern Nevada Water Authority
USGS	U.S. Geological Survey
WRFS	White River Flow System

ABBREVIATIONS

afy	acre-feet per year
ft	foot
Ga	billion years
km	kilometer
m	meter
Ma	million years
mg	milligram
mGal	milliGal
mi	mile

THIS PAGE INTENTIONALLY LEFT BLANK

1.0 INTRODUCTION

This report describes the geologic framework of an area of east-central and southeastern Nevada and adjacent western Utah. Included is a description of the geologic and hydrogeologic data compilation, map and cross section development, and hydrogeologic framework completed in support of the Southern Nevada Water Authority's (SNWA) Clark, Lincoln, and White Pine Counties Groundwater Development Project. This report and related work products were used in developing hydrogeologic conceptual models and a three-dimensional regional groundwater flow model for selected basins of eastern Nevada and western Utah.

1.1 PROJECT BACKGROUND

The Clark, Lincoln, and White Pine Counties Groundwater Development Project (hereafter referred to as the Project) proposes to develop unused groundwater resources within selected basins of eastern Nevada where SNWA holds groundwater rights and applications. These basins include Coyote Spring, Cave, Dry Lake, Delamar, Spring, and Snake valleys (hereafter referred to as the Project Basins), and are depicted in Figure 1-1.

In 2004, SNWA applied to the Bureau of Land Management (BLM) for issuance of rights of way to construct Project facilities, most of which will be located on public lands administered by the BLM. These facilities include groundwater production wells, water conveyance facilities, water storage and regulating reservoirs, and power facilities. BLM issuance of these rights of way to construct, maintain, and operate these facilities requires a federal action for which the National Environmental Policy Act and Endangered Species Act must be considered. BLM has determined that preparation of an Environmental Impact Statement is required to assess the potential environmental effects that may result from permitting the rights of way, including the potential indirect effects of the proposed groundwater development. This report was prepared in support of that assessment.

1.2 PURPOSE AND SCOPE OF GEOLOGIC INVESTIGATION

The purposes of this report are to (1) provide an overview of the geology for an area encompassing the Project Basins, including a description of how that geology relates to the hydrogeology of the area; (2) present the geologic and hydrogeologic framework of the Project Basins and surrounding area; and (3) evaluate the potential continuity of groundwater flow.

The scope of this geologic investigation included significant data compilation and acquisition, and development of geologic and hbydrogeologic surface maps and cross sections. This investigation also included gravity surveys of the Project Basins conducted by the U.S. Geological Survey (USGS) through joint funding agreements with SNWA. Significant fieldwork was conducted to improve the geologic understanding of selected areas. The scope of work was defined, in part, to differentiate between aquifers and aquitards, that is, hydrogeologic units (HGUs) with high and low hydraulic conductivity, respectively. The geologic investigation also focused on identifying areas where aquitards of sufficient thickness are present and inhibit groundwater flow.

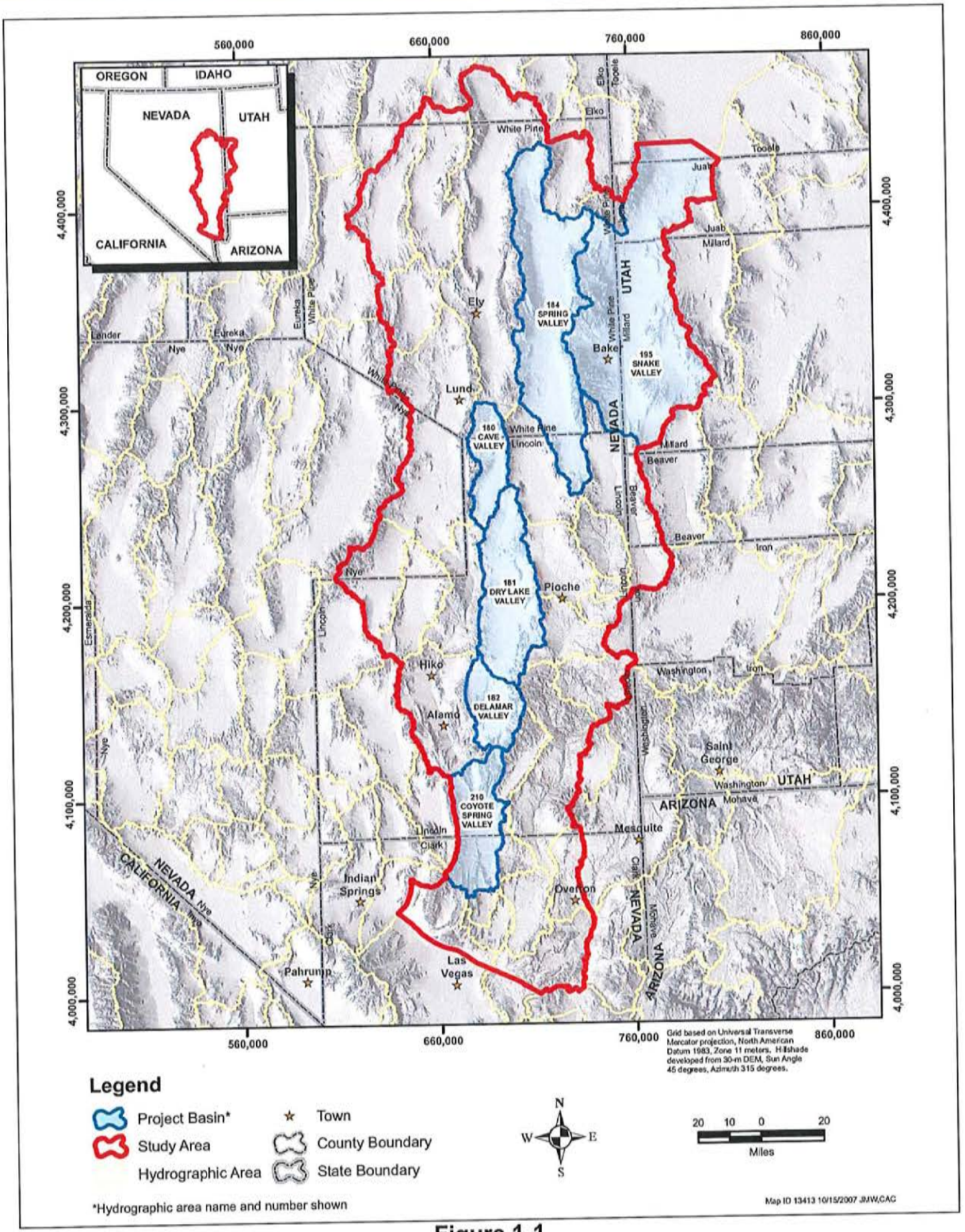

Figure 1-1
Location of Project Basins

1.3 DOCUMENT ORGANIZATION

This document consists of the following seven sections and Appendix A showing general photos of the study area.

- Section 1.0 provides a description of the Project background, the purpose and scope of the geologic investigation, and an overview of the contents of this report.
- Section 2.0 describes the geologic study area and physiographic setting of the area, including a discussion on the regional geologic features and regional flow systems.
- Section 3.0 describes the methodology applied in the geologic analysis, including a description of the objectives of the analysis and technical approach.
- Section 4.0 discusses the geology and hydrogeology of the geologic study area and some of the surrounding basins and ranges that could be in hydrogeologic connection with the basins of the geologic study area. Section 4.0 is divided into subsections describing the various aspects of the geology and hydrogeology, as follows:
  - Section 4.1 discusses the geology and stratigraphy of the geologic study area of this report, including the geologic units in the study area.
  - Section 4.2 discusses the HGUs of the geologic study area and how they relate to the geologic units.
  - Section 4.3 discusses the evolution of the geologic structure in the geologic study area and how that structure impacts the hydrogeology.
  - Section 4.4 describes the geology of the mountain ranges and adjacent basins within the geologic study area and how the specific geology in these areas affects the hydrogeology.
- Section 5.0 discusses the geophysics of the geologic study area.
- Section 6.0 is a summary of the general geology and general hydrogeology of the geologic study area.
- Section 7.0 provides a list of references cited in the document as well as a list of references used in making the geologic maps and cross sections.

THIS PAGE INTENTIONALLY LEFT BLANK

2.0 DESCRIPTION OF GEOLOGIC STUDY AREA

The area of study for the geologic investigation encompasses the Project Basins and additional basins that comprise regional groundwater flow systems in which the Project Basins reside. The physiographic setting of the geologic study area is presented, followed by summary descriptions of the regional groundwater flow systems comprising the geologic study area.

2.1 GEOLOGIC STUDY AREA

The area covered by this geologic investigation, hereafter referred to as the geologic study area, includes all hydrographic areas within the White River Flow System (WRFS). The geologic study area also includes adjacent basins that may be in hydraulic connection with basins within the WRFS. The geologic study area is delineated by a thick red line on Figure 2-1. The purpose of including such a large area is to allow investigation of the potential hydraulic continuity or discontinuity between these basins due to geologic influences. In addition, geology of the same scale was compiled, and cross sections extended, over an even larger area whose boundary is identified by a thick black line seen outside the boundary of the geologic study area (Figure 2-1). This was done to assess the broader geologic framework in order to determine the best model area and to provide additional data should the boundaries of the model area later change.

More specifically, the geologic study area includes all of the basins in Lincoln and White Pine counties, Nevada, except for certain basins in southwestern and southeastern Lincoln County and along the northern edge of White Pine County. Several basins in adjacent counties are included, such as basins overlapping into Elko County, basins in Eureka, northern Nye, and northern Clark counties, Nevada, and basins in the western areas of Juab, Millard, Beaver, and Iron counties, Utah. These basins are also delineated on Figure 2-1.

The groundwater flow systems incorporated in this evaluation are delineated on Figure 2-1. These systems include all of the WRFS, which covers much of eastern Nevada from just beyond the Elko/White Pine county line to Lake Mead. The WRFS (Eakin, 1966), as used here, was called the Colorado Flow System by Harrill and Prudic (1998; see also Belcher, 2004). The Meadow Valley Flow System (MVFS) subset of the Colorado Flow System is included. This flow system originates north of Pioche at the Lincoln/White Pine county border, in Nevada, and extends to Moapa in northern Clark County, Nevada, where it joins the WRFS. A portion of the Great Salt Lake Desert Flow System (GSLDFS) is covered in this investigation. This flow system originates in the Snake Range of eastern Nevada and surrounding basins, extending eastward into Utah and then northward to the Great Salt Lake Desert.

Other flow systems in the geologic study area are the southern Goshute Valley Flow System (GVFS) of White Pine and Elko counties, Nevada; the eastern edges of the Ruby Valley, Newark Valley, and Railroad Valley flow systems of western White Pine, Eureka, and northern Nye counties, Nevada; the eastern edge of the Penoyer Valley area of Lincoln and Nye counties, Nevada; the northeastern portion of the Death Valley Flow System (DVFS) in Lincoln and Nye counties, Nevada; the northeastern part of the Las Vegas Valley of the Colorado Flow System; the western edge of the Virgin River Flow System of the Mesquite, Nevada, area; and the western edge of the Sevier Lake

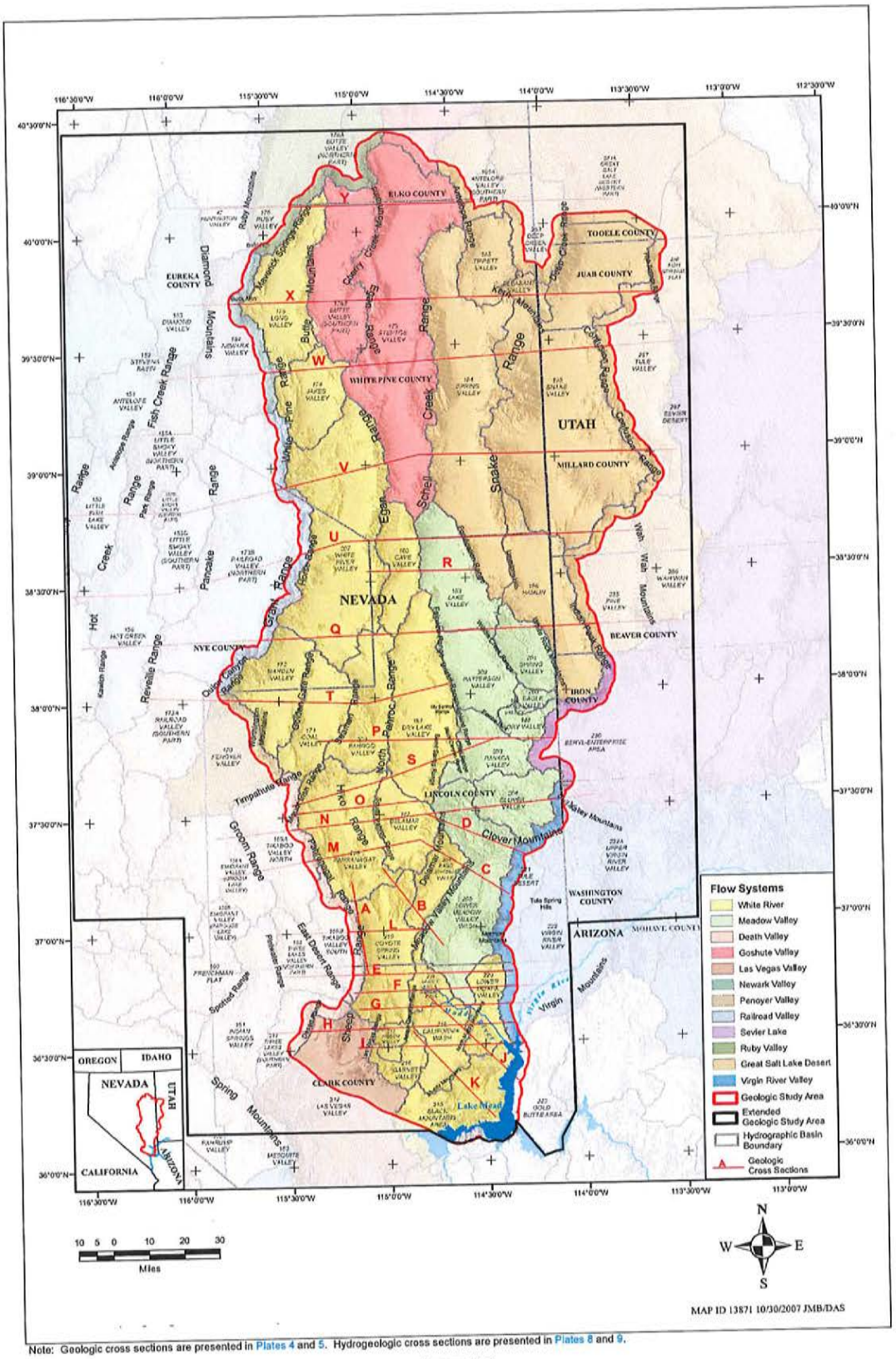

Note: Geologic cross sections are presented in Plates 4 and 5. Hydrogeologic cross sections are presented in Plates 8 and 9.

FIGURE 2-1
HYDROGRAPHIC BASINS, RANGES AND FLOW SYSTEMS WITHIN THE GEOLOGIC STUDY AREA

Flow System of western Utah. These flow systems are defined by Eakin (1966), Harrill et al. (1988), and Harrill and Prudic (1998).

2.2 Physiographic Setting and Background

The geologic study area (Figure 2-1) is within the Great Basin physiographic province, characterized by north-trending basins and ranges that are formed by generally north-striking basin-range normal faults. The area has been subjected to several periods of deformation since Precambrian time. The most recent episode of deformation, which produced the present topography, is the basin-range episode of normal faulting. This topography consists of a number of closed basins and partially closed basins, typical of the Great Basin region where surface-water flow is restricted to within that region. Exceptions occur only along the Great Basin boundary along the Colorado River, where a few basins have surface water exiting to the Colorado River. These exceptions include the Virgin River, Muddy River, Las Vegas Wash, and the associated basins in which these streams occur.

During wetter periods of Pleistocene time, the latest of which was about 10,000 to 15,000 years before present, ancestral streams connected some closed basins, commonly through a series of ancestral lakes. For instance, the White River and its tributaries flowed southward through much of the western portion of the map area and integrated many of these basins, apparently by overflowing closed basins one by one (Figure 2-2) (Tschanz and Pampeyan, 1970). During this time, the White River joined other streams that flowed southward to join the Colorado River at the vicinity of present-day Lake Mead, at the southern edge of the area. At the present time, over most of its course and as far south as Moapa, Nevada, the descendant drainages of the White River are intermittent.

Despite the intermittent nature of surface water, groundwater occurs at different depths beneath most of the map area. The groundwater exists in aquifers within and between a number of groundwater basins, and it flows through these aquifers in the defined regional groundwater flow systems (Figure 2-1). These systems may include a dozen or more closed or integrated topographic basins that are interconnected in the subsurface. These regional flow systems are defined by evidence that their groundwater flow paths pass beneath topographic divides and continue beneath adjacent basins and ranges (Eakin, 1966; Winograd and Thordarson, 1975; Harrill et al., 1988; Harrill and Prudic, 1998).

The primary regional aquifers in the flow systems consist of Paleozoic carbonate rocks, volcanic rocks (generally Tertiary ash-flow tuffs), and Miocene to Holocene basin-fill sediments. The primary regional aquitards within the flow systems are Precambrian to Cambrian schist, quartzite, slate, and shale, Mississippian shale, Mesozoic clastic sedimentary rocks, and Jurassic to Tertiary plutonic rocks.

The direction and magnitude of groundwater flow is generally enhanced by faulting, specifically along damage zones as defined by Caine et al. (1996), which consist of small faults and extensional fractures on both sides of the interior "core zone" of a fault, where most deformation has taken place. The damage zones of fractures along the outer portion of fault zones are generally parallel to the faults that formed them. Where the damage zones are in carbonate rocks, solution of the carbonate rocks along the fractures can create substantially larger groundwater flow paths. Fault-based barriers to flow include fault gouge zones that typically occur along the interior core zones of fault zones (Caine et al., 1996; Dixon and Katzer, 2002; Fairley and Hinds, 2004; Rowley and Dixon, 2004; Page et al., 2005a).

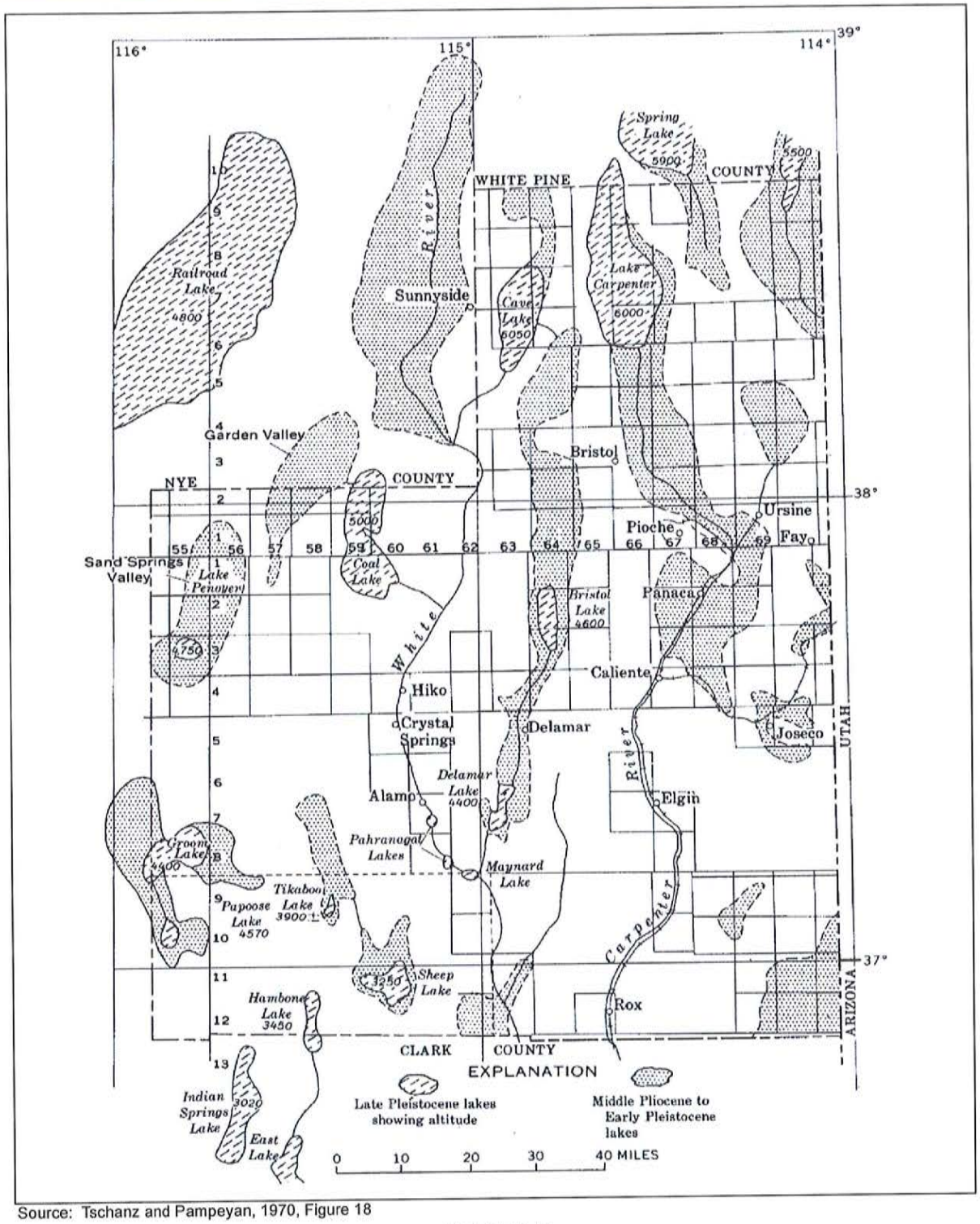

Source: Tschanz and Pampeyan, 1970, Figure 18

FIGURE 2-2
MAP OF PLIOCENE AND PLEISTOCENE LAKES AND STREAMS IN LINCOLN COUNTY AND ADJACENT AREAS, NEVADA

3.0 METHODOLOGY

The objectives of the geologic analysis and the methods applied in developing the work products accompanying this report are described in the following sections. Work products developed as part of this analysis include 1:250,000-scale digital geologic maps (Plates 1 and 2), an explanation of map units (Plate 3), and cross sections (Plates 4 and 5). Hydrogeologic units (HGUs) were derived by combining geologic stratigraphic units based on their hydraulic properties and spatial distribution, then the digital geologic maps were simplified accordingly to construct hydrogeologic maps (Plates 6 and 7) and cross sections (Plates 8 and 9). The geologic map area (red line, Figure 2-1) covers most of White Pine County and Lincoln County, Nevada, as well as large parts of adjacent counties in Nevada and Utah.

3.1 OBJECTIVES

The primary objective of this geological analysis is to develop a digital geologic and hydrogeologic framework in support of a groundwater model of a portion of the area covered by this geologic analysis. The geologic information compiled provides data on reasonable model boundaries, reasonable internal boundaries, extents of HGUs, and potential groundwater flow paths and flow barriers. Hydrologic interpretations that depend on these geologic data are given in accompanying hydrologic reports. The geologic framework also provides aquifer and aquitard thickness for the modeled area. Geologic evaluations outside of the model area (black line, Figure 2-1) provide a basis for interpreting groundwater interactions across model boundaries, including potential groundwater interactions between groundwater flow systems internal to the model and groundwater flow systems outside of the modeled area. This geologic analysis was manifested through the creation of geologic and hydrogeologic maps and cross sections of the geologic study area.

The objective of the geologic maps and geologic cross sections is to provide, in digital form, the geologic framework for the eastern carbonate aquifer systems of Nevada and western Utah as an aid in developing numerical models of groundwater flow systems. Framework data that were acquired include the distribution, geometry, thickness, composition, and physical properties of geologic units used to define HGUs and potential aquifers and aquitards (confining units). Such information will assist in ascertaining the rock units that are most likely to provide pathways for groundwater flow and which rock units are most likely to retard or divert flow.

An important aspect of the geologic maps is the portrayal of the distribution and attitude of faults, especially those formed during the youngest (basin-range) episode of deformation. Faults may serve as barriers and/or conduits to groundwater flow. In the geologic study area, most faults trend northerly, parallel to the general southward topographic gradient of the WRFS. Thus for the WRFS, basin-range faults serve as significant conduits to groundwater flow in this direction. In other flow systems in the geologic study area, basin-range faults may either direct groundwater flow through a system of barriers and fault conduits and/or impede groundwater flow toward otherwise down-gradient groundwater basins. Part of the objective of this report is to evaluate the potential for these faults to influence groundwater flow, especially how they may act as either barriers or conduits to groundwater flow. Another objective of this report is to evaluate which faults are most likely to

provide conduits and/or barriers to groundwater flow so that they can be properly incorporated into a groundwater model of the region.

3.2 Technical Approach

The approach used in this investigation was to combine published and unpublished geologic information from dozens of references collected, compiled, and reviewed by authors familiar with the geology of the region. In addition, an evaluation was conducted of borehole information from oil and gas test wells, monitor wells, such as those drilled during the U.S. Air Force's MX missile-siting program of the early 1980s, and borehole information from monitor holes drilled by SNWA for the Project. Other sources of information were geophysical studies of the region published by USGS and other entities, particularly data from gravity surveys performed by USGS in 2003 to 2005 (Mankinen et al., 2006; McPhee et al., 2005, 2007; Scheirer, 2005). These latter studies have given insight as to the thickness of basin fill and depth to underlying rocks within several basins in Lincoln and White Pine counties, Nevada. A final source of evidence is geologic field work performed over the area by the authors of this report.

Based on the evaluation of the compiled data and the expertise of the geologists involved in this investigation, geologic maps were constructed for the area of the groundwater model (Plates 1 and 2). Geologic cross sections were constructed (Plates 4 and 5) and tied into the geologic maps. Because of the complexity of the geology of eastern Nevada, these maps and cross sections represent a work in progress, inasmuch as new data on crosscutting faults, bedding surfaces, intrusions, volcanic sequences, and other geologic units and geologic relationships must be continuously evaluated as new information becomes available.

The geologic units were combined into HGUs of similar hydraulic properties and spatial extent. These broad units make up the aquifers, aquitards, and units of intermediate permeability of the area described by this report. These HGUs are displayed in Plates 6 and 7. Cross sections of these units were compiled using the geologic cross sections of Plates 4 and 5 as a basis; these hydrogeologic cross sections are displayed in Plates 8 and 9. Based on the hydrogeologic maps and cross sections, the extents of aquifers, aquitards, and intermediate-permeability rocks could be evaluated, along with potential fault barriers and fault conduits to groundwater flow. The hydrogeologic maps, cross sections, and hydrogeologic interpretations were used to compile the geologic framework for the groundwater model. The hydrogeologic maps and cross sections were also interpreted to evaluate probable groundwater flow paths and flow barriers.

3.3 Geologic Data Compilation

The compilation of geologic data was derived from a number of sources, including literature review, review of State Engineer's records, oil and gas test well and other borehole data, evaluation of drilling data and information from SNWA monitor wells, evaluation of studies performed by USGS, and consultation with geologic experts in the area. This literature was reviewed and compared with other literature and other sources of geologic information prior to incorporation into the geologic maps and cross sections.

Geologic data from wells were compiled from reports to the State Engineer, when available, and data on oil and gas test wells drilled within the geologic study area, and from monitor wells drilled by

SNWA in 2003 and 2005 in upper Moapa, Coyote Spring, Cave, Dry Lake, and Delamar valleys. Not every well had geologic information, but most of them did have useful information to assist in compiling the geologic and hydrogeologic cross sections.

3.4 PREPARATION OF GEOLOGIC MAPS AND SECTIONS

A large portion of the map area is underlain by the WRFS (Figure 2-1). The geology of the southern part of the WRFS and adjacent systems (Figure 3-1) has been discussed by Page et al. (2005a) and in this report is digitally mapped at 1:250,000 scale (Plate 2). The digital geologic and tectonic maps of the DVFS (Figure 3-1), to the west of the WRFS, were also published at a 1:250,000 scale (Workman et al., 2002 and 2003). The DVFS includes much of the southwestern portions of Plates 1 and 2. The geologic maps of both the DVFS and southern WRFS included significant new and unpublished geologic mapping.

For the maps (Plates 1 and 2), much of the surface geology was based on county 1:250,000-scale geologic maps and the Utah 1:500,000-scale state geologic map (Hintze, 1980; Hintze et al., 2000). From west to east and north to south, the Nevada counties covered by these maps are southern Elko County (Roberts et al., 1967), eastern Nye County (Cornwall, 1972; Kleinhampl and Ziony, 1985), White Pine County (Hose and Blake, 1976), Lincoln County (Tschanz and Pampeyan, 1970), and Clark County (Longwell et al., 1965). The Utah counties covered by these maps are southwestern Tooele County, western Juab County, western Millard County (Hintze and Davis, 2002a and b, and 2003), and western Beaver County (Hintze, 1980 and 1988; Hintze and Davis, 2002a).

Nearly all county maps and reports were published decades ago. Many revisions and reinterpretations have been made to the geology of portions of those maps since that time. A significant part of the entire map area was compiled by Terrascan Group, Inc. (1987), but it used the same county maps used in the present map. The entire map area is also covered by state geologic maps at 1:500,000-scale (Stewart and Carlson, 1978; Hintze, 1980; Hintze et al., 2000), but some of the geology on these maps has also been subsequently revised and reinterpreted. These revisions and reinterpretations of the geology are from many more recent, commonly more detailed, published Nevada and Utah geologic maps and reports, and this new information has been incorporated into the maps of Plates 1 and 2 and in the discussions in this report. Not all of these maps and reports are cited in the text because of their large number, although all of them are listed in Section 7.0 of this report. Small-scale geologic maps used for the creation of Plates 1 and 2 are indexed in Figure 3-1. In addition, the present maps (Plates 1 and 2) include some new, unpublished field observations, though no new mapping was conducted specifically for this report and associated maps.

The geologic maps of Plates 1 and 2 include many changes of specific geologic units throughout the geologic study area. In many places, facies changes resulted in major changes in the lithology of a specific unit, and in other places, different formation names were used essentially for the same unit. In some instances, a specific unit thinned in certain areas and was included as a member of another unit or as an inconsequential bed within another unit. An example is the Mississippian Chainman Shale, which is a major shale confining unit in the north, as in White Pine County (Hose and Blake, 1976), but a generally inconsequential shale horizon included within other units in the southern map area, as in Clark County (Longwell et al., 1965). During compilation of the geologic map, separate stratigraphic columns were commonly used for different counties, along with a stratigraphic column for units within western Utah. Correlations between specific geologic units are commonly given in

FIGURE 3-1
INDEX MAP OF PREVIOUS SMALL-SCALE MAPPING USED IN THE GEOLOGIC EVALUATIONS AND TO CREATE THE GEOLOGIC AND HYDROGEOLOGIC MAPS OF Plates 1, 2, 6, AND 7

the literature and these correlations were generally used to associate units of the same or similar age in different parts of the map area. An example is the correlation between the Devonian Guilmette Formation and the Devils Gate Limestones (Hose and Blake, 1976).

During map compilation, a hard copy of the available digital file—generally the county map—was modified by hand, then digitized. Before this compilation, we accumulated, assimilated, and evaluated all available new geologic data about the area. The new data included reports, different concepts, detailed or regional maps, geophysics, and well logs, etc. Conflicts necessarily resulted over interpretations and placement of contacts and faults. Decisions on the eventual linework were based on what appeared to be scientifically the most reasonable and depended primarily on the judgement and experience of the authors.

The maps (Plates 1 and 2) include 25 new geologic cross sections (Plates 4 and 5), most of which generally trend east-west. These cross sections are roughly evenly spaced across the map area at the same scale as the map and at locations chosen to best show specific geologic and structural relationships important to the interpretation of the exposed geology. In addition, hydrogeologic maps (Plates 6 and 7) and hydrogeologic cross sections (Plates 8 and 9) were constructed, where geologic units with similar hydrologic properties such as porosity and permeability were combined into HGUs, distinct from the geologic units that comprise them. Few of the reports and maps used to compile the geologic maps had associated geologic cross sections, so the cross sections for this report are based on interpretations of the county geologic maps along with all other available maps and reports of the map areas. A geologic map by Terrascan Group, Inc. (1987) presented associated cross sections that were referred to in making the cross sections for the maps in this report. In addition, the geologic map of Elko County (Coats, 1987) was used to help interpret Cross Section Y—Y' (Plate 4), along the northern edge of the map area. The cross sections of Page et al. (2006) aided us in making our cross sections in the southern part of the geologic study area. The cross section of Smith et al. (1991) was useful in constructing Cross Section X—X' (Plate 4) near the northern margin of the geologic study area.

Unlike compilation of the geologic map, most cross sections are newly authored for this report, so there was no need to resolve conflicts arising from other work in the area. The first step in the construction of cross sections is to satisfy the three-dimensional geometry of the rocks at depth based on the types, attitudes, and thicknesses of rocks and structures on the surface. The most difficult part of making cross sections is dealing with the near absence of subsurface information. Therefore, geophysics and well logs near the line of section are precious. Fortunately, aeromagnetic and gravity geophysical data were available for much of the area. Unfortunately, well logs and audiomagnetotelluric (AMT) and seismic profiles are rare. Where local information on the third dimension is not available, analogies are made with areas in other parts of the Great Basin where seismic and drill-log data provide ideas about how the rocks and structures look at depth. And here, as in compilation of geologic maps, the judgment and experience of the authors are of paramount importance.

All cross sections incorporated lithologic information from available oil- and water-well logs. Oil-well logs in Nevada are available online from the Nevada Bureau of Mines and Geology or through their publications. Garside et al. (1988) compiled geologic data from oil and gas wells drilled in Nevada from 1907 through 1988. This compilation was supplemented by Hess (2001). This information was supplemented again in 2004 (Hess, 2004). Oil-well logs in Utah were obtained from

the Utah Division of Oil, Gas, and Mining website (UDOGM, 2006). Water-well logs in Utah were obtained from the Utah Division of Water Rights website (UDWR, 2006).

Geophysical studies, notably gravity maps (Saltus, 1988a and b; Cook et al., 1989; Ponce, 1992; Saltus and Jachens, 1995; Ponce et al., 1996), aeromagnetic maps (Hildenbrand and Kucks, 1988a and b), and seismic sections (Allmendinger et al., 1983; Hauser et al., 1987), were used to aid in the interpretation of geologic cross sections and structure sections. Gravity maps and electromagnetic profiles were completed by USGS as part of USGS/SNWA joint funding agreements (Mankinen et al., 2006; McPhee et al., 2005 and 2007; Scheirer, 2005). The gravity data were converted to depth-to-basement data and were used to aid in constructing the cross sections.

4.0 CONCEPTUAL GEOLOGIC MODEL

4.1 GEOLOGY AND STRATIGRAPHY

4.1.1 OVERVIEW

The geology of the geologic study area (Figure 2-1, Plates 1 and 2) is characterized by a thick stratigraphic sequence of rocks from Proterozoic to Holocene age that has been structurally deformed during several tectonic episodes. The thick sequence includes three major assemblages that are important aquifers:

- Carbonate aquifer of Paleozoic age
- Volcanic rocks of Tertiary age
- Basin-fill sediments of Tertiary to Quaternary age.

Along with the aquifers are moderate to thick confining units or low-permeability units, including:

- Early to Late-Proterozoic metamorphic and igneous rocks
- Late Proterozoic to Lower Cambrian quartzite and shale
- Shale, sandstone, and conglomerate of Mississippian age
- Triassic to Cretaceous shale, siltstone, and sandstone
- Mesozoic to Cenozoic plutons.

Three tectonic episodes, plus an intervening episode of extensive volcanism, have affected the hydrogeology of the region. The oldest tectonic episode is the Antler deformation (Late Devonian to Late Mississippian). This episode included east-verging thrust sheets. The second tectonic episode was the Sevier deformation (Jurassic through early Cenozoic) that resulted in east-verging thrust sheets in which Paleozoic carbonate rocks were placed over each other and over younger rocks.

In Eocene to middle Miocene time, volcanism resulted in the development of thick blankets of ash-flow tuff and related lava flows, including many scattered calderas that were the sources of the tuff. The caldera margins formed new groundwater flow paths and barriers.

The third tectonic episode is the middle Miocene to Holocene basin-range deformation that shaped the current topography of the Great Basin, including most of Nevada and parts of western Utah and southeastern California. Basin-range faulting produced graben and horst topography, resulting in deep basins and relatively high mountain ranges, generally oriented north-south. The mountain ranges provided areas of groundwater recharge, and accumulations of alluvial fill within the basins provided areas of aquifer storage and avenues of groundwater flow. Basin-range faults may provide hydrogeologic barriers to groundwater flow. But more commonly, basin-range faults provide conduits to groundwater flow, especially from north to south. These north-south conduits may double as barriers to east or west flow in certain flow systems such as the GSLDFS.

The age of the rocks in the geologic study area is summarized in a Geologic Time Scale chart (Figure 4-1). The oldest rocks are Early and Late Proterozoic metamorphic and igneous units. These rocks are overlain by thick sequences of quartzite and subordinate shale, which are locally

ERA	PERIOD	EPOCH	TIME	PROCESSES AND ROCK TYPES
Cenozoic	Quaternary	Holocene Pleistocene	Present 1.8 Ma	Valley-Fill Alluvium
	Tertiary	Pliocene Miocene	*5 Ma*	Start Basin-Range Faulting (20 Ma) Volcanics and Older Sediments
		Oligocene Eocene Paleocene	*38 Ma* 65 Ma	Emplacement of Calderas
Mesozoic	Cretaceous Jurassic Triassic		248 Ma	Sevier Orogeny, Intrusions Continental Sediments
Paleozoic	Permian Pennsylvanian Mississippian Devonian Silurian Ordovician Cambrian		543 Ma	Antler Orogeny, Intrusions Chainman Shale, Carbonates Quartzite and shale
Precambrian			4.5 Ga	

Source: Adapted from Geological Society of America, 1999

FIGURE 4-1
GEOLOGIC TIME SCALE, INCLUDING ROCK TYPE AND TECTONIC EVENTS

metamorphosed to slate and schist, of Late Proterozoic age. The Proterozoic rocks pass conformably upward into rocks of similar type and thickness, though less metamorphosed, that are Late Proterozoic to Early Cambrian in age. During Middle Cambrian time, carbonate deposition was initiated, and thick sequences of marine limestone and dolomite were deposited from the Middle Cambrian through the Permian Periods. These rocks make up the carbonate aquifer of Nevada and adjacent parts of Utah and range in thickness between 5,000 and 30,000 ft throughout this area (Harrill and Prudic, 1998).

Locally, marine sandstone and shale are intertongued with the carbonates. These units generally do not form significant impediments to regional groundwater flow, with the exception of the Chainman Shale and related shale and sandstone of Late Mississippian age. This unit locally exceeds 2,000 ft in thickness, and in all but the southern part of the geologic study area, this unit divides the carbonate aquifer into two distinct aquifers, the lower and upper carbonate aquifers. The Chainman Shale and related clastic units were derived from erosion of a structural highland, the Antler Highland, in and northwest of the geologic study area. The highland, made up in large part of the Roberts Mountain allochthon, was produced by the Antler compressive deformational event.

Mesozoic rocks in the geologic study area are largely clastic, nonmarine, and thin where deposited, but in most places they have been removed by erosion. Mesozoic and older rocks were deformed during the Sevier deformational event. At this time, the geologic study area was a highland, also known as a hinterland, and an episode of erosion of the area removed most Mesozoic rocks.

Plutons of Late Jurassic to Paleocene age were intruded during pulses during Sevier deformation. These plutons probably had associated extrusive volcanic units, but all of these units have been removed by erosion. Mesozoic plutons commonly led to significant mineralization in the geologic study area.

Middle Tertiary (Eocene to middle Miocene) time marked the beginning of calc-alkaline intrusion and resulting volcanism, the terminal product of subduction beneath western North America that began in the Triassic Period (Atwater, 1970; Lipman et al., 1972; Hamilton, 1995). Above individual source plutons, vent deposits included andesitic and dacitic lava flows and volcanic mudflow breccia that locally exceeded several thousand feet of thickness. Caldera deposits consist of dacitic to rhyolitic ash-flow tuffs, which are similarly thick within individual calderas. Farther outward from the vents above the plutons, lava flows are sparse because they do not flow more than a few miles from their vents, but outflow ash-flow tuffs accumulated to aggregate thicknesses exceeding 1,000 ft in most of the geologic study area.

Starting at about 20 Ma ago (middle Miocene), subduction ceased and extensional deformation increased in the map area (Christiansen and Lipman, 1972; Christiansen and Yeats, 1992; Rowley and Dixon, 2001). Basin-range deformation, characterized by vertical (normal) faulting, began to form alternating mountain ranges and valley basins. The main pulse of this basin-range faulting began about 10 Ma ago, during which time the present topography formed. As valleys formed, they were filled by debris eroded from the adjacent mountain range, creating basin-fill deposits.

Individual rock units, structures, basins, and ranges are described in the following sections. Thicknesses of most units are from the county reports of the area where the unit is exposed. The relationships between geologic units in the different areas of the map can be determined from Figures 4-2 to 4-5. These figures illustrate geologic columns for Lincoln (Figure 4-2), White Pine

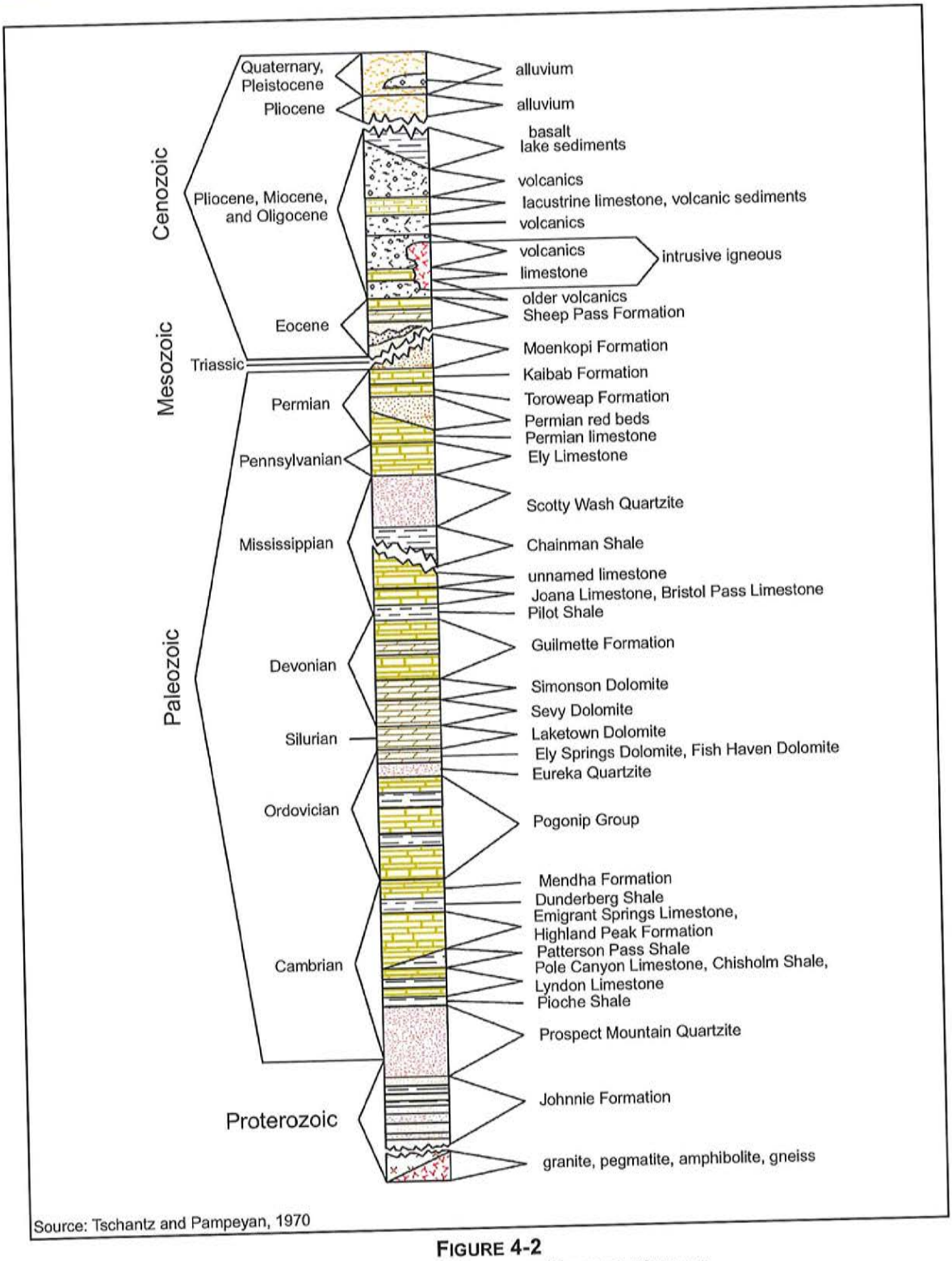

FIGURE 4-2
GEOLOGIC UNITS OF LINCOLN COUNTY, NEVADA

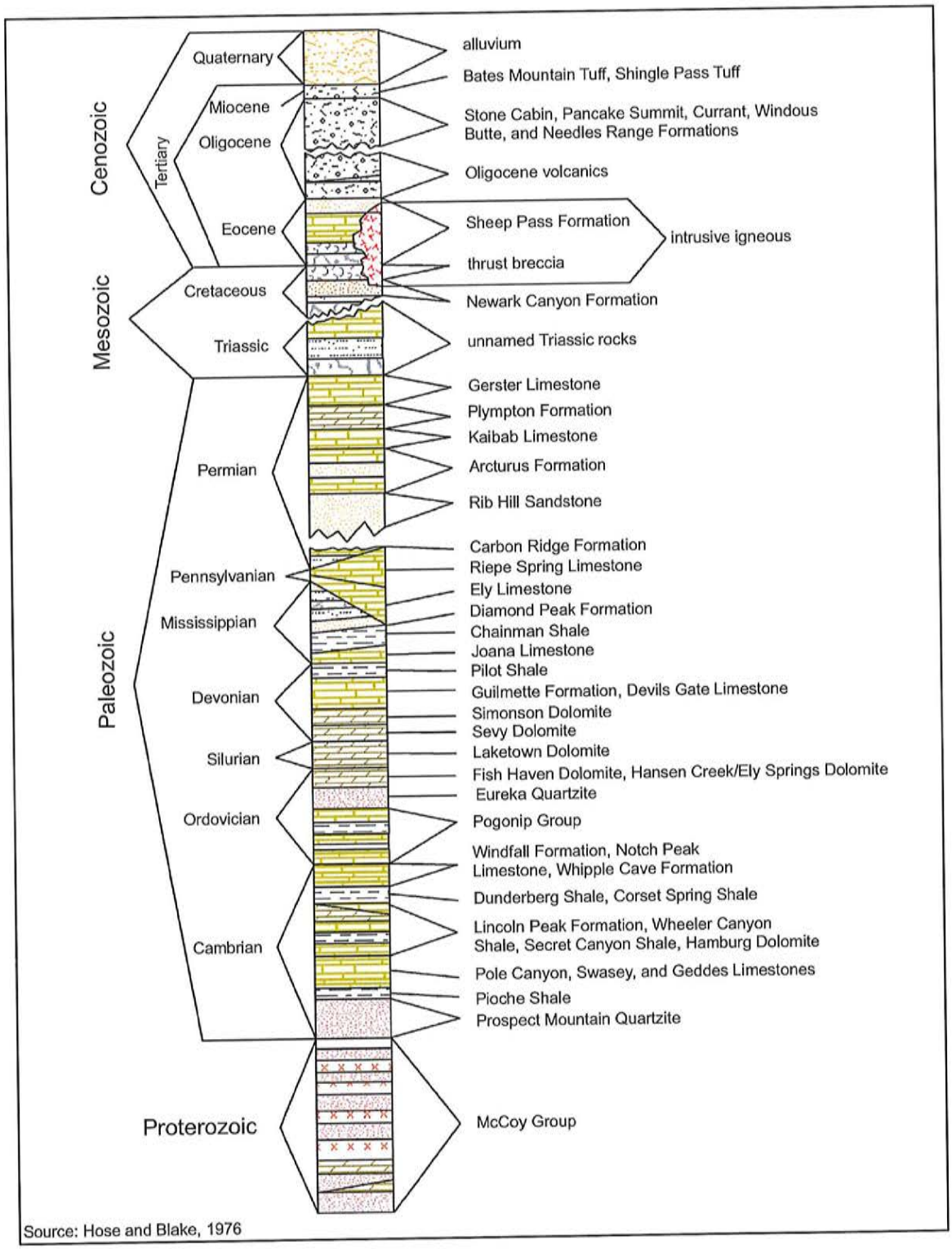

Source: Hose and Blake, 1976

FIGURE 4-3
GEOLOGIC UNITS OF WHITE PINE COUNTY, NEVADA

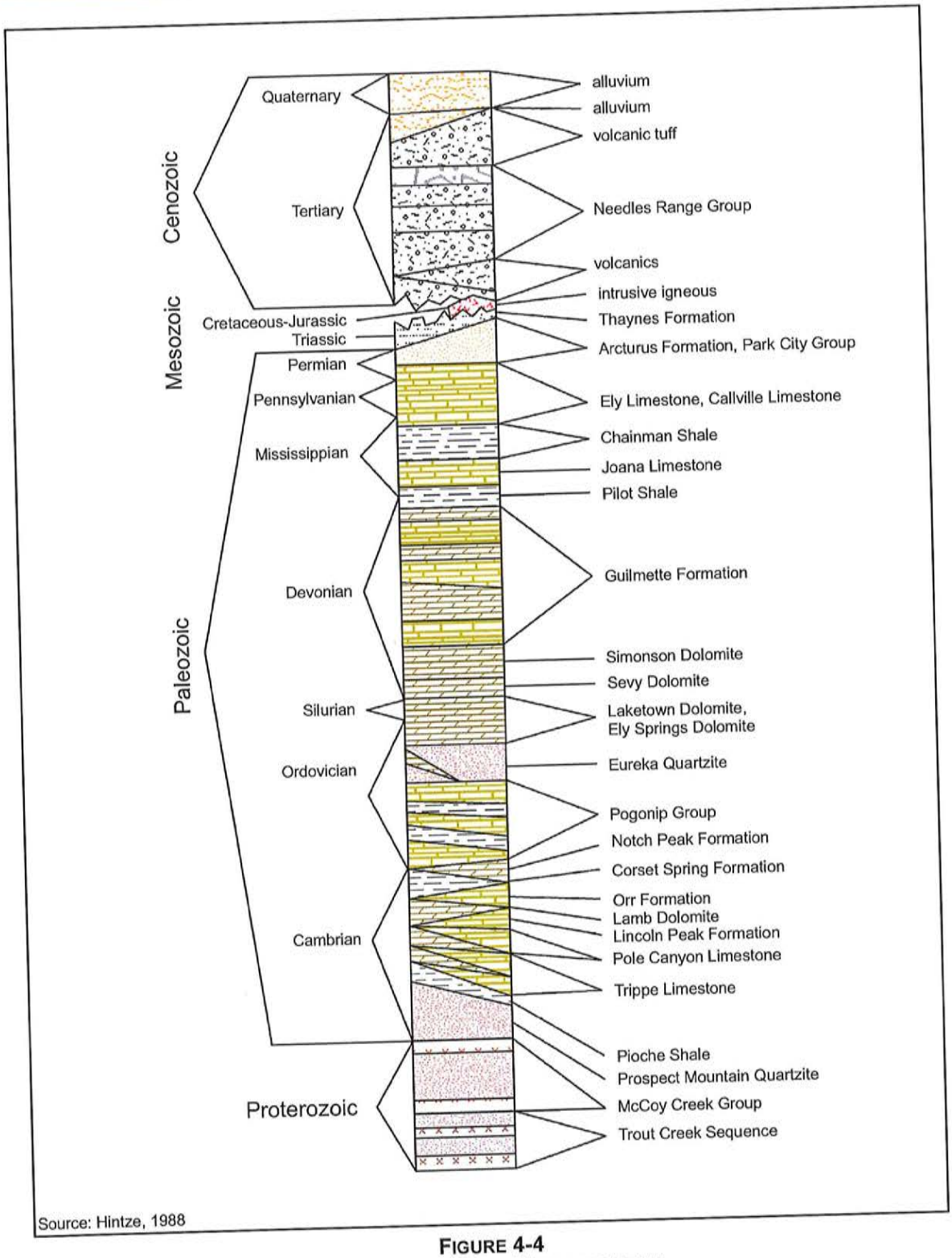

FIGURE 4-4
GEOLOGIC UNITS OF WESTERN UTAH

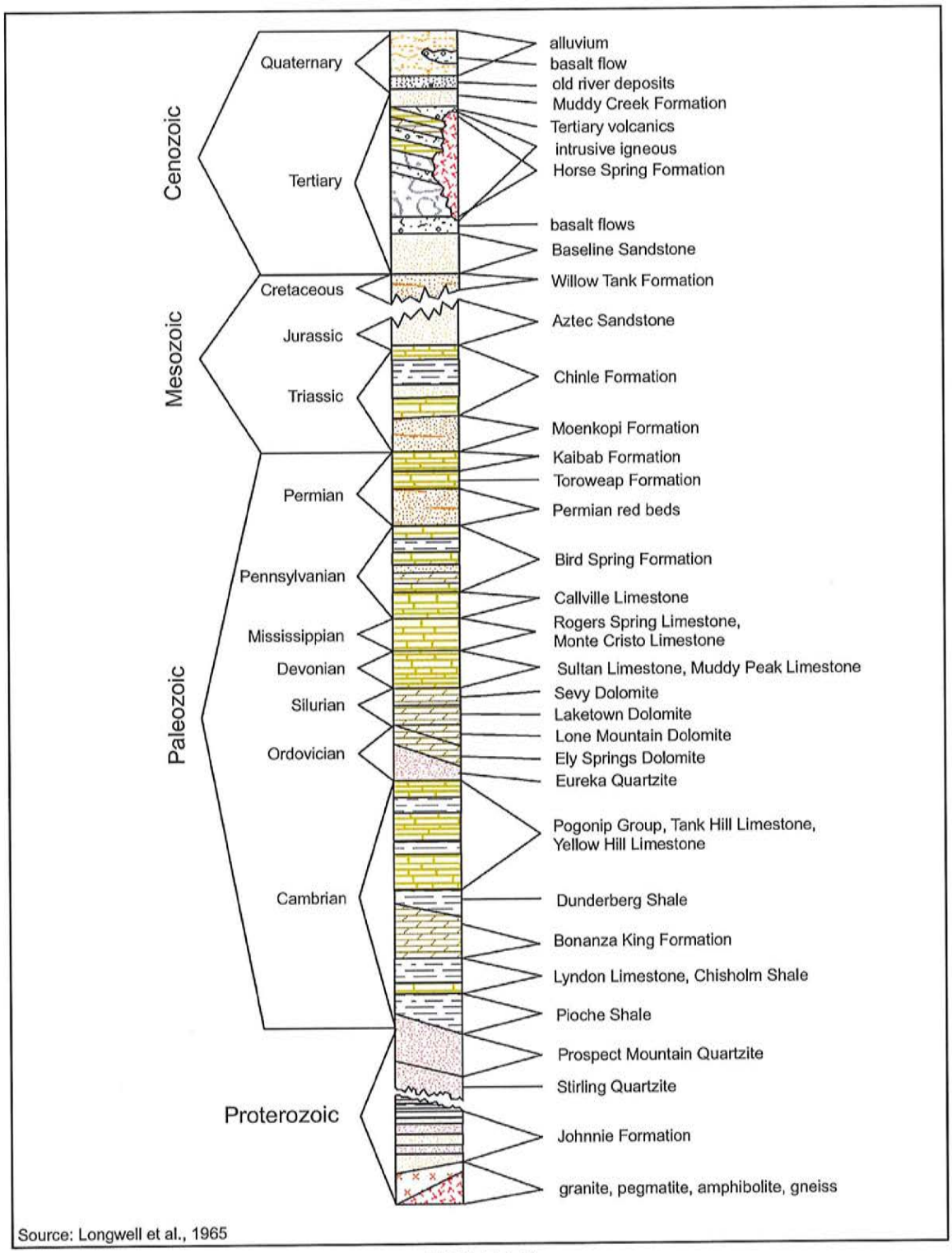

FIGURE 4-5
GEOLOGIC UNITS OF CLARK COUNTY, NEVADA

(Figure 4-3), and Clark counties (Figure 4-5), Nevada, and western Utah (Figure 4-4). The Utah area consists of western Iron, Beaver, and Millard counties and the southwestern corner of Juab County.

4.1.2 PROTEROZOIC ROCKS

The oldest rocks are in and adjacent to the southern part of the geologic study area in the Beaver Dam Mountains, Mormon Mountains, Virgin Mountains, northeastern Spring Mountains, and the Desert Range (Plate 2) (Tschanz and Pampeyan, 1970; Longwell et al., 1965). These rocks are crystalline metamorphic rocks of Early Proterozoic age (Page et al., 2005a) that we have mapped as Precambrian rocks (p€). Over most of the geologic study area, however, the oldest rocks are Late Proterozoic to Lower Cambrian quartzite. These Late Proterozoic to Cambrian units appear to be the initial deposits of the Cordilleran miogeocline, a western belt of offshore carbonate-shelf and intertidal deposits (Page et al., 2005a). These units were deposited in shallow marine waters along a passive continental margin of what is now western North America (Stewart and Poole, 1972; Stewart, 1976).

In White Pine County and adjacent Utah, the principal Late Proterozoic unit is the McCoy Creek Group. The assemblage consists of well-bedded, resistant feldspathic quartzite and subordinate slate and argillite more than 9,000 ft thick in the Schell Creek Range (Plate 1) and about 7,600 ft thick in the Deep Creek Range, Utah. The metamorphic grade of these units is low to moderate, locally producing schist. The unit is mapped in the Deep Creek Range with the underlying Trout Creek Group, also of Late Proterozoic age and similar in appearance. The Trout Creek Group is estimated at 11,600 ft thick (Hintze, 1988) and of higher metamorphic grade. Link et al. (1993) concluded that both of these sequences range in age from 780 to 560 Ma and that the upper part of the McCoy Creek Group may be correlative with the Johnnie Formation of southern Nevada, which is as much as 4,000 ft thick. In Lincoln County and at least in parts of White Pine County, the basal units of the overlying Prospect Mountain Quartzite are considered to be partly Proterozoic. The McCoy Creek and Trout Creek units are mapped in the geologic study area as Precambrian rocks (p€).

4.1.3 PALEOZOIC ROCKS

4.1.3.1 CAMBRIAN ROCKS

The Prospect Mountain Quartzite (Cambrian to Precambrian sedimentary rocks, €p€s) overlies the McCoy Creek Group in White Pine County. The Prospect Mountain consists of well-bedded, resistant quartzite and subordinate shale, commonly weakly metamorphosed. It has been generally considered to be Early Cambrian, although it is not well characterized by age or correlation from place to place, and at least in the southern part of the geologic study area is partly Late Proterozoic. In the study area, complete sections are uncommon, but the unit ranges from 3,000 to nearly 8,000 ft thick (Tschanz and Pampeyan, 1970). Thickness decreases southward to just a few hundred feet in the Mormon Mountains. The Prospect Mountain Quartzite in the southern half of the geologic study area is correlated with three units mapped in and west of the southern part of the geologic study area: the Stirling Quartzite (Late Proterozoic and Early Cambrian), the Wood Canyon Formation (Early Cambrian), and the Zabriskie Quartzite (Early Cambrian) (Stewart, 1970, 1974, and 1984; Rowley et al., 1994).

In the southern part of the geologic study area, the Stirling Quartzite is at least 2,000 ft thick and its base is not exposed. Link et al. (1993) considered the Stirling Quartzite to postdate the Late

Proterozoic McCoy Creek Group. In the Desert Range and above the Gass Peak thrust in the Las Vegas Range, the Wood Canyon Formation, a quartzite, is 1,000 to 3,000 ft thick.

Above the Prospect Mountain Quartzite are, from base to top, the Pioche Shale (Lower and Middle Cambrian, 200 to 1,000 ft thick), Lyndon Limestone (Middle Cambrian, 150 to 400 ft thick), and Chisholm Shale (Middle Cambrian, 100 to 300 ft thick). These three units are combined in many places with the Prospect Mountain Quartzite, as €p€s in White Pine County. These rocks are partly correlative with the Carrara Formation at the Nevada Test Site and in portions of Clark County.

Cambrian carbonate rocks range in thickness from about 7,500 ft just southwest of the geologic study area to almost 5,000 ft over most of the geologic study area. The map unit is shown as the middle part of Cambrian rocks, or €m. In the southern half of the geologic study area, the most widespread and best studied of the Cambrian carbonate rocks is the Highland Peak Formation, consisting of Middle and Late Cambrian, well-bedded limestone and dolomite about 4,500 ft thick (Tschanz and Pampeyan, 1970). To the west, as in the Groom mining district, it is 5,400 ft thick.

In the northern part of the geologic study area, the Cambrian carbonate rocks consist of many named units of generally similar lithology, total thickness, and age (Hose and Blake, 1976). Just to the northwest, these were originally named, from base to top, the Eldorado Dolomite, the Geddes Limestone, the Secret Canyon Shale, and the Hamburg Dolomite. In the Snake Range, these are, from base to top, the Pole Canyon Limestone, the Lincoln Peak Formation, and the Johns Wash Limestone. These latter names are now preferred in the northwestern part of the geologic study area and areas to the west. In the Cherry Creek Mountains of Nevada and in Utah, the units making up the entire sequence of Middle Cambrian carbonate rocks are, from base to top, the Dome Formation, Swasey Limestone, Wheeler Shale, Marjum Limestone, Weeks Limestone, Trippe Limestone, Wah Wah Summit Formation, Orr Formation, and others (Hose and Blake, 1976; Hintze and Davis, 2003). The overall Cm sequence is roughly equivalent to the Bonanza King Formation to the south (Longwell et al., 1965). See Figures 4-2 to 4-5 for geologic sections in different areas of the map.

Above the Middle Cambrian carbonate section in Nevada is an Upper Cambrian to Lower Ordovician(?) sequence that includes a lower unit, the Dunderberg Shale, and an unnamed upper unit of limestone and dolomite (Tschanz and Pampeyan, 1970). The rocks are mapped as an upper part of the Cambrian section (€u); in some cross sections, the map unit is combined with €m as Cambrian carbonate rocks, undivided (€c). In White Pine County and in Utah, the €u limestone unit has been variously referred to as the Windfall Formation, Orr Formation, Notch Peak Limestone, and Whipple Cave Formation. In the southern part of the geologic study area, the €u limestone unit is the Nopah Limestone. See Figures 4-2 to 4-5 for geologic sections. The Dunderberg Shale generally is about 300 ft thick over most of the geologic study area, but it is as much as 1,400 ft thick in the southern Ruby Mountains (Hose and Blake, 1976). The overlying limestone ranges in thickness from 400 to 4,000 ft, generally being thickest on the western side of the geologic study area (Tschanz and Pampeyan, 1970).

4.1.3.2 ORDOVICIAN TO DEVONIAN ROCKS

The Ordovician to Silurian parts of the rock column in the geologic study area are shown as a lower unit (Middle and Lower Ordovician, symbol Ol) and an upper unit (Silurian and Upper Ordovician, symbol SOu). The lower unit in the area consists in ascending order of the Pogonip Group and the

Eureka Quartzite. The Pogonip Group consists of interbedded thick-bedded limestone, sandy to silty limestone, conglomerate, and shale, generally about 2,000 to 3,500 ft thick in the geologic study area. The Eureka Quartzite is a distinctive white, resistant, brittle, vitreous, fine- to medium-grained quartzite that thins southward from 600 to 800 ft thick in the Confusion Range to 200 ft in southern Lincoln County (Hose and Blake, 1976; Tschanz and Pampeyan, 1970). The Eureka unit is a major marker bed throughout most of the geologic study area (Plates 1 and 2). Just northwest of the geologic study area, the lower unit includes the Vinini and Valmy formations.

The upper unit (SOu) generally consists in ascending order of the Hansen Creek Formation, Ely Springs Dolomite, Fish Haven Dolomite, and Laketown Dolomite. The Ely Springs Dolomite is mostly a poorly resistant, gray to dark-gray carbonate unit that occurs over most of the area of Plate 1 in Lincoln County (Tschanz and Pampeyan, 1970). The Ely Springs Dolomite in Lincoln County overlaps into northern Nye and Eureka counties, where it is locally called the Hansen Creek Formation, a dark dolomite and/or limestone unit that thins southward from 500 to 100 ft (Tschanz and Pampeyan, 1970; Kleinhampl and Ziony, 1985). In White Pine County, the Ely Springs Dolomite is called the Fish Haven Dolomite and ranges between 200 and 850 ft thick. The Silurian Laketown Dolomite is lithologically similar to the Ely Springs Dolomite and Fish Haven Dolomite and ranges between 600 and 1,850 ft thick.

In Eureka and Nye counties, the Laketown Dolomite is underlain by, and partly equivalent in age to, the Lone Mountain Formation, a unit with limestone and dolomite that is not present farther east in Lincoln and White Pine counties (Kleinhampl and Ziony, 1985). In Nye County, these units, particularly the Lone Mountain Formation, overlie and interfinger with the Roberts Mountain Formation. The Roberts Mountain is gradational to western facies deep-water sediments and is comprised of shaly limestone, dolomite, and shale with a thickness of 500 to 1,900 ft (Kleinhampl and Ziony, 1985). See Figures 4-2 to 4-5 for geologic sections in different areas of the map.

Devonian carbonate rocks over most of the geologic study area consist of, in ascending order, the Sevy Dolomite, Simonson Dolomite, and Guilmette Formation. Where combined, they are mapped as Devonian rocks, undivided (Du). In the southern part of the geologic study area, this map unit includes the Muddy Peak Limestone (Upper and Middle [?] Devonian). In most places, however, the three formations are mapped as the Simonson and Sevy Dolomites (Ds) and Guilmette Formation (Dg). The Sevy Dolomite is a resistant, gray dolomite, commonly argillaceous and with a sandstone unit near the top. This dolomite increases in thickness southward across the geologic study area from about 450 ft in the Snake Range to 1,300 ft in the Limestone Hills and southward (Tschanz and Pampeyan, 1970). This thickness decreases south of the Pahranagat Range, and the unit disappears south of the Delamar Mountains. The Simonson Dolomite is resistant, dark- and light-gray dolomite about 900 to 1,200 ft thick over most of the geologic study area, but it thins to less than 700 ft in the southeastern part of the map area, continuing to decrease in thickness farther south. The Simonson Dolomite is about 500 ft thick in the Snake Range (Tschanz and Pampeyan, 1970), although both the Simonson and Sevy dolomites may be reduced in thickness by faulting.

The Guilmette Formation (Dg) is a mostly resistant, fossiliferous limestone and dolomite, with biostromes and bioherms, and commonly sandy with minor sandstone layers. The unit ranges in thickness from about 1,050 to 3,500 ft and appears to decrease in thickness in all directions from its thickest occurrences in north-central Lincoln County (Tschanz and Pampeyan, 1970; Hose and Blake, 1976). In Clark County, the Guilmette map unit includes the Sultan Limestone, which is made up of

a lower dolomite unit and an upper limestone unit with a thickness of 1,800 ft (Longwell et al., 1965). The Sultan Limestone is equivalent to the Muddy Peak Limestone in the Muddy Mountains.

In Eureka County and northern Nye County, the rocks of the Sevy, Simonson, and lower Guilmette units are called the Nevada Formation (Dn), which is about 2,500 ft thick. This map unit locally includes the Cockalorum Wash Formation. In Eureka and northern Nye counties, the upper Guilmette Formation is called the Devils Gate Limestone (Dd), which is about 2,000 ft thick (Roberts et al., 1967; Hose and Blake, 1976; Kleinhampl and Ziony, 1985).

4.1.3.3 MISSISSIPPIAN TO LOWER PERMIAN ROCKS

In White Pine County, a distinctive sequence of rocks consists, in ascending order, of the Pilot Shale, Joana Limestone, Chainman Shale (Mc), and Diamond Peak Formation (Md). In Lincoln County, only the Pilot Shale is recognized (Tschanz and Pampeyan, 1970). These map units represent products of the Antler deformation, which took place in Late Devonian to Late Mississippian time and resulted in the Antler Highland located along the western side and northwest of the geologic study area. The basin of deposition of these units was to the east of the highland (Poole and Sandberg, 1977 and 1991; Larson and Langenheim, 1979, Figures 7 and 8). Where these four units are thin, they are categorized on the map as Mississippian to Devonian rocks (MDd). But in most places, Chainman Shale and Diamond Peak Formation are mapped separately and Pilot Shale and Joana Limestone are combined as unit MD. The Pilot Shale, Late Devonian to Early Mississippian, is mostly a poorly resistant, gray, thin-bedded dolomitic siltstone and limestone containing little shale. This unit is generally from 100 to 400 ft thick, but locally, in northern White Pine County and western Utah, it is 500 to 900 ft thick (Hose and Blake, 1976; Tschanz and Pampeyan, 1970; Hintze and Davis, 2002a and b). The Joana Limestone (Lower Mississippian) is a mostly resistant, bluish-gray limestone about 100 to 1,000 ft thick.

The Monte Cristo Group of southern Nevada, which is Upper and Lower Mississippian, is considered equivalent to the Joana Limestone. The Monte Cristo Group overlies the Sultan Limestone. The Monte Cristo is a dark-gray to light-gray limestone containing abundant chert and is about 750 ft thick. In the Muddy Mountains, the Mississippian Rogers Spring Limestone has a similar lithology and is considered to be equivalent in age to the Monte Cristo (Longwell et al., 1965). The general equivalent of the Chainman Shale southwest of the geologic study area is the Eleana Formation (Mississippian and Upper Devonian), which is several thousand feet thick (Workman et al., 2003). In mapping, the Monte Cristo, Rogers Spring, and Eleana are included with the MD map unit. The map unit also includes local units Mercury Limestone and Bristol Pass Limestone (both mostly in White Pine County), Webb Formation (Elko County), Ochre Mountain Limestone (Utah), and West Range Limestone (Upper Devonian) in northern Lincoln County, Nevada.

The Upper Mississippian Chainman Shale is a soft, black, impermeable shale that is between 200 and 2,000 ft thick. This unit is mapped as unit Mc over the northern part of the geologic study area, but the Chainman is thin in the southern part of the geologic study area and here is included within a sequence of more permeable carbonate rocks. It is a regional confining unit (called the "upper aquitard") separating the lower carbonate aquifer from the upper carbonate aquifer over all except the southern part of the geologic study area. Paleotopography during deposition and post-depositional erosion resulted in substantial variations in Chainman thickness. The unit was mapped (Hintze and Davis, 2002b) in the Confusion Range as having thicknesses greater than 2,000 ft. A similar

thickness is reported from an oil-well log in Lake Valley (Hess, 2004). Although these two locations are distal from the source area, they represent localized depositional basins.

In the northwestern part of the geologic study area, the Upper Mississippian Diamond Peak Formation is mapped as unit Md above the Chainman Shale. The Diamond Peak Formation is a poorly resistant, gray siltstone, claystone, sandstone, and conglomerate that ranges in thickness from 600 to 2,500 ft (Hose and Blake, 1976; Kleinhampl and Ziony, 1985). The unit thins and pinches out eastward in north-central White Pine County. The Diamond Peak Formation is derived from erosion of the Antler Highland and generally included in the upper aquitard with Chainman. The Diamond Peak is generally equivalent to the Scotty Wash Quartzite in the southern part of the geologic study area. The Scotty Wash Quartzite is made up of interbedded sandstone, shale, and local limestone of limited extent. The Scotty Wash is included with the Md map unit.

Much of the geologic study area is underlain by the Ely Limestone, which is mostly Pennsylvanian but includes Mississippian rocks at its base and Permian rocks at its top. The Ely Limestone is mapped as Pennsylvanian rocks (IP). In the Utah part of the geologic study area, the Ely Limestone is 1,850 to 2,000 ft thick (Hintze and Davis, 2002a and b). The map unit is called the Wildcat Peak Formation in the northwestern part of the geologic study area and the Callville Limestone in the southern and eastern part of the geologic study area. The Ely Limestone is overlain by a Lower Permian limestone of similar lithology in northern White Pine County (Hose and Blake, 1976). All units are resistant, gray limestone sequences that collectively range in thickness from 1,900 to 3,000 ft thick. The overlying Lower Permian limestone is called the Riepe Spring Limestone. Where both Ely and Riepe Spring are mapped together in the northern part of the geologic study area, they are shown as Permian and Pennsylvanian rocks, undivided (PIP). The rocks in the PIP unit are unnamed in Lincoln County and range from 3,500 to more than 5,000 ft thick (Tschanz and Pampeyan, 1970). The Ely and Riepe Spring Limestones are overlain by, and partly equivalent to, the Carbon Ridge Formation, a Lower Permian, nonresistant, thin-bedded limestone and shale that is 1,400 to 2,300 ft thick. The Carbon Ridge is locally mapped separately in the northwestern part of the geologic study area as Pc, or where thinner is included within the PIP map unit.

The Bird Spring Formation is an Upper Mississippian to Lower Permian limestone in the southern part of the geologic study area that is roughly equivalent in age to the combined Ely Limestone, Riepe Spring Limestone, and Carbon Ridge Formation of White Pine County (Longwell et al., 1965; Tschanz and Pampeyan, 1970). The Bird Spring is a sequence of limestone beds with sandstone and dolomitic limestone layers. The formation is as much as 8,000 ft thick in the Spring Mountains and Las Vegas Range (Page et al., 2005b) and at least 5,400 ft thick in the Meadow Valley Mountains (Pampeyan, 1993). The Bird Spring is included in the PIP map unit, as is the Brock Canyon Formation in the northwestern part of the geologic study area and the Oquirrh Group (Lower Permian and Pennsylvanian) in the northeastern part of the geologic study area.

The Lower Permian Rib Hill Sandstone (Pr) overlies the Carbon Ridge Formation in the northwestern part of the geologic study area (Hose and Blake, 1976). The Rib Hill is a nonresistant sandstone and dolomite 500 to 1,400 ft thick. In northern White Pine County and adjacent parts of Utah, the Lower Permian Arcturus Formation (Pa) is named for a sequence of poorly resistant, gray limestone, sandstone, and siltstone that is 2,700 to 3,400 ft thick (Hose and Blake, 1976). In the northwestern part of the geologic study area, the Arcturus Formation overlies the Rib Hill Sandstone. Where the two are combined in the mapping, they are shown as unit Par. In Elko County, this map unit includes

the Pequop Formation. In the southern part of the geologic study area, this same Par map unit includes a redbed sequence, and in the southeastern part of the map, the map unit includes the Queantoweap Sandstone.

4.1.3.4 PARK CITY GROUP

The Park City Group (Pp) is a distinctive, resistant, light-gray Lower Permian limestone and dolomite sequence that is exposed only locally. The scattered nature of the outcrops suggests that the unit was originally fairly extensive in the geologic study area but has been partly removed by erosion over most its original extent. In White Pine County and adjacent western Utah, the group is made up, from base to top, of the Kaibab Limestone, Plympton Formation, and Gerster Limestone. The Kaibab Limestone is 50 to 600 ft thick, the Plympton is 700 to 900 ft thick, and the Gerster is as thick as 1,100 ft (Hose and Blake, 1976). These rocks are not found in Eureka or Nye counties.

In Lincoln County and east of the geologic study area in Utah, the east platform part of the sequence consists of the Toroweap Formation, the Kaibab Limestone, and locally the Plympton Formation (Tschanz and Pampeyan, 1970). In Lincoln County, these units have a combined thickness of between 250 and 450 ft. The Toroweap is a cherty, thin-bedded, shaly limestone, and the Kaibab limestone is a cherty, sandy, light-gray limestone. The Kaibab Limestone and Toroweap Formation in Clark County have a maximum combined thickness of 1,300 ft in the Muddy Mountains (Bohannon, 1983). In Clark County, their lithology is dominated by cherty limestone, sandstone, and red shale, with local gypsum beds (Bohannon, 1983; Page et al., 2005b).

4.1.4 MESOZOIC ROCKS

Mesozoic rocks were deposited locally or have been largely removed by erosion in the geologic study area. However, they are exposed in some ranges and are widespread east and south of the map area. Most of these rocks are continental clastic rocks deposited in fluvial, lacustrine, eolian, and marginal marine environments. The Thaynes Formation (Lower Triassic) is a soft, gray, thin-bedded claystone and limestone that is locally about 1,900 ft thick in western Utah in the northeastern part of the geologic study area (Hintze and Davis, 2002b). The overlying Moenkopi Formation (Lower Triassic) is a mostly soft, red and gray, thin-bedded siltstone, limestone, sandstone, and shale, commonly gypsiferous, and locally about 2,000 ft thick in western Utah. The Thaynes and Moenkopi Formations are thin in the Nevada portion of Plate 1 and are not separated on this map. In Clark County, however, the Moenkopi Formation is about 2,000 ft thick and of similar lithology, with gypsum beds in the upper part of the formation (Page et al., 2005b).

The Upper Triassic Chinle Formation includes a basal unit, the Shinarump Conglomerate Member, which is a resistant gray sandstone and conglomerate that ranges from 10 to 250 ft thick. The balance of the formation is of soft, variegated mudstone and siltstone that is widely exposed above the Moenkopi in the southern part of the geologic study area (Bohannon, 1983; Page et al., 2005b). This mudstone and siltstone have been measured to be about 1,000 to 3,300 ft thick within the geologic study area. The Luning Formation (Upper Triassic) is locally exposed northwest of the area. All Triassic rocks in the geologic study area have been combined as Triassic sedimentary rocks (Ŧs).

Jurassic sedimentary rocks (Js) are exposed in the southern part of the geologic study area. These rocks are dominated by the Lower Jurassic Aztec Sandstone, a brick-red, buff, and light-gray, fine- to

medium-grained eolian sandstone containing large-scale cross beds. The Aztec is 600 to 3,600 ft thick. The equivalent Navajo Sandstone is about 2,000 ft thick in the southeastern part of the geologic study area. It is here underlain by the Moenave (lower) and Kayenta (upper) Formations, both of Early Jurassic age and mostly made up of fine-grained sandstone and siltstone of eolian and fluvial origin, with a combined thickness of 500 to 3,000 ft. The Navajo is here overlain by the Temple Cap (lower) and Carmel (upper) Formations, both of Middle Jurassic age and made up of sandstone, limestone, siltstone, and shale of mostly marginal marine origin and with a combined thickness of about 900 ft. The map unit also includes the Dunlap Formation (Lower Jurassic) in the northwestern part of the geologic study area.

Cretaceous synorogenic sedimentary rocks (Ks) are present but uncommon in the geologic study area. Most of this area was a highland undergoing erosion at that time. The Lower Cretaceous Newark Canyon Formation is exposed in the northwestern part of the geologic study area as a poorly exposed, reddish-brown to gray, fresh-water limestone, siltstone, conglomerate, and sandstone from 1,400 to 1,800 ft thick (Hose and Blake, 1976). Upper Cretaceous sedimentary rocks, shed east from erosion of Sevier highlands in and north of the geologic study area, are thin and patchy in the map area but extensive and thick east and south of the area. Upper Cretaceous through Paleocene fault breccias, primarily from thrust faults related to Sevier deformation, are locally exposed in the geologic study area.

In Clark County, Cretaceous sedimentary units include from oldest to youngest the Willow Tank Formation (Lower Cretaceous) and the Baseline Sandstone. The Willow Tank Formation is 300 to 450 ft thick and consists of a basal conglomerate and overlying fine-grained sediments, including bentonitic clay, and is primarily restricted to the Muddy Mountains. The Baseline Sandstone consists of about 3,000 to 5,000 ft of gray and red, well-bedded sandstone and conglomerate. In the southeastern (Utah) part of the geologic study area, the Upper Cretaceous Cedar Mountain Formation and overlying Iron Springs Formation consist of mudstone, shale, sandstone, and conglomerate about 3,000 ft thick.

Plutonic rocks related to the Middle Jurassic through Paleocene Sevier deformational event are exposed locally throughout the geologic study area (Maldonado et al., 1988). Of these, Jurassic quartz monzonite and diabase have been identified in the House Range and in the Burbank Hills, respectively, both in Utah near the eastern edge of the geologic study area (Hintze and Davis, 2002a and b, and 2003). Other plutons of quartz monzonite to granodiorite, mostly of Middle Jurassic age, form a north-trending belt along the eastern edge of White Pine County, Nevada, extending from the southern Snake Range to the Clifton Hills of western Utah. A north-trending plutonic belt of Cretaceous age is exposed in eastern White Pine County, Nevada, extending into the Deep Creek Range of western Utah and including the main mass of the large Kern Mountains granite pluton of apparent Cretaceous and Eocene age (Best et al., 1974; Miller et al., 1999). An east-trending string of small Lower Cretaceous plutons extends from Eureka through Ely, Nevada.

4.1.5 CENOZOIC ROCKS

Cenozoic rocks in the geologic study area belong to three main sequences: (1) locally exposed, mostly thin, older continental sedimentary rocks; (2) generally voluminous, calc-alkaline volcanic rocks and their source plutons; and (3) rocks that formed during regional basin-range extension, namely thin bimodal-composition (basalt and high-silica rhyolite) lava flows and locally thick

basin-fill sediments. On the geologic maps, most of these rocks are separated into several rock types based on age, following the mapping strategy of Ekren et al. (1977). The basalts and basin-fill sedimentary rocks, including surficial sediments, of the youngest of the three main sequences, however, are mapped respectively as Quaternary to Late Tertiary basaltic rocks (QTb) and Quaternary to late Tertiary alluvium (QTa).

4.1.5.1 UPPER CRETACEOUS(?) TO MIOCENE SEDIMENTARY ROCKS

The oldest Cenozoic sedimentary rocks (Ts1) are thin and poorly exposed in the geologic study area but are more common in eastern Clark County and southwestern Utah. These units were unconformably deposited on rocks deposited and deformed during the Sevier orogeny. In eastern Nevada, the principal Ts1 unit is the Sheep Pass Formation of Eocene to Oligocene age (Hose and Blake, 1976). The Sheep Pass Formation occupies a basin about 15,000 mi^2 in size over an area extending south from Ely and Eureka, Nevada, to Penoyer and northern Pahranagat valleys (Fouch et al., 1991). The unit is mostly nonresistant, gray conglomerate, sandstone, mudstone, and limestone, with a thickness of 600 to 3,000 ft in the geologic study area.

In the southeastern part of the geologic study area, the mostly resistant Grapevine Wash Formation and overlying Claron Formation are included within the Ts1 map unit. The Grapevine Wash Formation, poorly constrained in age as Late Cretaceous(?) to early Tertiary but considered by Hintze et al. (1994) to postdate Sevier deformation, consists of as much as 2,000 ft of gray, tan, and red conglomerate and sandstone. The Claron Formation, also poorly constrained in age but likely of a restricted age ranging between Paleocene and Oligocene, is sandstone, limestone, and conglomerate as much as 2,000 ft thick.

Similar sedimentary rocks (Ts2, Ts3, and Ts4) of various names and ages, from Oligocene to Miocene, are exposed in the geologic study area. These include the Gilmore Gulch Formation of about 30 Ma (Ts2), exposed in the northwestern part of the area. The Horse Spring Formation, about 12 to 20 Ma, and the red sandstone unit, 11 to 12 Ma, that overlies it are mapped as Ts4 in the southern part of the geologic study area (Bohannon, 1983 and 1984). The Horse Spring Formation consists of conglomerate, sandstone, siltstone, claystone, limestone, dolomite, tuff, and gypsum as much as 10,000 ft thick.

4.1.5.2 TERTIARY VOLCANIC ROCKS

Volcanic rocks make up the primary Cenozoic rock type in the geologic study area. The older (Eocene to middle Miocene) sequence of calc-alkaline rocks consists of andesite to low-silica rhyolite that are mapped as different units separated by rock type and age. Tertiary plutonic rocks, which are the sources for the volcanic rocks, are mapped as unit Ti whether of calc-alkaline or bimodal origin.

The calc-alkaline sequence is made up largely of regional ash-flow tuff sheets derived from widely scattered calderas. The oldest tuffs are mapped as Tt1 (Eocene and Oligocene) that predate the Needles Range Group (about 32 Ma). The next younger group of tuffs, consisting mostly of the Needles Range Group, is mapped as Tt2 (Oligocene), from about 32 Ma to 27 Ma, the latter the age of the Isom Formation. The next younger tuffs are mapped as Tt3 (Oligocene and Miocene), ranging in age from that of the Shingle Pass Tuff (about 27 Ma) to the youngest calc-alkaline tuffs (about 18 Ma). Individual calderas are filled with thick intracaldera ash-flow tuffs that are at least several

thousand feet thick. Their outflow sheets are generally thin, generally less than 1,000 ft, but the aggregate thickness of all of these tuffs is considerable in most places.

The outflow tuffs are interspersed with locally distributed but thick central stratovolcano deposits made up of lava flows and volcanic mudflow breccia generally deposited above their source plutons. Where these calc-alkaline flows and breccia are largely andesite, they are mapped as Ta1, Ta2, Ta3, and Ta4 based on ages that correspond to those of the ash-flow tuffs. Unit Ta4 is made up of andesitic (calc-alkaline) flows of post-18 Ma that are exposed in the southern part of the geologic study area. Where calc-alkaline flows and breccia are largely low-silica rhyolite, they are mapped as Tr1, Tr2, and Tr3 based on ages that correspond to those of the tuffs.

The tectonic environment during calc-alkaline magmatism was generally one of east-west extension in the Great Basin. The direction of principal maximum compressive stress was generally north-south, creating an environment of strike-slip and oblique-slip faults. The orientation and size of mountains during this time are poorly known, but the outpouring of large volumes of volcanic ash-flow tuff probably resulted in a subdued landscape with topographic variations caused by the uneven distribution of these units.

In the Great Basin, vents—notably calderas—for Tertiary calc-alkaline volcanic rocks occur in generally east-west igneous belts that become younger from north to south (Ekren et al., 1976 and 1977; Stewart and Carlson, 1976; Stewart et al., 1977; Rowley, 1998; Rowley and Dixon, 2001). These igneous belts are partly controlled by transverse zones of faulting and underlain by batholiths whose cupolas provide the main vent areas for the volcanic rocks. The oldest volcanic rocks in the map area belong to the Ely-Tintic igneous belt (belt names from Rowley [1998]) in the northern part of the geologic study area. The ages of vents in this belt are about 38 Ma and locally older (Eocene) along the northern margin of the area, and 36 Ma farther south (Rowley, 1998). An east-west gap in vent areas, about 30 to 60 mi wide, occurs south of Ely and Preston, Nevada, although a volcanic plain of thin outflow tuffs underlies the gap. To the south, the Pioche-Marysvale igneous belt crosses near Pioche, Nevada. The volcanic centers here are about 32 to 31 Ma on the northern side of the belt and about 28 to 27 Ma along the southern part. About 12 mi south of the Pioche-Marysvale belt is the Delamar-Iron Springs igneous belt, of about 24 Ma along its northern side and 16 Ma along its southern side. Its southern edge is just south of the latitude of Pahranagat Valley, Nevada.

In the Ely-Tintic igneous belt, the most voluminous volcanic unit is the Kalamazoo Tuff (35 Ma), an ash-flow tuff sequence deposited over an east-west elongated area 90-mi-long and 25 mi wide. Its caldera has not been found but may underlie the Red Hills or adjacent northern Spring Valley (Gans et al., 1989) near the center of deposition. Other ash-flow tuffs and lava flows underlie and overlie the Kalamazoo Tuff, and the overall thickness of the volcanic rocks in the igneous belt is about 500 to 1,500 ft. Plutons of a 45 to 30 Ma age range are scattered throughout the belt; most of these represent source areas of volcanic rocks that have since been removed by erosion. One of these plutons, roughly 45 to 30 Ma in age (Best et al., 1974), is at the eastern end of the composite-age Kern Mountains pluton.

In the Pioche-Marysvale belt, volcanic rocks are thicker and more widespread than in the Ely-Tintic belt because calderas are more abundant and larger and the volcanic rocks are somewhat younger and thus less eroded. Most volcanic rocks are regional ash-flow tuffs from calderas, but lava flows and mudflow breccia erupted from volcanoes in and along the margins of calderas or from isolated

volcanoes such as the Seaman Range volcanic center. The largest vent area in the belt is the Indian Peak caldera complex (Best et al., 1989a) in the southeastern part of the geologic study area. It erupted ash-flow tuffs and related rocks of the Needles Range Group (Oligocene, about 32 to 28 Ma) and the Isom Formation (27 to 26 Ma). This may be the largest caldera complex in the world; ash-flow tuffs from this complex are spread over an area of about 200 mi east-west by 150 mi north-south.

A cluster of smaller calderas west of the Indian Peak caldera complex also belongs to the Pioche-Marysvale igneous belt. These calderas produced, from oldest to youngest and generally from north to south, regional ash-flow tuffs known as the Stone Cabin Formation (35.3 Ma), Pancake Summit Tuff (34.8 Ma), Windous Butte Formation (31.3 Ma), tuff of Hot Creek Canyon (29.7 Ma), Monotony Tuff (27.3 Ma), tuff of Orange Lichen Creek (26.8 Ma), Shingle Pass Tuff (26.7 to 26 Ma), tuff of Lunar Cuesta (25.4 Ma), tuff of Goblin Knobs (25.4 Ma), tuff of Big Ten Peak (25 Ma), Pahranagat Tuff (22.6 Ma), and Fraction Tuff (18.3 Ma) (Best et al., 1989b and 1993). Most of this cluster of calderas was referred to as the "central Nevada caldera complex" (Best et al., 1993; Scott et al., 1995). However, the feature is not a classic caldera complex because all of it has not subsided following tuff eruptions, but instead individual calderas (subsided areas) are locally separated by pre-caldera Phanerozoic sedimentary rocks that are currently exposed outside the margins of individual calderas. Within calderas in the geologic study area, intracaldera ash-flow tuffs and subordinate lava flows and mudflow breccia are several thousand feet thick and are underlain by intracaldera source plutons. Outside the calderas, the thickness of volcanic rocks in the belt in the area is about 1,500 to 3,000 ft, but locally more. A few plutons of the same age range, likely representing sources for volcanic rocks that have been removed by erosion, occur in the Grant Range and many other parts of the geologic study area.

In the Delamar-Iron Springs igneous belt, at the southern edge of the geologic study area, the largest igneous centers are the Caliente and Kane Springs Wash caldera complexes. The Caliente caldera complex erupted ash-flow tuffs that spread over an area about 150 mi east-west by 100 mi north-south. It had an unusually long history of activity, at least 10 Ma. The regional ash-flow tuffs derived from it include the Swett (23.7 Ma) and Bauers (22.8 Ma) Tuff Members of the Condor Canyon Formation, Racer Canyon Tuff (18.7 Ma), Hiko Tuff (18.3 Ma), tuff of Tepee Rocks (17.8 Ma), tuff of Dow Mountain (17.4 Ma), tuff of Acklin Canyon (17.1 Ma), tuff of Rainbow Canyon (15.6 Ma), tuff of Etna (14.0 Ma), Ox Valley Tuff (13.5 Ma), and probably the Leach Canyon Formation (23.8 Ma) (Rowley et al., 1995; Scott and Swadley, 1995; Snee and Rowley, 2000). The Kane Springs Wash caldera complex, just to the south, erupted the tuff of Narrow Canyon (15.8 Ma), tuff of Boulder Canyon (15.1 Ma), and Kane Wash Tuff (14.7 to 14.4 Ma) (Scott et al., 1995 and 1996; Scott and Swadley, 1995). The total thickness of volcanic rocks in the igneous belt generally does not exceed 1,000 ft outside the caldera complexes.

The bimodal sequence is made up of small basalt lava flows and cinder cones as well as small high-silica rhyolite volcanic domes, lava flows, ash-flow tuffs, and airfall tuffs. The basalts are categorized on the geologic map as unit QTb, rhyolite domes and flows as Tr4, and tuffs as Tt4. All the volcanic rocks derived from the Kane Springs Wash caldera complex, and those that postdate the tuff of Tepee Rocks from the Caliente caldera complex, are included within the bimodal assemblage. The tectonic environment during bimodal magmatism was east-west extension, with the direction of principal maximum compressive stress generally oriented vertically, creating an environment of north-south normal faults. Bimodal magmatism coincided with basin-range deformation, in which

the present topography was created and previous tectonic features and topography were deformed and obscured.

4.1.5.3 MIOCENE TO HOLOCENE SEDIMENTS

With the start of basin-range deformation at about 20 Ma, north-striking normal faults created the present ranges and basins. Erosion of the ranges, as they were faulted up, resulted in basin-fill sediments that accumulated to thicknesses of locally more than 10,000 ft in down-faulted basins. In most places, the basin-fill sediments are unnamed. These units are referred to as Holocene through middle Miocene alluvium (QTa) and are considered to be aquifers, especially where fractured by faulting.

The bimodal volcanic rocks that were deposited at the same time were either high-silica rhyolite lava flows and tuffs or basalt lava flows and tuffs. Their distribution in the geologic study area is spotty and their thickness is rarely more than several hundred feet, except for their source volcanic domes or cinder cones. Where thin, they may be combined in the cross sections with the older, much thicker calc-alkaline volcanic rocks or with thick interbedded basin-fill sediments.

The basin-fill sediments (QTa) were largely deposited by streams in closed basins. In general, coarse-grained materials accumulated around the edges of the mountain fronts, whereas finer materials accumulated toward the center of the basins. In some basin interiors, fine-grained sediments accumulated in ephemeral playa lakes. The largest playa lakes are Plio-Pleistocene in age, including the latest Pleistocene Bonneville and Lahontan lakes that had water depths of as much as 1,000 ft, resulting in deposition of clay and saline sediments in many basins (Mifflin and Wheat, 1979). These lakes, however, were short lived and produced fine-grained materials that rarely exceeded a few tens of feet in thickness. Because of the vagaries of the sizes of storms, of climate changes, of integration of some basins, and of timing of the deformation of basin-bounding versus within-basin faults, the stratigraphy of basin-fill sediments is characterized by a complex intertonguing of beds of all lithologies. Within-basin faults commonly produced horsts (hills) of soft basin-range sediments that were then eroded away by streams and redeposited as younger basin-fill sediments. As with the older basin-fill sediments, Quaternary deposits are dominated by stream alluvium but also include the deposits from landslides, playas, and springs that are not individually separated in this report or on the maps due to their limited extent.

In some places the basin-fill sediments have local names that were categorized as QTa on the geologic map. One such local unit is the Muddy Creek Formation of 5 to 11 Ma in southern Lincoln and Clark counties. The Muddy Creek consists of locally gypsiferous sandstone, siltstone, conglomerate, and limestone. Another named unit is the Panaca Formation, about 2 to 10 Ma and located in the central part of the geologic study area (Rowley and Shroba, 1991). Others are the Horse Camp Formation in the northwestern part of the area (Brown and Schmitt, 1991) and the Salt Lake Formation northeast of the area. All these units are generally more than 1,000 ft thick and locally as much as 10,000 ft thick.

4.2 HYDROGEOLOGIC UNITS

HGUs are rock units grouped so that they are more useful for hydrogeologic studies. They provide a bridge between geologic units and groundwater modeling units. As such, they are used to construct groundwater flow models, that is, to approximate spatially complex geology with groupings that can

be readily simulated with mathematical modeling techniques. HGUs, as given on Plates 6 and 7 and listed in Table 4-1, are a set of geologic formations that are grouped based on physical properties of the units. The geologic units (Plate 3) that make up each HGU are listed below under the discussion of HGUs. This grouping reflects lithologic properties rather than more traditional geologic groups based on genetic sequences.

TABLE 4-1
BRIEF SUMMARY OF HYDROGEOLOGIC UNITS

QTs	Quaternary and Tertiary sediments - Includes sediments younger than the volcanic section but may include older sediments where volcanic rocks are minor or nonexistent. Also includes playa deposits. Generally moderate permeability but may be high where fractured.
QTb	Quaternary and Tertiary basalt - Quaternary and late Tertiary mafic volcanic rocks. Generally permeable but not hydrologically significant regionally because mostly thin.
Tv	Tertiary volcanic rocks - Miocene to Eocene volcanic rocks. Good to moderate permeability, commonly a significant aquifer.
Tos	Older Tertiary sediments - Primarily created for the cross sections; includes the older Tertiary alluvial and lacustrine section below the volcanic section. Of moderate permeability where fractured.
TJi	Tertiary to Jurassic intrusive rocks - Includes all plutons. Generally impermeable except where fractured.
KTs	Cretaceous to Triassic siliciclastic rocks - Thicker where near the Colorado Plateau and generally of low permeability. More abundant in the southern part of the geologic study area. A confining unit of limited extent.
PPc	Permian and Pennsylvanian carbonate rocks - Includes Ely Limestone, Bird Spring Formation, Park City Group, and other units. May include thin Triassic carbonate rocks in the Butte Mountains. Also includes Permian red beds, undifferentiated. A highly permeable aquifer.
Ms	Mississippian siliciclastic rocks - Includes Chainman Shale, Scotty Wash Quartzite, Diamond Peak Formation, and Eleana Formation. The Chainman Shale and Scotty Wash Quartzite are not differentiated in Lincoln County, except in the Egan and Schell Creek Ranges. Where mapped, is a confining unit of low permeability.
MOc	Mississippian to Ordovician carbonate rocks - Joana Limestone (Monte Cristo Formation) to Pogonip Group, also includes thin Chainman Shale in most of Lincoln and Clark counties. The Pilot Shale, Eureka Quartzite, Guilmette Formation, Simonson Dolomite, Sevy Dolomite, and Laketown Dolomite are also included. A highly permeable aquifer.
€c	Cambrian carbonate rocks - Includes the Bonanza King, Highland Peak, Lincoln Peak, and Pole Canyon formations. A highly permeable aquifer.
€p€s	Cambrian and Precambrian siliciclastic rocks - Includes the Wood Canyon Formation, Prospect Mountain and Stirling quartzites, Chisholm Shale, Lyndon Limestone, and Pioche Shale. Generally impermeable except where fractured.
p€m	Precambrian metamorphic rocks - Precambrian X, Y, and Z high-grade metamorphic rocks, generally Early Proterozoic. It also includes the Johnnie Formation in the south and the McCoy Creek and Trout Creek groups in the Schell Creek, Deep Creek, and Snake ranges. Impermeable except where fractured.

HGUs must be distinguished from hydrostratigraphic units (Maxey, 1964; Seaber, 1992; Donovan, 1996), which are based on the material properties of porosity and permeability. Hydrostratigraphic units are independent of age, formation boundaries, and saturation, yet they follow stratigraphic procedures and principles.

HGUs, as opposed to hydrostratigraphic units, reflect geologic history, conform to informal and formal formation boundaries, and define many of the large-scale differences and spatial distributions

of porosity and permeability. HGUs largely define units that could be called regional aquifers and confining units (aquitards) and would be of Group or Supergroup rank in formal stratigraphic terminology because they contain many units of formation rank. These formal distinctions are not critical in the context of this report because the units are informal and conform to geologic unit boundaries, but this discussion should give the reader a sense of the purpose, scale, and general approach used to develop the units and the challenges in developing traditional geologic correlations. The geologic and hydrogeologic maps and cross sections were developed concurrently in preparation of this report.

4.2.1 Precambrian Metamorphic Rocks

Precambrian rock units (p€m) consist primarily of moderately to intensely metamorphosed Precambrian "basement" rocks, forming the most significant aquitard in the geologic study area. The largest exposure in the area of Plate 6 is on the eastern side of the Schell Creek Range, north of U.S. Highway 50 and on the western side of the Snake Range, north and south of U.S. Highway 50. This unit includes the Proterozoic rock units up through the McCoy Group. The permeability of the unit is low, except in areas where fractured or weathered. Additional Precambrian basement rocks are on Plate 7 in the southern part of the geologic study area in the Mormon Mountains, the Desert Range, and the Black Mountains at Lake Mead. These rocks include Precambrian metamorphic and crystalline rocks, the McCoy Creek Group, Trout Creek Group, and the Johnnie Formation. On the geologic maps and cross sections (Plates 1 and 2), map unit has the symbol p€.

4.2.2 Cambrian to Precambrian Siliciclastic Rocks

The Cambrian to Precambrian clastic rock unit (€p€s) is non-metamorphosed to moderately metamorphosed siliciclastic rock deposited in the Late Proterozoic and Early Cambrian. The unit is quartzite with a substantial thickness of shale also present, thus a major aquitard. The unit is thickest in the southwest where it is estimated to exceed 10,000 ft, and it is thinnest in the north and southeast where it is estimated to be about 5,000 ft thick or locally less. The thickness of the unit is approximate because the base is rarely exposed, but the estimate is consistent with the amount of section that is exposed. In most places, the youngest formation within this unit is the Pioche Shale, and the bulk of the unit is mapped as the Prospect Mountain Quartzite. The permeability of the unit is low except in areas where fractured or weathered. The difference in permeability between p€m and €p€s in exposed sections is considered minor, although the €p€s unit is expected to be slightly more permeable than the older p€m (Belcher and Elliott, 2001). On the geologic maps and cross sections, unit consists of the symbol €p€s.

4.2.3 Cambrian Carbonate Rocks

The Cambrian carbonate unit (€c) consists of Middle and Upper Cambrian carbonate rocks, notably the Bonanza King, Highland Peak, and Pole Canyon formations. The units are interpreted to be thicker in the south (~8,000 ft) and thinner (~5,000 ft) in the north. This unit is mostly carbonate with a limited thickness of clastic sections. It has high permeability, especially where faulted, and therefore is a major aquifer. In the southern part of the geologic study area, the unit constitutes about half the thickness of the Paleozoic section. The Cambrian carbonate aquifer includes a thin, spatially limited confining unit, the Dunderberg Shale. This unit is of limited extent and is too thin to be considered capable of limiting flow on a regional basis. On the geologic maps and sections, unit

consists of the rocks with the symbols of both €m and €u and, on the cross sections, also the rocks with the symbol €c.

4.2.4 MISSISSIPPIAN TO ORDOVICIAN CARBONATE ROCKS

The Mississippian to Ordovician carbonate rock unit (MOc) consists of the middle part of the Paleozoic carbonate section. The unit can exceed 12,000 ft as on Plate 8, Cross Section P—P' but has a wide variation in thickness as on Plate 8, Cross Section N—N' due to paleotopographic influences during deposition and post-depositional erosion. The unit includes the section from the Mississippian Joana or Monte Cristo Limestone to the Ordovician Pogonip Group or Antelope Valley Formation and therefore includes the Pilot Shale and Eureka Quartzite. This unit is characterized as carbonate with limited clastic rocks. It is generally very permeable, especially where faulted.

The Mississippian to Ordovician carbonate aquifer includes the Ordovician Eureka Quartzite and Pilot Shale, which are aquitards. Neither of these formations is considered a significant aquitard at the scale of Plates 6 to 9, and the Eureka Quartzite, where fractured, can be an aquifer nearly as permeable as the carbonates. This section of rocks also includes the Guilmette, Sultan, Sevy, and Simonson formations of Devonian Age and the Lone Mountain Dolomite of Silurian age. These rocks are predominately dolomite. From oldest to youngest, the symbols for the rocks on the geologic maps and sections that are combined in this HGU are the following: Ol, SOu, SO, Ds, Dg, Dn, Dd, Du, DO, DS, MD, and MDd.

4.2.5 MISSISSIPPIAN SILICICLASTIC ROCKS

The Mississippian clastic rock unit (Ms) includes the Diamond Peak Formation, Chainman Shale, Scotty Wash Quartzite, and equivalent siliciclastic rock units. The first two formations listed are not differentiated in this report in Lincoln County, except in the Egan and Schell Creek ranges, and are not differentiated in Clark County because they are thin. The clastic rock unit is derived from erosion of highlands in north-central Nevada associated with the Antler upland. It is thickest (about 3,500 ft) on the western side of Plate 8, Cross Section Y—Y'. The permeability of the unit is low, and the unit is an important confining layer in the Paleozoic section north of the North Pahroc Range (about 38 degrees north latitude). In the Snake Range, the rock unit is too thin to comprise a confining unit. On the geologic maps and sections, the unit consists of the rocks with the symbols Mc and Md.

4.2.6 PERMIAN AND PENNSYLVANIAN CARBONATE ROCKS

The Permian and Pennsylvanian carbonate unit (PIPc) includes the Ely Limestone and Bird Spring Formation. It is nominally equivalent to the upper carbonate aquifer of Winograd and Thordarson (1975) at the Nevada Test Site. In the northern part of the geologic study area, these rocks are continuous with the Arcturus and Park City groups, which are predominantly carbonate rocks. In the Butte Mountains in the northwestern part of the area, a small section of Triassic rocks is included in this unit. The unit is thickest near Robinson Summit in the Egan Range, with a thickness of ~10,000 ft at Plate 8, Cross Section W—W'. This unit is mostly carbonate, with a minimal thickness of clastic rocks. It is generally very permeable on a regional scale, especially where faulted. It is hydrologically similar to the lower carbonate section but separated from it by the Mississippian confining unit, unit Ms. The unit includes Permian carbonate and red beds in the southern part of the

geologic study area. From oldest to youngest, the symbols for the rocks on the geologic maps and sections that are combined in this HGU are the following: IP, PIP, Pr, Pa, Par, and Pp.

4.2.7 Cretaceous to Triassic Siliciclastic Rocks

The Cretaceous to Triassic clastic unit (KTrs) consists of Mesozoic rocks in eastern Lincoln and Clark counties. The unit includes the Triassic Moenkopi and Chinle formations and the Jurassic Aztec and Navajo sandstones. These units are locally beneath thrust faults that carry overlying older Paleozoic carbonates thrust from the west during Sevier deformation, and this unit may be 10,000 ft thick or more. The rocks of this unit are generally much less permeable than the carbonate aquifers. The symbols for the rocks on the geologic maps and sections that are combined in this HGU are Trs and Ks.

4.2.8 Tertiary to Jurassic Intrusive Rocks

The Tertiary to Jurassic intrusive unit (TJi) includes all plutons in the geologic study area. Mesozoic plutons form either a significant part of, or the bulk of, several large ranges in the northeastern part of the area, including the Snake, Schell Creek, Egan, and Kern ranges. In addition, extensive Tertiary plutons exist beneath all calderas. The permeability of the unit is low except in areas where fractured or weathered. The symbols for the rocks on the geologic maps and sections that are combined in this HGU are Ji, Ki, TKi, and Ti.

4.2.9 Older Tertiary Sediments

The older Tertiary sedimentary unit (Tos) consists mostly of older Tertiary clastic sediments (Eocene to Oligocene age) below the volcanic section. The unit reaches a maximum thickness of 4,000 ft in Railroad Valley, west of the geologic study area, and a similar thickness in the southern part of the area. The permeability is moderate, especially where well fractured. On the geologic map and cross sections, the unit consists of the rocks with the symbol Ts1 where they underlie the Tertiary volcanic rocks HGU.

4.2.10 Tertiary Volcanic Rocks

The Tertiary volcanic unit (Tv) includes large volumes of middle Tertiary (Eocene to middle Miocene), mostly intermediate to felsic volcanic rocks. It also includes thin sedimentary rocks and local tuffaceous sediments that are interbedded with the volcanic units. Most of the exposed bedrock in Delamar, Dry Lake, Patterson, Little Spring, Rose, Eagle, Kane Spring, and Clover valleys are of volcanic rock. Outflow rocks are generally less than 3,000 ft thick, but intracaldera rocks may locally be more than 10,000 ft thick.

The Tertiary volcanic unit consists of a number of units of variable permeabilities: ash-flow tuffs are brittle and generally permeable, whereas lava flows are less permeable. In general, the permeability is considered good to moderate, but where faulted, the unit is more permeable and in some places, it may be an important aquifer. From oldest to youngest, the symbols for the rocks on the geologic maps that are combined in this HGU are the following: Tmb, Ta1, Ta2, Ta3, Ta4, Tr1, Tr2, Tr3, Tr4, Tt1, Tt2, Tt3, and Tt4. The symbol for the rocks on the geologic sections is Tv.

4.2.11 QUATERNARY AND TERTIARY BASALT

The Quaternary and Tertiary basalt unit (QTb) resulted from Quaternary and late Tertiary mafic volcanism. The deposits are thin but locally cover significant areas. The unit is of possible hydrologic significance as a separate unit only where divided from the older volcanic rocks by alluvium. It is separated from the alluvium largely because it is a distinct rock type. The largest outcrops are located in north-central Nye County (Plate 1), and there are also extensive outcrops of this unit in southern Lincoln and northern Clark counties (Plate 2). Basalt is brittle and has high permeability, but because of the limited thickness and distribution, it does not have regional significance. On the geologic maps and cross sections, the unit consists of the rocks with the same symbol (QTb).

4.2.12 QUATERNARY AND TERTIARY SEDIMENTS

The Quaternary and Tertiary sedimentary sequence (QTs) consists mostly of basin-fill sediments younger than the volcanic section. This unit may include older Tertiary sediments where the volcanic rocks are thin or nonexistent and these older units are too thin or too localized to separate out. In some places, these older units consist of sands and gravels that are difficult to distinguish from the younger alluvial sediments, and these units are, therefore, lumped together.

The QTs unit is interpreted to be thicker than 10,000 ft in some down-faulted grabens (valleys), such as Dry Lake and Panaca valleys on Plate 8, Cross Section P—P'. The unit is composed of conglomerate, fresh-water limestone, sand, silt, gravel, and clay, and therefore it has a large range of permeability. Also included in this unit are playa deposits that are too thin to show on cross sections but are an obvious surface feature throughout the Great Basin. Overall, the map unit has moderate permeability but may be high where fractured. The symbols for the rocks on the geologic maps that are combined in this HGU are Ts2, Ts3, Ts4, and QTa. On the cross sections, the symbol for the rocks in this HGU is QTa.

4.3 STRUCTURAL GEOLOGY

This section discusses the structural framework of the geologic study area. This presentation is followed by an analysis of the effect of specific structures on the hydrogeology of the region. This analysis covers structures as both groundwater flow conduits and flow barriers, in other words how they guide flow along and across a general flow path.

4.3.1 EVOLUTION OF THE REGIONAL STRUCTURE

Three main structural events affected the geologic study area: (1) Late Devonian to Late Mississippian Antler compressive deformation, (2) Late Jurassic to early Tertiary Sevier compressive deformation, and (3) late Cenozoic basin-range extensional deformation. In addition to these structural events, middle Cenozoic time was characterized by mild extension (Rowley, 1998; Miller et al., 1999; Rowley and Dixon, 2001) and voluminous calc-alkaline volcanism that profoundly affected the topography and hydrology of the geologic study area.

The Late Devonian to Late Mississippian Antler compressive deformation affected the northwestern part of the geologic study area, creating a north-trending highland (Larson and Langenheim, 1979; Carpenter et al., 1994; Poole and Sandberg, 1977 and 1991). This event formed folds and thrusts of

the Roberts Mountain allochthon, which was at least 8,000 ft thick and passed through the western side of Eureka, Nevada (Carpenter et al., 1994; Saucier, 1997). The thrusts transported deeper-water sedimentary rocks eastward as much as 100 mi. Coarse synorogenic siliceous clastic detritus was shed from the highland into the foreland basin to the east, transitioning to shale farther east. The main synorogenic rock units that resulted were the Chainman Shale and Diamond Peak Formation, and farther south the Scotty Wash Quartzite.

The second structural event, the Middle Jurassic to early Tertiary Sevier compressive deformation, resulted in generally north- to north-northeast-striking, east-verging folds and thrust faults. Scattered Middle Jurassic to lower Tertiary plutons were emplaced in many mountain ranges of the geologic study area. Eastward-directed overthrusts emplaced Late Proterozoic to middle Paleozoic rocks over Late Proterozoic to Mesozoic rocks (Armstrong, 1968). At least a half dozen large thrusts are well exposed in the Las Vegas area, each with displacements ranging from several to 20 mi (Page et al., 2005b). Tectonic shortening caused by thrusting in southern Nevada is at least 22 to 45 mi (Stewart, 1980; Burchfiel et al., 1974). Except for the southern part of the geologic study area, most of the area has been considered to be the western hinterland of the deformation. In other words, the leading edges of most major thrusts are east of the map area, and the deformation created highlands within the hinterland of the map area that in turn eroded and shed clastic material primarily to the east. Some of the thrusts, including the Gass Peak, however, have been projected northward into the hinterland in the central and northern part of the geologic study area, including the Timpahute Range, Worthington Mountains, Golden Gate Range, Grant Range, Pancake Range, and Newark Valley (Vandervoort and Schmitt, 1990; Dobbs et al., 1994; Taylor et al., 2000). Sevier-type deformation is shown schematically on Figure 4-6, and the Sevier-age Glendale/Muddy Mountains thrust in the Muddy Mountains is shown on Figure 4-7.

East-striking faults and folds, alignments of plutons and volcanic vents, alignments of geophysical anomalies, local alignments of basins and ranges, hot springs, hydrothermally altered rocks, and mineral deposits have been noted in the Great Basin for years, primarily by geologists of the mining industry. Ekren et al. (1976 and 1977), Rowley et al. (1978), and Stewart et al. (1977) called these alignments "lineaments" with an origin similar to transform faults in the ocean basins. Ekren et al. (1976) also suggested that the lineaments began to form in the Cretaceous, if not earlier, and continued to be active throughout both Tertiary calc-alkaline magmatism and basin-range deformation. Like transform faults, these lineaments seem to represent boundaries between areas to the north and south that had different amounts, rates, and types of structural deformation. Rowley (1998) and Rowley and Dixon (2001) referred to them as transverse zones, and we follow their terminology here. They are poorly known and have been mapped in detail only locally, so they are projected with limited evidence between these areas where they are known. Therefore, transverse zones are delineated as speculative zones of potential disruption on Plates 1 and 2.

Transverse zones bound parts of most igneous belts in the Great Basin. They also define the northern and southern sides of the Caliente caldera complex, representing structures by which this caldera spread east and west to a degree much more profound than most other calderas in the Great Basin. Transverse zones may both provide barriers to the southward flow of groundwater and act as conduits to east or westward flow of groundwater (Prudic et al., 1995; Rowley, 1998; Rowley et al., 2001).

The third structural event, the basin-range episode of extensional deformation, began at about 20 Ma and continues today. It is characterized by east-west extension and resulted primarily in

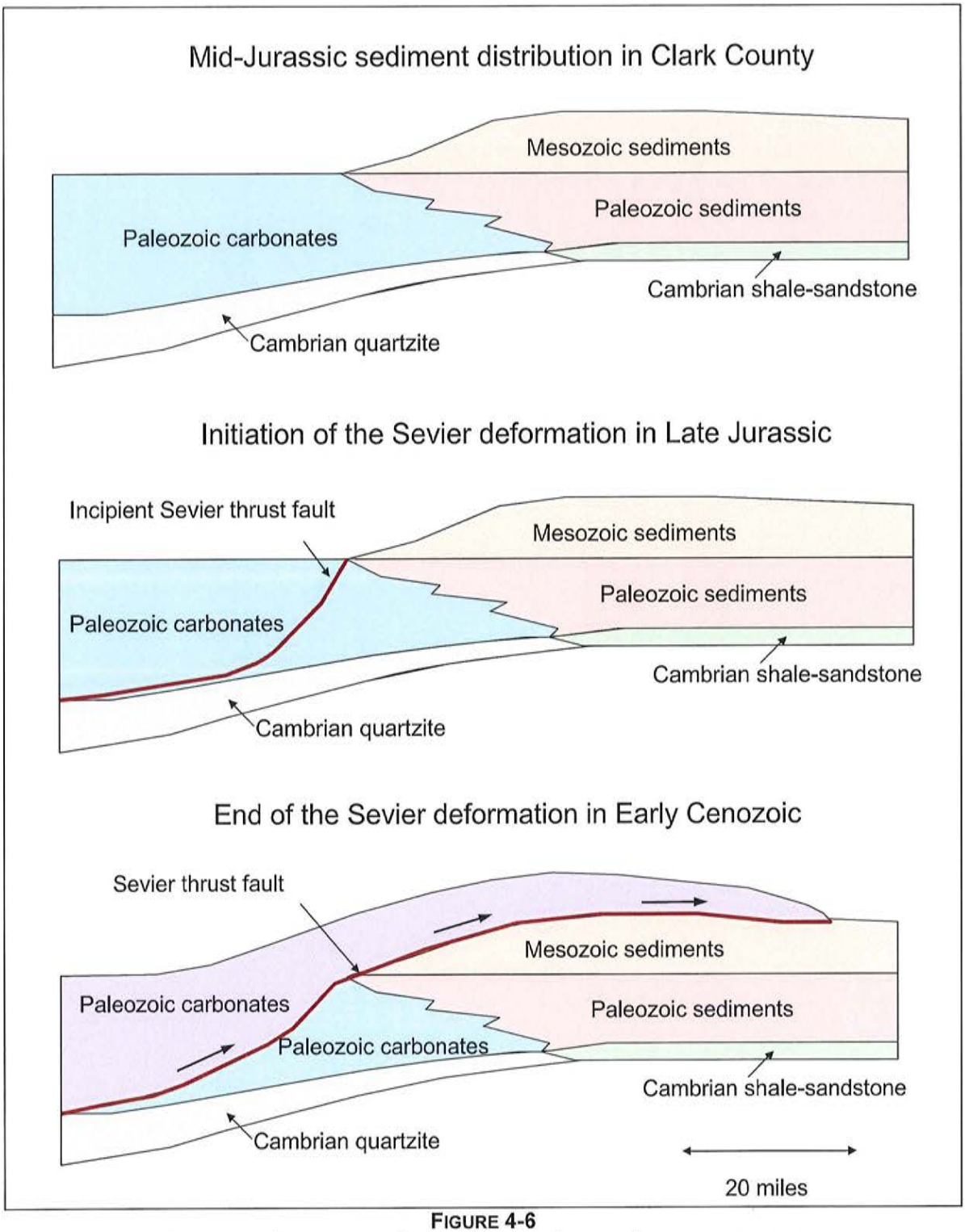

FIGURE 4-6
SCHEMATIC DIAGRAM OF SEVIER THRUST SHEETS, ILLUSTRATING THE MOVEMENT OF PALEOZOIC CARBONATES OVER CRATONIC SEDIMENTS

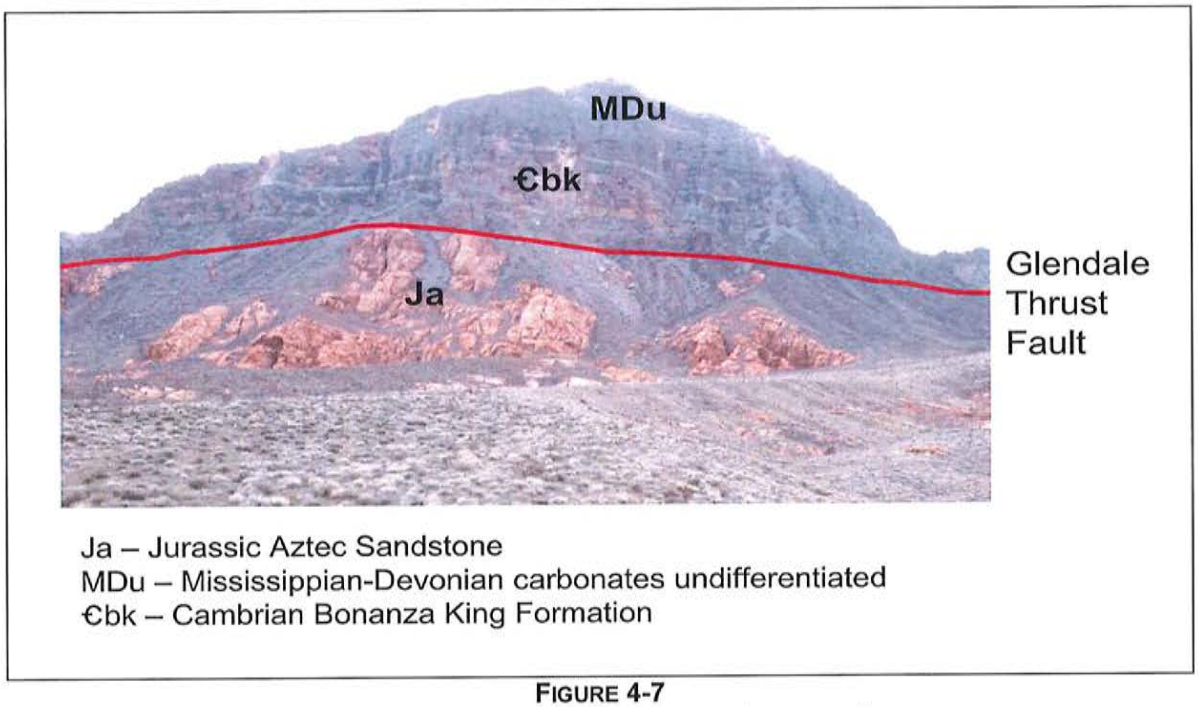

FIGURE 4-7
PALEOZOIC CARBONATES THRUST OVER JURASSIC AZTEC SANDSTONE IN THE MUDDY MOUNTAINS NEAR MUDDY PEAK

north-striking normal faults. Over some parts of the Great Basin, early phases of this deformation produced north-striking basins and ranges due partly to gentle folding. Sediments were deposited in basins formed by these early faults and broad warps, but these basins were not necessarily in the same locations as they are today. The present topography was produced later, during the main pulse of basin-range deformation that began after 10 Ma for most parts of the Great Basin. The axes of basins and ranges since 10 Ma were commonly different from those created during the early phase of deformation. Some parts of the older basins were uplifted as part of the new ranges and some parts of the older ranges were downthrown as part of the new basins. An example is the presence of Miocene lacustrine limestones and associated clastics in the North Pahroc and Pahranagat ranges (Tschanz and Pampeyan, 1970) that were originally deposited in one or more basins.

The dominant fault type since major deformation began (about 10 Ma) continued to be north-striking normal faults, but locally strike-slip and oblique-slip faults accommodated the east-west extension. Examples of such accommodation zones are the east-northeast, left-lateral Pahranagat shear zone at the southern end of Pahranagat Valley and the northeast-trending, left-lateral Kane Spring fault zone west of the Meadow Valley Mountains (Ekren et al., 1977). East-striking transverse faults continued to be active at the same time, segmenting the Great Basin into broad east-trending corridors of different types and amounts of east-west pulling apart.

In some parts of the map area, low-angle faults were previously mapped as thrust faults. These faults, however, place younger rocks on older rocks. In some places, the direction of movement of the upper plates of these faults is westward rather than eastward. We consider that most of these faults are much younger, Tertiary in age, expressions of structural extension and that most formed during the basin-range deformational event. We interpret the faults to be detachment faults, although the general

synonyms "attenuation" or "denudation faults" that were used by some early workers who first recognized them (Moores et al., 1968; Armstrong, 1972) are more appropriate in places where many subhorizontal faults are present, notably the Eureka area. In these areas, rapid uplift of ranges resulted in their tops being structurally stripped (or attenuated or denuded) by low-angle faults that verged into the adjacent low areas, much like large gravity slides.

One major fault to which the name "detachment" fault is appropriate is the well-known Snake Range decollement. Although originally considered to be a thrust fault that placed Middle Cambrian and younger rocks over Middle Cambrian and older rocks (for example, Nelson, 1966), the fault was later mapped in greater detail and reinterpreted as an Eocene to middle Miocene low-angle fault caused by stretching and thinning during uplift of a metamorphic core complex (Miller et al., 1983; Gans et al., 1985 and 1989). This detachment may represent the ductile/brittle transition zone uplifted by the core complex, as illustrated schematically in Figure 4-8 (Miller et al., 1983; Gans et al., 1985; Gans, 2000b). Rocks have been thinned by the elimination of strata due to the faulting. Later work indicated that, while the decollement had an older (late Eocene and early Oligocene) history, most displacement on it was middle Miocene and later, coinciding with basin-range deformation (Miller et al., 1999). The core-complex uplift that formed the decollement included the Kern Mountains and southern Deep Creek Range (Miller et al., 1999). Finally, Miller et al. (1999, p. 902) suggested that the Snake Range decollement may not be a normal fault at all but instead a "highly complex structural boundary developed above a rising and extending mass of hot crystalline rocks."

4.3.2 EFFECT OF STRUCTURES ON GROUNDWATER FLOW

This section evaluates the effect of the three episodes of structural deformation and one episode of volcanism on the groundwater flow in the geologic study area.

4.3.2.1 THE ANTLER DEFORMATION

The Antler episode of compressive deformation probably had the least direct effect on groundwater flows of any structural event. Most of the thrust faults associated with this tectonic event are west and northwest of the geologic study area. Instead, the deformational event had more of an effect on the types of sediment deposited than on any structural controls on groundwater flow. The deformation created a highland west of the map region, and sandstone and shale, including the Chainman Shale, were deposited within the northern half of the geologic study area, forming a lithologic aquitard. Most of the tectonic features developed during this event were themselves deformed and changed in subsequent tectonic episodes.

4.3.2.2 THE SEVIER DEFORMATION

The Sevier episode of compressive deformation had a stronger effect on groundwater flow in the region than the Antler event. The Sevier event resulted in major thrust faults, especially in the southern part of the geologic study area but locally in the central and northern part of the area. Gouge and mylonitic zones along these thrusts created barriers to groundwater flow, particularly in the Sheep Range, the Pahranagat Range, the Delamar Mountains, and in several other ranges in the southern part of the area. Furthermore, these thrust faults brought western assemblage carbonates over eastern assemblage cratonic clastic sedimentary rocks of Triassic through Cretaceous age. These cratonic confining units generally also are flow barriers. Some of these geologic barriers to flow are several

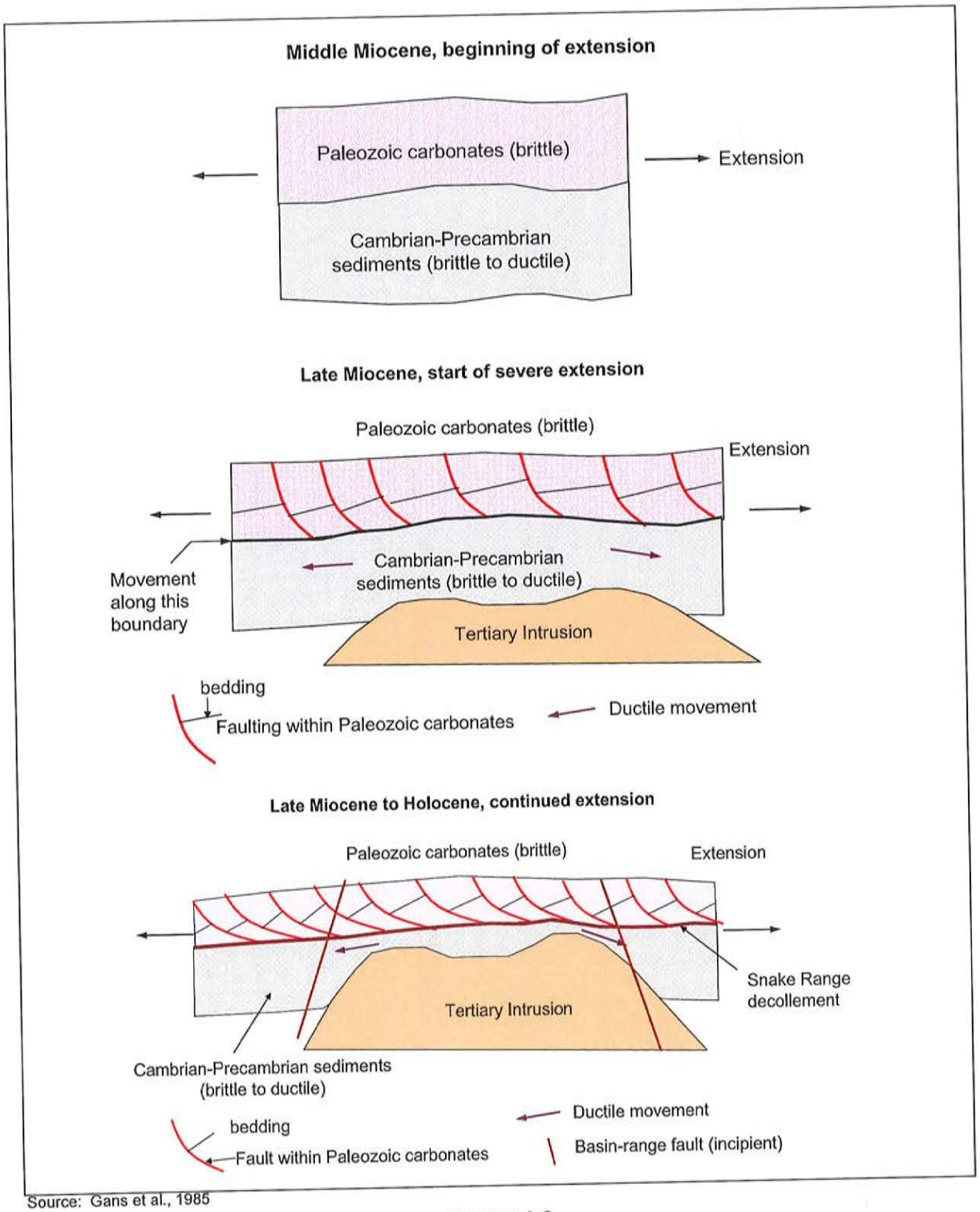

Source: Gans et al., 1985

FIGURE 4-8
ONE SCENARIO FOR DEVELOPMENT OF THE
SNAKE RANGE DECOLLEMENT DURING LATE CENOZOIC EXTENSION

thousand feet thick, as in the Muddy, Meadow Valley, and Clover mountains. In other places, thrust faults brought Precambrian and Cambrian siliciclastic rocks over the carbonate units, as in the Sheep and Las Vegas ranges along the Gass Peak thrust and in the Delamar Mountains along the Delamar thrust. In contrast to barriers to flow caused by the Sevier deformation, northerly conduits may have resulted from a concentration of fractures developed along the axes of open shallow anticlines, most of which trend north.

4.3.2.3 THE EOCENE-MIOCENE EPISODE OF CALC-ALKALINE VOLCANISM

The third episode of landscape change was during the Eocene, Oligocene, and Miocene epochs, when the area was drastically affected by voluminous calc-alkaline volcanism, mild extension, and high-angle strike-slip faults and high- to low-angle normal faults. The topography became dominated by calderas, which capped mountainous areas formed by uplift and inflation of the crust due to the rise of underlying source batholiths and stocks. Ash-flow tuffs that erupted from the calderas blanketed and subdued the topography. Stratovolcanoes and other volcano edifices fed lava flows and mudflows. The geometry, extent, strike, size, and type of structure that formed during this time are poorly known but likely included strike-slip and normal faults, including detachment faults. The region was characterized by mild extension and wrench tectonics. Strike-slip faults probably had northeast and northwest strikes. The caldera complexes and their associated ring faults and other margin structures provided mostly barriers to groundwater flow. Perhaps more important than the caldera margins themselves are the intracaldera intrusions that underlie the calderas, which caused hydrothermal clay to form by heating and convective overturn of ancient groundwater and contact metamorphism of intracaldera ash-flow tuff. Faults and associated joints that postdate and cut the calderas locally provide conduits for groundwater flow through the calderas.

4.3.2.4 THE MIOCENE-QUATERNARY BASIN-RANGE EPISODE OF EXTENSION

The basin-range episode of extensional faulting began in the middle Miocene and is continuing today. The faults that formed during this episode are generally moderate to steeply dipping normal faults that are generally north trending. They formed most of the topography we see today. High-angle oblique-slip and local strike-slip faults that formed as accommodation zones during the same east-west extension also were important. The north-striking high-angle faults and resultant fractures generally provide conduits to groundwater flow north or south along the hydraulic gradient, rather than flow barriers (e.g., Rowley and Dixon, 2004). In areas where groundwater flow is directly across these fault zones, such as between Spring and Hamlin valleys, groundwater flow may be limited by gouge in the core zones of the faults but not prevented by these structures (Figure 4-9). Along the WRFS where flow is from north to south, parallel to these structures, flow is enhanced in the north-south direction by these faults (Figure 4-9). The hydrologic effect produced by faults largely results from joints that the faults cause, with larger-displacement faults resulting in more joints and thus greater fracture flow. However, for brittle rocks such as carbonates, ash-flow tuff, and basalt flows, even small faults—which are many times more abundant in the Great Basin than the large faults we have mapped—will create rock fractures, acting like a hammer on a plate of glass. These brittle rocks in the Great Basin cannot help but be significantly fractured throughout, commonly creating important aquifers (Winograd and Thordarson, 1975; Dettinger, 1992; Dettinger et al., 1995; Burbey, 1997; Rowley and Dixon, 2004).

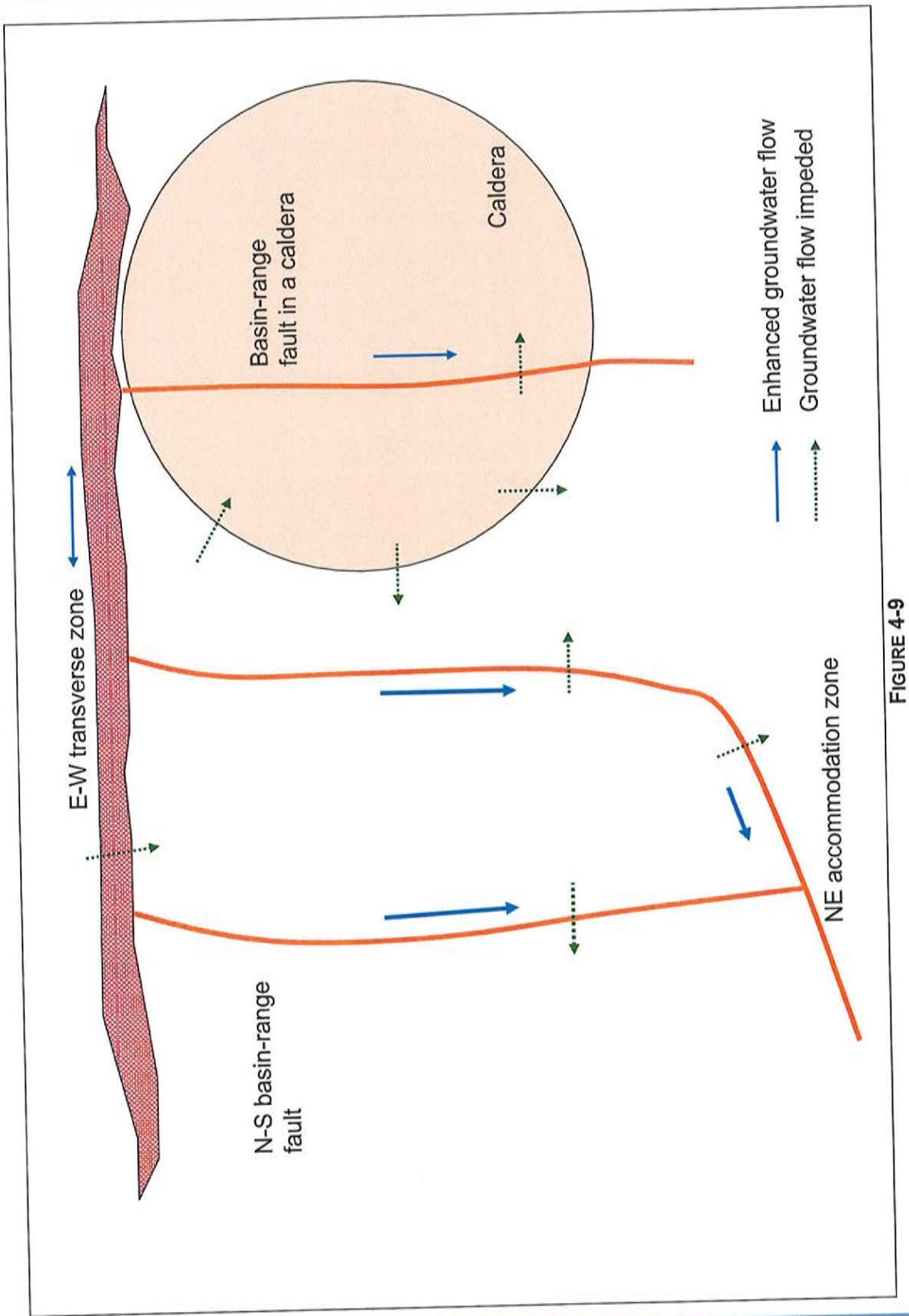

FIGURE 4-9
DIAGRAMMATIC MAP SHOWING ENHANCEMENT OR IMPEDANCE OF GROUNDWATER FLOW ALONG OR ACROSS FAULTS, TRANSVERSE ZONES, AND CALDERAS

Some normal faults are low-angle—that is, detachment or attenuation faults. Their effect on groundwater flow is much less important than that from high-angle faults. These detachment zones may be either from brittle or plastic deformation, resulting respectively in gouge or mylonitic zones along the faults. Gouge and mylonite may provide barriers to groundwater flow. An example is the Snake Range decollement that formed as the Snake and Schell Creek ranges were uplifted and intruded. The detachment faults of the Snake Range decollement may locally prevent rainfall from infiltrating the range. But a more profound effect on infiltration is caused by the underlying Proterozoic and Cambrian metamorphic rocks and quartzite, which also provide barriers to east or west flow through the ranges.

4.4 DESCRIPTIONS OF BASINS AND RANGES AND POTENTIAL FOR INTERBASIN GROUNDWATER FLOW

This section describes basins and ranges and the potential for interbasin groundwater flow between the basins within a series of hydrologic regional flow systems. Most flow systems were defined by Harrill et al. (1988) and Harrill and Prudic (1998). The most extensive flow systems within and adjacent to the geologic study area are the WRFS and DVFS, the boundaries of which are defined on Figures 2-1 and 3-1, respectively, and the GSLDFS, part of the boundary for which is defined on Figure 2-1. Adjacent to these flow systems are the Penoyer Valley, Newark Valley, Railroad Valley, Diamond Valley, Humboldt, Ruby Valley, Goshute Valley, Virgin River, and Sevier Lake flow systems (Figure 2-1). The MVFS is considered a separate system by some workers, but in this report, this flow system is interpreted to be part of the WRFS to which it is tributary. In subsequent sections, the MVFS is included in the WRFS.

This study concentrated on specific basins or hydrographic areas within or adjacent to the model area, which includes the WRFS, the MVFS, and the southwest portion of the GSLDFS. Mountain ranges adjacent to these basins are described in more detail than the valleys themselves due to their greater exposures of pre-Quaternary geologic units. Because of this, the discussion below is organized by ranges, and the adjacent basins are discussed within these sections. Basins and bounding mountain ranges in adjacent flow systems are shown to give regional context and are described in less detail.

Basins and ranges are described in this section to better understand their structure and extent within individual flow systems. The features are first described for the WRFS and MVFS, going from west to east and north to south, starting in the northwestern part of the map. For adjacent flow systems, basins and ranges are described for the western edge north to south, then the eastern edge north to south.

The potential for interbasin groundwater flow is discussed within the text and is illustrated by Figure 4-10. The figure shows the likelihood of interbasin groundwater flow based on lithology and structure. The potential for interbasin groundwater flow was classified, geologically, as likely, permissible, or unlikely. The hydrographic area boundaries identified as likely or permissible zones for groundwater flow are approximate locations and are not meant to represent the exact location of interbasin groundwater flow.

As defined, boundaries of the flow systems are inferred from available water-level data, mass-balance calculations, geochemical signatures, and geologic features that control groundwater movement. Probable flow pathways of the flow systems are defined by geologic features, which are critical in understanding flow routing between the valleys of the flow systems.

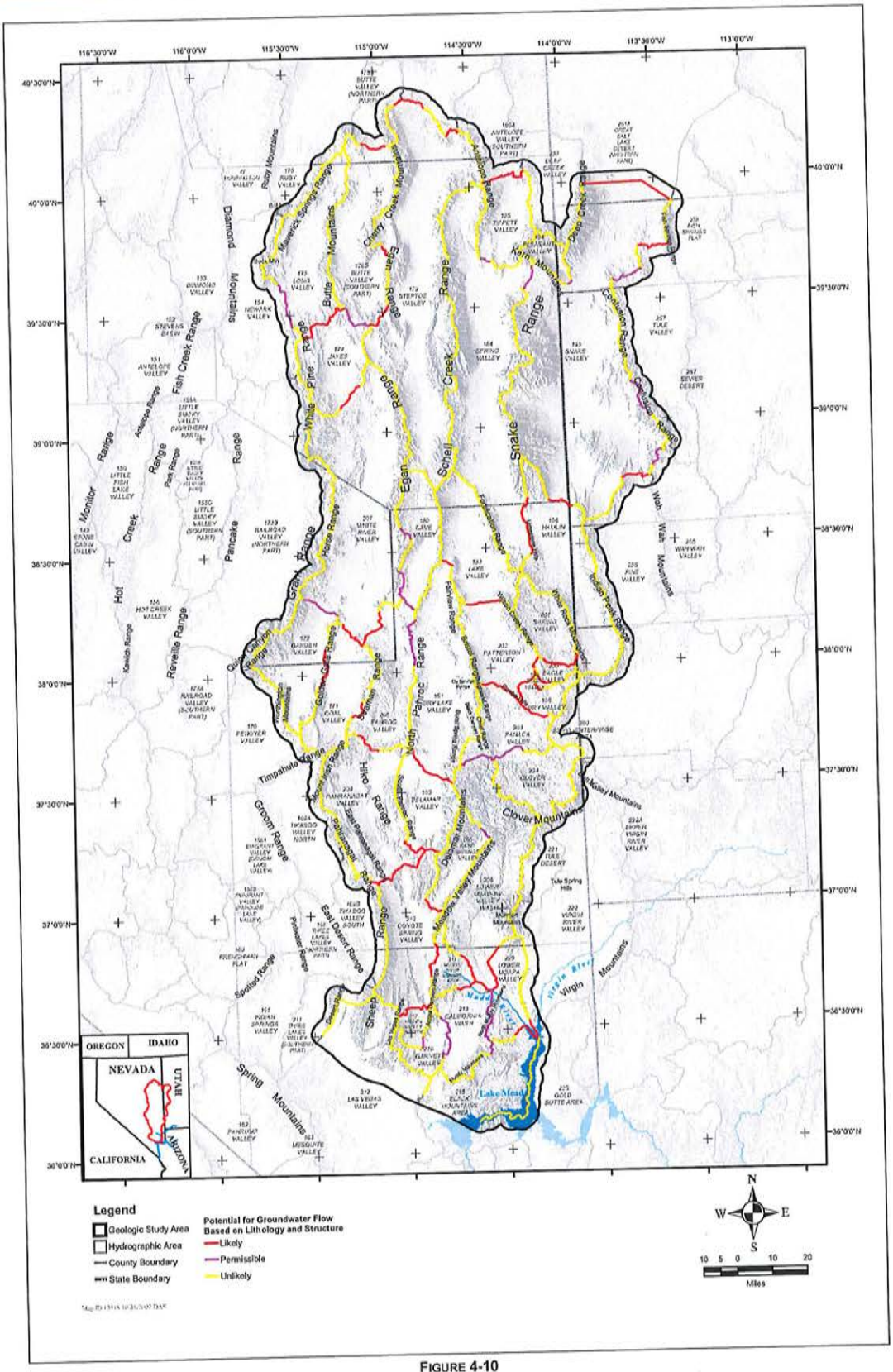

FIGURE 4-10
POTENTIAL FOR INTERBASIN GROUNDWATER FLOW WITHIN THE GEOLOGIC STUDY AREA

4.4.1 BASINS AND RANGES ALONG AND WITHIN THE WHITE RIVER FLOW SYSTEM

This section discusses the geology and hydrogeology of basins and ranges along the sides and interior of the WRFS. Basins and ranges of the MVFS are included in the discussion. The order of ranges is generally from north to south and west to east.

4.4.1.1 RUBY MOUNTAINS, BALD MOUNTAIN, AND BUCK MOUNTAIN

The mountain ranges at and near the northwestern parts of the WRFS are the southern Ruby Mountains, Bald Mountain, and Buck Mountain. These ranges bound Long Valley, the northernmost valley of the WRFS; Ruby Valley, the southernmost valley of the Ruby Valley Flow System; Huntington Valley, a southern valley in the Humboldt River Flow System; and Newark Valley, the northern and downstream end of the Newark Valley Flow System (Figure 2-1). The Ruby Mountains, just west of the geologic study area, is a horst in which large amounts of vertical uplift resulted in detachment (attenuation) faults along the margins. In other words, the range is a metamorphic core complex (Howard et al., 1979; Wright and Snoke, 1993). Most rocks in the range dip east and are early Paleozoic in age. The Ruby Mountains is cored by a Jurassic to Miocene batholith and Precambrian to Cambrian aquitards.

Bald Mountain consists of east-dipping lower Paleozoic rocks cored by Jurassic intrusions that formed major deposits of gold, silver, and other metals (Hitchborn et al., 1996). Bald Mountain joins Buck Mountain, a horst of subhorizontal middle Paleozoic rocks. A south-trending narrow arm of Buck Mountain joins the White Pine Range to the south, and flow is permissible from Long Valley into Newark Valley (Figure 4-10). The intrusions provide a barrier to flow across Bald Mountain, thereby allowing separation of the Ruby, White River, and Newark flow systems at this location.

Ruby Valley is a deep graben bounded by the Ruby Mountains to the west, the Maverick Springs Range (Section 4.4.1.2) to the east, and Bald Mountain to the south. This graben is locally about 5,000 ft deep. On the western side of the Ruby Mountains and Bald Mountain is Huntington Valley, a graben that is several thousand feet deep. This valley is bounded on the west by the Diamond Mountains. A groundwater divide is present between Huntington Valley and Newark Valley (Harrill et al., 1988). Newark Valley is bounded by the Diamond Mountains to the west and by Bald and Buck mountains to the east. This valley is another graben with locally more than 5,000 ft of valley fill (Plates 4 and 8, Cross Section X—X'); it is further described in Section 4.4.1.3. Seismic profiles disclose Sevier thrusts beneath the basin-fill deposits (Dobbs et al., 1994).

4.4.1.2 MAVERICK SPRINGS RANGE

The Maverick Springs Range of northern White Pine County, Nevada, is a low, northeast-trending range of mostly east-dipping upper Paleozoic rocks uplifted along a normal fault on the western side. The range forms part of the northern edge of the WRFS and the southeastern edge of Ruby Valley. The eastern side of the Maverick Springs Range is bounded by a normal fault, down to the east, that separates it from Long Valley to the east. The northern end of the Maverick Springs Range is cored by a Tertiary pluton (Plates 4 and 8, Cross Section Y—Y') that continues north into Elko County, Nevada, as a broad series of hills, floored by cupolas of a Tertiary stock or batholith. The southern half of the Maverick Springs Range joins Buck Mountain to the south, separated by a down-to-the-west normal fault in the Alligator Ridge area, site of a major gold deposit (Nutt, 2000).

The pluton in the Maverick Springs Range is a barrier to groundwater flow east or west across the northern part of the range, and flow is theoretically possible but considered unlikely through carbonate rocks above and around the pluton. The east dip of the beds would preferentially cause mountain recharge to flow eastward.

Long Valley, at the northern end of the WRFS, is narrow and shallow at its northern end but it widens and deepens to at least 3,000 ft to the south. The fault zone that bounds the western side of the Maverick Springs Range in Ruby Valley passes through Mooney Basin to the western side of Long Valley and is potentially a conduit for groundwater flow between southern Ruby Valley and Long Valley. Groundwater in Long Valley flows southward along north-trending faults and fractures in the valley, then is permissible to move along faults and fractures of the same trend in the northern White Pine Range, then into Jakes Valley to the southeast (Figure 4-10) (Harrill et al., 1988).

4.4.1.3 Butte Mountains and White Pine Range

The Butte Mountains is located east of Long Valley along the northeastern margin of the WRFS. The range is a 40-mi-long, north-trending horst of east-dipping to anticlinically folded, upper Paleozoic sedimentary rocks. Southward, the Butte Mountains joins the eastern side of the north-trending, 50-mi-long White Pine Range across a low range of hills of upper Paleozoic carbonate and Tertiary volcanics rocks. The southern end of the Butte Mountains also joins with the Egan Range (Section 4.4.1.9) to the east across a similar low range of hills. At this divide, flow is likely to the southeast into Steptoe Valley and permissible to the southwest into Jakes Valley (Figure 4-10).

The northern White Pine Range is a generally low, broad series of horsts and grabens (Gans, 2000a). One of the grabens becomes Long Valley to the north, and the eastern horst becomes the Butte Mountains to the north. The northern White Pine Range is underlain largely by upper Paleozoic rocks, but middle Paleozoic rocks underlie some of the horsts (Lumsden et al., 2002) and Tertiary volcanic rocks underlie some of the grabens (Plates 4 and 8, Cross Section W—W'). The southern end of the White Pine Range has considerable elevation (as much as 11,500 ft) and is made up mostly of east-dipping, lower to middle Paleozoic rocks. The range here has a large eastward bulge, the White River caldera, which includes an underlying resurgent dome that doubtless is responsible for the high relief of the range here (Plates 4 and 8, Cross Section V—V'). West of the caldera, the rocks include Cambrian to Precambrian siliciclastic rocks intruded by a Tertiary pluton. The north-trending axis of the caldera contains a narrow, north-striking graben; it is geologically likely that the graben may be a groundwater conduit between Jakes Valley and the White River Valley (Figure 4-10), respectively, west and south of the caldera. The siliciclastic and intrusive rocks of the White Pine Range form a groundwater barrier between the White River Valley and Railroad Valley, and east-dipping sedimentary rocks may allow recharge to flow preferentially eastward from the range into the White River Valley.

Basins surrounding the Butte Mountains and White Pine Range include the previously described Long Valley, southern Butte Valley, Jakes Valley, northern White River Valley, and southern Newark Valley. Butte Valley, east of the Butte Mountains, is a graben similar to Long Valley but is part of the GVFS. Butte Valley contains upper Paleozoic rocks at shallow depth, with overlying Tertiary volcanic rocks in the southern part of the valley. The valley fill is a maximum of about 4,000 ft thick, overlying less than 1,000 ft of Tertiary volcanic rocks. A narrow horst is within the northern end of Butte Valley (Plates 4 and 8, Cross Section Y—Y'). Jakes Valley, south of the Butte Mountains, may

be as deep as 6,500 ft (Plates 4 and 8, Cross Section W—W'), with Tertiary volcanic rocks and upper Paleozoic carbonate rocks beneath about 5,000 ft of basin-fill sediments. Jakes Valley is the second northernmost valley within the WRFS.

West of the White Pine Range, Newark Valley is a shallow graben, narrowing and becoming shallower to the south; it is further described in Section 4.4.1.1. West of the southern end of the White Pine Range, Newark Valley opens out southward into Railroad Valley, a broad deep graben and the upper eastern end of the Railroad Valley Flow System. East of the axis of the White Pine caldera, the White Pine Range is dropped down by many down-to-the-east normal faults that also create White River Valley to the east, which is part of the WRFS. Although relatively shallow at this latitude, near Preston and Lund, Nevada, the White River Valley widens and becomes a deep, broad graben to the south, with a depth of more than 5,000 ft (see Section 4.4.1.4).

4.4.1.4 HORSE, GRANT, AND QUINN CANYON RANGES

At the southern side of the White River caldera in northern Nye County, Nevada, the east-striking, oblique-slip Currant Summit fault zone (Moores et al., 1968; Williams and Taylor, 2002), part of the Prichards Station transverse zone, structurally separates the White Pine Range to the north from the small, 20-mi-long, north-trending Horse Range to the south. The Horse Range consists of east-dipping, lower to middle Paleozoic sedimentary rocks (Plates 4 and 8, Cross Section U—U'). The Horse Range is uplifted on its western side against thick, east-dipping volcanic rocks and basin-fill sediments to the west. The basin-fill sediments fill Horse Camp Basin (Moores et al., 1968; Brown and Schmitt, 1991), and the volcanic rocks form the eastern flank of the northern Grant Range and underlie the basin.

The Grant Range is 40-mi-long, increasing in width southward. It, in turn, passes into the high, broad Quinn Canyon Range to the south, which is 15 mi north-south by 20 mi east-west. All these ranges are bounded on the west by the deep graben of Railroad Valley. The crests of the Horse, Grant, and Quinn Canyon ranges thus define the boundary between the Railroad Valley Flow System to the west and the WRFS to the east. On the east, the Horse and Grant ranges are bounded by the large, deep graben of White River Valley. The Grant Range is underlain mostly by east-dipping Cambrian through Permian carbonate rocks (Lumsden et al., 2002) cut by several east-verging Sevier thrust faults (Taylor et al., 2000) and, in turn, intruded by a large Tertiary pluton in the central and southern parts of the range (Plates 4 and 8, Cross Section Q—Q'). Low-angle Tertiary detachment faults dip into Railroad Valley from both sides, especially the Grant Range on the east. Many subsurface detachments were detected during widespread exploration for oil in Railroad Valley (Lund et al., 1991; Schalla and Johnson, 1994; French and Schalla, 1998; Ehni and Faulds, 2002). The carbonate rocks plunge generally northward in the range, so Cambrian and Precambrian siliciclastic rocks and the Tertiary intrusive rocks form the core of the southern Grant Range and likely act as a barrier to groundwater flow between Railroad and White River valleys.

The Quinn Canyon Range, south of the Grant Range, is bordered by Garden Valley to the east, the southern end of Railroad Valley to the north and northwest, and Penoyer Valley (Sand Spring Valley) to the south. Garden Valley is a narrow graben several thousand feet deep, between the Quinn Canyon and Golden Gate Ranges (Plates 4 and 8, Cross Sections T—T' and Q—Q'). The Quinn Canyon Range is underlain by all or parts of several calderas (E.B. Ekren, 2002 to 2004, unpublished mapping), making up the southeastern part of what is referred to on Plate 1 as the central Nevada

caldera complex. This feature, called a caldera complex by Best et al. (1993) and Scott et al. (1995), is not, however, a true caldera complex because not all of it has subsided as a caldera; instead, individual calderas are separated by pre-caldera rocks, so it might better be considered a cluster of adjacent calderas. The southwestern end of the Quinn Canyon Range, including the southern edge of the "caldera complex," passes into Lincoln County, where it is a narrow prong of outflow volcanic rocks. East of this prong and south of the main massive part of the range underlain by the caldera is Penoyer Valley (Sand Spring Valley), which is the single-basin Penoyer Valley Flow System (Harrill et al., 1988).

The calderas of the main mass of the Quinn Canyon Range are underlain by intracaldera (resurgent) plutons (see Plates 4 and 8, Cross Section T—T') that likely limit east-west groundwater flow between Railroad Valley and White River/Garden valleys. Geologically permissible fault conduits between Railroad Valley and Penoyer Valley are likely limited due to the presence of a buried caldera margin and perhaps the strong range-front fault along the western side of the Quinn Canyon Range. White River Valley is a broad, deep graben within the WRFS. Gravity surveys on its eastern side (Scheirer, 2005) suggest that it is underlain by many thousands of feet of basin-fill sediments and volcanic and carbonate rocks. We interpret that the White River Valley contains as much as 5,000 ft of valley fill (Plates 4 and 8, Cross Section T—T'). It is geologically permissible that groundwater passes from southwestern White River Valley to Garden Valley.

4.4.1.5 WORTHINGTON MOUNTAINS AND TIMPAHUTE RANGE

The northern end of the narrow, 15-mi-long, north-trending Worthington Mountains is just southeast of the Quinn Canyon Range. The Worthington Mountains define the northeastern side of Penoyer Valley and the western side of southern Garden Valley. The Worthington Mountains is mostly west-dipping Ordovician through Mississippian rocks that are uplifted along a north-striking fault on the eastern side of the range. The range contains the east-verging Freiburg thrust, which placed Ordovician rocks on Ordovician and Devonian rocks during Sevier deformation (Taylor et al., 2000).

The Worthington Mountains extend southward into the Timpahute Range, an east-trending block of heavily faulted mountains. The two ranges form the boundary between the WRFS on the east and the Penoyer Valley Flow System on the west. The Timpahute Range separates the southeastern side of Penoyer Valley from northern Tikaboo Valley. The Timpahute Range is underlain by Upper Cambrian through Permian sedimentary rocks, unconformably overlain by Tertiary volcanic rocks. The Paleozoic rocks are cut by several Sevier thrusts, the lowest of which places Devonian rocks over Devonian through Permian rocks. The uppermost thrust places Cambrian through Ordovician rocks above younger rocks (Taylor et al., 1994). The western end of the range includes the Tem Piute mining district of tungsten and silver, associated with two Tertiary granite stocks. The range is heavily broken by north-south basin-range faults and synchronous east-west faults. The east-west faults, which define the southern margin of the range, are part of the Timpahute transverse zone, which also controls the northern side of the Caliente caldera complex.

Garden Valley, east of the Worthington Mountains, terminates southward against the eastern Timpahute Range. Garden Valley is a graben containing about 3,000 ft of basin-fill sediment (Plates 4 and 8 Cross Section T—T'). Penoyer Valley is bounded on the east by a range-front fault and on the south by the east-west Timpahute transverse zone. Penoyer Valley probably contains several thousand feet of basin-fill sediments.

Groundwater flow to the west is possible through the carbonate rocks of the southern Worthington Mountains because of the north-northeast-striking faults connecting Garden Valley with Penoyer Valley at the northern end of the Worthington Mountains. This flow, however, has been considered minor by Belcher (2004) and for the purposes of this study is deemed unlikely (Figure 4-10). The eastern Timpahute Range is underlain by a granitic pluton and, therefore, groundwater flow between Garden Valley and the eastern arm of northern Tikaboo Valley is unlikely.

4.4.1.6 GOLDEN GATE RANGE, MOUNT IRISH, PAHRANAGAT RANGE, AND NORTHERN SHEEP RANGE

The Golden Gate Range is a 40-mi-long, low string of north-trending faulted hills that passes southward into Mount Irish, a 10-mi by 10-mi massif bounded by east-striking faults. Mount Irish is the northernmost part of the larger, 35-mi-long Pahranagat Range, which continues southward to the 50-mi-long Sheep Range. The northern end of the Golden Gate Range, located in Nye County, Nevada, forms the western side of White River Valley and the eastern side of Garden Valley. The main part of this range forms the boundary between Garden and Coal valleys in Nye and Lincoln counties. In Nye County, the Golden Gate Range consists of Devonian through Pennsylvanian rocks overlain by Tertiary volcanic rocks. Here and farther south, the range is a west-tilted horst; the main controlling normal fault is on the eastern side. In Lincoln County, the rocks of the Golden Gate Range are Devonian to Pennsylvanian sedimentary deposits, of which Ordovician through Devonian rocks are thrust over Devonian to Mississippian rocks (Plates 4 and 8, Cross Section T—T'). In the central Golden Gate Range, the range is cross cut by two faults related gaps that would allow groundwater to flow in a west to east direction into Coal Valley.

The Mount Irish Range is a stubby, east-trending block that is the eastern continuation of the Timpahute Range and is controlled by east-striking faults of the Timpahute transverse zone. Mount Irish is made up of Ordovician through Mississippian rocks containing the same thrusts that occur in the Timpahute Range (Plates 4 and 8, Cross Section S—S') (Taylor et al., 1994 and 2000). The Mount Irish block closes the southern end of Coal Valley and it is unlikely that north-striking faults through the block allow groundwater flow between Coal Valley and Pahranagat Valley to the south.

The Pahranagat Range, including a separate parallel structural block along the eastern side that is called the East Pahranagat Range, is bounded by Tikaboo Valley on the west and shallow Pahranagat Valley on the east. At their southern ends, the Pahranagat and East Pahranagat Ranges are separated from the northern Sheep Range by a series of east-northeast-striking splays of the left-lateral Pahranagat shear zone. The southern splay is the Maynard Lake fault zone (Plates 5 and 9, Cross Section A—A') (Jayko, 1990). The western part of the splay is interpreted to join the main north-south normal fault that defines the western side of the Sheep Range. Under this interpretation, the Maynard Lake zone is an accommodation or transfer fault that transfers east-west pulling apart into left-lateral shear. In this scenario, in those places where faults strike north, all east-west extension is taken up by normal movement down the dip of the fault plane, and where faults strike northeast, east-west pulling apart is taken up by oblique (left-lateral and normal) movement. The Pahranagat Range is a horst bounded on both sides by major normal faults (Plates 4 and 8, Cross Sections M—M' and N—N'). In the north, the range dips gently west but in the south it is a syncline. The east-verging Gass Peak thrust of Sevier age runs the length of the range, placing Middle Cambrian to Devonian rocks on Devonian to Mississippian rocks. The East Pahranagat Range locally consists of an overturned fold of Devonian to Pennsylvanian rocks. Tertiary volcanic rocks

unconformably overlie the folded and thrust-faulted Paleozoic rocks and are thickest where downfaulted into a graben between the Pahranagat Range and East Pahranagat Range.

The northern Sheep Range is a simple, narrow, and abrupt horst of Cambrian and Ordovician sedimentary rocks. The Pahranagat and Sheep ranges are the boundary between the WRFS on the east and the DVFS on the west, so flow between them is generally unlikely. It is geologically likely, however, that the subparallel faults of the Pahranagat shear zone provide conduits from southern Pahranagat Valley through the Pahranagat Range to Tikaboo Valley South.

4.4.1.7 Southern Sheep Range, Las Vegas Range, and Elbow Range

The southern Sheep Range is generally composed of Cambrian through Devonian carbonate rocks that dip mostly eastward (Plates 5 and 9, Cross Sections G—G', H—H', and I—I') (Guth, 1980). The range is a large horst block defined by north-striking, normal basin-range faults on its eastern and western sides, the eastern fault having the greatest offset. Within the range, minor north-striking faults dominate, but some cross-faults that strike east to east-northeast also have been mapped. The low-angle Gass Peak thrust underlies most of the range. It has transported Late Proterozoic to Cambrian quartzite and Cambrian to Ordovician carbonate rocks eastward over Cambrian to Mississippian rocks.

A small north-trending range, the northern end of which terminates against the Maynard Lake fault zone, lies just east of the northern end of the Sheep Range. This basin-range tilt block consists largely of east-dipping volcanic rocks (Jayko, 1990) that rest unconformably on Pennsylvanian and Permian carbonate rocks. North-striking normal faults on its western side and within this range pass into the Maynard Lake fault zone and transfer the normal slip to oblique slip. The buried north-striking trace of the Gass Peak thrust fault passes beneath the normal faults. In concert with the faults of the Pahranagat shear zone, it is likely that the normal faults carry groundwater from southern Pahranagat Valley to Coyote Spring Valley.

The Las Vegas Range northwest of Apex is defined by the Gass Peak thrust, which transported rocks as old as the Cambrian Wood Canyon Formation eastward over Mississippian, Pennsylvanian, and Permian carbonate rocks of the Bird Spring Formation (Plates 5 and 9, Cross Section F—F') (Maldonado and Schmidt, 1991). Most of the range is made up of folded Bird Spring limestone, with the Gass Peak thrust exposed along its western side (Maldonado and Schmidt, 1991; Page, 1998). The small Elbow Range, which bounds the Las Vegas Range on the northeast, is made up of thrusted and folded Bird Spring Formation (Page and Pampeyan, 1996). The folds and thrusts in the Las Vegas and Elbow ranges strike north and it is geologically likely that they provide conduits for groundwater flow.

4.4.1.8 Cherry Creek Range

The Cherry Creek Range is in northern White Pine and southern Elko Counties, just northeast of the WRFS. The range is a large horst of gently west-dipping Precambrian through Permian sedimentary rocks. Basin-range faults separate it from Butte Valley on the west and from Steptoe Valley on the east; the bigger fault is on the east. The high range separates two north-flowing basins, with the Ruby Valley Flow System on the west and the GVFS on the east. Butte Valley is part of the GVFS (Harrill et al., 1988).

A thin sliver of bedrock cored by a Tertiary intrusion connects the Cherry Creek Mountains with the northern Egan Range. A northeast-striking oblique-slip, also left-lateral and down-to-the-west, cuts through the southern end of this sliver. It is geologically permissible that this fault provides an avenue for minor groundwater to flow between Butte Valley South and Steptoe Valley (Figure 4-10). The Tertiary intrusion north of this fault localized the Cherry Creek mining district, which produced gold, silver, and base metals. This pluton, along with Precambrian and Cambrian quartzite into which it was intruded, form a likely barrier to groundwater flow north of the fault. The west dip of the rocks in the Cherry Creek Mountains would facilitate flow of recharge westward toward Butte Valley.

4.4.1.9 NORTHERN EGAN RANGE

Like the Cherry Creek Mountains to the north, the Egan Range is a high, north-trending horst of Precambrian through Permian rocks, unconformably overlain by Tertiary volcanic rocks. The major basin-range fault zone that uplifted the Egan Range is along the eastern side. The vertical displacement along this fault is as much as 20,000 ft. The range continues southward for 70 mi in White Pine County, then another 40 mi in Lincoln County. In the northern end of the range, the rocks dip westward and are intruded by Tertiary stocks. The Snake Range decollement is present here as a thin skin of Paleozoic rocks at the crest of the range and along its western slope (Plates 4 and 8, Cross Section X—X'). The decollement is a Tertiary detachment fault that transported rocks as old as Middle Cambrian eastward and placed them on top of older rocks. Butte Valley is to the west and Steptoe Valley is to the east of the northern Egan Range.

About 20 mi south of the northern end of the Egan Range, the range becomes considerably wider and lower as the Butte Mountains join it from the west and Butte Valley closes. Here the range is broken into a series of horsts and grabens (Plates 4 and 8, Cross Section W—W'). The downthrown areas on the western side of the Egan Range are underlain by Tertiary volcanic rocks that form low ridges and hills that connect with the southeastern Butte Mountains. The towns of Ely and Ruth, Nevada, occur in this broad, low, heavily faulted part of the Egan Range, in areas called Copper Flat and Smith Valley. A major mining district, the Robinson District, was developed on a series of east-trending ore deposits of copper, lead, zinc, silver, and gold associated with a Cretaceous pluton. Barren Tertiary plutons also are present in the area and extend to Ely on the eastern side of the Egan Range adjacent to Steptoe Valley (Brokaw and Shawe, 1965; Brokaw and Heidrich, 1966; Brokaw and Barosh, 1968; Brokaw, 1973, Brokaw et al., 1973; Jones, 1996). Southwest of the mining district, a series of low hills extends southwest to the White River caldera of the White Pine Range. These hills provide the southeastern margin of Jakes Valley and the north-northwestern margin of White River Valley (Figure 2-1).

South of the Robinson mining district, the Egan Range continues southward for almost 30 mi to the latitude of Lund as a single, high horst of east-dipping Cambrian through Permian rocks that together are more than 30,000 ft thick (Plates 4 and 8, Cross Section V—V') (Kellogg, 1963 and 1964; Taylor et al., 1991). Patches of volcanic rocks overlie the Paleozoic rocks on the eastern edge of the range. Several small plutons also are exposed. Major faults of the horst separate the Egan Range from the White River Valley in the WRFS to the west and southern Steptoe Valley to the east.

Steptoe Valley is a deep graben with as much as 8,000 ft of basin-fill sediments in it. Thus, it is one of the deepest grabens in the central Great Basin. Steptoe Valley is part of the GVFS, in which groundwater flows north (Harrill et al., 1988).

4.4.1.10 SOUTHERN EGAN RANGE

At the latitude of Lund, Nevada, a narrow ridge of Cambrian to Permian rocks extends southeastward from the main part of the Egan Range to the Schell Creek Range to the east. This ridge forms the southern end of Steptoe Valley and the northern end of Cave Valley, which continues southward. The Egan and Schell Creek Ranges continue southward, with Cave Valley between them. Along the western side of Cave Valley (Plates 4 and 8, Cross Section U—U'), the Egan Range is a complexly faulted horst of east-dipping Cambrian to Permian rocks, overlain by Tertiary volcanic rocks. White River Valley is east of the Egan Range. Halfway southward down Cave Valley, at a latitude about 20 mi south of Lund, a northeast-striking oblique-slip fault passes through the Egan Range at Shingle Pass (Plates 4 and 8, Cross Section R—R'). Farther south, the Egan Range remains an east-tilted horst of Cambrian through Tertiary rocks then bends southeast to join the southern end of the Schell Creek Range. Here Cave Valley terminates where the Egan and Schell Creek ranges join each other in a complex of north-northeast- and north-northwest-striking normal and oblique-slip faults. Farther south, the combined Egan and Schell Creek ranges become a low, narrow, north-northwest-striking horst of faulted Paleozoic sedimentary rocks and Tertiary volcanic rocks (Plates 4 and 8, Cross Section Q—Q') that topographically continues southward to the northern end of the North Pahroc Range.

Cave Valley is part of the WRFS and consists of two distinct but connected portions, separated by the oblique-slip fault at Shingle Pass. One of these portions, northern Cave Valley, is a narrow graben with mostly east-dipping Cambrian rocks at shallow depth and containing relatively thin basin-fill sediments (Plates 4 and 8, Cross Section U—U'). It is geologically permissible that the fault at Shingle Pass provides a conduit for groundwater flow from northern Cave Valley into White River Valley (Figure 4-10). Gravity data (Scheirer, 2005) and oil test well logs (Hess, 2004) indicate that the base of combined basin-fill sediments and volcanic rocks is about 3,000 ft below the valley floor.

The other portion of the valley, southern Cave Valley in Lincoln County, is a tilt block bounded by the high fault scarp of the Schell Creek Range to the east. In other words, the east-dipping Cambrian through Permian succession of the Egan Range passes beneath the valley to terminate against the range-front fault of the Schell Creek Range (Plates 4 and 8, Cross Section R—R'). Nonetheless, a groundwater connection between northern and southern Cave Valley is likely because of the north-striking range-front fault of the Egan Range; however, the southeast-dipping strike ridge south of the Shingle Pass fault continues across Cave Valley and contains the Chainman Shale based on oil test well drilling and gravity surveys (Hess, 2004; Mankinen et al., 2006; Scheirer, 2005). Southern Cave Valley generally contains less than 3,000 ft of basin-fill sediments and volcanic rocks. In a narrow, central, north-trending axial part of the valley, however, these Cenozoic rocks are 6,000 ft or more thick. McPhee et al. (2005 and 2007) provided information on faults on the eastern side of the basin based on AMT profiles. At the southern end of Cave Valley, a series of northwest-trending right-lateral faults forms the boundary between southern Cave Valley, northern Pahroc Valley, and northern Dry Lake Valley. These faults provide permissible groundwater pathways out of southern Cave Valley into northern Pahroc Valley, and then potentially into northern Dry Lake Valley.

4.4.1.11 SEAMAN RANGE

The 35-mi-long, heavily-faulted Seaman Range, located in Nye and Lincoln counties, trends north and northwest and joins the Golden Gate Range at the northern end of both ranges (Section 4.4.1.6).

Coal Valley, between the two ranges, is a graben containing several thousand feet of basin-fill sediments (Plates 4 and 8, Cross Section T—T'). The valley is bounded on the south by the Timpahute Range. At its northern end, the Seaman Range is low and bounds the southern end of the White River Valley. In Nye County, the Seaman Range is made up of Devonian to Pennsylvanian sedimentary rocks, overlain unconformably by Tertiary volcanic rocks (du Bray and Hurtubise, 1994). In Lincoln County, the Seaman Range is made up of gently west-dipping Ordovician to Pennsylvanian rocks that are unconformably overlain by Tertiary volcanic rocks. The Tertiary volcanic rocks include the dacitic to rhyolitic Seaman volcanic center of flows and subordinate tuffs and a central plug (du Bray and Hurtubise, 1994). The Seaman Range is within the central part of the WRFS, and it is geologically likely that northwest-trending faults along Seaman Wash (southern end of the range) likely form conduits for movement of groundwater between Coal Valley and Pahroc Valley (Figure 4-10).

4.4.1.12 NORTH PAHROC, SOUTH PAHROC, AND HIKO RANGES

The North Pahroc Range extends south from the junction with the southern Egan and Schell Creek ranges for 40 mi. It is separated from the smaller South Pahroc Range by an east-trending belt of faulted rocks of low relief formed by the east-striking Timpahute transverse zone. The belt of faulted rocks is the boundary between Dry Lake Valley to the north and Delamar Valley to the south. The Seaman (Section 4.4.1.11) and the North Pahroc ranges join together at their southern ends, and the Hiko Range continues south of this intersection. The Hiko Range is a small range parallel to and west of the South Pahroc Range and east of northern Pahranagat Valley. The South Pahroc Range extends southward from the North Pahroc Range and forms the western boundary of Delamar Valley. The South Pahroc Range connects with the Hiko Range at their southern ends to form the eastern boundary of southern Pahranagat Valley. The ephemeral channel of the White River flows from White River Valley along the western side of the North Pahroc Range. The channel is deeply incised through Tertiary volcanic rocks at White River Narrows then enters the Pahranagat Valley north of the town of Hiko, where the ephemeral channel is called Pahranagat Wash. Pahranagat Valley is a graben west of the Hiko Range that contains volcanic and Paleozoic bedrock at shallow depth (Plates 4 and 8, Cross Sections S—S', O—O', and N—N').

The North Pahroc Range consists of upper Paleozoic rocks overlain by Tertiary volcanic rocks. These rocks dip west off major faults along the eastern side of the range. The South Pahroc Range is a series of west-tilted blocks of volcanic rocks; the main faults are on the eastern side of the range. The Hiko Range consists of Devonian rocks and overlying volcanic rocks that dip east, off the normal fault that separates the range from the floor of Pahranagat Valley. The South Pahroc and Pahranagat ranges terminate to the south against the east-northeast-trending Pahranagat shear zone, which also terminates Pahranagat and Delamar valleys.

Dry Lake Valley is a deep graben (Plates 4 and 8, Cross Sections T—T', P—P', and S—S') east of the North Pahroc Range that contains in most places 3,000 to 5,000 ft of basin-fill sediments (Mankinen et al., 2006) but locally along the axis of the graben as much as 10,000 ft of sediments and underlying downfaulted volcanic and carbonate rocks (Scheirer, 2005). Delamar Valley, just south of Dry Lake Valley, is a southward-deepening graben with a general maximum thickness of more than 3,000 ft of basin-fill sediments east of the South Pahroc Range (Mankinen et al., 2006) but locally as much as 5,000 ft of sediments and underlying downfaulted volcanic and carbonate rocks (Scheirer, 2005). All

these basins and ranges are within the WRFS. Groundwater flow is southward in Dry Lake and Delamar valleys (Brothers et al., 1996).

4.4.1.13 SCHELL CREEK RANGE

The northern end of the Schell Creek Range is just south of the northern border of White Pine County. The range continues south for 120 mi, mostly as a high, narrow, north-striking horst. Steptoe and Cave valleys are on the west, and Spring Valley, northern Lake Valley, and northern Dry Lake Valley (Muleshoe Valley) are on the east. The northern part of the Schell Creek Range is made up of a west-dipping sequence of Precambrian through Permian rocks (Lumsden et al., 2002), with overlying Tertiary volcanic rocks along the faulted western flank of the range (Plates 4 and 8, Cross Section X—X'). Small Tertiary intrusions are exposed locally along the range. The main bounding basin-range fault is on the eastern side of the range. The Snake Range decollement is locally exposed at the crest of the Schell Creek Range. This detachment transported Middle Cambrian and younger rocks eastward over Lower Cambrian and older rocks (Figure 4-8). About 10 mi northeast of Ely, two north-northeast-striking faults form a graben, Duck Creek Valley, in the range (Plates 4 and 8, Cross Section W—W'). The southern half of the Schell Creek Range along Cave Valley contains a narrow, heavily faulted sequence of Precambrian through Tertiary rocks that dips east. Here the dominant fault is on the western flank of the range. West of the Geyser Ranch (Plates 4 and 8, Cross Section U—U') the rocks are mostly Late Proterozoic and Cambrian quartzite (Van Loenen, 1987), but farther south the rocks are dropped down along an east-trending fault at Patterson Pass and are mostly of middle to upper Paleozoic and Tertiary age (Plates 4 and 8, Cross Section R—R'). Where the Schell Creek Range joins the Egan Range, a Tertiary pluton has mineralized adjacent carbonate rocks at the Silver King Mine (Plates 4 and 8, Cross Section Q—Q').

Spring Valley is a broad, deep graben within the GSLDFS that is discussed in Section 4.4.2.4. On the southwestern side of Spring Valley, a thin ridge of gently northeast-dipping Pennsylvanian and Permian carbonate rocks extends southeast from the central Schell Creek Range to the Fortification Range. Spring Valley continues southeast on the eastern side of the Fortification Range. South of the thin carbonate ridge is Lake Valley, between the Schell Creek Range and the Fortification Range. Lake Valley contains at least 2,000 ft of basin-fill sediments throughout its 60-mi length but locally the sediments may be much thicker (Plates 4 and 8, Cross Sections U—U', R—R', and Q—Q') (Scheirer, 2005). Lake Valley is part of the MVFS, a subsystem of the WRFS. At the thin ridge between the Fortification Range and the Schell Creek Range, the combination of carbonate rocks here and a north-south fault cutting through would seem to create the potential for groundwater flow between southern Spring and northern Lake valleys, but the Chainman Shale, at shallow depth beneath the thin ridge, probably creates a barrier to flow, and we consider flow unlikely. The Schell Creek Range forms the northwestern boundary of Lake Valley for about 20 mi southward until it bends south-southwest to join the Egan Range.

Because much of the Schell Creek Range is covered by Precambrian to Cambrian quartzite, the range forms a barrier to flow between much of Steptoe Valley and Spring Valley. The only geologically possible groundwater routes between these valleys is around the northern end of the Schell Creek Range, along the faults that define and continue northeast from Duck Creek Valley, or through middle to upper Paleozoic carbonate rocks at and south of Conners Pass where U.S. Highway 50 crosses the range, but we consider significant flow as unlikely. On the eastern side of northern Cave Valley, the Schell Creek Range is also cored by Precambrian to Cambrian quartzite, creating a likely barrier to

flow between northern Cave Valley and Lake Valley (Figure 4-10). South of Patterson Pass, the quartzite sequence is down-faulted and carbonate and volcanic rocks and cross faults are present, but it is unlikely that groundwater flows between southern Cave Valley and Lake and northern Dry Lake valleys. Range-front faults on both sides of the southern Schell Creek Range likely inhibit this flow.

Northern Dry Lake Valley contains at least several thousand feet of basin-fill sediments (Plates 4 and 8, Cross Section Q—Q'), and gravity surveys (Scheirer, 2005) indicate that about 3,000 to more than 6,000 ft of basin-fill sediments plus underlying downfaulted volcanic rocks underlie most of the valley. It is geologically likely that some groundwater flows southward from Lake Valley through fault conduits at Muleshoe Pass, between the Schell Creek Range and the northern Fairview Range (Figure 4-10). It is permissible that groundwater locally follows paths in carbonate rocks, cross faults, and the caldera margin in the northern Fairview Range (Rowley, 1998). From northern Dry Lake Valley, groundwater passes south along fault conduits into the main part of Dry Lake Valley (Harrill et al., 1988).

4.4.1.14 FAIRVIEW, BRISTOL, WEST, ELY SPRINGS, HIGHLAND, BLACK CANYON, BURNT SPRING, AND CHIEF RANGES, AND PIOCHE HILLS

From north to south, the Fairview, Bristol, Highland, and Chief Ranges are a 60-mi-long group of north-trending, heavily faulted ranges of mostly east-dipping rocks. These in-line horsts and tilt blocks lie west of Lake and Panaca (Meadow) valleys. From north to south, the West, Ely Springs, Black Canyon, and Burnt Spring ranges are small horsts along the western side of the Bristol, Highland, and Chief ranges. Northern Dry Lake (Muleshoe) Valley is west of the Fairview Range, and the rest of Dry Lake Valley is west of the West, Ely Springs, Black Canyon, and Burnt Spring ranges. The Pioche Hills, which extends southeast from the eastern side of the southern Bristol Range, separates Lake Valley on the north from Panaca (Meadow) Valley on the south. All the ranges are separated by normal and oblique-slip (left-lateral and right-lateral, normal) faults.

The Fairview Range touches the Schell Creek Range across Muleshoe Pass, through which runs the range-front faults for both the Schell Creek and Fairview Ranges. The Fairview Range is a horst made up of Devonian to Pennsylvanian rocks at both the northern and southern ends of the range. The central part of the range consists of the western lobe of the Indian Peak caldera complex. The low pass between the Fairview Range and the Bristol Range is cut by numerous east-striking faults of the Blue Ribbon transverse zone, which crosses the entire Great Basin at about this latitude (Rowley, 1998; Rowley and Dixon, 2001).

The Bristol Range is a horst that consists mostly of an east-dipping sequence of Cambrian carbonate rocks. The range is cored by a Tertiary pluton on the northern end that is associated with silver deposits of the Jackrabbit and Bristol districts. A low angle, west-dipping detachment or gravity-slide fault that placed Devonian rocks on Cambrian rocks is exposed in the northwestern part of the range (Page and Ekren, 1995). The Highland Range, the southward continuation of the Bristol Range, consists of east-dipping Cambrian carbonate rocks, underlain by Precambrian and Cambrian quartzite. A west-dipping, west-verging, moderately dipping fault on the western side of the range, the breakaway part of the Highland detachment fault, placed the younger carbonate rocks on the older quartzite. The Chief Range, south of the Highland Range, is made up of east-dipping Precambrian and Cambrian quartzite that is unconformably overlain by Tertiary volcanic rocks and cut by a Tertiary pluton that controls the small Chief gold district. The faults that lift the range on the western

side consist of an oblique-slip fault (right lateral and normal) and the west-dipping Highland detachment fault (Rowley et al., 1994).

The small West Range, to the west of the northern Bristol Range, consists of Devonian sedimentary rocks and Tertiary volcanic rocks on which Devonian rocks are emplaced by a low-angle fault that can be interpreted as either a detachment fault or a gravity-slide plane (Plates 4 and 8, Cross Section T—T') (Page and Ekren, 1995). The Ely Springs Range, south of the West Range and northwest of the Highland Range, consists of Cambrian through Silurian rocks, overlain by Tertiary volcanic rocks. The Black Canyon Range, south of the Ely Springs Range and southwest of the Highland Range, consists of Cambrian sedimentary rocks and Tertiary volcanic rocks (Plates 4 and 8, Cross Section P—P'). The Burnt Springs Range, southwest of the Black Canyon Range, consists of Cambrian sedimentary rocks unconformably overlain by Tertiary volcanic rocks (Plates 4 and 8, Cross Section S—S').

The Pioche Hills consists of Cambrian sedimentary rocks unconformably overlain to the northeast by Tertiary volcanic rocks. The hills contain the major Pioche lead-zinc-silver mining district, which is controlled by its proximity to the margin of the Indian Peak caldera complex. The margin includes caldera-collapse megabreccia and caldera ring dikes. Panaca (Meadow) Valley, south of the Pioche Hills, is probably at least 5,000 ft thick (Plates 4 and 8, Cross Section P—P') and is filled with Pliocene to upper Miocene basin-fill sediments of the Panaca Formation (Rowley and Shroba, 1991).

The presence in the Bristol, Highland, and Chief ranges of near-surface Late Proterozoic to Cambrian quartzite results in a likely barrier to groundwater flow between Lake, Patterson (southern Lake) and Panaca (Meadow) valleys to the east and Dry Lake Valley to the west (Figure 4-10). In the Fairview Range, a likely barrier to flow may result from the Indian Peak caldera complex due to probable subsurface intracaldera intrusions and their contact metamorphic and hydrothermal products. Geologically likely conduits to flow through and around the Fairview Range include the faults between Lake and northern Dry Lake valleys, through Muleshoe Pass (Figure 4-10). East-striking faults of the Blue Ribbon transverse zone are mapped between the Fairview and Bristol ranges; however, their hydrologic significance is unknown (Prudic et al., 1995; Rowley, 1998; Rowley et al., 2001). The Pioche Hills could likely form a partial flow barrier due to the presence of Proterozoic to Cambrian shale and quartzite in the range, but this barrier is localized and likely serves only to direct groundwater around the Pioche Hills along fault zones bounding and within the range.

4.4.1.15 DELAMAR MOUNTAINS

The Delamar Mountains extends southward for 40 mi from the Burnt Springs Range, forming the western side of Delamar Valley and continuing to Coyote Spring Valley. The boundary between the Delamar and Burnt Spring ranges is the western extension of the northern caldera wall of the Caliente caldera complex, here controlled by the east-trending Timpahute transverse zone (Ekren et al., 1976; Swadley and Rowley, 1994; Rowley, 1998). The eastern side of the northern Delamar Mountains is the perennial, south-flowing Meadow Valley Wash, which drains Panaca (Meadow) Valley, passes south through Caliente, Nevada, and then creates beautiful Rainbow Canyon that separates the Delamar Mountains from the Clover Mountains to the east. The stream becomes ephemeral at the southern end of Rainbow Canyon, but in the Pleistocene it was part of through-flowing drainage that joined the Muddy River at Glendale, Nevada, and from there to the Colorado River. The eastern side

of the southern Delamar Mountains is Kane Springs Valley, to the east of which is the Meadow Valley Mountains.

The Delamar Mountains consists of east-dipping Late Proterozoic to Cambrian rocks and Tertiary volcanic rocks. The range, however, is dominated by Tertiary caldera complexes. The western end of the Caliente caldera complex is in the northern part of the range, and the Kane Springs Wash caldera complex is in the central part of the range (Plates 4 and 8, Cross Sections N—N', D—D', and C—C') (Rowley et al., 1995; Scott et al., 1995 and 1996). The main bounding fault of the Delamar Mountains is the down-to-the-west normal fault on the western side, and this is joined from the southwest by several splays of the left-lateral Pahranagat shear zone (Ekren et al., 1977). In Kane Springs Valley, the bounding fault is the oblique (left-lateral and normal down-to-the-west) Kane Springs Wash fault zone (Swadley et al., 1994). Flow from southern Delamar Valley is likely through the Pahranagat shear zone and north-striking normal faults into Pahranagat and Coyote Springs valleys (see Figure 4-10).

Late Proterozoic to Cambrian quartzite and shale and Tertiary caldera complexes form an effective barrier to groundwater flow between Delamar Valley and valleys to the east (Figure 4-10). The calderas are barriers primarily because of their underlying intracaldera intrusions and both hydrothermal clays and contact-metamorphic rocks formed by emplacement of the intrusions into intracaldera tuffs. North- and northeast-striking basin-range faults just west of the calderas provide geologically likely conduits for groundwater to Pahranagat and Coyote Springs Valleys.

4.4.1.16 MEADOW VALLEY MOUNTAINS

The Meadow Valley Mountains constitute a narrow, generally low, north-northeast-trending range about 40-mi-long. The northern 30 mi of the range consists mostly of outflow ash-flow tuffs and part of the Kane Springs Wash caldera complex (Plates 4 and 8, Cross Section C—C'). The southern end of the Meadow Valley Mountains, just east of Coyote Spring Valley, is made up of mostly thrust-faulted and normally faulted Paleozoic rocks (Plates 4 and 8, Cross Sections C—C', Plates 5 and 9, Cross Sections B—B', E—E', and F—F') (Pampeyan, 1993; LVVWD, 2001). The Meadow Valley Mountains is separated from the Delamar Mountains on the west by Kane Springs Valley, a shallow valley underlain along the eastern side by the oblique-slip (normal, left-lateral) Kane Springs Wash fault zone (Swadley et al., 1994; Harding et al., 1995; Scott et al., 1996). The broad, deep valley of Meadow Valley Wash lies east of the Meadow Valley Mountains and west of the Mormon Mountains (Schmidt, 1994).

It is likely that the Tertiary caldera, north-northeast-striking oblique faults, and thrusts prevent groundwater flow between Kane Springs Valley and the valley of Meadow Valley Wash east of the Mormon Mountains.

4.4.1.17 ARROW CANYON RANGE

The Arrow Canyon Range is a sharp, narrow, north-trending range consisting of a syncline of Cambrian to Mississippian carbonate rocks. It is uplifted along its western side by normal faults of the Arrow Canyon Range fault zone (Plates 5 and 9, Cross Section I—I') (Schmidt and Dixon, 1995; Page and Pampeyan, 1996; Page, 1998). The trace of the north-striking Dry Lake thrust, which carries Cambrian rocks over Silurian through Permian carbonate rocks, is exposed and projected

north just east of the range (Page and Dixon, 1992; Schmidt and Dixon, 1995; LVVWD, 2001). East of the Dry Lake thrust, the Silurian through Permian rocks form a series of low, unnamed, north-trending hills. These hills are controlled by north-striking normal faults, along some of which are Pleistocene carbonate spring-mound deposits that indicate that the faults formerly carried significant groundwater (Schmidt and Dixon, 1995).

The range is within the WRFS. Coyote Spring Valley, on the western side of the Arrow Canyon Range, is underlain by thin basin-fill sediments, generally less than 1,000 ft deep (Plates 5 and 9, Cross Sections L—L', E—E', F—F', and G—G'). Groundwater moves south beneath Coyote Spring Valley (Harrill et al., 1988). It also flows southeast, passing north of the Arrow Canyon Range as well as through the range in its carbonate rocks. The southeast-flowing groundwater is the principal source of the Muddy River Springs Area and the Muddy River (Schmidt and Dixon, 1995).

4.4.1.18 Fortification Range, Wilson Creek Range, and White Rock Mountains

The Fortification Range is a narrow, locally high, north-northwest-trending range about 20-mi-long. The range is a horst bounded on both sides by normal faults. Northern Lake Valley is on the west, and the southern end of Spring Valley is on the east. The northern half of the Fortification Range is a series of faulted, upper Paleozoic carbonate rocks including, at the northern end, a narrow, low, north-northwest-trending, northeast-dipping cuesta that joins the eastern side of the Schell Creek Range. This low ridge, which separates Spring Valley on the northeast from Lake Valley on the southwest, is a groundwater divide, as noted in Section 4.4.1.13. Geological reasons for the ridge being a groundwater divide is that it is bounded on the northeastern side by a northwest-striking fault and the ridge is underlain by the Chainman Shale, which is probably more than 1,000 ft thick (Plates 4 and 8; Cross Sections U—U'). The northern Fortification Range is complexly faulted and contains repeated sections of the Chainman Shale beneath the surface. The presence of the Chainman in the fault blocks likely restricts groundwater flow through the northern half of the range.

The southern half of the Fortification Range consists of east-dipping volcanic rocks (Loucks et al., 1989), part of which we interpret to be intracaldera rocks of the Indian Peak caldera complex. Due to the Chainman Shale in the northern part of the range and the caldera in the southern part, the range likely marks a groundwater divide between the WRFS and the GSLDFS. The Fortification Range connects at its southern end with the broad Wilson Creek Range beyond a low pass. This pass at the mining town of Atlanta, Nevada, is partly underlain by an east-striking fault, so it is geologically possible that some groundwater moves along it.

The Wilson Creek Range is a complexly faulted, north-northwest-trending range that forks southward, with the continuation of the Wilson Creek Range on the west and with the White Rock Mountains on the east. A small central valley (graben) named Spring Valley separates the two ranges. This valley is called "little" Spring Valley in this report to distinguish it from the much larger Spring Valley to the north. The Wilson Creek Range and White Rock Mountains are each about 35-mi-long and consist entirely of intracaldera volcanic rocks, probably floored by an intracaldera (resurgent) intrusion of the Indian Peak caldera complex (Willis et al., 1987; Best et al., 1989c). The western side of the Wilson Creek Range is bounded by a major normal fault. The valleys to the west of the range are northern Lake and Patterson (southern Lake) valleys; the southern half of northern Lake Valley and all of Patterson Valley are within the Indian Peak caldera. The southern ends of the Wilson Creek Range and White Rock Mountains pass into a series of mostly unnamed, generally low fault blocks of

intracaldera volcanic rocks (Best and Williams, 1997; Williams et al., 1997). These fault blocks continue southward for 10 mi to the southern wall of the Indian Peak caldera. More fault blocks extend southward another 15 mi as outflow volcanic rocks to the Clover Mountains, which is underlain by the Caliente caldera complex. Panaca Summit, traversed by Nevada State Route 319, is a pass through these hills of outflow volcanic rocks.

Because of its underlying intracaldera intrusions, it is geologically likely that the Indian Peak caldera complex is a low-permeability unit with limited groundwater flow through it. However, north-south faults, particularly the range-front faults along Lake, Patterson, and Hamlin valleys, likely provide conduits for southward (Lake and Patterson valleys) and northward (Hamlin Valley) groundwater flow (Figure 4-10).

4.4.1.19 CLOVER MOUNTAINS AND BULL VALLEY MOUNTAINS

The Clover Mountains, Bull Valley Mountains, and Delamar Mountains represent a poorly defined, broad, east-trending, 60-mi-long massif of low mountains made up of heavily faulted volcanic rocks. North-south Rainbow Canyon is a narrow erosional cut made by Meadow Valley Wash near the western part of the massif. The Clover Mountains extends from Rainbow Canyon on the west to about 30 mi to the Utah/Nevada border on the east and from the Panaca (Meadow) Valley on the north to about 25 mi to the Tule Desert on the south. The Bull Valley Mountains extends eastward about 20 mi from the Utah/Nevada border and is about 20 mi north to south. The entire east-trending massif passes into north-trending ranges on all sides. This massif gets its unusual easterly trend because it is cored by the 50-mi by 20-mi Caliente caldera complex (Ekren et al., 1977; Rowley et al., 1995), one of the largest calderas in the United States.

The east-elongated caldera complex is bounded on the north and south by east-trending transverse zones, the Timpahute on the north and the Helene on the south. Locally, the transverse zones are caldera margins. These transverse zones facilitated differential east-west growth (spreading) of the caldera, driven by east-west extension and caldera eruptions. Rowley and Anderson (1996) referred to the complex as a syntectonic caldera. The caldera complex is floored by an intracaldera intrusion of batholithic dimensions, but it is exposed in few places (Plates 4 and 8, Cross Sections N—N' and D—D'). South of the caldera complex, the Clover Mountains is underlain by Paleozoic carbonate rocks cut by a Sevier thrust fault and many high-angle normal faults, but these rocks are blanketed by a thick cover of outflow ash-flow tuff, and they are remote and poorly studied and mapped.

The batholith and the east-trending faults present a likely barrier to southward groundwater flow, but the entire massif is heavily cut by north- and northwest-trending faults, so it is geologically possible that these provide conduits to some flow. Rainbow Canyon allows surface water to move southward via Meadow Valley Wash.

4.4.1.20 MORMON MOUNTAINS

The Mormon Mountains is a nearly circular range, about 18 mi across, east of lower Meadow Valley Wash. The Mormon Mountains represents a dome of mostly Cambrian to Permian rocks, underlain by Early Proterozoic crystalline metamorphic rocks. East-verging Sevier thrust faults placed Cambrian rocks above Cambrian to Mississippian rocks. The range subsequently underwent major uplift, and it now is underlain by prominent positive aeromagnetic and gravity anomalies. Wernicke

et al. (1985) interpreted the range to contain west-verging detachment faults that resulted from late Tertiary extension above a metamorphic core complex. Wernicke et al. (1985) suggested that these detachment faults followed thrust faults within the mountains. Anderson and Barnhard (1993) disputed the detachment hypothesis, and they instead emphasized footwall deformation along normal and oblique-slip, generally high-angle faults that flatten upward and formed during the major domal uplift. Carpenter and Carpenter (1994a) also disputed the detachment hypothesis, partly on seismic data unavailable to Wernicke and colleagues. Carpenter and Carpenter argued for Tertiary extension along high-angle normal faults and explained Wernicke's low-angle structures as representing gravity slides. These interpretations have been largely adopted by Page et al. (2005a) and by this report.

The broad valley of Meadow Valley Wash, to the west and northwest of the Mormon Mountains, is underlain by about 3,000 ft of valley-fill sediments (Plates 5 and 9, Cross Section E—E'). Northwest of the Mormon Mountains, two buried thrust faults have been hypothesized (Plates 4 and 8, Cross Section C—C'). Southwest of the Mormon Mountains, buried Paleozoic carbonate rocks may be present beneath Meadow Valley Wash (Plates 5 and 9, Cross Section B—B'). In this part of lower Meadow Valley Wash, the basin-fill sediments are about 2,000 ft thick. A band of hills continuing southward from the Mormon Mountains is underlain by Paleozoic sedimentary rocks that are cut by Sevier thrust faults, including the Glendale/Muddy Mountains thrust (Plates 5 and 9, Cross Sections E—E' and F—F').

The Mormon Mountains massif represents a barrier to groundwater flow between the eastern side of Meadow Valley Wash and the Tule Desert to the east. However, the low divide north of the Mormon Mountains may provide geological structures that make flow possible in this area. Northwest of the Mormon Mountains, thrust faults may also likely restrict groundwater flow to the east. Southwest of the Mormon Mountains, flow is likely from lower Meadow Valley Wash to the Glendale basin (Section 4.4.1.21) to the south.

4.4.1.21 North Muddy Mountains, Muddy Mountains, and Dry Lake Range

The southeastern end of the geologic study area contains the North Muddy Mountains and, to the south, the Muddy Mountains (Plates 5 and 9, Cross Sections H—H', I—I', and K—K') (Bohannon, 1983). The North Muddy Mountains separate the Glendale basin on the west from the Mesquite basin on the east. The Muddy Mountains occupy the northern side of Lake Mead. West of the Muddy Mountains, the map area includes the small Dry Lake Range east of Apex. This range is made up mostly of Bird Spring carbonate rocks. A narrow arm of bedrock extending west from Apex connects with the southern Arrow Canyon Range/Las Vegas Range. A thin finger of Quaternary sediments at Apex, just west of the Dry Lake Range, most probably was a pathway for Tertiary and Quaternary basin-fill sediments entering the Las Vegas Valley just southwest of the map area. The finger also is along the trace of the north-northeast-striking Dry Lake thrust (Page and Dixon, 1992). Basin-fill sediments to the northeast along the I-15 corridor (Glendale basin) are not connected with those in the Las Vegas Valley and, based on limited mapping in the area, are not correlated with those in the Las Vegas Valley.

In the Muddy Mountains and North Muddy Mountains, high-angle faults strike north-northeast (Bohannon, 1983), and the east-west gap between the two ranges, now occupied by Tertiary and Quaternary basin-fill sediments, likely also is underlain by fractures of the same strike. The northern Muddy Mountains and North Muddy Mountains contain significant Jurassic sedimentary rocks

(Bohannon, 1983), including the Aztec Formation. The Aztec Formation and other Jurassic sandstone units have low permeability and thus form a confining zone. The northwestern side of the North Muddy Mountains is made up of upper Paleozoic carbonate rocks, which suggests that it is geologically permissible that they allow southward and southeastward groundwater flow (Figure 4-10) (Eichhubl et al., 2004). Mesozoic sedimentary rocks in the eastern North Muddy Mountains and the Muddy Mountains may also allow southward flow to Lake Mead. A possible flow barrier is provided by east-striking faults of the northern Muddy Mountains. These faults include the northeast-verging Glendale/Muddy Mountains thrust (Figures 4-6 and 4-7) (Bohannon, 1983; Carpenter and Carpenter, 1994b). Bohannon interpreted this structure as the northern continuation of the Keystone thrust zone, which has been displaced approximately 40 mi right laterally by the Las Vegas Valley shear zone. As with the Keystone/Glendale/Muddy Mountains thrust zone, the Dry Lake thrust just west of the Keystone/Glendale/Muddy Mountains thrust has been displaced 40 mi by the same shear zone; its southern equivalent is the Deer Creek thrust in the Spring Mountains. Farther east in the North Muddy Mountains, the Summit/Willow Tank thrust is exposed (Plates 5 and 9, Cross Section J—J') (Bohannon, 1983, 1984, and 1992; Carpenter and Carpenter, 1994b).

The southeastern edge of the geologic study area, where the Muddy and Virgin rivers enter the Overton Arm of Lake Mead, is probably an area of groundwater discharge. Basin-fill sediments, dominated at the surface by resistant Quaternary calcretes, underlie Mormon Mesa and its northward extension. This prominent calcrete is underlain by Pliocene to upper Miocene basin-fill deposits making up the southwestern end of the Mesquite basin. The Black Mountains and Gold Butte areas, respectively west and east of Lake Mead, contain Proterozoic metamorphic rocks that extend northward to the southwestern Virgin Mountains. Numerous fault zones have been mapped here and in the northeastern end of the Muddy Mountains, including northeast-striking faults that are discharge points for Rogers and Blue Point springs in the Lake Mead National Recreation Area. These faults most likely are related to a series of faults that strike northeast, have oblique-slip (left-lateral and normal) motion, and are part of the Lake Mead fault zone (Anderson and Barnhard, 1993).

4.4.2 Basins and Ranges West and East of the White River Flow System

This section discusses the geology and hydrogeology of basins and ranges outside the WRFS and MVFS. The areas are described generally from north to south and west to east.

4.4.2.1 Antelope Range, White Pine County

The Antelope Range, in northeastern White Pine County, Nevada, is a relatively small, low range of faulted, mostly Tertiary volcanic rocks that unconformably overlie mostly west-dipping Silurian to Permian sedimentary rocks, dominantly carbonate rocks. It is a horst between the narrow, northern part of Spring Valley on the west, and Tippett Valley (Antelope Valley) on the east. At its northern end, Spring Valley contains about 2,000 ft of basin-fill sediments. Tippett Valley contains at least 1,000 ft of basin-fill sediments, with thick volcanic rocks beneath these sediments; geophysical data indicate that the depth to the pre-volcanic rocks locally are as much as 5.5 km. The Antelope Range and its bounding valleys are within the GSLDFS. The range likely is a barrier to groundwater flow through it (Figure 4-10), for flow in northern Spring Valley appears to head mostly south, whereas flow in Tippett Valley appears to head mostly north (Harrill et al., 1988).

4.4.2.2 KERN MOUNTAINS AND ADJACENT SMALL RANGES

The Kern Mountains is a 17-mi-long, east-trending range that was structurally controlled by the Sand Pass transverse zone. East-striking faults occur on both the northern and southern sides of the range. The granite core of the Kern Mountains is made up of three separate plutons. These plutons are all biotite-bearing; the largest pluton also contains primary muscovite. The plutons range in age from 75 to 35 Ma (Best et al., 1974; Ahlborn, 1977; Miller et al., 1999). A separate, shallow Tertiary pluton that erupted lava flows occurs on the southeastern side of the range (Gans et al., 1989). A small north-trending range north of the western side of the Kern Mountains and east of Tippett (Antelope) Valley consists mostly of Tertiary volcanic rocks. A small valley, Pleasant Valley, separates the Kern Mountains and the Deep Creek Range to the north. This valley may have as much as 3,000 ft of valley fill (Plates 4 and 8, Cross Section X—X'). Another valley south of the Kern Mountains appears to be shallow.

The Kern Mountains and associated ranges are within the GSLDFS. Because of its core of plutonic rocks, the Kern Mountains forms a likely barrier to groundwater flow through it. However, it is geologically permissible that limited eastward flow may take place along east-striking fault conduits and carbonate rocks south of the mountain block (Figure 4-10).

4.4.2.3 DEEP CREEK RANGE, UTAH

The Deep Creek Range is a north-trending range about 40-mi-long just east of the Nevada-Utah border and northeast of the Kern Mountains. The Deep Creek Range is a horst bounded by north-striking normal faults on either side that separate it from Deep Creek Valley to the west and northern Snake Valley to the southeast. The fault on the eastern side of the Deep Creek Range appears to be the main basin-range fault controlling the range, but the basin-range fault on the western side is also significant, for it drops down Deep Creek Valley, which contains as much as 5,000 ft of basin-fill sediments.

Geologic mapping of the Deep Creek Range began with Nolan's (1935) classic report on the Gold Hill mining district at the northern end of the range. Here, Jurassic, Eocene, and Miocene plutons formed gold, tungsten, arsenic, silver, lead, copper, and zinc deposits in limestone of mostly Pennsylvanian and Mississippian age (Nolan, 1935; Robinson, 1993). Nolan mapped many east-striking faults that he called "transverse faults" and recognized that they cut the range in many places. Rocks in the northern part of the mountains dip east and range from Proterozoic to Cambrian quartzite on the east to Devonian dolomite on the west. In the central part of the range, another Tertiary pluton, the Ibapah granite of 39 Ma (Miller et al., 1999) spans the width of the range. The southern part of the range consists of highly deformed Late Proterozoic quartzite and schist of the McCoy Creek and Trout Creek groups. These Precambrian units have a combined thickness estimated at 19,000 ft (Hintze, 1988; Nutt et al., 1990). West of the southern part of the range, Paleozoic sedimentary rocks dip westward. These rocks range from Late Proterozoic and Cambrian quartzite through Cambrian and Devonian carbonate rocks and Mississippian Chainman Shale. They are cut by many low- to high-angle faults subparallel to the north-northeast-striking beds. The faults include detachments that may represent attenuation deroofing of the Deep Creek Range during its uplift as a core complex (Miller et al., 1999).

The quartzite and plutons that make up the core of the Deep Creek Range form a likely barrier to groundwater flow between Snake and Deep Creek valleys (Figure 4-10). Nonetheless, the range and its bounding valleys are part of the GSLDFS. Groundwater flows north in these valleys. In fact, Snake Valley passes northward into the Great Salt Lake Desert at the latitude of the central Deep Creek Range. The Great Salt Lake Desert is the ultimate sink for groundwater in the flow system (Harrill et al., 1988).

4.4.2.4 SNAKE RANGE AND LIMESTONE HILLS

The Snake Range is a broad, high, north-trending range. It contains Wheeler Peak, more than 13,000 ft high and within Great Basin National Park. The range is about 65-mi-long, nearly all of it in White Pine County, but with the low southern end in Lincoln County. The range is a horst, bounded on both sides by major high-angle normal fault zones. Spring Valley, west of the Snake Range, is a major graben defined by basin-range faults of at least 10,000 ft of vertical displacement. Snake Valley, east of the Snake Range, is a graben containing about 5,000 ft of basin-fill deposits but local holes in the basin contain deposits thicker than this (Plates 4 and 8, Cross Sections X—X', W—W', V—V', and U—U') (Allmendinger et al., 1983; Saltus and Jachens, 1995; Kirby and Hurlow, 2005). Hamlin Valley, southeast of the Snake Range and south of Snake Valley, is similar to Snake Valley in structural size. The Limestone Hills is a narrow, low, heavily faulted cuesta extending about 20 mi south of the Snake Range.

Except for the southern end, the Snake Range is cored by Late Proterozoic to Cambrian quartzite, intruded by a massive batholith of apparent Jurassic age (Whitebread, 1970; Miller et al., 1994 and 1995). The range is a metamorphic core complex, which rose rapidly and formed the Snake Range decollement, a detachment fault (Miller et al., 1999). This low-angle Tertiary detachment formed over an extended period as the range uplifted and stretched the roof rocks apart (Figure 4-8) (Gans, 2000b). The fault places complexly faulted Middle Cambrian carbonate and younger rocks over a lower plate of Middle Cambrian carbonate rocks, Lower Cambrian clastic rocks, and older rocks. The decollement is exposed on the top and eastern side of the northern half of the range. The central part of the Snake Range is narrower and lower. On the eastern side of Sacramento Pass, north-striking, down-to-the-east listric normal faults drop down a thick section of Tertiary volcanic and basin-fill rocks (Gans et al., 1989; Miller et al., 1994, 1995, and 1999). The southern end of the range consists of south-plunging tilt blocks of Paleozoic rocks as young as Mississippian. These tilt blocks become lower in elevation to the south, and the eastern tilt blocks plunge beneath the valley fill. The western tilt blocks continue southward to become the Limestone Hills, which consists mostly of east-dipping Devonian carbonate rocks bounded by normal faults on the western and eastern sides. The Limestone Hills continues southward into the Wilson Creek Range (Section 4.4.1.18). The southern end of the Limestone Hills forms part of the northern wall of the Indian Peak caldera complex.

Spring Valley is a 100-mi-long, broad, deep graben containing about 6,000 ft of basin-fill sediments (Plates 4 and 8, Cross Sections X—X', W—W', V—V', and U—U'). Snake Valley is a similarly long, broad, deep graben that passes southward into Hamlin Valley. Basin-fill sediments are locally more than 5,000 ft thick beneath Snake Valley (Plates 4 and 8, Cross Sections X—X', W—W', and V—V') (Davis, 2005).

The Snake Range and Spring, Hamlin, and Snake valleys are part of the GSLDFS. In northern Spring Valley, groundwater flows partly along north-striking basin-range faults and related fractures but appears to pool in northern Spring Valley (Harrill et al., 1988). Gravity data support a groundwater divide between northern and central Spring Valley, coinciding with a surface-water divide (Mankinen et al., 2006). McPhee et al. (2005 and 2007) used gravity data and an AMT profile across southern Spring Valley, west from the Limestone Hills, to identify many previously unknown faults in the basin-fill sediments, which here are as thick as 3,000 ft. Some of the groundwater in southern Spring Valley flows east through the Limestone Hills into Hamlin Valley (Harrill et al., 1988). From Hamlin Valley, groundwater flows mostly northward into Snake Valley (Davis, 2005) then farther northward to the Great Salt Lake Desert (Harrill et al., 1988). Because of its core of plutons and quartzite, the Snake Range is a groundwater barrier to east or west flow for nearly its entire length. In the Sacramento Pass area in the center of the range, however, it is geologically possible that minor groundwater might flow through it along an east-striking fault and adjacent carbonate and volcanic rocks near Osceola, Nevada. But we consider such flow unlikely because any flow would be at least 1,500 ft below the surface at Osceola. The carbonate rocks and faults that form the Limestone Hills provide the only significant pathway for groundwater flow from southern Spring Valley to Hamlin Valley and from there to southern Snake Valley (Figure 4-10). Hood and Rush (1965) estimated a flow of 4,000 afy through the Limestone Hills.

Fracture flow, as elsewhere in the Great Basin, explains movement of groundwater in Snake Valley. In other words, we interpret that northward groundwater flow beneath Snake Valley is along mostly high-angle, north-striking normal faults in both the basin-fill and carbonate-rock aquifers, few of which can be shown on Plates 1 and 4 because of the scale. We also interpret that these faults formed Snake Valley, resulting in a deep graben, as supported by geophysics and logs of oil wells. Allmendinger et al. (1983) and Kirby and Hurlow (2005), however, suggested that the eastern frontal fault of the Snake Range, separating the range from Snake Valley, is the low-angle Snake Range decollement. The straight range front argues for our interpretation of a high-angle normal fault. Miller et al. (1999), who have studied the Snake Range decollement in the most detail, agree with us and showed (Miller et al., 1999, Figure 10) such a high-angle fault cutting the decollement (Plates 4 and 8, Cross Section W—W').

4.4.2.5 Confusion Range, Conger Range, Burbank Hills, and Tunnel Spring Mountains

The Confusion Range and small ranges of similar rocks form the entire eastern (Utah) side of Snake Valley. The area includes hills (Middle Range) connected to and east of the northern end of the Confusion Range. The Confusion Range proper is 60-mi-long, with a general northerly trend. The Conger Range is a 15-mi-long, southwest-diverging fork in the southern Confusion Range, located northeast of the small communities of Baker, Nevada, and Garrison, Utah. Tule Valley is east of the Confusion Range. The Burbank Hills is a 15-mi-long range south of the Conger Range and southeast of Baker and Garrison. The Burbank Hills is separated from the Conger Range by a northwest-trending valley known as the Ferguson Desert; the Desert may contain several thousand feet of basin-fill deposits (Plates 4 and 8, Cross Section V—V'). The Tunnel Spring Mountains is a narrow, 20-mi-long range southeast of the Burbank Hills and east of northern Pine Valley. Northern Pine Valley connects with the southeastern end of the Ferguson Desert.

All of these ranges consist almost entirely of folded, thrusted, and attenuated, middle to upper Paleozoic rocks that together form a synclinorium, in other words a combination of synclines and

anticlines that overall appear as a broad syncline (Plates 4 and 8, Cross Sections W—W' and V—V') (Hose, 1977; Hintze and Davis, 2002a and b, and 2003). The Mississippian Chainman Shale, 1,000 to 2,000 ft thick in the area, is repeated and thus exposed on both sides of and beneath all these ranges because it is deformed into north-striking folds (Hintze and Davis, 2002a and b, and 2003). Tertiary regional ash-flow tuffs formerly covered most of the area to a thickness of as much as 500 ft, but erosion has left only patches of these tuffs, notably the Oligocene Needles Range Group, derived from the Indian Peak caldera complex. Basin-range faults cut all these ranges, but most are of small magnitude so individual stratigraphic units are remarkably coherent and continuous over this large area. The most significant basin-range fault is the northerly-trending fault zone that defines the eastern side of Snake Valley. Basin-range faults that separate the Confusion Range from Tule Valley have moderate vertical offset.

The Confusion Range and adjacent ranges and valleys are within the GSLDFS. The Chainman Shale underlies at shallow depth all of these areas accept the southern Confusion Range. In fact, the Chainman is folded along north-striking trends so it is repeated over the area. The entire area is underlain at shallow depth by north-striking thrust faults. The folded Chainman, and perhaps the thrusts, probably are significant barriers to groundwater flow to the east or west. Other barriers to east or west flow are the north-striking faults, which provide conduits for northward flow. The only flow from west to east that is permissible is in the southern Confusion Range, where lower Paleozoic carbonate rocks are exposed and the range is low (Harrill et al., 1988).

4.4.2.6 NEEDLE RANGE AND WAH WAH MOUNTAINS

The Needle Range, just east of the Nevada-Utah state line, is about 50-mi-long and consists of two subranges, the Mountain Home Range to the north and the Indian Peak Range to the south. The Mountain Home Range merges with the Burbank Hills to the north. Hamlin Valley, to the west, separates the Needle Range from the southern Snake Range, Limestone Hills, and White Rock Mountains to the west. To the east of the Needle Range is Pine Valley and to the south is the Escalante Desert. The Wah Wah Mountains is a parallel tilt block of similar length to, and located east of, the Needle Range, near the eastern margin of the geologic study area. The Wah Wah Mountains is the southward continuation of the Confusion Range. Wah Wah Valley is east of the Wah Wah Mountains and west of the San Francisco Mountains.

The northern part of the Needle Range consists of folded, middle to upper Paleozoic rocks (Hintze and Davis, 2002a). Locally lower Paleozoic carbonate rocks are thrusted over upper Paleozoic carbonate rocks (Best et al., 1987a and b). Most of the Needle Range, however, consists of east-dipping outflow ash-flow tuffs derived primarily from the Indian Peak caldera complex. The eastern caldera margin passes through much of the southern part of the range (Williams et al., 1997). The Needle Range is a faulted horst, with the main basin-range fault separating Hamlin Valley from the Needle Range (Plates 1 and 6, Cross Sections U—U' and Q—Q'). Hamlin Valley contains at least 4,000 ft of basin-fill sediments (Plates 4 and 8, Cross Sections U—U' and Q—Q'). The basin-fill sediments in the southern half of Hamlin Valley are underlain by the Indian Peak caldera complex (Plates 4 and 8, Cross Section Q—Q'). A significant basin-range fault separates the eastern side of the Needle Range from Pine Valley.

The northern Wah Wah Mountains, like the southern Confusion Range just to the north, consists of gently folded and locally thrusted, lower to middle Paleozoic carbonate rocks. Farther south,

east-dipping Late Proterozoic to Cambrian quartzite and overlying Cambrian carbonate rocks form most of the range (Hintze and Davis, 2002a). An oil well drilled by Hunt Oil Company in the southern Wah Wah Mountains was spudded in the Prospect Mountain Quartzite and penetrated 12,500 ft of rocks, including several thrust zones (Erskine, 2001). Other thrust faults that place lower Paleozoic rocks over middle and upper Paleozoic rocks are well exposed and unconformably overlain by east-dipping, Tertiary ash-flow tuffs (Abbott et al., 1983). Near the southern end of the range, other Sevier thrusts place Cambrian rocks above the Jurassic Navajo Sandstone (Best et al., 1987c). The southeastern part of the Indian Peak caldera complex cuts the southwestern end of the Wah Wah Mountains (Williams et al., 1997). As with the Needle Range, the dominant structure controlling the range is a basin-range fault zone on the western margin, beneath Pine Valley. Pine Valley is a graben underlain by basin-fill sediments perhaps as much as several thousand feet thick but generally less (Davis, 2005). The southern ends of both the Needle Range and Wah Wah Mountains merge with each other (Best et al., 1987c) and, still farther southwest, these merge with the White Rock Mountains. These southern range margins form the northern margin of Escalante Desert and the southern margin of the Indian Peak caldera complex (Best, 1987).

Hamlin, Pine, and Wah Wah valleys are part of the GSLDFS, likely with northward groundwater flow into Snake Valley (Harrill et al., 1988). Except for their southern edges, the Needle Range and Wah Wah Mountains also are within the GSLDFS. These southern edges and the Escalante Desert are part of the Sevier Lake Flow System of Harrill et al. (1988), where groundwater flow is eastward then northward to its sump at Sevier Lake, east of the House Range. Groundwater flow from Pine Valley to Wah Wah Valley is permissible through the northern Wah Wah Mountains because of its carbonate rocks and perhaps even through the southern part of the Wah Wah Mountains because of its outflow volcanic rocks and local cross faults (Harrill et al., 1988). The presence of Late Proterozoic to Cambrian quartzite in the central part of the range, however, likely prevents flow through the range here. Wah Wah Valley may receive flow from the Sevier Lake Flow System to the east (Harrill et al., 1988). Nonetheless, northward flow likely dominates in all these valleys, following conduits provided by the basin-range faults.

4.4.2.7 Fish Springs and House Ranges

The 20-mi-long Fish Springs Range, near the northeastern edge of the geologic study area, extends south from the Great Salt Lake Desert. The southward continuation of the Fish Springs Range is the 60-mi-long House Range. The two ranges form the eastern boundary of Tule Valley, which contains basin-fill sediments that in most places are 1,000 to 2,000 ft thick (Plates 4 and 8, Cross Sections W—W' and V—V') but have been estimated to be locally more than 6,000 ft thick (Davis, 2005).

The Fish Springs Range is a highly faulted but generally gently west-dipping horst consisting of lower Paleozoic carbonate rocks (Plates 4 and 8, Cross Section X—X') (Hintze, 1980; Hintze et al., 2000). The range is bounded by large basin-range faults on its western and eastern sides. The high House Range is a tilt block, bounded on the western side by a major basin-range fault beneath eastern Tule Valley. The fault uplifts the range and tilts it several degrees east (Hintze and Davis, 2002b). The range, famous among paleontologists for its trilobites, consists mostly of Cambrian strata, which include clastic sedimentary rocks at the western base of the range and carbonate rocks above. The central part of the range is intruded by the Notch Peak quartz monzonite pluton of Jurassic age.

The Fish Springs Range and the valleys east (Fish Springs Flat) and west (Tule Valley) of it are within the GSLDFS. The House Range marks the eastern side of this flow system. Late Proterozoic to Cambrian quartzite along the western side of the Fish Springs and House ranges forms a likely eastward groundwater barrier between Tule Valley and the valleys to the east, including the Sevier Desert. Some eastward groundwater flow, however, is permissible through Sand Pass between the Fish Springs and House ranges (Harrill et al., 1988). Southern Tule Valley receives flow from the Sevier Lake Flow System to the east (Harrill et al., 1988). Northward flow, of course, likely dominates in this entire area in conduits provided by basin-range faults, including the fault zone along the western side of the Fish Springs and House ranges (Stephens, 1977). In northern Tule Valley, this northward flow is shown as likely, and northwestward flow is considered permissible (Figure 4-10).

THIS PAGE INTENTIONALLY LEFT BLANK

5.0 GEOPHYSICS

5.1 GRAVITY

Analysis of gravity anomalies in east-central Nevada defines the overall shape of their basins, provides estimates of the depth to pre-Cenozoic basement rocks, and identifies buried structures beneath the sedimentary cover.

USGS collected gravity observations at 1,013 new sites to supplement about 5,000 previous stations in this area (Snyder et al., 1981; Bol et al., 1983; Snyder et al., 1984; Ponce, 1992 and 1997; Scheirer, 2005; Mankinen et al., 2006). At gravity stations on bedrock, samples were collected for density and magnetic susceptibility properties. In this section, we use metric measurements because they were used in the USGS studies.

Values of observed gravity were calculated at the new stations by accounting for fluctuations related to tidal accelerations and for instrument drift constrained at the beginning and end of each day. New gravity stations were collected within coverage gaps of the prior data, especially in the ranges adjacent to the basins of concern. Gravity observations were processed to account for the predictable effects of latitude, elevation, and terrain variations, yielding isostatic gravity observations that primarily reflect density variations in the upper and middle crust.

Gridded isostatic gravity anomaly data were used to guide the gravity analysis in two modes: (1) to detect significant lateral density interfaces in the subsurface using a maximum horizontal gradient technique (Blakely and Simpson, 1986) and (2) to create models of the depth to pre-Cenozoic basement using the anomaly separation technique of Jachens and Moring (1990). The magnitude of the gradient is a function of the depth to the density boundary and the size of the density contrast.

The depth-to-basement technique involves two steps: (1) to separate contributions to the isostatic gravity anomaly that arise from Cenozoic sedimentary and volcanic deposits and those from pre-Cenozoic rocks and (2) to convert the contributions from the lower density deposits into a model of basin depth (Jachens and Moring, 1990).

Because available gravity data for the study area were made by many different observers at different times, the data set was examined to remove duplicate entries. Major station elevations were compared with elevations interpolated from 10- and 30-m digital elevation models. Large elevation differences indicate possible errors in station location or elevation, and each station so identified was examined individually to confirm the discrepancy before omitting it from the data set. The revised data set, including all new gravity observations, was gridded at a spacing of 0.5 km using a minimum curvature algorithm (Webring, 1985). The resulting isostatic gravity field emphasizes features that reflect local density variations in the middle and upper crust. Gravity lows (cool colors) generally indicate low-density sedimentary and volcanic rocks in basin fill; gravity highs (warm colors) generally reflect pre-Cenozoic basement rocks in the basin.

The isostatic residual gravity field reflects a pronounced contrast between dense pre-Cenozoic rocks and significantly less dense overlying strata. Because of this relationship, the gravity inversion method (Jachens and Moring, 1990) can be used to separate the isostatic residual anomaly into

pre-Cenozoic "basement" and younger "basin" fields, thus allowing an estimate of thickness of Cenozoic alluvial fill and underlying Tertiary volcanic rocks within the area. The accuracy of thickness estimates derived by the gravity inversion technique is dependent on (1) the assumed density-depth relation of the Cenozoic valley fill and (2) the initial density assigned to the basement rocks. Density of basement rocks is generally assumed to be 2.67 mg/m^3, and this value is considered appropriate in this area, where major exposures consist of Late Precambrian through upper Paleozoic marine carbonate and siliciclastic sedimentary rocks. Subvolcanic Cenozoic intrusions are included here as part of the basement because their physical properties are similar to most of the older rocks, and they differ strongly from those of the eruptive and basin-fill sequences. The density-depth function used here is the same as used in an earlier basin-depth analysis of the Basin and Range province (Saltus and Jachens, 1995). The gravity inversion method also allows the input of basement depths determined from deep drill-holes and seismic data.

5.1.1 Gravity Data for Spring and Snake Valleys

As discussed by Mankinen et al. (2006 and 2007), a total of 545 new gravity stations (Figure 5-1) were collected for Spring and Snake valleys (Figure 5-2). The isostatic gravity field for Spring and Snake valleys is shown on Figure 5-3. The depth to basement, calibrated by oil and gas wells (dots in Figure 5-4) is shown on Figure 5-4. The topographic contour interval in these figures is 200 m.

In general, the gravity inversion method indicates that the maximum thickness of basin fill (alluvium and volcanics) in the principal valleys of interest is generally 2 km or more (Figure 5-4). Note, however, that the deepest areas of Spring and Hamlin valleys are much narrower than the deepest areas in both Steptoe and Snake valleys. Maximum depths to pre-Cenozoic basement in Spring, Steptoe, and Hamlin valleys are between 3 and 3.5 km. The northernmost areas of Steptoe and Spring valleys (39°45' N to 40° N) have maximum depths near 4 km. The approximately 4 km of fill in these areas are comparable to the deepest parts of Snake Valley. Maximum depths in Duck Creek Valley northeast of McGill range from approximately 1.5 to 2.0 km. There appears to be a particularly deep basin beneath Antelope Valley (Tippett Valley) where depths are generally greater than 3 km, and in some areas these extend to between 5 and 5.5 km.

5.1.2 Gravity Data for Cave, Dry Lake, and Delamar Valleys

In 2003 and 2004, USGS collected gravity observations at 468 new sites (Scheirer, 2005; Mankinen et al., 2006 and 2007) in Cave, Dry Lake, and Delamar valleys to supplement the prior compilation of ~3,500 stations in this area (Figure 5-5) (Snyder et al., 1981; Bol et al., 1983; Snyder et al., 1984; and Ponce, 1992 and 1997).

Analysis of gravity anomalies in Cave, Dry Lake, and Delamar valleys defines the shape of their basins, estimates the depth to pre-Cenozoic basement rocks, and identifies buried faults (Figure 5-6 [Scheirer, 2005, Figure 2]). In all cases, the basins are asymmetric in their cross section and in their placement beneath the valley, reflecting the extensional tectonism that was initiated during Miocene time in this area. Absolute values of basin depths are estimated using a density-depth profile calibrated by deep oil and gas wells and one MX well (red and white dots and red triangle, respectively, in Figures 5-5 and 5-6), some of which penetrated pre-Cenozoic basement. In Figure 5-6, the red and white dashed lines show the outlines of the alluvial valleys. The left image of Figure 5-6 shows the basin gravity anomaly derived from the depth-to-basement algorithm, the

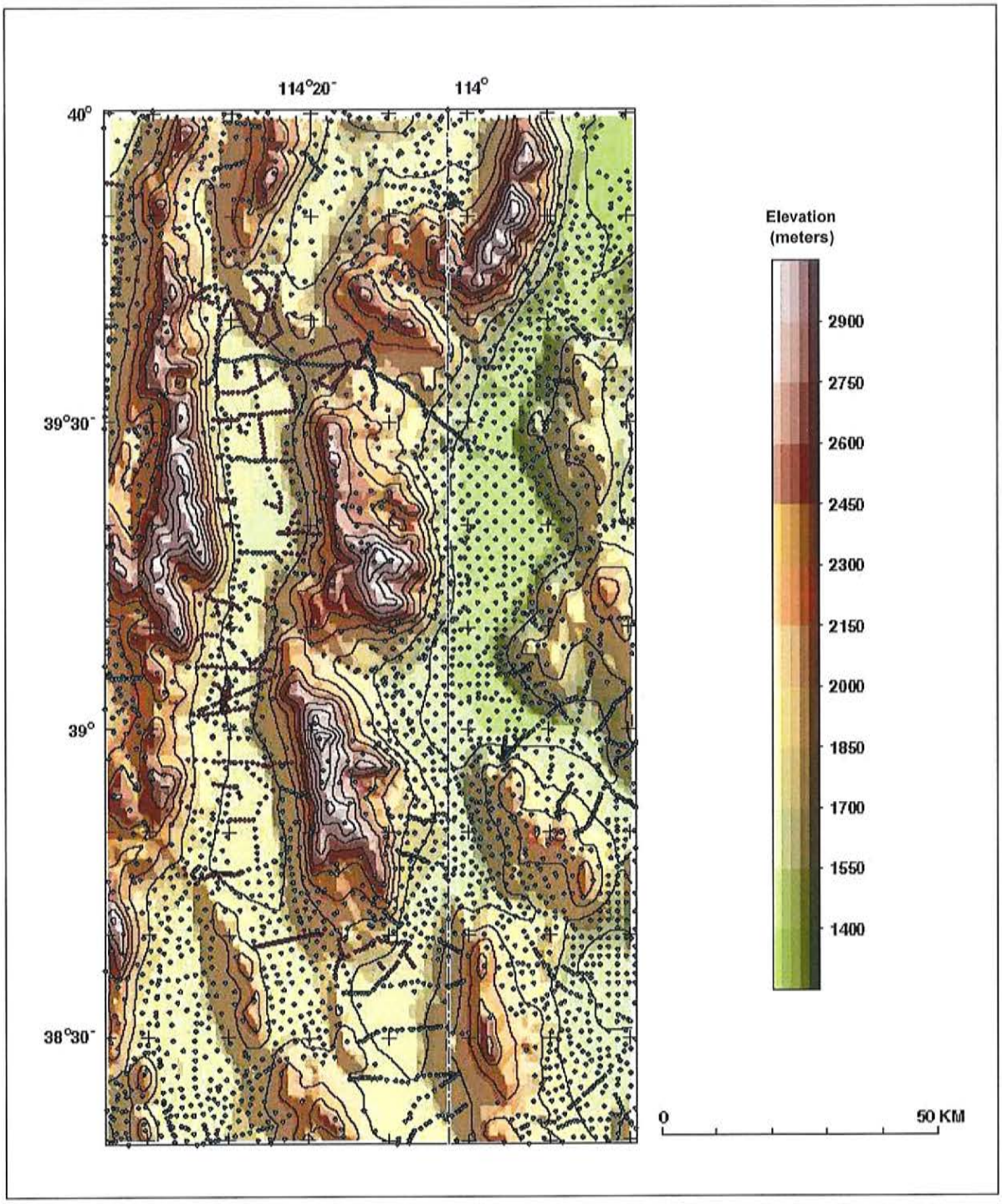

Source: after Mankinen et al., 2006

Figure 5-1
Previously Available Gravity Stations (Green Dots) and Gravity Stations Established During the 2004/2005 Field Seasons (Red Dots) in Spring and Snake Valleys, Nevada and Utah

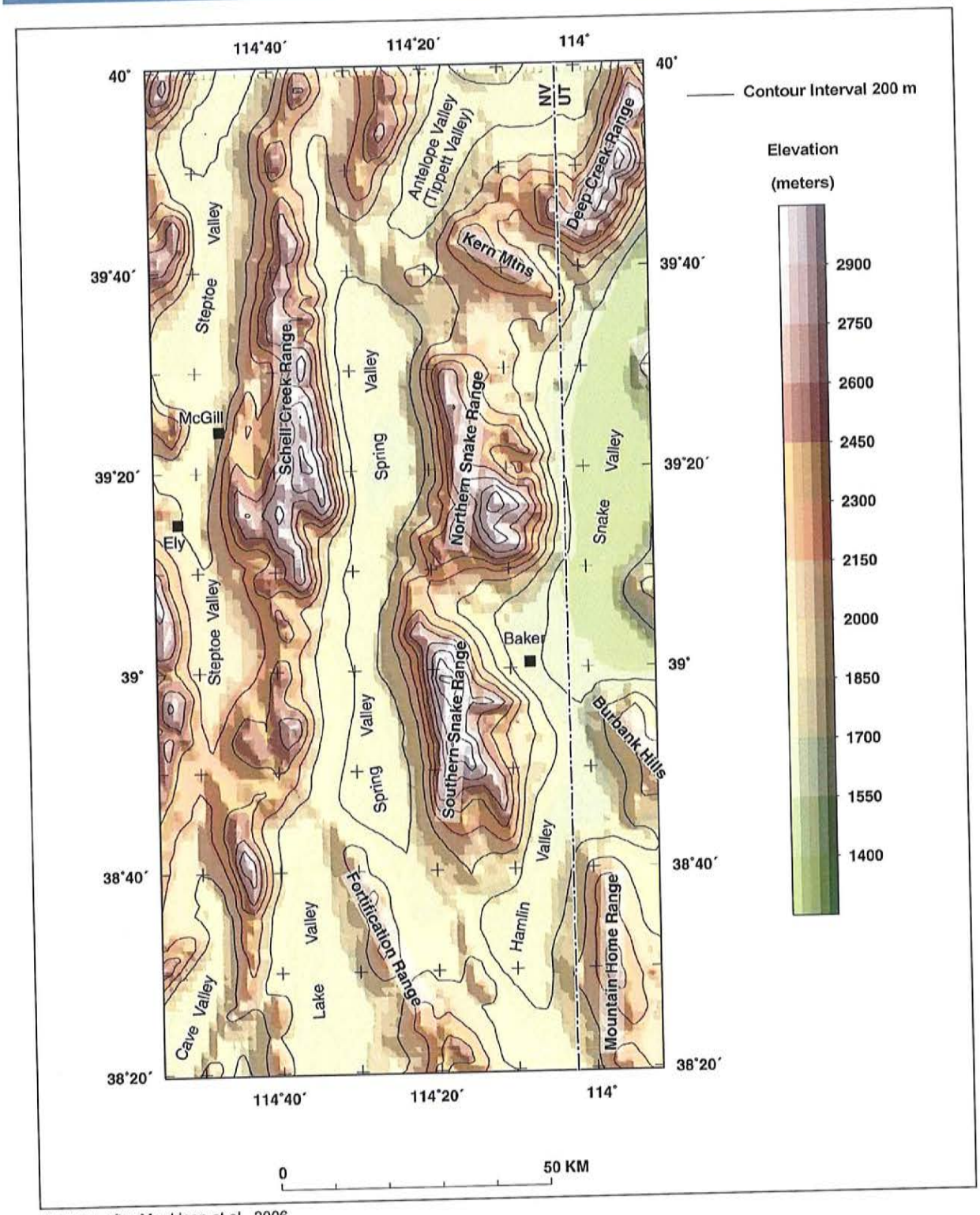

Source: after Mankinen et al., 2006

FIGURE 5-2
INDEX MAP TO THE SPRING VALLEY, NEVADA, STUDY AREA

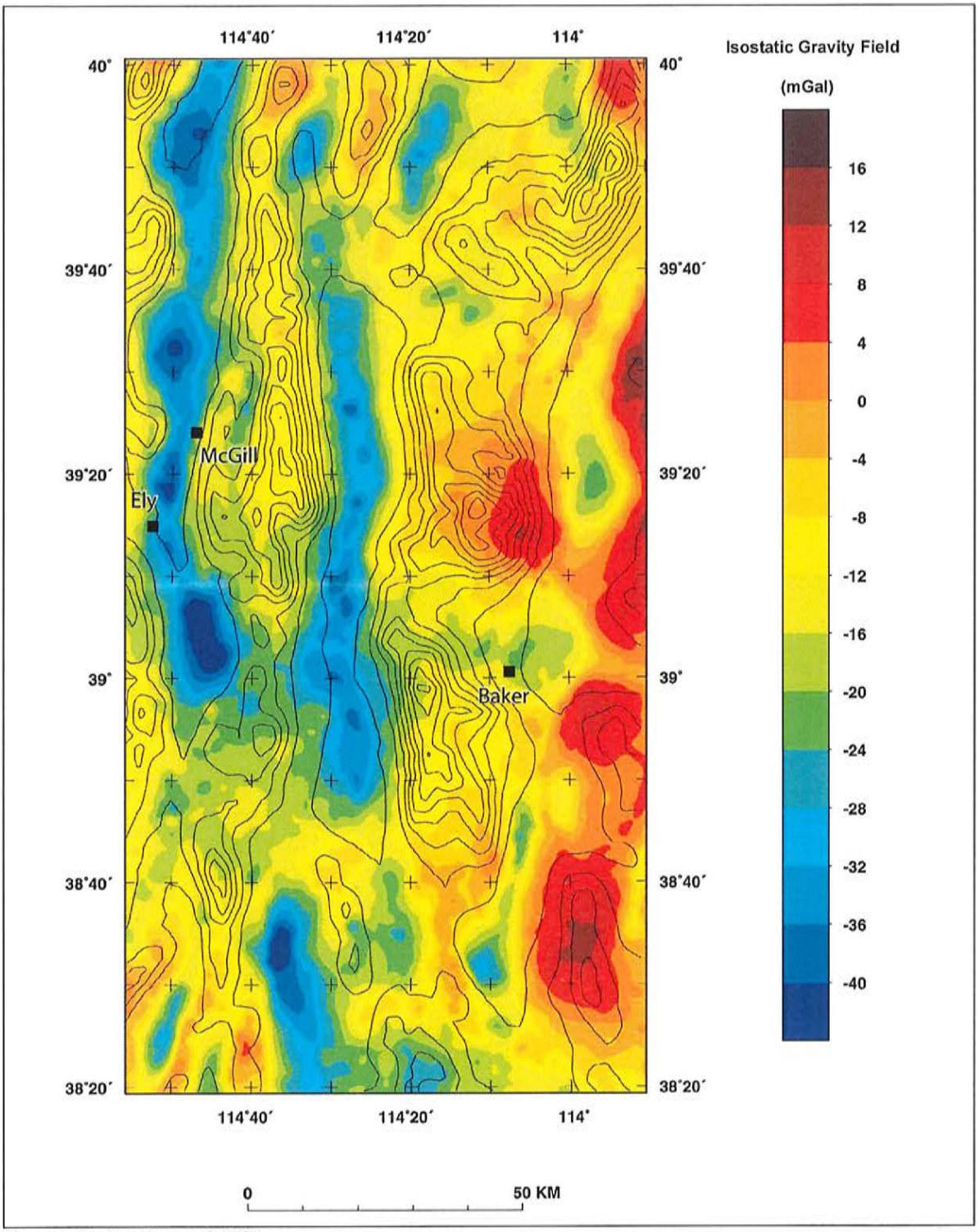

Source: after Mankinen et al., 2006

FIGURE 5-3
ISOSTATIC RESIDUAL GRAVITY FIELD

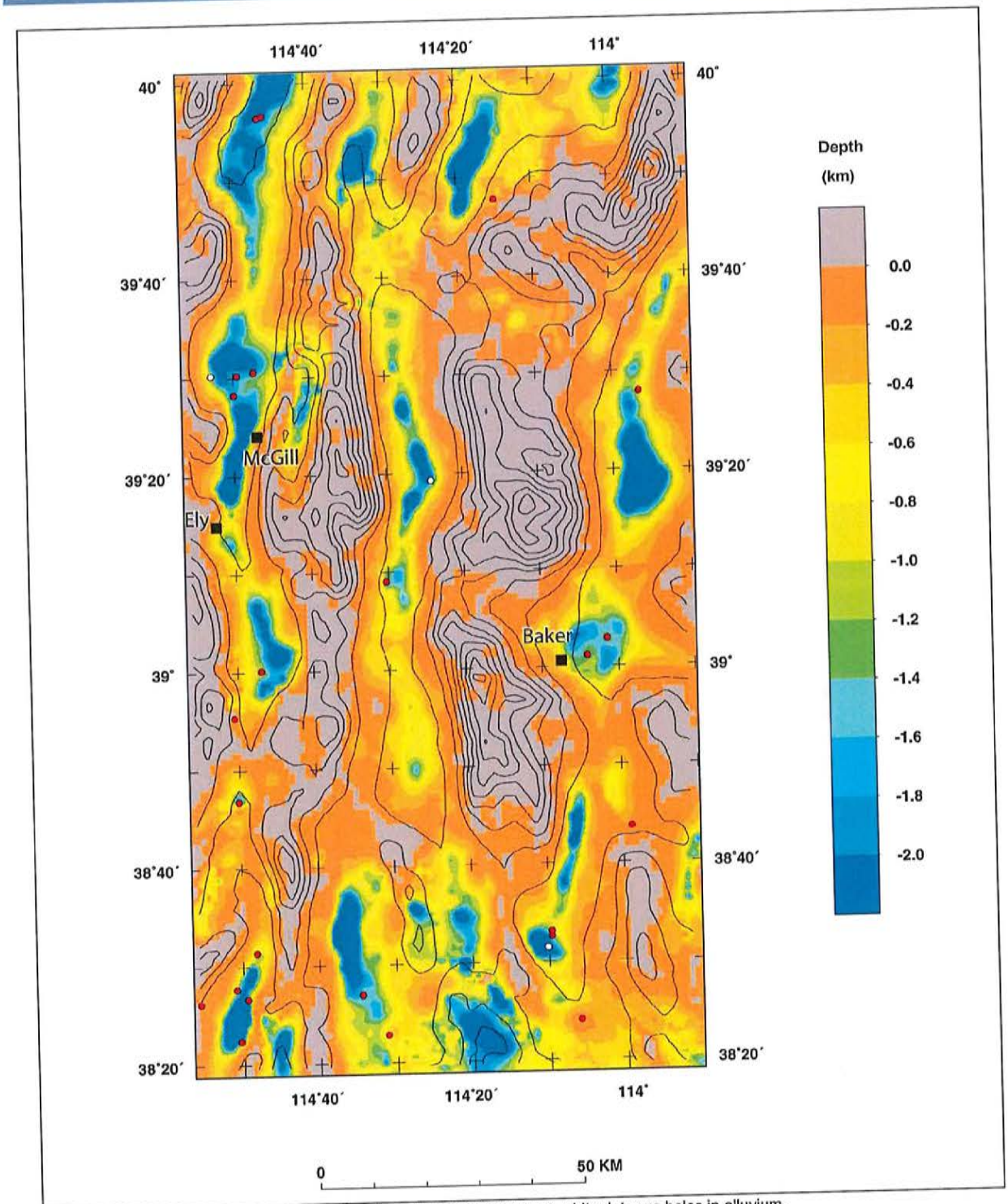

Note: Red dots are drill holes that encountered pre-Cenozoic basement; white dots are holes in alluvium.
Source: after Mankinen et al., 2006

FIGURE 5-4
DEPTH TO PRE-CENOZOIC BASEMENT IN THE SPRING VALLEY STUDY AREA

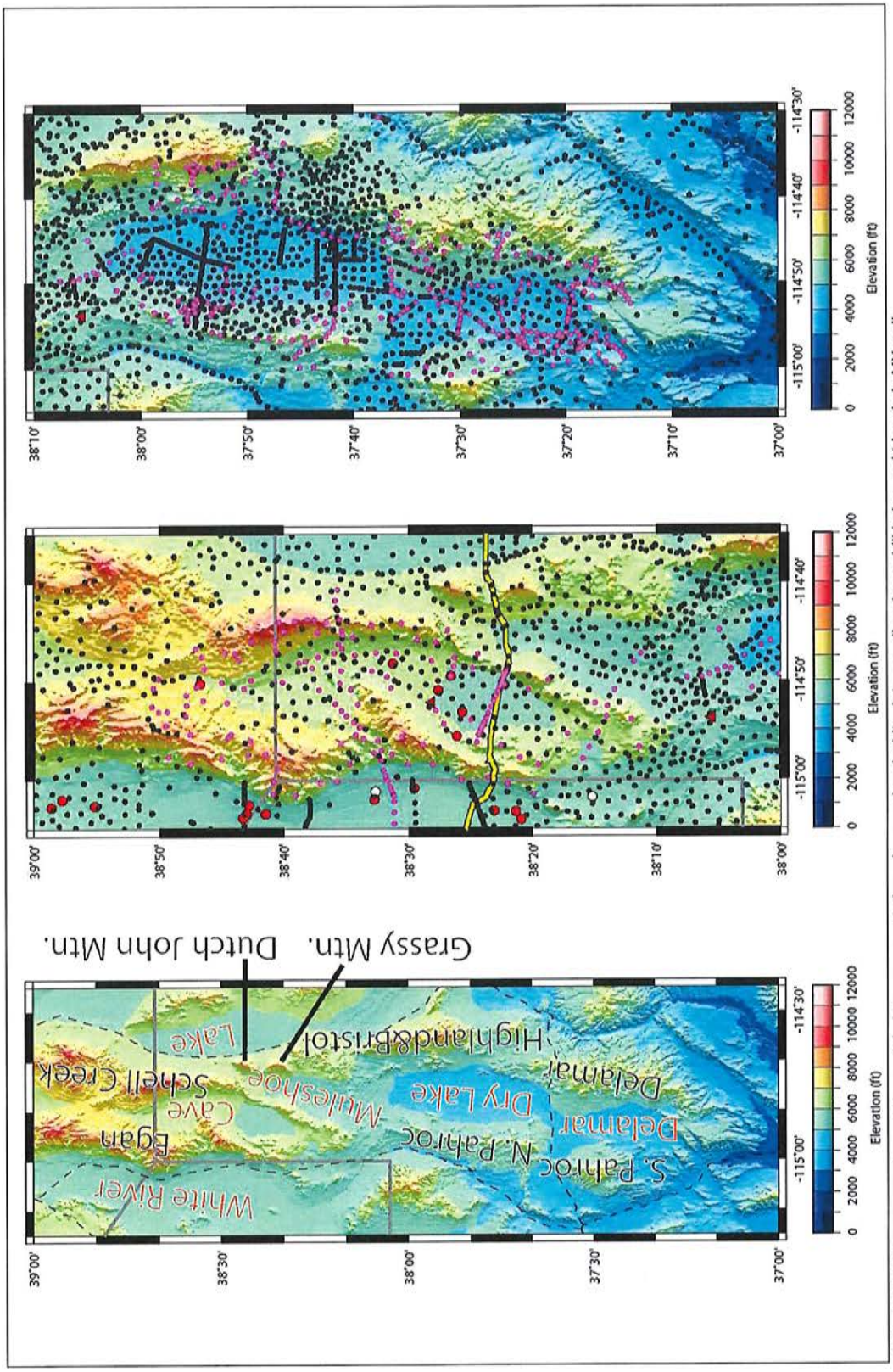

Note: Black dots are previous stations, pink dots are new stations, large red and white dots are oil and gas drill holes, red triangle is MX well.
Source: after Scheirer, 2005

FIGURE 5-5
INDEX MAP, SHOWING GRAVITY STATIONS, OF CAVE, DRY LAKE, AND DELAMAR VALLEYS WITHIN THE GEOLOGIC STUDY AREA

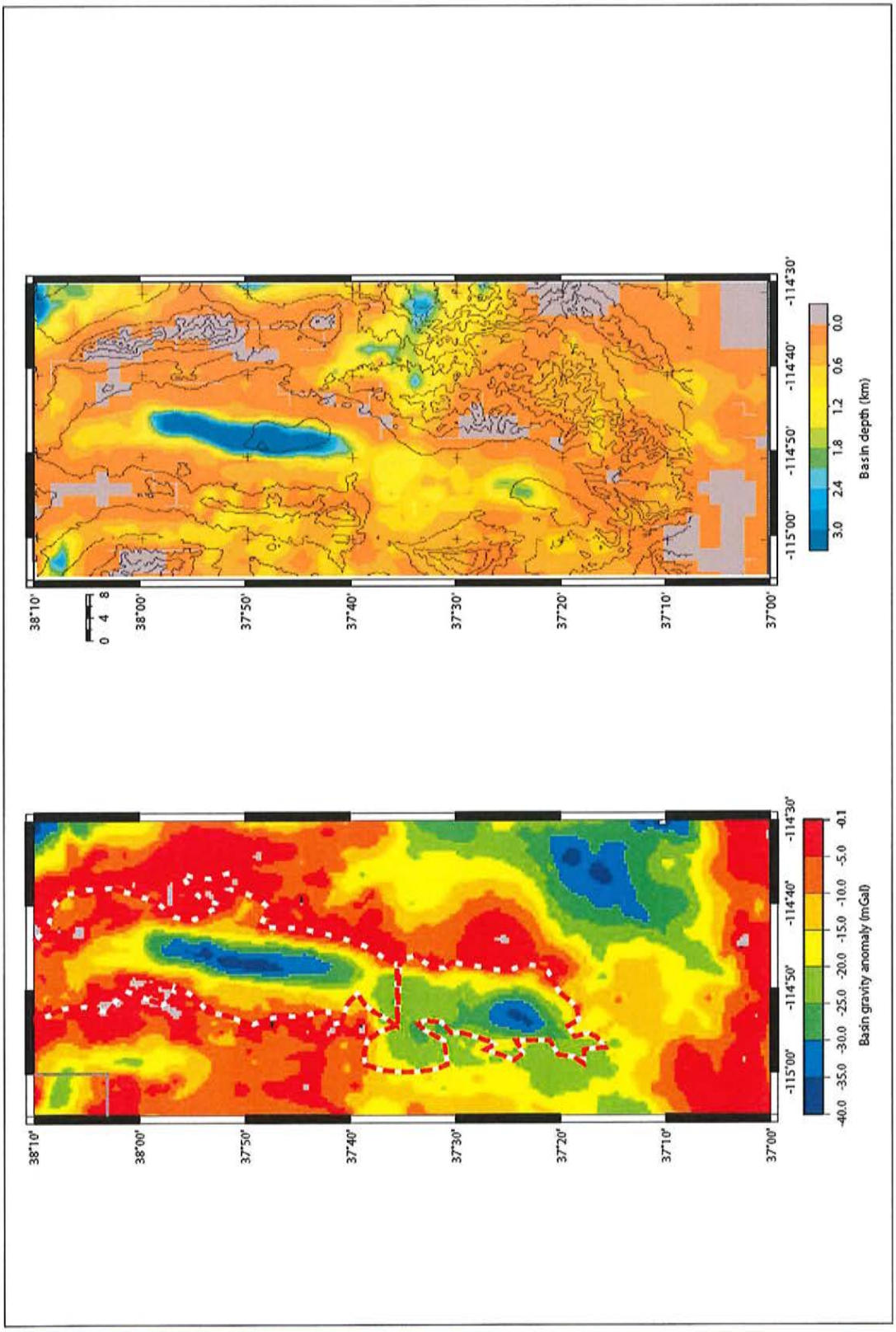

Source: after Scheirer, 2005; Mankinen et al., 2006 and 2007.

FIGURE 5-6
CAVE, DRY LAKE, AND DELAMAR VALLEY BASIN GRAVITY ANOMALIES DERIVED FROM DEPTH-TO-BASEMENT ALGORITHM

image shows the calculated basin depth based on the basin gravity anomaly. The basin beneath southern Cave Valley extends down to 3 to 5 km, that beneath Dry Lake Valley to 3 to 5 km, and that beneath Delamar Valley to 2 to 3 km. The ranges surrounding Dry Lake and Delamar valleys are dominated by volcanic units that may produce lower-density basin infill, which, in turn, would make the maximum depth estimates somewhat less. Dry Lake Valley is characterized by a slot-like graben in its center, whereas the deep portions of Cave and Delamar valleys are more bowl-shaped. Significant portions of the basins are shallow (less than 1 km deep) as are the transitions between each of these valleys. A seismic reflection image across southern Cave and northern Dry Lake (Muleshoe) valleys (yellow line in central image of Figure 5-5) confirms the basin shapes inferred from gravity analysis. The architecture of these basins inferred from gravity aided in interpretation of the hydrogeologic framework of Cave, Dry Lake, and Delamar valleys by placing estimates on the volume and connectivity of potential unconsolidated alluvial aquifers and by identifying faults buried beneath basin deposits.

5.1.3 GRAVITY DATA FOR COYOTE SPRING VALLEY

USGS conducted gravity surveys in the Coyote Springs Valley and vicinity in Clark and Lincoln counties, Nevada (Phelps et al., 2000). These gravity measurements (224 measurements spaced 660 ft apart) were made along 5 profiles across parts of the Coyote Spring Valley to aid in modeling the depth and shapes of the underlying basins and to locate faults concealed beneath the basin fill (Figure 5-7).

The isostatic residual gravity field defined by the new data is shown in Figure 5-8. The results of the depth to pre-Cenozoic basement analysis are shown in Figure 5-9. The results show two deep basins (the northern crossed by profile N2 and the southern crossed by profiles S1 and S3) beneath the axis of Coyote Spring Valley, both reaching maximum depths greater than about 3,300 ft. The deepest parts of both basins are aligned north-south and are separated from each other by a north-northwest-trending, shallowly-buried, bedrock edge that is the northward continuation of the Arrow Canyon Range. A smaller basin (maximum depth of about 1,600 ft) lies beneath the valley containing Dead Man Wash and part of Pahranagat Wash and appears to be the southern continuation of the northern basin beneath Coyote Spring Valley.

5.2 AUDIOMAGNETOTELLURICS STUDIES

In conjunction with the gravity studies of Scheirer (2005), Mankinen et al. (2006), and Phelps et al. (2000), AMT technology was tested to see whether it is a feasible approach for mapping the structure and to contribute to the regional hydrological model in a typical Basin and Range setting. In particular, faults and stratigraphy within the valleys, as well as estimates of depth to pre-Cenozoic basement, are valuable targets. AMT technology is used to detect variations in shallow, subsurface electrical resistivity, which is largely dependent on the fluid content, porosity, fracturing, and conductive mineral content of the subsurface geology. We concluded that it may serve as a valuable tool for mapping subsurface faults and lithology at shallow levels of basins (~1,000 m).

The AMT data were collected along two profiles in Spring Valley by McPhee et al. (2005) and shown on Figure 5-10. The models along Profile A (Figure 5-11) and Profile B (Figure 5-12) in Spring Valley show detailed fault structure (black lines in Profile A, red lines in Profile B) revealed by the inversion model within the alluvial basin. A clear transition between unsaturated (200 to 500 ohm-m)

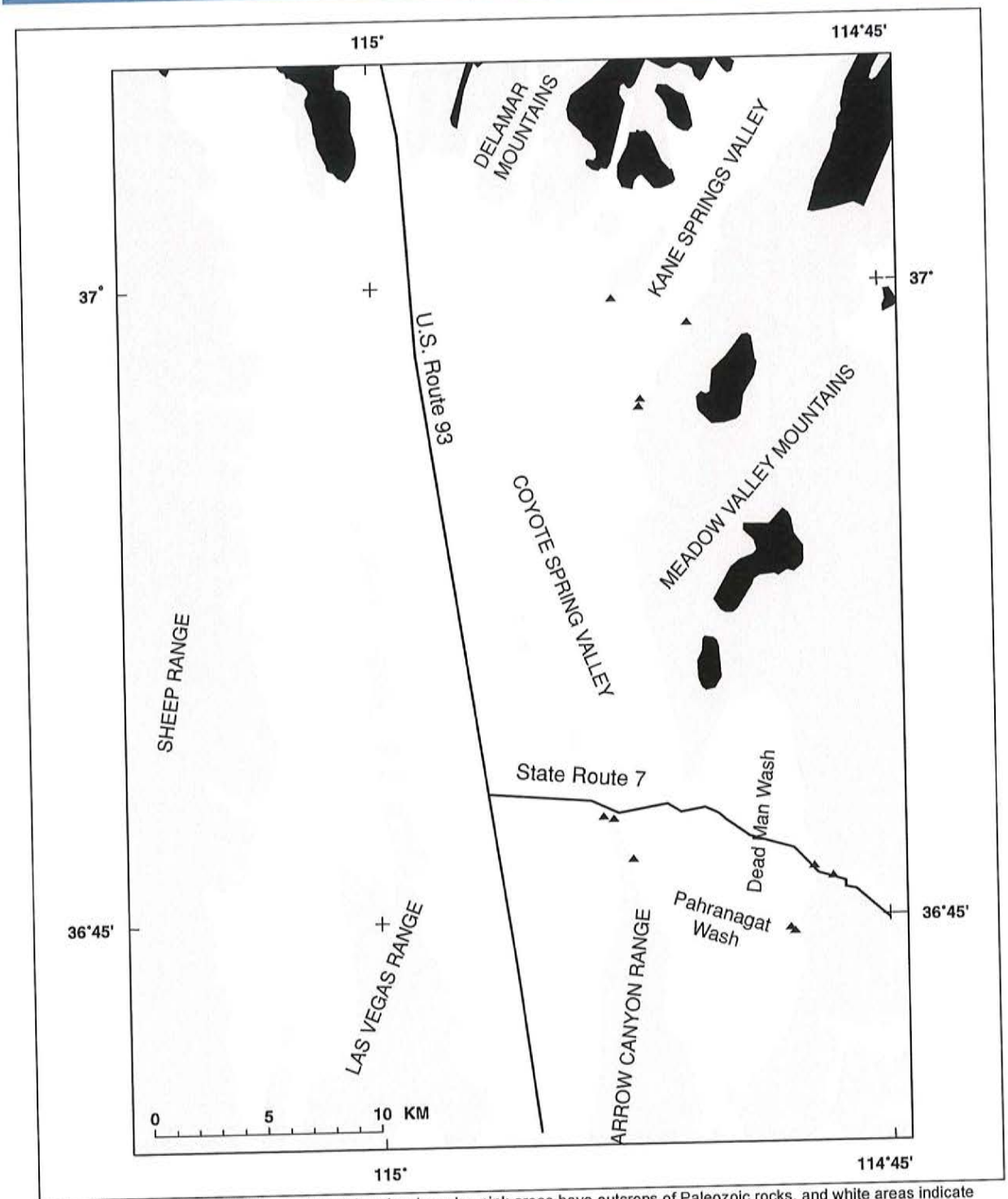

Note: Black areas have outcrops of Cenozoic volcanic rocks, pink areas have outcrops of Paleozoic rocks, and white areas indicate areas covered by Cenozoic basin fill. Solid triangles indicate locations where samples of Paleozoic rock were collected for density measurements. Source: after Phelps et al., 2000

FIGURE 5-7
INDEX MAP SHOWING COYOTE SPRING VALLEY STUDY AREA AND VICINITY

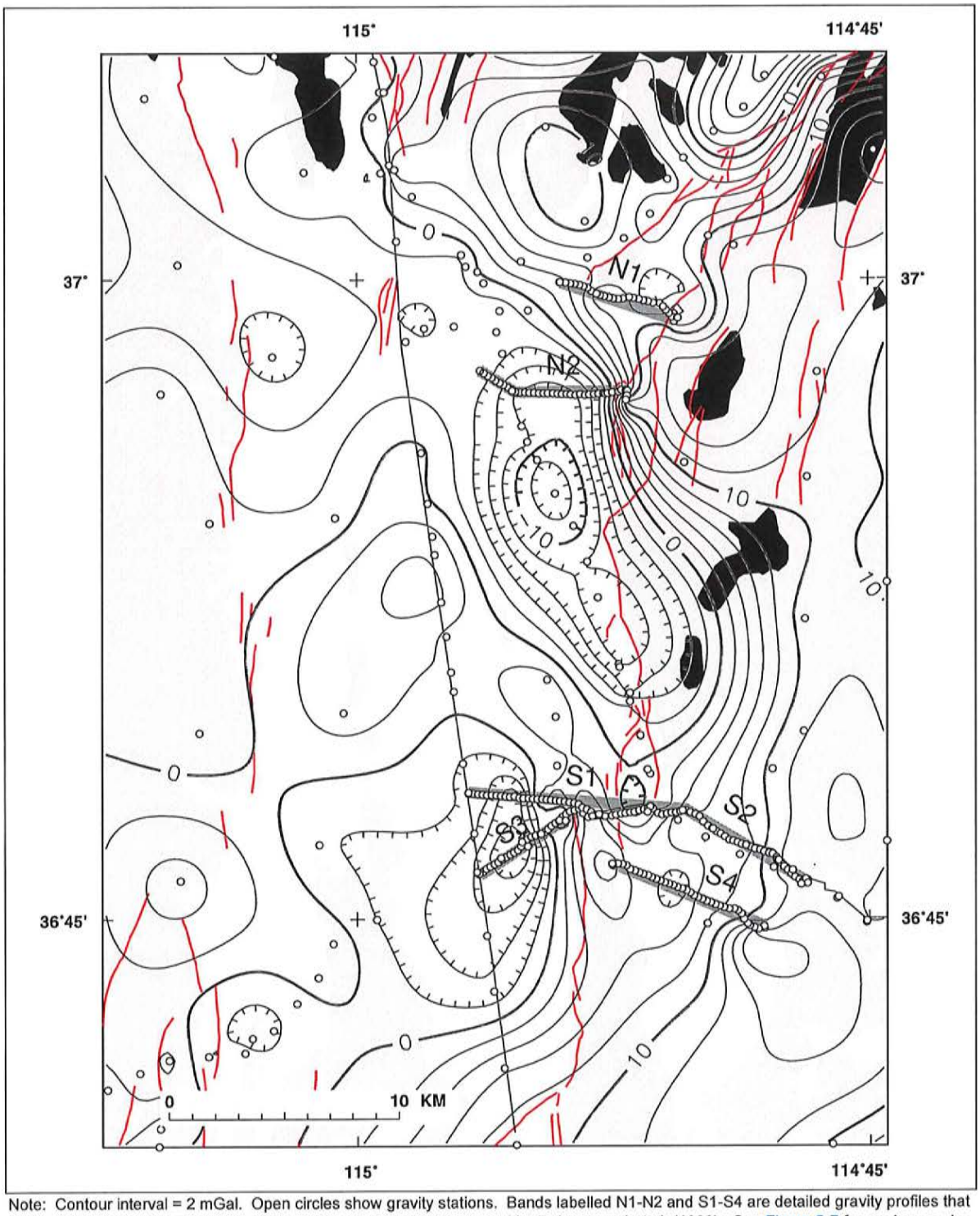

Note: Contour interval = 2 mGal. Open circles show gravity stations. Bands labelled N1-N2 and S1-S4 are detailed gravity profiles that were modeled to define basin shape. Red lines indicate faults mapped by Dohrenwend et al. (1996). See Figure 5-7 for geology and culture. Source: after Phelps et al., 2000

Figure 5-8
Isostatic Residual Gravity Contours for Coyote Spring Valley and Vicinity

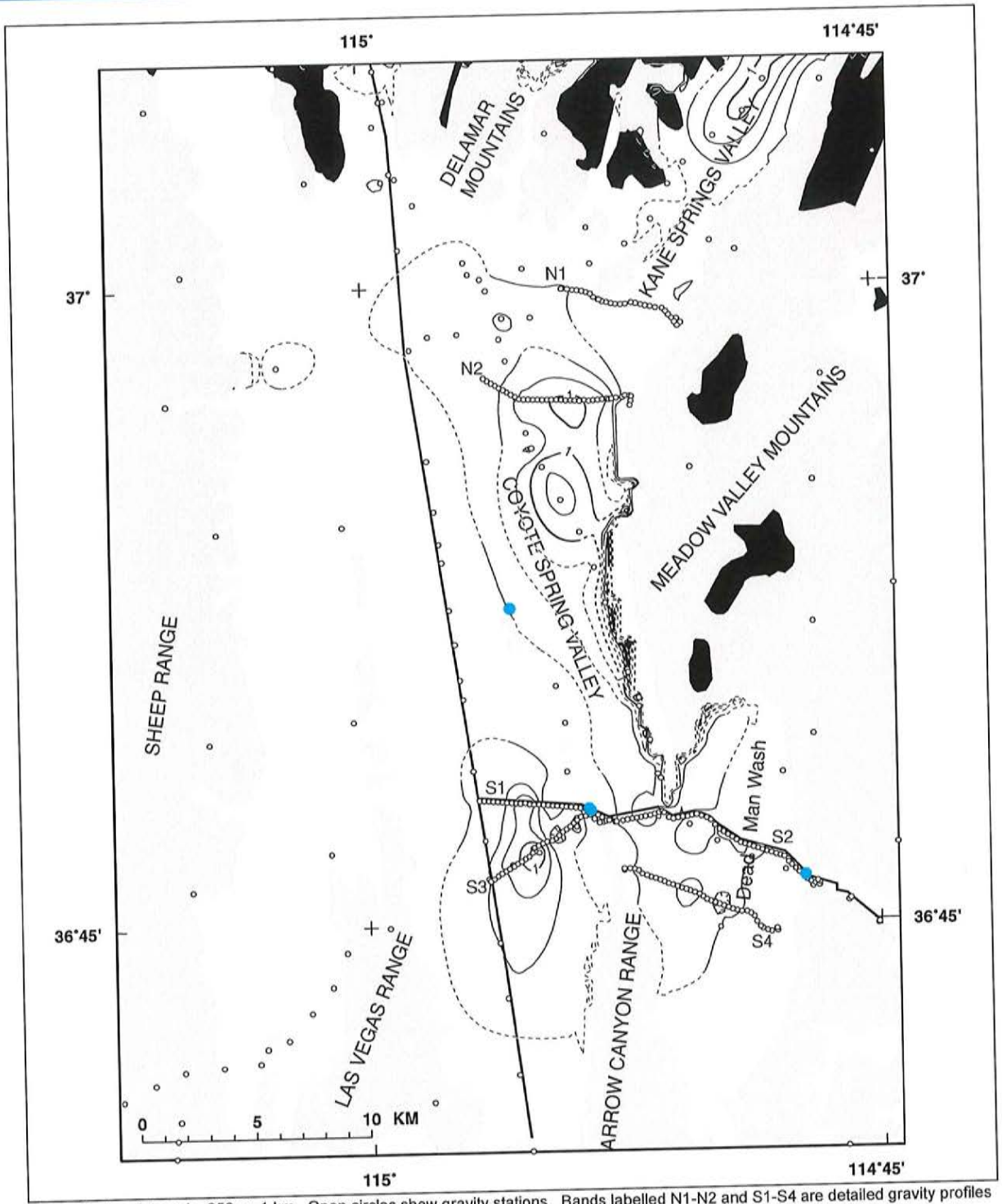

Note: Contour intervals, 250 m, 1 km. Open circles show gravity stations. Bands labelled N1-N2 and S1-S4 are detailed gravity profiles that were modeled to define basin shape. Contours dashed where poorly constrained. Blue dots, wells that penetrate pre-Cenozoic basement. See Figure 5-7 for geology and culture. Source: after Phelps et al., 2000

FIGURE 5-9
BASIN THICKNESS MAP OF THE STUDY AREA

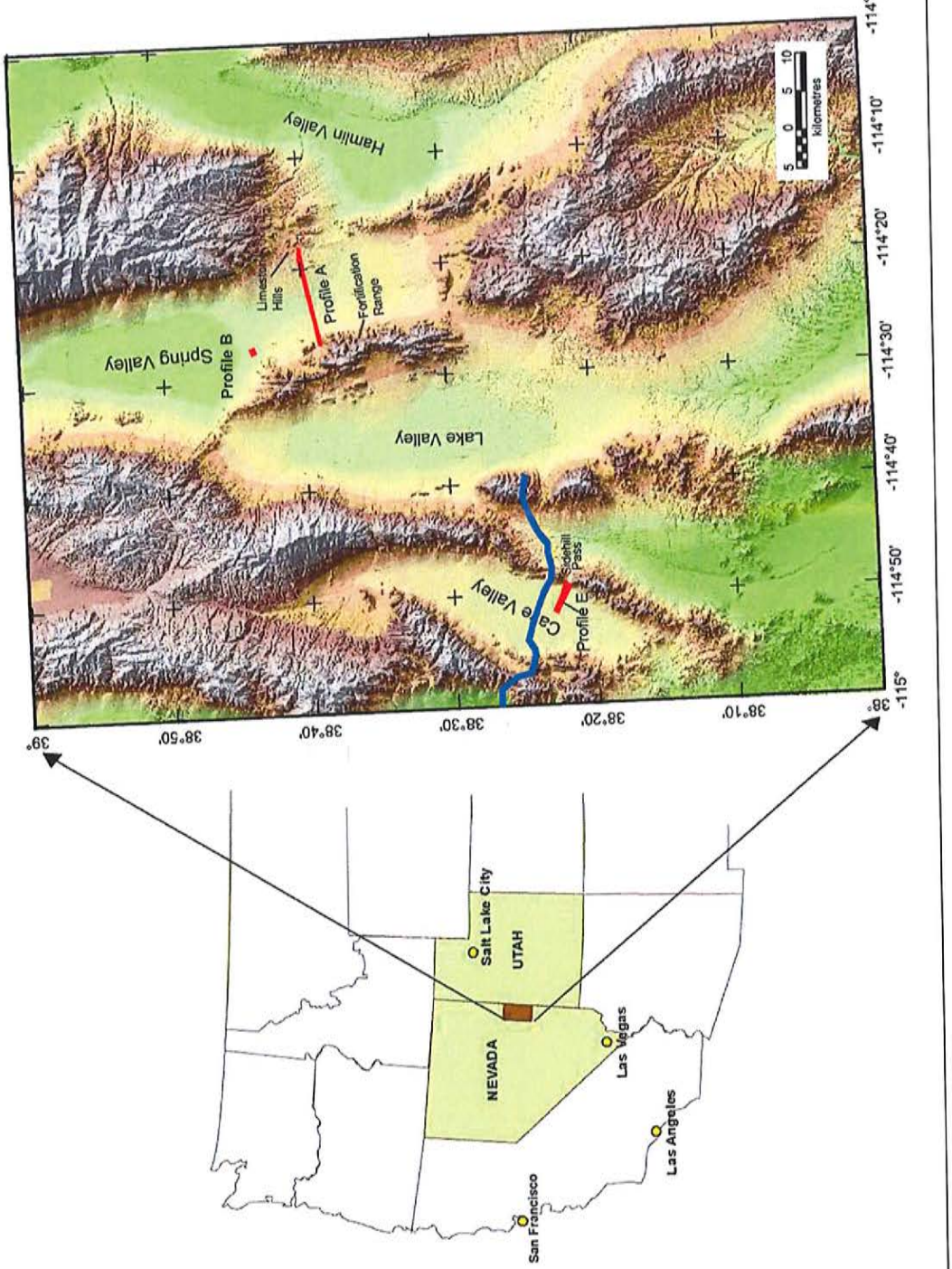

FIGURE 5-10
LOCATIONS OF AMT PROFILES (RED) AND ECN-01 SEISMIC LINE (BLUE) PERFORMED IN THE GEOLOGIC STUDY AREA

Source: after McPhee et al., 2005

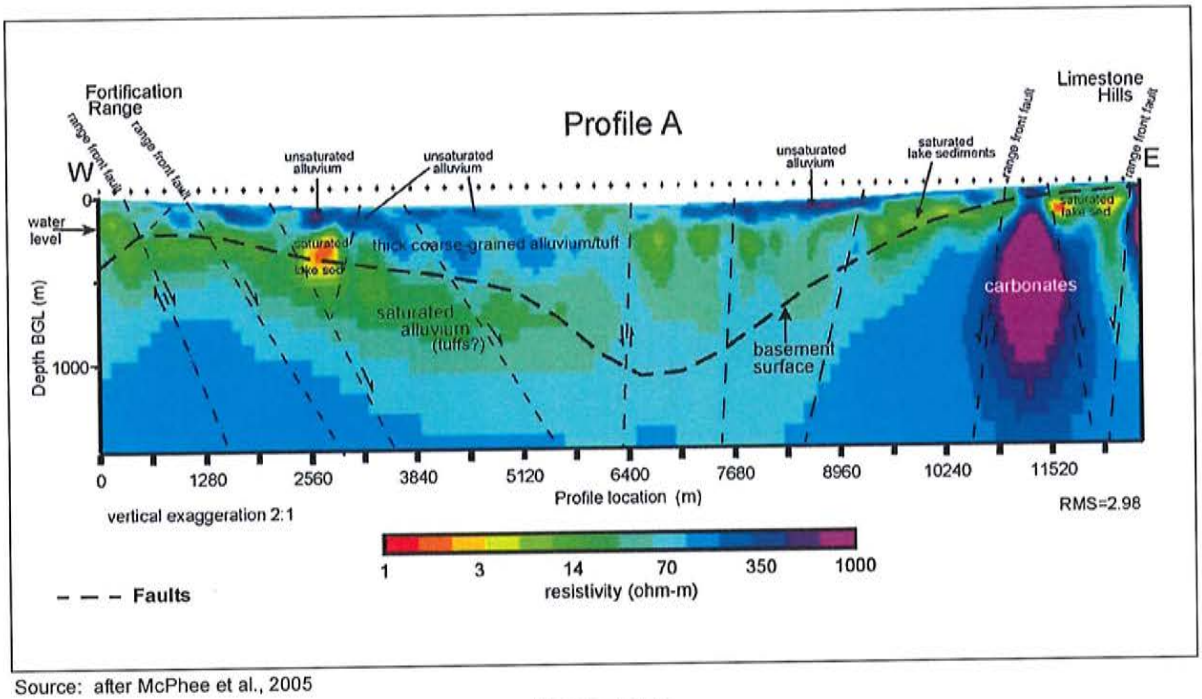

Source: after McPhee et al., 2005

FIGURE 5-11
AMT MODEL ALONG PROFILE A ACROSS SOUTHERN SPRING VALLEY, NEVADA

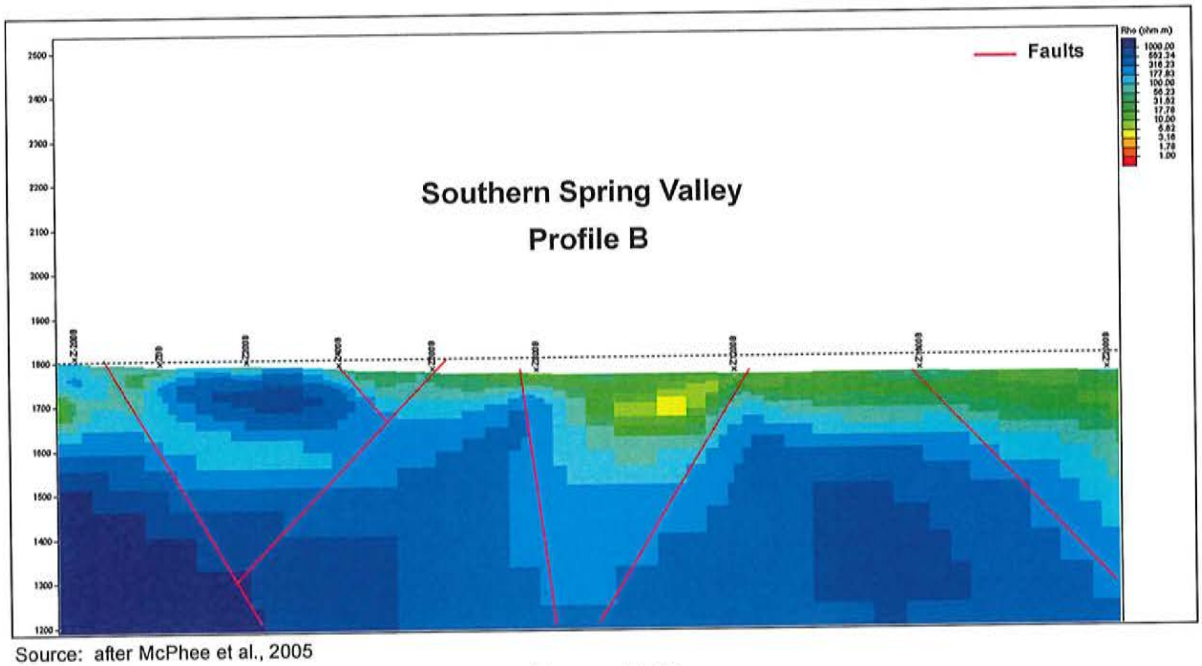

Source: after McPhee et al., 2005

FIGURE 5-12
AMT MODEL ALONG PROFILE B ACROSS SOUTHERN SPRING VALLEY, NEVADA

and saturated alluvium/volcanic rocks (20 to 50 ohm-m) is present at roughly 100 m depth in Profile A. High-resistive (greater than 1,000 ohm-m) carbonate rocks are clearly defined at the eastern end of Profile A under the Limestone Hills, and the locations and dips of several range-front and interbasin faults that lack surface expression can be interpreted throughout the upper 1-km portion of the section image. The interpreted surface of the pre-Cenozoic basin is shown by the heavy dashed line in Figure 5-11.

McPhee et al. (2005 and 2007) provided information on faults on the eastern side of the southern part of Cave Valley, based on AMT profiles (Figure 5-10 and Figure 5-13). The data collected along this Profile E (Figure 5-13) were "noisier" than those collected along Profiles A and B in Spring Valley. The upper several hundred meters of the valley shows more conductive alluvial fill (3 to 20 ohm-m) than was observed in Spring Valley, perhaps due to the additional presence of clays in the valley. Clearly delineated structure within the basin includes other interbasin faults as well.

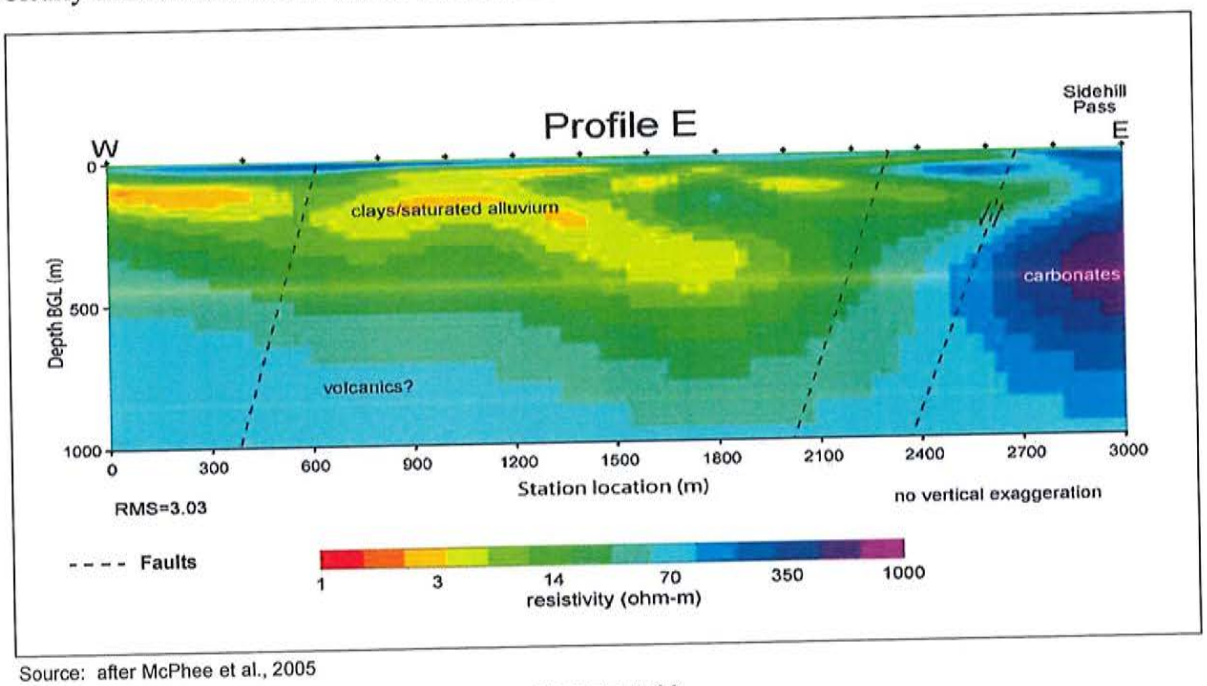

Source: after McPhee et al., 2005

FIGURE 5-13
AMT MODEL ALONG PROFILE E ACROSS CENTRAL CAVE VALLEY, NEVADA

An abrupt contrast between the resistive limestones on the east side of Cave Valley in the Sidehill Pass area and the more conductive valley fill agrees with the sharp gravity gradient observed by Scheirer (2005), who calculated a steep eastern basin margin that is likely bounded by a range-front fault. The depth to basement beyond the eastern margin of Profile E extends deeper than the resolution of our AMT model (Scheirer, 2005).

When compared to the basement-surface estimates derived from the inversion of the gravity data (Scheirer, 2005; Mankinen et al., 2006), AMT technology proves successful at estimating the depth to bedrock. That the AMT data is consistent with the gravity data enhances confidence in these depth estimates.

Several AMT profiles were attempted in Coyote Spring Valley, but due to significant electronic noise from local construction activities, no usable data were obtained.

5.3 SEISMIC STUDIES

An additional view into the subsurface structure of southern Cave Valley and northern Dry Lake (Muleshoe) Valley is provided by a portion of the industry-shot ECN-01 seismic reflection line (Scheirer, 2005) (Figure 5-14a). The seismic line crosses near the maximum depth position of Cave Valley. The seismic reflection image illustrates the asymmetric character of Cave Valley, with a steeper eastern side where the range-front fault of the Schell Creek Range lies and a less-steep western floor leading up to the dip-slope of the Egan Range. Strong reflectors mark the base of Cave Valley, and a discordant and more horizontal packet of reflectors characterizes much of the deeper valley fill. Weaker subhorizontal reflectors are present in the upper valley fill. The reflectors in the shallow portions of Muleshoe Valley are weak or absent, but in its deeper section they exhibit characteristics similar to those of the Cave Valley reflectors.

These seismic data are displayed in travel time, so a quantitative appraisal of seismic depths to basement is not possible. Nevertheless, the basin structure inferred from gravity analysis (Figure 5-14b) shares a number of similarities with the seismic image: Cave Valley is asymmetric and reminiscent of a half-graben (Scheirer, 2005). The overall shapes of Cave versus Muleshoe, in deeper portions, appear similar in the seismic and gravity models. Location and depth of American Petroleum Institute (API) well 27-017-05221 are superimposed schematically on Figure 5-14b to illustrate its general agreement with the gravity depth-to-basement estimate and to show its position with respect to the seismic structures.

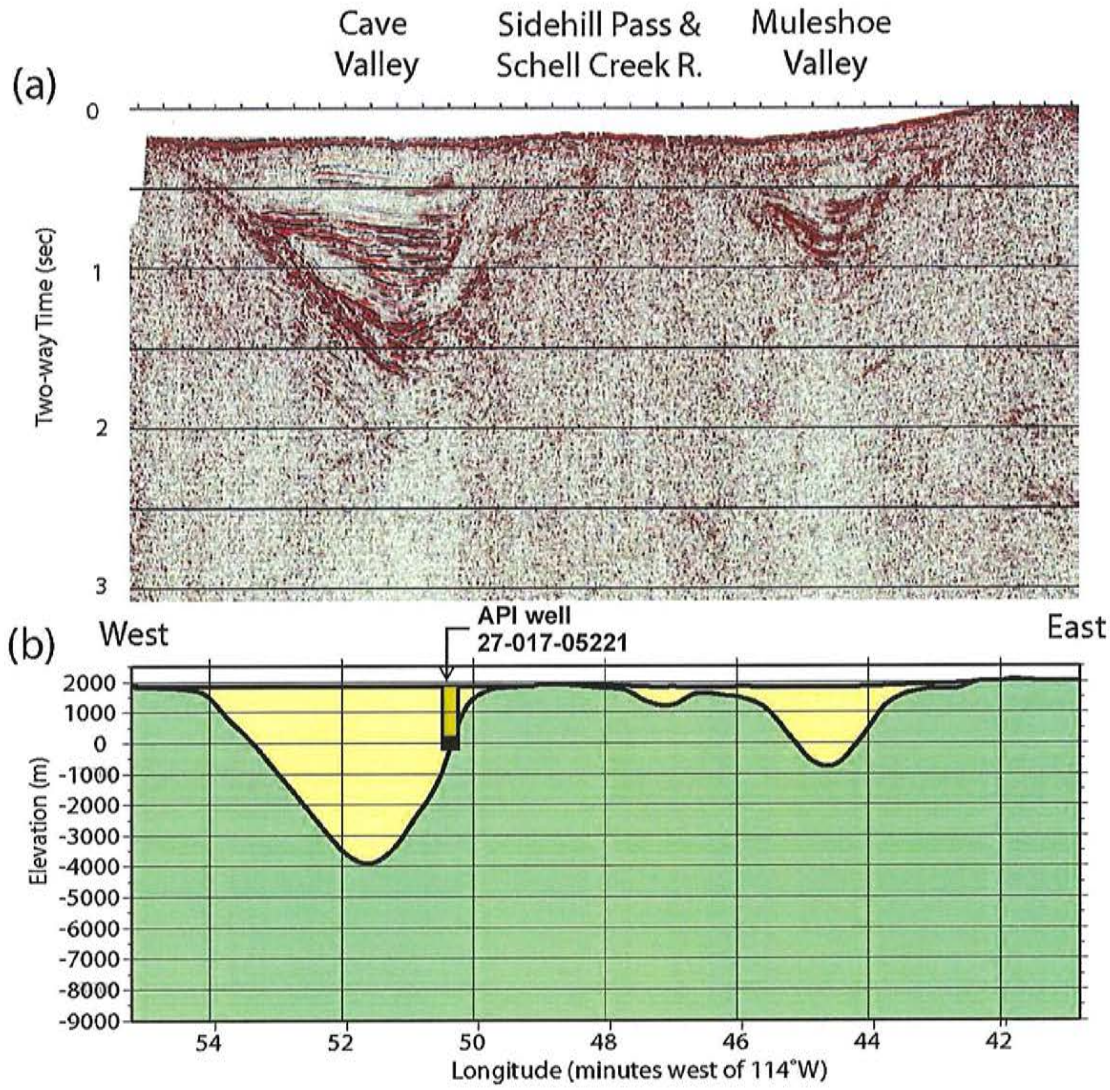

(a) Cross section of southern Cave and northern Muleshoe valleys ECN-01 seismic reflection section displayed in time. (b) Results of gravity depth-to-basement inversion with low-density basin fill in yellow. API well 27-017-05221 is displayed on the section, and its alluvial interval is shown in dark yellow. Vertical exaggeration = 1.5.

Source: after Scheirer, 2005

FIGURE 5-14
(A) ECN-01 SEISMIC REFLECTION SECTION DISPLAYED IN TIME
(B) RESULTS OF GRAVITY DEPTH-TO-BASEMENT

THIS PAGE INTENTIONALLY LEFT BLANK

6.0 SUMMARY

6.1 GENERAL GEOLOGY OF THE STUDY AREA

Eastern Nevada and adjacent parts of Utah were the sites of deposition of thick quartzite and other clastic rocks in Late Proterozoic and Early Cambrian time. These rocks, the initial deposits of the Cordilleran miogeocline, were deposited in shallow marine water along a passive continental margin of what is now western North America. Middle Cambrian through Lower Permian rocks record a shift in deposition to predominantly carbonate sedimentation, resulting in 30,000 ft or locally more of mostly limestone and dolomite, the great carbonate aquifer. All these rocks can be grouped into two facies that are gradational over time and place: (1) a western facies of the Cordilleran miogeocline, now exposed in most of the map area, that represents a Late Proterozoic through Devonian offshore carbonate shelf and intertidal environment of deposition and an overlying Mississippian to Permian carbonate platform; and (2) a thinner eastern facies that includes cratonic platform rocks (Colorado Plateau) in the extreme southeastern part of the geologic study area that are mostly shallow marine but includes near-shore through continental environments of deposition.

In Late Devonian to Late Mississippian time, thrust faults and folds of the Antler compressive deformational event transported deeper-marine rocks eastward to about the longitude of Eureka, Nevada, and created a highland there. Clastic sediments, which included the Chainman Shale, were deposited in a foreland marine basin east of the Antler Highland. Carbonate deposition resumed by Late Mississippian time and continued through the Pennsylvanian and into the Permian.

Triassic, Jurassic, and Cretaceous rocks in the geologic study area are mostly continental clastic units deposited only in the eastern part of the area. In fact, the entire geologic study area was characterized by erosion during and after deposition of these units, so they are spotty in distribution and collectively were less than several thousand feet thick. From Middle Jurassic through the early Paleocene, thrust faults, folds, and intrusions of the Sevier compressive deformational event were emplaced. The thrusts transported western facies rocks eastward onto thinner eastern, more cratonic facies. A series of thrusts are well exposed throughout the southern part of the area, and some of these continue into the central and northern part of the map area. But most thrusts strike north-northeast and therefore pass east of the northern part of the map area. The deformation created a highland over most of the area that shed clastic sediment eastward.

During and following the waning stages of the Sevier deformation in the Paleocene, erosional stripping of the Sevier highland that included the northern part of the map area led to sedimentation mostly east of the map area. Only the post-deformational Sheep Pass Formation in mostly White Pine County and the Claron Formation in the extreme southeastern part of the area remain as patches in the geologic study area. These rocks, as well as the deeply eroded underlying Paleozoic and Mesozoic rocks, were inundated by voluminous Eocene to Miocene calc-alkaline, subduction-related volcanic rocks. Most of these rocks are ash-flow tuff, derived from many scattered calderas in the area, but andesitic to dacitic lava flows and mudflow breccia from stratovolcanoes were also deposited. Depositional thickness of overall outflow ash-flow tuffs and flows ranged from about 1,000 to 6,000 ft thick over most of the area, but intracaldera tuffs were thicker. Intrusions, the ultimate sources of the volcanic rocks, are abundant. The locations and types of post-Sevier faults that

deformed the lower to middle Tertiary sedimentary and volcanic rocks are uncertain but doubtless included oblique-slip high-angle faults. East-trending transverse zones, which began to form in the Mesozoic, deformed the calc-alkaline rocks and continued throughout the Cenozoic.

By middle to late Miocene, subduction ceased and the area began to be deformed by extensional tectonics, during which time the rocks were pulled apart in an east-west direction. North-trending normal basin-range faults began to form. By about 10 Ma ago, this deformation intensified and the present topography began to form. North-trending ranges were, and continue to be, uplifted on one side as tilt blocks or on both sides as horsts, and north-trending basins similarly went down as tilt blocks or grabens. The ranges were stripped by erosion and the basins were filled by the erosional debris. The resulting basin-fill sediments accumulated to many thousands of feet thick until the present time. Bimodal (basalt and rhyolite) volcanic rocks, generally thin, are intertongued with the basin-fill sediments.

6.2 General Hydrogeology of the Study Area

Each succeeding episode of deposition and deformation had increasingly greater effects on the hydrogeology of the study area. Most of the hydrogeologic effects for Paleozoic events, including the Antler deformational event, resulted from deposition of the various sediments that would become the aquifers and aquitards of eastern Nevada. The greatest of these aquifers is the carbonate aquifer. On the other hand, deposition of clastic sediments predominated throughout the Mesozoic, resulting primarily in aquitards or low-permeability sedimentary rocks. The Sevier deformational event created barriers to groundwater flow in the southern part of the geologic study area.

During the middle Cenozoic, emplacement of calderas and associated intracaldera intrusions created areas of low permeability within the region but, especially where fractured ash-flow tuffs dominate, the thick calc-alkaline volcanic rocks are major aquifers. Some volcanic rocks sandwiched between valley fill above and carbonate rocks below may have reduced the interconnection of the carbonate aquifer and the valley fill in a few basins. The result is that carbonate aquifers beneath the volcanic rocks may be under artesian pressure or at least have a piezometric head higher than that of the basin fill. Some springs may result from this. During Mesozoic to late Cenozoic time, east-west transverse zones developed. These zones may provide potential conduits or barriers to groundwater flow, but their hydrologic significance is unknown at this time.

From middle Miocene to Holocene time, basin-range extensional tectonics resulted in the dominantly north-south faults of the Great Basin. These north-trending structures are excellent conduits to north or south groundwater flow. Gouge in the core zone of these north-south faults acted as partial to complete barriers, however, to east or west flow. During this tectonism, all rocks became fractured, but brittle units such as ash-flow tuffs, carbonate rocks, and basalt and rhyolite flows became shattered throughout and thus became local to regional aquifers. In carbonate rocks, groundwater dissolution resulted in even larger and more interconnected fracture conduits.

7.0

REFERENCES

The following geologic maps and reports are cited in the text of the report.

Abbott, J.T., Best, M.G., and Morris, H.T., 1983, Geologic map of the Pine Grove—Blawn Mountain area, Beaver County, Utah: U.S. Geological Survey Miscellaneous Investigations Series Map I-1479, scale 1:24,000.

Ahlborn, R.C., 1977, Mesozoic-Cenozoic structural development of the Kern Mountains, eastern Nevada—western Utah: Brigham Young University Geology Studies, v. 24, pt. 2, p. 117–131.

Allmendinger, R.W., Sharp, J.W., Von Tish, D. Serpa, L. Brown, L. Kaufman, S., Oliver, J. and Smith, R.B., 1983, Cenozoic and Mesozoic structure of the eastern Basin and Range province, Utah, from COCORP seismic-reflection data: Geology, v. 11, p. 532–536.

Anderson, R.E., and Barnhard, T.P., 1993, Heterogeneous Neogene strain and its bearing on horizontal extension and horizontal and vertical contraction at the margin of the extensional orogen, Mormon Mountains area, Nevada and Utah: U.S. Geological Survey Bulletin 2011, 43 p.

Armstrong, R.L., 1968, Sevier orogenic belt in Nevada and Utah: Geological Society of America Bulletin, v. 79, p. 429–458.

Armstrong, R.L., 1972, Low-angle denudation faults, hinterland of the Sevier orogenic belt, eastern Nevada and western Utah: Geological Society of America Bulletin, v. 83, p. 1729–1754.

Atwater, T., 1970, Implications of plate tectonics for the Cenozoic tectonic evolution of western North America: Geological Society of America Bulletin, v. 81, p. 3513–3536.

Belcher, W.R., ed., 2004, Death Valley regional ground-water flow system, Nevada and California—Hydrogeologic framework and transient ground-water flow model: U.S. Geological Survey Scientific Investigations Report 2004–5205, 408 p.

Belcher, W.R., and Elliott, P.E., 2001, Hydraulic-property estimates for use with a transient ground-water flow model of the Death Valley regional ground-water flow system, Nevada and California: U.S. Geological Survey Water-Resources Investigations Report 01-4210, CD-ROM; http.//water.usgs.gov/pubs/wri/wri014210/.

Best, M.G., 1987, Geologic map and sections of the area between Hamlin Valley and Escalante Desert, Iron County, Utah: U.S. Geological Survey Miscellaneous Investigations Series Map I-1774, scale 1:50,000.

Best, M.G., Armstrong, R.L., Graustein, W.C., Embree, G.F., and Ahlborn, R.C., 1974, Mica granites of the Kern Mountains pluton, eastern White Pine County, Nevada—Remobilized basement of the Cordilleran miogeosyncline: Geological Society of America Bulletin, v. 85, p. 1277–1286.

Best, M.G., Christiansen, E.H., and Blank, R.H., Jr., 1989a, Oligocene caldera complex and calc-alkaline tuffs and lavas of the Indian Peak volcanic field, Nevada and Utah: Geological Society of America Bulletin, v. 101, p. 1076–1090.

Best, M.G., Christiansen, E.H., Deino, A.L., Gromme, C.S., McKee, E.H., and Noble, D.C., 1989b, Eocene through Miocene volcanism in the Great Basin of the western United States: New Mexico Bureau of Mines and Mineral Resources Memoir 47, p. 91–133.

Best, M.G., Grant, S.K., Hintze, L.F., Cleary, J.G., Hutsinpiller, A., and Saunders, D.M., 1987a, Geologic map of the Indian Peak (southern Needle Range), Beaver and Iron Counties, Utah: U.S. Geological Survey Miscellaneous Investigations Series Map I-1795, scale 1:50,000.

Best, M.G., Hintze, L.F., and Homes, R.D., 1987b, Geologic map of the southern Mountain Home and northern Indian Peak Ranges (central Needle Range), Beaver County, Utah: U.S. Geological Survey Miscellaneous Investigations Series Map I-1796, scale 1:50,000.

Best, M.G., Morris, H.T., Kopf, R.W., and Keith, J.D., 1987c, Geologic map of the southern Pine Valley area, Beaver and Iron Counties, Utah: U.S. Geological Survey Miscellaneous Investigations Series Map I-1794, scale 1:50,000.

Best, M.G., Scott, R.B., Rowley, P.D., Swadley, W.C., Anderson, R.E., Gromme, C.S., Harding, A.E., Deino, A.L., Christiansen, E.H., Tingey, D.G., and Sullivan, K.R., 1993, Oligocene-Miocene caldera complexes, ash-flow sheets, and tectonism in the central and southeastern Great Basin, *in* Lahren, M.M., Texler, J.H., Jr., and Spinosa, Claude, eds, Crustal evolution of the Great Basin and Sierra Nevada: Field Trip Guide, Geological Society of America, Cordilleran and Rocky Mountain sections meeting, p. 285–311.

Best, M.G., Toth, M.I., Kowallis, J.B., Willis, J.B., and Best, V.C., 1989c, Geologic map of the northern White Rock Mountains-Hamlin Valley area, Beaver County, Utah, and Lincoln County, Nevada: U.S. Geological Survey Miscellaneous Investigations Series Map I-1881, scale 1:50,000.

Best, M.G., and Williams, V.S., 1997, Geologic map of the Rose Valley quadrangle, Lincoln County, Nevada: U.S. Geological Survey Geologic Quadrangle Map GQ-1765, scale 1:24,000.

Blakely, R.J., and Simpson, R.W., 1986, Approximating edges of source bodies from magnetic or gravity anomalies: Geophysics, v. 51, p. 1494–1498.

Bohannon, R.G., 1983, Geologic map, tectonic map and structure sections of the Muddy and Northern Black Mountains, Clark County, Nevada: U.S. Geological Survey Miscellaneous Investigations Series Map I-1406, scale 1:62,500.

Bohannon, R.G., 1984, Nonmarine sedimentary rocks of Tertiary age in the Lake Mead region, southeastern Nevada and northwestern Arizona: U.S. Geological Survey Professional Paper 1259, 72 p.

Bohannon, R.G., 1992, Geologic map of the Weiser Ridge quadrangle, Clark County, Nevada: U.S. Geological Survey Geologic Quadrangle Map GQ-1714, scale 1;24,000.

Bol, A.J., Snyder, D.B., Healey, D.L, and Saltus, R.W., 1983, Principal facts, accuracies, sources, and base station descriptions for 3672 gravity stations in the Tonopah and Lund 1° × 2° quadrangles, Nevada: National Technical Information Service, NTIS-PB83-202671.

Brokaw, A.L., 1973, Geologic map of the Ely quadrangle, White Pine County, Nevada: U.S. Geological Survey Geologic Quadrangle Map GQ-697, scale 1:24,000.

Brokaw, A.L., and Barosh, P.J., 1968, Geologic map of the Riepetown quadrangle, White Pine County, Nevada: U.S. Geological Survey Geologic Quadrangle Map GQ-758, scale 1:24,000.

Brokaw, A.L., Bauer, H.L., and Breitrick, R.A., 1973, Geologic map of the Ruth quadrangle, White Pine County, Nevada: U.S. Geological Survey Geologic Quadrangle Map GQ-1085, scale 1:24,000.

Brokaw, A.L., and Heidrich, T., 1966, Geologic map and sections of the Giroux Wash quadrangle, White Pine County, Nevada: U.S. Geological Survey Geologic Quadrangle Map GQ-476, scale 1:24,000.

Brokaw, A.L., and Shawe, D.R., 1965, Geologic map of the Ely 3 quadrangle, White Pine County, Nevada: U.S. Geological Survey Miscellaneous Geological Investigations Map I-449, scale 1:24,000.

Brothers, K., Katzer, T., and Johnson, M., 1996, Hydrology and steady state ground-water model of Dry Lake and Delamar Valleys, Lincoln County, Nevada: Las Vegas, Nevada, Cooperative Water Project Report No. 16, Las Vegas Valley Water District, 48 p.

Brown, C.L., and Schmitt, J.G., 1991, Horse Camp Formation—Record of Miocene-Pliocene extensional basin development, northern Grant Range, Nevada, *in* Flanigan, D.M.H., Hansen, M., and Flanigan, T.E., eds., Geology of White River Valley, the Grant Range, eastern Railroad Valley and western Egan Range, Nevada: Nevada Petroleum Society 1991 Field Trip Guidebook, p. 7–13.

Burbey, T.J., 1997, Hydrogeology and potential for ground-water development, carbonate-rock aquifers, southern Nevada and southeastern California: U.S. Geological Survey Water-Resources Investigations Report 95-4168, 65 p.

Burchfiel, B.C., Fleck, R., Secor, D.T., Vincelette, R.R., and Davis, G.A., 1974, Geology of the Spring Mountains, Nevada: Geological Society of America Bulletin, v. 85, p. 1013–1022.

Caine, J.S., Evans, J.P., and Forster, C.B., 1996, Fault zone architecture and permeability structure: Geology, v. 24, p. 1025–1028.

Carpenter, J.A., and Carpenter, D.G., 1994a, Analysis of basin-range and fold-thrust structure, and reinterpretation of the Mormon Peak detachment and similar features as gravity slide systems, southern Nevada, southwest Utah, and northwest Arizona, *in* Dobbs, S.W., and Taylor, W.J., eds., Structural and stratigraphic investigations and petroleum potential of Nevada, with special emphasis south of the Railroad Valley producing trend: Nevada Petroleum Society 1994 conference volume II (book 1), p. 15–52.

Carpenter, J.A., and Carpenter, D.G., 1994b, Fold-thrust structure, synorogenic rocks, and structural analysis of the North Muddy and Muddy Mountains, Clark County Nevada, *in* Dobbs, S.W., and Taylor, W.J., eds., Structural and stratigraphic investigations and petroleum potential of Nevada, with special emphasis south of the Railroad Valley producing trend: Nevada Petroleum Society 1994 conference volume II (book 1), p. 65–94.

Carpenter, J.A., Carpenter, D.G., and Dobbs, S.W., 1994, Antler orogeny—Paleostructural analysis and constraints on plate tectonic models with a global analogue in southeast Asia, *in* Dobbs, S.W., and Taylor, W.J., eds., Structural and stratigraphic investigations and petroleum potential of Nevada, with special emphasis south of the Railroad Valley producing trend: Nevada Petroleum Society 1994 conference volume II (book 2), p. 187–240.

Christiansen, R.L., and Lipman, P.W., 1972, Cenozoic volcanism and plate tectonic evolution of the western United States—II. Late Cenozoic: Royal Society of London Philosophical Transactions (A), v. 271, p. 249–284.

Christiansen, R.L., and Yeats, R.S., 1992, Post-Laramide geology of the U.S. Cordilleran region, *in* Burchfiel, B.C., Lipman, P.W., and Zoback, M.L., eds., The Cordilleran orogen—Conterminous U.S.: Boulder, Colorado, Geological Society of America, Geology of North America, v. G-3, p. 261–406.

Coats, R.R., 1987, Geology of Elko County, Nevada: Nevada Bureau of Mines and Geology Bulletin 101, 112 p., scale 1:250,000.

Cook, K.L., Bankey, V., Mabey, D.R., and DePangher, M., 1989, Complete Bouguer gravity anomaly map of Utah: Utah Geological and Mineral Survey Map 122, scale 1:500,000.

Cornwall, H.R., 1972, Geology and mineral deposits of southern Nye County, Nevada: Nevada Bureau of Mines and Geology Bulletin 77, 49 p.

Davis, F.D., 2005, Water resources of Millard County, Utah: Utah Geological Survey Open-File Report 447, 27 p.

Dettinger, M.D., 1992, Geohydrology of areas being considered for exploratory drilling and development of the carbonate-rock aquifers in southern Nevada--preliminary assessment: U.S. Geological Survey Water Resources Investigations Report 90-4077, 35 p.

Dettinger, M.D., Harrill, J.R., Schmidt, D.L., and Hess, J.W., 1995, Distribution of carbonate rock aquifers and the potential for their development, southern Nevada and adjacent parts of California, Arizona and Utah: U.S. Geological Survey Water-Resources Investigations Report 91-4146, 100 p.

Dixon, G.L., and Katzer, T.C., 2002, Geology and Hydrology of the lower Virgin River Valley in Nevada, Arizona, and Utah: Virgin Valley Water District, Mesquite, Nevada, Report No. VVWD-01, 126 p.

Dobbs, S.W., Garbee, J.J., Jr., Stuart, C.K., and Nelson, S.L., 1994, Intergrated [sic] geological and geophysical interpretation in the Newark Valley area, Eureka fold-and-thrust belt, east-central Nevada, *in* Dobbs, S.W., and Taylor, W.J., eds., Structural and stratigraphic investigations and petroleum potential of Nevada, with special emphasis south of the Railroad Valley producing trend: Nevada Petroleum Society 1994 conference volume II (book 2), p. 241–253.

Dohrenwend, J.C., Schell, B.A., Menges, C.M., Moring, B.C., and McKittrick, M.A., 1996, Reconnaissance photogeologic map of young (Quaternary and late Tertiary) faults in Nevada: Nevada Bureau of Mines and Geology Open-File Report 96-2.

Donovan, D.J., 1996, Hydrostratigraphy and allostratigraphy of the Cenozoic alluvium in the northwestern part of Las Vegas Valley, Clark County, Nevada: Las Vegas, Nevada, unpublished M.S. thesis, University of Nevada, Las Vegas, 199 p.

du Bray, E.A., and Hurtubise, D.O., 1994, Geologic map of the Seaman Range, Lincoln and Nye Counties, Nevada: U.S. Geological Survey Miscellaneous Investigations Series Map I-2282, scale 1:50,000.

Eakin, T.E., 1966, A regional interbasin groundwater system in the White River area, southeastern Nevada: Water Resources Research, v. 2, p. 251–271.

Ehni, W., and Faulds, J., eds., 2002, Detachment and attenuation in eastern Nevada and its application to petroleum exploration: Reno, Nevada Petroleum Society 2002 Field Trip Guidebook, 163 p.

Eichhubl, P., Taylor, W.L., Pollard, D.D., Aydin, A., 2004, Paleo-fluid flow and deformation in the Aztec Sandstone at the Valley of Fire, Nevada—Evidence for the coupling of hydrogeologic, diagenetic, and tectonic processes: Geological Society of America Bulletin, v. 116, p. 1120–1136.

Ekren, E.B., Bucknam, R.C., Carr, W.J., Dixon, G.L., and Quinlivan, W.D., 1976, East-trending structural lineaments in central Nevada: U.S. Geological Survey Professional Paper 986, 16 p.

Ekren, E.B., Orkild, P.P., Sargent, K.A., and Dixon, G.L., 1977, Geologic map of Tertiary rocks, Lincoln County, Nevada: U.S. Geological Survey Miscellaneous Investigations Series Map I-1041, scale 1:250,000.

Erskine, M.C., 2001, Structural overlap of passive continental margin stratigraphic packages onto the Colorado Plateau cratonic package in southwestern Utah, *in* Erskine, M.C., Faulds, J.E., Bartley, J.M., and Rowley, P.D., eds., The geologic transition, High Plateaus to Great Basin—A symposium and field guide (The Mackin Volume): Utah Geological Association and Pacific Section of the American Association of Petroleum Geologists: Utah Geological Association Publication 30, p. 365–377.

Fairley, J.P., and Hinds, J.J., 2004, Rapid transport pathways for geothermal fluids in an active Great Basin fault zone: Geology, v. 32, p. 825–828.

Fouch, T.D., Lund, K., Schmitt, J.G., Good, S.C., and Hanley, J.H., 1991, Late Cretaceous(?) and Paleogene sedimentary rocks and extensional(?) basins in the region of the Egan and Grant ranges, and White River and Railroad valleys, Nevada—Their relation to Sevier and Laramide contractional basins in the southern Rock Mountains and Colorado Plateau, *in* Flanigan, D.M.H., Hansen, M., and Flanigan, T.E., eds., Geology of White River Valley, the Grant Range, eastern Railroad Valley and western Egan Range, Nevada: Nevada Petroleum Society 1991 Field Trip Guidebook, p. 15–28.

French, D.E., and Schalla, R.A., eds., 1998, Hydrocarbon habitat and special geologic problems of the Great Basin: Reno, Nevada Petroleum Society 1998 Field Trip Guidebook, 102 p.

Gans, P.B., 2000a, The northern White Pine Range, *in* Gans, P.B., and Seedorff, Eric, eds., Geology and Ore Deposits 2000, Field Trip 11, Geological Society of Nevada, p. 83–95.

Gans, P.B., 2000b, The Snake Range metamorphic core complex—Geologic overview of the northern Snake Range, *in* Gans, P.B., and Seedorff, Eric, eds., Geology and Ore Deposits 2000, Field Trip 11, Geological Society of Nevada, p. 99–117.

Gans, P.B., Miller, E.L., McCarthy, J., Ouldcott, M.L., 1985, Tertiary extensional faulting and evolving ductile-brittle transition zones in the northern Snake Range and vicinity—New insights from seismic data: Geology, v. 13, p. 189–193.

Gans, P.B., Mahood, G.A., and Schermer, E., 1989, Synextensional magmatism in the Basin and Range province—A case study from the eastern Great Basin: Geological Society of America Special Paper, v. 233, 53 p.

Garside, L.J., Hess, R.H., Fleming, K.L., and Weimer, B.S., 1988, Oil and gas developments in Nevada: Nevada Bureau of Mines and Geology Bulletin 104, 136 p.

Geological Society of America, 1999, 1999 Geologic Time Scale, Product Code CTS004, accessed at http://www.geosociety.org/science/timescale/timescl.pdf.

Guth, P.L., 1980, Geology of the Sheep Range, Clark County, Nevada: Boston, Massachusetts Institute of Technology, unpublished Ph.D. dissertation, 189 p.

Hamilton, W.B., 1995, Subduction systems and magmatism, *in* Smellie, J.L., ed., Volcanism associated with extension of consuming plate margins: Geological Society Special Publications 81, p. 3–28.

Harding, A.E., Scott, R.B., Mehnert, H.H., and Snee, L.W., 1995, Evidence of the Kane Springs Wash caldera in the Meadow Valley Mountains, southeastern Nevada, *in* Scott, R.B., and Swadley, W.C., eds., Geologic studies in the Basin and Range—Colorado Plateau transition in southeastern Nevada, southwestern Utah, and northwestern Arizona, 1992: U.S. Geological Survey Bulletin 2056, p. 135–180.

Harrill, J.R., Gates, J.S., and Thomas, J.M., 1988, Major ground-water flow systems in the Great Basin region of Nevada, Utah, and adjacent states: U.S. Geological Survey Hydrologic Investigations Atlas HA-694-C, scale 1:1,000,000.

Harrill, J.R., and Prudic, D.E., 1998, Aquifer systems in the Great Basin region of Nevada, Utah, and adjacent states—Summary report: U.S. Geological Survey Professional Paper 1409A, 61 p.

Hauser, E., Potter, C., Hauge, T., Burgess, S., Burtch, S., Mutschler, J., Allmendinger, R., Brown, L., Kaufman, S., and Oliver, J., 1987, Crustal structure of eastern Nevada from COCORP deep seismic reflection data: Geological Society of America Bulletin, v. 99, p. 833–844.

Hess, R., 2001, Nevada oil and gas well database map: Nevada Bureau of Mines and Geology Open-File Report 01-7, PDF file + CD-ROM.

Hess, R., 2004, Nevada oil and gas well database: Nevada Bureau of Mines and Geology Open-File Report 04-1, PDF file, http://www.nbmg.unr.edu/lists/oil/oil.htm.

Hildenbrand, T.G., and Kucks, R.P., 1988a, Total intensity magnetic anomaly map of Nevada: Nevada Bureau of Mines and Geology Map 93A, scale 1:750,000.

Hildenbrand, T.G., and Kucks, R.P., 1988b, Filtered magnetic anomaly maps of Nevada: Nevada Bureau of Mines and Geology Map 93B, scale 1:750,000.

Hintze, L.F., 1980, Geologic map of Utah: Utah Geological and Mineralogical Survey, scale 1:500,000.

Hintze, L.F., 1988, Geologic history of Utah: Brigham Young University Geology Studies, Special Publication 7, 202 p.

Hintze, L.F., Anderson, R.E., and Embree, G.F., 1994, Geologic map of the Motoqua and Gunlock quadrangles, Washington County, Utah: U.S. Geological Survey Miscellaneous Investigations Series Map I-2427, scale 1:24,000.

Hintze, L.F., and Davis, F.D., 2002a, Geologic map of the Wah Wah Mountains North 30' × 60' quadrangle and part of the Garrison 30' × 60' quadrangle, southwest Millard County and part of Beaver County, Utah: Utah Geological Survey Map 182, scale 1:100,000.

Hintze, L.F., and Davis, F.D., 2002b, Geologic map of the Tule Valley 30' × 60' quadrangle and parts of the Ely, Fish Springs, and Kern Mountains 30' × 60' quadrangles, northwest Millard County, Utah: Utah Geological Survey Map 186, scale 1:100,000.

Hintze, L.F., and Davis, F.D., 2003, Geology of Millard County, Utah: Utah Geological Survey Bulletin 133, 305 p.

Hintze, L.F., Willis, G.C., Laes, D.Y.M., Sprinkel, D.A., and Brown, K.D., 2000, Digital geologic map of Utah, Utah Geological Survey Map 179DM, scale 1:500,000.

Hitchborn, A.D., Arbonies, D.G., Peters, S.G., Connors, K.A., Noble, D.C., Larson, L.T., Beebe, J.S., and McKee, E.H., 1996, Geology and gold deposits of the Bald Mountain mining district, White Pine County, Nevada, *in* Coyner, A.R., and Fahey, P.L., eds., Geology and ore deposits of the American Cordillera: Geological Society of Nevada Symposium Proceedings, v. 1, p. 505–546.

Hood, J.W., and Rush, F.E, 1965, Water-Resources Appraisal of the Snake Valley Area, Utah and Nevada, Water Resources – Reconnaissance Series Report 34, U.S. Geological Survey in cooperation with the State of Nevada Department of Conservation and Natural Resources, 43 p.

Hose, R.K., 1977, Structural geology of the Confusion Range, west-central Utah: U.S. Geological Survey Professional Paper 971, 9 p.

Hose, R.K., and Blake, M.C., Jr., 1976, Geology and mineral resources of White Pine County, Nevada, Part 1, Geology: Nevada Bureau of Mines and Geology Bulletin 85, p. 1–35.

Howard, K.A., Kistler, R.W., Snoke, A.W., and Willden, R., 1979, Geologic map of the Ruby Mountains, Nevada: U.S. Geological Survey Miscellaneous Investigations Series Map I-1136, scale 1:125,000.

Jachens, R.C., and Moring, B.C., 1990, Maps of the thickness of Cenozoic deposits and the isostatic residual gravity over basement for Nevada: U.S. Geological Survey Open-File Report 90-404, 15 p.

Jayko, A.S., 1990, Shallow crustal deformation in the Pahranagat area, southern Nevada, *in* Wernicke, B.P., ed., Basin and Range extensional tectonics near the latitude of Las Vegas, Nevada: Geological Society of America Memoir 176, p. 213–236.

Jones, A.E., ed., 1996, Geology and gold deposits of eastern Nevada, 1996 Spring Field Trip Guidebook: Geological Society of Nevada Special Publication No. 23, 166 p.

Kellogg, H.E., 1963, Paleozoic stratigraphy of the southern Egan Range, Nevada: Geological Society of America Bulletin, v. 74, p. 685–708.

Kellogg, H.E., 1964, Cenozoic stratigraphy and structure of the southern Egan Range, Nevada: Geological Society of America Bulletin, v. 75, p. 949–968.

Kirby, S., and Hurlow, H., 2005, Hydrogeologic setting of the Snake Valley hydrologic basin, Millard County, Utah, and White Pine and Lincoln Counties, Nevada—Implications for possible effects of proposed water wells: Utah Geological Survey Report of Investigations 254, CD-ROM.

Kleinhampl, F.J., and Ziony, J.I., 1985, Geology of northern Nye County, Nevada: Nevada Bureau of Mines and Geology Bulletin 99A, 172 p.

Larson, E.R., and Langenheim, R.L., Jr., 1979, The Mississippian and Pennsylvanian (Carboniferous) systems in the United States—Nevada: U.S. Geological Survey Professional Paper 1110-BB, p. BB1–19.

Las Vegas Valley Water District, 2001, Water resources and ground-water modeling in the White River and Meadow Valley flow systems, Clark, Lincoln, Nye and White Pine Counties, Nevada: Las Vegas Valley Water District, 11 chapters + appendices.

Link, P.K., Christie-Blick, N., Devlin, W.J., Elston, D.P., Horodyski, R.J., Levy, M., Miller, J.M.G., Pearson, R.C., Prave, A., Stewart, J.H., Winston, D., Wright, L.A., and Wrucke, C.T., 1993, Middle and Late Proterozoic stratified rocks of the western U.S. Cordillera, Colorado Plateau, and Basin and Range province, Chap. 6, *in* Reed, J.C., Jr., and others, eds., Precambrian—Conterminous U.S.: Geological Society of America, The Geology of North America, v. C-2, p. 463–595.

Lipman, P.W., Prostka, H.J., and Christiansen, R.L., 1972, Cenozoic volcanism and plate tectonic evolution of the western United States—I. Early and middle Cenozoic: Royal Society of London Philosophical Transactions (A), v. 271, p. 217–248.

Longwell, C.R., Pampeyan, E.H., Bowyer, B., and Roberts, R.J., 1965, Geology and mineral deposits of Clark County, Nevada: Nevada Bureau of Mines and Geology Bulletin 62, 218 p., scale 1:250,000.

Loucks, M.D., Tingey, D.G., Best, M.G., Christiansen, E.H., and Hintze, L.F., 1989, Geologic map of the Fortification Range, Lincoln and White Pine Counties, Nevada: U.S. Geological Survey Miscellaneous Investigations Series Map I-1866, scale 1:50,000.

Lumsden, W.W., Walker, C.T., and Francis, R.D., 2002, The Precambrian and Paleozoic stratigraphy of the White Pine, Grant and Schell Creek Ranges in eastern Nevada—The key to interpreting structures formed by extension and attenuation, *in* Ehni, W., and Faulds, J., eds., 2002, Detachment and attenuation in eastern Nevada and its application to petroleum exploration: Nevada Petroleum Society 2002 Field Trip Guidebook, p. 33–72.

Lund, K., Beard, L.S., and Perry, W.J., Jr., 1991, Structures of the northern Grant Range and Railroad Valley, Nye County, Nevada—Implications for oil occurrences, *in* Flanigan, D.M.H., Hansen, M., and Flanigan, T.E., eds., Geology of White River Valley, the Grant Range, eastern Railroad Valley and western Egan Range, Nevada: Nevada Petroleum Society 1991 Field Trip Guidebook, p. 1–6.

LVVWD, see Las Vegas Valley Water District.

Maldonado, F., Spengler, R.W., Hanna, W.F., and Dixon, G.L., 1988, Index of granitic rock masses in the State of Nevada: U.S. Geological Survey Bulletin 1831, 81 p.

Maldonado, F., and Schmidt, D.L., 1991, Geologic map of the southern Sheep Range, Fossil Ridge, and Castle Rock area, Clark County, Nevada: U.S. Geological Survey Miscellaneous Investigations Series Map I-2086, scale 1:24,000.

Mankinen, E.A., Roberts, C.W., McKee, E.H., Chuchel, B.A., and Moring, B.C., 2006, Geophysical Data from the Spring and Snake Valleys Area, Nevada and Utah. U.S. Geological Survey Open File Report 2006-1160, 36 p.

Mankinen, E.A., Roberts, C.W., McKee, E.H., Chuchel, B.A., and Morin, R.L., 2007, Geophysical Data from Spring Valley to Delamar Valley, east-central Nevada: U.S. Geological Survey Open File Report 2007-1190 [http://pubs.usgs.gov/of/2007/1190/].

Maxey, G.B., 1964, Hydrostratigraphic units: Journal of Hydrology, v. 2, p. 124–129.

McPhee, D.K., Pellerin, L., Chuchel, B., and Dixon, G.L., 2005, Resistivity imaging of Spring Valley, Nevada, using the audiomagnetotelluric method: Eos Transactions, American Geophysical Union, v. 86, no. 18, Joint Assembly Supplement, Abstract NS23B-06.

McPhee, D.K., Pellerin, L., Chuchel, B., Tilden, J., and Dixon, G.L., 2007, Resistivity imaging in eastern Nevada using the audiomagnetotelluric method for hydrogeologic framework studies, *in* Proceedings of the 19th Annual Symposium on the Application of Geophysics to Engineering and Environmental Problems (SAGEEP), Seattle, WA., April 2–6, 2006.

Mifflin, M.D., and Wheat, M.M., 1979, Pluvial lakes and estimated pluvial climates of Nevada: Nevada Bureau of Mines and Geology Bulletin 94, 57 p.

Miller, E.L., Dumitru, T.A., Brown, R.W., and Gans, P.B., 1999, Rapid Miocene slip on the Snake Range-Deep Creek Range fault system, east-central Nevada: Geological Society of America Bulletin, v. 111, p. 886–905.

Miller, E.L., Gans, P.B., and Garing, J., 1983, The Snake Range decollement—An exhumed mid-Tertiary ductile-brittle transition: Tectonics, v. 2, p. 239–263.

Miller, E.L., Gans, P.B., and Grier, S.P., 1994, Geologic map of Windy Peak 7.5' quadrangle, White Pine County, Nevada: U.S. Geological Survey Open-File Report 94-687, scale 1:24,000.

Miller, E.L., Grier, S.P., and Brown, J.L., 1995, Geologic map of the Lehman Caves quadrangle, White Pine County, Nevada: U.S. Geological Survey Geologic Quadrangle Map GQ-1758, scale 1:24,000.

Moores, E.M., Scott, R.B., and Lumsden, W.W., 1968, Tertiary tectonics of White Pine-Grant Range region, east-central Nevada, and some regional implications: Geological Society of America Bulletin, v. 79, p. 1703–1726.

Nelson, R.B., 1966, Structural development of northernmost Snake Range, Kern Mountains, and Deep Creek Range, Nevada and Utah: American Association of Petroleum Geologists Bulletin, v. 50, p. 921–951.

Nolan, T.B., 1935, The Gold Hill mining district, Utah: U.S. Geological Survey Professional Paper 177, 172 p.

Nutt, C.J., 2000, Geologic map of the Alligator Ridge area, including the Buck Mountain East and Mooney Basin Summit quadrangles and parts of the Sunshine Well NE and Long Valley Slough quadrangles, White Pine County, Nevada: U.S. Geological Survey Geologic Investigations Series Map I-2691, scale 1:24,000.

Nutt, C.J., Zimbelman, D.R., Campbell, D.L., Duval, J.S., and Hannigan, B.J., 1990, Mineral resources of the Deep Creek Mountains Wilderness Study Area, Juab and Tooele Counties, Utah: U.S. Geological Survey Bulletin 1745-C, 40 p.

Page, W.R., 1998, Geologic map of the Arrow Canyon NW quadrangle, Clark County, Nevada: U.S. Geological Survey Geologic Quadrangle Map GQ-1776, scale 1:24,000.

Page, W.R., and Dixon, G.L., 1992, Northern terminus of Mesozoic Dry Lake thrust fault, Arrow Canyon Range, southeastern Nevada: Geological Society of America Abstracts with Programs, v. 24, no. 6, p. 56.

Page, W.R., Dixon, G.L., Rowley, P.D., and Brickey, D.W., 2005a, Geologic map of parts of the Colorado, White River, and Death Valley groundwater flow systems, Nevada, Arizona, and Utah: Nevada Bureau of Mines & Geology Map 150, scale 1:250,000.

Page, W.R., and Ekren, E.B., 1995, Preliminary geologic map of the Bristol Well quadrangle, Lincoln County, Nevada: U.S. Geological Survey Open-File Report 95-580, 27 p.

Page, W.R., Lundstrom, S.C., Harris, A.G., Langenheim, V.E., Workman, J.B., Mahan, S.A., Paces, J.B., Dixon, G.L., Rowley, P.D., Burchfiel, B.C., Bell, J.W., and Smith, E.I., 2005b, Geologic and geophysical maps of the Las Vegas 30' × 60' quadrangle, Clark and Nye Counties, Nevada, and Inyo County, California: U.S. Geological Survey Scientific Investigations Map 2814, 55 p., scale 1:100,000.

Page, W.R., and Pampeyan, E.H., 1996, Preliminary geologic map of the Paleozoic rocks in the Wildcat Wash SE and Wildcat Wash SW quadrangles, Lincoln and Clark Counties, Nevada: U.S. Geological Survey Open-File Report 96-26, 18 p., scale 1:24,000.

Page, W.R., Scheirer, D.S., and Langenheim, V.E., 2006, Geologic cross sections of parts of the Colorado, White River, and Death Valley regional ground-water flow systems, Nevada, Utah, and Arizona: U.S. Geological Survey Open-File Report 2006-1040, scale 1:250,000.

Pampeyan, E.H., 1993, Geologic map of the Meadow Valley Mountains, Lincoln and Clark Counties, Nevada: U.S. Geological Survey Miscellaneous Investigations Series Map I-2173, scale 1:50,000.

Phelps, G.A., Jewel, E.B., Langenheim, V.E., and Jachens, R.C., 2000, Principal Facts for Gravity Stations in the Vicinity of Coyote Spring Valley, Nevada with Initial Gravity Modeling Results: U.S. Geological Survey Open-File Report 00-420.

Ponce, D.A., 1997, Gravity data of Nevada: U.S. Geological Survey Digital Data Series DDS-42, CD-ROM, 27 p.

Ponce, D.A., 1992, Bouguer gravity map of Nevada, Ely sheet: Nevada Bureau of Mines and Geology Map 99, scale 1:250,000.

Ponce, D.A., Morin, R.L., and Robbins, S.L., 1996, Bouguer gravity map of Nevada, Elko sheet: Nevada Bureau of Mines and Geology Map 107, scale 1:250,000.

Poole, F.G., and Sandberg, C.A., 1977, Mississippian Paleogeography and tectonics of the Western United States, *in* Stewart, J.H., Stevens, C.H., and Fritsche, A.E., eds., Paleozoic paleogeography of the western United States: Pacific Section, Society of Economic Paleontologists and Mineralogists, p. 67–85.

Poole, F.G., and Sandberg, C.A., 1991, Mississippian paleogeography and conodont biostratigraphy of the western United States, *in* Cooper, J.D., and Stevens, C.H., eds., Paleozoic paleogeography of the western United States—II: Pacific Section, Society of Economic Paleontologists and Mineralogists, v. 67, p. 107–136.

Prudic, D.E., Harrill, J.R., and Burbey, T.J., 1995, Conceptual evaluation of regional ground-water flow in the carbonate-rock province of the Great Basin, Nevada, Utah, and adjacent states: U.S. Geological Survey Professional Paper 1409-D, 102 p.

Roberts, R.J., Montgomery, K.M., and Lehner, R.E., 1967, Geology and mineral resources of Eureka County, Nevada: Nevada Bureau of Mines and Geology Bulletin 64, 152 p., scale 1:250,000.

Robinson, J.P., 1993, Provisional geologic map of the Gold Hill quadrangle, Tooele County, Utah: Utah Geological Survey Map 140, scale 1:24,000.

Rowley, P.D., 1998, Cenozoic transverse zones and igneous belts in the Great Basin, western United States--their tectonic and economic implications, *in* Faulds, J.E., and Stewart, J.H., eds., Accommodation zones and transfer zones--The regional segmentation of the Basin and Range province: Geological Society of America Special Paper 323, p. 195–228.

Rowley, P.D., and Anderson, R.E., 1996, The syntectonic caldera—A new caldera type bounded by synchronous linear faults (abs.): Geological Society of America Abstracts with Programs, v. 28, no. 7, p. A-449.

Rowley, P.D., and Dixon, G.L., 2001, The Cenozoic evolution of the Great Basin area, U.S.A.—New interpretations based on regional geologic mapping, *in* Erskine, M.C., Faulds, J.E., Bartley, J.M., and Rowley, P.D., eds., The geologic transition, High Plateaus to Great Basin—A symposium and field guide (The Mackin Volume): Utah Geological Association and Pacific Section of the American Association of Petroleum Geologists: Utah Geological Association Publication 30, p. 169–188.

Rowley, P.D., and Dixon, G.L., 2004, The role of geology in increasing Utah's ground-water resources from faulted terranes—Lessons from the Navajo Sandstone, Utah, and the Death Valley flow system, Nevada-California, *in* Spangler, L.E., ed., Ground water in Utah—Resource, protection, and remediation: Utah Geological Association Publication 31, p. 27–41.

Rowley, P.D., Lipman, P.W., Mehnert, H.H., Lindsey, D.A., and Anderson, J.J., 1978, Blue Ribbon lineament, an east-trending structural zone within the Pioche mineral belt of southwestern Utah and eastern Nevada: U.S. Geological Survey Journal of Research, v. 6, p. 175–192.

Rowley, P.D., Nealey, L.D., Unruh, D.M., Snee, L.W., Mehnert, H.H., Anderson, R.E., and Gromme, C.S., 1995, Stratigraphy of Miocene ash-flow tuffs in and near the Caliente caldera complex, southeastern Nevada and southwestern Utah, *in* Scott, R.B., and Swadley, W.C., eds., Geologic studies in the Basin and Range—Colorado Plateau transition in southeastern Nevada, southwestern Utah, and northwestern Arizona, 1992: U.S. Geological Survey Bulletin 2056, p. 43–88.

Rowley, P.D., and Shroba, R.R., 1991, Geologic map of the Indian Cove quadrangle, Lincoln County, Nevada: U.S. Geological Survey Geologic Quadrangle Map GQ-1701, scale 1:24,000.

Rowley, P.D., Shroba, R.R., Simonds, F.W., Burke, K.J., Axen, G.J., and Olmore, S.D., 1994, Geologic map of the Chief Mountain quadrangle, Lincoln County, Nevada: U.S. Geological Survey Geologic Quadrangle Map GQ-1731, scale 1:24,000.

Rowley, P.D., Snee, L.W., Anderson, R.E., Nealey, L.D., Unruh, D.M., and Ferris, D.E., 2001, Field trip to the Caliente caldera complex, east-striking transverse zones, and nearby mining districts in Nevada-Utah—Implications for petroleum, ground-water, and mineral resources, *in* Erskine, M.C., Faulds, J.E., Bartley, J.M., and Rowley, P.D., eds., The geologic transition, High Plateaus to Great Basin—A symposium and field guide (The Mackin Volume): Utah Geological Association and Pacific Section of the American Association of Petroleum Geologists: Utah Geological Association Publication 30, p. 401–418.

Saltus, R.W., 1988a, Bouguer gravity anomaly map of Nevada: Nevada Bureau of Mines and Geology Map 94A, scale 1:750,000.

Saltus, R.W., 1988b, Regional, residual, and derivative gravity maps of Nevada: Nevada Bureau of Mines and Geology Map 94B, scale 1:750,000.

Saltus, R.W., and Jachens, R.C., 1995, Gravity and basin-depth maps of the Basin and Range province, western United States: U.S. Geological Survey Geophysical Investigations Map GP-1012, scale 1:2,500,000.

Saucier, A.E., 1997, The Antler thrust system in northern Nevada, *in* Perry, A.J., and Abbott, E.W., eds., The Roberts Mountains thrust, Elko and Eureka Counties, Nevada: Nevada Petroleum Society 1997 Field Trip Guidebook, p. 1–16.

Schalla, R.A., and Johnson, E.H., eds., 1994, Oil fields of the Great Basin: Reno, Nevada Petroleum Society, 380 p.

Scheirer, D.S., 2005, Gravity studies of Cave, Dry Lake, and Delamar Valleys, east-central Nevada: U.S. Geological Survey Open-File Report 2005-1339, 27 p.

Schmidt, D.L., 1994, Preliminary geologic map of the Farrier quadrangle, Clark and Lincoln Counties, Nevada: U.S. Geological Survey Open-File Report 94-625, scale 1:24,000.

Schmidt, D.L., and Dixon, G.L., 1995, Geology and aquifer system of the Coyote Spring Valley area, southeastern Nevada: U.S. Geological Survey Open-File Report 95-579, 47 p.

Scott, R.B., Gromme, C.S., Best, M.G., Rosenbaum, J.G., and Hudson, M.R., 1995, Stratigraphic relationships of Tertiary volcanic rocks in central Lincoln County, southeastern Nevada, *in* Scott, R.B., and Swadley, W.C., eds., Geologic studies in the Basin and Range—Colorado Plateau transition in southeastern Nevada, southwestern Utah, and northwestern Arizona, 1992: U.S. Geological Survey Bulletin 2056, p. 5–42.

Scott, R.B., and Swadley, W.C., eds., 1995, Geologic studies in the Basin and Range—Colorado Plateau transition in southeastern Nevada, southwestern Utah, and northwestern Arizona, 1992; U.S. Geological Survey Bulletin 2056, 275 p.

Scott, R.B., Rowley, P.D., Snee, L.W., Anderson, R.E., Harding, A.E., Unruh, D.M., Nealey, L.D., Hudson, M.R., Swadley, W.C., and Ferris, D.E., 1996, Synchronous Oligocene and Miocene extension and magmatism in the vicinity of caldera complexes in southeastern Nevada, *in* Thompson, R.A., Hudson, M.R., and Pillmore, C.L., eds., Geologic excursions to the Rocky Mountains and beyond, Field Trip Guidebook for the 1996 annual meeting, Geological Society of America, Denver, Colorado, October 28-31: Colorado Geological Survey Special Publication 44, 36 p. (CD-ROM).

Seaber, P.R., 1992, Proposed addition to the North American stratigraphic code, hydrostratigraphic units: unpublished manuscript presented by Commissioner Seaber at the 1992 annual meeting of the North American Code of Stratigraphic Nomenclature, Annual GSA meeting (complete text in Donovan, 1996).

Smith, D.L., Gans, P.B., and Miller, E.L., 1991, Palinspastic restoration of Cenozoic extension in the central and eastern Basin and Range province at latitude 39-40° N, *in* Raines, G.L., Lisle, R.E., Schafer, R.W., and Wilkinson, W.H., eds., Geology and the deposits of the Great Basin, Geological Society of Nevada, v. 1, p. 75–86.

Snee, L.W., and Rowley, P.D., 2000, New $^{40}Ar/^{39}Ar$ dates from the Caliente caldera complex, Nevada-Utah—At least 10 million years of Tertiary volcanism in one of the World's largest caldera complexes (abs.): Geological Society of America Abstracts with Programs, v. 32, no. 7, p. A-461.

Snyder, D.B., Healey, D.L., and Saltus, R.W., 1984, Bouguer gravity map of Nevada – Lund sheet: Nevada Bureau of Mines and Geology Map 80, scale 1:250,000.

Snyder, D.B., Wahl, R.R., and Currey, F.E., 1981, Bouguer gravity map of Nevada – Caliente sheet: Nevada Bureau of Mines and Geology Map 70, scale 1:250,000.

Stephens, J.C., 1977, Hydrologic Reconnaissance of the Tule Valley Drainage Basin, Juab and Millard Counties, Utah: Utah Department of Natural Resources Technical Publication No. 56, 37 p.

Stewart, J.H., 1970, Upper Precambrian and Lower Cambrian strata in the southern Great Basin, California and Nevada: U.S. Geological Survey Professional Paper 620, 206 p.

Stewart, J.H., 1974, Correlation of uppermost Precambrian and Lower Cambrian strata from southern to east-central Nevada: U.S. Geological Survey Journal of Research, v. 2, p. 609–618.

Stewart, J.H., 1976, Late Precambrian evolution of North America—Plate-tectonic implications: Geology, v. 4, p. 11–15.

Stewart, J.H., 1980, Geology of Nevada, a discussion to accompany the geologic map of Nevada: Nevada Bureau of Mines and Geology Special Publication 4, 136 p.

Stewart, J.H., 1984, Stratigraphic sections of Lower Cambrian and upper Proterozoic rocks in Nye, Lander, and Lincoln Counties, Nevada, and Sonora, Mexico: U.S. Geological Survey Open-File Report 84-691, 53 p.

Stewart, J.H., and Carlson, J.E., 1976, Cenozoic rocks of Nevada: Nevada Bureau of Mines and Geology Map 52, scale 1:1,000,000.

Stewart, J.H., and Carlson, J.E., 1978, Geologic map of Nevada: U.S. Geological Survey, scale 1:500,000.

Stewart, J.H., Moore, W.J., and Zietz, I., 1977, East-west patterns of Cenozoic igneous rocks, aeromagnetic anomalies, and mineral deposits, Nevada and Utah: Geological Society of America Bulletin, v. 88, p. 67–77.

Stewart, J.H., and Poole, F.G., 1972, Lower Paleozoic and uppermost Precambrian Cordilleran miogeocline, Great Basin, western United States, *in* Dickinson, W.R., ed., Tectonics and sedimentation: Society of Economic Paleontologists and Mineralogists Special Publication 22, p. 28–57.

Swadley, W.C., Page, W.R., Scott, R.B., and Pampeyan, E.H., 1994, Geologic map of the Delamar 3 SE quadrangle, Lincoln County, Nevada: U.S. Geological Survey Geologic Quadrangle Map-GQ-1754, scale 1:24,000.

Swadley, W.C., and Rowley, P.D., 1994, Geologic map of the Pahroc Spring SE quadrangle, Lincoln County, Nevada: U.S. Geological Survey Geologic Quadrangle Map GQ-1752, scale 1:24,000.

Taylor, M.E., Poole, F.G., and Cook, H.E., 1991, Summary of Paleozoic stratigraphy in the southern Egan and Schell Creek ranges, east central Nevada, *in* Flanigan, D.M.H., Hansen, M., and Flanigan, T.E., eds., Geology of White River Valley, the Grant Range, eastern Railroad Valley and western Egan Range, Nevada, Nevada Petroleum Society 1991 Field Trip Guidebook, p. 29–35.

Taylor, W.J., Bartley, J.M., Martin, M.W., Geissman, J.W., Walker, J.D., Armstrong, P.A., and Fryxell, J.E., 2000, Relations between hinterland and foreland shortening—Sevier orogeny, central North American Cordillera: Tectonics, v. 19, p. 1124–1143.

Taylor, W.J., Dobbs, S.W., Nelson, S.L., and Armstrong, P.A., 1994, Generation of four-way closure through multiple tectonic events—Structures of the Timpahute Range, southern Nevada, *in* Dobbs, S.W., and Taylor, W.J., eds., Structural and stratigraphic investigations and petroleum potential of Nevada, with special emphasis south of the Railroad Valley producing trend: Nevada Petroleum Society 1994 conference volume II (book 2), p. 141–156.

Terrascan Group, Inc., 1987, Geologic map of the eastern Great Basin, Nevada and Utah, scale 1:250,000.

Tschanz, C.M., and Pampeyan, E.H., 1970, Geology and Mineral deposits of Lincoln County, Nevada: Nevada Bureau of Mines and Geology Bulletin 73, 188 p.

UDOGM, see Utah Division of Oil, Gas, and Mining.

UDWR, see Utah Division of Water Rights.

Utah Division of Oil, Gas, and Mining, 2006, Online oil and gas information system, well logs, Database as accessed at http://utstnrogmsg/3.state.ut.us/utahrbdmsweb/logs.htm on March 8, 2006.

Utah Division of Water Rights, 2006, Well drilling database, Database as accessed at http://nrwrt1.nr.state.ut.us/cgi/bin/wellview.exe on March 8, 2006.

Vandervoort, D.S., and Schmitt, J.G., 1990, Cretaceous to early Tertiary paleogeography in the hinterland of the Sevier thrust belt, east-central Nevada: Geology, v. 18, p. 567–570.

Van Loenen, R.E., 1987, Geologic map of the Mount Grafton wilderness study area, Lincoln and White Pine Counties, Nevada: U.S. Geological Survey Miscellaneous Field Studies Map MF-1938, scale 1:50,000.

Webring, M., 1985, SAKI-FORTRAN program for generalized linear inversion of gravity and magnetic profiles: U.S. Geological Survey Open-File Report 85-122, 29 p.

Wernicke, B., Walker, J.D., and Beaufait, M.S., 1985, Structural discordance between Neogene detachments and frontal Sevier thrusts, central Mormon Mountains, southern Nevada: Tectonics, v. 4, no. 2, p. 213–246.

Whitebread, D.H., 1970, Geologic map of the Wheeler Peak and Garrison quadrangles, Nevada and Utah: U.S. Geological Survey Miscellaneous Geologic Investigations Map I-578, scale 1:48,000.

Williams, N., and Taylor, W.J., 2002, Extensional oblique-slip barrier transfer fault—The Currant Summit fault, east-central Nevada, *in* Ehni, William and Faulds, James, eds., 2002, Detachment and attenuation in eastern Nevada and its application to petroleum exploration: Nevada Petroleum Society 2002 Field Trip Guidebook, p. 149–163.

Williams, V.S., Best, M.G., and Keith, J.D., 1997, Geologic map of the Ursine-Panaca Summit-Deer Lodge area, Lincoln County, Nevada, and Iron County, Utah: U.S. Geological Survey Miscellaneous Investigations Series Map I-2479, scale 1:50,000.

Willis, J.B., Best, M.G., Kowallis, B.J., and Best, V.C., 1987, Preliminary geologic map of the northern Wilson Creek Range, Lincoln County, Nevada: U.S. Geological Survey Miscellaneous Field Studies Map MF-1971, scale 1:50,000.

Winograd, I.J., and Thordarson, W., 1975, Hydrogeologic and hydrogeochemical framework, south-central Great Basin, Nevada-California, with special reference to the Nevada Test Site: U.S. Geological Survey Professional Paper 712-C, 126 p.

Workman, J.B., Menges, C.M., Page, W.R., Ekren, E.B., Rowley, P.D., and Dixon, G.L., 2002, Tectonic map of the Death Valley ground-water model area, Nevada and California: U.S. Geological Survey Miscellaneous Field Studies Map MF-2381-B, 58 p.

Workman, J.B., Menges, C.M., Page, W.R., Taylor, E.M., Ekren, E.B., Rowley, P.D., Dixon, G.L., Thompson, R.A., and Wright, L.A., 2003, Geologic map of the Death Valley ground water model area, Nevada and California: U.S. Geological Survey Miscellaneous Field Studies MF-2381-A, scale 1:250,000.

Wright, J.E., and Snoke, A.W., 1993, Tertiary magmatism and mylonitization in the Ruby-East Humboldt metamorphic core complex, northeastern Nevada -- U-Pb geochronology and Sr, Nd, and Pb isotope geochemistry: Geological Society of America Bulletin, v. 105, p. 935–952.

Map Bibliography

The following geologic maps and reports were used in the compilation of the geologic maps and cross sections. Many of these are not cited in the text of the report.

Abbott, J.T., Best, M.G., and Morris, H.T., 1983, Geologic map of the Pine Grove—Blawn Mountain area, Beaver County, Utah: U.S. Geological Survey Miscellaneous Investigations Series Map I-1479, scale 1:24,000.

Ahlborn, R.C., 1977, Mesozoic-Cenozoic structural development of the Kern Mountains, eastern Nevada—western Utah: Brigham Young University Geology Studies, v. 24, pt. 2, p. 117–131.

Anderson, R.E., 2003, Geologic map of the Callville Bay quadrangle, Clark County, Nevada, and Mohave County, Arizona: Nevada Bureau of Mines and Geology Map 139, scale 1:24,000.

Anderson, R.E., and Hintze, L.F., 1993, Geologic map of the Dodge Spring quadrangle, Washington County, Utah, and Lincoln County, Nevada: U.S. Geological Survey Geologic Quadrangle Map GQ-1721, scale 1:24,000.

Armstrong, P.A., 1991, Displacement and deformation associated with lateral thrust propagation—An example from the Golden Gate Range, southern Nevada: Salt Lake City, University of Utah, M.S. Thesis, 162 p.

Bartley, J.M., Axen, G.J., Taylor. W.J., and Fryxell, J.E., 1988, Cenozoic tectonics of a transect through eastern Nevada near 38° N latitude, *in* Weide, D.L., and Faber, M.L., eds., This extended land, geological journeys in the southern Basin and Range, Geological Society of America, Cordilleran section, Field Trip Guidebook: University of Nevada, Las Vegas, Department of Geoscience Special Publication no. 2, p. 1–20.

Best, M.G., 1987, Geologic map and sections of the area between Hamlin Valley and Escalante Desert, Iron County, Utah: U.S. Geological Survey Miscellaneous Investigations Series Map I-1774, scale 1:50,000.

Best, M.G., Armstrong, R.L., Graustein, W.C., Embree, G.F., and Ahlborn, R.C., 1974, Mica granites of the Kern Mountains pluton, eastern White Pine County, Nevada—Remobilized basement of the Cordilleran miogeosyncline: Geological Society of America Bulletin, v. 85, p. 1277–1286.

Best, M.G., Christiansen, E.H., and Blank, R.H., Jr., 1989, Oligocene caldera complex and calc-alkaline tuffs and lavas of the Indian Peak volcanic field, Nevada and Utah: Geological Society of America Bulletin, v. 101, p. 1076–1090.

Best, M.G., Christiansen, E.H., Deino, A.L., Gromme, C.S., McKee, E.H., and Noble, D.C., 1989, Eocene through Miocene volcanism in the Great Basin of the western United States: New Mexico Bureau of Mines and Mineral Resources Memoir 47, p. 91–133.

Best, M.G., Grant, S.K., Hintze, L.F., Cleary, J.G., Hutsinpiller, A., and Saunders, D.M., 1987, Geologic map of the Indian Peak (southern Needle Range), Beaver and Iron Counties, Utah: U. S. Geological Survey Miscellaneous Investigations Series Map I-1795, scale 1:50,000.

Best, M.G., Hintze, L.F., Deino, A.L., and Maughan, L.L., 1998, Geologic map of the Fairview Range and Grassy Mountain, Lincoln County, Nevada: Nevada Bureau of Mines and Geology Map 114, 7 p., scale 1:24,000.

Best, M.G., Hintze, L.F., and Homes, R.D., 1987, Geologic map of the southern Mountain Home and northern Indian Peak Ranges (central Needle Range), Beaver County, Utah: U.S. Geological Survey Miscellaneous Investigations Series Map I-1796, scale 1:50,000.

Best, M.G., Morris, H.T., Kopf, R.W., and Keith, J.D., 1987, Geologic map of the southern Pine Valley area, Beaver and Iron Counties, Utah: U.S. Geological Survey Miscellaneous Investigations Series Map I-1794, scale 1:50,000.

Best, M.G., Scott, R.B., Rowley, P.D., Swadley, W.C., Anderson, R.E., Gromme, C.S., Harding, A.E., Deino, A.L., Christiansen, E.H., Tingey, D.G., and Sullivan, K.R., 1993, Oligocene-Miocene caldera complexes, ash-flow sheets, and tectonism in the central and southeastern Great Basin, *in* Lahren, M.M., Texler, J.H., Jr., and Spinosa, C., eds., Crustal evolution of the Great Basin and Sierra Nevada: Field Trip Guide, Geological Society of America, Cordilleran and Rocky Mountain sections meeting, p. 285–311.

Best, M.G., Toth, M.I., Kowallis, J.B., Willis, J.B., and Best, V.C., 1989, Geologic map of the northern White Rock Mountains-Hamlin Valley area, Beaver County, Utah, and Lincoln County, Nevada: U.S. Geological Survey Miscellaneous Investigations Series Map I-1881, scale 1:50,000.

Best, M.G., and Williams, V.S., 1997, Geologic map of the Rose Valley quadrangle, Lincoln County, Nevada: U.S. Geological Survey Geologic Quadrangle Map GQ-1765, scale 1:24,000.

Bohannon, R.G., 1983, Geologic map, tectonic map and structure sections of the Muddy and Northern Black Mountains, Clark County, Nevada: U.S. Geological Survey Miscellaneous Investigations Series Map I-1406, scale 1:62,500.

Bohannon, R.G., 1992, Geologic map of the Weiser Ridge quadrangle, Clark County, Nevada: U.S. Geological Survey Geologic Quadrangle Map GQ-1714, scale 1;24,000.

Brokaw, A.L., 1973, Geologic map of the Ely quadrangle, White Pine County, Nevada: U.S. Geological Survey Geologic Quadrangle Map GQ-697, scale 1:24,000.

Brokaw, A.L., and Barosh, P.J., 1968, Geologic map of the Riepetown quadrangle, White Pine County, Nevada: U.S. Geological Survey Geologic Quadrangle Map GQ-758, scale 1:24,000.

Brokaw, A.L., Bauer, H.L., and Breitrick, R.A., 1973, Geologic map of the Ruth quadrangle, White Pine County, Nevada: U.S. Geological Survey Geologic Quadrangle Map GQ-1085, scale 1:24,000.

Brokaw, A.L., and Heidrich, T., 1966, Geologic map and sections of the Giroux Wash quadrangle, White Pine County, Nevada: U.S. Geological Survey Geologic Quadrangle Map GQ-476, scale 1:24,000.

Brokaw, A.L., and Shawe, D.R., 1965, Geologic map of the Ely 3 quadrangle, White Pine County, Nevada: U.S. Geological Survey Miscellaneous Geological Investigations Map I-449, scale 1:24,000.

Brown, C.L., and Schmitt, J.G., 1991, Horse Camp Formation—Record of Miocene-Pliocene extensional basin development, northern Grant Range, Nevada, *in* Flanigan, D.M.H., Hansen, M., and Flanigan, T.E., eds., Geology of White River Valley, the Grant Range, eastern Railroad Valley and western Egan Range, Nevada: Nevada Petroleum Society 1991 Field Trip Guidebook, p. 7–13.

Carpenter, J.A., and Carpenter, D.G., 1994, Analysis of basin-range and fold-thrust structure, and reinterpretation of the Mormon Peak detachment and similar features as gravity slide systems, southern Nevada, southwest Utah, and northwest Arizona, *in* Dobbs, S.W., and Taylor, W.J., eds., Structural and stratigraphic investigations and petroleum potential of Nevada, with special emphasis south of the Railroad Valley producing trend: Nevada Petroleum Society 1994 conference volume II (book 1), p. 15–52.

Carpenter, J.A., Carpenter, D.G., and Dobbs, S.W., 1994, Antler orogeny—Paleostructural analysis and constraints on plate tectonic models with a global analogue in southeast Asia, *in* Dobbs, S.W., and Taylor, W.J., eds., Structural and stratigraphic investigations and petroleum potential of Nevada, with special emphasis south of the Railroad Valley producing trend: Nevada Petroleum Society 1994 conference volume II (book 2), p. 187–240.

Castor, S.B., Faulds, J.E., Rowland, S.M., and de Polo, C.M., 2000, Geologic map of the Frenchman Mountain quadrangle, Clark County, Nevada and Mohave County, Arizona: Nevada Bureau of Mines and Geology Map 127, scale 1:24,000.

Coats, R.R., 1987, Geology of Elko County, Nevada: Nevada Bureau of Mines and Geology Bulletin 101, 112 p., scale 1:250,000.

Cornwall, H.R., 1972, Geology and mineral deposits of southern Nye County, Nevada: Nevada Bureau of Mines and Geology Bulletin 77, 49 p.

Dixon, G.L., Hedlund, D.C., and Ekren, E.B., 1972, Geologic map of the Pritchards Station quadrangle, Nye County, Nevada: U.S. Geological Survey Miscellaneous Geologic Investigations Map I-728, scale 1:48,000.

Dixon, G.L., and Katzer, T.C., 2002, Geology and Hydrology of the lower Virgin River Valley in Nevada, Arizona, and Utah: Virgin Valley Water District, Mesquite, Nevada, Report No. VVWD-01, 126 p.

du Bray, E.A., and Hurtubise, D.O., 1994, Geologic map of the Seaman Range, Lincoln and Nye Counties, Nevada: U.S. Geological Survey Miscellaneous Investigations Series Map I-2282, scale 1:50,000.

Duebendorfer, E.M., 2003, Geologic map of the Government Wash quadrangle, Clark County, Nevada: Nevada Bureau of Mines and Geology Map 140, scale 1:24,000.

Ekren, E.B., Anderson, R.E., Rogers, C.L., and Noble, D.C., 1971, Geology of northern Nellis Air Force Base Bombing and Gunnery Range, Nye County, Nevada: U.S. Geological Survey Professional Paper 651, 91 p.

Ekren, E.B., Bath, G.D., Dixon, G.L., Healey, D.L., and Quinlivan, W.D., 1974, Tertiary history of Little Fish Lake Valley, Nye County, Nevada, and implications as to the origin of the Great Basin: U.S. Geological Survey Journal of Research, v. 2, no. 1, p. 105–118.

Ekren, E.B., Bucknam, R.C., Carr, W.J., Dixon, G.L., and Quinlivan, W.D., 1976, East-trending structural lineaments in central Nevada: U.S. Geological Survey Professional Paper 986, 16 p.

Ekren, E.B., Hinrichs, E.N., and Dixon, G.L., 1972, Geologic map of The Wall quadrangle, Nye County, Nevada: U.S. Geological Survey Miscellaneous Geologic Investigations Map I-719, scale 1:48,000.

Ekren, E.B., Hinrichs, E.N., Quinlivan, W.D., and Hoover, D.L., 1973, Geologic map of the Moores Station quadrangle, Nye County, Nevada: U.S. Geological Survey Miscellaneous Geologic Investigations Map I-756, scale 1:48,000.

Ekren, E.B., Orkild, P.P., Sargent, K.A., and Dixon, G.L., 1977, Geologic map of Tertiary rocks, Lincoln County, Nevada: U.S. Geological Survey Miscellaneous Investigations Series Map I-1041, scale 1:250,000.

Ekren, E.B., and Page, W.R., 1995, Preliminary geologic map of the Coyote Spring quadrangle, Lincoln County, Nevada: U.S. Geological Survey Open-File Report 95-550, 19 p., scale 1:24,000.

Ekren, E.B., Quinlivan, W.D., Snyder, R.P., and Kleinhampl, F.J., 1974, Stratigraphy, structure, and geologic history of the Lunar Lake caldera of northern Nye County, Nevada: U.S. Geological Survey Journal of Research, v. 2, no. 5, p. 599–608.

Ekren, E.B., Rogers, C.L., and Dixon, G.L., 1973, Geologic and bouguer gravity map of the Reveille quadrangle, Nye County, Nevada: U.S. Geological Survey Miscellaneous Investigations Series Map I-806, scale 1:48,000.

Elliott, P.E., Beck, D.A., and Prudic, D.E., 2006, Characterization of surface-water resources in the Great Basin National Park area and their susceptibility to ground-water withdrawals in adjacent valleys, White Pine County, Nevada: U.S. Geological Survey Scientific Investigations Report 2006-5099, 156 p.

Erskine, M.C., 2001, Structural overlap of passive continental margin stratigraphic packages onto the Colorado Plateau cratonic package in southwestern Utah, *in* Erskine, M.C., Faulds, J.E., Bartley, J.M., and Rowley, P.D., eds., The geologic transition, High Plateaus to Great Basin—A symposium and field guide (The Mackin Volume): Utah Geological Association and Pacific Section of the American Association of Petroleum Geologists: Utah Geological Association Publication 30, p. 365–377.

Fouch, T.D., Lund, K., Schmitt, J.G., Good, S.C., and Hanley, J.H., 1991, Late Cretaceous(?) and Paleogene sedimentary rocks and extensional(?) basins in the region of the Egan and Grant ranges, and White River and Railroad valleys, Nevada—Their relation to Sevier and Laramide contractional basins in the southern Rock Mountains and Colorado Plateau, *in* Flanigan, D.M.H., Hansen, M., and Flanigan, T.E., eds., Geology of White River Valley, the Grant Range, eastern Railroad Valley and western Egan Range, Nevada: Nevada Petroleum Society 1991 Field Trip Guidebook, p. 15–28.

Gans, P.B., 2000, The northern White Pine Range, *in* Gans, P.B., and Seedorff, E., eds., Geology and Ore Deposits 2000, Field Trip 11, Geological Society of Nevada, p. 83–95.

Gans, P.B., 2000, The Snake Range metamorphic core complex—Geologic overview of the northern Snake Range, *in* Gans, P.B., and Seedorff, E., eds., Geology and Ore Deposits 2000, Field Trip 11, Geological Society of Nevada, p. 99–117.

Gans, P.B., Mahood, G.A., and Schermer, E., 1989, Synextensional magmatism in the Basin and Range province—A case study from the eastern Great Basin: Geological Society of America Special Paper, v. 233, 53 p.

Gans, P.B., Miller, E.L., Huggins, C.C., and Lee, J., 1999, Geologic map of the Little Horse Canyon quadrangle, Nevada: Nevada Bureau of Mines and Geology Field Studies Map 20, scale 1:24,000.

Gans, P.B., Miller, E.L., and Lee, J., 1999, Geologic map of the Spring Mountain quadrangle, Nevada: Nevada Bureau of Mines and Geology Field Studies Map 18, scale 1:24,000.

Gans, P.B., Miller, E.L., McCarthy, J., Ouldcott, M.L., 1985, Tertiary extensional faulting and evolving ductile-brittle transition zones in the northern Snake Range and vicinity—New insights from seismic data: Geology, v. 13, p. 189–193.

Guth, P.L., 1980, Geology of the Sheep Range, Clark County, Nevada: Boston, Massachusetts Institute of Technology, unpublished Ph.D. dissertation, 189 p.

Harding, A.E., Scott, R.B., Mehnert, H.H., and Snee, L.W., 1985, Evidence of the Kane Springs Wash caldera in the Meadow Valley Mountains, southeastern Nevada, *in* Scott, R.B., and Swadley, W.C., eds., Geologic studies in the Basin and Range—Colorado Plateau transition in southeastern Nevada, southwestern Utah, and northwestern Arizona, 1992: U.S. Geological Survey Bulletin 2056, p. 135–180.

Hauser, E., Potter, C., Hauge, T., Burgess, S., Burtch, S., Mutschler, J., Allmendinger, R., Brown, L., Kaufman, S., and Oliver, J., 1987, Crustal structure of eastern Nevada from COCORP deep seismic reflection data: Geological Society of America Bulletin, v. 99, p. 833–844.

Hintze, L.F., 1980, Geologic map of Utah: Utah Geological and Mineralogical Survey, scale 1:500,000.

Hintze, L.F., 1988, Geologic history of Utah: Brigham Young University Geology Studies, Special Publication 7, 202 p.

Hintze, L.F., Anderson, R.E., and Embree, G.F., 1994, Geologic map of the Motoqua and Gunlock quadrangles, Washington County, Utah: U.S. Geological Survey Miscellaneous Investigations Series Map I-2427, scale 1:24,000.

Hintze, L.F., and Axen, G.J., 1995, Geologic map of the Scarecrow Peak quadrangle, Washington County, Utah, and Lincoln County, Nevada: U.S. Geological Survey Geologic Quadrangle Map GQ-1759, scale 1:24,000.

Hintze, L.F., and Axen, G.J., 2001, Geologic map of the Lime Mountain quadrangle, Lincoln County, Nevada: Nevada Bureau of Mines and Geology Map 129, scale 1:24,000.

Hintze, L.F., and Davis, F.D., 2002, Geologic map of the Tule Valley 30' × 60' quadrangle and parts of the Ely, Fish Springs, and Kern Mountains 30' × 60' quadrangles, northwest Millard County, Utah: Utah Geological Survey Map 186, scale 1:100,000.

Hintze, L.F., and Davis, F.D., 2002, Geologic map of the Wah Wah Mountains North 30' × 60' quadrangle and part of the Garrison 30' × 60' quadrangle, southwest Millard County and part of Beaver County, Utah: Utah Geological Survey Map 182, scale 1:100,000.

Hintze, L.F., and Davis, F.D., 2003, Geology of Millard County, Utah: Utah Geological Survey Bulletin 133, 305 p.

Hintze, L.F., Grant, S.K., Weaver, C.L., and Best, M.G., 1994, Geologic map of the Blue Mountain-Lund area, Beaver and Iron Counties, Utah: U.S. Geological Survey Miscellaneous Investigations Map I-2361, scale 1:50,000.

Hintze, L.F., and Hammond, B.J., 1994, Geologic map of the Shivwits quadrangle, Washington County, Utah: Utah Geological Survey Map 153, 21 p., scale 1:24,000.

Hintze, L.F., Willis, G.C., Laes, D.Y.M., Sprinkel, D.A., and Brown, K.D., 2000, Digital geologic map of Utah, Utah Geological Survey Map 179DM, scale 1:500,000.

Hitchborn, A.D., Arbonies, D.G., Peters, S.G., Connors, K.A., Noble, D.C., Larson, L.T., Beebe, J.S., and McKee, E.H., 1996, Geology and gold deposits of the Bald Mountain mining district, White Pine County, Nevada, *in* Coyner, A.R., and Fahey, P.L., eds., Geology and ore deposits of the American Cordillera: Geological Society of Nevada Symposium Proceedings, v. 1, p. 505–546.

Hose, R.K., 1977, Structural geology of the Confusion Range, west-central Utah: U.S. Geological Survey Professional Paper 971, 9 p.

Hose, R.K., and Blake, M.C., Jr., 1976, Geology and mineral resources of White Pine County, Nevada, Part 1, Geology: Nevada Bureau of Mines and Geology Bulletin 85, p. 1–35.

Howard, K.A., Kistler, R.W., Snoke, A.W., and Willden, R., 1979, Geologic map of the Ruby Mountains, Nevada: U.S. Geological Survey Miscellaneous Investigations Series Map I-1136, scale 1:125,000.

Jayko, A.S., 1990, Shallow crustal deformation in the Pahranagat area, southern Nevada, *in* Wernicke, B.P., ed., Basin and Range extensional tectonics near the latitude of Las Vegas, Nevada: Geological Society of America Memoir 176, p. 213–236.

Keith, J.D., Tingey, D.G., and Best, M.G., 1994, Geologic map of the Rice Mountain quadrangle, Nevada and Utah: Nevada Bureau of Mines and Geology Field Studies Map 7, scale 1:24,000.

Kellogg, H.E., 1963, Paleozoic stratigraphy of the southern Egan Range, Nevada: Geological Society of America Bulletin, v. 74, p. 685–708.

Kellogg, H.E., 1964, Cenozoic stratigraphy and structure of the southern Egan Range, Nevada: Geological Society of America Bulletin, v. 75, p. 949–968.

Kleinhampl, F.J., and Ziony, J.I., 1985, Geology of northern Nye County, Nevada: Nevada Bureau of Mines and Geology Bulletin 99A, 172 p.

Lee, J., Gans, P.B., and Miller, E.L., 1999, Geologic map of the Mormon Jack Pass quadrangle, Nevada: Nevada Bureau of Mines and Geology Field Studies Map 17, scale 1:24,000.

Lee, J., Gans, P.B., and Miller, E.L., 1999, Geologic map of the Third Butte East quadrangle, Nevada: Nevada Bureau of Mines and Geology Field Studies Map 16, scale 1:24,000.

Lee, J., Miller, E.L., Gans, P.B., and Huggins, C.C., 1999, Geologic map of the Mount Moriah quadrangle, Nevada: Nevada Bureau of Mines and Geology Field Studies Map 19, scale 1:24,000.

Link, P.K., Christie-Blick, N., Devlin, W.J., Elston, D.P., Horodyski, R.J., Levy, M., Miller, J.M.G., Pearson, R.C., Prave, A., Stewart, J.H., Winston, D., Wright, L.A., and Wrucke, C.T., 1993, Middle and Late Proterozoic stratified rocks of the western U.S. Cordillera, Colorado Plateau, and Basin and Range province, Chap. 6, *in* Reed, J.C., Jr., and others, eds., Precambrian—Conterminous U.S.: Geological Society of America, The Geology of North America, v. C-2, p. 463–595.

Longwell, C.R., Pampeyan, E.H., Bowyer, B., and Roberts, R.J., 1965, Geology and mineral deposits of Clark County, Nevada: Nevada Bureau of Mines and Geology Bulletin 62, 218 p., scale 1:250,000.

Loucks, M.D., Tingey, D.G., Best, M.G., Christiansen, E.H., and Hintze, L.F., 1989, Geologic map of the Fortification Range, Lincoln and White Pine Counties, Nevada: U.S. Geological Survey Miscellaneous Investigations Series Map I-1866, scale 1:50,000.

Lund, K., Beard, L.S., and Perry, W.J., Jr., 1991, Structures of the northern Grant Range and Railroad Valley, Nye County, Nevada—Implications for oil occurrences, *in* Flanigan, D.M.H., Hansen, M., and Flanigan, T.E., eds., Geology of White River Valley, the Grant Range, eastern Railroad Valley and western Egan Range, Nevada: Nevada Petroleum Society 1991 Field Trip Guidebook, p. 1–6.

Maldonado, F., and Schmidt, D.L., 1991, Geologic map of the southern Sheep Range, Fossil Ridge, and Castle Rock area, Clark County, Nevada: U.S. Geological Survey Miscellaneous Investigations Series Map I-2086, scale 1:24,000.

Maldonado, F., Spengler, R.W., Hanna, W.F., and Dixon, G.L., 1988, Index of granitic rock masses in the State of Nevada: U.S. Geological Survey Bulletin 1831, 81 p.

Miller, E.L., and Gans, P.B., 1999, Geologic map of The Cove quadrangle, Nevada and Utah: Nevada Bureau of Mines and Geology Field Studies Map 22, scale 1:24,000.

Miller, E.L., Gans, P.B., and Garing, J., 1983, The Snake Range decollement—An exhumed mid-Tertiary ductile-brittle transition: Tectonics, v. 2, p. 239–263.

Miller, E.L., Gans, P.B., and Grier, S.P., 1994, Geologic map of Windy Peak 7.5' quadrangle, White Pine County, Nevada: U.S. Geological Survey Open-File Report 94-687, scale 1:24,000.

Miller, E.L., Gans, P.B., Grier, S.P., Huggins, C.C., and Lee, J., 1999, Geologic map of the Old Mans Canyon quadrangle, Nevada and Utah: Nevada Bureau of Mines and Geology Field Studies Map 21, scale 1:24,000.

Miller, E.L., Grier, S.P., and Brown, J.L., 1995, Geologic map of the Lehman Caves quadrangle, White Pine County, Nevada: U.S. Geological Survey Geologic Quadrangle Map GQ-1758, scale 1:24,000.

Nelson, R.B., 1966, Structural development of northernmost Snake Range, Kern Mountains, and Deep Creek Range, Nevada and Utah: American Association of Petroleum Geologists Bulletin, v. 50, p. 921–951.

Nolan, T.B., 1935, The Gold Hill mining district, Utah: U.S. Geological Survey Professional Paper 177, 172 p.

Nolan, T.B., Merriam, C.W., and Blake, M.C., Jr., 1974, Geologic map of the Pinto Summit quadrangle, Eureka and White Pine Counties, Nevada: U.S. Geological Survey Miscellaneous Investigations Series Map I-793, scale 1:31,680.

Nolan, T.B., Merriam, C.W., and Brew, D.A., 1971, Geologic map of the Eureka quadrangle, Eureka and White Pine Counties, Nevada: U.S. Geological Survey Miscellaneous Investigations Series Map I-612, scale 1:31,680.

Nutt, C.J., 2000, Geologic map of the Alligator Ridge area, including the Buck Mountain East and Mooney Basin Summit quadrangles and parts of the Sunshine Well NE and Long Valley Slough quadrangles, White Pine County, Nevada: U.S. Geological Survey Geologic Investigations Series Map I-2691, scale 1:24,000.

Nutt, C.J., 2004, Geologic map of the Big Bald Mountain quadrangle and part of the Tognini Spring quadrangle, White Pine County, Nevada: Nevada Bureau of Mines and Geology Map 145, scale 1:24,000.

Nutt, C.J., Zimbelman, D.R., Campbell, D.L., Duval, J.S., and Hannigan, B.J., 1990, Mineral resources of the Deep Creek Mountains Wilderness Study Area, Juab and Tooele Counties, Utah: U.S. Geological Survey Bulletin 1745-C, 40 p.

Page, W.R., 1992, Preliminary geologic map of the Arrow Canyon quadrangle, Clark County, Nevada: U.S. Geological Survey Open-File Report 92-681, scale 1:24,000.

Page, W.R., 1998, Geologic map of the Arrow Canyon NW quadrangle, Clark County, Nevada: U.S. Geological Survey Geologic Quadrangle Map GQ-1776, scale 1:24,000.

Page, W.R., Dixon, G.L., Rowley, P.D., and Brickey, D.W., 2005, Geologic map of parts of the Colorado, White River, and Death Valley groundwater flow systems, Nevada, Arizona, and Utah: Nevada Bureau of Mines & Geology Map 150, scale 1:250,000.

Page, W.R., Lundstrom, S.C., Harris, A.G., Langenheim, V.E., Workman, J.B., Mahan, S.A., Paces, J.B., Dixon, G.L., Rowley, P.D., Burchfiel, B.C., Bell, J.W., and Smith, E.I., 2005, Geologic and geophysical maps of the Las Vegas 30' × 60' quadrangle, Clark and Nye Counties, Nevada, and Inyo County, California: U.S. Geological Survey Scientific Investigations Map 2814, 55 p., scale 1:100,000.

Page, W.R., and Pampeyan, E.H., 1996, Preliminary geologic map of the Paleozoic rocks in the Wildcat Wash SE and Wildcat Wash SW quadrangles, Lincoln and Clark Counties, Nevada: U.S. Geological Survey Open-File Report 96-26, 18 p., scale 1:24,000.

Page, W.R., Scheirer, D.S., and Langenheim, V.E., 2006, Geologic cross sections of parts of the Colorado, White River, and Death Valley regional ground-water flow systems, Nevada, Utah, and Arizona: U.S. Geological Survey Open-File Report 2006-1040, scale 1:250,000.

Page, W.R., Swadley, W.C., and Scott, R.B., 1990, Preliminary geologic map of the Delamar 3 SW quadrangle, Lincoln County, Nevada: U.S. Geological Survey Open-File Report 90-366, scale 1:24,000.

Pampeyan, E.H., 1993, Geologic map of the Meadow Valley Mountains, Lincoln and Clark Counties, Nevada: U.S. Geological Survey Miscellaneous Investigations Series Map I-2173, scale 1:50,000.

Poole, F.G., and Sandberg, C.A., 1977, Mississippian Paleogeography and tectonics of the Western United States, *in* Stewart, J.H., Stevens, C.H., and Fritsche, A.E., eds., Paleozoic paleogeography of the western United States: Pacific Section, Society of Economic Paleontologists and Mineralogists, p. 67–85.

Poole, F.G., and Sandberg, C.A., 1991, Mississippian paleogeography and conodont biostratigraphy of the western United States, *in* Cooper, J.D., and Stevens, C.H., eds., Paleozoic paleogeography of the western United States—II: Pacific Section, Society of Economic Paleontologists and Mineralogists, v. 67, p. 107–136.

Quinlivan, W.D., and Rogers, C.L., 1974, Geologic map of the Tybo quadrangle, Nye County, Nevada: U.S. Geological Survey Miscellaneous Investigations Series Map I-821, scale 1:48,000.

Quinlivan, W.D., Rogers, C.L., and Dodge, H.W., Jr., 1974, Geologic map of the Portuguese Mountain quadrangle, Nye County, Nevada: U.S. Geological Survey Miscellaneous Investigations Series Map I-804, scale 1:48,000.

Roberts, R.J., Montgomery, K.M., and Lehner, R.E., 1967, Geology and mineral resources of Eureka County, Nevada: Nevada Bureau of Mines and Geology Bulletin 64, 152 p., scale 1:250,000.

Robinson, J.P., 1993, Provisional geologic map of the Gold Hill quadrangle, Tooele County, Utah: Utah Geological Survey Map 140, scale 1:24,000.

Rowley, P.D., 1998, Cenozoic transverse zones and igneous belts in the Great Basin, western United States--their tectonic and economic implications, *in* Faulds, J.E., and Stewart, J.H., eds., Accommodation zones and transfer zones--The regional segmentation of the Basin and Range province: Geological Society of America Special Paper 323, p. 195–228.

Rowley, P.D., and Dixon, G.L., 2001, The Cenozoic evolution of the Great Basin area, U.S.A.—New interpretations based on regional geologic mapping, *in* Erskine, M.C., Faulds, J.E., Bartley, J.M.,

and Rowley, P.D., eds., The geologic transition, High Plateaus to Great Basin—A symposium and field guide (The Mackin Volume): Utah Geological Association and Pacific Section of the American Association of Petroleum Geologists: Utah Geological Association Publication 30, p. 169–188.

Rowley, P.D., Lipman, P.W., Mehnert, H.H., Lindsey, D.A., and Anderson, J.J., 1978, Blue Ribbon lineament, an east-trending structural zone within the Pioche mineral belt of southwestern Utah and eastern Nevada: U.S. Geological Survey Journal of Research, v. 6, p. 175–192.

Rowley, P.D., Nealey, L.D., Unruh, D.M., Snee, L.W., Mehnert, H.H., Anderson, R.E., and Gromme, C.S., 1995, Stratigraphy of Miocene ash-flow tuffs in and near the Caliente caldera complex, southeastern Nevada and southwestern Utah, *in* Scott, R.B., and Swadley, W.C., eds., Geologic studies in the Basin and Range—Colorado Plateau transition in southeastern Nevada, southwestern Utah, and northwestern Arizona, 1992: U.S. Geological Survey Bulletin 2056, p. 43–88.

Rowley, P.D., and Shroba, R.R., 1991, Geologic map of the Indian Cove quadrangle, Lincoln County, Nevada: U.S. Geological Survey Geologic Quadrangle Map GQ-1701, scale 1:24,000.

Rowley, P.D., Shroba, R.R., Simonds, F.W., Burke, K.J., Axen, G.J., and Olmore, S.D., 1994, Geologic map of the Chief Mountain quadrangle, Lincoln County, Nevada: U.S. Geological Survey Geologic Quadrangle Map GQ-1731, scale 1:24,000.

Rowley, P.D., Williams, V.S., Vice, G.S., Maxwell, D.J., Hacker, D.B., Snee, L.W., and Mackin, J.H., in press, Geologic map of the Cedar City 30' × 60' quadrangle, Iron and Washington Counties, Utah: Utah Geological Survey Map, scale 1:100,000.

Sargent, K.A., and Roggensack, K., 1984, Map showing outcrops of pre-Quaternary ash-flow tuffs and volcaniclastic rocks, Basin and Range province, Nevada: U.S. Geological Survey Water-Resources Investigations Report WRIR 83-4119-E, scale 1:500,000.

Saucier, A.E., 1997, The Antler thrust system in northern Nevada, *in* Perry, A.J., and Abbott, E.W., eds., The Roberts Mountains thrust, Elko and Eureka Counties, Nevada: Nevada Petroleum Society 1997 Field Trip Guidebook, p. 1–16.

Scheirer, D.S., 2005, Gravity studies of Cave, Dry Lake, and Delamar Valleys, east-central Nevada: U.S. Geological Survey Open-File Report 2005-1339, 27 p.

Schmidt, D.L., 1994, Preliminary geologic map of the Farrier quadrangle, Clark and Lincoln Counties, Nevada: U.S. Geological Survey Open-File Report 94-625, scale 1:24,000.

Schmidt, D.L., Page, W.R., and Workman, J.B., 1996, Preliminary geologic map of the Moapa West quadrangle, Clark County, Nevada: U.S. Geological Survey Open-File Report 96-521, scale 1:24,000.

Scott, R.B., Gromme, C.S., Best, M.G., Rosenbaum, J.G., and Hudson, M.R., 1995, Stratigraphic relationships of Tertiary volcanic rocks in central Lincoln County, southeastern Nevada, *in* Scott, R.B., and Swadley, W.C., eds., Geologic studies in the Basin and Range—Colorado Plateau transition in southeastern Nevada, southwestern Utah, and northwestern Arizona, 1992: U.S. Geological Survey Bulletin 2056, p. 5–42.

Scott, R.B., Harding, A.E., Swadley, W.C., and Pampeyan, E.H., 1991, Preliminary geologic map of the Vigo NW quadrangle, Lincoln County, Nevada: U.S. Geological Survey Open-File Report 91-389, scale 1:24,000.

Scott, R.B., Novak, S.W., and Swadley, W.C., 1990, Preliminary geologic map of the Delamar 3 NE quadrangle, Lincoln County, Nevada: U.S. Geological Survey Open-File Report 90-33, scale 1:24,000.

Scott, R.B., Page, W.R., and Swadley, W.C., 1990, Preliminary geologic map of the Delamar 3 NW quadrangle, Lincoln County, Nevada: U.S. Geological Survey Open-File Report 90-405, scale 1:24,000.

Scott, R.B., Rowley, P.D., Snee, L.W., Anderson, R.E., Harding, A.E., Unruh, D.M., Nealey, L.D., Hudson, M.R., Swadley, W.C., and Ferris, D.E., 1996, Synchronous Oligocene and Miocene extension and magmatism in the vicinity of caldera complexes in southeastern Nevada, *in* Thompson, R.A., Hudson, M.R., and Pillmore, C.L., eds., Geologic excursions to the Rocky Mountains and beyond, Field Trip Guidebook for the 1996 annual meeting, Geological Society of America, Denver, Colorado, October 28-31: Colorado Geological Survey Special Publication 44, 36 p. (CD-ROM).

Scott, R.B., Swadley, W.C., and Novak, S.W., 1993, Geologic map of the Delamar Lake quadrangle, Lincoln County, Nevada: U.S. Geological Survey Geologic Quadrangle Map GQ-1730, scale 1:24,000.

Scott, R.B., Swadley, W.C., and Page, W.R., 1991, Preliminary geologic map of the Gregerson Basin quadrangle, Lincoln County, Nevada: U.S. Geological Survey Open-File Report 90-646, scale 1:24,000.

Slate, J.L., Berry, M.E., Rowley, P.D., Fridrich, C.J., Williams, V.S., Morgan, K.S., Workman, J.B., Young, O.D., Dixon, G.L., Swadley, W.C., McKee, E.H., Ponce, D.A., Hildenbrand, T.G., Ekren, E.B., Warren, R.G., Cole, J.C., Fleck, R.J., Lanphere, M.A., Lundstrom, S.C., Grunwald, D.J., Laczniak, R.J., Menges, C.M., Yount, J.C., and Jayko, A.S., 1999, Digital geologic map of the Nevada Test Site and vicinity, Nye, Lincoln, and Clark Counties, Nevada, and Inyo County, California: U.S. Geological Survey Open-File Report 99-554-A, 53 p., CD-ROM, scale 1:100,000.

Smith, D.L., Gans, P.B., and Miller, E.L., 1991, Palinspastic restoration of Cenozoic extension in the central and eastern Basin and Range province at latitude 39-40° N, *in* Raines, G.L., Lisle, R.E., Schafer, R.W., and Wilkinson, W.H., eds., Geology and the deposits of the Great Basin, Geological Society of Nevada, v. 1, p. 75–86.

Snyder, R.P., Ekren, E.B., and Dixon, G.L., 1972, Geologic map of the Lunar Crater quadrangle, Nye County, Nevada: U.S. Geological Survey Miscellaneous Geologic Investigations Map I-700, scale 1:48,000.

Stewart, J.H., 1980, Geology of Nevada, a discussion to accompany the geologic map of Nevada: Nevada Bureau of Mines and Geology Special Publication 4, 136 p.

Stewart, J.H., and Carlson, J.E., 1978, Geologic map of Nevada: U.S. Geological Survey, scale 1:500,000.

Swadley, W.C., Page, W.R., Scott, R.B., and Pampeyan, E.H., 1994, Geologic map of the Delamar 3 SE quadrangle, Lincoln County, Nevada: U.S. Geological Survey Geologic Quadrangle Map-GQ-1754, scale 1:24,000.

Swadley, W.C., and Rowley, P.D., 1994, Geologic map of the Pahroc Spring SE quadrangle, Lincoln County, Nevada: U.S. Geological Survey Geologic Quadrangle Map GQ-1752, scale 1:24,000.

Swadley, W.C., and Scott, R.B., 1990, Preliminary geologic map of the Delamar NW quadrangle, Lincoln County, Nevada: U.S. Geological Survey Open-File Report 90-622, scale 1:24,000.

Taylor, M.E., Poole, F.G., and Cook, H.E., 1991, Summary of Paleozoic stratigraphy in the southern Egan and Schell Creek ranges, east central Nevada, *in* Flanigan, D.M.H., Hansen, M., and Flanigan, T.E., eds., Geology of White River Valley, the Grant Range, eastern Railroad Valley and western Egan Range, Nevada, Nevada Petroleum Society 1991 Field Trip Guidebook, p. 29–35.

Taylor, W.J., Dobbs, S.W., Nelson, S.L., and Armstrong, P.A., 1994, Generation of four-way closure through multiple tectonic events—Structures of the Timpahute Range, southern Nevada, *in* Dobbs, S.W., and Taylor, W.J., eds., Structural and stratigraphic investigations and petroleum potential of Nevada, with special emphasis south of the Railroad Valley producing trend: Nevada Petroleum Society 1994 conference volume II (book 2), p. 141–156.

Terrascan Group, Inc., 1987, Geologic map of the eastern Great Basin, Nevada and Utah, scale 1:250,000.

Tschanz, C.M., and Pampeyan, E.H., 1970, Geology and Mineral deposits of Lincoln County, Nevada: Nevada Bureau of Mines and Geology Bulletin 73, 188 p.

Van Loenen, R.E., 1987, Geologic map of the Mount Grafton wilderness study area, Lincoln and White Pine Counties, Nevada: Miscellaneous Field Studies Map MF-1938, scale 1:50,000.

Vikre, P.G., 1998, Intrusion-related, polymetallic carbonate replacement deposits in the Eureka district, Eureka County, Nevada: Nevada Bureau of Mines and Geology Bulletin 110, 52 p.

Wernicke, B., Walker, J.D., and Beaufait, M.S., 1985, Structural discordance between Neogene detachments and frontal Sevier thrusts, central Mormon Mountains, southern Nevada: Tectonics, v. 4, no. 2, p. 213–246.

Whitebread, D.H., 1970, Geologic map of the Wheeler Peak and Garrison quadrangles, Nevada and Utah: U.S. Geological Survey Miscellaneous Geologic Investigations Map I-578, scale 1:48,000.

Williams, V.S., 1996, Preliminary geologic map of the Mesquite quadrangle, Clark County, Nevada: U.S. Geological Survey Open-File Report 96-676, scale 1:24,000.

Williams, V.S., Best, M.G., and Keith, J.D., 1997, Geologic map of the Ursine-Panaca Summit-Deer Lodge area, Lincoln County, Nevada, and Iron County, Utah: U.S. Geological Survey Miscellaneous Investigations Series Map I-2479, scale 1:50,000.

Williams, V.S., Bohannon, R.G., and Hoover, D.L., 1997, Geologic map of the Riverside quadrangle, Clark County, Nevada: U.S. Geological Survey Geologic Quadrangle Map GQ-1770, scale 1:24,000.

Williams, V.S., Schmidt, D.L., and Bohannon, R.G., 1997, Preliminary geologic map of the Moapa East quadrangle, Clark County, Nevada: U.S. Geological Survey Open-File Report 97-449, scale 1:24,000.

Willis, J.B., Best, M.G., Kowallis, B.J., and Best, V.C., 1987, Preliminary geologic map of the northern Wilson Creek Range, Lincoln County, Nevada: U.S. Geological Survey Miscellaneous Field Studies Map MF-1971, scale 1:50,000.

Workman, J.B., Menges, C.M., Page, W.R., Ekren, E.B., Rowley, P.D., and Dixon, G.L., 2002, Tectonic map of the Death Valley ground-water model area, Nevada and California: U.S. Geological Survey Miscellaneous Field Studies Map MF-2381-B, 58 p.

Workman, J.B., Menges, C.M., Page, W.R., Taylor, E.M., Ekren, E.B., Rowley, P.D., Dixon, G.L., Thompson, R.A., and Wright, L.A., 2003, Geologic map of the Death Valley ground water model area, Nevada and California: U.S. Geological Survey Miscellaneous Field Studies MF-2381-A, scale 1:250,000.

THIS PAGE INTENTIONALLY LEFT BLANK

Appendix A

General Photos of the Study Area

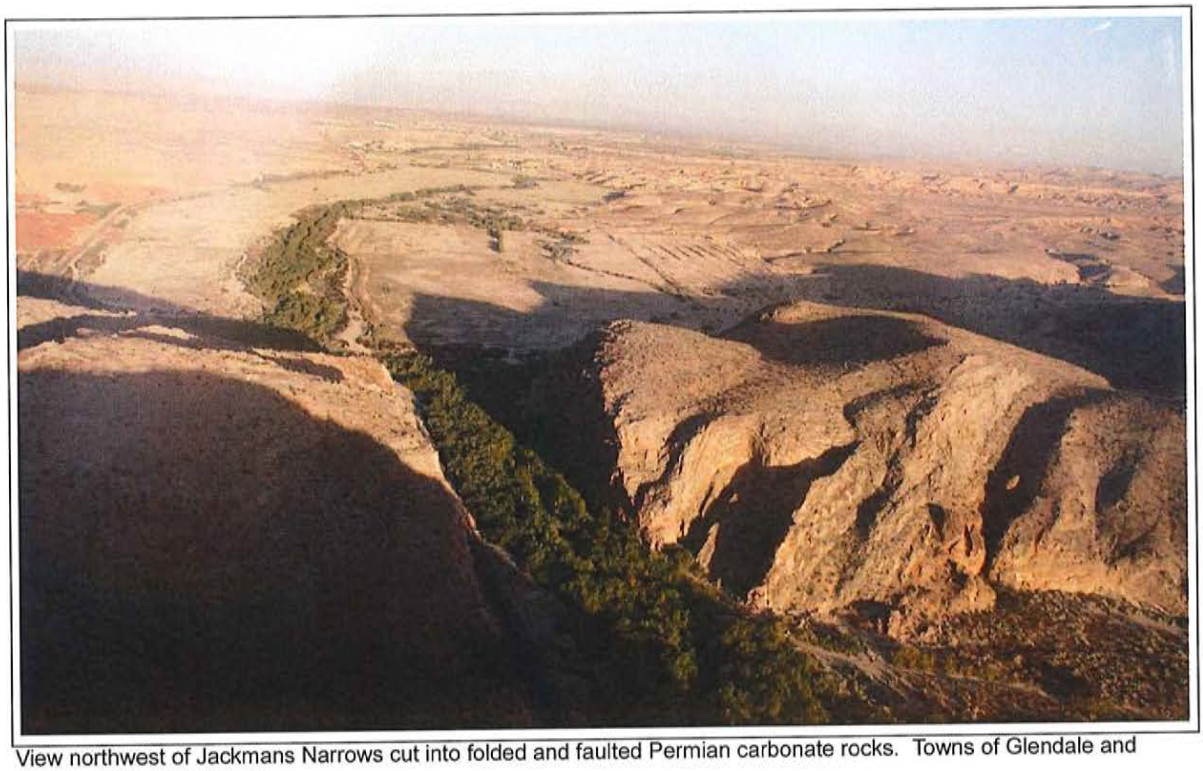

View northwest of Jackmans Narrows cut into folded and faulted Permian carbonate rocks. Towns of Glendale and Moapa in the background.

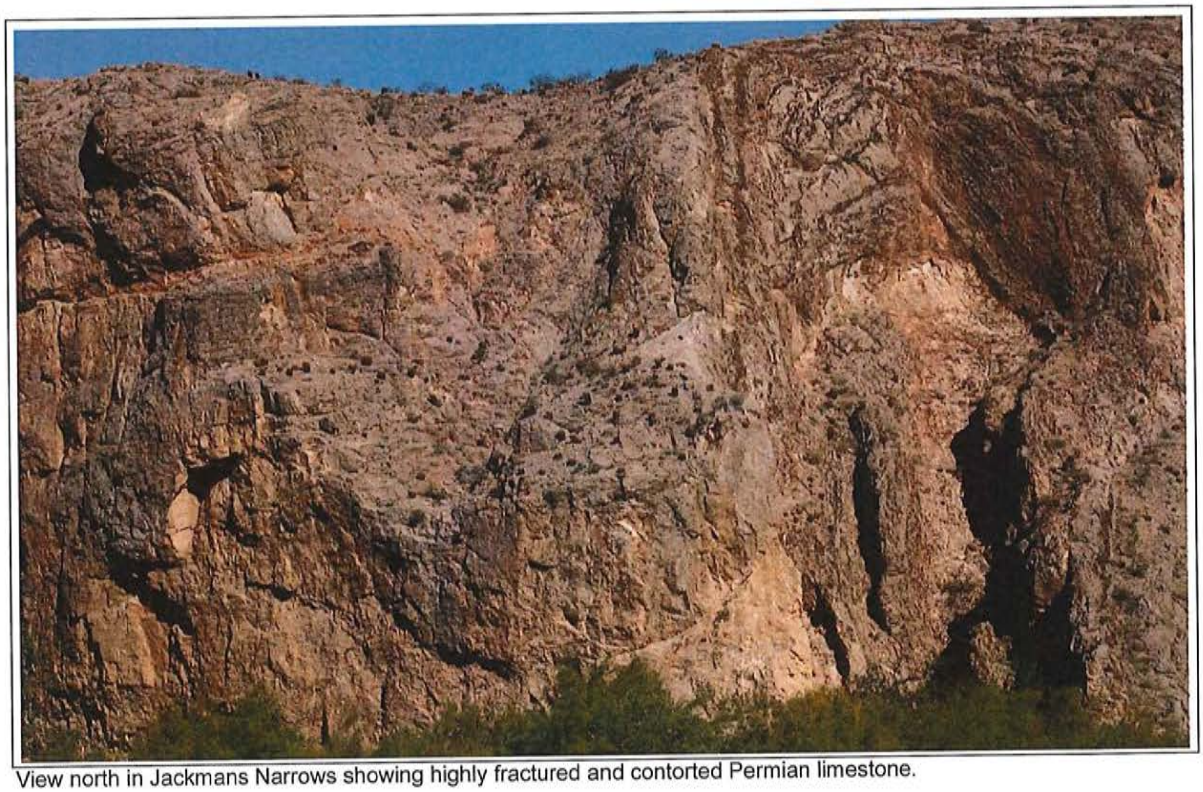

View north in Jackmans Narrows showing highly fractured and contorted Permian limestone.

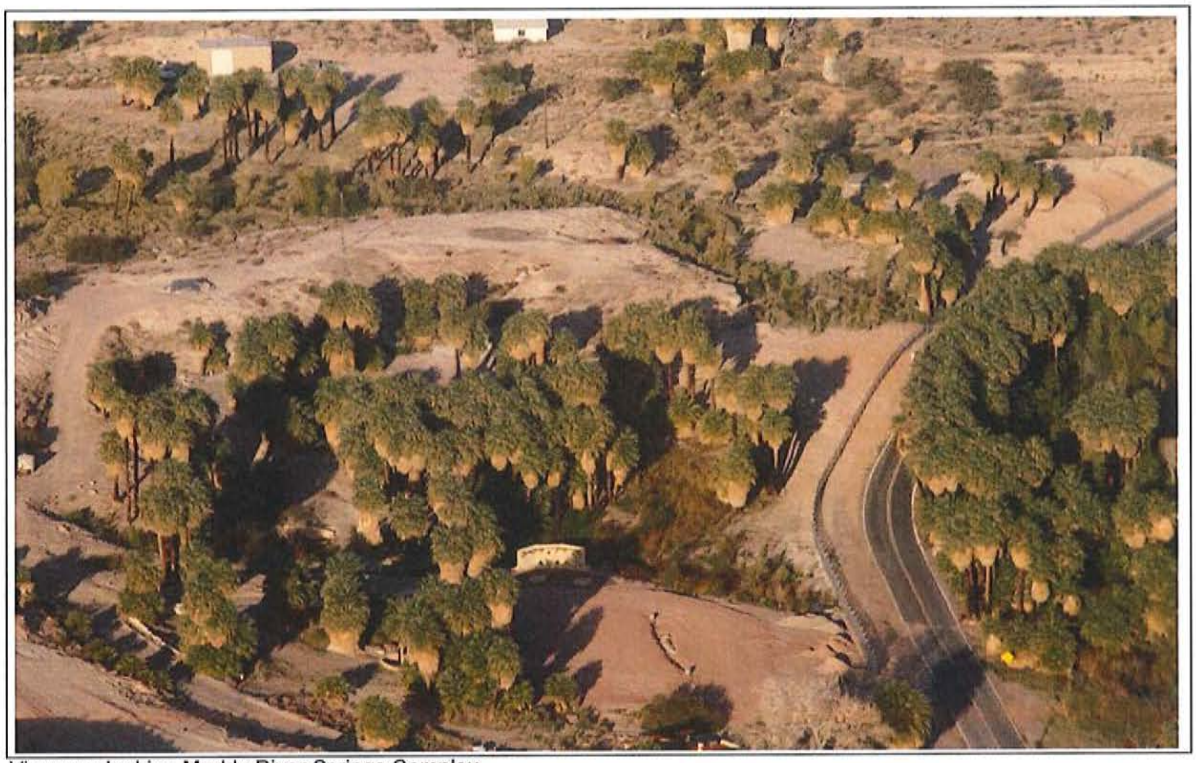

View overlooking Muddy River Springs Complex.

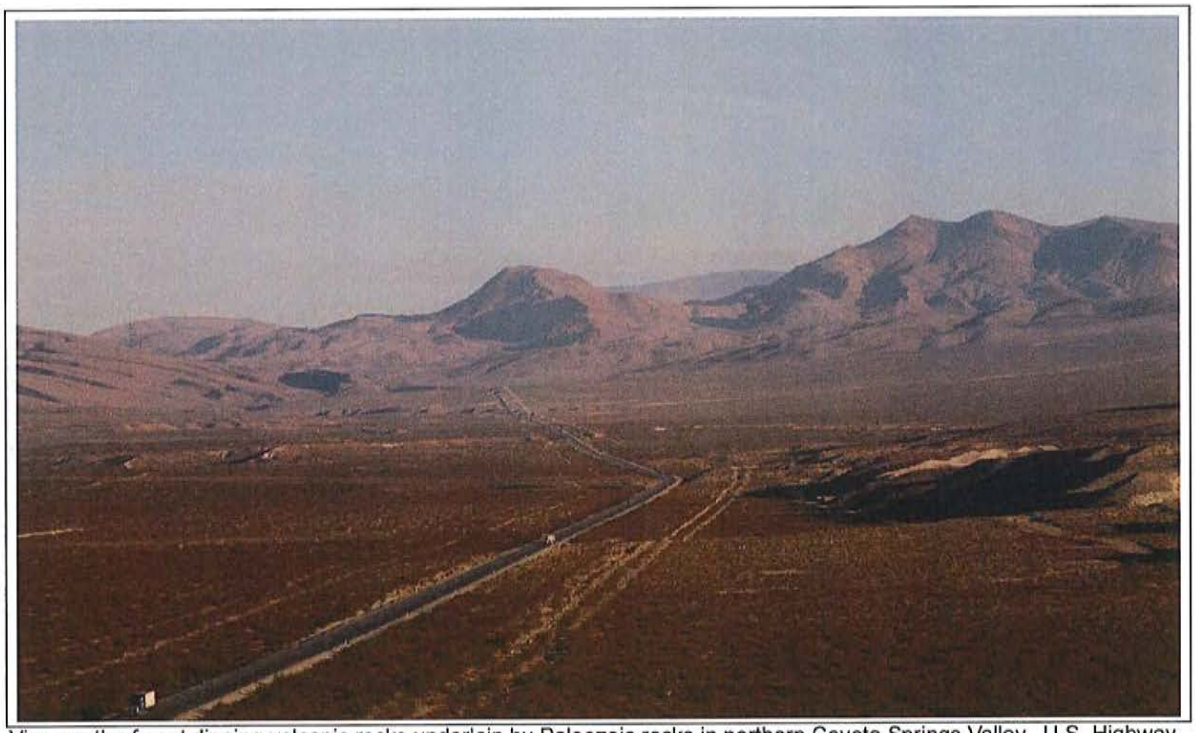

View north of east dipping volcanic rocks underlain by Paleozoic rocks in northern Coyote Springs Valley. U.S. Highway 93 in center of photograph.

View north into southern Delamar Valley. Delamar Lake in left center of photograph. Maynard Lake strand of the Pahranagat shear zone forms the scarp that is in shadows in the foreground, whereas the Delamar Lake strand passes beneath Delamar Lake and north of the hills on the left side of the photograph.

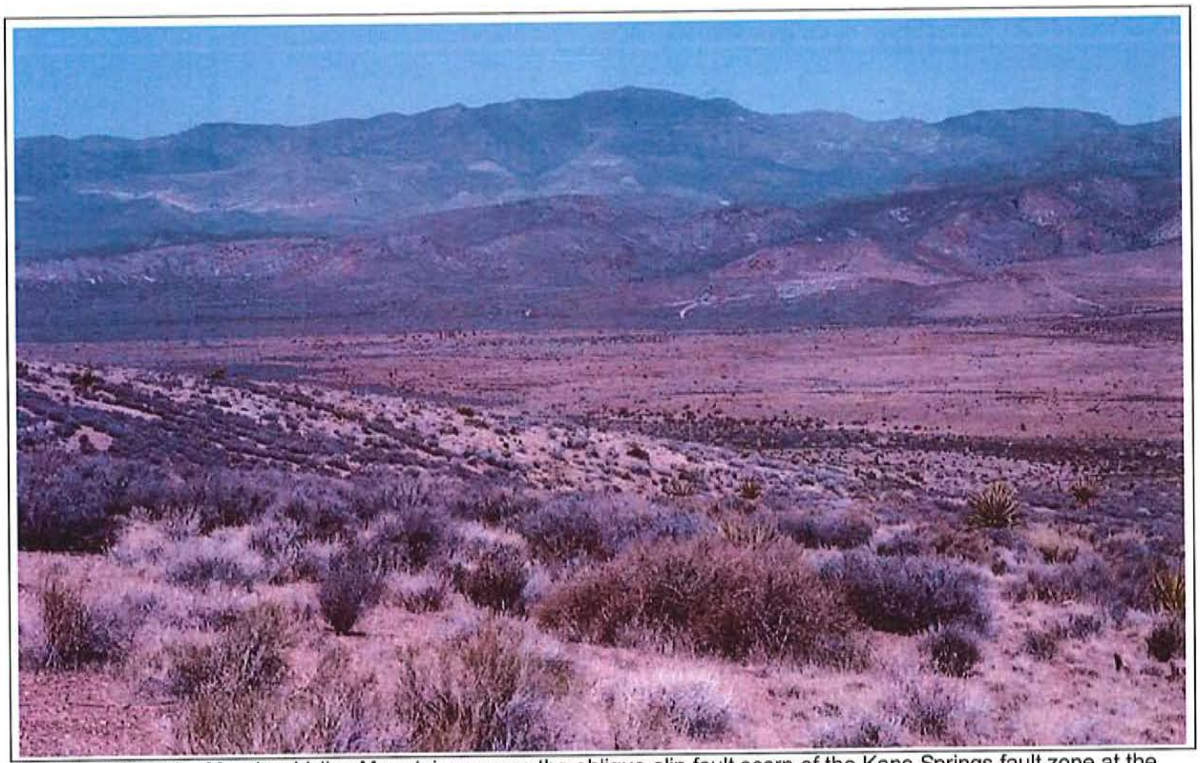

View west from the Meadow Valley Mountains across the oblique-slip fault scarp of the Kane Springs fault zone at the Kane Springs Wash caldera complex in the Delamar Mountains.

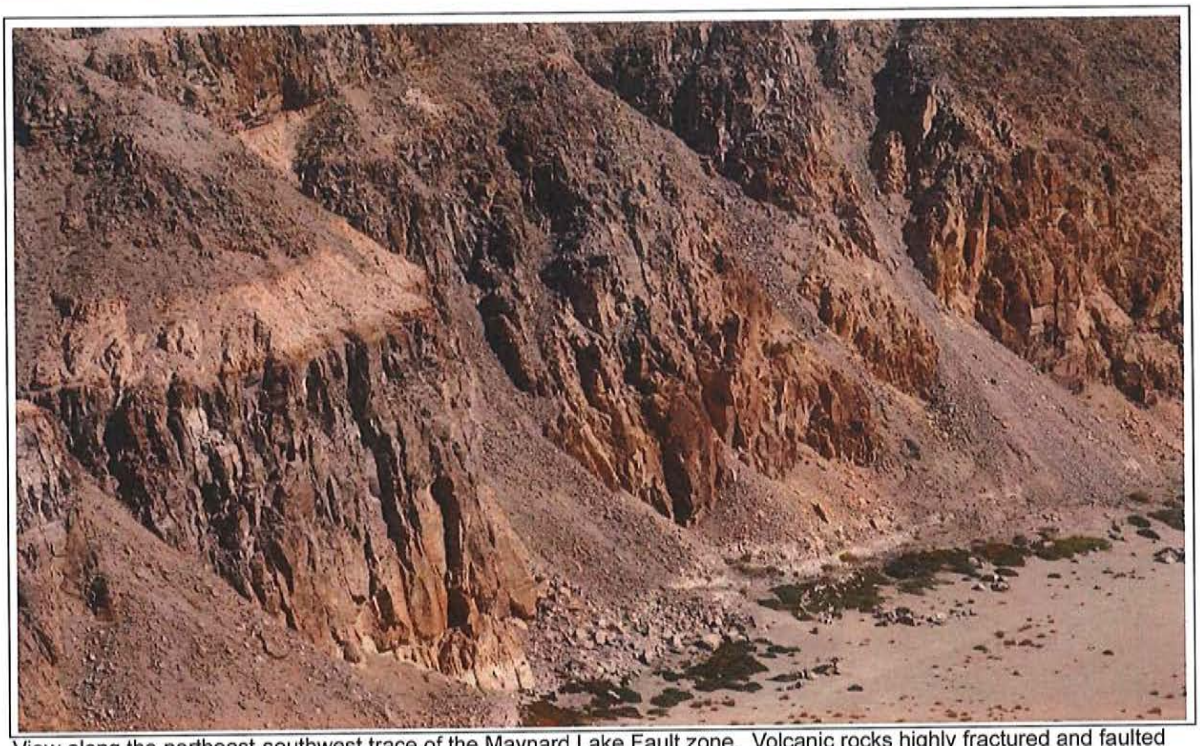

View along the northeast-southwest trace of the Maynard Lake Fault zone. Volcanic rocks highly fractured and faulted along fault zone. Maynard Lake (dry) in bottom of photograph.

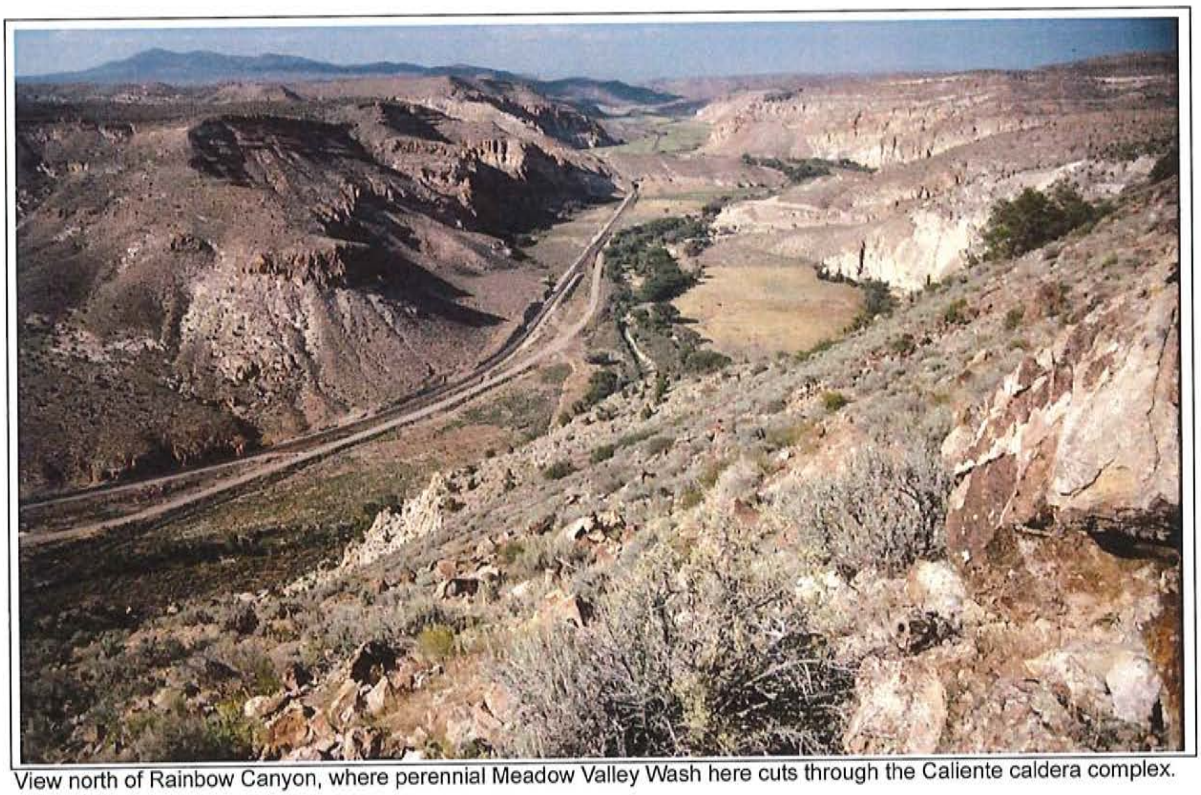

View north of Rainbow Canyon, where perennial Meadow Valley Wash here cuts through the Caliente caldera complex.

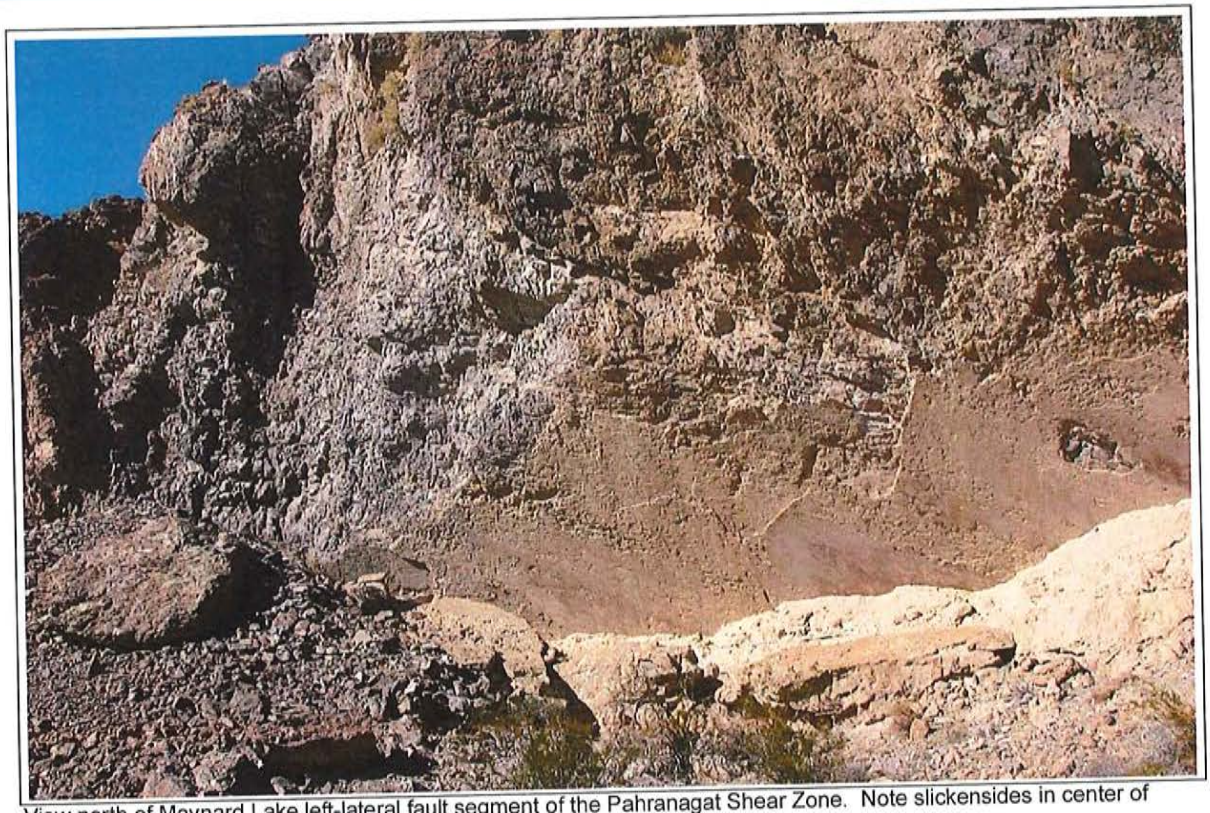

View north of Maynard Lake left-lateral fault segment of the Pahranagat Shear Zone. Note slickensides in center of photograph and brecciated volcanic rocks adjacent to fault.

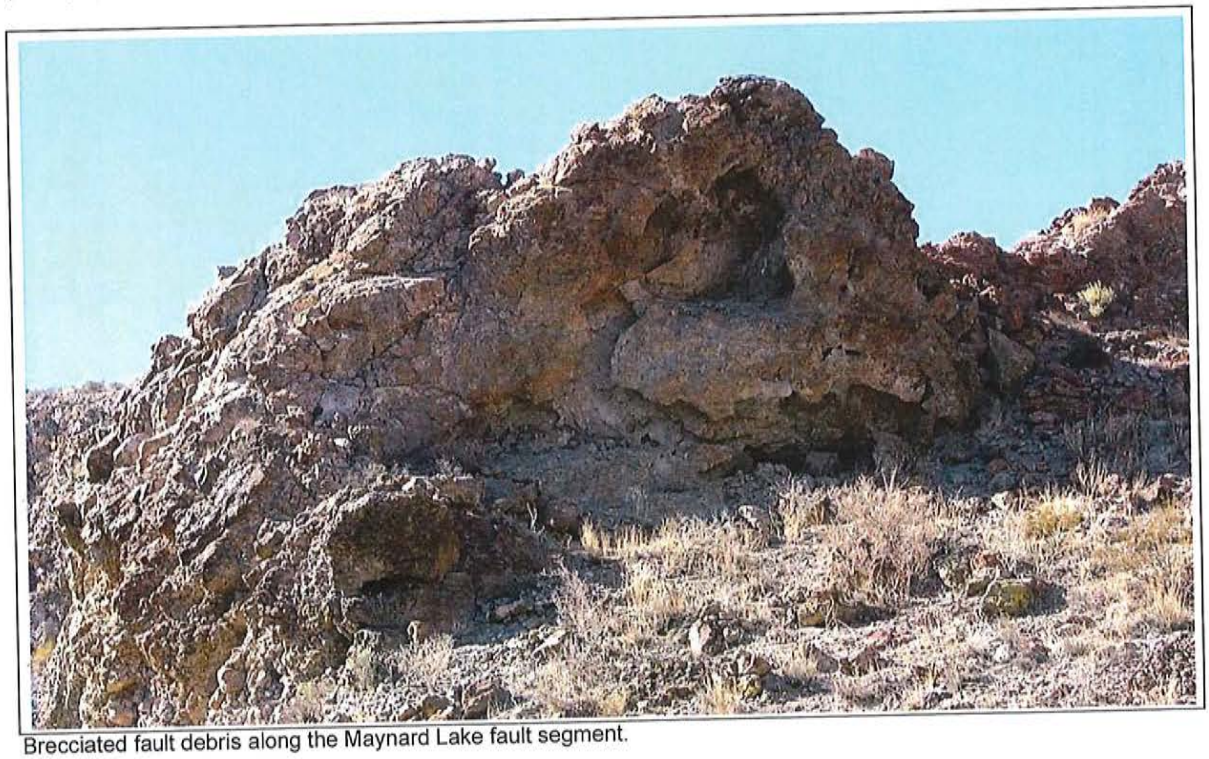

Brecciated fault debris along the Maynard Lake fault segment.

View west-northwest of Delamar mining district and northern Delamar Valley. Although Nevada's largest gold district from 1895 to 1910, now only a few walls of buildings remain along the main street.

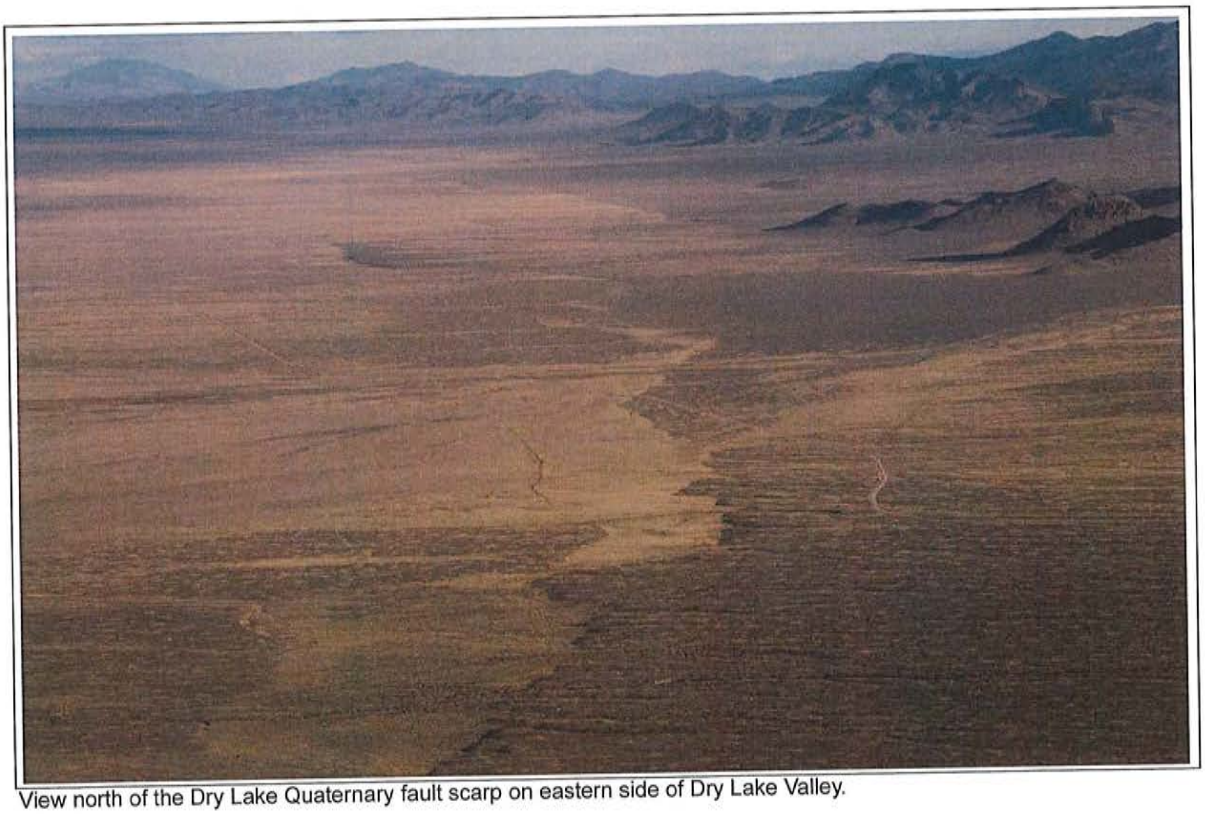

View north of the Dry Lake Quaternary fault scarp on eastern side of Dry Lake Valley.

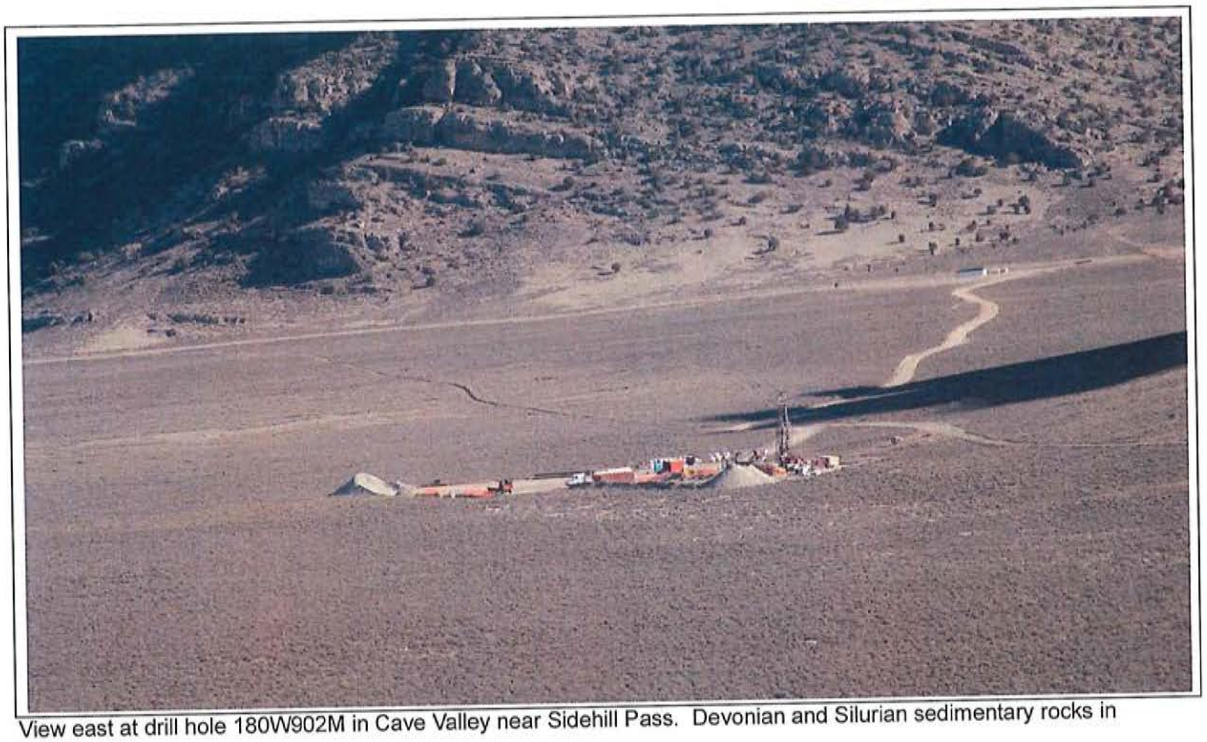

View east at drill hole 180W902M in Cave Valley near Sidehill Pass. Devonian and Silurian sedimentary rocks in background.

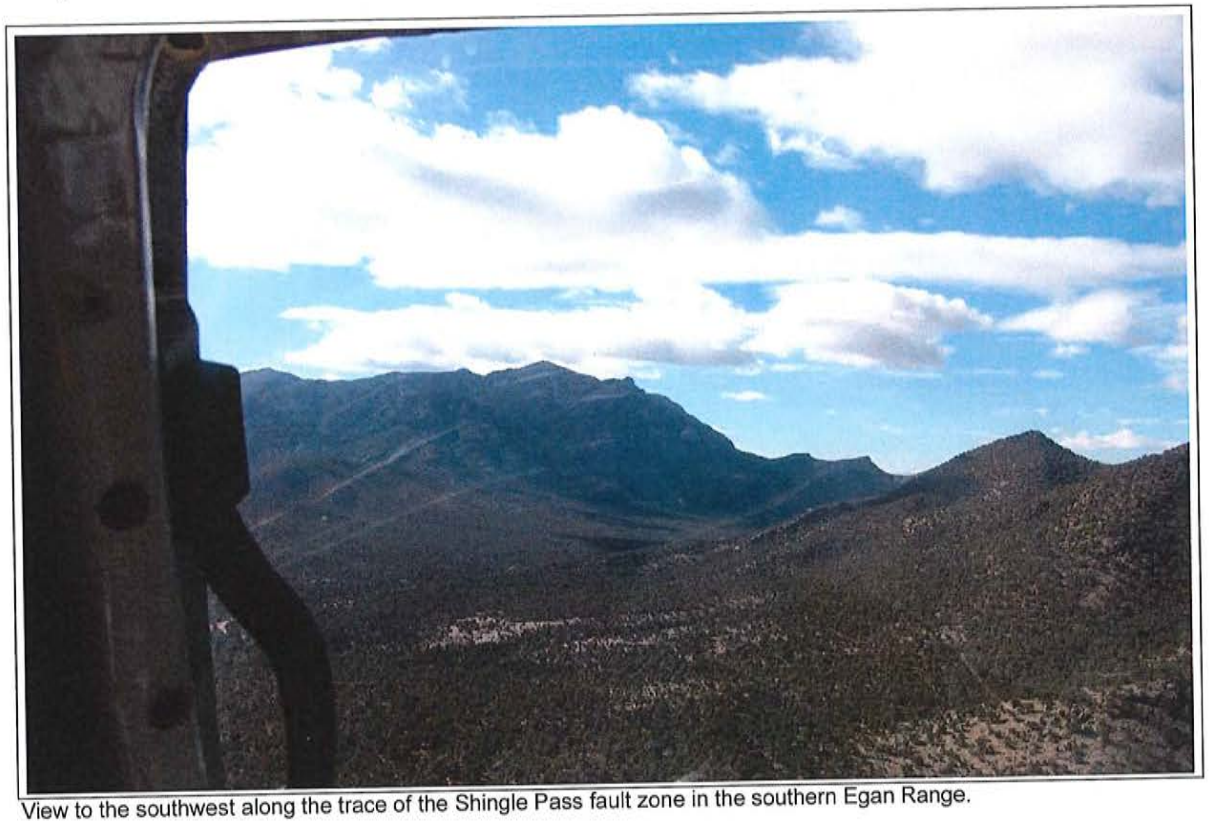

View to the southwest along the trace of the Shingle Pass fault zone in the southern Egan Range.

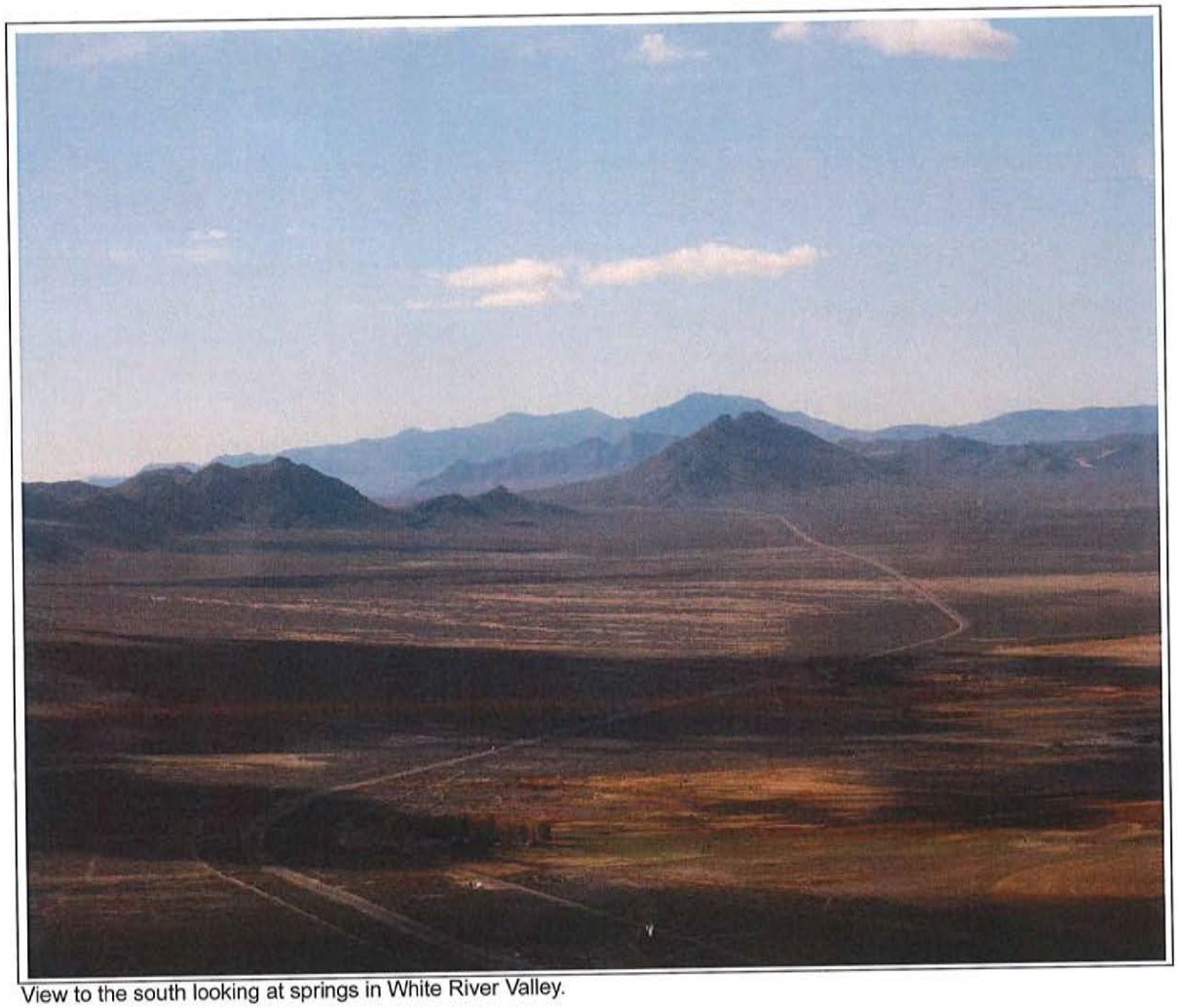

View to the south looking at springs in White River Valley.

Plates

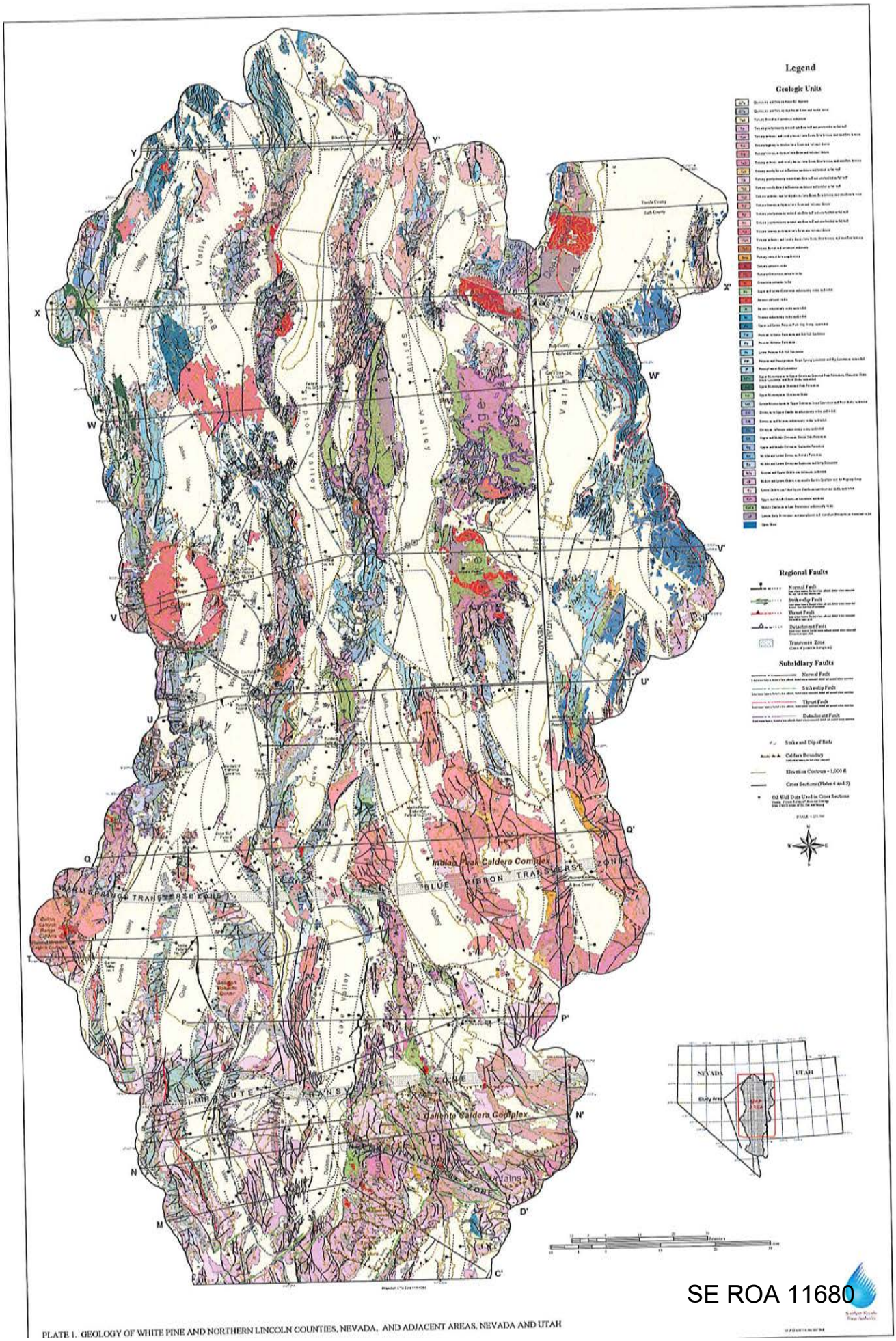

PLATE 1. GEOLOGY OF WHITE PINE AND NORTHERN LINCOLN COUNTIES, NEVADA, AND ADJACENT AREAS, NEVADA AND UTAH

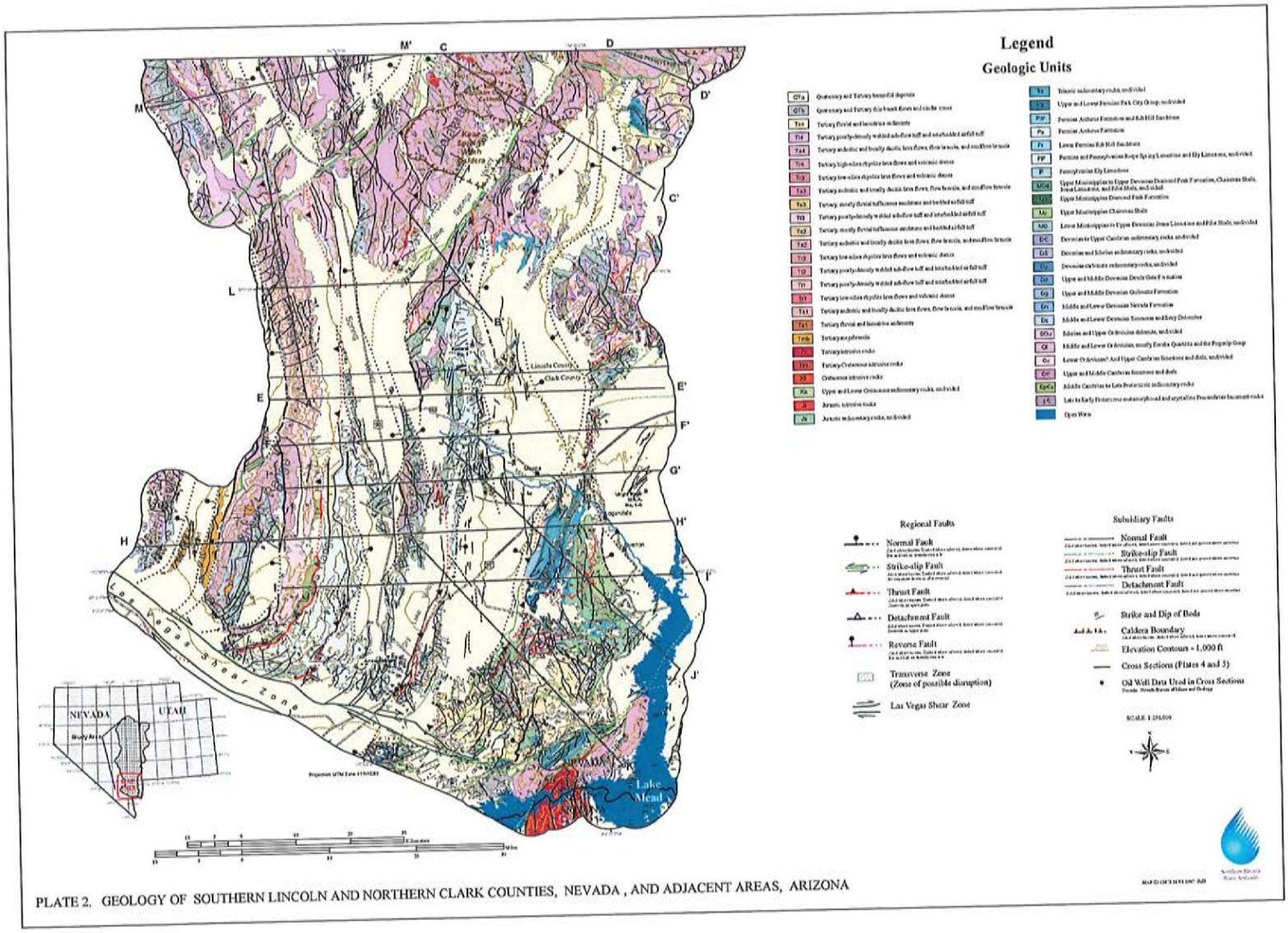

PLATE 2. GEOLOGY OF SOUTHERN LINCOLN AND NORTHERN CLARK COUNTIES, NEVADA , AND ADJACENT AREAS, ARIZONA

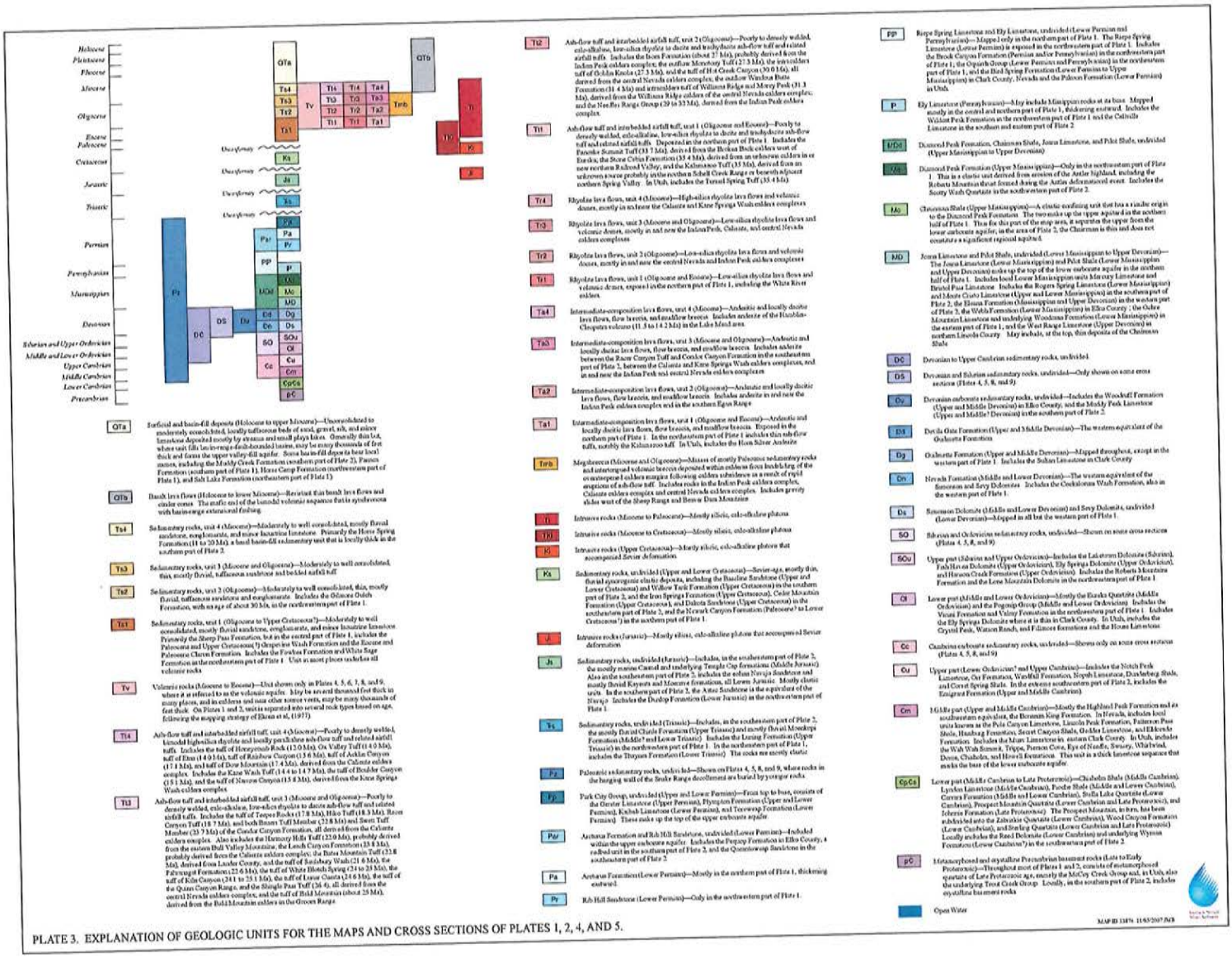

QTa Surficial and basin-fill deposits (Holocene to upper Miocene)—Unconsolidated to moderately consolidated, locally tuffaceous beds of sand, gravel, silt, and minor limestone deposited mostly by streams and small playa lakes. Generally thin but, where unit fills late-to-mid-Cenozoic fault-bounded basins, may be many thousands of feet thick and forms the upper valley-fill aquifer. Some basin-fill deposits bear local names, including the Muddy Creek Formation (southern part of Plate 2), Panaca Formation (southern part of Plate 1), Horse Camp Formation (northwestern part of Plate 1), and Salt Lake Formation (northeastern part of Plate 1)

QTb Basalt lava flows (Holocene to lower Miocene)—Reviewed thin basalt lava flows and cinder cones. The mafic end of the bimodal volcanic sequence but is synchronous with basin-range extensional faulting.

Ts4 Sedimentary rocks, unit 4 (Miocene)—Moderately to well consolidated, mostly fluvial sandstone, conglomerate, and minor lacustrine limestone. Primarily the Horse Spring Formation (14 to 20 Ma), a basal basin-fill sedimentary unit that is locally thick in the southern part of Plate 2.

Ts3 Sedimentary rocks, unit 3 (Miocene and Oligocene)—Moderately to well consolidated, thin, mostly fluvial, tuffaceous sandstone and bedded tuffaß

Ts2 Sedimentary rocks, unit 2 (Oligocene)—Moderately to well consolidated, thin, mostly fluvial, tuffaceous sandstone and conglomerate. Includes the Grouse Gulch Formation, with an age of about 30 Ma, in the northeastern part of Plate 1.

Ts1 Sedimentary rocks, unit 1 (Oligocene to Upper Cretaceous?)—Moderately to well consolidated, mostly fluvial sandstone, conglomerate, and minor lacustrine limestone. Primarily the Sheep Pass Formation, but in the central part of Plate 1, includes the Paleocene and Upper Cretaceous(?) Oregonian Wash Formation and the Eocene and Paleocene Claron Formation. Includes the Fowkes Formation and White Sage Formation in the northeastern part of Plate 1. Unit in most places underlies all volcanic rocks

Tv Volcanic rocks (Miocene to Eocene)—Unit shown only in Plates 4, 5, 6, 7, 8, and 9, where it is referred to as the volcanic aquifer. May be several thousand feet thick in many places, and in caldrons and near source vents, may be many thousands of feet thick. On Plates 1 and 3, unit is separated into several rock types based on age, following the mapping strategy of Ekren et al. (1977)

Tr4 Ash-flow tuff and interbedded airfall tuff, unit 4 (Miocene)—Poorly to densely welded, bimodal high-silica rhyolite and locally peralkaline ash-flow tuff and related airfall tuffs. Includes the tuff of Honeycomb Rock (12.0 Ma), Ox Valley Tuff (14.0 Ma), tuff of Elan (14.9 Ma), tuff of Rainbow Canyon (13.6 Ma), tuff of Ackles Canyon (17.1 Ma), and tuff of Dow Mountain (17.4 Ma), derived from the Caliente caldera complex. Includes the Kane Wash Tuff (14.4 to 14.7 Ma), the tuff of Boulder Canyon (15.1 Ma), and the tuff of Narrow Canyon (15.4 Ma), derived from the Kane Springs Wash caldera complex

Tr3 Ash-flow tuff and interbedded airfall tuff, unit 3 (Miocene and Oligocene)—Poorly to densely welded, calc-alkalian, low-silica rhyolite to dacite ash-flow tuff and related airfall tuffs. Includes the tuff of Teapot Rocks (17.8 Ma), Hiko Tuff (18.3 Ma), Racer Canyon Tuff (18.7 Ma), and both Bearpaw Tuff Member (32.8 Ma) and Swett Tuff Member (33.7 Ma) of the Condor Canyon Formation, all derived from the Caliente caldera complex. Also includes the Harmony Hills Tuff (23.0 Ma), probably derived from the eastern Bull Valley Mountains; the Leach Canyon Formation (25.8 Ma), probably derived from the Caliente caldera complex; the Bates Mountain Tuff (23.8 Ma), derived from Lander County, and the tuff of Antelope Wash (21.6 Ma), the Fraycraft Formation (23.6 Ma), the tuff of White Blotch Spring (24 to 25 Ma), the tuff of Kiln Canyon (24.1 to 25.1 Ma), the tuff of Lunar Crater (24.6 Ma), the tuff of the Quinn Canyon Range, and the Shingle Pass Tuff (26.4), all derived from the central Nevada caldera complex, and the tuff of Bald Mountain (about 25 Ma), derived from the Bald Mountain caldera in the Grouse Range

Tr2 Ash-flow tuff and interbedded airfall tuff, unit 2 (Oligocene)—Poorly to densely welded, calc-alkaline, low-silica rhyolite to dacite and trachydacite ash-flow tuff and related airfall tuffs. Includes the Isom Formation (about 27 Ma), probably derived from the Indian Peak caldera complex; the outflow Mercury Tuff (27.3 Ma), the intracaldera tuff of Ocklin Knolls (27.3 Ma), and the tuff of Hot Creek Canyon (30.0 Ma), all derived from the central Nevada caldera complex; the outflow Windous Butte Formation (31.4 Ma) and intracaldera tuff of Williams Ridge and Mount Peak (31.3 Ma), derived from the Williams Ridge caldera of the central Nevada caldera complex; and the Needles Range Group (29 to 33 Ma), derived from the Indian Peak caldera complex.

Tr1 Ash-flow tuff and interbedded airfall tuff, unit 1 (Oligocene and Eocene)—Poorly to densely welded, calc-alkaline, low-silica rhyolite to dacite and trachydacite ash-flow tuff and related airfall tuffs. Deposits in the northern part of Plate 1. Includes the Pancake Summit Tuff (33.7 Ma), derived from the Broken Back caldera west of Eureka; the Stone Cabin Formation (35.4 Ma), derived from an unknown caldera in or near northern Railroad Valley; and the Kalamazoo Tuff (35 Ma), derived from an unknown source probably in the northern Schell Creek Range or beneath adjacent northern Spring Valley. In Utah, includes the Needles Range Group (29 to 33 Ma), derived from the Indian Peak caldera complex.

Tr4 Rhyolite lava flows, unit 4 (Miocene)—High-silica rhyolite lava flows and volcanic domes, mostly in and near the Caliente and Kane Springs Wash caldera complexes

Tr3 Rhyolite lava flows, unit 3 (Miocene and Oligocene)—Low-silica rhyolite lava flows and volcanic domes, mostly in and near the Indian Peak, Caliente, and central Nevada caldera complexes

Tr2 Rhyolite lava flows, unit 2 (Oligocene)—Low-silica rhyolite lava flows and volcanic domes, mostly in and near the central Nevada and Indian Peak caldera complexes

Tr1 Rhyolite lava flows, unit 1 (Oligocene and Eocene)—Low-silica rhyolite lava flows and volcanic domes, exposed in the northern part of Plate 1, including the White River caldera

Ta4 Intermediate-composition lava flows, unit 4 (Miocene)—Andesitic and locally dacitic lava flows, flow breccia, and mudflow breccia. Includes andesite of the Hamblin-Cleopatra volcano (11.5 to 14.2 Ma) in the Lake Mead area.

Ta3 Intermediate-composition lava flows, unit 3 (Miocene and Oligocene)—Andesitic and locally dacitic lava flows, flow breccia, and mudflow breccia. Includes andesite between the Racer Canyon Tuff and Condor Canyon Formation in the southeastern part of Plate 2, between the Caliente and Kane Springs Wash caldera complexes, and in and near the Indian Peak and central Nevada caldera complexes

Ta2 Intermediate-composition lava flows, unit 2 (Oligocene)—Andesitic and locally dacitic lava flows, flow breccia, and mudflow breccia. Includes andesite in and near the Indian Peak caldera complex and in the southern Egan Range

Ta1 Intermediate-composition lava flows, unit 1 (Oligocene and Eocene)—Andesitic and locally dacitic lava flows, flow breccia, and mudflow breccia. Exposed in the northeastern part of Plate 1. In the northeastern part of Plate 1 includes thin ash-flow tuffs, notably the Kalamazoo tuff. In Utah, includes the Rose Knob Andesite

Tmb Megabreccia (Miocene and Oligocene)—Masses of mostly Paleozoic sedimentary rocks and interstratified volcanic breccia deposited within caldrons from landsliding of the overlapped caldera margins following caldera subsidence as a result of rapid eruptions of ash-flow tuff. Includes rocks in the Indian Peak caldera complex, Caliente caldera complex and central Nevada caldera complex. Includes gravity slides west of the Sheep Range and Arrow Canyon Range

Ti Intrusive rocks (Miocene to Paleocene)—Mostly silicic, calc-alkaline plutons

TKi Intrusive rocks (Miocene to Cretaceous)—Mostly silicic, calc-alkaline plutons

Ki Intrusive rocks (Upper Cretaceous)—Mostly silicic, calc-alkaline plutons that accompanied Sevier deformation

Ks Sedimentary rocks, undivided (Upper and Lower Cretaceous)—Sevier-age, mostly thin, flat-lying orogenic clastic deposits, including the Baseline Sandstone (Upper and Lower Cretaceous) and Willow Tank Formation (Upper Cretaceous) in the southern part of Plate 2, and the Iron Springs Formation (Upper Cretaceous), Cedar Mountain Formation (Upper Cretaceous), and Dakota Sandstone (Upper Cretaceous) in the southeastern part of Plate 2, and the Newark Canyon Formation (Paleocene? to Lower Cretaceous?) in the southern part of Plate 1.

J Intrusive rocks (Jurassic)—Mostly silicic, calc-alkaline plutons that accompanied Sevier deformation

Js Sedimentary rocks, undivided (Jurassic)—Includes, in the southeastern part of Plate 2, the mostly marine Carmel and underlying Temple Cap formations (Middle Jurassic). Also in the southeastern part of Plate 2, includes the eolian Navajo Sandstone and mostly fluvial Kayenta and Moenave formations, all Lower Jurassic. Mostly clastic units. In the southern part of Plate 2, the Aztec Sandstone is the equivalent of the Navajo. Includes the Dunlap Formation (Lower Jurassic) in the northeastern part of Plate 1.

Ts Sedimentary rocks, undivided (Triassic)—Includes, in the southeastern part of Plate 2, the mostly fluvial Chinle Formation (Upper Triassic) and mostly fluvial Moenkopi Formation (Middle? and Lower Triassic). Includes the Luning Formation (Upper Triassic) in the northwestern part of Plate 1. In the northeastern part of Plate 1, includes the Thaynes Formation (Lower Triassic). The rocks are mostly clastic

Pz? Paleozoic sedimentary rocks, undivided—Shown on Plates 4, 5, 8, and 9, where rocks in the hanging wall of the Snake Range decollement are buried by younger rocks

PPc Park City Group, undivided (Upper and Lower Permian)—From top to base, consists of the Grenier Limestone (Upper Permian), Phosphoria Formation (Upper and Lower Permian), Kaibab Limestone (Lower Permian), and Toroweap Formation (Lower Permian). These make up the top of the upper carbonate aquifer.

Pzu Arcturus Formation and Rib Hill Sandstone, undivided (Lower Permian)—Included within the upper carbonate aquifer. Includes the Pequop Formation in Elko County, a ridge-forming unit in the southern part of Plate 2, and the Quartzite-ridge Sandstone in the southeastern part of Plate 2.

Pa Arcturus Formation (Lower Permian)—Mostly in the northern part of Plate 1, thickening eastward.

Pr Rib Hill Sandstone (Lower Permian)—Only in the northeastern part of Plate 1.

PP Riepe Spring Limestone and Ely Limestone, undivided (Lower Permian and Pennsylvanian)—Mapped only in the northern part of Plate 1. The Riepe Spring Limestone (Lower Permian) is exposed in the northeastern part of Plate 1. Includes the Brock Canyon Formation (Permian and/or Pennsylvanian) in the northeastern part of Plate 1; the Oquirrh Group (Lower Permian and Pennsylvanian) in the northeastern part of Plate 1; and the Bird Spring Formation (Lower Permian to Upper Mississippian) in Clark County, Nevada and the Pilot Formation (Lower Permian) in Utah.

P Ely Limestone (Pennsylvanian)—May include Mississippian rocks at its base. Mapped mostly in the central and northern part of Plate 1, thickening eastward. Includes the Wildcat Peak Formation in the northwestern part of Plate 1 and the Callville Limestone in the southern and eastern part of Plate 2.

MDd Diamond Peak Formation, Chainman Shale, Joana Limestone, and Pilot Shale, undivided (Upper Mississippian to Upper Devonian)

Dd Diamond Peak Formation (Upper Mississippian)—Only in the northwestern part of Plate 1. This is a clastic unit derived from erosion of the Antler highland, including the Roberts Mountain thrust formed during the Antler deformational event. Includes the Scotty Wash Quartzite in the southwestern part of Plate 2.

Mc Chainman Shale (Upper Mississippian)—A clastic confining unit that has a similar origin to the Diamond Peak Formation. The two rocks up the upper aquifer in the northern half of Plate 1. This fix this part of the map area, it separates the upper from the lower carbonate aquifer, in the area of Plate 2, the Chainman is thin and does not constitute a significant regional aquitard.

MD Joana Limestone and Pilot Shale, undivided (Lower Mississippian to Upper Devonian)—The Joana Limestone (Lower Mississippian) and Pilot Shale (Lower Mississippian and Upper Devonian) make up the top of the lower carbonate aquifer in the northern half of Plate 1. Includes local Lower Mississippian units Mercury Limestone and Bristol Pass Limestone. Includes the Rogers Spring Limestone (Lower Mississippian) and Monte Cristo Limestone (Upper and Lower Mississippian) in the southern part of Plate 2, the Elosa Formation (Mississippian and Upper Devonian) in the western part of Plate 2, the Webb Formation (Lower Mississippian) in Elko County; the Osino Mountain Limestone and underlying Woodman Formation (Lower Mississippian) in the eastern part of Plate 1, and the West Range Limestone (Upper Devonian) in northern Lincoln County. May include, at the top, thin deposits of the Chainman Shale

DC Devonian to Upper Cambrian sedimentary rocks, undivided

DS Devonian and Silurian sedimentary rocks, undivided—Only shown on some cross sections (Plates 4, 5, 8, and 9)

Dv Devonian carbonate sedimentary rocks, undivided—Includes the Woodruff Formation (Upper and Middle Devonian) in Elko County, and the Muddy Peak Limestone (Upper and Middle? Devonian) in the southern part of Plate 2.

Dd Devils Gate Formation (Upper and Middle Devonian)—The western equivalent of the Guilmette Formation

Dg Guilmette Formation (Upper and Middle Devonian)—Mapped throughout, except in the western part of Plate 1. Includes the Sultan Limestone in Clark County

Dn Nevada Formation (Middle and Lower Devonian)—The western equivalent of the Simonson and Sevy Dolomites. Includes the Cooksonia Wash Formation, also in the western part of Plate 1.

Ds Simonson Dolomite (Middle and Lower Devonian) and Sevy Dolomite, undivided (Lower Devonian)—Mapped in all but the western part of Plate 1.

SO Silurian and Ordovician sedimentary rocks, undivided—Shown on some cross sections (Plates 4, 5, 8, and 9)

SOu Upper part (Silurian and Upper Ordovician)—Includes the Laketown Dolomite (Silurian), Fish Haven Dolomite (Upper Ordovician), Ely Springs Dolomite (Upper Ordovician), and Hanson Creek Formation (Upper Ordovician). Includes the Roberts Mountains Formation and the Lone Mountain Dolomite in the northwestern part of Plate 1

Ol Lower part (Middle and Lower Ordovician)—Mostly the Eureka Quartzite (Middle Ordovician) and the Pogonip Group (Middle and Lower Ordovician). Includes the Vinini Formation and Valmy Formation in the northeastern part of Plate 1. Includes the Ely Springs Dolomite where it is thin in Clark County. In Utah, includes the Crystal Peak, Watson Ranch, and Fillmore formations and the Hound Limestone

Cc Cambrian carbonate sedimentary rocks, undivided—Shown only on some cross sections (Plates 4, 5, 8, and 9)

Cu Upper part (Lower Ordovician? and Upper Cambrian)—Includes the Notch Peak Limestone, Orr Formation, Windfall Formation, Nopah Limestone, Dunderberg Shale, and Carrara Spring Shale. In the extreme southeastern part of Plate 2, includes the Emigrant Formation (Upper and Middle Cambrian)

Cm Middle part (Upper and Middle Cambrian)—Mostly the Highland Peak Formation and its southeastern equivalent, the Bonanza King Formation. In Nevada, includes local units known as the Pole Canyon Limestone, Lincoln Peak Formation, Palmetto Pass Shale, Hamburg Formation, Secret Canyon Shale, Geddes Limestone, and Hillcreek Formation. Includes the Muav Limestone in eastern Clark County. In Utah, includes the Weh Weh Summit, Teppe, Pierson Cove, Eye of Needle, Swasey, Whirlwind, Dotsa, Chisholm, and Howell formations. This unit is a thick limestone sequence that marks the base of the lower carbonate aquifer.

CpCs Lower part (Middle Cambrian to Late Proterozoic)—Chisholm Shale (Middle Cambrian), Lyndon Limestone (Middle Cambrian), Poode Shale (Middle and Lower Cambrian), Carrara Formation (Middle and Lower Cambrian), Stella Lake Quartzite (Lower Cambrian), Prospect Mountain Quartzite (Lower Cambrian and Late Proterozoic), and Inferno Formation (Late Proterozoic). The Prospect Mountain, in turn, has been subdivided into the Zabriskie Quartzite (Lower Cambrian), Wood Canyon Formation (Lower Cambrian), and Stirling Quartzite (Lower Cambrian and Late Proterozoic). Locally includes the Reed Dolomite (Lower Cambrian) and underlying Wyman Formation (Lower Cambrian?) in the southernmost part of Plate 2.

pC Metamorphosed and crystalline Precambrian basement rocks (Late to Early Proterozoic)—Throughout most of Plates 1 and 2, consists of metamorphosed quartzite of Late Proterozoic age, mostly the McCoy Creek Group and, in Utah, also the underlying Trout Creek Group. Locally, in the southern part of Plate 2, includes pre-Belted basement rocks

Open Water

MAP ID 11874 11/03/2017 JWB

PLATE 3. EXPLANATION OF GEOLOGIC UNITS FOR THE MAPS AND CROSS SECTIONS OF PLATES 1, 2, 4, AND 5.

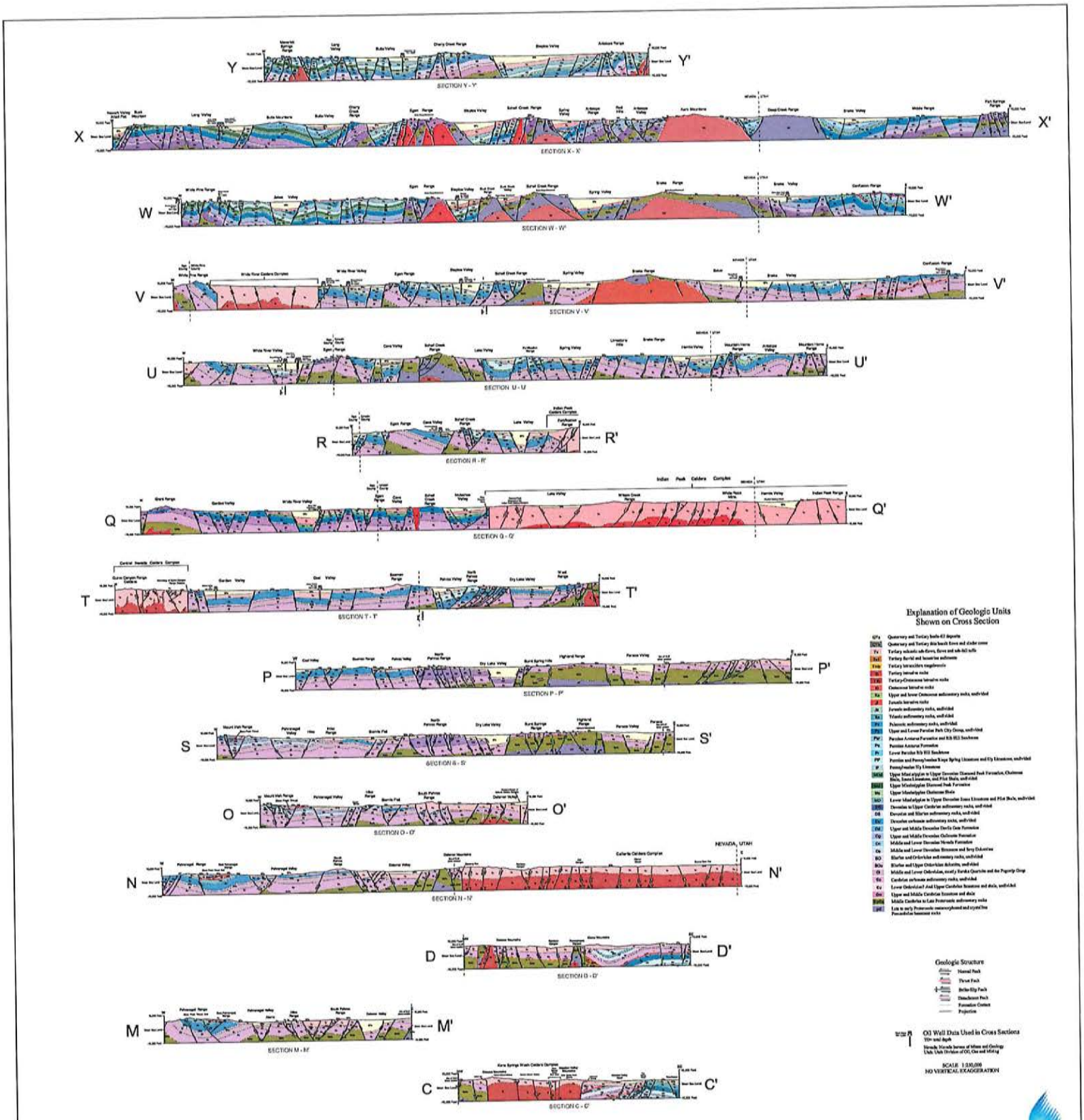

PLATE 4. CROSS SECTIONS SHOWING GEOLOGY OF WHITE PINE AND NORTHERN LINCOLN COUNTIES, NEVADA, AND ADJACENT AREAS, NEVADA AND UTAH

Explanation of Geologic Units Shown on Cross Section

QTa	Quaternary and Tertiary basin-fill deposits
QTb	Quaternary and Tertiary thin basalt flows and cinder cones
Tv	Tertiary volcanic ash-flows, flows and ash-fall tuffs
Ts	Tertiary fluvial and lacustrine sediments
Tmb	Tertiary intrusive megabreccia
Ti	Tertiary intrusive rocks
TKi	Tertiary-Cretaceous intrusive rocks
Ki	Cretaceous intrusive rocks
Ks	Upper and lower Cretaceous sedimentary rocks, undivided
Ji	Jurassic intrusive rocks
Js	Jurassic sedimentary rocks, undivided
Ts	Triassic sedimentary rocks, undivided
Pz	Paleozoic sedimentary rocks, undivided
PzU	Upper and Lower Permian Park City Group, undivided
PzA	Permian Arcturus Formation and Rib Hill Sandstone
Pa	Permian Arcturus Formation
Pr	Lower Permian Rib Hill Sandstone
PP	Permian and Pennsylvanian Riepe Spring Limestone and Ely Limestone, undivided
P	Pennsylvanian Ely Limestone
MDM	Upper Mississippian to Upper Devonian Diamond Peak Formation, Chainman Shale, Joana Limestone, and Pilot Shale, undivided
MDd	Upper Mississippian Diamond Peak Formation
Mc	Upper Mississippian Chainman Shale
MD	Lower Mississippian to Upper Devonian Joana Limestone and Pilot Shale, undivided
DC	Devonian to Upper Cambrian sedimentary rocks, undivided
DS	Devonian and Silurian sedimentary rocks, undivided
Dc	Devonian carbonate sedimentary rocks, undivided
Dd	Upper and Middle Devonian Devils Gate Formation
Dg	Upper and Middle Devonian Guilmette Formation
Dn	Middle and Lower Devonian Nevada Formation
Ds	Middle and Lower Devonian Simonson and Sevy Dolomites
SO	Silurian and Ordovician sedimentary rocks, undivided
SOu	Silurian and Upper Ordovician dolomite, undivided
Ol	Middle and Lower Ordovician, mostly Eureka Quartzite and the Pogonip Group
Cc	Cambrian carbonate sedimentary rocks, undivided
Cu	Lower Ordovician? And Upper Cambrian limestone and shale, undivided
Cm	Upper and Middle Cambrian limestone and shale
CpCu	Middle Cambrian to Late Proterozoic sedimentary rocks
pC	Late to early Proterozoic metamorphosed and crystalline Precambrian basement rocks

Geologic Structure

- Normal Fault
- Thrust Fault
- Strike-Slip Fault
- Detachment Fault
- Formation Contact
- Projection

Oil Well Data Used in Cross Sections
TD= total depth

SCALE 1:250,000
NO VERTICAL EXAGGERATION

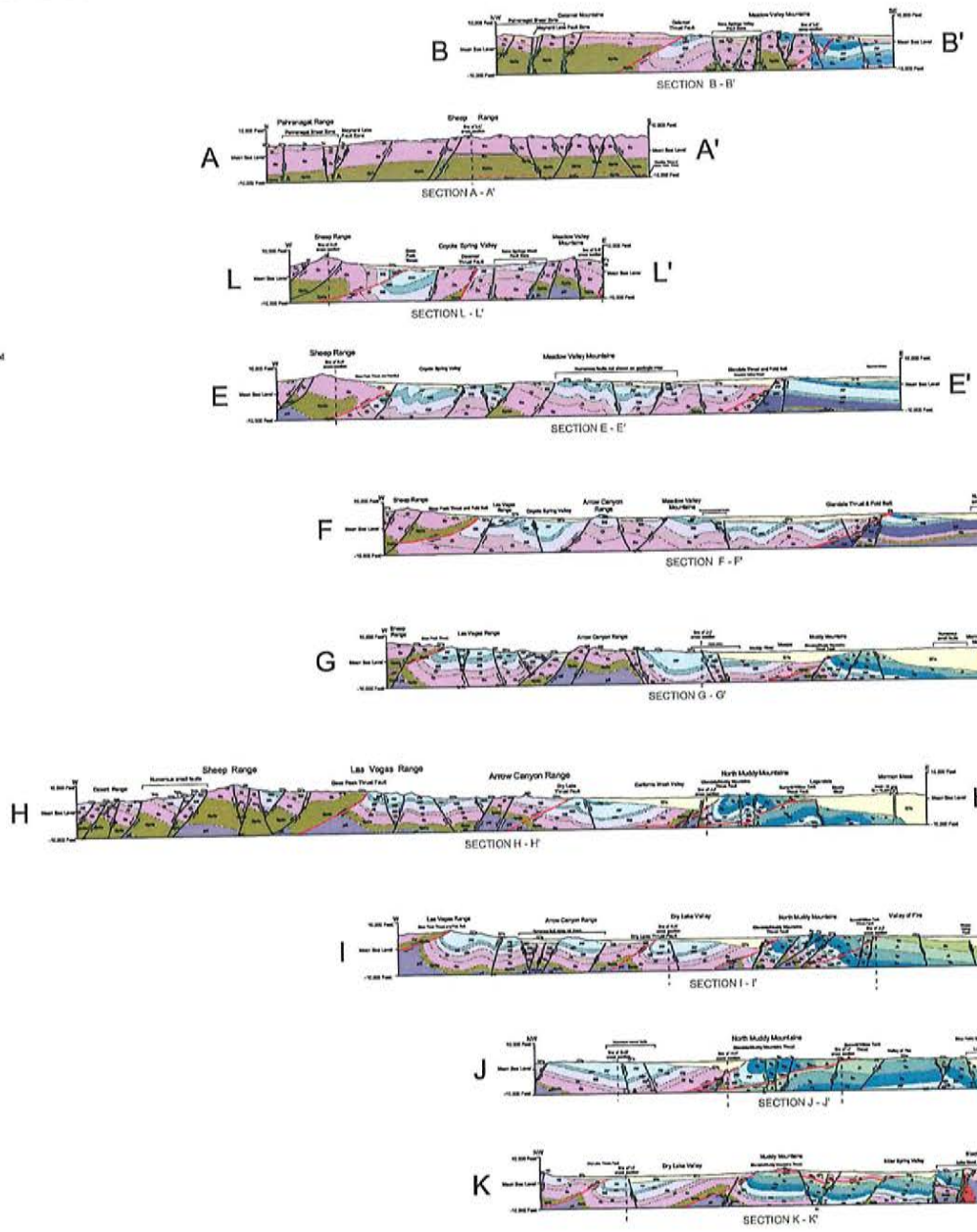

PLATE 5. CROSS SECTIONS SHOWING GEOLOGY OF SOUTHERN LINCOLN AND NORTHERN CLARK COUNTIES, NEVADA

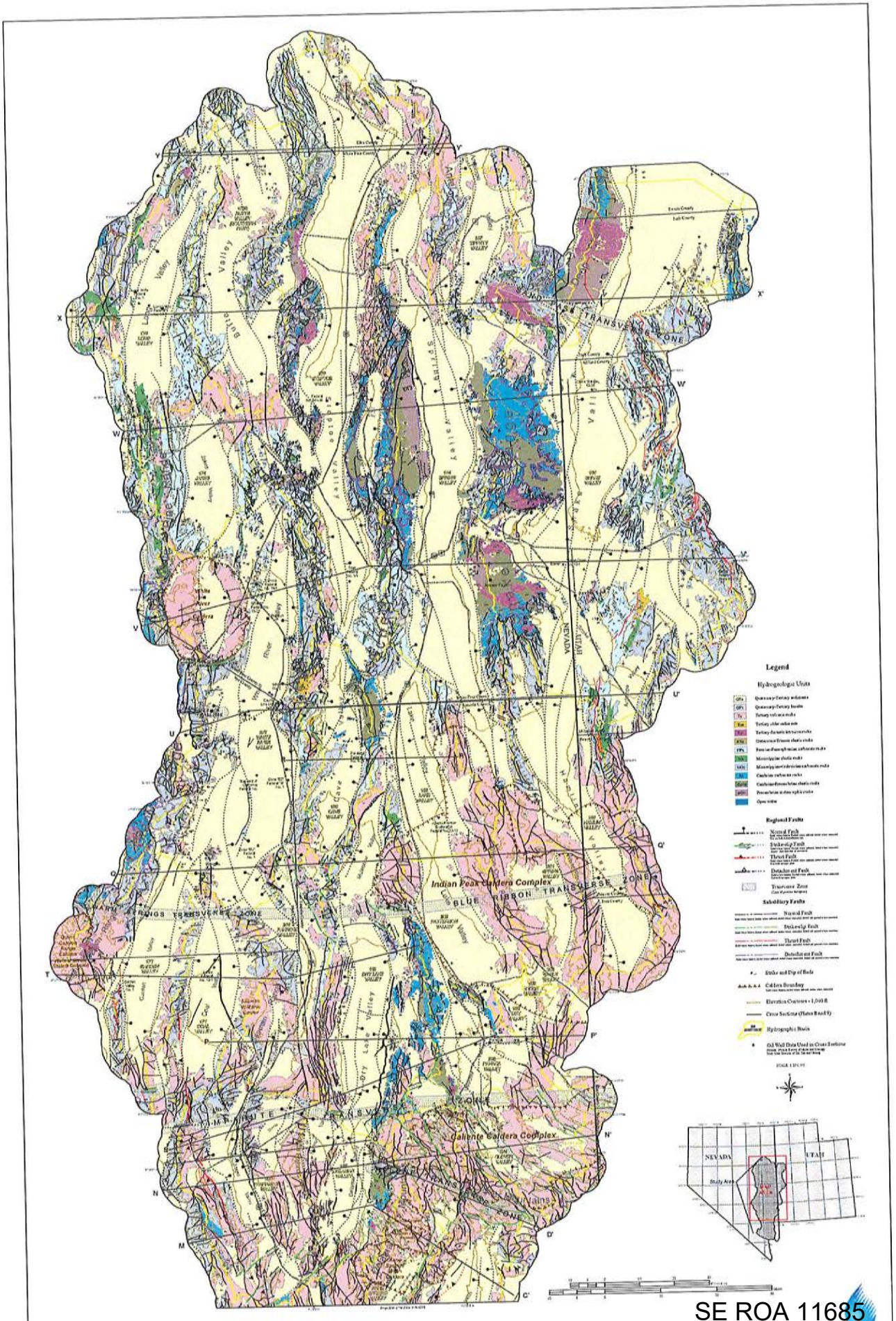

PLATE 6. HYDROGEOLOGY OF WHITE PINE AND NORTHERN LINCOLN COUNTIES, NEVADA, AND ADJACENT AREAS, NEVADA AND UTAH

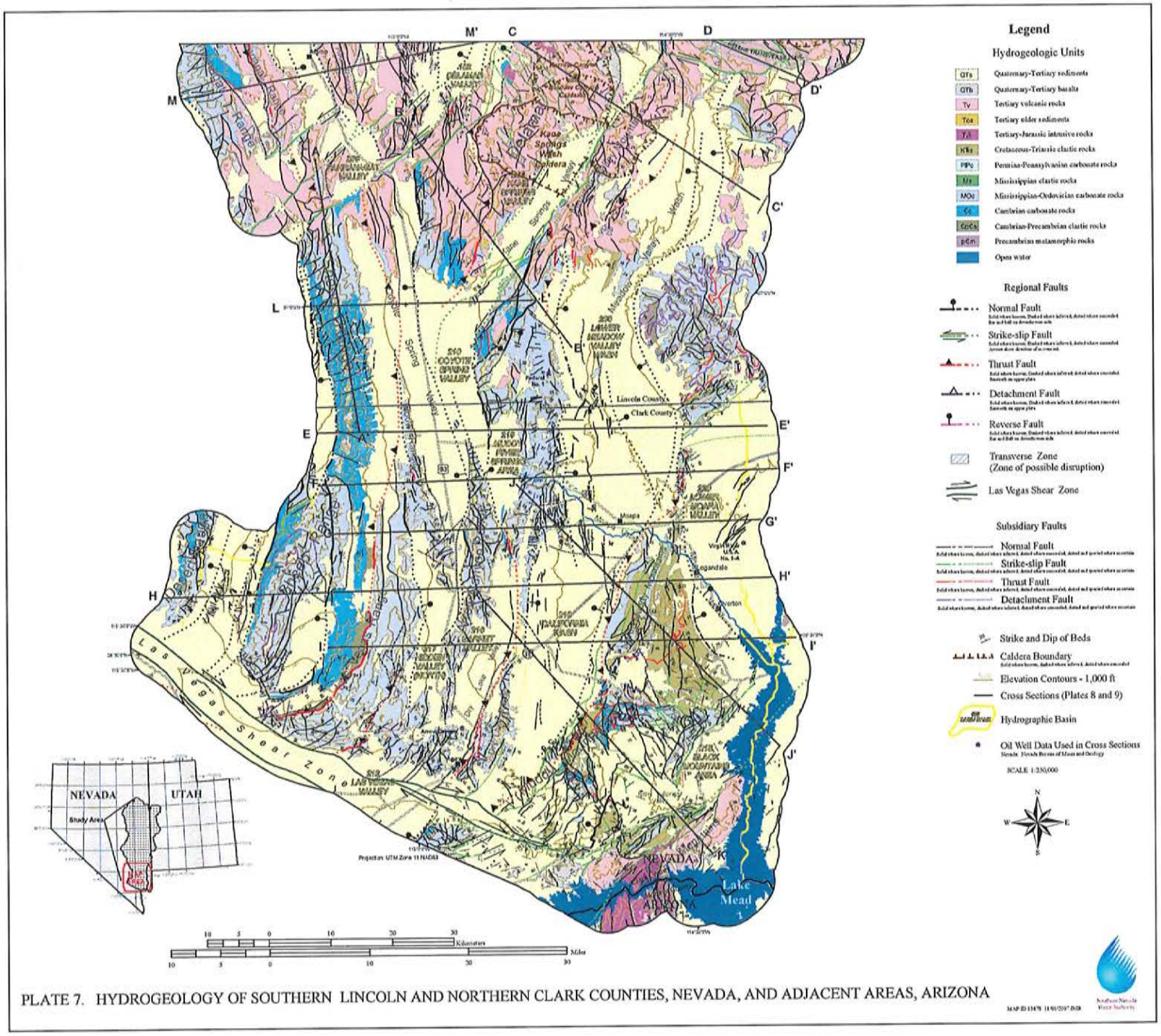

PLATE 7. HYDROGEOLOGY OF SOUTHERN LINCOLN AND NORTHERN CLARK COUNTIES, NEVADA, AND ADJACENT AREAS, ARIZONA

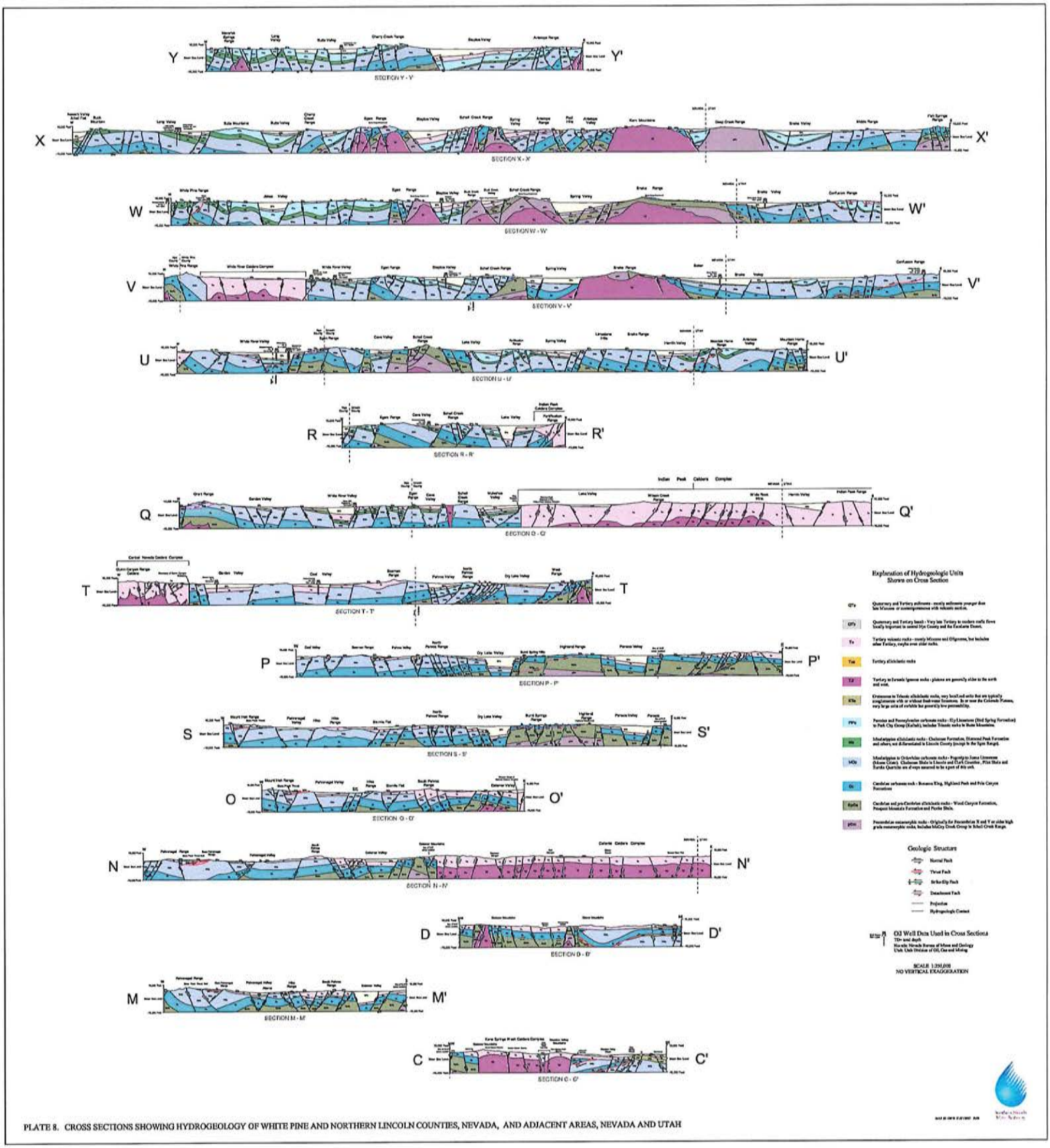

PLATE 8. CROSS SECTIONS SHOWING HYDROGEOLOGY OF WHITE PINE AND NORTHERN LINCOLN COUNTIES, NEVADA, AND ADJACENT AREAS, NEVADA AND UTAH

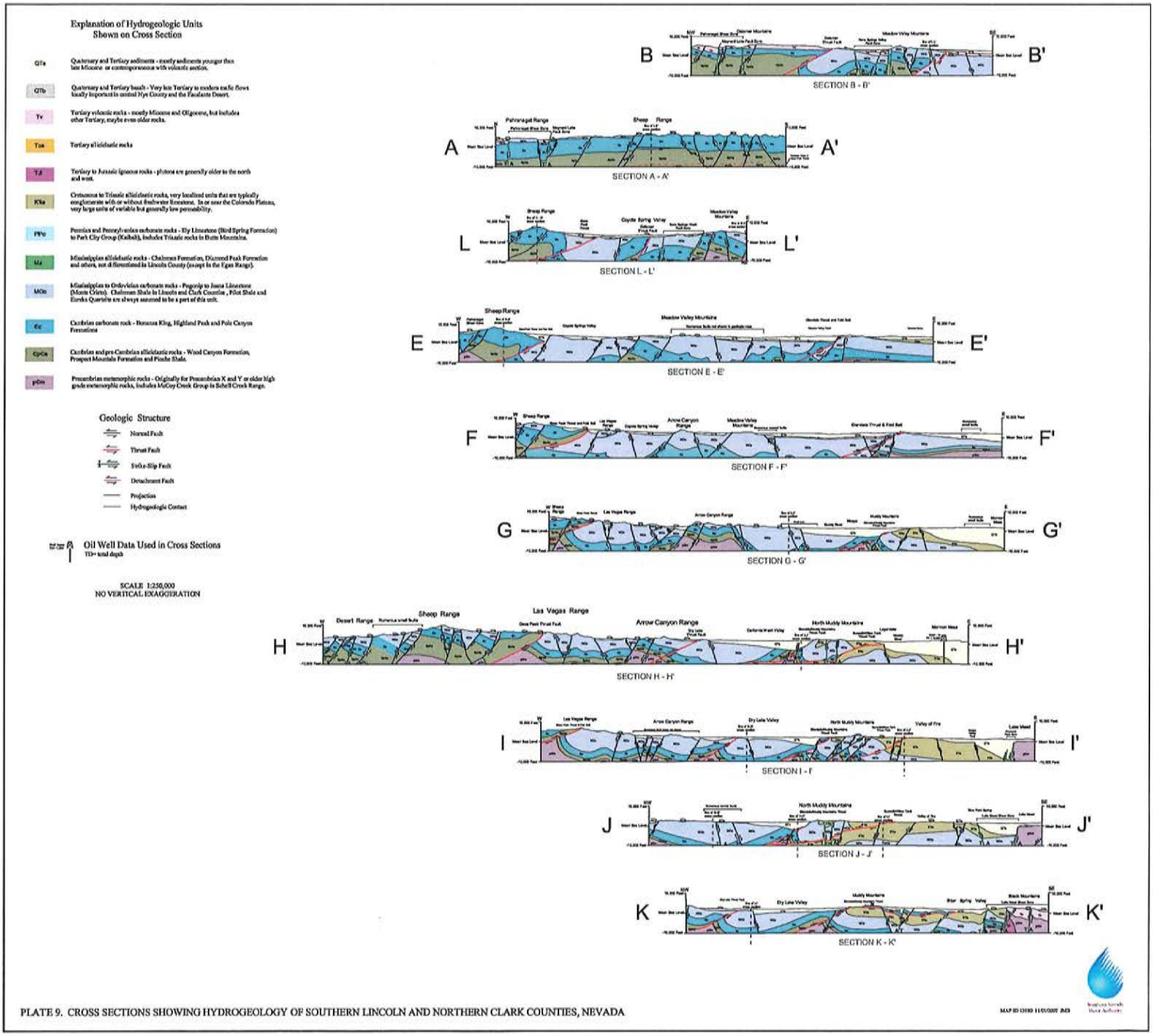
Explanation of Hydrogeologic Units
Shown on Cross Section
QTa
Quaternary and Tertiary sediments - mostly sediments younger than late Miocene or contemporaneous with volcanic section.
QTb
Quaternary and Tertiary basalt - Very late Tertiary to modern mafic flows locally important in central Nye County and the Escalante Desert.
Tv
Tertiary volcanic rocks - mostly Miocene and Oligocene, but includes other Tertiary, maybe even older rocks.
Tsk
Tertiary siliciclastic rocks
Ti
Tertiary to Jurassic igneous rocks - plutons are generally older to the north and west.
KTa
Cretaceous to Triassic siliciclastic rocks, very localized units that are typically conglomeratic with or without freshwater limestone. In or near the Colorado Plateau, very large units of variable but generally low permeability.
PPe
Permian and Pennsylvanian carbonate rocks - Ely Limestone (Bird Spring Formation) to Park City Group (Kaibab), includes Triassic rocks in Butte Mountains.
Mz
Mississippian siliciclastic rocks - Chainman Formation, Diamond Peak Formation and others, not differentiated in Lincoln County (except in the Egan Range).
MDe
Mississippian to Ordovician carbonate rocks - Pogonip to Joana Limestone (Adams Units). Chainman Shale in Lincoln and Clark Counties , Pilot Shale and Eureka Quartzite are always assumed to be a part of this unit.
Cc
Cambrian carbonate rock - Bonanza King, Highland Peak and Pole Canyon Formations
CpCa
Cambrian and pre-Cambrian siliciclastic rocks - Wood Canyon Formation, Prospect Mountain Formation and Pioche Shale.
pCm
Precambrian metamorphic rocks - Originally for Precambrian X and Y or older high grade metamorphic rocks, includes McCoy Creek Group in Schell Creek Range.
Geologic Structure
Normal Fault
Thrust Fault
Strike-Slip Fault
Detachment Fault
Projection
Hydrogeologic Contact
Oil Well Data Used in Cross Sections
TD= total depth
SCALE 1:250,000
NO VERTICAL EXAGGERATION
B
B'
SECTION B - B'
A
A'
Pahranagat Range
Sheep Range
SECTION A - A'
L
L'
Sheep Range
Coyote Spring Valley
Meadow Valley Mountains
SECTION L - L'
E
E'
Sheep Range
Meadow Valley Mountains
SECTION E - E'
F
F'
Sheep Range
Arrow Canyon Range
Meadow Valley Mountains
SECTION F - F'
G
G'
SECTION G - G'
H
H'
Desert Range
Sheep Range
Las Vegas Range
Arrow Canyon Range
North Muddy Mountains
SECTION H - H'
I
I'
Las Vegas Range
Arrow Canyon Range
Dry Lake Valley
North Muddy Mountains
Valley of Fire
Lake Mead
SECTION I - I'
J
J'
North Muddy Mountains
SECTION J - J'
K
K'
Muddy Mountains
Dry Lake Valley
Black Mountains
SECTION K - K'
PLATE 9. CROSS SECTIONS SHOWING HYDROGEOLOGY OF SOUTHERN LINCOLN AND NORTHERN CLARK COUNTIES, NEVADA